DE-FC21-93MC30256--99

The Extraction of Bitumen From Western Oil Sands
Volume I

Final Report
November 26, 1997

By
Alex G. Oblad; Donald A. Dahlstrom
Milind D. Deo; John V. Fletcher
Francis V. Hanson; Jan D. Miller
J.D. Seader

Work Performed Under Contract No.: DE-FC21-93MC30256

For
U.S. Department of Energy
Office of Fossil Energy
Federal Energy Technology Center
P.O. Box 880
Morgantown, West Virginia 26507-0880

By
University of Utah
Department of Chemical and Fuels Engineering
Department of Metallurgical Engineering
Salt Lake City, Utah 84112

Disclaimer

TABLE OF CONTENTS

LIST OF FIGURES

INFORMATION REQUIRED FOR THE NATIONAL ENVIRONMENTAL POLICY ACT (NEPA)

WATER BASED RECOVERY OF BITUMEN

FLUIDIZED BED PYROLYSIS OF OIL SANDS IN A THREE-INCH DIAMETER FLUIDIZED BED

FLUIDIZED BED PYROLYSIS OF OIL SANDS IN A LARGE DIAMETER REACTOR

IN-SITU TECHNOLOGIES: STEAM ASSISTED GRAVITY DRAINAGE (SAGD)

UINTA BASIN BITUMEN HYDROTREATING: A COMPARISON OF CATALYTIC AND THERMAL EFFECTS DURING HYDROTREATING OF BITUMEN-DERIVED HEAVY OILS

HYDROTREATING KINETIC STUDY FOR PR SPRING BITUMEN-DERIVED HEAVY OILS OVER HDN AND HDM CATALYSTS

UINTA BASIN BITUMEN HYDROTREATING: CATALYTIC UPGRADING OF THE ASPHALT RIDGE BITUMEN

LIST OF TABLES

WATER-BASED RECOVERY OF BITUMEN

SUPERCRITICAL FLUID EXTRACTION OF OIL SAND BITUMENS FROM THE UINTA BASIN, UTAH

UINTA BASIN BITUMEN HYDROTREATING: THERMAL CONVERSION OF THE PR SPRING BITUMEN-DERIVED HEAVY OIL IN THE PRESENCE OF NA/ALUMINA

UINTA BASIN BITUMEN HYDROTREATING: A COMPARISON OF CATALYTIC AND THERMAL EFFECTS DURING HYDROTREATING OF BITUMEN-DERIVED HEAVY OILS

HYDROTREATING KINETIC STUDY FOR PR SPRING BITUMEN-DERIVED HEAVY OILS OVER HDN AND HDM CATALYSTS

UINTA BASIN BITUMEN HYDROTREATING: CATALYTIC UPGRADING OF THE ASPHALT RIDGE BITUMEN

EXECUTIVE SUMMARY

Principal Investigator: A.G. Oblad

The Oil Sand Research and Development Group at the University of Utah revised and updated the environmental assessment of the impact of projected program-related activities for the 1994-1996 contract period in accordance with the requirements of the National Environmental Policy Act.

The surface tension of toluene-extracted bitumens from the Whiterocks, Sunnyside, PR Spring, Asphalt Ridge, and Circle Cliffs oil sands was determined by the Wilhelmy plate technique and found to be 20.6 mNm^{-1}, 21.3 mNm^{-1}, 31.2 mNm^{-1}, 28.9 mNm^{-1}, and 29.3 mNm^{-1} at 333 K, respectively. No apparent correlation between the bitumen surface tension and fractional composition of bitumen was observed.

A linear relationship between the bitumen surface tension and temperature was found for Utah bitumens examined in the temperature range of 310-356 K (depending on bitumen sample). The temperature coefficient for surface tension was calculated to be -0.077 $mNm^{-1}deg^{-1}$, -0.063 $mNm^{-1}deg^{-1}$, -0.097 $mNm^{-1}deg^{-1}$, -0.078 $mNm^{-1}deg^{-1}$, and -0.093 $mNm^{-1}deg^{-1}$, for the Whiterocks, Sunnyside, PR Spring, Asphalt Ridge, and Circle Cliffs bitumen, respectively.

The contact angles for water drops at the surface of bitumen films were measured and the bitumen surface tension at 294 K was calculated from Neumann's equation-of-state. The contact angle technique provided comparable values for the bitumen surface tension at room temperature

for the Whiterocks, Sunnyside, and PR Spring samples. Significant discrepancies between the bitumen surface tension values as obtained from the contact angle technique and as obtained from direct measurements with the Wilhelmy plate technique were found for the Asphalt Ridge and Circle Cliffs bitumens. In this regard, the contact angle technique, which is based on Neumann's equation-of-state and contact angle measurements, may not be valid and, in any event, is limited to a small temperature range.

The supercritical fluid extraction (SFE) of bitumens from the Whiterocks, Asphalt Ridge, PR Spring and Sunnyside oil sand deposits of the Uinta Basin has been investigated in a semi-continuous system. The extraction experiments were performed at five different operating conditions: a combination of three pressures and three temperatures using commercial propane as the solvent. The results indicted that the cumulative extraction yields increased with an increase in pressure at constant temperature and decreased with increase in temperature at constant pressure. The extraction yields increased with an increase in solvent density.

The composition of the feedstock was a major factor in controlling the extraction yields. The four bitumens varied significantly in their physical and chemical properties. The extraction yields were inversely proportional to the bitumen asphaltene content and directly proportional to the bitumen resin content. The cumulative extraction yields increased with an increase in bitumen volatility and saturates and aromatic contents for the Whiterocks, PR Spring and Sunnyside bitumens. The asphaltenes appeared to concentrate in the residual fraction and were not extracted. Furthermore, they hindered the extraction of other solubility classes. The extracted phases were upgraded liquids compared to original bitumen feedstocks and the volatilities of the extract phases were considerably higher than those of the original bitumens. The fractionation of the residual

fractions into solubility fractions indicated that the saturates and aromatic were preferentially extracted from the bitumen relative to asphaltenes and resins. This phenomena was confirmed by reduction in the H/C ratio of the residual fractions.

The SFE of Asphalt Ridge and Sunnyside bitumen was modeled using continuous thermodynamics principles and the Peng-Robinson equation of state. A process flow diagram was suggested to upgrade bitumens using supercritical fluid extraction and separation technology. Suitable operating conditions such as pressure, temperature and solvent-to-feed ratio were identified for the proposed extraction and separation process concept. The modeling successfully fit the experimental observations.

A high temperature simulated distillation technique was developed along with software to extend the ASTM D2887 and D5307 techniques to estimate the boiling point of heavy oils from 811 K to 973 K.

The residual drum quantity samples of the mined oil sand ores from the Circle Cliffs, Whiterocks, Asphalt Ridge, PR Spring and Sunnyside oil sands deposits which were obtained for use in the University of Utah Oil Sand Research and Development Program have been discarded. The contents of the drums were transferred to a dump truck and were taken to Staker Asphalt for use as feedstock for the preparation of hot mix asphalt paving material. The drums were cleaned and recycled as scrap metal.

The studies related to the 3-inch diameter flluidized bed oil sand pyrolysis reactor included coked sands and oil sands feeding using a bin discharge auger feeder, the withdrawal of solids from a fluidized bed using a modified L-valve, fluidization-defluidization experiments using different fluidization modes, and the determination of minimum fluidization velocities at ambient

and elevated temperatures and pyrolysis of the PR Spring oil sands.

The feeder study results indicated that the modified Acrison bin discharge feeder with a water cooled E-auger provided linear and reproducible oil sands feed rates from 1 to 10% of the full range of the feeder motor speed controller. The feeder study confirmed that predictable and reproducible feed rates were possible with a solid fight C-auger when feeding coked sands.

The coked sands withdrawal device was a modified pneumatic L-valve with an auxiliary aeration port. The variables studied included the lengths of the vertical and horizontal sections, the location of the primary gas injection port, and the injection gas flow rates. The results indicated that the effect of the length of the vertical section on solids withdrawal rate was not a significant variable. Solids flowed freely due to gravity when the length of the horizontal section was less than two times its diameter. The solids flow rate decreased as the length of the horizontal section increased. The maximum solids flow rate was obtained when the injection gas port was located 1.3 cm behind the center line of the vertical section. The solids flow rate decreased when the gas injector was moved in either direction.

Fluidization studies were conducted with the coked sands produced from previous oil sands pyrolysis experiments. The fluidization experiments indicated that the coked sands, which were group B particles according to Geldart's classification system, had a minimum fluidization velocity of 1.41 cm/s in the regular fluidization mode, 1.35 cm/s in the reduced pressure fluidization mode, and 1.62 cm/s in the pull fluidization mode. Three different fluidization modes have been identified and the pressures in the reactor for the three modes have also been analyzed. The fluidization curves obtained with a tapered gas distributor have been obtained. Fluidization studies at elevated temperatures (>373 K) indicated that empirical minimum fluidization velocity

correlations developed at ambient temperatures were incapable of predicting minimum fluidization velocities at elevated temperatures. An alternative relationship was developed in this study in which the minimum fluidization velocity was determined to be $2.03\text{-}2.02\times10^{-3}T$ cm/s in the temperature range from 297 to 623 K.

The mined oil sands ore used in the pyrolysis studies was obtained from the PR Spring oil sands deposit. The influence of reactor temperature and solids retention time on the product distribution and yields and on the total liquid product qualities was determined in the pyrolysis process variable study. The total liquid yields increased as the reactor temperature increased in the range from 723 to 773 K at a fixed solids retention time of 30 minutes. A maximum yield of 84.2 wt% was obtained at a reactor temperature of 773 K. The liquid yields decreased slightly as the reactor temperature was increased from 773 to 798 K. The coke yields decreased as the reactor temperature increased from 723 to 773 K. The coke yield was insensitive to the reactor temperature above 773 K. The hydrocarbon gas (C_1 to C_4) yields increased with reactor temperature from 723 to 798 K.

The total liquid product yields ranged from 80 to 84 wt% based on bitumen fed to the reactor as the solids retention time increased from 18.5 to 39 min at a constant reactor temperature of 773 K. The coke yields increased slightly with solids retention time. The hydrocarbon gas (C_1 to C_4) yields were insensitive to solids retention time. The shortest solids retention time achieved for the pyrolysis of the PR Spring oil sands in this system was 18.5 min. The reactor had a tendency to plug with unreacted oil sands at solids retention times below about 20 min.

The total liquid produced in the pyrolysis studies were significantly upgraded relative to the bitumen.

Pyrolysis experiments with PR Spring oil sands were also conducted in a 6-inch diameter pilot scale fluidized bed reactor. The effect of reactor temperature and solids residence time on product distribution and yields was investigated. The liquid products (C5+) were analyzed to determine the extent of bitumen upgrading achieved in the process and to study the effect of process variables on the quality of the liquid product. The reactor temperature varied between 723 and 808 K and the solids residence time varied between 20 and 50 min. The fluidization gas flow rate was maintained constant at 5380$\pm$141 SCFH (approximately five times the minimum fluidization velocity) in all experiments.

The liquid yields obtained in this investigation were significantly higher than those obtained with laboratory scale reactors and a pilot scale rotary kiln reactor (77 to 82 wt% as compared to 45 to 70 wt%, respectively). Concomitant with the increase to liquid yields was a decrease in light gas (C1 to C4) yields (1-6 wt% as compared to 15-22 wt%, respectively). The product distribution and yields did not exhibit discernible trends with reactor temperature and solids residence time. These results were presumed to be related to suppression of secondary cracking reactions due to rapid removal of primary cracked pyrolysis products from the reactor. It is proposed that the superior quality of fluidization and elimination of slugging due to the "pull" mode of fluidization and larger diameter of the reactor were responsible for better mixing and increased mass transfer rate between the emulsion and bubble phases in the fluidized bed. This led to a reduction in the effective residence time of the primary pyrolysis products and a suppression of secondary cracking reactions.

The liquid products obtained in this investigation were upgraded compared to the bitumen in terms of volatility, viscosity, molecular weight, pour point, Conradson carbon residue,

asphaltenes content, and trace metals (Ni and V) contents. The nitrogen and sulphur contents of the total liquid products were also reduced relative to the bitumen. The reactor temperature had a minor effect on the liquid product quality. The liquid products obtained at high reactor temperatures (>748K) were only slightly more upgraded than those produced at low reactor temperatures (<748K). The solids residence time did not appear to exert any influence on liquid product quality.

Based on the results of this study, the following set of process conditions are recommended for fluidized bed pyrolysis of PR Spring oil sands: reactor temperature, 748K; solids residence time, 20 min; fluidization gas velocity, 5 time Umf; and settled reactor height to diameter ratio (H/D), 1.9.

A thermal process involving coupled fluidized-bed reactors has been developed at the University of Utah for thermal extraction of tar sand bitumen and has been described in previous reports. During this reporting period, the development of a comprehensive model for the process was completed, which incorporates sub-models for fluidization hydrodynamics, pyrolysis and combustion kinetics, mass and heat transfer, material and energy balances, and the heat pipes that couple the two fluidized beds.

The model was used to determine optimal process conditions for maximizing oil yields and minimizing process energy requirements. The model predicts that a pyrolysis temperature of 475°C and a combustion temperature of 600°C are optimum. The model accounts for differences in yields of different tar sands on the basis of the chemical nature of compounds present in the bitumen. However, due to the complexity of the pyrolysis process, more information about the chemistry of pyrolysis of bitumen is needed for making predictions with more certainty.

Experiments were carried out to verify the model and the predicted optimal operating conditions. The simulation results compared well with experimental results obtained for Whiterocks tar sand. Material balances on the experimental data included quantifying the amount of light gases (by gas chromatography), liquid product, and coke formed on the sand. Energy balances were used to determine the effectiveness of the head pipes. The two main operating parameters predicted by the model and verified by experiments were the pyrolysis temperature and sand residence time. The quality of the liquid product was determined by measuring its specific gravity, viscosity, pour point, Conradson Carbon Residue, and simulated distillation fractions. Using the ASPEN Plus simulator, a cost analysis was completed for a hydrotreating plant to upgrade the oil produced from the bitumen.

A heat recovery flowsheet was added to the scaled-up version of the model and the entire process was optimized. The optimal pyrolysis temperature, pyrolysis sand residence time, and combustion temperature were obtained. An optimal control strategy was developed, using experimental data, to find the optimal trajectories for the pyrolysis temperature and residence time, while minimizing a selected cost function.

The steam assisted gravity drainage (SAGD) method of thermal in situ oil recovery from bitumen bearing sandstones has been evaluated for potential application to Utah oil sands. Sensitivity studies were conducted using a thermal reservoir simulator. A gravity driven process such as SAGD is expected to be sensitive to the grid size in the vertical direction. A comprehensive set of simulations were performed to examine the effect of grid size on simulation results. In a process where the injectors and producers are placed in close proximity, the injection and reservoir pressure are of importance. Hence these parameters were studied. Permeabilities,

both vertical and horizontal are also expected to play a significant role.

Grid size sensitivity studies revealed that using blocks of six to ten feet thickness provided adequate resolution without requiring inordinate amounts of computer time. Best results were obtained by using grid blocks of various size. Regions of high activity such as near the well bore consisted of five foot thick grid blocks, while areas near the edge of the reservoir were adequately represented with 20 foot thick grid blocks.

Several sensitivity comparisons were made between the source-sink model and the discretized well bore model. A discretized well bore model allocates space within the simulation to account for the actual physical presence of the well bore. This method is much more rigorous, but also much more time intensive, than the source-sink model. Results indicated no significant differences in the output data between the two models.

Changes in reservoir pressures did not noticeably effect the amount of oil recovered as long as the pressure difference between injector and reservoir was greater than 50 psi. Smaller pressure differences greatly reduced the recovery efficiencies. Output from the simulations indicates a strong correlation between high recovery efficiencies and high reservoir permeability. This relationship is most noticeable at lower permeability levels, where a permeability increase of just 0.1 Darcy, in the vertical direction, resulted in a four-fold increase in recovery efficiency.

A comparison of two main types of well patterns -- vertical injector / horizontal producer and horizontal injector / horizontal producer was made. The study compared the recovery efficiencies associated with one-, two-, and three- well patterns during a 7-year project lifetime. Efficiencies were calculated based on the percent recovery of the original oil in place (%OOIP). Additionally, comparisons of the volume of water injected versus the volume of oil recovered

(water-to-oil ratio) were made. On an efficiency basis, the best results of the wells patterns studied were obtained in the closely spaced (100 ft), 3 horizontal pairs system. While the 3 vertical injector / one horizontal producer system consistently produced at a lower efficiency than the 3 horizontal pairs system, the difference was small enough to suggest that from an economic standpoint, the former process might be preferable to the latter. Similar results were found among the four and two well systems.

PR Spring bitumen was hydrotreated in a fixed-bed reactor over a commercial Mo/alumina hydrodemetallation (HDM) catalyst. Hydrodenitrogenation (HDN), hydrodesulfurization (HDS), hydrodemetallation, Conradson carbon residue (CCR) reduction, and residuum conversion were studied as a function of process operating conditions (T=625-685K, WHSV=0.26-1.55 h^{-1} and reactor pressure=11.1-16.6 Mpa). The hydrogen-to-oil ratio was fixed at 890 m^3/m^3 (5000 scf H_2/bbl). The degree of sulfur removal was greater than residuum conversion and nitrogen removal with increasing temperature and contact time. Nitrogen conversion was lower than the conversions of the other species in all cases. Reactor pressure did not exert a significant influence on nitrogen and sulfur removal and CCR and residuum conversion.

The hydrotreating of PR Spring bitumen-derived heavy oils was studied in a fixed-bed reactor over a presulfided commercial NiMo/alumina hydrodenitrogenation catalysts. The extent of heteroatom and metal removal and of Conradson carbon (CCR) and residuum (>811 K) conversion were determined in terms of process operating variables. The operating variables investigated were temperature (625-685 K) and liquid hourly space velocity (0,14-0.80 h^{-1}). Pressure and hydrogen-to-oil ratio were fixed at 13.7 Mpa and 890 m^3/m^3 (5000 scf H_2/bbl); respectively, in all experiments.

Product distributions and yields of the hydrotreated bitumen-derived heavy oils were determined. The degree of nickel, nitrogen and sulfur removal and of CCR and residuum conversion was significant as reciprocal LHSV increased at a fixed temperature and as temperature increased at a fixed LHSV. The residuum fraction (>811K) conversion increased significantly with residence time concomitantly the yields of gas oil (617-811K), distillate (477-617K), naphtha (IBP-477K) and C_1-C_4 gases increased. Residuum conversion to volatiles was significant at higher temperatures. The yield of distillate, naphtha and gas increased rapidly at higher temperatures.

The thermal cracking of PR Spring bitumen-derived heavy oils in the presence of hydrogen was studied in a fixed-bed reactor as a function of process operating variables. The reactor was filled with a catalytically inert sodium exchanged alumina. The packing consisted of an alumina hydrodenitrogenation catalyst support which had been impregnated with 2 wt% sodium to reduce the acidity of the alumina. Thermal reactions were investigated with regard to denitrogenation, desulfurization, demetallation, Conradson carbon residue (CCR) reduction and residuum conversion. The process operating variables investigated were temperature (642-683 K), and WHSV (0.25-0.74 h^{-1}). The reactor pressure and hydrogen-to-oil ratio were fixed at 13.7 MPa and 890 m^3/m^3 (5000 scf H_2/bbl); respectively, in all experiments The product distributions and yields were also determined as a function of process operating variables.

Residuum conversion over the sodium-impregnated catalyst support was greater in all cases relative to nitrogen and sulfur removal due to thermal cracking of the residuum. Only low levels of heteroatom conversion were possible via thermal reactions. The extent of nitrogen removal over the sodium-impregnated catalyst support was lower than that of all other classes of component-types. Significant levels of CCR conversion were obtained despite the absence of metal sulfides on the

alumina and were attributed to hydrothermal conversion.

The relative magnitude of catalytic and thermal reactions during the hydrotreating of PR Spring bitumen-derived heavy oil was evaluated in a fixed-bed reactor as a function of temperature, residence time and catalyst selection. The relative effects of thermal and catalytic reactions were evaluated by hydrotreating the PR Spring bitumen-derived heavy oil over three catalysts: sulfided NiMo/alumina HDN catalyst, Mo/alumina HDM catalyst and sodium-impregnated alumina. Catalytic and thermal effects for each of the catalysts were evaluated under a range of temperature (625-685 K) and liquid hourly space velocity (0.14-0.81 h^{-1}). The reactor pressure, 13.7 MPa, and the hydrogen-to-oil ratio, 890 m^3/m^3 (5000 scf H_2/bbl), were fixed in all experiments.

The catalysts activities were ranked as follows: HDN catalyst > HDM catalyst > sodium-impregnated alumina based on their activities for nitrogen, sulfur and nickel removal as well as for the conversion of Conradson carbon residue (CCR) and residuum. The catalyst activities were strongly dependent on the metal loading and were dependent, to a lesser extent, on the acidity of the alumina support. CCR and residuum conversion was closely linked relative to heteroatom and metal removal. This is attributed to a significant overlap between moieties which are classified as CCR precursors and moieties which are classified as residuum. Catalyst selection significantly affected residuum conversion. This is because the high catalyst densities employed in packed bed reactors accentuate catalytic reactions relative to thermal reactions. Although sulfur was generally more reactive than nitrogen, sulfur conversions in excess of 70% were difficult to achieve. It was presumed that 30-40% of the sulfur was asphaltic in nature and exhibited low reactivity. For this reason it was easy to achieve significant sulfur conversion as low severities, but difficult to achieve deep desulfurization at high severities. The deactivation rates of HDN and HDM catalysts were 0.06 and

0.02°API/day, respectively.

The kinetics of removal of nitrogen, sulfur and metals, as well as, conversion of Conradson carbon residue (CCR) and residuum were studied in a fixed-bed reactor. These studies were performed with commercial NiMo/alumina hydrodenitrogenation and Mo/alumina hydrodemetallation catalysts. Bitumen-derived heavy oils from the PR Spring oil sand were hydrotreated under a range of process conditions. The process conditions included reactor temperature (625-685 K), space velocity (0.14-0.81 h^{-1}) and total reactor pressure (11.1-16.6 Mpa).

Conversion data were modeled with a pseudo nth order kinetic model and a parallel-consecutive reaction model. It was found that hydrodenitrogenation over HDN and HDM catalysts followed pseudo nth order kinetics. Hydrodesulfurization and hydrodemetallation and CCR and resid conversion data were correlated with a parallel-consecutive reaction model.

The bitumen extracted from Asphalt Ridge oil sands was hydrotreated over three sulfided NiMo/γ-Alumina hydrodenitrogenation catalysts in a fixed bed reactor to study the extent of upgrading as a function of process variables and catalyst. The process variables investigated were temperature (619-685 K), liquid hourly space velocity (0.18-0.95 h^{-1}), and pressure (11.1-15.3 Mpa). The hydrogen/oil ratio was fixed at 890 m^3/m^3 in all experiments.

The effects of process variables and catalyst on hydrodenitrogenation, hydrodesulfurization, and hydrodemetallation, and on Conradson carbon residue (CCR), asphaltenes, and residuum conversion, viscosity reduction, and yields and product distribution were investigated. Temperature and space velocity exerted a greater influence on heteroatom reduction and conversion than pressure. High surface area was a dominant factor for species conversion in the lower temperature regime, whereas high surface area and wide pore size distribution appeared to exert equivalent effects at

temperatures above 684 K.

Significant upgrading of the bitumen was achieved after secondary hydrotreating of the liquid product produced at the severest conditions (temperature of 684 K, LHSV of 0.2 h^{-1}, pressure of 13.7 Mpa) in primary hydrotreating. The total conversions of sulfur, CCR, nitrogen, asphaltenes, and residuum were 99.5, 95.0, 94.8, 92.2, and 79.8 wt%, respectively. The viscosity, measured at 313 K, was reduced by a factor in excess of four orders of magnitude. The total weight fraction of naphtha plus distillate was 48% and increased fourfold compared with that of the bitumen.

It was concluded that the refractory fraction, 20 wt%, of the residuum contained little CCR and asphaltenes and was more difficult to convert than asphaltenes.

The conversions of sulfur, nitrogen, CCR, and residuum in bitumen were successfully modeled by nth power rate law kinetics and by a distributed activation energy model using a normal distribution function. Higher-order kinetics was required to represent the conversions of lumped sulfur, nitrogen, CCR and residuum. The asymptotic lumped kinetic model used to describe hydrodesulfurization was supported experimentally.

The hydropyrolysis reactor system was reassembled and preliminary pressure and flow tests were conducted with a modified mixing nozzle design. Regrettably, no funding was available to carry out actual hydropyrolysis experiments.

INFORMATION REQUIRED FOR THE NATIONAL ENVIRONMENTAL POLICY ACT (NEPA)

Principal Investigator: A.G. Oblad
Co-Principal Investigators: M. D. Deo
F.V. Hanson

INTRODUCTION

The information required for compliance with the National Environmental Protection Act (NEPA) has been documented in this section. This final report has been prepared to reflect the research and development activities performed under the cooperative agreement 94MC30256 between the University of Utah, Department of Chemical and Fuels Engineering and the U.S. Department of Energy. Detailed descriptions of the individual projects, process flow diagrams for the various oil sand recovery technologies, laboratory locations, environmental impacts, health and safety procedures, etc. have been documented in detail in the 1991-92 final report for the cooperative agreement 89MC26268(1). An updated NEPA checklist and the information required for a CX-B exclusion determination were reported in the 1992-1993 final report for the cooperative agreement 89MC26268(2). The proposed program for the current contract does not include any experimental activity which would result in the generation of additional gaseous, liquid and solid wastes over and above those indicated in the detailed [1] and updated [2] reports submitted previously. All liquid and solid waste materials produced during the course of the experimental program will be processed through the EPA approved University of Utah Safety Services disposal system.

This section includes an NEPA checklist and a brief description of the 1993-1994 University of Utah oil sand research and development program and its overall environmental

impact. The information provided essentially qualifies the program for CX-B exclusion determination.

NEPA CHECKLIST

1.	Date: 7-16-96	NEPA Number
2.	Activity/Project Name	Recovery of Bitumen from Western Sands
3.	Project Manager/Branch/Division	J.D. Westhoff, LFT Br., FRM Div
4.	Project/Activity Description	Include purpose, location, site map (proved figure or map if appropriate) construction requirements, schedule, operation processes.

This action is in response to the (DE-FC-21-93 MC30256) application for the cooperative agreement with the University of Utah, Department of Chemical and Fuels Engineering. A similar cooperative agreement was in place between the U.S. DOE and the Department of Fuels Engineering, University of Utah (89MC26286) since 1989. The Department of Chemical Engineering and the Department of Fuels Engineering merged in September of 1992 and now exist as a single department. NEPA approval for the program and the activities conducted under the former cooperative agreement (89MC26286) has been documented in a memo (dated Nov. 1990). The current program is a continuation of the effort to develop commercial processes for the recovery of oil from the extensive tar sand resource base in Utah and for the upgrading of the oil recovered. During the past 15 years, the program has produced a comprehensive body of scientific and engineering data related to the

characterization and processing of the Utah tar sands and has evaluated numerous options for bitumen upgrading.

The program is composed of 20 projects, of which 17 are laboratory bench or laboratory pilot scale processes or computer process simulations that are performed in existing facilities on the University of Utah campus in north-east Salt Lake City. These tasks are:

1. Coupled fluidized-bed bitumen recovery and coked sand combustion
2. Water-based recovery of bitumen
3. Oil sand pyrolysis in a continuous rotary kiln reactor
4. Oil sand pyrolysis in a large diameter fluidized bed reactor
5. Oil sand pyrolysis in a small diameter fluidized bed reactor
6. Combustion of spent sand in a transport reactor
7. Recovery and upgrading of oil sand bitumen using solvent extraction methods
8. Fixed-bed hydrotreating of Uinta Basin bitumens and bitumen-derived hydrocarbon liquids
9. Ebullieted bed hydrotreating of bitumen and bitumen derived liquids
10. Bitumen upgrading by hydropyrolysis
11. Evaluation of Utah's major oil sand deposits for the production of asphalt, high-energy jet fuels and other specialty products
12. Characterization of the bitumens and reservoir rocks from the Uinta Basin oil sand deposits
13. Bitumen upgrading pilot plant recommendations
14. Liquid-solid separation and fine tailings thickening
15. In-situ production of heavy oil from Uinta Basin oil sand deposits
16. Oil sand research and development group analytical facility
17. Process economics

A site map showing the location of the project laboratories on the University of Utah campus is attached as Figure 1. There are no earth moving or construction requirements for the program or its projects. The Departments of Chemical and Fuels Engineering and

Figure 1. Location site map University of Utah

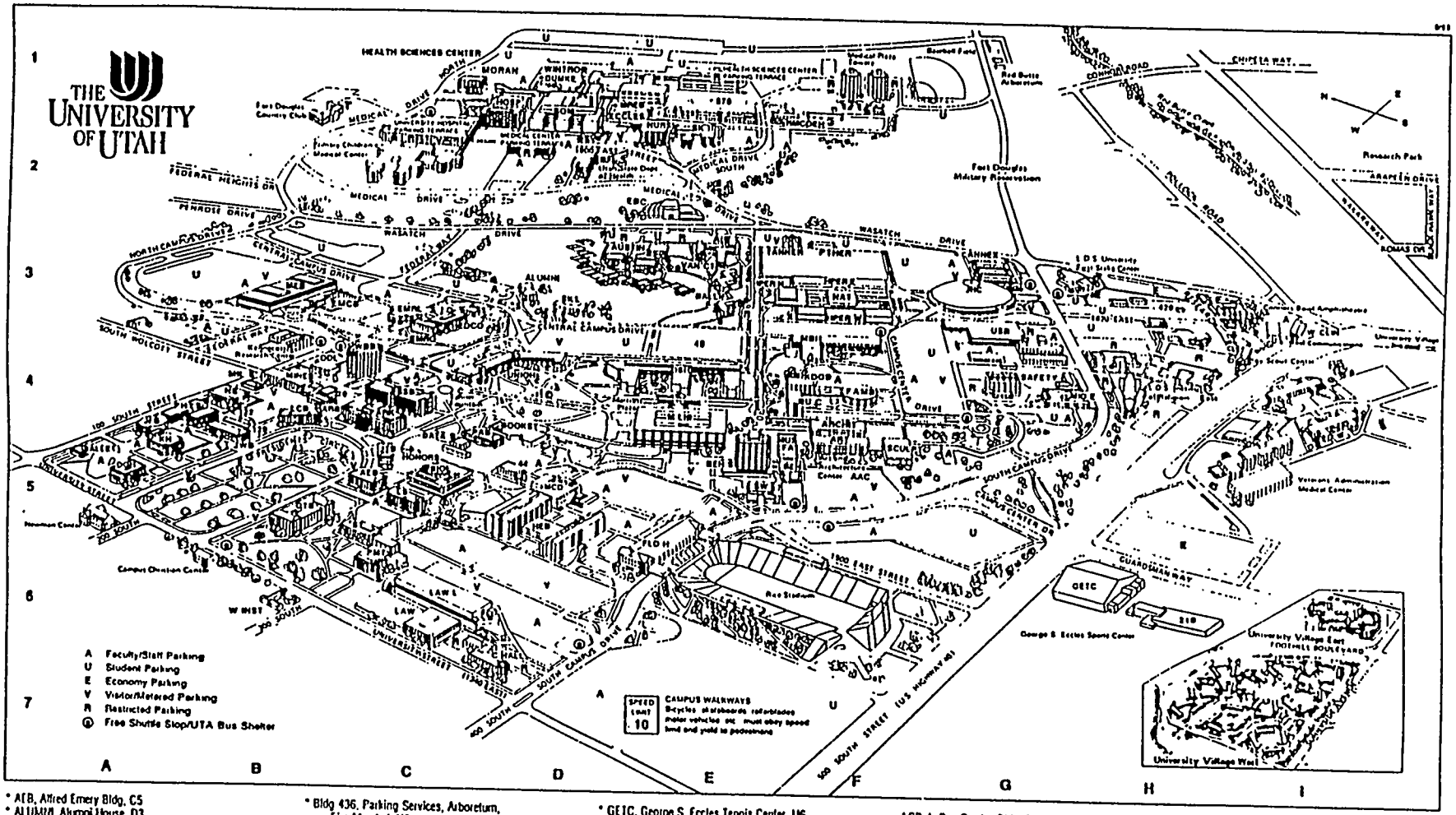

* AEB, Alfred Emery Bldg, C5
* ALUMNI, Alumni House, D3
* ANNEX, Annex Bldg, G3
  ARB, Applied Research Bldg, B4
* ARCHI, Architecture Bldg, F4
* ART, Art Bldg, F4
* AUSTN, Austin Hall, E2
  OPERA, Opera Studio, A5
* BALLR, Ballr Hall, E3
* BEHL, Social & Behavioral Science Lecture Hall, F5
* BEHS, Social & Behavioral Science Tower, E4
* BIOL, Biology Bldg, C5
  Bldg 20, Physics Offices/Lab, B4
* Bldg 44, Office Annex, D5
* Bldg 49, Language/Communications Bldg (under construction), E4
  Bldg 122, Math Office Bldg, B4
* Bldg 129, Math Offices, Communication Lab, B4
* Bldg 210, D Glenn Smith Athletic Center, H6
* Bldg 420, Outdoor Program Bldg, I3
* Bldg 436, Parking Services, Arboretum, Fire Marshal, H3
* Bldg 528, Health Sciences Bookstore, Credit Union, E1
* Bldg 570, Biomedical Polymers Research Bldg (under construction), E1
* BOOKST, University Bookstore, D4
* BUC, Business Classroom Bldg, F4
  CHAEL, Carlson Hall, D6
* DATA S, Data Services Bldg, C4
* DGH, David Gardner Hall, A5
* DUMKE, Dumke Biomedical Engr Research Bldg, D1
* EBC, Dolores Dore Eccles Broadcast Center, E2
* ECCLES, Eccles Health Sciences Library, D1
* ENG, Eccles Institute of Human Genetics, D1
* EMCB, Engineering & Mines Classroom Bldg, C3
* EMRL, Energy & Minerals Research Lab, C4
* EMRO, Energy & Minerals Research Office Bldg, C3
* FAMB, Francis A Madsen Bldg, F4
* HDH, Ernst Nielsen Field House, E5
* GEIC, George S Eccles Tennis Center, H6
* GIB, George Thomas Bldg (Museum of Natural History), B5
* HEB, Henry Eyring Bldg, D5
* HEDCO, Hedco Bldg, C4
  HONORS, Honors Program, C4
* INTRAE, Health, Physical Education & Recreation East Bldg, F3
* INTRAN, Health, Physical Education & Recreation North Bldg, F3
* INTRAW, Health, Physical Education & Recreation West Bldg, F3
* JFB, James Fletcher Bldg, A4
* JHC, Jon Huntsman Center, G3
  JTB, James Talmage Bldg, C4
* JWB, John Widstoe Bldg, B4
* KDGB, Kendall D Gaff Bldg, F4
  KH, Kingsbury Hall, A5
* LAW, Law Bldg C6
* LAWL, Law Library, C6
  LCB, LeRoy Cowles Bldg, B4
* LS, Life Science Bldg, C5
* MBH, Milton Bennion Hall, F3
* MCD, Marriott Center for Dance, D5
* MEB, Merrill Engineering Bldg, B3
  MIDE, Middle East Center, G4
  MIL S, Military Science Bldg, B4
  MINES, Mines Bldg, B4
* M LIB, Marriott Library, E4
* MORAN, John A Moran Eye Center, C1
* MREB, Medical Research & Education Bldg, D1
* MUSFA, Museum of Fine Arts, Utah, F4
* NAT, Natatorium, F3
  NS, Naval Science Bldg, B4
* NURS, Nursing Bldg, E1
  ODL, Ore Dressing Lab, B4
* OSH Olson Spencer Hall, E3
* PAB, Performing Arts Bldg, D4
* PARK, Park Bldg, C4
  PHYS, Physics Bldg B4
* PMT, Pioneer Memorial Theatre, C6
* P THER, Physical Therapy Bldg, F2
* RMCOEH, Rocky Mountain Center for Occupational & Environmental Health, E2
  SAFETY, Public Safety, H3
* SCULPT, Sculpture Bldg, F4
* SILL, Sterling Sill Home Living Center, U3
* SKH, Skaggs Hall, E1
* SOM, School of Medicine Bldg, D1
* SSB, Student Services Bldg, C4
  ST, Stewart Bldg C5
* SW, Social Work Bldg E5
  TANNER, Virginia Tanner Dance Bldg, F2
* U HOSP, University Hospital, D1
* UNION, Olpin Union D3
* USB University Services Bldg, G3
* VAN CT, Van Cott Hall, E2
* WBB, William Browning Mineral Science Bldg, C4
* W CLIN University Wasatch Clinics, I3
  W INST, LDS Institute of Religion (West), B6
* WINTRO, Wintrobe Research Bldg, D1

Metallurgical Engineering operate under the University of Utah, Department of Safety Services, which is responsible for compliance with the U.S. EPA, state an city permits. Hazardous waste management and Chemical Hygiene programs are operated by the University of Utah Department of Safety Services. The air and water effluents from the University are monitored by the city and the state. The hazardous waste disposal program is monitored by the U.S. EPA and the chemical hygiene program is monitored by OSHA.

5. Brief Description of Affected Environment — State if previously disturbed occupied, or vacant. Indicate in a few words the type of cover (e.g. grasslands, woods, natural, landscaped), or habitat types known.

The program and all the projects are located at the University of Utah campus in north-east Salt Lake City. The University of Utah is a major public educational a research institution with an enrollment of about 26,000 students. The University of Utah employs 3,400 full-time faculty and 30,000 personnel in its various facilities. The campus has 233 buildings, including about 1,400 research laboratories all of which are located on 1,480 acres.

6. Environmental Concerns Will the project/activity, either during construction or operation, result in changes or disturbances to the following entities? Provide brief explanations to any "yes" answers.

6.1 Threaten a violation of applicable statutory, regulatory, or permit requirements for environment, safety, and health requirements for DOE orders?

Yes____ No X Unknown

6.2 Require siting and construction or major expansion of waste storage, disposal recovery, or treatment facilities?

Yes____No _X_ Unknown

6.3 Uncontrolled or unpermitted releases resulting from hazardous substances, pollutants or CERCLA-excluded petroleum and natural gas products that preexist in the environment?

Yes____ No _X_ Unknown

6.4 Adversely affect environmentally sensitive resources including:

4.a Threatened/Endangered Species or Critical Habitat Areas

Yes____ No _X_ Unknown

4.b Flood Plains/Wetlands

Yes____ No _X_ Unknown

4.c Archaeological/Cultural Resources

Yes____ No _X_ Unknown

4.d Prime, Unique or Important Farmland

Yes____ No _X_ Unknown

4.e Special sources of Groundwater (sole source aquifer, etc.)

Yes____ No _X_ Unknown

4.f Tundra, Coral Reefs, Rain Forests, Coastal Zones

Yes____ No _X_ Unknown

4.h National Parks, Wild and Scenic Rivers, Waters of the State, etc.

Yes____ No _X_ Unknown

4.i CAA Criteria Pollutants (7)

Yes____No____Unknown _X_

Cumulative gaseous emissions under the current operating conditions will be about 500 kg per year of which 97% would be comprised of carbon dioxide and water vapor. The composition of the remaining 3% or 15 kg per year of he emissions is speculative.

7. Additional Information Will the project/activity...

7.1 affect water use and quality, including sedimentation, and discharge of point/nonpoint source pollutants to surface or ground water?

Yes___ No X Unknown

7.2 control or modify the water, streambed, or shoreline of any stream or water body?

Yes___ No X Unknown

7.3 result in the generation, transportation, and disposal of any hazardous or toxic materials as defined by Federal or applicable state regulations?

Yes___ No X Unknown

Product liquids from process experiments are stored in tightly-sealed drums for upgrading and characterization research. The waste sand is stored for combustion and residual carbon research and is eventually hauled back to the mine of origin for disposal. The solid and liquid hazardous wastes (petroleum products) are collected by the University Department of Safety Services and are disposed of according to state and federal guidelines by their contractor-APTUS Environmental. The University of Utah Safety Services provides a hazardous waste management program including a clear and concise flow-chart for management of hazardous materials from the point of identification to disposal. The office has a US EPA number for hazardous waste handling and disposal and it carefully administers the University waste management activity.

7.4 affect any aspect of the human environment besides those mentioned above either directly or indirectly (e.g. visibility, noise, aesthetic and socioeconomic impacts; public facilities and services or exposure to toxic and hazardous material)?

The program activities are performed in existing buildings. In the worst-case scenario, with three of the reactors operating simultaneously, the noise level in the vicinity of the reactors was measured to be 75-80 db. For operation in the noise intensive areas, hearing protection is provided and used. Visibility and aesthetic effects due to the processes are non existent. A rigorous hazard communication protocol, with formal safety workshops and informal equipment training is in place. The exposure of personnel to hazardous and toxic substances is monitored by the University Safety Services under a comprehensive Chemical Safety and Hygiene plan. The Salt Lake City Office of OSHA (Occupational Safety and Health Administration) monitors the University Department of Safety Services.

7.5 generate public controversy?

Yes____ No X Unknown

Please write all explanations of any "yes" answer on an attached page.

8. Is the Project/Activity specifically called out in the procedures as a categorical exclusion?

Yes X No____ Unknown

State Specific category CX-B 3.10

9. Recommended NEPA Determination: CX_A ____CX-B X EA

EIS____None needed

Original Signed

Signature of Project Manager Date

Original Signed

Signature of Environmental Project Manager Date

Original Signed

Signature of METC NCO Date

RECOVERY OF BITUMEN FROM WESTERN TAR SANDS

Environmental Impact Summary: Categorical Exclusion (CX_B)Determination:

Proposed Action: Renewal of the existing cooperative agreement DE-FC-21-93MC30256 with the University of Utah Department of Chemical and Fuels Engineering.

Location: University of Utah, Department of Chemical and Fuels Engineering, 3290 Merrill Engineering Building, Salt Lake City, Utah, 84112

Proposed by: Morgantown Energy Technology Center, U.S. Department of Energy

Description of the proposed action:

The U.S. DOE and the University of Utah, Department of Chemical and Fuels Engineering, entered into cooperative agreement DE-FC-21-93MC30256 to conduct research and development to create a body of scientific and engineering data necessary to develop commercially viable processes for the recovery and utilization of the extensive tar sand deposits in the United States. All research, development, small-scale fabrication and testing activities will be conducted in existing facilities. The operations will be inspected and monitored by the University Safety and Environmental Personnel, who are responsible to the local state and U.S. EPA regulations. The following is a subject breakdown of the 17 laboratory-scale processes or computer process simulations and calculations that are being performed on the University of Utah campus.

- Thermal recovery
- Water-assisted recovery
- Other recovery processes; solvent extraction and in-situ
- Resource/bitumen characterization/analytical facilities

- Upgrading/specialty chemicals
- Economics

The laboratory equipment being used to carry out the program tasks consists of:

1. Coupled fluidized-bed, pyrolysis-combustion reactor
2. Rotary kiln
3. Small, screening fluidized bed pyrolysis reactor
4. Six-inch fluidized-bed reactor
5. Digestor, separator and associated equipment for water-
6. assisted recovery of bitumen
7. Continuous solvent extractor
8. Hydropyrolysis reactor system
9. Hydrotreater
10. Ebullieted bed hydrocracker-hydrodynamic studies unit
11. Three-phase gravity classifier/thickener
12. Transport reactor for coked sand combustion

The experimental program consists of characterization of the bitumen and of the products of various recovery processes, process variable study of several possible recovery processes and a comprehensive evaluation of the upgrading options.

Feedstock use, product fate, and cumulative waste management are discussed below:

A. Feedstock: A maximum of 6 tons of tar sands will be processed during the current year in all of the experiments. The feedstock will contain approximately 7-12% by weight of the hydrocarbon material or bitumen. The remaining 88-93% of the material will contain predominantly sand (silica) and some clay.

B. Produced Bitumen: The processing is expected to produce about 500 kg of bitumen which will be stored in polyethylene-line containers and will either be used for upgrading research or will be disposed of through the university hazardous waste management system. Conservatively, 95-97% of the hydrocarbon are captured and it is estimated that the maximum hydrocarbon losses are 75 kg for the year.

C. Off Gases: The pyrolytic processes produced vapor streams which are condensed into a lighter product. The lighter gases in the vapor stream are flared to form CO_2 and H_2O. The coked sand combustion is carried out under excess air conditions an generates mostly CO_2 and H_2O and small amounts of CO. At the maximum, the program will generate 500 kg of off-gasses, 485 kg of off gases which would be CO2 and H2O. The remaining 15 kg would be unburned hydrocarbon gasses and CO.

D. Water Wastes: The water assisted recovery processes use process water. Remaining operations use water mainly for cooling the classifier and thickener operations use a closed loop system where there will be no liquid wastes during the operation. The three closed-loop experiments planned for the thickener study are expected to use a total 7,500 kg of water. Once these experiments are complete the products will be down loaded into 55 gallon drums and will be handed over to the University Safety services for appropriate disposal. The water-assisted recovery process studies are expected to use 2500 kg of water. The water used in this process is recycled 10 times after which it is pumped to a water-tight sump and is disposed of as hazardous waste.

E. Solid and Liquid Hazardous Wastes: The spent sand from the pyrolysis reactors is either used for combustion research or is disposed to the mine site of origin. It is not classified as hazardous material. The bitumen and oil produced in the recovery processes are either used in upgrading research or disposed of as hazardous liquid wastes through the university hazardous waste management service. If required the oils are stored in polyethylene lined barrels. The waste solvents resulting due to analytical activity are also stored and disposed in a similar manner. Guidelines described in the University of Utah hazardous waste management manual are strictly adhered to in handling and disposing all hazardous material. The proposed action is a variety of small-scale laboratory research and development projects performed at existing facilities. Its is thus within the threshold limits of the U.S. DOE National Environmental Policy Act (NEPA). The action meets all of the eligibility requirements for categorical exclusions as set forth in 10 CFR 1021, section 410, and all the integral elements of the classes of Actions in Appendix B.

WATER-BASED RECOVERY OF BITUMEN

SURFACE TENSION OF BITUMENS FROM UTAH OIL SANDS AS DETERMINED BY WILHELMY PLATE AND CONTACT ANGLE TECHNIQUES

Principal Investigator:	J.D. Miller
Res. Assoc. Professor:	J. Hupka
Post Doctoral Fellow:	J. Drelich
Research Associate:	R. Bokotko
Graduate Students:	D. Lelinski
	Ch. Holbert

INTRODUCTION

As the conventional crude oil deposits are rapidly being depleted, there is a greater need to develop other petroleum resources. One such resource is oil sand, a bitumen-impregnated sandy material, which is successfully mined and processed in Canada. Bitumen is separated from sand using the hot-water process, and further upgraded to synthetic crude oil. At the University of Utah researchers have developed both water-based separation processes and thermal processes for bitumen recovery from the Utah oil sand deposits, however, these technologies have not been commercialized yet (3).

Processing of oil sands involves several steps in which the physico-chemical properties of the bitumen may be of particular significance in its recovery and upgrading. In particular, properties such as surface tension, interfacial tension, and electrical charge at the bitumen/air and bitumen/water interfaces may affect the efficiency of bitumen separation from oil sands using the hot-water process (4-6). Also, bitumen surface tension may be an important property in upgrading processes such as hydrotreating and hydrocracking when three-phase ebullited bed

reactors are used (7). In this regard, there is a need for basic research leading to specification of the physical and chemical properties of bitumen. This task has received more attention at the University of Utah, in recent years, and the surface properties of Utah oil sand bitumens have been studied. Electrophoretic properties of bitumen emulsions have been reported for Asphalt Ridge (8), Sunnyside (8), and Whiterocks (6) bitumens. The bitumen/air surface tension and the bitumen/aqueous phase interfacial tension for Whiterocks bitumen have been examined also (5, 6). In this contribution the surface tension of toluene-extracted bitumens from the Whiterocks, Asphalt Ridge, Sunnyside, PR Spring, and Circle Cliffs oil sands were measured and the results are presented herein.

Literature Survey of Surface Tension Data

Only a limited amount of experimental data has been reported in the literature on the surface tension of bitumens, and most of these measurements were carried out for Canadian bitumens (4-6, 9-11). Bowman (4), and Isaacs and Smolek (9) measured the surface tension of bitumen recovered from the Athabasca oil sand. Results presented by Bowman (4) have only limited practical significance as they were obtained for nonequilibrated systems and the procedure used was not well-defined. Isaacs and Smolek (9) reported the surface tension value of bitumen which was obtained from the commercial hot water processing of Athabasca oil sand, using du Nouy ring tensiometry. The bitumen surface tension was reported to be 29.6 mNm^{-1} at 64°C which decreased to 25 mNm^{-1} at 112°C. Potoczny et al. (10) measured the surface tension of several Canadian bitumen samples from different sites using the Wilhelmy plate technique. The surface tension values of these samples varied from about 23 mNm^{-1} to 32 mNm^{-1} at 40°C, depending on the location of the oil sand sample and solvent type used for the bitumen extraction. Vargha-Butler et al. (11) proposed that the surface tension of bitumen at room temperature can be determined

from contact angle measurements using Neumann's equation-of-state for surface tension (12). The surface tension of bitumens, as determined from contact angle measurements was reported to be in the range of 24.4 mNm^{-1} to 33.8 mNm^{-1} at 23°C, depending on the sample origin and the experimental procedure used in the bitumen preparation. This new technique for the bitumen surface tension determination based on contact angle measurements was examined for five different Utah oil sand bitumens and the results are presented in this report. The theoretical background for the relationship between the bitumen surface tension and contact angle data is briefly reviewed in the following section.

Equation-of-State for Interfacial Tensions

The force balance at a solid surface involving a three-phase system in which the equilibrium contact angle is established, can be resolved in terms of the interfacial free energies by using the Young equation (13):

$$\gamma_{SV} - \gamma_{SL} = \gamma_{LV} \cos\theta \qquad (1)$$

$$\gamma_{SV} = \gamma_S - \pi \qquad (1a)$$

where γ_S, γ_{SV}, γ_{SL}, γ_{LV} are the surface free energy of solid in contact with vacuum, surface free energy of solid in contact with saturated liquid vapor, interfacial free energy of the solid/liquid interface, and liquid/vapor surface tension, respectively; θ is the contact angle; π is the equilibrium film pressure of the adsorbate (adsorbed liquid vapors), which is assumed to be zero for low energy solid surfaces.

A difficulty in the application of the Young equation (1) is that there are two parameters, γ_{SV} and γ_{SL}, which cannot be measured directly. In this regard, several researchers have tried to estimate the surface free energy of solids based on contact angle data for various liquids, and

calculation methods based on the dispersive and nondispersive theory of interaction between phases have been proposed (14), including Neumann's equation-of-state (12).

Girifalco and Good[15] suggested that if two phases are immiscible and interact only through additive dispersion forces the interfacial free energy can be expressed by the following equation:

$$\gamma_{SL} = \gamma_S + \gamma_{LV} - 2\phi(\gamma_S \gamma_{LV})^{\frac{1}{2}} \quad (2)$$

where Φ is the correction factor called the interaction parameter.

According to Neumann et al. (12), there is a relationship between the surface free energy of the solid, γ_S, of the liquid, γ_{LV}, and the solid/liquid interfacial free energy, γ_{SL}:

$$\gamma_{SL} = f(\gamma_S, \gamma_{LV})$$

It was assumed that the interaction parameter, Φ, is a function of the interfacial free energy of the solid/liquid interface, γ_{SL}:

$$\phi = -\alpha\gamma_{SL} + 1 \quad (3)$$

where α is a constant with a value of 0.0075 m^2/mJ, as determined from contact angle data for hydrophobic surfaces.

Substituting the value of Φ and the Young equation (1) into equation (2), and neglecting the contribution of π, Neumann et al. (12) obtained the following equation-of-state in terms of the appropriate interfacial tensions:

$$\cos\theta = \frac{2(\alpha\gamma_S - 1)(\gamma_S \gamma_{LV})^{\frac{1}{2}} + \gamma_{LV}}{\gamma_{LV}[2\alpha(\gamma_S \gamma_{LV})^{\frac{1}{2}} - 1]} \quad (4)$$

Vargha-Butler and others (11) have proposed that the equation-of-state (4) can be used for determination of the surface tension of bitumens at room temperature. Advancing contact angles for water and glycerol drops placed on Canadian bitumen films were measured. They found that for most bitumens the surface tension data calculated from equation (4) were in good agreement with surface tension data obtained from direct measurements using the Wilhelmy plate technique. However, in a few cases the differences in the surface tension values by these two methods exceeded 2 mNm^{-1}.

A disadvantage of the equation-of-state (4) lies in the discontinuity of the dependence of $\cos\Theta = f(\gamma_S)$ when $2\alpha(\gamma_S\gamma_{LV})^{1/2}$ approaches 1. In order to overcome this disadvantage the above equation-of-state was revised and a new equation was derived by Li and Neumann (16, 17):

$$\cos\theta = 2\left(\frac{\gamma_S}{\gamma_{LV}}\right)^{\frac{1}{2}} e^{-\beta(\gamma_{LV}-\gamma_S)^2} - 1 \qquad (5)$$

where β is a constant with a value of 0.0001247 $(m^2/mJ)^2$, which was determined from contact angle data for low energy solids (17).

The principal advantage of the equation-of-state for interfacial tension is that it allows for the determination of γ_S (the surface tension of bitumen in our case) from a measurement of the contact angle using only one liquid. The applicability of the equation-of-state for bitumen surface characterization was examined in this study. The surface tension values calculated from equation (5) using contact angle measurements for water drops placed on bitumen films are compared with the surface tension data obtained from direct tensiometric measurements.

EXPERIMENTAL

Bitumen Samples

Oil sand samples used in this investigation were obtained from the Whiterocks, Sunnyside, PR Spring, Asphalt Ridge, and Circle Cliffs deposits of Utah. The bitumen was extracted from the oil sand samples using spectrograde toluene (EM Science, U.S.A.). The extractions were carried out for 24 hours at 385-390 K in a Dean-Stark apparatus with Whatman cellulose thimbles, as described in a previous contribution (18). Shark skin filter paper was wrapped around the thimble to retain fine mineral particles which penetrated through the thimble wall. The toluene/bitumen solutions were subjected to 12-14 hours vacuum distillation on the rotary evaporator, 20 torr and 358 K. The residual toluene in the bitumen was less than 0.2 wt%, as determined by gas chromatography. The bitumen samples were stored in a dark place in air-tight glass containers to avoid bitumen oxidation before use.

The physical and chemical characteristics of toluene-extracted bitumens from the Whiterocks, Sunnyside, PR Spring, Asphalt Ridge, and Circle Cliffs deposits, as reported in the literature, are shown in Table 1 and 2, respectively.

Wilhelmy Plate Technique

The surface tension of bitumens was measured on a Digital-Tensiometer K10T (KRUSS, GmbH; Germany) with a fine platinum roughened plate. The tensiometer was connected to a constant temperature water bath to maintain the desired temperature. A 10 mL bitumen sample was placed in the sample container, which was installed in the tensiometer and the sample was allowed to reach thermal equilibrium. The instrument with the attached platinum plate was calibrated before being brought in contact with the bitumen sample. The sample container was raised against the bottom edge of the platinum plate until the plate became moistened by the

Table 1. Physical Properties of Extracted Bitumens from Utah Oil Sands[3,19-21]

Property	Whiterocks	Sunnyside	PR Spring	Asphalt Ridge	Circle Cliffs
bitumen content, wt%	7.1-8.3	8.5-10	5-14	10.9-13.1	2.8[A]
specific gravity	0.981	1.033	1.016	0.970	ND
gravity, °API	12.7	5.5	7.8	14.4	14.3
Conradson carbon, wt%	8.8	14.8	14.0	ND	23.3
ash, wt%	0.24	2.4	3.3	0.04	0.06
viscosity (323K), Pa·s	32	1500	280	80	258[A]

ND = not determined, [A] K. Bukka, unpublished data

Table 2. Fractional Composition (wt %) of the Utah Oil Sand Bitumens[19,22,23]

Bitumen Fraction	Whiterocks	Sunnyside	PR Spring	Asphalt Ridge	Circle Cliffs[A]
saturates	29.5	24.9	26.6	32.4	23.8
aromatics	22.2	18.1	25.7	22.4	19.2
resins	42.4	30.0	31.7	37.6	28.8
asphaltenes	3.3	23.7	16.0	7.3	28.1
atomic H/C ratio	1.60	1.45	1.57	1.56	1.37
molecular weight	500	588	820	490	744

[A] K. Bukka, unpublished data

sample. The resulting force, due to the wetting, was then measured. The accuracy of the measurements was within 0.2 mNm^{-1} of the reported value. The results were recorded when no change in the surface tension was observed, typically after 20-30 min.

Contact Angle Measurements

A film of bitumen was spread mechanically on a clean and warm (323-333 K) glass slide to form a thickness of less than 5-6 μm, as estimated from the difference in the weight of a clean glass slide and that covered by the bitumen film. The glass slide with the bitumen film was cooled to room temperature (294$\pm$1 K). The bitumen films, as prepared, were uniform and smooth. It is important to note that viscous bitumens, in particular Sunnyside bitumen, could only be uniformly deposited on the glass slide at an elevated temperature.

A 4-6 mm diameter water drop was placed on the bitumen film and the contact angle was measured on both sides of the drop with an NRL Goniometer (Rame-Hart Inc., U.S.A.) with an accuracy of 2 degrees. In all experiments, distilled water with a specific conductivity of less than 10^{-6} S/cm, pH=5.8$\pm$0.1, and a surface tension of 72.6$\pm$0.1 mNm^{-1}, was used. In each case 5 to 10 water drops were placed on 2-3 slides, each covered with freshly prepared bitumen films, and then the contact angles were measured. Only the average values of the contact angles and confidence intervals for the experimental data are reported. In selected experiments with the Whiterocks and Circle Cliffs bitumens, the contact angle variation with time was recorded, whereas in other experiments the contact angle was measured immediately, i.e. 15-20 seconds, after the water drop had been placed on the bitumen film.

RESULTS AND DISCUSSION

Direct Measurement of Surface Tensions

Results from the temperature dependence of surface tension for the Whiterocks, Sunnyside, PR Spring, Asphalt Ridge, and Circle Cliffs bitumens, using the Wilhelmy plate technique, are presented in Figure 2. Surface tension measurements were carried out in the temperature range of 310-356 K. It was found that the surface tension values were reproducible in this temperature range. Further, in no case was hysteresis observed during temperature cycling. Always, for a given bitumen, the same linear relationship between surface tension and temperature was observed regardless of whether the temperature was increased or decreased during the experiments. Reproducibility of the results suggests that such phenomena as evaporation of light bitumen fractions, oxidation of asphaltenes, or chemical reactions at the platinum/bitumen interface, if such reactions are significant, did not affect the surface tension during the time of these measurements.

For each bitumen at a certain low temperature, the measured surface tension value was not reproducible, and the recorded values were always higher than expected from the linear relationship of $\gamma_B = f(T)$. This limiting low temperature was observed to vary with bitumen source. The low temperature limits for the bitumens under study were as follows: $T < 310$ K for Whiterocks bitumen, $T < 320$ K for PR Spring and Asphalt Ridge bitumens, $T < 325$ K for Circle Cliffs bitumen, and $T < 340$ K for Sunnyside bitumen. The higher viscosity of bitumen at low temperatures could contribute to the experimental error in the surface tension measurements with the Wilhelmy plate, as suggested in the literature (10).

Linear relationships between the surface tension of the bitumen and temperature were obtained for bitumen samples in the range of temperatures examined, 310-356 K (Figure 2), and were in general agreement with surface tension data reported in the literature for Canadian

Figure 2. Effect of temperature on the surface tension of bitumens separated from the Utah oil sands.

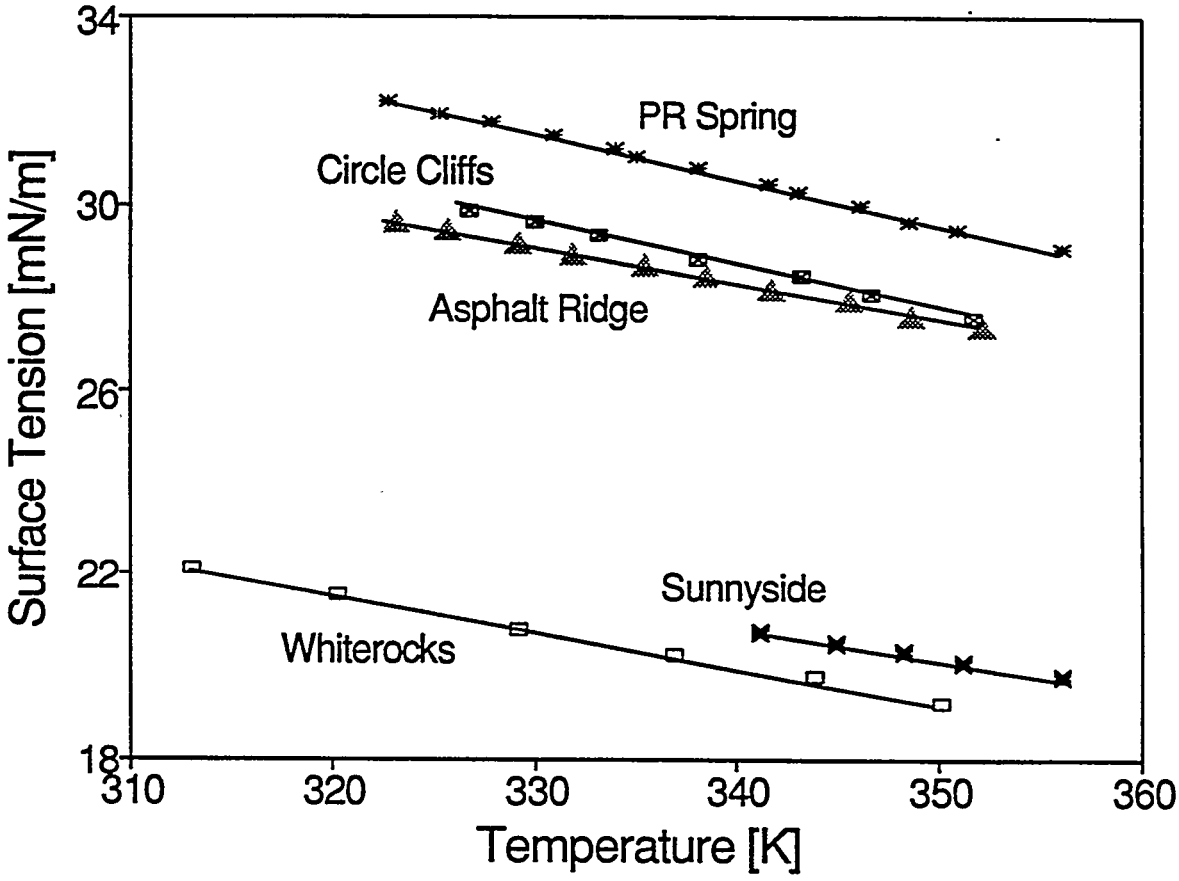
34
30
26
22
18
Surface Tension [mN/m]
PR Spring
Circle Cliffs
Asphalt Ridge
Sunnyside
Whiterocks
310
320
330
340
350
360
Temperature [K]

bitumens (10). The surface tensions of toluene-extracted bitumen samples from Utah oil sands were found to vary from 20.6 mNm^{-1} to 31.2 mNm^{-1} at 333 K, and are comparable to values reported for Canadian bitumens, 22.0-30.9 mNm^{-1} at 333 K (see Table 3). The results presented in Figure 2 can be described by the following equation:

$$\gamma_B(T) = \frac{d\gamma_B}{dT} T + \gamma_B(T=0) \qquad (6)$$

For each bitumen the temperature coefficient of the surface tension, $d\gamma_B/dT$, was calculated from the linear relationship (Figure 1), and presented in Table 3. The temperature coefficient values varied from -0.063 $mNm^{-1}deg^{-1}$ to -0.097 $mNm^{-1}deg^{-1}$, depending on the bitumen sample. Similar values of the temperature coefficient for bitumen surface tensions have been reported for Canadian bitumens (-0.044 $mNm^{-1}deg^{-1}$ to -0.095 $mNm^{-1}deg^{-1}$) (Table 3).

There was no apparent relationship between the bitumen surface tension (Table 3) and fractional composition of the bitumen examined (Table 2). Also, there seems to be no correlation of the bitumen surface tension and average molecular weight of the bitumen when data from Table 3 are compared with data from Table 2.

Bitumen Surface Tension from Contact Angle Measurements

The applicability of the equation-of-state (5) for bitumen surface tension determination was examined, and the advancing contact angles were measured for water drops resting on a bitumen film. The contact angles were measured immediately (15-20 seconds) after placement of the water drops at the bitumen film surface. Rapid measurement of contact angle was required in order to minimize the effect of liquid penetration and chemical interaction between the two phases on the contact angle measurement (11). Interactions at the interphase cause a decrease in the contact

Table 3. Surface Tension Values for North America Bitumens

Bitumen	Surface Tension at 333 K (60°C) mNm^{-1}	Temperature Coefficient of Surface Tension $mNm^{-1}deg^{-1}$	Literature
		Utah Bitumens	
Whiterocks	20.6±0.2	-0.077±0.002 (313 K to 350 K)	This work
Sunnyside	21.3±0.2	-0.063±0.001 (341 K to 356 K)	This work
PR Spring	31.2±0.2	-0.097±0.001 (322 K to 356 K)	This work
Asphalt Ridge	28.9±0.2	-0.078±0.001 (323 K to 352 K)	This work
Circle Cliffs	29.3±0.2	-0.093±0.002 (326 K to 352 K)	This work
		Canadian Bitumens	
Athabasca	~27.2	~-0.19 (313 K to 368 K)	[2]
	29.6 (64°C)	-0.095 (337 K to 385 K)	[7]
Peace River	22.0-29.2	-(0.048-0.072) (313 K to 363 K)	[8]
Pelican Lake	24.0-30.9	-(0.044-0.078) (313 K to 363 K)	[8]
Fort McMurray	22.2-30.6	-(0.050-0.082) (313 K to 363 K)	[8]

angle value with time as shown in Figure 3 for the Whiterocks and Circle Cliffs bitumens.

The results of contact angle measurements and the bitumen surface tension values calculated from equation (5) are presented in Table 4. The surface tension of the bitumen was found to vary in a narrow range of values from 23.9 mNm^{-1} for Whiterocks bitumen to 26.7 mNm^{-1} for Sunnyside bitumen. However the surface tension of the PR Spring bitumen was found to be significantly greater, 32.2 mNm^{-1}, than for the other Utah bitumens. As shown in Table 4, the average values for the surface tension calculated from contact angle data using equation-of-state (5) are close to the extrapolated values at 294 K from direct measurements using the Wilhelmy plate technique for Whiterocks, Sunnyside, and PR Spring bitumens. Significant discrepancies between data obtained by the two different techniques was observed for the Asphalt Ridge and Circle Cliffs bitumens. Vargha-Butler et al., (11) noted similar discrepancies for Canadian bitumens which were found to differ from 0.4 mNm^{-1} to 5.3 mNm^{-1}; but there was no systematic trend in this difference.

There is no reason to assume that the linear surface tension/temperature relationship, which is a characteristic property of liquids (13) and also melted polymers (24), does not exist for bitumens. The high bitumen viscosity in the 294-310 K temperature region makes surface tension measurements difficult with the Wilhelmy plate technique, nevertheless, the bitumens still exhibit liquid properties in this temperature range. In this regard, it is believed that the extrapolation procedure used for determination of the bitumen surface tension at room temperature could not account for such large discrepancies between surface tension values obtained with the two different techniques, Wilhelmy plate tensiometry and contact angle measurements.

It should be noted that special precaution was taken to avoid overheating the bitumen during film preparation. The bitumen was spread on a warm glass slide and immediately cooled

Figure 3. Variation of contact angle with respect to contact time for a water drop placed on the surface of the bitumen film.

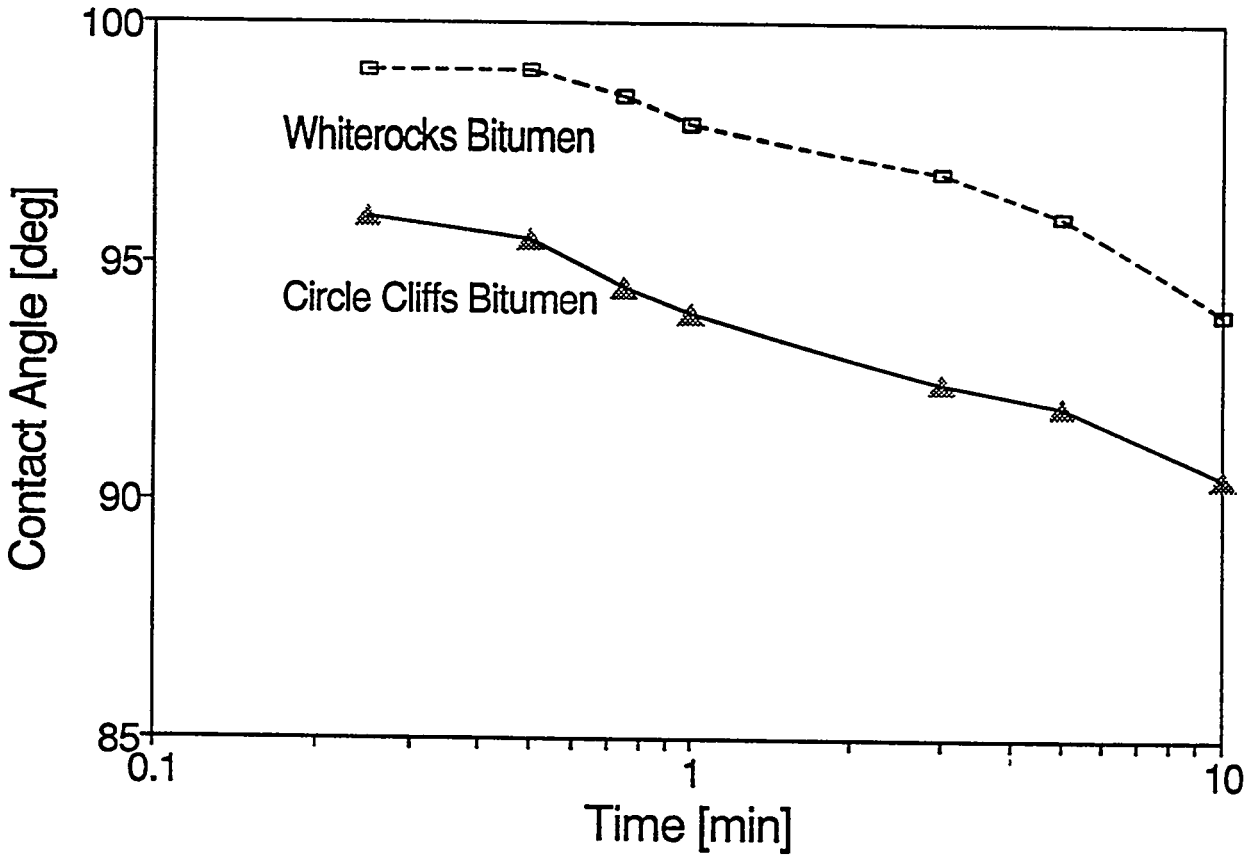
100
95
90
85
Contact Angle [deg]
Whiterocks Bitumen
Circle Cliffs Bitumen
0.1
1
10
Time [min]

Table 4. Comparison of Bitumen Surface Tension Values Calculated from Contact Angle Measurements with Bitumen Surface Tension Determined by Wilhelmy Plate Measurements (21°C)

	bitumen:				
	Whiterocks	Sunnyside	PR Spring	Asphalt Ridge	Circle Cliffs
contact angle for water drop at bitumen film at 294 K, [deg]	98.3±1.8	93.8±2.2	85.1±2.9	98.0±2.4	95.8±1.2
calculated bitumen surface tension, [mNm^{-1}]	23.9±1.2	26.7±1.5	32.2±1.9	24.2±1.5	25.5±0.8
bitumen surface tension after extrapolation of experimental data in Figure 1 to 294 K,[mNm^{-1}]	23.5±0.2	23.7±0.2	35.0±0.2	31.9±0.2	33.0±0.2
difference in determination of the bitumen surface tension by both methods, direct measurement and using contact angle data, [mNm^{-1}]	+0.4	+3.0	-2.8	-6.9	-7.5
	(-1.0 to +1.8)	(+1.7 to +4.7)	(-4.9 to -0.7)	(-9.4 to -6.4)	(-8.5 to -6.9)

to room temperature to minimize the destructive effect of the thermal energy on the bitumen composition. In our preliminary experiments, Whiterocks and Asphalt Ridge bitumens were deposited on a glass slide at room temperature. For such bitumen films, as prepared, the advancing contact angle as measured for a water drop was found to be in close agreement with that measured for a water drop placed on the bitumen film prepared at an elevated temperature. These experiments suggest that annealing of the bitumen films, during the time of the experiment has no significant effect on the surface properties of the bitumen films. The bitumen samples used in the tensiometric measurements were also subjected to elevated temperatures. In this regard, the thermal energy could affect the bitumen samples in a similar way in both techniques.

Vargha-Butler et al. (11) suggested that the presence of clay particles in bitumen can affect the energetic state of the bitumen surface, and thus, may be responsible for the difference in the surface tension as measured directly and those calculated from contact angle data. The procedure for bitumen extraction from oil sand samples and bitumen purification from solvent, as used in these studies, suggest that clay particles are probably not responsible for the observed difference.

Some interaction between molecules of water and bitumen occured rapidly during the contact angle measurements as presented in Figure 2. This may involve reorientation of molecules or some groups of bitumen molecules at the bitumen/water interface which affect the contact angle. Also, factors such as solubility of bitumen compounds in water and/or water in bitumen, deformation of the bitumen film at the three-phase contact line, and spreading of bitumen or bitumen constituents at the water drop surface, could affect the contact angle measurements. These effects caused difficulties in the selection of an appropriate time for contact angle measurements, and thus, thermodynamic equilibrium for the three-phase system could not be defined. In this regard, the contact angle measurements for liquid drops at a bitumen film surface may involve

some uncertainty. Also, it was pointed out recently that the equation-of-state has several limitations, such as applicability to apolar systems involving only physisorption (25). Apolar liquids such as hydrocarbons can not be used in the characterization of the bitumen surface due to the mutual solubility of the phases (6). In this regard, the bitumen surface tension determination based on contact angle measurements using polar liquids, such as water in our studies or water and glycerol in the studies of Vargha-Butler et al. (11), may account for some inaccuracy in the surface tension determination of the bitumens. Also, inaccuracy in the bitumen surface characterization using the equation-of-state may point to the weakness of the theoretical considerations used in the derivation of equation (5). (Note that additional proofs of the weakness of Neumann's approach for the surface tension determination of low-energy surfaces based on contact angle measurements were recently recognized in our laboratory during surface tension measurements of polymers (26).

Finally, another disadvantage of the contact angle technique is its limitation in the determination of the bitumen surface tension at room or lower temperatures when the bitumen becomes a semi-solid. In practice, oil sands are processed at elevated temperatures, mostly from 323 K to 358 K, and thus, the bitumen surface tension at higher temperatures is of more practical importance..

SUMMARY AND CONCLUSIONS

The surface tension of toluene-extracted bitumens from the Whiterocks, Sunnyside, PR Spring, Asphalt Ridge, and Circle Cliffs oil sands was determined by the Wilhelmy plate technique and found to be 20.6 mNm^{-1}, 21.3 mNm^{-1}, 31.2 mNm^{-1}, 28.9 mNm^{-1}, and 29.3 mNm^{-1} at 333 K, respectively. No apparent correlation between the bitumen surface tension and fractional

composition of bitumen was observed.

A linear relationship between the bitumen surface tension and temperature was found for Utah bitumens examined in the temperature range of 310-356 K (depending on bitumen sample). The temperature coefficient for surface tension was calculated to be -0.077 mNm^{-1} deg^{-1}, -0.063 $mNm^{-1}deg^{-1}$, -0.097 $mNm^{-1}deg^{-1}$, -0.078 $mNm^{-1}deg^{-1}$, and -0.093 $mNm^{-1}deg^{-1}$, for the Whiterocks, Sunnyside, PR Spring, Asphalt Ridge, and Circle Cliffs bitumen, respectively.

The contact angles for water drops at the surface of bitumen films were measured and the bitumen surface tension at 294 K was calculated from Neumann's equation-of-state. The contact angle technique provided comparable values for the bitumen surface tension at room temperature for the Whiterocks, Sunnyside, and PR Spring samples. Significant discrepancies between the bitumen surface tension values as obtained from the contact angle technique and as obtained from direct measurements with the Wilhelmy plate technique were found for the Asphalt Ridge and Circle Cliffs bitumens. In this regard, the contact angle technique, which is based on Neumann's equation-of-state and contact angle measurements, may not be valid and, in any event, is limited to a small temperature range. Several possible reasons for the discrepancies between surface tension values determined by direct measurements and those calculated from contact angle data were discussed in this contribution, however, the weakness of the theory, expressed by equation (5), especially its limitations to apolar systems involving only physisorption, seems to be the most reasonable explanation to account for such discrepancies.

CHARACTERIZATION AND STABILITY OF OIL-IN-WATER EMULSIONS

INTRODUCTION

Bitumen droplets in a successfully digested tar sand slurry exhibit a broad size distribution

with droplets from a few micrometers to 1 mm in size. Large bitumen droplets can be rapidly separated in a gravity cell assuming that they contain a sufficient amount of entrapped air. Fine bitumen droplets and bitumen-sand aggregates are either caught in the fast settling tailings or form a middlings layer, which requires flotation for fast and complete recovery.

There are two stages in the removal of dispersed oil from oil-in-water emulsions during flotation: contact and coalescence. These involve air bubbles and filming phenomena (27, 28). Contact is sensitive to long range forces between the droplets and bubbles as they approach each other. The contact or air bubble/oil droplet attachment can be controlled by adjusting the zeta potential of the droplets and bubbles. The zeta potential of a bubble and a droplet (or two droplets) should be close to the isoelectric point such that repulsion is weak.

The attachment involves rupture of the aqueous film and depends on the thermodynamic properties of the interfacial films and on the degree of irreversibility of film desorption. The possibility of filming can be estimated by calculation of the spreading coefficient for the system. A positive spreading coefficient is necessary for the filming process to occur.

Oil droplet size distribution and oil-in-water emulsion stability were investigated and will be discussed with respect to the deemulsification process. The results of this research support a general consensus that the interfacial chemistry for such dispersed systems plays a dominant role in phase separation processes and the bitumen-in-water system is no exception.

Oil Droplet Size Distribution Measurements

It is quite uncommon for any emulsion to have a uniform droplet size distribution. An emulsion consisting mostly of fine droplets exhibits maximum stability, all other things being equal (29). In this regard, suitable droplet size measurements as well as their description, are of critical importance. There are, in general, four different methods by which the droplet size

distribution may be determined. These methods include microscopic observation, sedimentation techniques, light-scattering measurements, and instrumental counting (29). It should be noted, however, that some of these methods do not actually yield distributions as such, but only average particle size.

Microscopic measurements have been used extensively for years and although laborious, they are the most accurate. Observation of the emulsion under a microscope fitted with a micrometer eyepiece permits the tabulation of the numbers of droplets in various size classes. From this, a distribution curve may be plotted. Alternatively, a photographic record of the emulsion may be made, from which the droplet sizes can be determined at a later time. In this way a permanent record of the emulsion is available. In much of the literature relating to the microscopic technique, undue emphasis has been placed on the necessity of counting a large number of droplets in order to get a meaningful size distribution. For example, Fischer and Harkins (30) made a direct microscopic count of 50,000 particles to obtain size distribution curves. Actually, however, statistically significant counts can be made with as little as 300 droplets. It can be shown (31) that a count of 300 droplets will result in a distribution in which the error at any size range will be less than 8% with a 95% confidence limit. Reduction of this expected error to 5%, at the same level of confidence, would require the counting 2960 droplets. In view of the other sources of error affecting such measurements, such a small reduction in error hardly seems worth the tenfold increase in effort.

The second type of measurement is based on sedimentation phenomena. If any emulsion creams at any sort of observable rate, measurement of the amount of creamed material per unit of time permits the construction of a size distribution curve. Most methods which depend on this phenomenon measure the change in density.

Droplet size can also be measured, in principle, by optical methods which depend either on measurement of the reduction in light transmitted through the dispersion (turbidimetric or nephelometric methods) or by light scattered at some definite angle (usually 90°) from the optical path. The method employed depends, to some degree, on the type of system being studied, direct transmission methods being more applicable to dispersions of higher turbidity.

Methods depending on direct counting have been developed recently. A flow counter which also gives particle size distributions is the Coulter Counter. In this device, the emulsion flows through a narrow orifice surrounded on either side by a conductivity electrode. In an oil-in-water emulsion, the conductivity of the dispersed oil droplets is, of course, much lower than that of the continuous phase. Consequently, each time a droplet passes through the orifice, a change in conductivity, whose magnitude is proportional to the droplet size, is recorded.

Since what is determined by most experimental measurements of size distribution is the population of various size ranges, the proper graphical representation of such data is by means of a histogram. For convenient discussion of particle-size data, it may be necessary to simplify matters somewhat by using average quantities. For example, the emulsion may be described in terms of an average particle diameter corresponding to that of a hypothetical monodispersed emulsion. However, this is not as simple a matter as it might seem, for the average diameter may be defined in a number of ways.

If, for example, one defines the total number of droplets in the emulsion as N, the total interfacial area as S, the volume of dispersed phase as V, and the sum of all globule diameters as D, six types of average diameter can be defined as shown below (29):

$$d_{10} = \frac{D}{N} = \frac{\sum d_i \, n_i}{\sum n_i} \tag{7}$$

$$d_{20} = \left(\frac{S}{\pi N}\right)^{\frac{1}{2}} = \left(\frac{\sum d_i^2 n_i}{\sum n_i}\right)^{\frac{1}{2}} \quad (8)$$

$$d_{30} = \left(\frac{6V}{\pi N}\right)^{\frac{1}{3}} = \left(\frac{\sum d_i^3 n_i}{\sum n_i}\right)^{\frac{1}{3}} \quad (9)$$

$$d_{21} = \frac{S}{\pi D} = \frac{\sum d_i^2 n_i}{\sum d_i n_i} \quad (10)$$

$$d_{31} = \left(\frac{6V}{\pi D}\right)^{\frac{1}{2}} = \left(\frac{\sum d_i^3 n_i}{\sum d_i^2 n_i}\right)^{\frac{1}{2}} \quad (11)$$

$$d_{32} = \frac{6V}{S} = \frac{\sum d_i^3 n_i}{\sum d_i^2 n_i} \quad (12)$$

where n_i is the number of droplets with a diameter of d_i.

Eq.(7) provides a simple arithmetic mean, while Eq.(12) yields mean volume-surface diameter (often called the Sauter diameter). The mean surface or interface area is also an index of the dispersity of the emulsion and is often employed. As indicated above, the most meaningful calculation of this quantity is from the volume-surface diameter.

Emulsion Stability Measurements

Emulsions are essentially unstable heterogeneous systems; they are partly dispersions, partly colloids. The properties of emulsions often depend largely on their composition and on their mode of preparation. The physical properties of the emulsion govern the stability of the system (29).

There are two stages in the collapse of emulsions: contact and coalescence. It should be noted that in a process consisting of two consecutive reactions, the overall reaction rate is determined by the slower of the two. For a very dilute oil-in-water emulsion the rate of contact can be made much slower than the rate of coalescence. As a consequence, the stability of the emulsion will be affected by the factors that affect the rate of contact. On the other hand, increasing the concentration of the oil phase in the emulsion will result in a slowly increasing rate of coalescence and a much faster increasing rate of contact. Thus, in highly concentrated emulsions, the coalescence can be rate-determining.

In a certain range of concentrations these two reaction rates can be roughly equivalent. Becher (29) has pointed out that even in very diluted emulsions, it is possible to make coalescence rate determining by the addition of surface active agents which may have little or no effect on the rate of contact while inhibiting coalescence.

In addition to the manner in which the droplet sizes are distributed in an emulsion, the total amount of the dispersed phase present would be expected to be important. However, the best and most direct indication of the stability of an emulsion is to measure the change in the dispersed phase concentration as a function of time under stagnant conditions. The results of this measurement can be presented as weight per cent, weight fraction, volume percent, volume fraction or molarity. In the present work the units of mg/dm^3 are used which are almost identical to ppm (parts per million) when the density of water is assumed to be 1 kg/m^3. The change in the emulsion density after the addition of oil and chemicals is negligible.

Generally, the oil phase sedimentation from o/w emulsions follows first order kinetics (27, 32-34). The sedimentation coefficient (k_s) as calculated from the following equation can be used as an indicator of emulsion stability (27).

$$\ln\frac{c}{c_o} = -k_s\, t \tag{13}$$

where c_0 - initial concentration
c - concentration after time t
k_s - sedimentation coefficient [1/s]
t - time [s]

The value of the sedimentation coefficient for very stable emulsions is smaller than $3 \cdot 10^{-7} s^{-1}$ and for unstable emulsions, k_s is larger than $5.6 \cdot 10^{-4} s^{-1}$.

EXPERIMENTAL

Oil Droplet Size Distribution Measurements

Hexadecane (Aldrich Chemical Co.) with a purity of 99% and a 20% Whiterocks bitumen-in-kerosene blend were used in this study as the organic phase (oil). Sodium dodecyl sulfate (SDS) with a purity of 95% (Sigma Chemical Co.) and PERCOL 592 (Allied Colloids, Inc.) were used as the surfactant and cationic polyelectrolyte, respectively.

The oil-in-water emulsions were prepared by emulsification of the oil samples in 5 L of water using the SILVERSON L4R homogenizer (5 min., 7200 rpm). The emulsion was diluted with water to 200 L in the conditioning tank in order to reach an oil concentration of 250 mg/dm^3. The surfactant and polyelectrolyte, if needed, were added to the conditioning tank. In each case, with or without chemical additions, the emulsion was equilibrated in the conditioning tank with a recirculating pump for 5 min. Next, chemicals were added (when both SDS and PERCOL 592 were added, SDS was added first) and the emulsion was equilibrated in the conditioning tank for an additional 15 min (when no chemicals were added the emulsion was equilibrated in the storage tank for the whole 20 min to maintain the identical conditions for each emulsion type).

A microscopic technique was adopted to determine the droplet size distribution. A sample of 200 cm^3 of emulsion was collected from the conditioning tank and immediately analyzed microscopically. An optical microscope, model AXIOPLAN (ZEISS, Germany) and microscopic slide with master scale (Fein-Optik in Jena, Germany) were used. Photographic records (12 of each sample) were made of each emulsion and droplet sizes were determined from these photographs. Four hundred fifty to five hundred droplets were counted to obtain the size distribution curve (5 to 6 photographs were selected for each distribution and every droplet on each photograph was counted).

Emulsion Stability

The kinetics of dispersed oil sedimentation were examined for model hexadecane-in-water and 20% Whiterocks bitumen/kerosene blend-in-water emulsions. Oil phases, added chemicals and their concentrations, as well as the procedure of emulsion preparation and the addition of chemicals, were identical to those described in previous section. Equilibration in the conditioning tank was done for 20 min.

After equilibration, a sample of 3.5 dm^3 of emulsion was taken from the conditioning tank. Next, the sample was left under quiescent conditions to allow gravity separation to occur. Samples of the emulsion were taken at various time intervals from the bottom of the container without disturbing the quiescent conditions of sedimentation. The time interval between successive sampling was set at 15 min. at the beginning and was increased to 12 hours toward the end of each experiment. The concentration of the dispersed oil phase was measured spectroscopically using a HORIBA OCMA-220 oil-in-water analyzer.

RESULTS AND DISCUSSION

Oil Droplet Size Distribution

The droplet size distributions for hexadecane are shown in Figures 4 to 7. The average droplet diameters for these emulsions are presented in Table 5 (formulas for each average diameter are given in Eqs 7 to 12).

As can be seen from Figures 4 to 7 there is, essentially, no change in the average droplet size after the addition of chemicals. When the surfactant and polyelectrolyte are added separately, the size distribution becomes narrower and shifts to smaller sizes whereas the average droplet diameters are very similar. The mechanisms by which SDS and PERCOL 592 bring about this

Figure 4. Droplet size distribution for hexadecane-in-water emulsion without the addition of chemicals

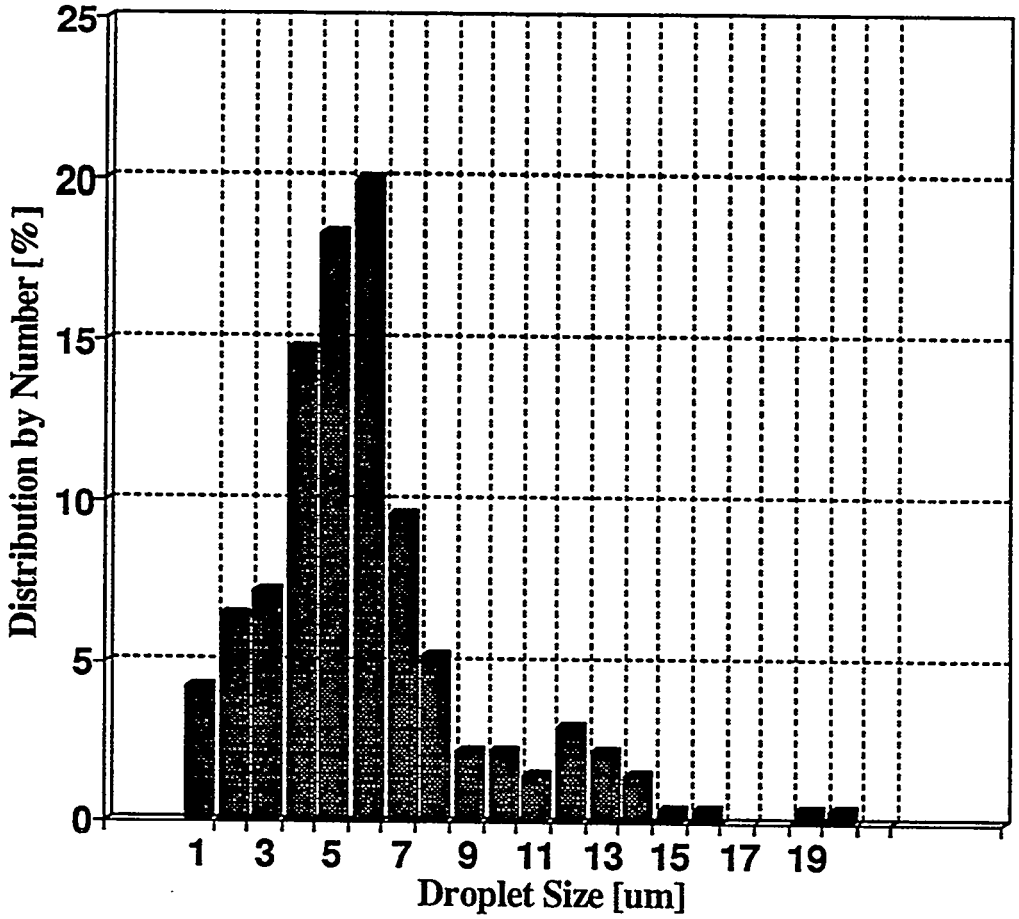
25
20
15
10
5
0
Distribution by Number [%]
1
3
5
7
9
11
13
15
17
19
Droplet Size [um]

Figure 5. Droplet size distribution for hexadecane-in-water emulsion with the addition of 30 mg/dm^3 of surfactant (SDS)

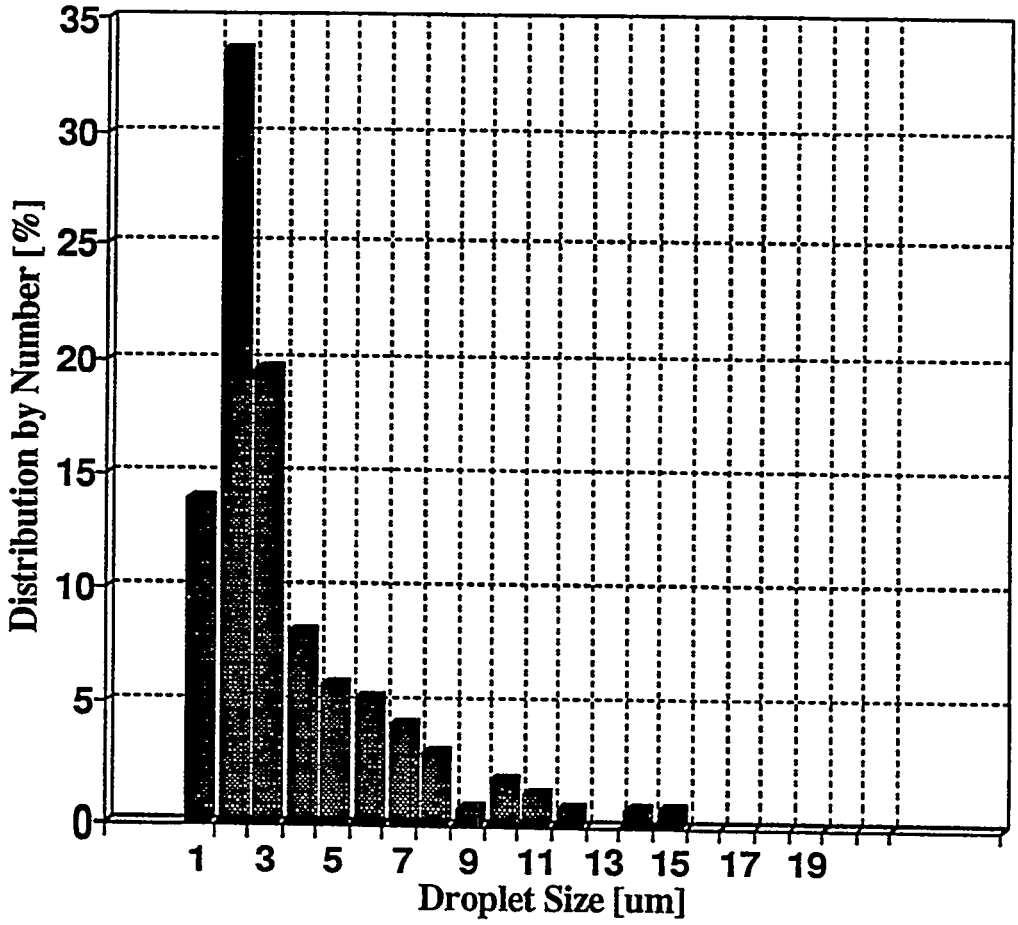
35
30
25
20
15
10
5
0
Distribution by Number [%]
1
3
5
7
9
11
13
15
17
19
Droplet Size [um]

Figure 6. Droplet size distribution for hexadecane-in-water emulsion with the addition of 2 mg/dm^3 of cationic polyelectrolyte (PERCOL 592)

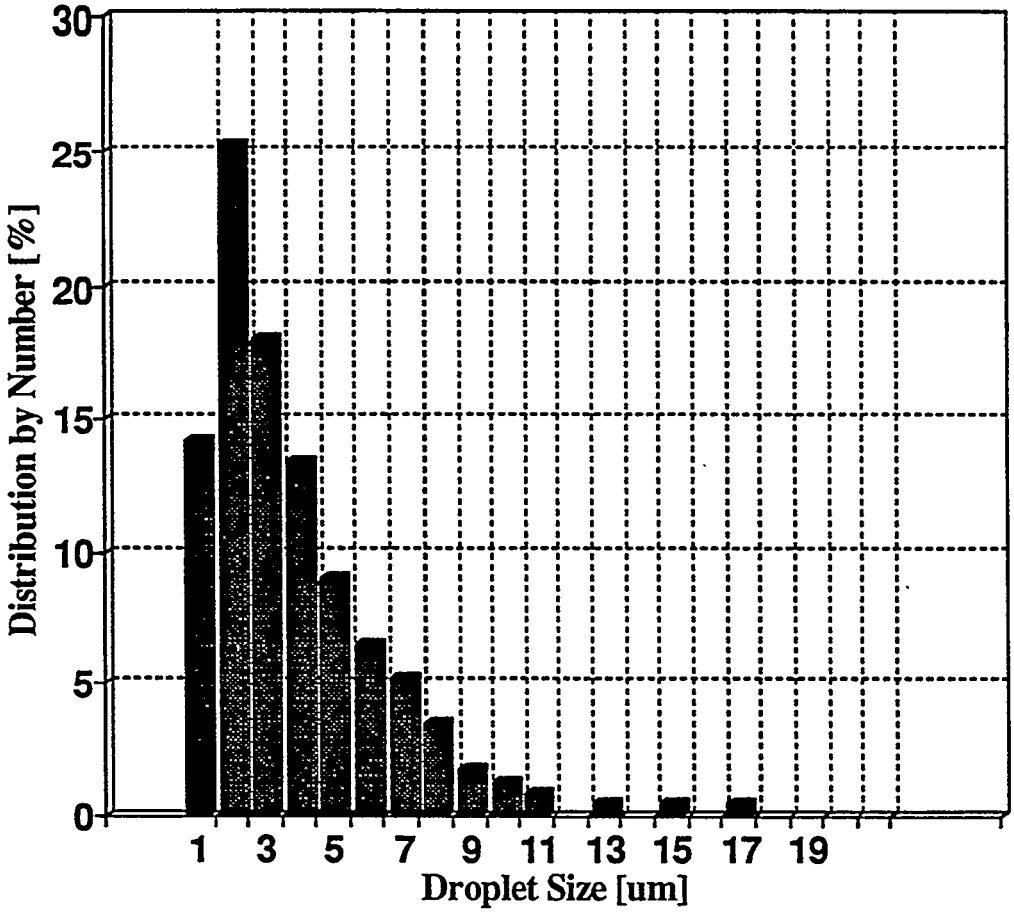
30
25
20
15
10
5
0
Distribution by Number [%]
1
3
5
7
9
11
13
15
17
19
Droplet Size [um]

Figure 7. Droplet size distribution for hexadecane-in-water emulsion with the addition of 30 mg/dm^3 of surfactant (SDS) and 2 mg/dm^3 of cationic polyelectrolyte (PERCOL 592)

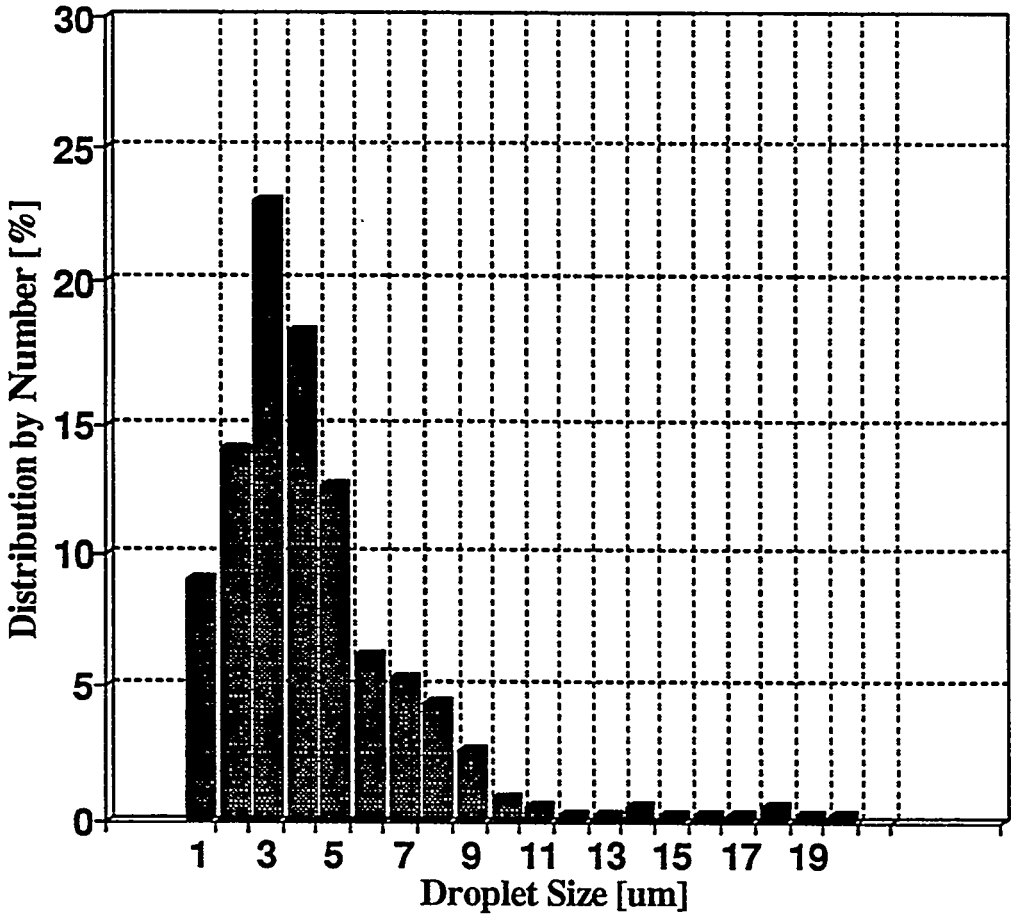
30
25
20
15
10
5
0
Distribution by Number [%]
1
3
5
7
9
11
13
15
17
19
Droplet Size [um]

Table 5. Average droplet diameter (μm) for hexadecane emulsions with different chemicals added (30 mg/dm^3 of SDS and 2 mg/dm^3 of PERCOL 592)

Average	No Additives	SDS	PE	SDS/PE
d_{10}	5.9	3.4	3.8	4.4
d_{20}	6.4	4.3	4.6	5.3
d_{30}	7.5	5.2	5.4	6.4
d_{21}	41.2	18.6	20.9	28.4
d_{31}	3.2	2.8	2.7	3.1
d_{32}	10.2	7.7	7.6	9.2

small change are quite different from each other. Addition of the surfactant to the water increases the susceptibility to emulsification and this makes the droplet diameters shift to smaller sizes. On the contrary, addition of the polyelectrolyte to the water causes coalescence and larger droplets are formed during the equilibration time. As a consequence, a layer of separated oil was observed at the top of the conditioning tank.

The oil concentration, especially at the beginning of the experiment, was the highest for the emulsion with the SDS addition, and as expected, the addition of PERCOL 592 decreased the oil concentration. The addition of PERCOL 592 together with SDS gave a broader size distribution and slightly larger average droplet diameter than the addition of PERCOL 592 alone. The addition of SDS and PERCOL 592 made the emulsion less stable and gravity separation was evident in this case.

It must be noted that the flocculation of oil drops may be reversible. Thus, in many cases the oil aggregates can be easily redispersed by stirring. This action of shearing forces can be enhanced by dilution with a solution of a suitable surface active agent. Furthermore, coagulation of an emulsion is a function not only of the rate of formation of these more or less reversible aggregates, but also of the rate at which the droplets coalesce to form larger droplets (29).

The droplet size distributions for a 20% bitumen in kerosene blend as an oil phase are shown in Figures 8 to 11. The average droplet diameters for these emulsions are presented in Table 6 (formulas for each average diameter are given in Equations 7 to 12).

Similar to the size distribution results for hexadecane emulsions, there is essentially no change in droplet size distribution for bitumen/kerosene emulsions with the addition of chemicals.

When the basic emulsions without the addition of chemicals were studied, the emulsion of the bitumen/kerosene blend as an oil phase was found to have a much narrower droplet size

Figure 8. Droplet size distribution for the 20% bitumen/kerosene blend-in-water emulsion without the addition of chemicals

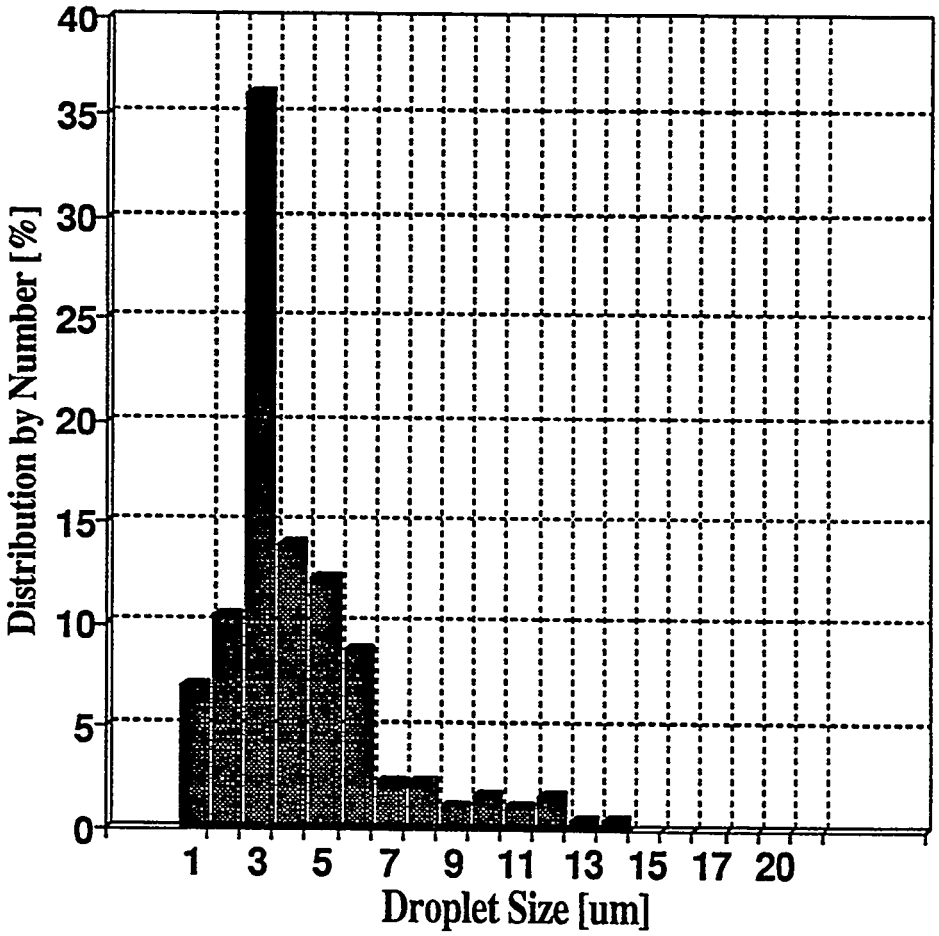
Distribution by Number [%]
40
35
30
25
20
15
10
5
0
1
3
5
7
9
11
13
15
17
20
Droplet Size [um]

Figure 9. Droplet size distribution for the 20% bitumen/ kerosene blend-in-water emulsion with the addition of 9 mg/dm^3 of surfactant (SDS)

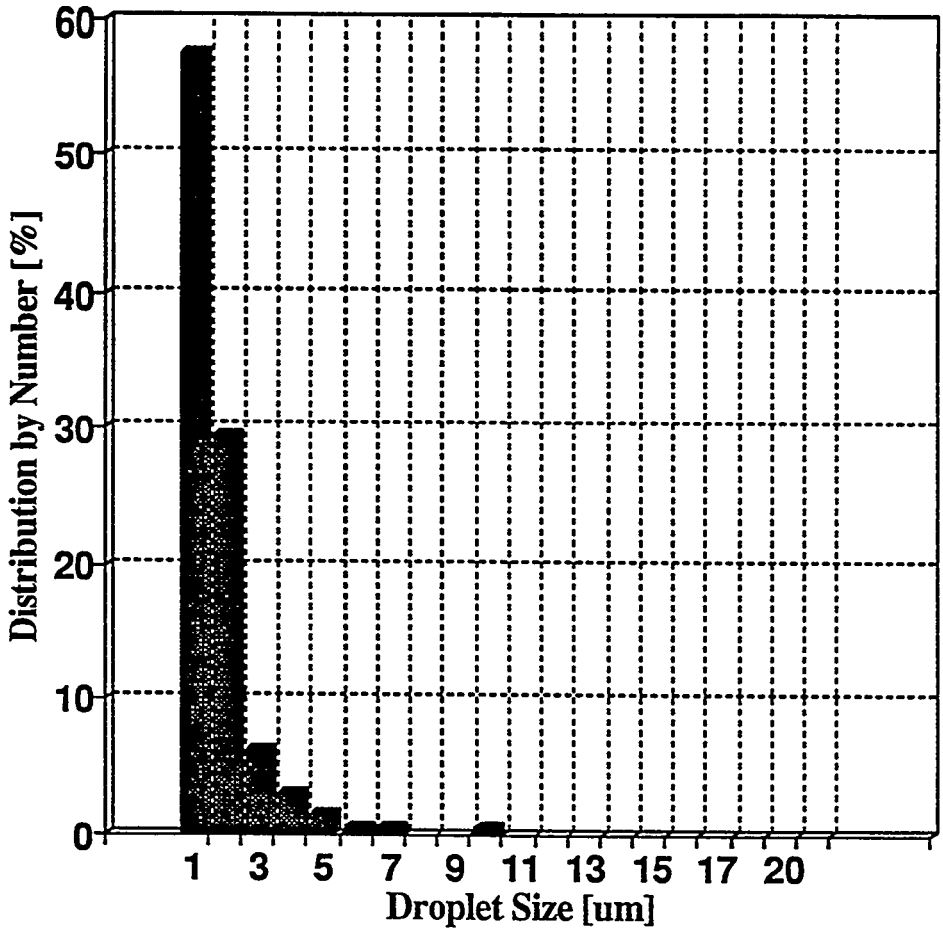
60
50
40
30
20
10
0
Distribution by Number [%]
1
3
5
7
9
11
13
15
17
20
Droplet Size [um]

Figure 10. Droplet size distribution for the 20% bitumen/ kerosene blend-in-water emulsion with the addition of 0.5 mg/dm^3 of cationic polyelectrolyte (PERCOL 592)

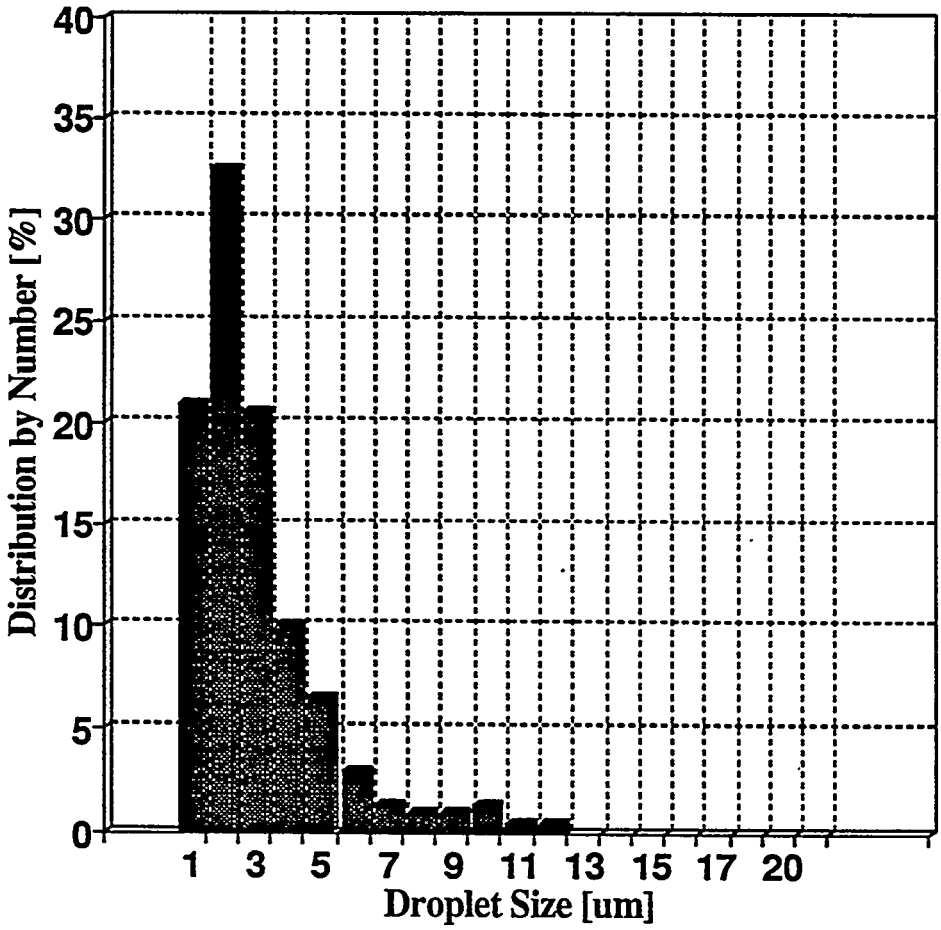
40
35
30
25
20
15
10
5
0
Distribution by Number [%]
1
3
5
7
9
11
13
15
17
20
Droplet Size [um]

Figure 11. Droplet size distribution for the 20% bitumen/ kerosene blend-in-water emulsion with the addition of 9 mg/dm^3 of surfactant (SDS) and 0.5 mg/dm^3 of cationic polyelectrolyte (PERCOL 592)

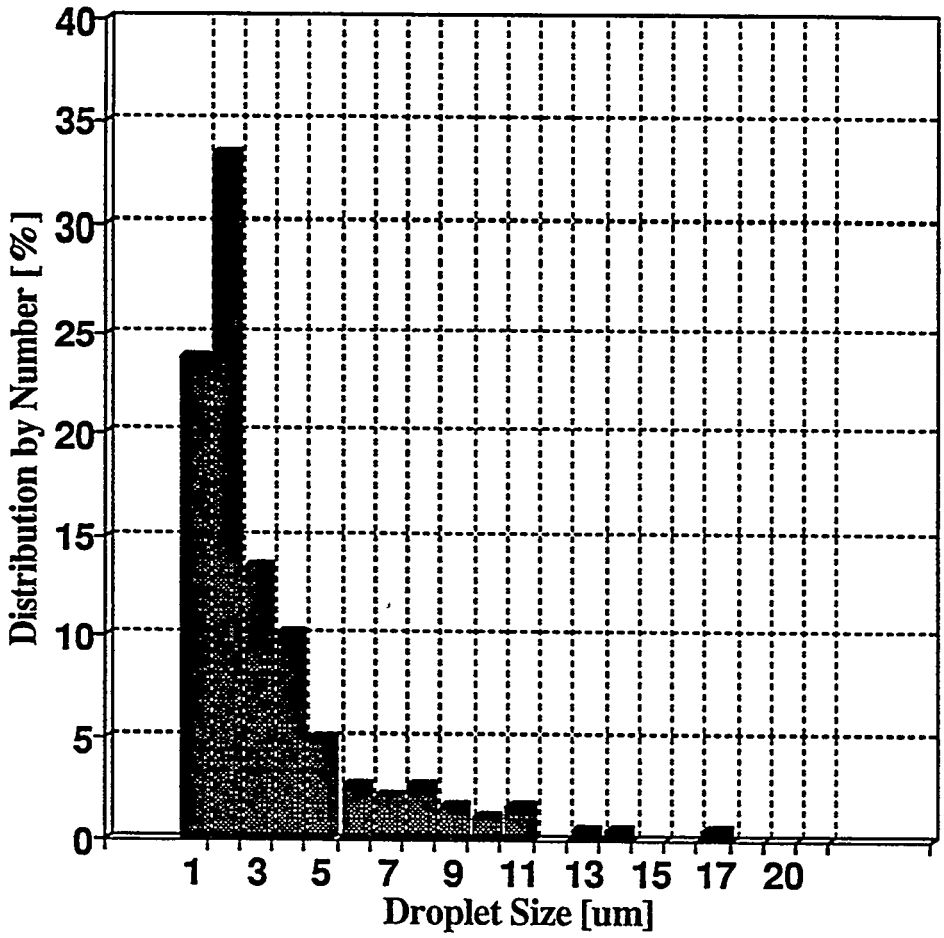
40
35
30
25
20
15
10
5
0
Distribution by Number [%]
1
3
5
7
9
11
13
15
17
20
Droplet Size [um]

Table 6. Average droplet diameter (μm) for bitumen/kerosene emulsions with different chemicals added (9 mg/dm^3 of SDS and 0.5 mg/dm^3 of PERCOL 592)

Average	No Additives	SDS	PE	SDS/PE
d_{10}	4.2	1.8	2.9	3.2
d_{20}	4.8	2.0	3.6	4.2
d_{30}	5.6	2.6	4.3	5.3
d_{21}	23.5	4.2	12.7	17.8
d_{31}	2.7	2.0	2.5	2.9
d_{32}	7.4	4.0	6.1	8.4

distribution range, as compared to the size distribution of the hexadecane emulsion. The size distribution difference between these two basic emulsions can be explained by taking into account the origin of the oil phase. Hexadecane is a pure hydrocarbon and an emulsion produced with it as an oil phase is a typical model emulsion. The bitumen in kerosene blend is a mixture of many different chemical compounds including the natural surfactants in bitumen. The other element which can have an influence on emulsion formation is the presence of fine particles - emulsion stabilizing agents (29) - such as clay and precipitated calcium carbonate (8) in bitumen. As pointed out by Becher (29), precipitates are, in general, better emulsifiers than substances added to the system and the physical state of the precipitates appears to be a very important factor. Generally, highly gelatinous or highly-dispersed fine precipitates are more efficient than granular ones. If the contact angle between a solid particle and two liquid phases is finite, a stable position for the particle is at the liquid-liquid interface. Coalescence is inhibited because work has to be done to displace the particle from the interface (13).

Emulsion Stability

The results of the measurements of dispersed oil concentration as a function of sedimentation time for hexadecane-in-water and bitumen/kerosene blend-in-water emulsions are presented in Figures 12 and 13, respectively. Both emulsion exhibit similar stability and a continuous reduction in oil concentration was evident during the course of the experiment. The emulsions with the addition of the polyelectrolyte (with and without surfactant) were less stable than the emulsions with no additives.

All emulsions were prepared using exactly the same amount of oil. The initial concentration differences came from the gravity separation during equilibration in the conditioning tank. A froth layer in the conditioning tank was observed, especially in the case of the hexadecane emulsion

Figure 12. Dispersed oil concentration vs. time for hexadecane-in-water emulsions

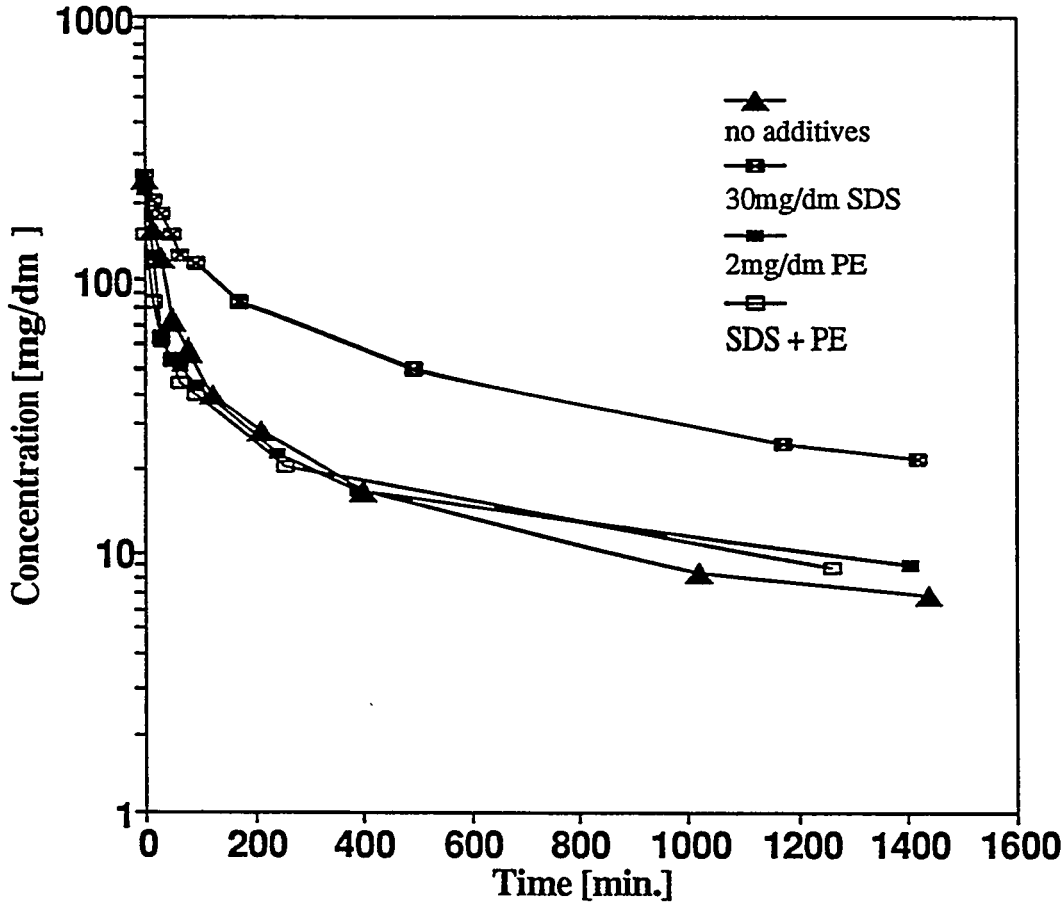
1000
100
10
1
Concentration [mg/dm]
0
200
400
600
800
1000
1200
1400
1600
Time [min.]
no additives
30mg/dm SDS
2mg/dm PE
SDS + PE

Figure 13. Dispersed oil concentration vs. time for the 20% bitumen/kerosene blend-in-water emulsions

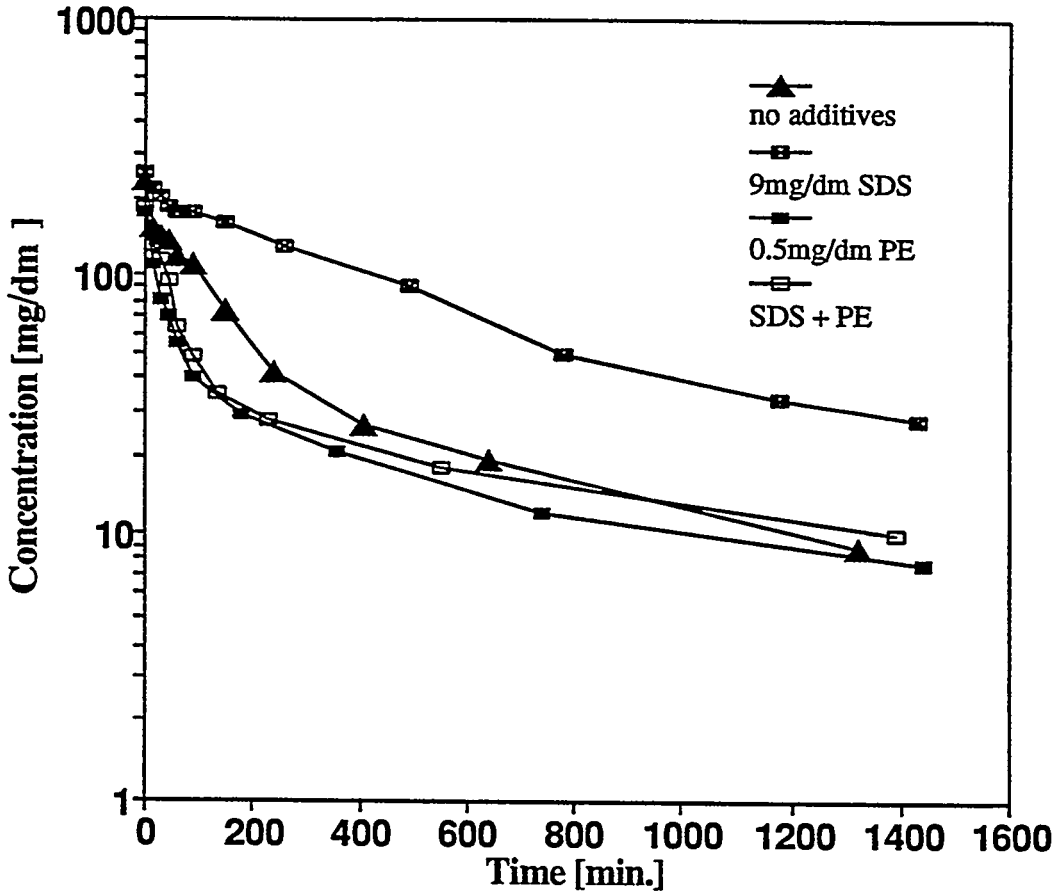
1000
100
10
1
Concentration [mg/dm]
0
200
400
600
800
1000
1200
1400
1600
Time [min.]
no additives
9mg/dm SDS
0.5mg/dm PE
SDS + PE

with the addition of SDS and PERCOL 592. In cases with the addition of only PERCOL 592, a thin oil layer at the surface was also observed.

In spite of the similar effects of the chemical additives, the two kinds of emulsions produced from the different oil phases can be easily distinguished from each other. The emulsion made from the bitumen/kerosene blend is more stable (i.e., higher oil concentration after a given period of time). The values of the sedimentation coefficient presented in Table 7 are calculated from Eq.(13). Two distinct stages of sedimentation can be distinguished in Figures 12 and 13. Consequently, data for the two periods of time before and after 60 minutes of sedimentation were taken for the calculations. Each stage can be approximated as a first order rate process. In the first stage, the rate of sedimentation is about an order of magnitude greater than after 60 minutes. This finding is very important because in the separation process the first period of 60 minutes is the most significant period of time, the time during which the emulsion is processed.

It can be concluded from the sedimentation coefficient calculations, that the bitumen/kerosene emulsion is more stable than the hexadecane emulsion (the smaller sedimentation coefficient, the more stable the emulsion). This can be seen especially for the first 60 minutes of sedimentation. When comparing the less stable emulsions (addition of SDS as well as SDS and PERCOL 592) with each other and with the more stable emulsions, the time of the conditioning process (30 minutes in the tank before sampling) has to be taken into consideration. The initial concentration was not the same in all cases. With the addition of SDS and PERCOL 592 the initial concentration was much lower than anticipated (250 mg/dm^3); for hexadecane, 149 mg/dm^3; and for bitumen/kerosene, 185 mg/dm^3. As a consequence, such an emulsion (with addition of SDS and PERCOL 592) is less stable than concluded from the data presented in Table 7. For a time period of over 60 minutes, all emulsions examined (with and without chemical

Table 7. Sedimentation coefficient calculated from the first order sedimentation rate equation for hexadecane and bitumen/kerosene emulsions with different chemicals added

Additives	Sedimentation Coefficient [s^{-1}]			
	Hexadecane		Bitumen/Kerosene	
	≤60 min	≥60 min	≤60 min	≥60 min
no additives	$4.3 \cdot 10^{-4}$	$2.6 \cdot 10^{-5}$	$1.7 \cdot 10^{-4}$	$3.3 \cdot 10^{-5}$
SDS	$1.9 \cdot 10^{-4}$	$2.1 \cdot 10^{-5}$	$9.4 \cdot 10^{-5}$	$2.4 \cdot 10^{-5}$
PE	$4.2 \cdot 10^{-4}$	$1.9 \cdot 10^{-5}$	$3.1 \cdot 10^{-4}$	$2.2 \cdot 10^{-5}$
SDS + PE	$3.2 \cdot 10^{-4}$	$2.0 \cdot 10^{-5}$	$2.7 \cdot 10^{-4}$	$2.0 \cdot 10^{-5}$

additions) had similar stability.

The reason for the greater stability of the bitumen/kerosene emulsion than the hexadecane emulsion is the presence of natural surfactants and fine particles as was discussed in first section. Addition of the surfactant makes the bitumen/kerosene emulsion more stable than the hexadecane emulsion. On the other hand, the addition of the polyelectrolyte reduces the stability of the bitumen emulsion. In the case of the hexadecane emulsion the reduction in stability due to the addition of PERCOL 592 is less evident.

SUMMARY AND CONCLUSIONS

Droplet size distribution and oil-in-water emulsion stability for hexadecane-in-water and 20% bitumen/kerosene-in-water systems were examined in this study. The emulsions were stabilized and destabilized with a surfactant (sodium dodecyl sulfate, SDS) and a cationic polyelectrolyte (PERCOL 592), respectively. The results of this investigation support a general consensus that phase separation for dispersed systems, such as for oil-in-water emulsions, can be stimulated by the surface chemistry of the oil-water interface.

It was found that adsorption of surface active compounds at the oil-water interface affects the oil droplet size distribution and the kinetics of droplet-droplet coalescence. Adsorbed SDS lowers the oil-water interfacial tension and increases the surface charge at the oil-water interface (27,28). As a consequence of the reduced oil-water interfacial tension, smaller sizes of oil droplets are generated in the homogenizer with constant hydrodynamic conditions. The mechanism of droplet-droplet coalescence is slower in such systems due to the increased surface charge at the interface.

The polyelectrolyte primarily reduces the surface charge at the oil-water interface and

enhances the kinetics of the droplet-droplet coalescence. Also, the polyelectrolyte may reduce the oil-water interfacial tension, however, this property was not examined in this research program as thoroughly as in previous studies (27, 28).

HIGH-SPEED VIDEO INVESTIGATION OF AIR BUBBLE FILMING WITH OIL

INTRODUCTION

Filming phenomena can be observed easily in the three phase air-water-oil system and is of particular importance in the separation of bitumen from tar sands in hot water processing, as will be demonstrated in the next chapter of this report. Filming of an air bubble with oil incorporates at least three important stages. Initially, the aqueous film occupies the gap between the colliding oil droplet and the air bubble. Next, after thinning and displacement, the aqueous film ruptures, and oil spreads at the air-water interface. The minimal time required for film drainage to a critical thickness and a spontaneous rupture is termed the induction time. The induction time depends on the surface chemistry and the hydrodynamics of the system. It is expected that the bubble adheres to the droplet when the bubble-droplet contact time is longer than the induction time.

At equilibrium, the condition for filming is expressed by the following thermodynamic criterion (35):

$$\gamma_W > \gamma_{OW} + \gamma_O \qquad (14)$$

corresponding to the positive value of the spreading coefficient, where γ_w, γ_o, γ_{ow} are the surface tension of water and oil, and the oil-water interfacial tension, respectively.

EXPERIMENTAL

Sodium dodecyl sulfate (95% purity, Sigma Chemical Co.) as the surfactant, n-dodecane (99% purity, Sigma Chemical Co.) as the oil and deionized water were used in all experiments.

Filming of the air bubble with oil was measured using the apparatus shown in Figure 13. A high-speed camera with a framing rate of 1000 frames per second and a 10 μs exposure time (Kodak EktaPro 1000 high-speed video system) was coupled with a Questar 100 long distance microscope. An air bubble and an oil droplet were put in contact by means of an electronic induction timer (Virginia Coal Mineral Services, Inc.). Figure 14 depicts the device for filming and measurement of the induction time. Two vertically oriented capillaries connected to microsyringes were used to form an oil droplet and an air bubble. The oil droplet was released from the upper capillary, while the air bubble was formed from the lower capillary. The upper capillary was attached to the induction timer. The oil droplet and the air bubble were generated in a rectangular glass cuvette filled with SDS solutions of varying concentrations. During the experiment, the position of the capillary with the air bubble was adjusted in such a manner that the bubble was in steady contact with the oil droplet. The volumes of the droplets and bubbles, controlled with microsyringes, were constant in all runs. The air bubble volume was 0.044 mm^3 (horizontal diameter 0.45 mm), and the oil droplet volume was 0.19 mm^3 (horizontal diameter 0.72 mm). The velocity of the bubble movement, resulting from the impulse, was also constant and equal to 2.1 mm/s. The distance between the bubble and droplet was set at 0.13 mm and was unchanged in all experiments. The filming time and the induction time were obtained from high-speed video tape recording.

Figure 14. Schematic diagram of the laboratory set-up used for measurements of the induction time: 1-electronic controller, 2-high-speed video camera, 3-long distance microscope, 4-electronic induction timer, 5-illuminators, 6-syringe with oil, 7-syringe with air, 8-upper capillary, 9-lower capillary, 10-glass cuvette, h-initial distance between the oil droplet and the air bubble.

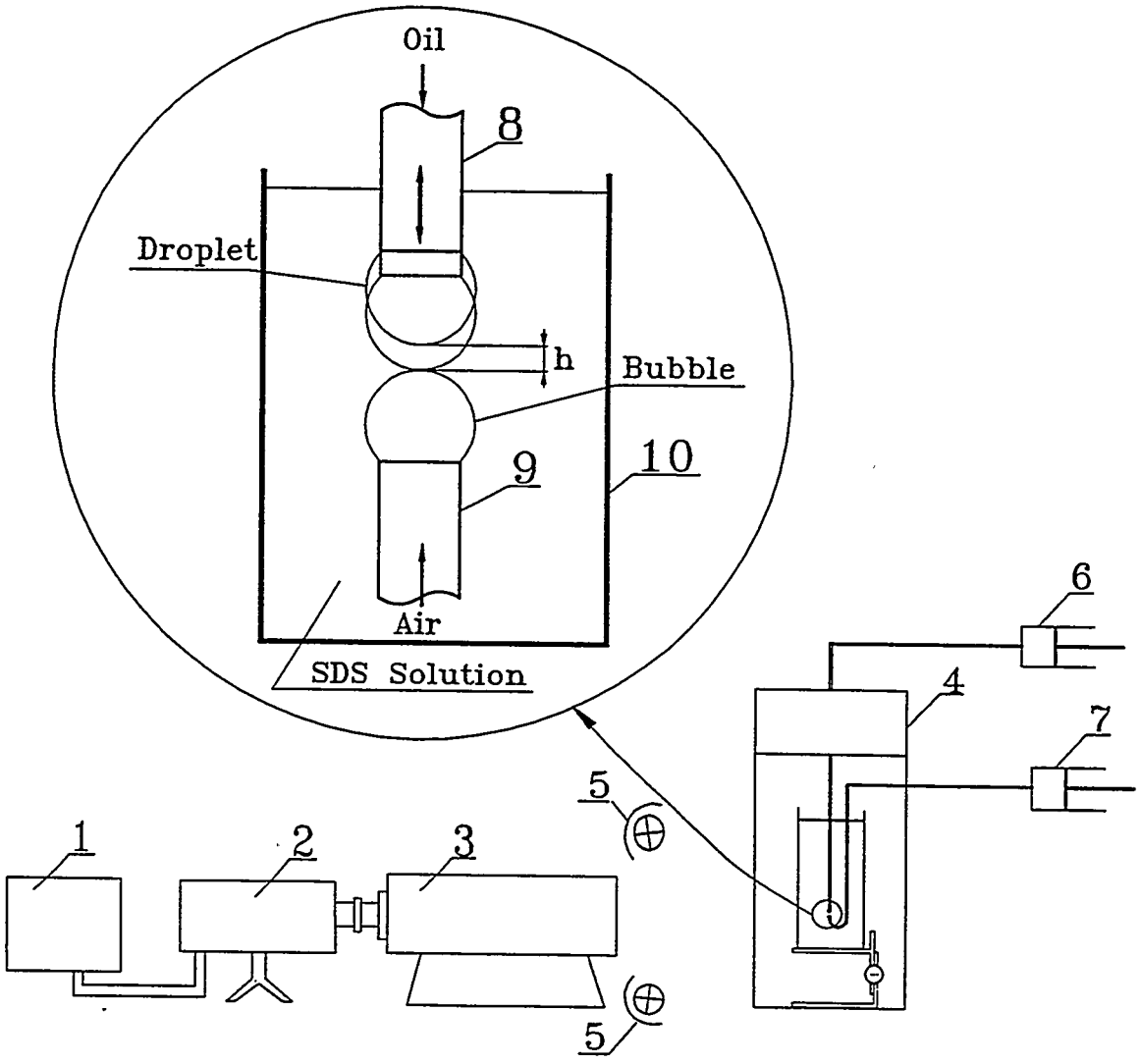
Oil
8
Droplet
h
Bubble
9
10
Air
SDS Solution
6
4
7
5
1
2
3
5

RESULTS AND DISCUSSION

Aging Effect on the Induction Time

The relationship between the induction time and the life time (conditioning time) of the bubble and droplet (which is the period elapsed from their release to rupture) was studied in a time range of 15 seconds to 5 minutes. Fifteeen seconds was the minimum bubble/droplet age that could be obtained in our experimental set-up. Figure 15 shows the effect of bubble/droplet age on the induction time for 10^{-7} M to 10^{-2} M aqueous SDS solutions. In all cases the induction time was practically constant which indicates that the coverage of newly formed surfaces with SDS molecules takes place in less than 15 seconds.

Induction and Filming Time as a Function of SDS Concentration

Figure 16 shows the results of the induction time measurements for the dodecane-air-aqueous solution systems with varying concentrations of SDS. The experimental data in Figure 16 represent the average values as calculated from at least 20 measurements for each SDS concentration. Large numbers of measurements were necessary because of the variation in the experimental data.

The induction time decreased steadily with an increasing SDS concentration (Figure 16). A minimum value of 0.59 second was obtained for approximately 10^{-4} M SDS. The induction time sharply increased for solutions with SDS concentrations larger than 10^{-4} M. In distilled water the induction time was 1.33 seconds.

The relationship between the spreading coefficient for dodecane and various SDS concentrations is presented in Figure 17. A comparison of Figure 16 with Figure 17 indicates a distinct correlation between the spreading coefficient and the induction time. The shortest induction time corresponding to the largest spreading coefficient indicates that thermodynamic

Figure 15. Relationship between induction time and age of air bubble/oil droplet system for varying SDS concentrations.

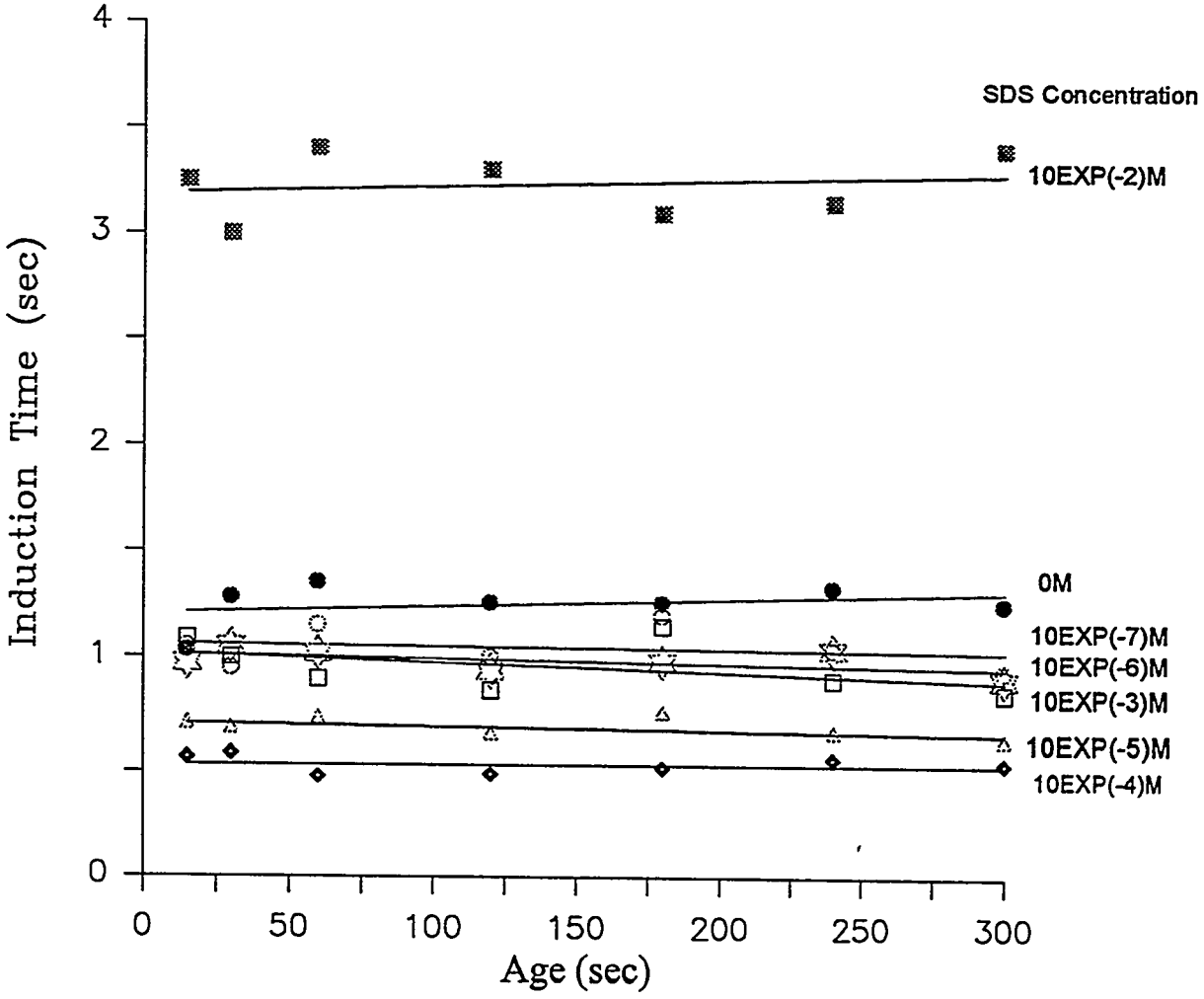
Induction Time (sec)
4
3
2
1
0
0
50
100
150
200
250
300
Age (sec)
SDS Concentration
10EXP(-2)M
0M
10EXP(-7)M
10EXP(-6)M
10EXP(-3)M
10EXP(-5)M
10EXP(-4)M

Figure 16. Relationship between induction time and SDS concentration.

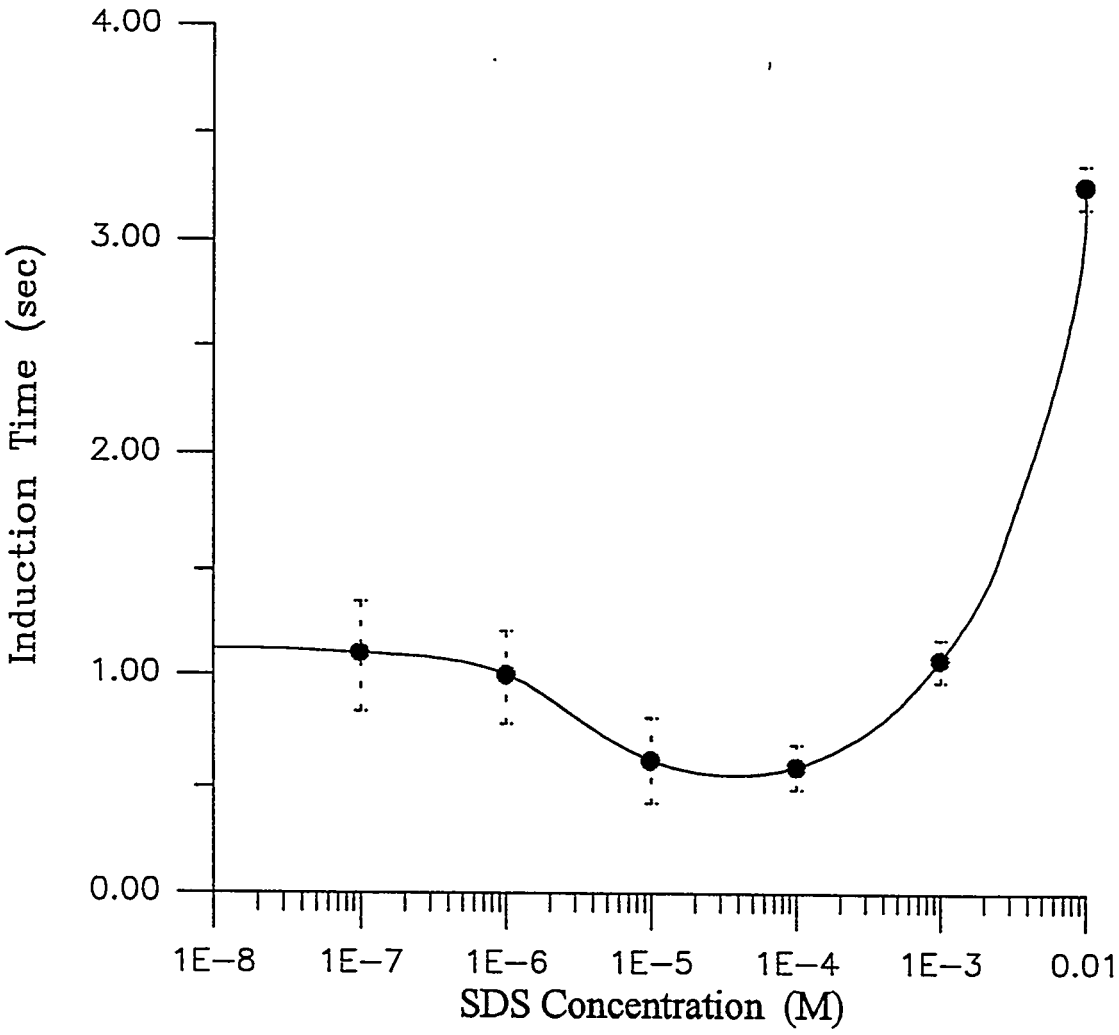
4.00
3.00
2.00
1.00
0.00
Induction Time (sec)
1E−8
1E−7
1E−6
1E−5
1E−4
1E−3
0.01
SDS Concentration (M)

Figure 17. Spreading coefficient for dodecane as a function of SDS concentration.

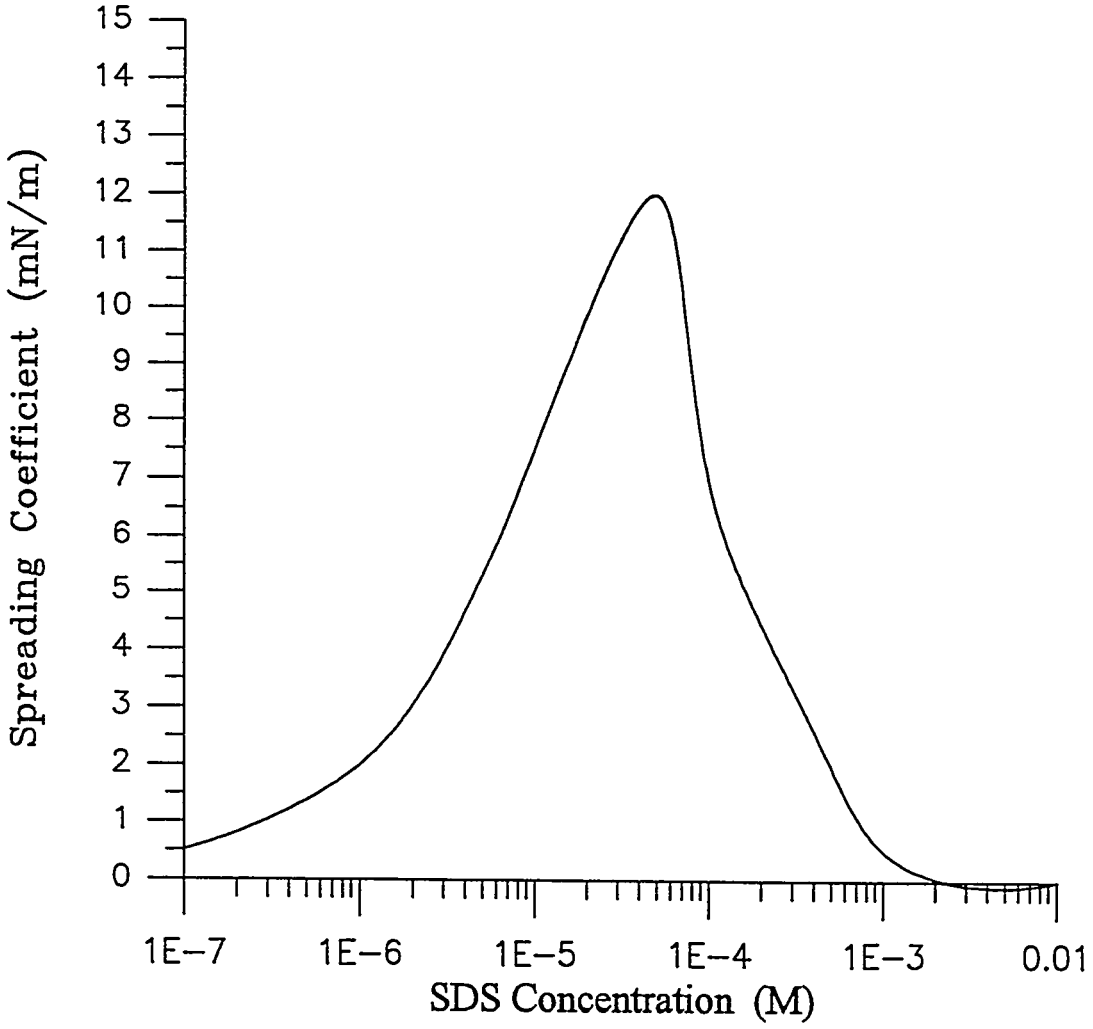
Spreading Coefficient (mN/m)
15
14
13
12
11
10
9
8
7
6
5
4
3
2
1
0
1E−7
1E−6
1E−5
1E−4
1E−3
0.01
SDS Concentration (M)

factors have substantial impact on filming phenomena, particularly on thinning and displacement of the aqueous phase between the air bubble and the oil droplet.

Hydrodynamic factors, namely the velocity of the moving bubble and droplet, or the vibrations of surfaces which are in contact, have a remarkable influence on the induction time. The rupture of the liquid film can occur before complete thinning. Factors which can initiate film rupture are small vibrations and sloshing of the liquid. A broad scatter of the experimental data in some measurements (Figure 15) supports this observation. Despite the fact that the diameters of the air bubbles and the oil droplets remained constant, as well as the velocity of the bubble approach to the oil droplet, at least 20-30 measurements for the SDS solution and about 50 for distlled water were necessary to obtain satisfactory results.

The measured values of the filming time are given in Figure 18. The relationship between the filming time and the SDS concentration corresponds very well to the induction time and the spreading coefficient. The results indicate that the filming time is controlled by the spreading coefficient - a thermodynamic property.

CONCLUSIONS

Induction time and filming time were measured for an air bubble-dodecane droplet-aqueous phase with varying SDS concentrations. A high-speed video camera (1000 frames per second, 10 μs exposure time) coupled with a long distance microscope were used to study the mechanism of the coalescence and spreading phenomena. It was found that the induction and filming times depended on the SDS concentration. With an increase in SDS concentration the induction time decreased and reached a minimum at a 10^{-4} M SDS solution. A similar relationship was observed for the filming time. The minimal values of the induction time and the filming time corresponded to the

Figure 18. Relationship between filming time and SDS concentration.

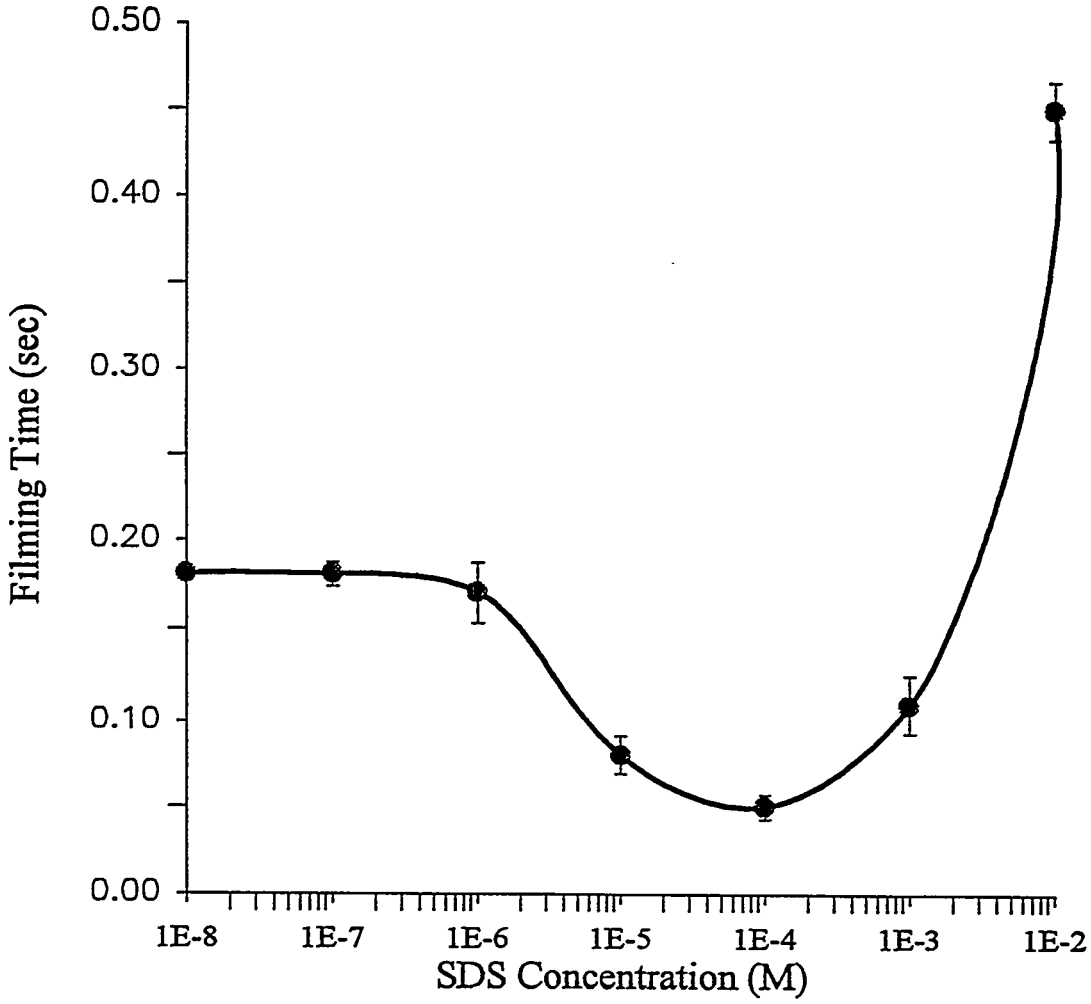
0.50
0.40
0.30
0.20
0.10
0.00
Filming Time (sec)
1E-8
1E-7
1E-6
1E-5
1E-4
1E-3
1E-2
SDS Concentration (M)

maximum value of the spreading coefficient, which indicates that thermodynamic properties of the system play an important role in spreading/filming phenomena.

ENHANCED BITUMEN SEPARATION FROM OIL SANDS IN THE PRESENCE OF GAS BUBBLES

INTRODUCTION

The modified water-based process developed at the University of Utah for domestic oil sands is presented in Figure 19. A pretreatment step which involves kerosene addition to the oil sand is necessary to reduce the bitumen viscosity below 1.5 Pa·s (20). The alkalinity of the aqueous phase in the digestion step is adjusted to a pH of 8.0 to 9.5 with sodium carbonate (Na_2CO_3); sodium tripolyphosphate ($Na_5P_3O_{10}$) is added to facilitate bitumen disengagement (36). The digestion temperature is maintained in the range of 323 to 333 K by saturation of the oil sand slurry with a mixture of steam and air. After several minutes of digestion, the slurry is discharged into a gravity separation cell and diluted with water. The bitumen concentrate is skimmed and the gravity tailings are transferred to a flotation cell to recover residual bitumen. The coarse sand particles are screened, and the tailings are subjected to sedimentation for 20-30 minutes. Finally, the tailings water is recycled to the digestion reactor (37). The bitumen concentrate thus prepared requires the removal of fine solids and dispersed/emulsified water before utilization and/or upgrading. The diluent-assisted hot-water process for bitumen recovery from oil sands as developed at the University of Utah satisfies basic practical requirements (high bitumen recovery, over 90%, and a good quality bitumen concentrate, 50-80 % bitumen on a dry weight basis) necessary for scale-up. However, it is believed that further improvements in bitumen recovery and the quality of the bitumen concentrate can be achieved by identification and control of the physico-

Figure 19. Flowsheet for the hot-water processing of Utah oil sands.

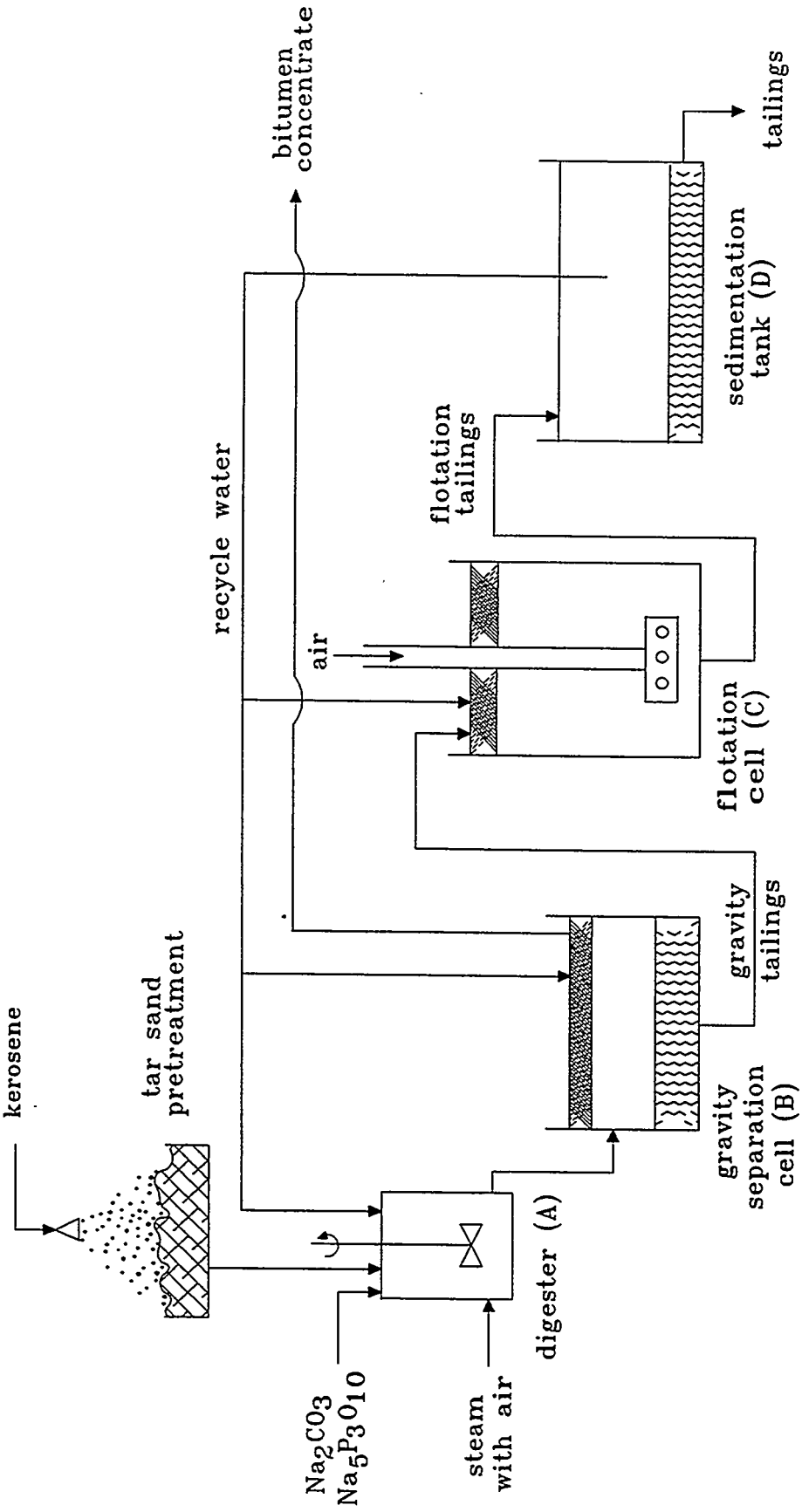
kerosene
tar sand pretreatment
Na_2CO_3
$Na_5P_3O_{10}$
steam with air
digester (A)
gravity separation cell (B)
gravity tailings
recycle water
air
flotation cell (C)
flotation tailings
sedimentation tank (D)
bitumen concentrate
tailings

chemical properties of such oil sand systems. Also, an appropriate identification and control of the physico-chemical properties of oil sand systems may lead to the development of new underground hot-water processing of oil sands.

For a long time, the digestion step was aimed at bringing the oil sand in contact with a hot alkaline-water solution in which the oil sand structure broke down to give water-wet sands and bitumen droplets displaced from mineral surfaces by the aqueous phase (similar to the mechanism of detergency). Bitumen dispersed in the alkaline solution was then recovered by flotation. Recently it has been discovered that gas injection during digestion improves the bitumen release from the oil sands and aerates the bitumen phase, thus facilitating the gravity separation of a high grade bitumen product (6, 38). Only aerated bitumen droplets can be separated by gravity because the difference in density between bitumen and water is generally insufficient to make an effective gravity concentration. Importantly, it was observed from these hot-water processing experiments that aeration of the oil sand slurry during digestion improves the quality of the bitumen concentrate.

Thus air injection during digestion plays an important role in bitumen release from oil sands. In this regard, the role of gas bubbles in the analysis of bitumen displacement from sand grains during digestion is important and its significance in the hot-water process is demonstrated in this contribution based on fundamental studies of model systems.

EXPERIMENTAL

Diluent-Assisted Hot-Water Experiments

The flowsheet for hot-water separation of bitumen from oil sand is presented in Figure 18. Oil sand samples from the North-West (7.0 wt% bitumen) or West-Central (6.0 wt% bitumen)

locations of the Whiterocks oil sand deposit were crushed, screened, and pretreated with 10 wt% kerosene (kerosene addition was based on the bitumen content). The kerosene was allowed to penetrate the oil sand for a period of 8 hours. Batch aqueous digestion (328-333 K, 75 wt% solids) experiments were conducted in a baffle stirred-tank reactor (A, 20 L) equipped with a double blade turbine impeller. Fresh tap water or recycled water (supernatant solution syphoned after 20 minutes of decantation from a 40 L sedimentation tank, D) with dissolved chemicals (Na_2CO_3, $Na_5P_3O_{10}$, NaCl), was used for digestion. A mixture of steam and air was used to raise the temperature of the oil sand slurry in the digester. After 5 minutes of digestion the resulting slurry was discharged into a gravity cell (B) and diluted with fresh tap water or recycled water (323 K, 40 wt% solids) for sand sedimentation and separation of the released bitumen concentrate. The suspension was gently stirred and the bitumen concentrate was skimmed from the surface of the process water. Batch flotation (15 wt% solids) in a Denver-type flotation cell (C, 38 L; air flow rate 5-6 L/min) was used for the final separation of the residual bitumen.

The grade of the bitumen concentrate from the gravity cell was determined by sample extraction with toluene using a Dean-Stark apparatus. Samples of the process water were withdrawn from the digester for measurement of the bitumen/water interfacial tension. The interfacial tension between the 10 wt% kerosene-in-bitumen and the process water was measured using the Wilhelmy plate technique with the K10T Digital-Tensiometer (KRUSS GmbH, Germany).

Significance of Aeration during Digestion

Crushed oil sand samples from the Whiterocks oil sand deposit (North-West location) were treated with kerosene (10 wt% of bitumen content) and allowed to equilibrate for 8-10 hours. Hot-water experiments were conducted in a Denver flotation cell (3 L) at a temperature of 325-330 K

with a 1 kg oil sand sample and 1.2 L water (45 wt% solids). Fresh tap water with dissolved Na_2CO_3 and $Na_5P_3O_{10}$ was used in all experiments.

In the first experimental procedure, the oil sand pulp was digested for 5 minutes (rotational speed of the stirrer was about 1000 rpm) and aerated with an air flow rate of 10-12 L/min. Subsequently, during gravity separation (5 min.) the bitumen concentrate was skimmed with a paddle and the froth composition was determined in terms of bitumen and solids content.

In the second experimental procedure, the oil sand pulp was digested at the same intensity but in the absence of aeration. After 5 minutes of digestion, gravity separation was attempted and the solids were separated from the supernatant liquid by decantation. The supernatant liquid was recycled to the flotation cell. The settling sands were washed with 1 L of fresh aqueous phase (warm tap water containing the same amount of chemicals as used in digestion) and discharged. The wash water was combined with the supernatant liquid and recycled to the digester (flotation cell). The supernatant liquid was subjected to flotation using conditions similar to those described in the first experimental procedure, viz., rotational speed of stirrer of 1000 rpm, air flow rate of 10-12 L/min, 5 minutes of flotation. Finally, the residual aerated bitumen concentrate in the supernatant was recovered for 5 minutes by gravity separation.

The bitumen content in the froth products was determined by the Dean-Stark analysis. The pH of the aqueous phase was measured using a pH-meter (model 520, Orion Research Inc., U.S.A.). The bituminous/aqueous phase interfacial tension was measured by the Wilhelmy plate technique (Digital-Tensiometer K10T, KRÜSS GmbH, Germany). Note that the 10 wt% kerosene-in-bitumen mixture was prepared separately for the interfacial tension measurements using kerosene (Chevron) and toluene-extracted bitumen from Whiterocks oil sands.

Microscopic Observations of Bitumen Spreading at the Gas Bubble Surface

Samples of the unconsolidated Whiterocks oil sand (North-West, 7.6 wt% bitumen) treated with 10 wt% kerosene (addition based on the bitumen content) were submerged in alkaline solutions in a glass cell. Changes in sample characteristics, especially bitumen spreading at the gas bubble surface, were observed through a stereoscopic microscope (Carl Zeiss Jena, Germany) and photographs taken as appropriate. The temperature in the glass cell was maintained at a constant level ($\pm$3 K) by using a hot plate, and the pH of the aqueous phase was measured using a pH-meter (model 520, Orion Research Inc.).

Whiterocks bitumen (either toluene-extracted or with 10 wt% kerosene) was spread mechanically on a quartz slide. The quartz slide was immersed in the aqueous phase at ambient or moderate temperatures. An air bubble, pushed through a microsyringe, was attached to the bitumen coated surface of the quartz slide. Bitumen spreading over the air bubble was observed and photographed through a stereoscopic microscope.

RESULTS AND DISCUSSION

Significance of Oil Sand Slurry Aeration

To demonstrate the significance of gas bubbles in bitumen release from mineral surfaces the following experiments were conducted. The Whiterocks oil sand was digested with process water in a Denver-type flotation cell. In the first experiment, air was sparged in the system (air flow rate was 10-12 L/min.) and after 5 minutes of gravity separation a bitumen concentrate was collected from the surface of the suspension. In the second experiment, oil sand was digested with process water under the same conditions but in the absence of aeration. After 5 minutes, sand and undigested oil sand were separated from the supernatant water, and washed with an additional

volume of the aqueous phase (same concentration of chemicals as for the aqueous phase used during oil sand digestion) to remove bitumen droplets entrapped in the slurry. The supernatant water from both steps of this experiment was combined and subjected to flotation (air flow rate of 10-12 L/min, 5 min., 1000 rpm). These two experiments were conducted to compare the efficiency of bitumen release from oil sand slurry during digestion in the presence and absence of aeration. In this way, it was possible to determine the role of air bubbles in the digestion step of the hot-water process. The experiments were conducted in a Denver flotation cell because aeration of the oil sand slurry could be controlled. The effect of oil sand slurry aeration during digestion on bitumen recovery and grade are presented in Table 8.

The results presented in Table 8 indicate the significance of the bitumen/water interfacial tension in the bitumen release from sand grains in the presence of air bubbles during oil sand digestion. The bitumen separation and the quality of bitumen concentrate increased with decreasing interfacial tension (Table 8). A significant bitumen recovery from Whiterocks oil sand was only observed when the oil sand slurry was sparged with air during digestion. This suggests that attachment of gas bubbles to bitumen at the surface of mineral particles and spreading of the bitumen at the gas bubble surface are important phenomena which account for the improved recovery of bitumen from oil sand.

The poor quality of bitumen concentrate obtained in experiments No 1-2 (Table 8) indicates that a significant amount of bitumen was strongly held by the solid particles and after air bubble attachment to the bituminous sand, agglomerates of air bubble-bitumen-solid particle are transported into the froth. A strong adhesion of bitumen to the mineral particle surfaces could not be overcome by hydrodynamics in the flotation cell, and a better bitumen separation was made possible only when the bitumen/water interfacial tension was lowered as in experiments No 3-5

Table 8. Bitumen recovery from Whiterocks oil sand in the presence and absence of aeration during digestion

Exp. No	Reagent Concentration Na_2CO_3 [M]	Reagent Concentration $Na_5P_3O_{10}$ [M]	pH	Interfacial Tension (60°C) [mNm^{-1}]	Recovery (Grade, dry basis) no aeration during digestion [wt%]	Recovery (Grade, dry basis) 10-12L/min air flow rate during digestion [wt%]
1.	$7.8 \cdot 10^{-3}$	$2.3 \cdot 10^{-3}$	7.9	11.7	<1 (ND)	20 (11)
2.	$1.2 \cdot 10^{-2}$	$3.4 \cdot 10^{-3}$	8.3	10.2	4 (33)	18 (15)
3.	$2.4 \cdot 10^{-2}$	$6.8 \cdot 10^{-3}$	8.7	9.2	5 (48)	29 (24)
4.	$3.9 \cdot 10^{-2}$	$1.1 \cdot 10^{-2}$	8.9	6.5	4 (51)	41 (32)
5.	$3.9 \cdot 10^{-2}$	$2.2 \cdot 10^{-2}$	9.0	4.4	7 (56)	47 (41)

ND - not determined

(Table 8).

Bitumen Release from Oil Sand - the Assistance of Gas Bubbles

It is evident from our experiments that gas bubbles aid bitumen release from mineral particles. The bitumen transfer from the oil sand to the gas bubble surface occurs during digestion of the oil sand slurry. Phenomena associated with bitumen release from coarse particle surfaces in the presence of air bubbles are revealed by the photographs presented in Figure 20. These photographs demonstrate how gas bubbles are enveloped by the bitumen. Gas (probably air saturated with volatile hydrocarbons), which is entrapped in the inter-particle space of the oil sand sample and in the pores of the mineral particles, appears to be displaced from the oil sand by penetration of the aqueous phase when the oil sand sample is immersed in an alkaline solution (6). The gas, displaced by the aqueous phase, forms bubbles at the oil sand surface which adhere to the mineral particle surfaces via bitumen bridges. In time, the bitumen spreads over the gas bubble surface to envelope the gas bubble as is evident for the systems shown in Figure 20. It is believed that in the digester the attachment of a gas bubble to a sessile bitumen droplet on the surface of a coarse particle may occur after inertial collision of the suspended phases. The kinetic energy for a collision between the bitumen-sand aggregate and the gas bubble should be much larger than for the collision between the bitumen droplet and the gas bubble due to a larger difference in density of the colliding bodies. Electrostatic repulsive forces between the charged dispersed phases, bitumen-sand aggregate and bubble, might play only a minor role in inhibiting such inertial collisions.

Bitumen spreading over the air bubble surface was also observed for the following model systems. A quartz slide was coated with Whiterocks bitumen, or kerosene (10 wt%)-in-bitumen mixture, and immersed in the aqueous phase. An air bubble was placed on the immersed quartz

Figure 20. Diluent pretreated Whiterocks oil sand sample (10 wt% kerosene based on the bitumen content) immersed in alkaline solution (A. pH=9.6, 0.001 M NaCl, T=338 K, t=3 min; B. pH=9.2, 0.05 M $Na_5P_3O_{10}$, T=328 K, t=4 min). Illustration of bitumen spreading over the gas bubble surface (A), and bitumen-enveloped gas bubbles (B). Photographs taken for stagnant conditions.

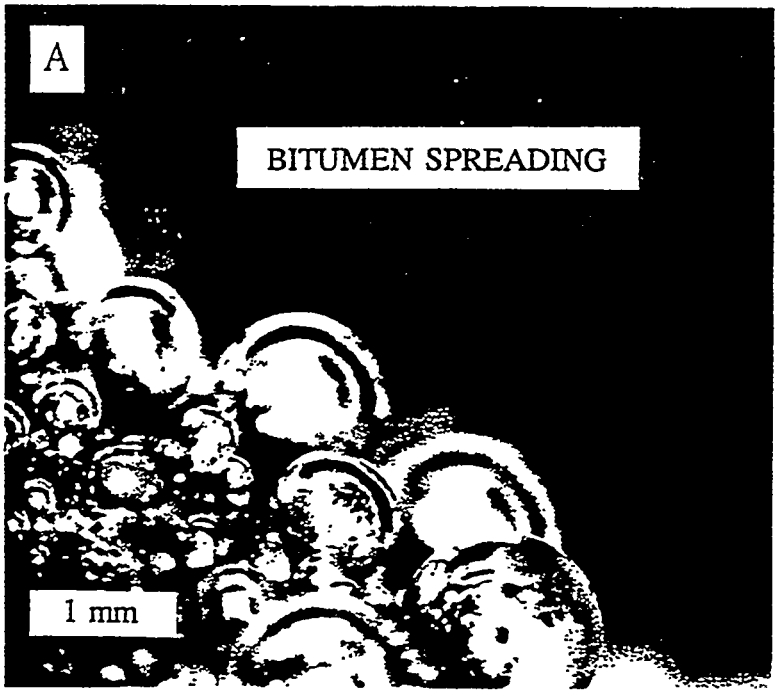
A
BITUMEN SPREADING
1 mm

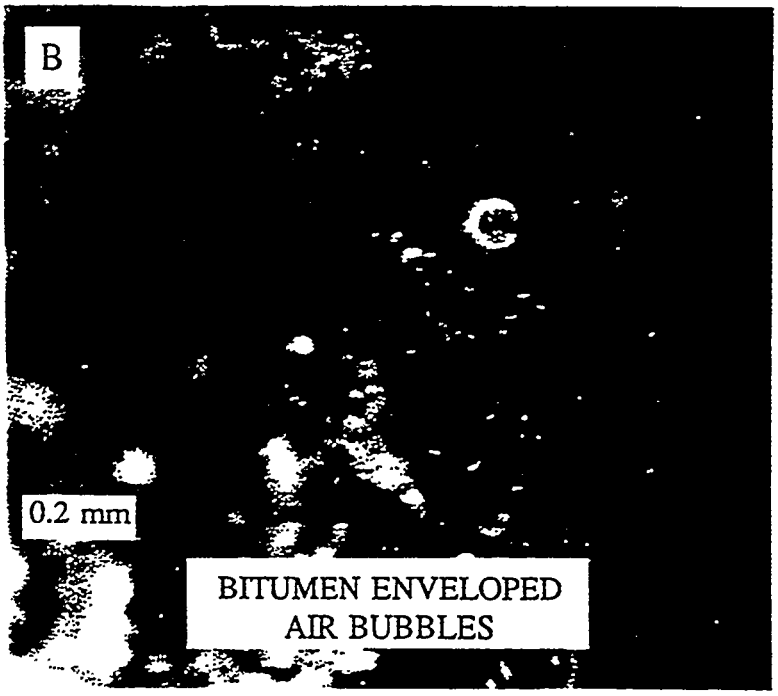
B
0.2 mm
BITUMEN ENVELOPED
AIR BUBBLES

slide using a microsyringe. The spreading of the bituminous phase over the bubble surface was observed and photographed through a stereoscopic microscope. Figure 21 illustrates the kinetics of bitumen spreading at the air bubble surface (additional photographs of bitumen spreading for similar model system are presented in Ref.(4)). It was observed that the bituminous phase covered the bubble surface in a variety of aqueous phase compositions: pH=7 to pH=11, 0 to 0.05 M $Na_5P_3O_{10}$ and 0 to 1 M NaCl concentrations, and temperatures from 293 K to 333K (6).

Bitumen spreading at the air bubble surface involves complex phenomena (6). First, it was observed that a precursor film always assisted the moving bituminous phase and this film covered the bubble surface in the first seconds of an experiment (a change in color of the air bubble surface in front of the bituminous phase was observed but the thickness of this film was impossible to estimate in these experiments). Second, the kinetics of bitumen spreading depended on the volume of bitumen in contact with the air bubble. When the air bubble was attached to a small bitumen lens, less than several hundred micrometers in diameter (bubbles with diameters larger than 1.5 mm were used in these experiments), the spreading of the bituminous phase was almost instantaneous and difficult to capture on photographs. Also, the bitumen spread rapidly when the temperature was greater than 300 K. Figure 21 illustrates the behavior of the system at ambient temperature, under which conditions the kinetics (60 seconds) of bitumen spreading did not significantly disturb the quality of the photographs.

Bitumen spreading and envelopment of the gas bubble, shown in Figures 20 and 21, indicate a positive spreading coefficient, $S>0$, where the spreading coefficient is expressed by the following equation (13):

$$S = \gamma_W - (\gamma_{BW} + \gamma_B) \qquad (15)$$

Figure 21. Spreading of bitumen (diluted with 10 wt% kerosene) at an air bubble surface pH=9.0-9.1, 0.001 M NaCl, T=293-295 K. Initially a bitumen film was deposited on a quartz slide and an air bubble was attached using a microsyringe.

1 mm

10 s

20 s

30 s

60 s

where γ_W, γ_B, γ_{BW} are the surface tension of the water, bitumen, and the bitumen/water interfacial tension, respectively. It was demonstrated in our previous contributions (5,6) (see also our 1992-1993 DOE report) that the spreading coefficient, S, as calculated based on equilibrium values of γ_B, γ_W, and γ_{BW}, remains positive for the Whiterocks bitumen/water systems with varying pH values from pH=7 to pH=11, and for varying concentrations of inorganic salts, from 0 to 0.1 M $Na_5P_3O_{10}$ and from 0 to 1 M NaCl, even if the surface tension of the processing water is reduced to 45 mN/m. However, bitumen spreading at a water surface is a dynamic process in which the driving force, the spreading coefficient, may vary with time. The spreading coefficient can change even for systems with pure single-component liquids. With time the initial positive spreading coefficient decreases to near zero or becomes negative when liquids are saturated with each other. Bitumen is a complex mixture of hydrocarbons. The equilibration of surface properties in bitumen/water systems requires time, and the spreading phenomena are even more complex than for pure systems. Microscopic observations, discussed in the previous section, showed that the precursor film (with a thickness of several micrometers or less, as expected after visual observations) always assists in the spreading of the bitumen. It was observed in our laboratory (6) that the surface tension of water in contact with bitumen decreased in time due to a screening effect created by the migration of bitumen, or selected bitumen components. Further, contact of bitumen with the aqueous phase also creates diffusional processes in which surface active compounds migrate at the bitumen/water interface to minimize the interfacial free energy (6). In this regard, the spreading coefficient for the bitumen/water system varies with time due to changes in the surface tension of the aqueous phase, affected by the spreading films of bitumen (or bitumen components), and changes of the bitumen/water interfacial tension. Bitumen spreading at the water surface occurs as long as the thermodynamic equilibrium in the system is not reached, i.e., there

is a positive spreading coefficient (note that the initial positive spreading coefficient was also demonstrated for a bitumen (20-40 wt%)/kerosene blend (27).

Hot-Water Processing of Oil Sands in the Presence of Dispersed Gas

The unique role of gas bubbles in bitumen separation from oil sands has been recognized in the commercialized hot water process used in Canada in which case 30 vol% of air is mixed with steam and injected during digestion to maintain an appropriate temperature for digestion (38). Thus, aerated bitumen droplets can be separated in the gravity cell. In the diluent-assisted hot-water experiments conducted at the University of Utah in a baffled stirred-tank reactor, air was also introduced into the digester with steam, but the amount of air was not controlled (6). Additionally, the intrinsic gas phase (air saturated with volatile compounds of bitumen) is released from oil sand during digestion. Atmospheric air may be incorporated into the oil sand slurry during digestion. Air from both sources is entrapped by bitumen in the oil sand slurry and causes the bitumen concentrate to float to the surface in the gravity separation cell.

The effect of bitumen/water interfacial tension on bitumen recovery in the gravity separation step, after oil sand digestion in the presence of air, is shown in Figure 22. The hot-water processing tests were carried out as described in the experimental section. A change in the bitumen/water interfacial tension was stimulated by varying the pH and/or the ionic strength of the aqueous phase (varying concentration of Na_2CO_3, $Na_5P_3O_{10}$, NaCl). See Ref.(4) and our 1992-1993 DOE report for more details. As previously mentioned, gravity separation of bitumen was possible in our experiments due to the entrapment of air during digestion. The gas phase was introduced with steam and also originated from the intrinsic gas released from the oil sand during digestion.

Based on the experimental results presented in Figure 22 it is evident, in addition to

Figure 22. Relationship between bitumen recovery from gravity separation and the bituminous phase (10 wt% kerosene-in-bitumen)/process water interfacial tension.

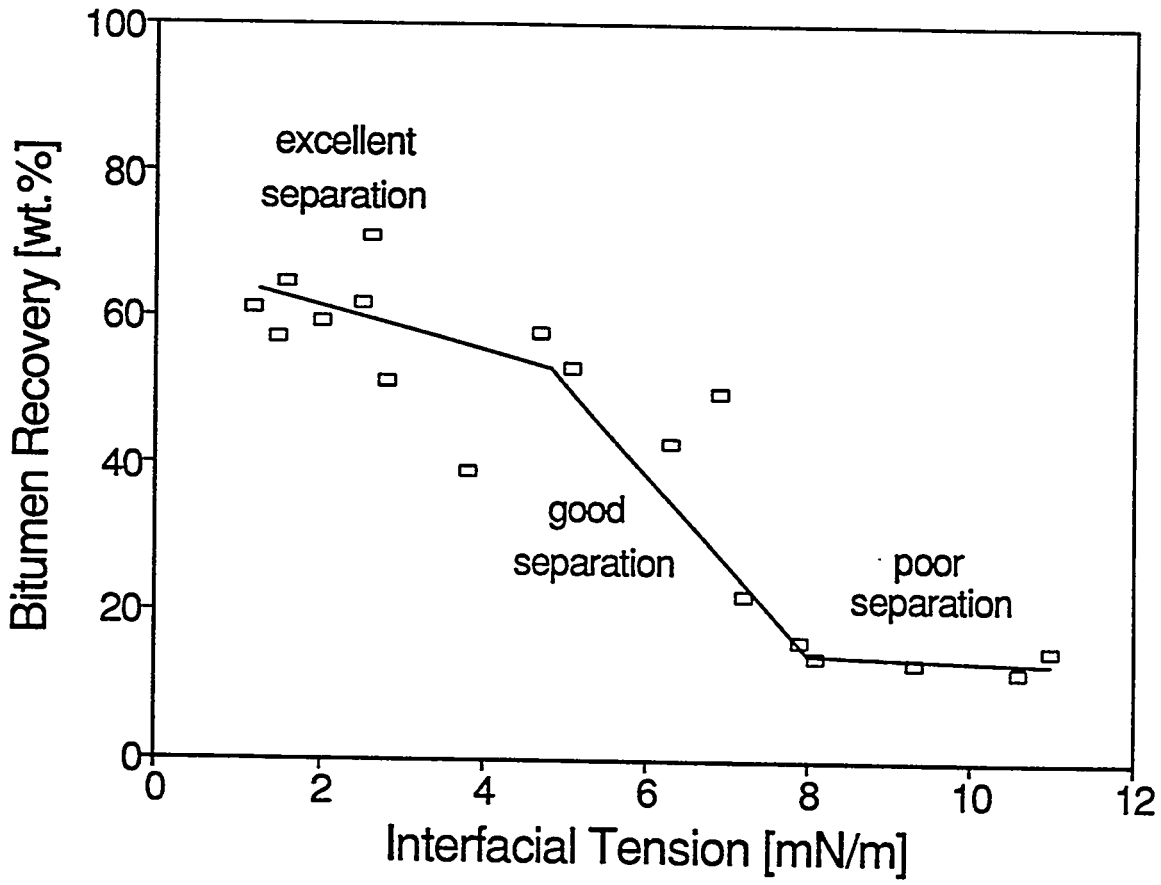
100
80
60
40
20
0
Bitumen Recovery [wt.%]
excellent
separation
good
separation
poor
separation
0
2
4
6
8
10
12
Interfacial Tension [mN/m]

aerated digestion, that the bitumen/water interfacial tension should be lowered to a value below 7 mN/m, preferably below 4 mN/m; for efficient Whiterocks bitumen recovery from the oil sand. These criteria are in agreement with our previous findings (5). However, it should be recognized that during oil sand processing the dynamic interfacial tension or the dynamic surface tension are difficult to predict and may differ slightly from values determined under equilibrium conditions.

CONCLUSIONS

Poor bitumen recovery from oil sands was observed when air (gas) was eliminated during digestion. A successful bitumen recovery from the Whiterocks oil sands was achieved when the oil sand pulp was saturated with dispersed air during the digestion step. The effective separation of bitumen from oil sands involves the mechanisms of gas bubble attachment to bitumen located at the surface of mineral particles, spreading of bitumen over the gas bubble surface, and detachment of bitumen-enveloped gas bubbles from the surfaces of coarse sand particles. All these steps are facilitated by decreasing the bitumen/water interfacial tension. A decrease in the bitumen/water interfacial tension can be accomplished by an increase in the pH and/or concentration of electrolyte.

Systematic studies of the process which combines oil sand digestion and flotation into one step seem to be of particular significance for future research activity. The optimal amount of injected air and air bubble size distribution needs to be identified in order to improve bitumen separation from oil sand.

BITUMEN PAVING MATERIAL WITH CRUMB RUBBER MODIFIER

INTRODUCTION

The amount of asphalt used annually is about 30 million tons of which approximately 24 million tons is used in paving applications (39). Refineries blend asphalt binders to meet the specification requirements of the design engineer. However, the current asphalt binder being supplied has not, in most cases, performed as expected. This is partially due to the decline in the supply of high quality asphalt from indigenous crudes. In addition, the performance of asphalt paving materials are constantly being challenged to withstand the strins of increasing traffic loads under widely differeing climatic conditions. In many circumstances, changing the mix design or aggregate types, or other conventional approaches have failed to solve the cracking and ruting problems exhibited by asphalt pavements. Recently, polymeric materials and other additives have been incorporated into asphalt binders to increase the viscoelastic behavior of pavements, thereby reducing permanent deformation while providing a tough, crack-resistant binder. In order to meet the increase demands and enhance the life-time of asphalt pavements, the development of high quality asphaltic materials is a must.

Tar sand bitumens represent an important potential petroleum resource that may serve the demand for the production of high asphaltic materials. The physical properties and elemental compositions of tar sand bitumens are quite similar to those reported for petroleum asphalts. In fact, the properties of several tar sand asphalts prepared in past studies by several different investigators compare favorable with petroleum-derived asphalts and ASTM specifications (39). In a previous investigation it was determined that the bitumen and a vacuum distillation residue from the Asphalt Ridge tar sand deposit in Utah met ASTM specifications as viscosity-graded asphalts, AC-5 and AC-30, respectively (41). A similar investigation with a vacuum distillation

residue of bitumen from the Whiterocks, Utah, deposit has classified it as a viscosity-graded AC-10 asphalt (41). The only commercial application of tar sand bitumen as a paving material has been limited to the direct use of run-of-mine tar sand as a surfacing material. The tar sands as obtained from quarries, however, do not meet existing specifications as a highway construction material.

Rubber is one type of polymeric material which can be used to modify the viscoelastic properties of asphalts. Enormous quantities of scrap tires are discarded around the world every year, almost 300 million tires in the United States alone (42), and represent a low-cost source of rubber. With the exception of Japan, where 92% of scrap tires are being utilized (42% in the form of crumb rubber), other countries dispose of the majority of waste tires in landfills or illegal dumps. In 1991, based on preliminary performance of rubber modified asphalt, the U.S. Congress included a provision in the Intermodal Surface Transportation and Efficiency Act (ISTEA, P.L. 102-240, Section 1038) addressing the use of scrap tire rubber in paving materials. The primary requirements of Section 1038 as they relate to rubber modified asphalt are: relax federal regulations to permit state and local agencies to use rubber in pavement construction; study the performance, recycling, and environmental aspects of rubber use in asphalt design; and satisfy a minimum rubber utilization requirement (MUR) beginning in 1994. The MUR requires that at least 5% of Federal Aid hot-mix projects in 1994 must include some form of recycled tire rubber (this has been delayed until 1995). The MUR increases 5% each year up to 20%.

In view of the foregoing, research was initiated to study the feasibility of blending scrap tire rubber with selected Utah tar sand bitumens. In this section of the report, high temperature consistency as measured by the Brookfield viscosity of the blended mixture is analyzed as a function of composition, and co-processing variables including reaction temperature and mixing

EXPERIMENTAL

Bitumen Samples

Hot water processing was used to obtain a bitumen concentrate from Asphalt Ridge tar sand (Uinta Basin, Utah) in large scale laboratory experiments according to procedures described in the previous section of this report. The bitumen concentrate originally contained 30 wt% dispersed water and about 5 wt% fine minerals. Both the contaminating phases were removed by 1 month sedimaentation at room temperature.

The Circle Cliffs tar sand (Uinta Basin, Utah) samples were used in several batches to obtain bitumen by the Dean-Stark toluene extraction method. The toluene extracts of the bitumen were subjected to vacuum distillation on the rotary evaporator, and the final traces of the solvent were removed at 90°C and a vacuum setting of 20 torr for more than 4 hours.

Crumb Rubber

Two types of commercially available crumb rubber were used in this study. One type consisted of whole-tire rubber and contained a small proportion of fibrous material. This fibrous material is believed to culminate fromthe reinforcing plies used in the construction of pneumatic tires, and is generally composed of polyester and polyamide fibers. The second type of crumb rubber consisted only of tread rubber and was relatively devoid of the fibrous material ubiquitous to whole-tire crumb. Both types of crumb were ambient ground and supplied by the manufacturer as minus 40 mesh material. Additional screening performed in the laboratory allowed for relatively narrow size fractions to be co-processed with the tar sand bitumen. The bitumen-rubber blends prepared with whole-tire rubber used crumb in the -100+140 mesh size interval; whereas, the blends containing tread rubber used -70+100 mesh crumb.

Viscosity Measurements

The viscosity measurements were made with a Brookfield Cone/Plate Viscometer, model 5XHBT, using 2 milliliters of sample and a 3.0° cone spindle. Viscosities of the bitumen-rubber blends were measured at shear rates of 1 to 40 sec^{-1} in the temperature range of 40 to 90°C.

Bitumen-Rubber Co-Processing

Co-processing of the crumb rubber and tar sand bitumen was performed in the temperature range of 200 to 380°C using a 150 cc autoclave (Autoclave Engineers). Reaction temperature was maintained within $\pm$2°C of the experimental temperature. Reaction time ranged from 0.5 to 4.0 hours not including the time associated with sample heat-up and cool-down periods. Sample heat-up times fluctuated according to the experimental temperature and ranged from 30 to 60 minutes. Sample cool-down was generally accomplished within 45 minutes.

A removable 100 milliliters 316L stainless steel sleave was machined and snugly fitted to the reaction chamber of the microclave to facilitate sample removal and cleaning operations. Approximately 36 grams of bitumen were used in each experiment, with crumb rubber additions ranging from 0 to 30% by weight of bitumen. The bitumen and crumb rubber were placed in the sleave in a layered configuration to optimize crumb rubber dispersion. Approximately one-half of the total bitumen was placed in the sleave immediately prior to and following crumb rubber addition. After the sample-filled sleave was sealed inside the autoclave, the system was purged three times at 1000 psig with nitrogenin order to remove oxygen from the reaction chamber. Mixing was accomplished with a straight four-blade turbine. Initial mixing intensity was set at 100 rpm and increased to 500 rpm when the sample temperature approached the temperature lower than 50°C of the experimental temperature. Lower boiling components were continuosly collected during each experimental run using a 5 mm diameter copper condenser connected to a sample port

located at the extreme top of the autoclave. To aid in the removal of the light fractions, nitrogen was slowly purged through the system during each experiment.

RESULTS AND DISCUSSION

The experimental conditions under which crumb rubber was co-processed with tar sand bitumen in the autoclave are outlined in Table 9. Two types of bitumen were examined - an oil extended bitumen concentration containing approximately 10 wt% kerosene and a refined Circle Cliffs bitumen, free of kerosene. The bitumens were blended with a whole-tire crumb rubber containing a small proportion of polyester and/or polyamide fibers, and a tread-rubber crumb relatively devoid of the fibrous material. In addition to the presence of the fibrous material, the whole-tire crumb probably contains a larger percentage of natural rubber than the tread-rubber crumb. Whole-tire crumb includes rubber from all components of a tire, including the sidewall which generally contains a large proportion of natural rubber to provide optimum flexibility. Whereas, tread-rubber requires a high resistance to abrasion and generally contains significant amounts of synthetic rubber compounds.

Viscosity measurements were made on the blended samples at shear rates of 1 to 40 sec^{-1} in the temperature range of 40 to 90°C. Unlike the empirical tests commonly performed on petroleum asphalts such as penetration and ductility, viscosity is a fundamental measurement of consistency that is generally unaffected by changes in testing conditions, such as instrumentation configuration or sample geometry. Viscosity measurements are capable of evaluating effects of temperature, heating, and rate of deformation of loading. Viscosity is probably the most important primary specification consideration since it is influential in determining the properties of the paving mixture during preparation and pavement construction, as well as, the properties of the

Table 9. Experimental conditions of tar sand bitumen-rubber samples prepared in the autoclave

Sample	Temperature [°C]	CRM Concentration* [%]	Reaction Time [hours]
Bitumen concentrate/whole-tire crumb 0.5	200		25
Bitumen concentrate/whole-tire crumb 1.0	200		25
Bitumen concentrate/whole-tire crumb 2.0	200		25
Bitumen concentrate/whole-tire crumb 4.0	200		25
Circle Cliffs bitumen/whole-tire crumb 2.0	200		25
Bitumen concentrate/whole-tire crumb 2.0	280		29
Bitumen concentrate	345	0	2.0
Bitumen concentrate/whole-tire crumb 2.0	345		24
Bitumen concentrate/whole-tire crumb 4.0	345		25
Bitumen concentrate/tread-rubber crumb 2.0	345		25
Circle Cliffs bitumen/whole-tire crumb 2.0	345		25
Bitumen concentrate/whole-tire crumb 2.0	350		30
Bitumen concentrate	380	0	2.0
Bitumen concentrate/whole-tire crumb 2.0	380		25

Crumb rubber modifier (CRM) concentration is based on weight of bitumen. Particle size of whole-tire crumb is -100+140 mesh and tread-rubber crumb is -70+100 mesh

finished pavement.

The flow properties of the bitumen-rubber samples generally exhibited non-Newtonian behavior, and at low measurement temperatures, the samples tended to behave as viscoelastic semi-solid materials. As the measurement temperature increased, the samples became Newtonian. In addition, the flow characteristics of the bitumen-rubber samples changed significantly with reaction temperature. At low reaction temperatures, sample viscosity decreased significantly with increasing shear rate. This is illustrated in Figure 23 where viscosity is plotted as a function of shear rate at constant measurement temperature for bitumen concentrate blended with 25 % crumb rubber at 200°C. However, the samples prepared at higher reaction temperatures (280 to 380°C) exhibited Newtonian flow behavior with increasing shear rate. This trend is evident in Figure 24 where viscosity is plotted as a function of shear rate at constant measurement temperature for bitumen concentrate blended with 25% crumb rubber for 2 hours at 200, 280, 345, and 380°C. The change in the flow behavior at higher reaction temperatures may presumably be a direct result of crumb rubber degradation. At mixing temperatures of 280°C and greater, the rubber particles are disintegrated and incorporated into the bitumen matrix; however, at 200°C rubber degradation does not occur to any appreciable extent, and the rubber particles swell under the action of the aromatic and naphthenic oils present in the bitumen. The texture of the blended samples also supports possible rubber disintegration and incorporation into the bitumen matrix. Rubber particles were easy to identify visually in the blended samples at 200°C but not in the samples prepared at 280, 345, and 380°C. The samples prepared at 200°C also exhibited a typical elastomeric properties.

It is important to note the significant increase in viscosity exhibited by the bitumen concentrate after blending with crumb rubber. For example, bitumen viscosity increases at 60°C

Figure 23. Viscosity as a function of shear rate at 60°C for bitumen concentrate blended with 25% whole-tire crumb at 200°C for various reaction times. Viscosity of unmodified bitumen is 4.4 Pa·sec.

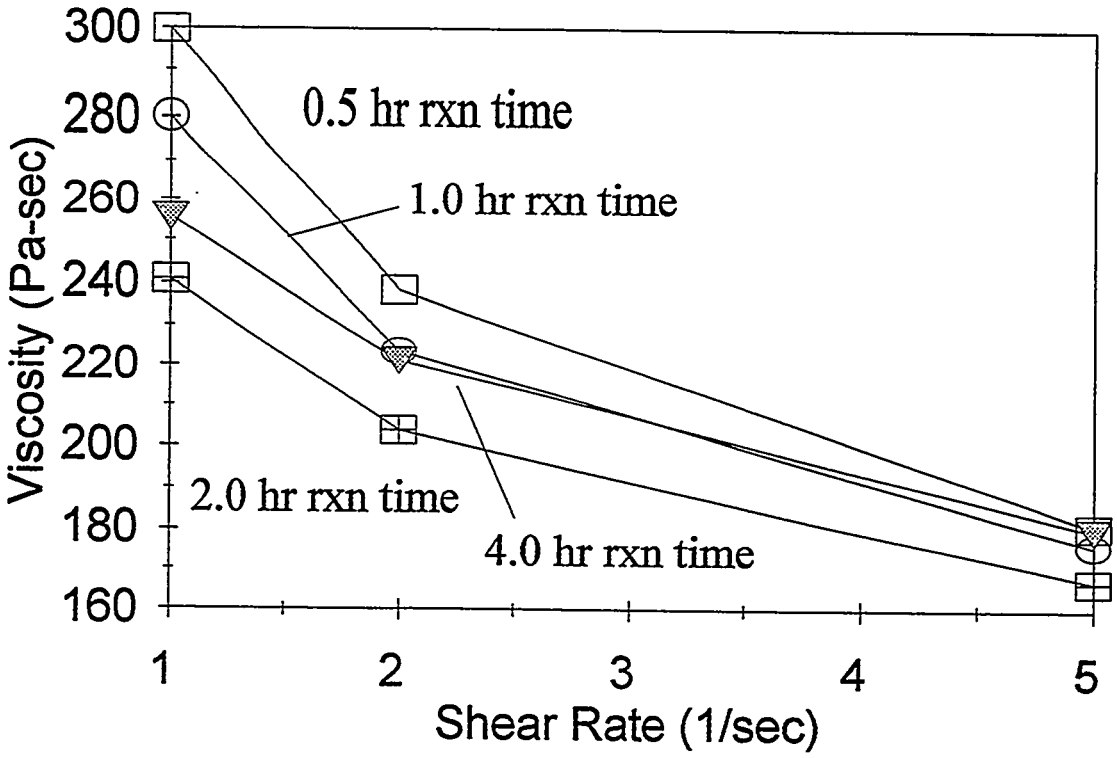
300
280
260
240
220
200
180
160
Viscosity (Pa-sec)
0.5 hr rxn time
1.0 hr rxn time
2.0 hr rxn time
4.0 hr rxn time
1
2
3
4
5
Shear Rate (1/sec)

Figure 24. Viscosity as a function of shear rate at 60°C for bitumen concentrate blended with 25% whole-tire crumb at 200, 280, 345, and 380°C for 2 hours. Viscosity of unmodified bitumen is 4.4 Pa·sec.

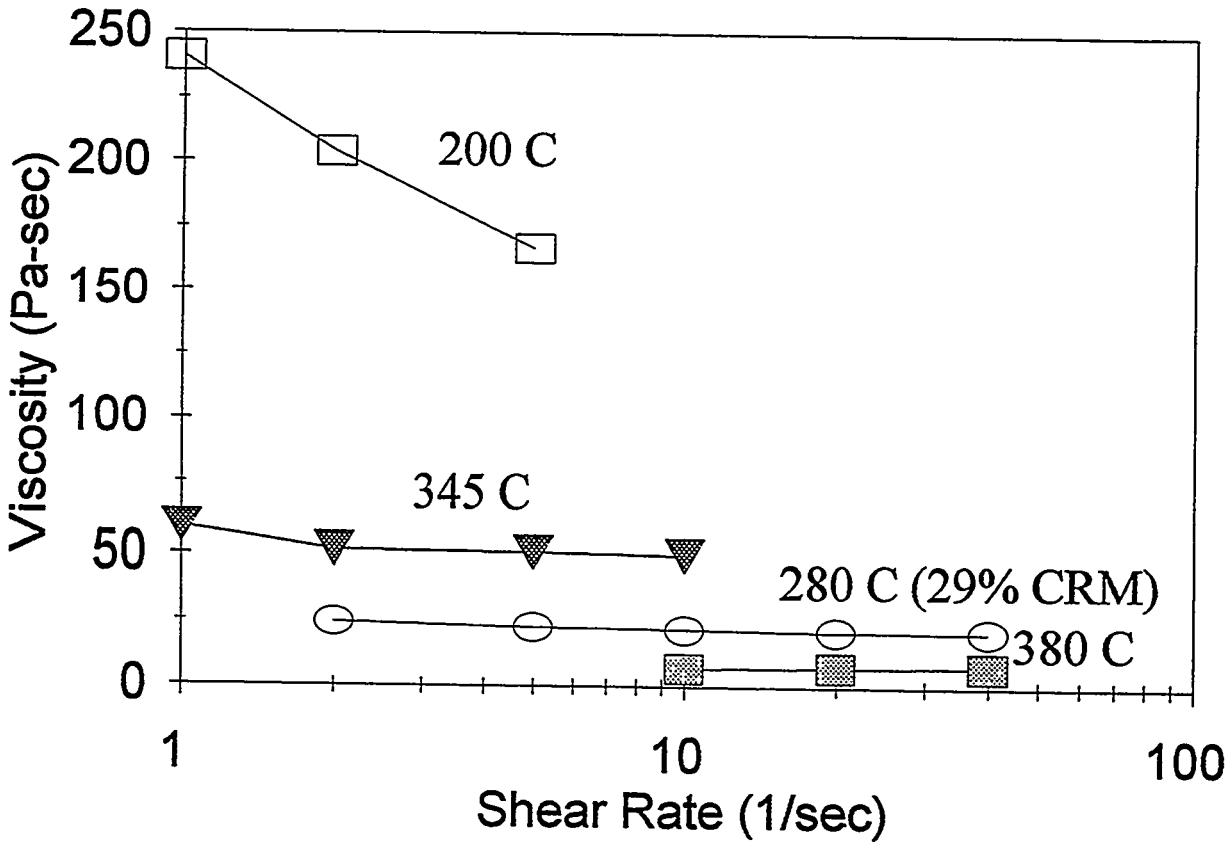
250
200
150
100
50
0
Viscosity (Pa-sec)
200 C
345 C
280 C (29% CRM)
380 C
1
10
100
Shear Rate (1/sec)

from 4.4 Pa·sec to a range of 241 to 167 Pa·sec (shear rate dependent) after 25% crumb rubber is blended with bitumen concentrate at 200°C for 2 hours (see Figure 24). Figure 25 illustrates the effect of reaction temperature on sample viscosity. As can be seen, the viscosity generally decreases with increasing reaction temperature. The one exception to this trend is the sample prepared at 280°C; however, experimental difficulties were experienced during the preparation of this particular sample. The largest increase in bitumen viscosity occurs at a reaction temperature of 200°C and is significantly higher than the samples prepared at 280, 345, and 380°C. This is presumable due to the presence of swollen rubber particles in the sample prepared at 200°C.

The effect of reaction time on the viscosity of bitumen-rubber samples prepared with 25% crumb rubber at 200°C is shown in Figures 26 through 28. The different figures represent viscosity measurements conducted at several shear rates. As the reaction time is increased from 0.5 to 2.0 hours, sample viscosity decreases. For a reaction time of 4.0 hours, however, no further decrease in sample viscosity is exhibited for measurement temperatures above approximately 70°C, and an increase in viscosity is experienced at temperatures below 70°C. The longer reaction times presumably increased crumb rubber degradation resulting in decreased viscosity. The increased viscosity of the 4 hour sample compared with the 2.0 hour sample at measurement temperatures below 70°C may be due to some sort of aging effects occuring within the bitumen matrix during mixing.

The increase in viscosity due to crumb rubber addition is most noticeable at low measurement temperatures. As the temperature is increased from 45 to 90°C, the viscosity of the rubber modified bitumen decreases dramatically (see Figure 26). Thus, the rubber modified bitumen provides the benefit of high viscosity at pavement temperatures experienced during summer months, without sacrificing processibility at temperatures normally used in pavement

Figure 25. Viscosity at 10 sec^{-1} shear rate as a function of measurement temperature for bitumen concentrate blended with 25% whole-tire crumb at 200, 280, 345, and 380°C for 2 hours.

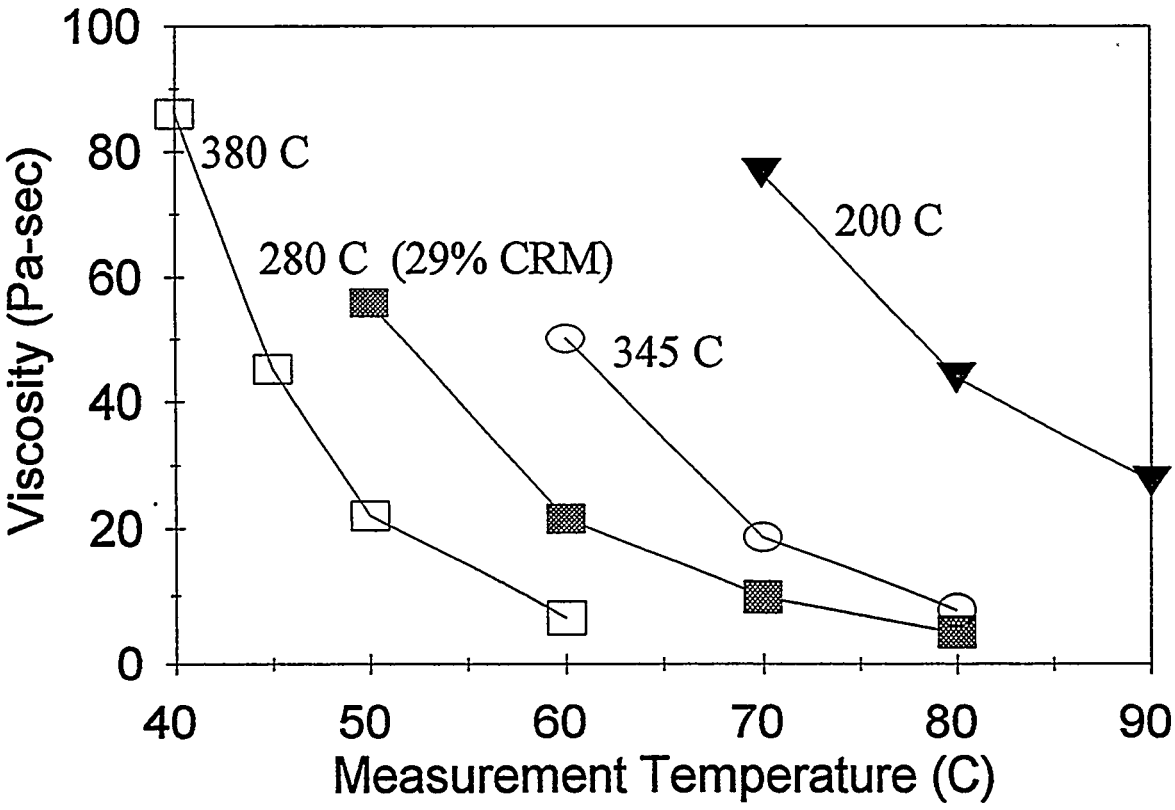
100
80
60
40
20
0
Viscosity (Pa-sec)
380 C
280 C (29% CRM)
345 C
200 C
40
50
60
70
80
90
Measurement Temperature (C)

Figure 26. Viscosity at 1 sec^{-1} shear rate as a function of measurement temperature for bitumen concentrate blended with 25% whole-tire crumb at 200°C for 0.5, 1.0, 2.0, and 4.0 hours.

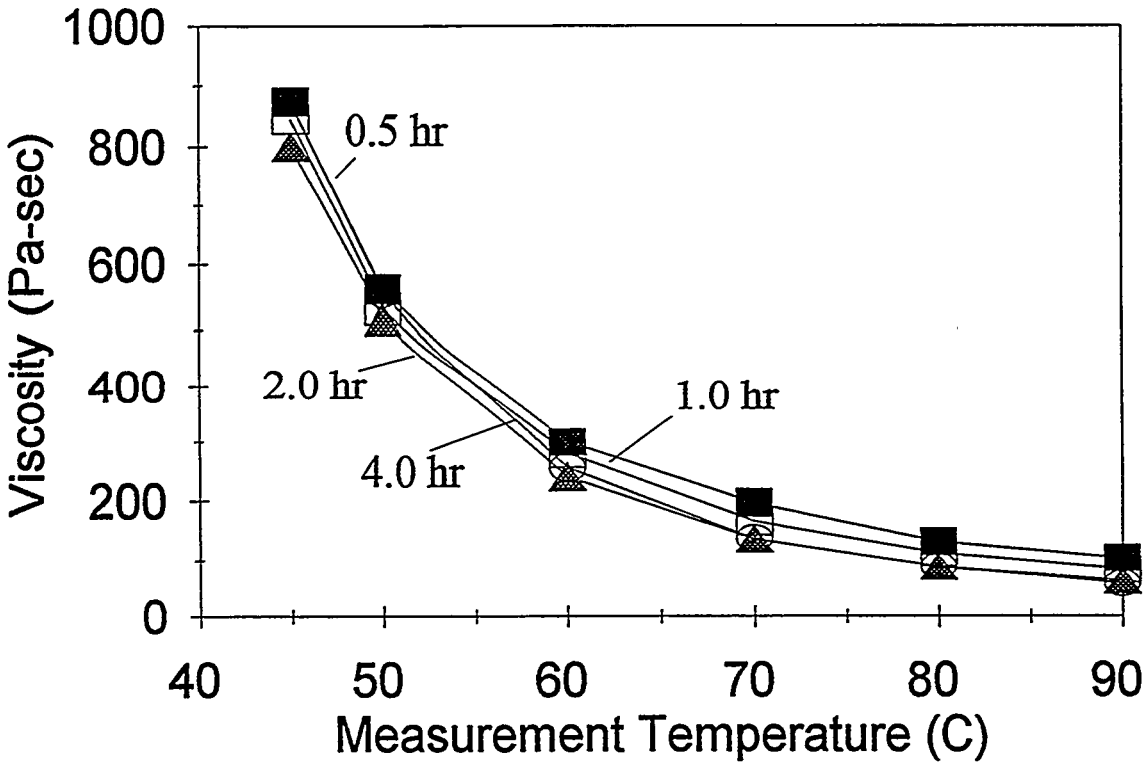
1000
800
600
400
200
0
Viscosity (Pa-sec)
0.5 hr
2.0 hr
1.0 hr
4.0 hr
40
50
60
70
80
90
Measurement Temperature (C)

Figure 27. Viscosity at 2 sec^{-1} shear rate as a function of measurement temperature for bitumen concentrate blended with 25% whole-tire crumb at 200°C for 0.5, 1.0, 2.0, and 4.0 hours.

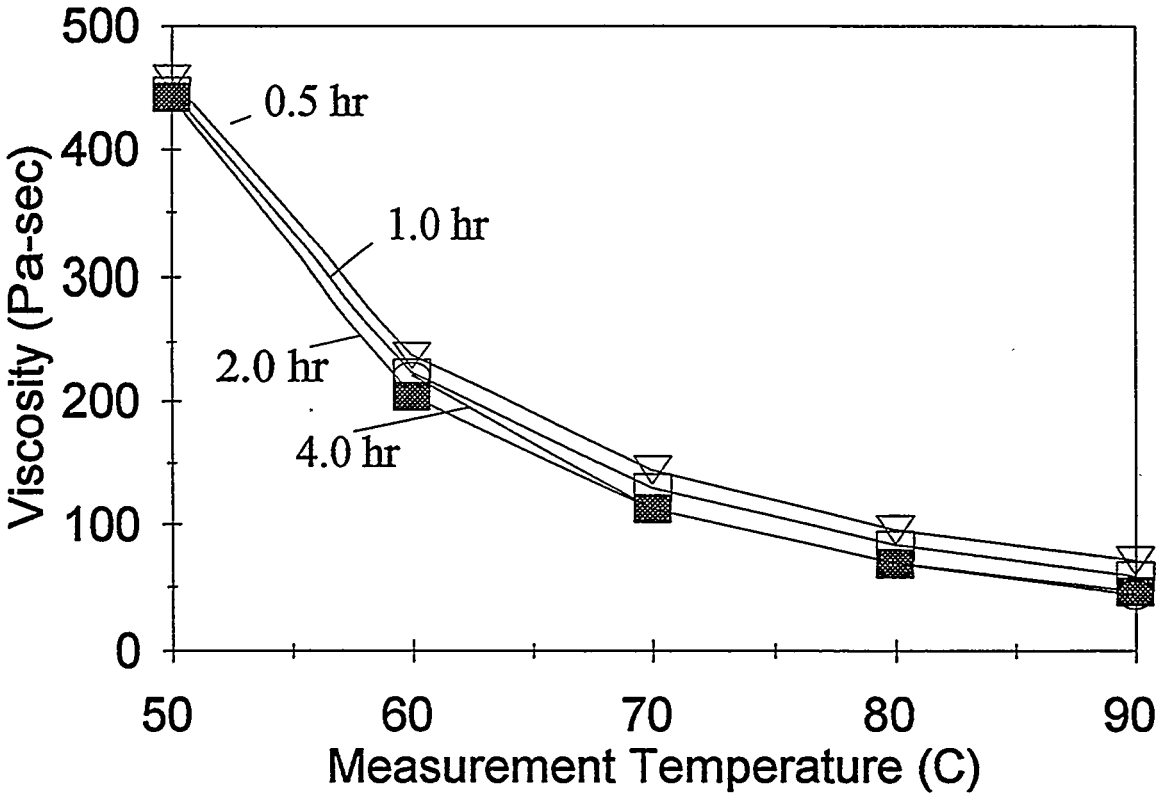
500
400
300
200
100
0
Viscosity (Pa-sec)
0.5 hr
1.0 hr
2.0 hr
4.0 hr
50
60
70
80
90
Measurement Temperature (C)

Figure 28. Viscosity at 5 sec^{-1} shear rate as a function of measurement temperature for bitumen concentrate blended with 25% whole-tire crumb at 200°C for 0.5, 1.0, 2.0, and 4.0 hours.

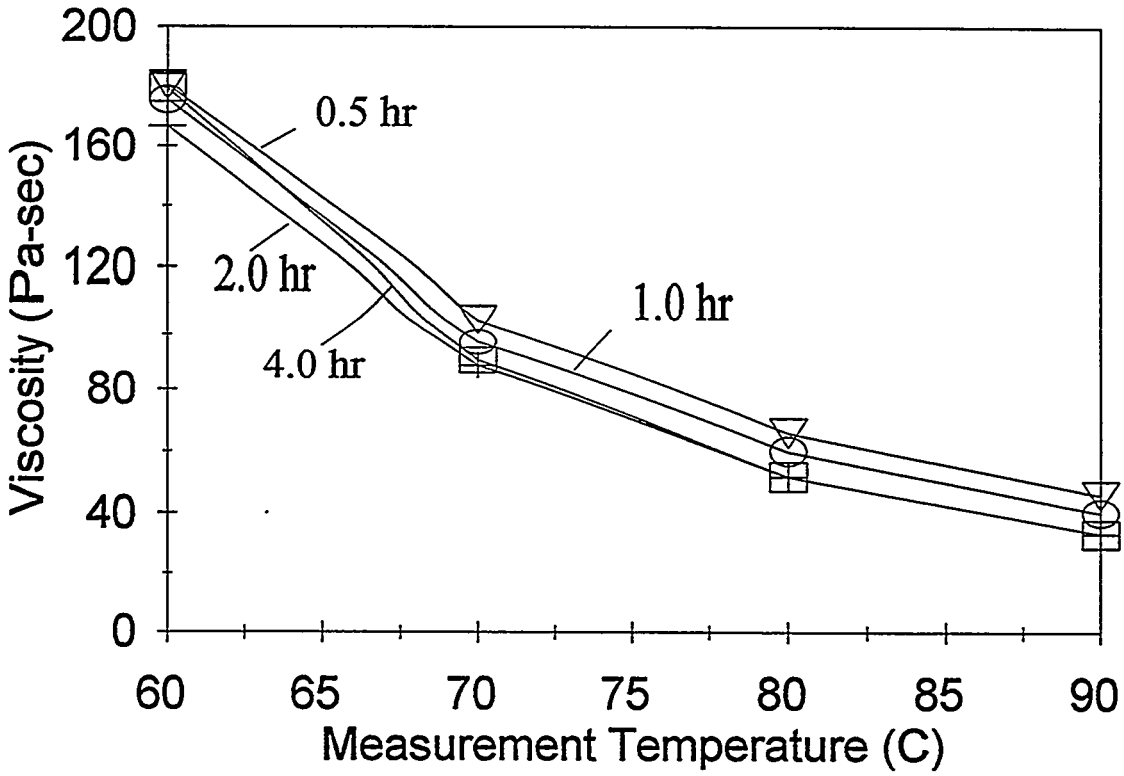
200
160
120
80
40
0
Viscosity (Pa-sec)
0.5 hr
2.0 hr
1.0 hr
4.0 hr
60
65
70
75
80
85
90
Measurement Temperature (C)

construction. Most importantly, the viscosity (at a shear rate of 1 sec^{-1}) of the bitumen-rubber samples prepared with 25% crumb rubber at 200°C meets the ASTM specification of 300±60 Pa·sec at 60°C for a viscosity-graded AC-30 asphalt binder (see Figure 23).

The effect of reaction time on the viscosity of bitumen-rubber samples prepared with 25% crumb rubber at 345°C is shown in Figure 29. The sample prepared at a reaction time of 4 hours exhibits a higher viscosity than 2 hour sample for measurement temperatures below 70°C. This is similar to the results obtained for samples prepared at 200°C and may be due to bitumen aging effects. Figures 30 and 31 illustrate the effects of crumb rubber concentration on the viscosity of samples prepared at 340 to 350°C for 2 hours. The viscosity of the bitumen-rubber samples increases with increasing crumb rubber concentration. The most dramatic increase in viscosity is experienced at measurement temperatures below 70°C. As the measurement temperature is raised near 80 to 90°C, the viscosity of the bitumen-rubber approaches that of the unmodified bitumen. As previously mentioned, this is beneficial for processibility at elevated temperatures.

An interesting effect occured when bitumen concentrate was blended with 25% crumb rubber at 380°C for 2 hours. The viscosity of the unmodified bitumen concentrate processed at these conditions exhibited higher viscosity values than the rubber modified bitumen processed under the same conditions. This is shown in Figure 32 where sample viscosity is plotted as a function of measurement temperature for both modified and unmodiified bitumen. At a measurement temperature of 60°C, the rubber modified bitumen has a viscosity (7.5 Pa·sec) approximately one-half that exhibited by the unmodified bitumen (15.6 Pa·sec). However, as the measurement temperature is increase, the vscosities of the two samples approach one another. For example, at 80°C the rubber modified bitumen has a viscosity of 1.7 Pa·sec compared to 2.5 Pa·sec for the unmodified bitumen. It appears that the addition of crumb rubber at 380°C exerts

Figure 29. Viscosity at 2 sec^{-1} shear rate as a function of measurement temperature for bitumen concentrate blended with 25% whole-tire crumb at 345°C for 2 and 4 hours. Corresponding blend prepared at 200°C included for comparison.

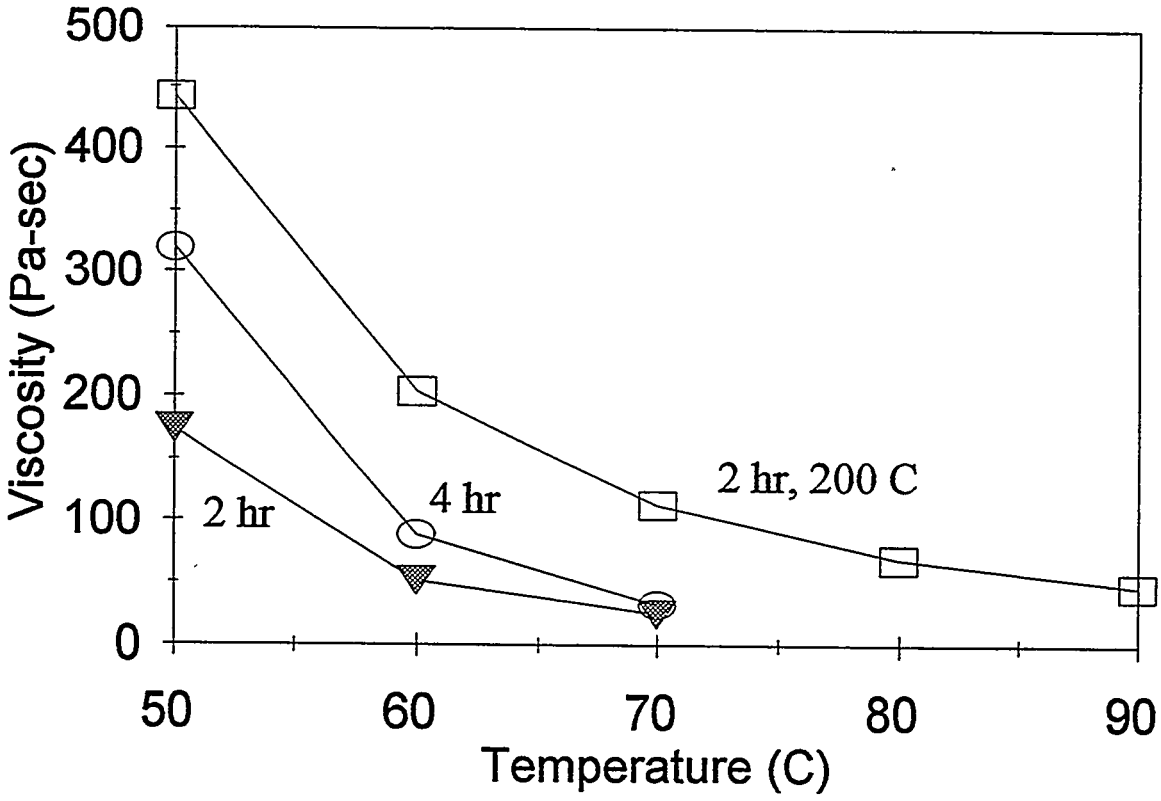
500
400
300
200
100
0
Viscosity (Pa-sec)
2 hr
4 hr
2 hr, 200 C
50
60
70
80
90
Temperature (C)

Figure 30. Viscosity at 40 sec^{-1} shear rate as a function of measurement temperature for bitumen concentrate blended with differing concentrations of whole-tire crumb at 340 to 350°C for 2 hours.

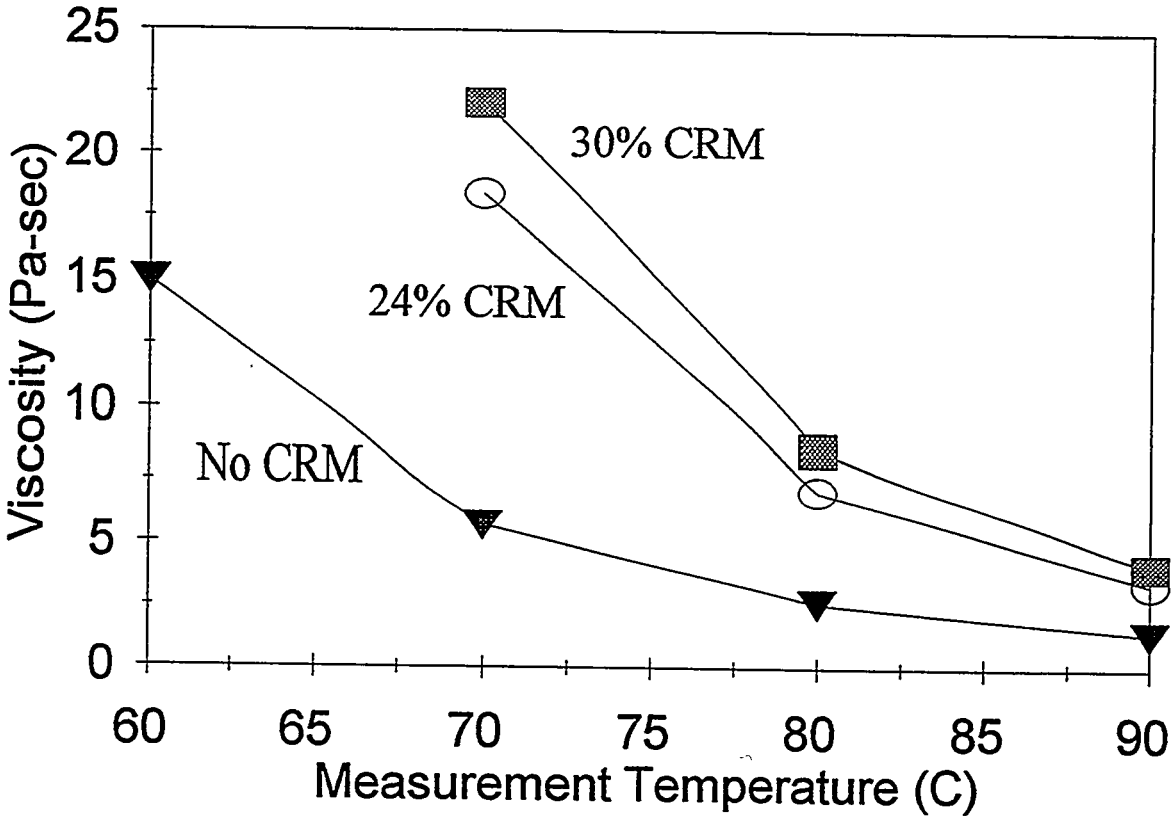
25
20
15
10
5
0
Viscosity (Pa-sec)
30% CRM
24% CRM
No CRM
60
65
70
75
80
85
90
Measurement Temperature (C)

Figure 31. Viscosity at 40 sec^{-1} shear rate as a function of whole-tire crumb concentration for bitumen-rubber blends prepared at 340 to 350°C for 2 hours.

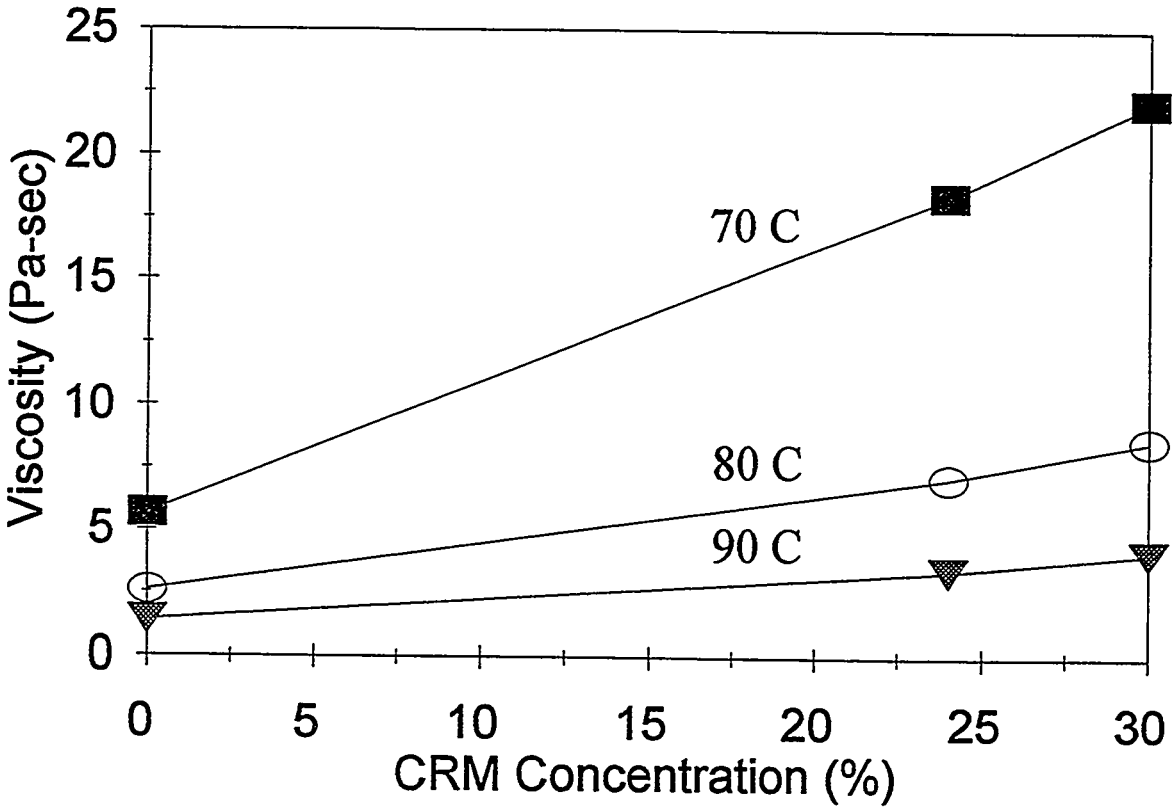
25
20
15
10
5
0
Viscosity (Pa-sec)
70 C
80 C
90 C
0
5
10
15
20
25
30
CRM Concentration (%)

Figure 32. Viscosity at 40 sec^{-1} shear rate as a function of measurement temperature for bitumen concentrate unmodified and modified with 25% whole-tire crumb at 380°C for 2 hours.

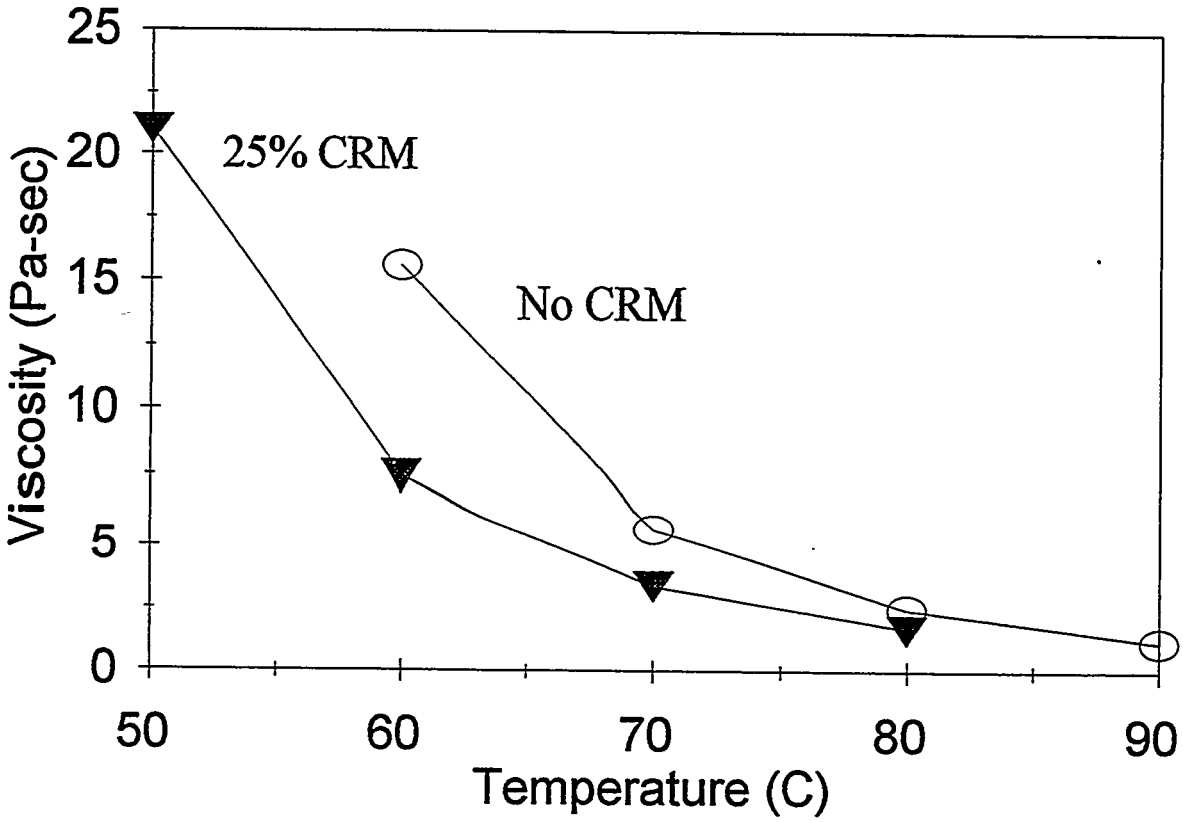
25
20
15
10
5
0
Viscosity (Pa-sec)
25% CRM
No CRM
50
60
70
80
90
Temperature (C)

a destructive effect on the bitumen matrix thereby reducing sample viscosity.

The effects on sample viscosity of bitumen and crumb rubber type for blends prepared at 340 to 350°C are shown in Figure 32. As is expected, the viscosity of the blend prepared with Circle Cliffs bitumen is significantly higher than the corresponding blend prepared with the oil extended bitumen concentrate. The viscosity of the Circle Cliffs blend, however, may actually be too high for adequate processibility and may cause serious problems during pavement construction. This is evident for Circle Cliffs-crumb rubber blends prepared at 200°C where the sample was extremely viscous and solid-like. The viscosity of the blends were also dependent upon the type of crumb rubber used to modify the bitumen. Bitumen modified with tread-rubber crumb exhibited higher viscosities than corresponding blends containing whole-tire crumb (see Figure 33). At a measurement temperature of 70°C, the viscosity of bitumen modified with tread-rubber crumb is 63.9 Pa·sec, compared with 19.7 Pa·sec for bitumen modified with whole-tire crumb. The difference in viscosity may be due to a potential difference in rubber composition of the two crumbs, or may be a result of the fibrous material present in the whole-tire crumb.

CONCLUSIONS

Co-processing of tar sand bitumens with crumb rubber at elevated temperatures has been shown to increase the viscosity of the blend with the exception of the bitumen-rubber sample prepared at 380°C. Optimum viscosity behavior is exhibited for an oil extended bitumen blended with crumb rubber at 200°C for 0.5 hours. The viscosity of the bitumen-rubber blend prepared under these conditions met ASTM specifications of a viscosity-graded AC-30 asphalt binder. In addition, the increase in viscosity is most noticeable at low measurement temperatures. As the measurement temperature is increased from 45 to 90°C, the viscosity of the rubber modified

Figure 33. Viscosity at 5 sec^{-1} shear rate as a function of measurement temperature for Circle Cliffs bitumen and bitumen concentrate blended with whole-tire (CRM) and tread-rubber crumb (Baker TR) at 340 to 350°C for 2 hours.

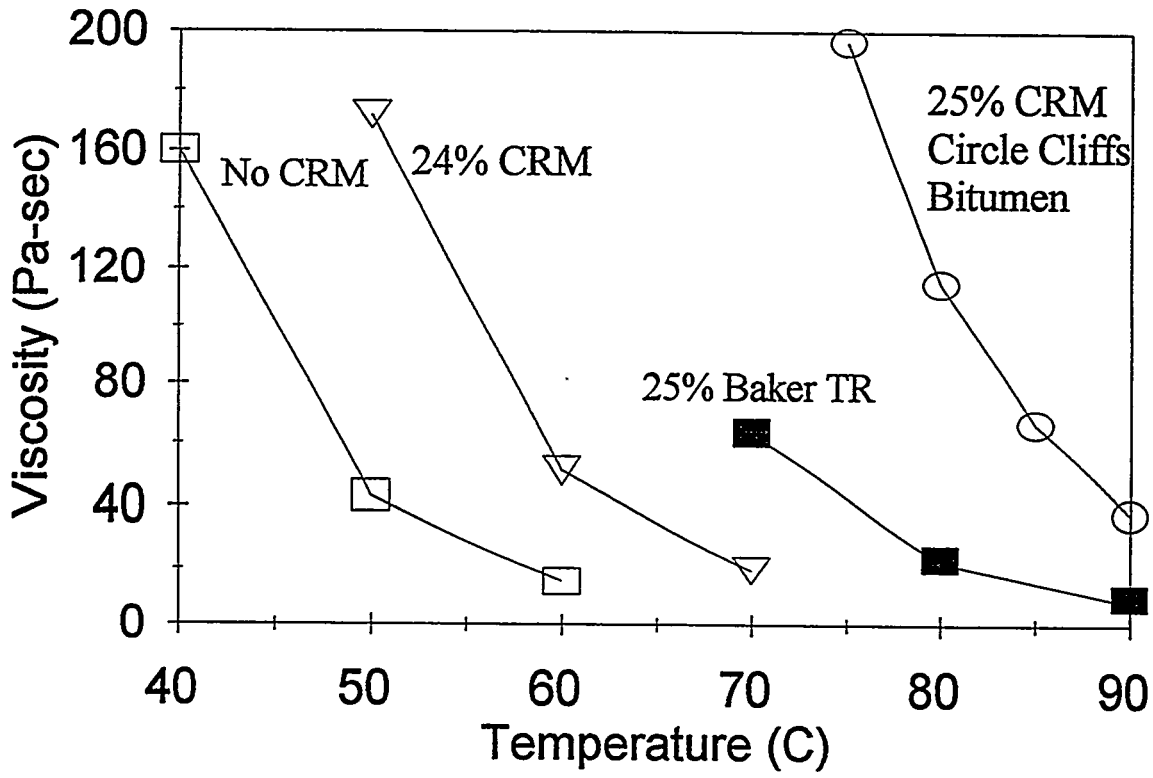
200
160
120
80
40
0
Viscosity (Pa-sec)
No CRM
24% CRM
25% CRM
Circle Cliffs
Bitumen
25% Baker TR
40
50
60
70
80
90
Temperature (C)

bitumen decreases dramatically. Thus, the rubber modified bitumen provides the benefit of high viscosity at pavement temperatures experienced during summer months, without concession of processibility at pavement construction temperatures. A difference in viscosity is observed between bitumen modified with whole-tire crumb and tread-rubber crumb. Evidently, this is due to the compositional differences that exist between the two materials.

SUPERCRITICAL FLUID EXTRACTION OF OIL SAND BITUMENS FROM THE UINTA BASIN, UTAH

Principal Investigator: F.V. Hanson
Graduate Student: M. Subramanian

INTRODUCTION

Mining-surface recovery processes for the recovery of bitumen from oil sands are recommended when the overburden-to-pay zone ratio is less than unity (43). The mined oil sands are transported to processing locations where the bitumen is extracted from oil sands by various surface processes: hot water process (44); solvent assisted aqueous method (28); solvent extraction (46-49); pyrolysis (50, 51); supercritical fluid extraction (52, 53); other thermal methods (54, 55).

The hot water and solvent assisted aqueous processes raise environmental concerns due to the need for an aqueous tailings pond. A tailings pond is necessary since several years are required for the settling and separation of fines (56). The solvent extraction process used for bitumen extraction from oil sands ores leaves behind residual solvent in the extracted sand and also poses potential environmental problems. Supercritical fluid extraction (SFE) (57) has been developed as an alternative to the conventional solvent extraction process. This process has several advantages over conventional processes: solvent and solute can be separated by depressurization; high selectivity in separation of solubility class compounds; and; selectivity can be varied by adjusting the pressure and temperature of the extraction process.

The bitumen feedstocks, extract samples, residual fractions and the solubility

fractions obtained from adsorption chromatography (58) of the bitumens were analyzed using an extended American Standards for Testing Material (ASTM) simulated distillation technique developed during this study. This technique (59) permitted the determination of the boiling point distribution up to 911 D. The bitumens, two SFE extract phase samples and the residual SFE fractions were subjected to adsorption chromatography to separate each into solubility fractions: asphaltenes, resins, aromatics and saturates to investigate the influence of the nature of the feedstocks on the SFE process. Elemental analyses were conducted on the bitumens and on the residual fractions. Continuous thermodynamics (60, 61) and the Peng-Robinson cubic equation of state (62) were used to model the extraction process. The Peng-Robinson EOS was selected since only a limited number of parameters were required for its application to the description of the bitumens and bitumen-derived heavy oils.

The present study focused on SFE of bitumens from the Asphalt Ridge and Sunnyside oil sands deposits using commercial propane as solvent. The extractions were carried out at the same operating conditions as those used for the Whiterocks (39) and PR Spring bitumens (40), so that meaningful comparisons could be made for the different bitumen feedstocks.

The specific objectives of this study included the following:

1) determination of the effect of pressure and temperature on extract yields and on the composition of the extract phases;
2) determination of the effect of pressure and temperature on extract yields and on the composition of the extract phases;
3) assess the influence of the nature of the bitumen on the extraction yields and

selectivity;

4) determination of the extent of asphaltene rejection during SFE; and

5) develop a preliminary mathematical model of the extraction process.

This work was a continuation of the SFE studies with the Whiterocks and PR Spring bitumens reported previously (63, 64).

EXPERIMENTAL

The supercritical fluid extraction (SFE) system was built by Autoclave Engineers Inc., Erie, Pennsylvania. This system was designed for semi-continuous extraction of complex hydrocarbon mixtures such as crude oil, heavy oils and coal liquids using carbon dioxide as the supercritical solvent. Detailed descriptions of the original experimental system and its components have been reported by Hwang (39) and Subramanian (40). The system was modified in the course of this study by the addition of a data acquisition system from Keithley Metrabyte to monitor flow rates and extract phase densities on a continuous basis. The pressure control valve originally located upstream of the extractor was moved to the downstream side of the densitometer to stabilize the system. The system can be conveniently divided into four subsystems: a) the supercritical fluid supply system; b) the extractor and densitometer assembly; c) the data acquisition system; and d) the separator assembly. A schematic of the supercritical fluid extraction system used in this study is presented in Figure 34.

The supercritical fluid supply system consisted of a high pressure, positive displacement pump and a dynamic, high pressure fluid circulation pump. The positive displacement system was acquired from D.B. Robinson Associates, Edmonton, Canada and

Figure 34.

Schematic of the Supercritical Fluid Extraction System

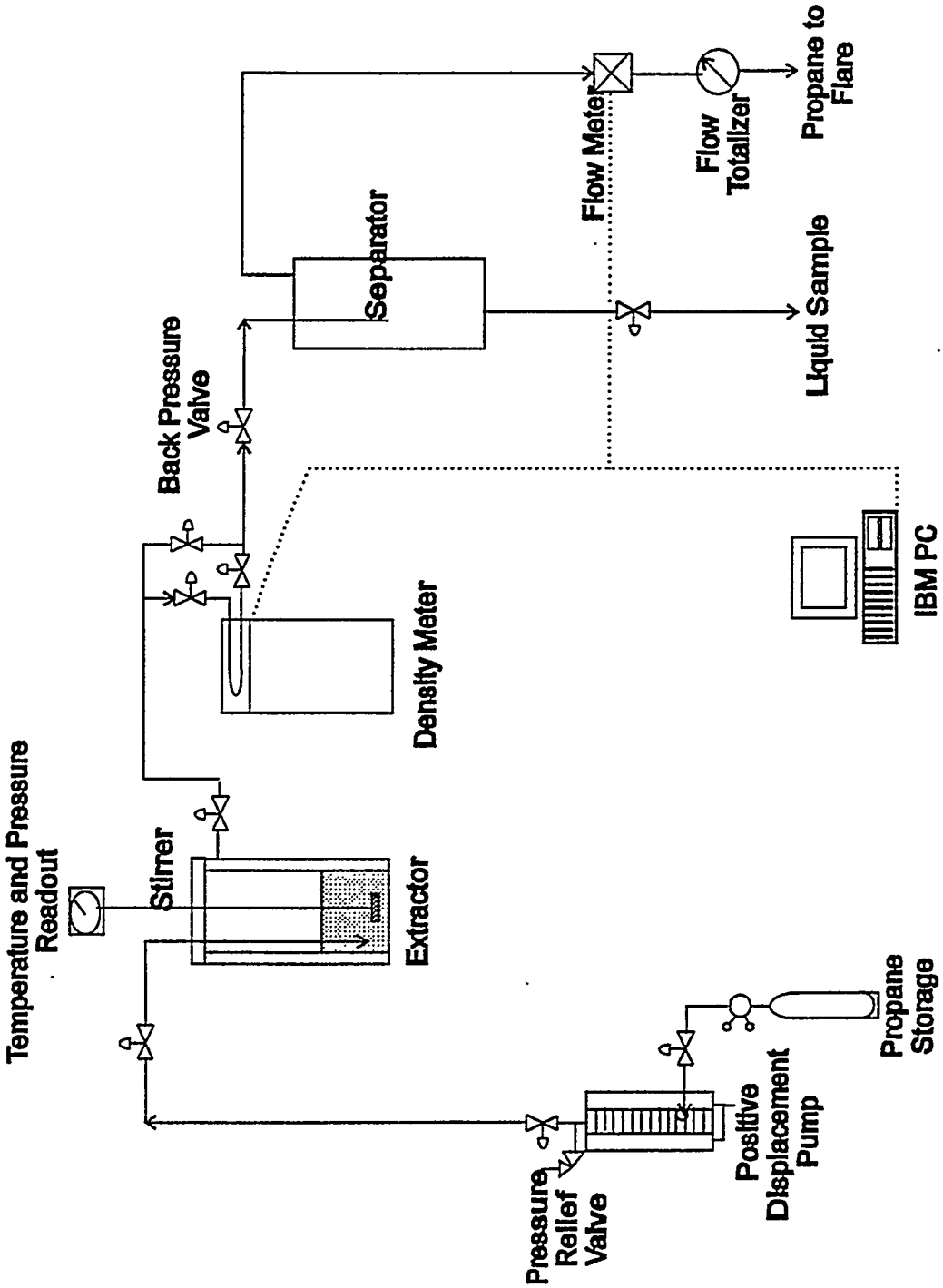
Temperature and Pressure Readout
Stirrer
Extractor
Density Meter
Back Pressure Valve
Separator
Flow Meter
Flow Totalizer
Propane to Flare
Liquid Sample
IBM PC
Propane Storage
Positive Displacement Pump
Pressure Relief Valve

consisted of a cylinder, piston, and power pack to pump the fluids at high pressures. The pump was designed to handle liquids at flow rates ranging from 0 to 1800 cm^3/h at a maximum pressure of 135 MPa and temperature of 1033 K. The volumetric capacity of the pump cylinder was 500 cm^3. The fluid was transferred from the storage tank into the pump cylinder, pressurized and pumped into the supercritical fluid extractor. This pump was capable of pumping fluid at a rate of one hundredth of a cm^3/min and the volume discharged by the pump could be measured to within 0.1 cm^3 accuracy.

The fluid pumping system consisted of a storage cylinder (CO_2 or propane), a nonreturn valve and line filter, a high pressure liquid circulation pump, and a circulating refrigerant bath to cool the pump head. The head of the circulation pump was maintained at 273 K by means of a circulating cooling bath (Fisher Scientific, Model 900) to prevent vapor lock.

The extractor assembly consisted of the extraction vessel, a flanged stainless steel closure, a magnetic-drive, packerless stirring device and a pressure gauge mounted on the flange-head. The 300 cm^3 extractor was rated for a working pressure of 37 Mpa at 616 K. The effective volume of the extractor with the stirring device assembly in place was 290 cm^3.

An electric furnace mounted on the outside of the extractor. A three-mode temperature controller provided with a type-K thermocouple was used to control the temperature inside the extractor. The control thermocouple was located in the thermowell adjacent to the stirrer blades.

The densitometer consisted of two parts: 1) an external measuring cell and 2) a display unit. The external measuring cell (Anton Paar K.G, model DMA 512) was placed on the downstream side of the extractor assembly to measure the extract phase densities at high

densitometer and the separator, a back pressure regulator valve, a separator vessel, the liquid sample withdrawal valve and a gas outlet line with a flow totalizer. The separator vessel had a capacity of 500 cm^3 and was constructed of 316 stainless steel. The maximum working pressure of the vessel was 13.7 MPa at 505 K. The cover of the vessel was fixed to the vessel with quick disconnect couplings and was sealed with Buna-N O-ring seals. A type-J thermocouple was used to monitor the temperature inside the separator. The ball valve mounted at the bottom outlet was used to withdraw the liquid phase samples from the separator. The extraction system pressure was maintained by a manually operated back pressure regulator (Haskel Engineering & Supply Co.) installed between the extractor-densitometer system and the separator. It also served as a pressure reduction valve through which the supercritical extract phase flowed to the separator where the solute was recovered when the extract phase flashed. The fluid transfer lines between the extractor, the densitometer and the separator were traced with heat tape to maintain the transfer line temperatures the same as that of the extractor.

The solvent separated from the solute in the separator was vented after passing through a flow meter and a flow totalizer. When propane was used as solvent, the vent line was connected to a flare in the evacuation hood where the propane was burned. An electronic flow meter (EG&G Flow Technology, model FTO-4NIYA-GHC-5) was used to measure the flow rate and cumulative volume of the solvent vented through the system.

Oil Sands Bitumen Preparation

The bitumens used in the SFE studies were recovered from crushed, screened and well-mixed ore samples by conventional Dean-Stark extraction apparatus using toluene as the

solvent. The ores were mined from the Whiterocks, PR Spring, Asphalt Ridge and Sunnyside oil sands deposits of the Uinta Basin (Utah). The extractions were carried out in a Dean-Stark apparatus with Whatman single thickness cellulose thimbles. Sharkskin filter paper was wrapped around the outside of the thimble to retain any fine mineral particles that penetrated the thimble wall.

Extraction was carried out at total reflux depending on the compaction and bitumen content of the oil sands ore. The solvent reservoir temperature was maintained between 385 and 389 K. A rotary evaporator was used in conjunction with a vacuum pump to evaporate the toluene from the concentrated toluene/bitumen solution. A sample was withdrawn from the bitumen-toluene solution for simulated distillation (SIMDIS) analysis to determine the residual toluene concentration.

A residual toluene concentration of less than 0.1 wt% was achieved for the PR Spring (64), Asphalt Ridge and Sunnyside bitumens after rotoevaporating for 20 hrs at 5.3 kPa with the water bath temperature held at 358 K.

Liquid Product Analysis

The Asphalt Ridge and Sunnyside bitumens, all extracts and the residues from the extraction experiments were analyzed using a simulated distillation technique to obtain the carbon number distribution up to C_{90}.

The samples were assigned carbon numbers based on the elution patterns of standard samples containing normal alkanes ranging from C_{10} to C_{90}. Three standard samples, namely, Polywax 655 (C_{20} to C_{110}), ASTM PS-12-60N (C_{12} to C_{60}) and ASTM PS-18-44N 60N (C_{18} to C_{44}) from Supelco, Inc. were used for calibration purposes. The uneluted portion was

determined using an internal standard (C_{14} to C_{17}) mixture. A Visual Basic computer program was developed to estimate the carbon number distributions.

The Conradson carbon residues and the pour points of the feedstocks were determined according to the procedures outlined in the ASTM D189-65 and ASTM D97-66 methods, respectively. The viscosities of the Whiterocks, Asphalt Ridge, PR Spring and Sunnyside bitumens were determined using a Brookfield cup-cone digital viscometer (Model DVT-II+). The viscosities were measured at four different temperatures to establish the relationships between temperature and viscosity for each bitumen. The densities of the bitumens were measured using the procedure developed by AOSTRA[191] for semisolids.

The saturate, aromatic, resin and asphaltene (SARA) contents of the feedstocks, extracts and residues were determined by an analytical method developed by Bukka et al. (58, 66). The most commonly used solvents to make the initial separation of bitumen into maltenes and asphaltenes are n-pentane and n-heptane. The solvating power of the alkane increases gradually with increase in the carbon chain length, thus pentane yields quantitatively more asphaltenes than heptane for a given hydrocarbon sample (65). Moreover, removal of pentane from the maltenes fraction by rotoevaporation can be accomplished at lower atmospheric equivalent temperature relative to heptane; hence, it has gained popularity as the standard solvent for asphaltene separation.

The elemental (C,H,N,S) analyses of the feedstocks and residual fractions and the molecular weight determinations for the feedstocks were carried out at Galbraith Laboratories, Inc., Knoxville, Tennessee. Galbraith used a Perkin Elmer 240 elemental analyzer. Molecular weights were determined by a three point vapor pressure osmometry method using toluene as the solvent.

Gas Analysis

The propane used for extraction studies was a commercial grade gas supplied by Wasatch Propane, Inc. The analyses of the feed gases are presented in Table 10.

Table 10

Analyses of the Gas Used as SFE Solvent

	Propane	
Supplier	Wasatch Propane, Inc.	
Grade	Commercial	
Cylinder Content	14 Kgs	
Saturation Pressure (@STP)	758 kPa	
Composition (vol%)	Methane:	0.2
	Ethane:	5.4
	Propane	93.9
	Butane :	0.5

RESULTS AND DISCUSSION

The bitumens from the Asphalt Ridge (AR) and Sunnyside (SS) oil sands deposits of the Uinta Basin, Utah were used in the SFE experiments using propane as solvent. The SFE of the bitumens from the Whiterocks (WR) and PR Spring (PRS) oil sands deposits was conducted by Hwang (63) and Subramanian (64), respectively. The four bitumens differ significantly in their physical and chemical characteristics. Thus, it was possible to compare the effect of pressure, temperature, solvent density and composition on the SFE extraction yields, the quality of the extract phases and the nature of the residual fractions for four oil sands bitumens from the Uinta Basin, Utah.

Feedstock Characterization

Four different bitumens from the WR, AR, PRS and SS oil sands deposits of the Uinta Basin (Utah), were used for the SFE experiments using propane as solvent. The physical and chemical properties of the bitumens are presented in Table 11.

Physical Properties

The specific gravities of the bitumens were measured using the procedure proposed by Syncrude Limited for semisolid hydrocarbons. The WR bitumen had a specific gravity (288 K/288 K) of 0.98, compared to 0.985 for the AR bitumen, 1.005 for the PRS bitumen and 1.015 for the SS bitumen. The WR and SS bitumen had the lowest and highest specific gravities, respectively. The AR and PRS bitumen specific gravities fell in-between with the AR density lower than that of the PRS bitumen. The viscosities of the bitumens were measured at 343 K to provide a direct comparison. The viscosity of the WR

Table 11
Physical and Chemical Properties of Uinta Basin Bitumens

Properties	Whiterocks Bitumen	Asphalt Ridge Bitumen	PR Spring Bitumen	Sunnyside Bitumen
Specific Gravity (288K/288 K)	0.980	0.985	1.005	1.015
API Gravity, °API	12.9	12.1	9.3	7.9
Conradson Carbon, Residue, wt %	9.5	13.9	14.17	15.0
Pour Point, K	327	320	319	348
Viscosity, cp @ 343 K	4,825	5,050	47,000	173,000
Asphaltenes[a], wt %	2.9	6.8	19.3	23.6
Saturates, wt %	35.7	39.2	33.4	20.0
Aromatics, wt %	7.0	9.0	3.6	15.1
Resins, wt %	54.5	44.1	43.8	36.8
Molecular Weight, g/gmol	653	426	670	593
Elemental Analysis[b]				
C, wt %	87.0	86.9	87.0	86.8
H, wt %	11.2	11.6	11.3	10.8
N, wt %	1.4	1.7	1.3	1.1
S, wt %	0.4	0.4	0.4	0.7
H/C Atomic Ratio	1.56	1.60	1.56	1.49
Simulated Distillation				
Volatility(<811 K), wt%	46.6	53.5	45.4	40.9
< 477 K	0.5	1.3	0.4	0.6
477 - 617 K	7.4	11.8	8.2	7.8
617 - 811 K	38.7	40.4	36.8	32.5
> 811 K	53.4	46.5	54.6	59.1

a) Pentane Insolubles
b) C,H,N,S analyses normalized to 100%

bitumen was lowest at 4825 cP compared to the SS bitumen at 173,000 cP and the viscosities of the AR (5050 cP) and PRS bitumens (47,000 cP) fell in between. The viscosities for these bitumens were measured in the temperature range from 318 to 353 K. In general, the viscosities of the four bitumens decreased with increase in temperature and the rate of decrease in viscosities were different for the different bitumens. The relationship between viscosity and inverse temperature is presented in Figure 35. It is observed from Figure 35 that the decrease in the viscosity of the SS bitumen was greatest with increase in temperature, the PRS and WR bitumen have similar slopes and the AR bitumen had the lowest decrease for a given increase in temperature. The activation energies, E_{act} for viscous flow for the four bitumens are presented in Table 12.

The pour points, a measure of the fluidity of the bitumens, of the AR and PRS bitumens were similar at around 320 K, the WR bitumen was 327 K and the SS bitumen was highest at 348 K.

Chemical Properties

The bitumen feedstocks were mixed with an excess of normal pentane (40 cc of pentane/gram of sample) to precipitate the asphaltenes fraction and to dissolve the maltene fraction. The procedure adopted by Bukka et al. (58, 66) was used to fractionate the bitumens, and the extract phases and residual fractions obtained from SFE. The maltenes were subjected to adsorption chromatography using Fuller's earth as the adsorbent and were sequentially eluted using solvents of increasing polarity to isolate saturates and aromatics, resins I and resins II. These compound classes were separated based on their solubility using solvents such as pentane, tetrahydrofuran and methanol. The saturates and

Figure 35.

Relationship Between Temperature and Viscosity for the Bitumens

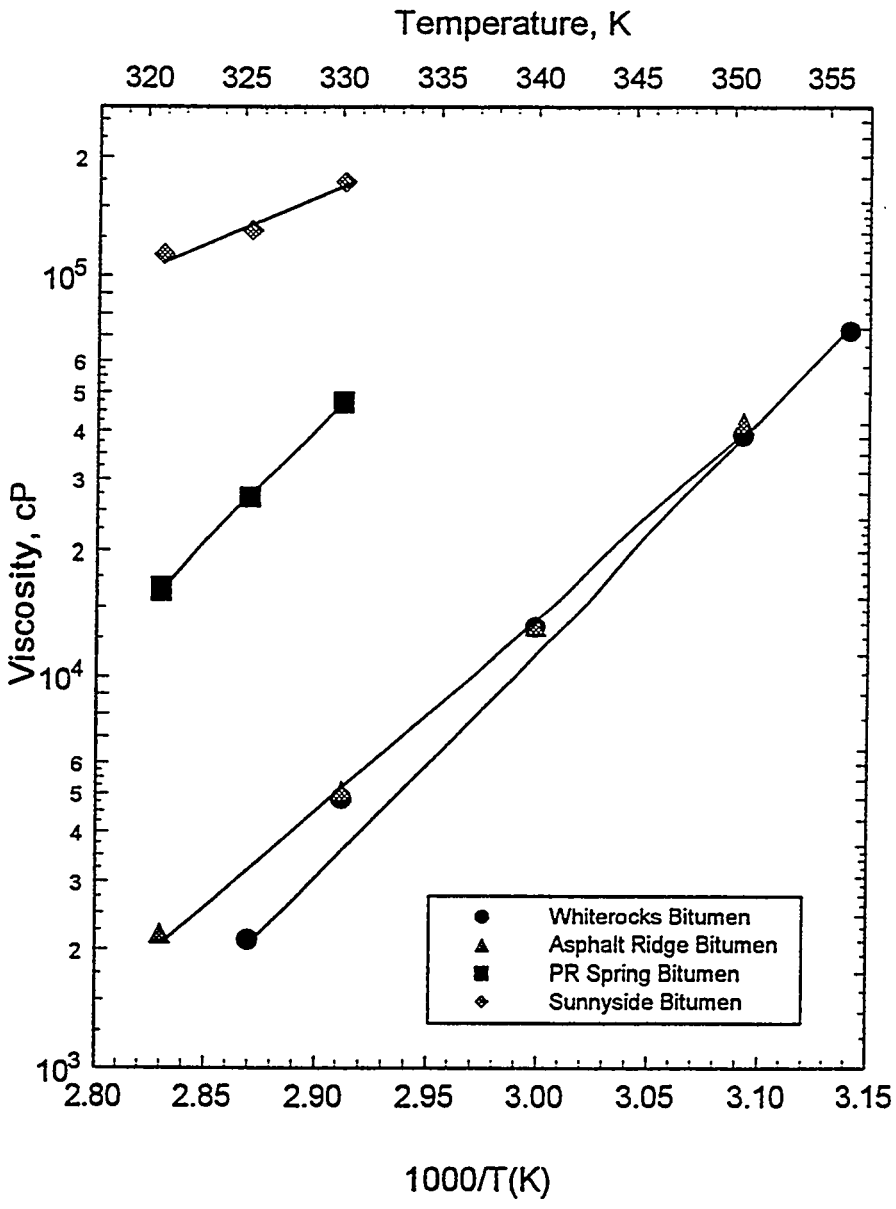
Temperature, K
320
325
330
335
340
345
350
355
Viscosity, cP
2
10^5
6
5
4
3
2
10^4
6
5
4
3
2
10^3
2.80
2.85
2.90
2.95
3.00
3.05
3.10
3.15
1000/T(K)
Whiterocks Bitumen
Asphalt Ridge Bitumen
PR Spring Bitumen
Sunnyside Bitumen

Table 12
The E_{act} for Viscous Flow for Four Bitumens from Uinta Basin (Utah)

Bitumen	k_o	E_{act}
Whiterocks Bitumen	5.2187×10^{-13}	-12.574
Asphalt Ridge Bitumen	2.8487×10^{-11}	-11.281
PR Spring Bitumen	2.6708×10^{-12}	-12.843
Sunnyside Bitumen	4.3948×10^{-02}	-5.207

Temperature "T" in Kelvin

aromatics were further adsorbed on neutral alumina and eluted using the same sequence of solvents mentioned above to isolate saturates, aromatics I and aromatics II. The aromatics I and II fractions and the resins I and II fractions were combined and were reported as aromatics and resins, respectively. The fractionation results obtained for the four different bitumen feedstocks are presented in Figure 36.

It is seen from Figure 36 that the asphaltene content of the WR bitumen was lowest at 2.9 wt%, and the asphaltene contents of AR (6.8 wt%), PRS (19.3 w%) and SS bitumens (23.6 wt%) were progressively greater. The saturates content of the SS bitumen was lowest at 20.0 wt% compared to the high value for the AR bitumen of 39.2 wt%. The PRS and WR bitumens saturates contents fell in the intermediate range at 33.4 and 35.7 wt%, respectively. The aromatics content of the SS bitumen was highest at 16 wt% and the aromatics content of the other three bitumens was less than 10 wt%. The resin content of the WR bitumen was highest at 54.5 wt%, the SS bitumen lowest at 36.8 wt%. The AR (44.1 wt%) and PRS bitumens (43.8 wt%) had intermediate resins contents with the AR resin content slightly higher than that of the PRS bitumen.

It is also observed from the chemical compositions of the bitumens that as the asphaltene content of the bitumens increased, the specific gravity, viscosity at 343 K and Conradson carbon of the four bitumens increased. Thus, the asphaltene content appears to have affected these properties of the bitumens under investigation.

The molecular weights of these bitumens were determined by Galbraith Laboratories, Inc., Knoxville, TN. The molecular weight of the AR bitumen was lowest at 426 g/gmol, the WR and PRS bitumens had similar molecular weights around 660 g/gmol and the SS bitumen had an intermediate molecular weight of 593 g/gmol.

Figure 36.

Comparison of the Solubility Fractions of the Bitumens

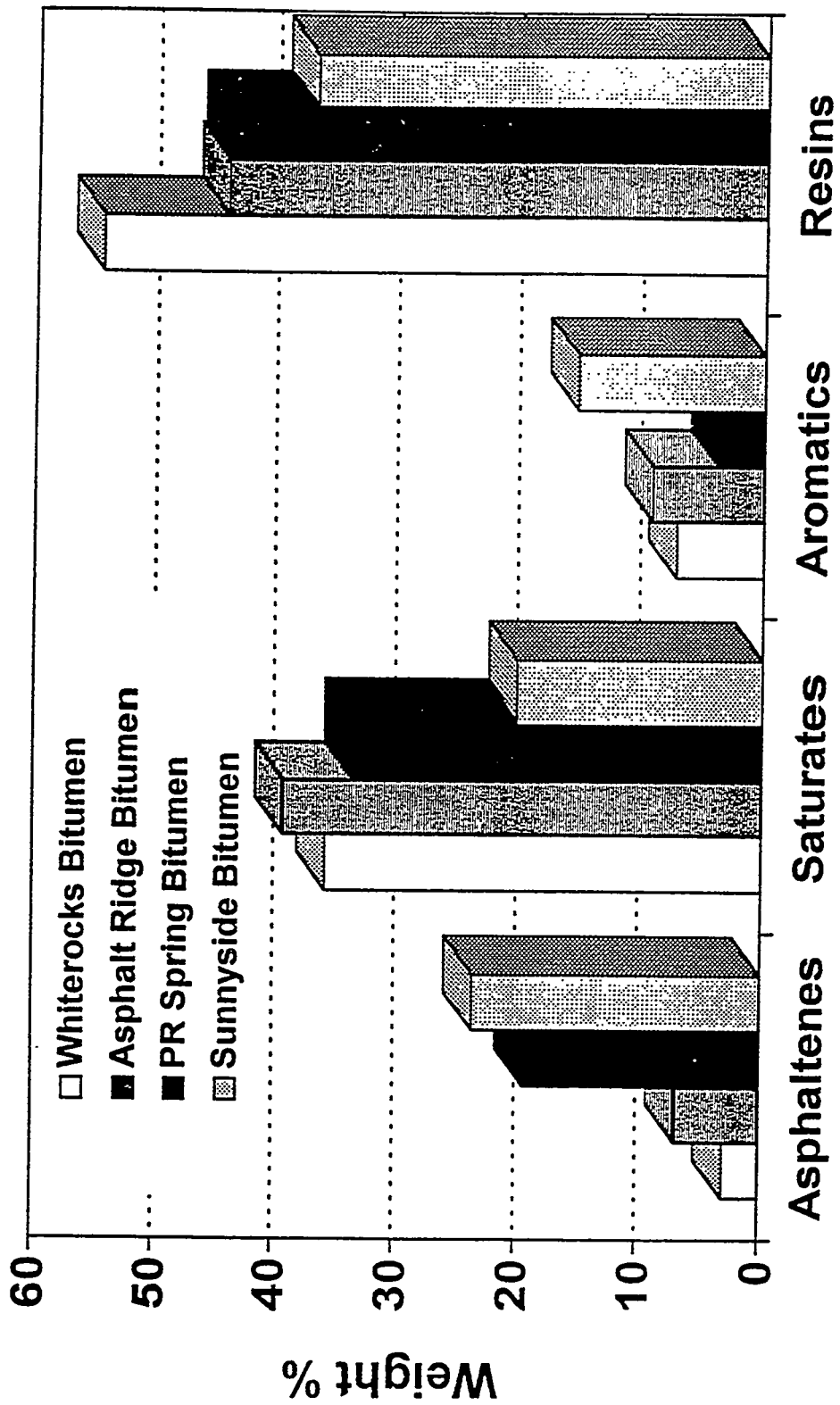
Weight %
60
50
40
30
20
10
0
Asphaltenes
Saturates
Aromatics
Resins
Whiterocks Bitumen
Asphalt Ridge Bitumen
PR Spring Bitumen
Sunnyside Bitumen

The elemental analyses for carbon, hydrogen, nitrogen and sulfur were also determined by Galbraith Laboratories, Inc. The carbon, hydrogen, nitrogen and sulfur contents of the bitumen were normalized and are reported in Table 11. The AR bitumen was more saturated than the other bitumens with a hydrogen/carbon (H/C) atomic ratio of 1.6. The WR and PRS bitumens had H/C ratios of 1.56. The SS bitumen was the least saturated with a H/C atomic ratio of 1.48. The H/C atomic ratio of these bitumens correlated with their saturates contents: the higher the saturates content, the higher the H/C ratio of the bitumen. The AR bitumen had the highest saturates content and the highest H/C atomic ratio. The nitrogen contents of the four bitumens were higher than their sulfur contents which is typical for fresh water origin hydrocarbon resources.

The quality ranking for the four bitumens as indicated by their physical and chemical properties is as follows:

Whiterocks < Asphalt Ridge < PR Spring < Sunnyside

Simulated Distillation

The boiling point or carbon number distributions of the bitumens were determined up to 973 K. The simulated distillation chromatograms and the boiling point distribution for the Whiterocks bitumen is presented in Figures 37 and 38, respectively. The simulated distillation analyses for the four bitumens are presented in Table 13.

Supercritial Fluid Extraction of Asphalt Ridge and Sunnyside Oil Sands Bitumens

SFE experiments were conducted using the AR and SS bitumens as a part of this study using commercial propane as the solvent. SFE of the WR and PRS bitumens were

Figure 37.

Chromatograms for Whiterocks Bitumen

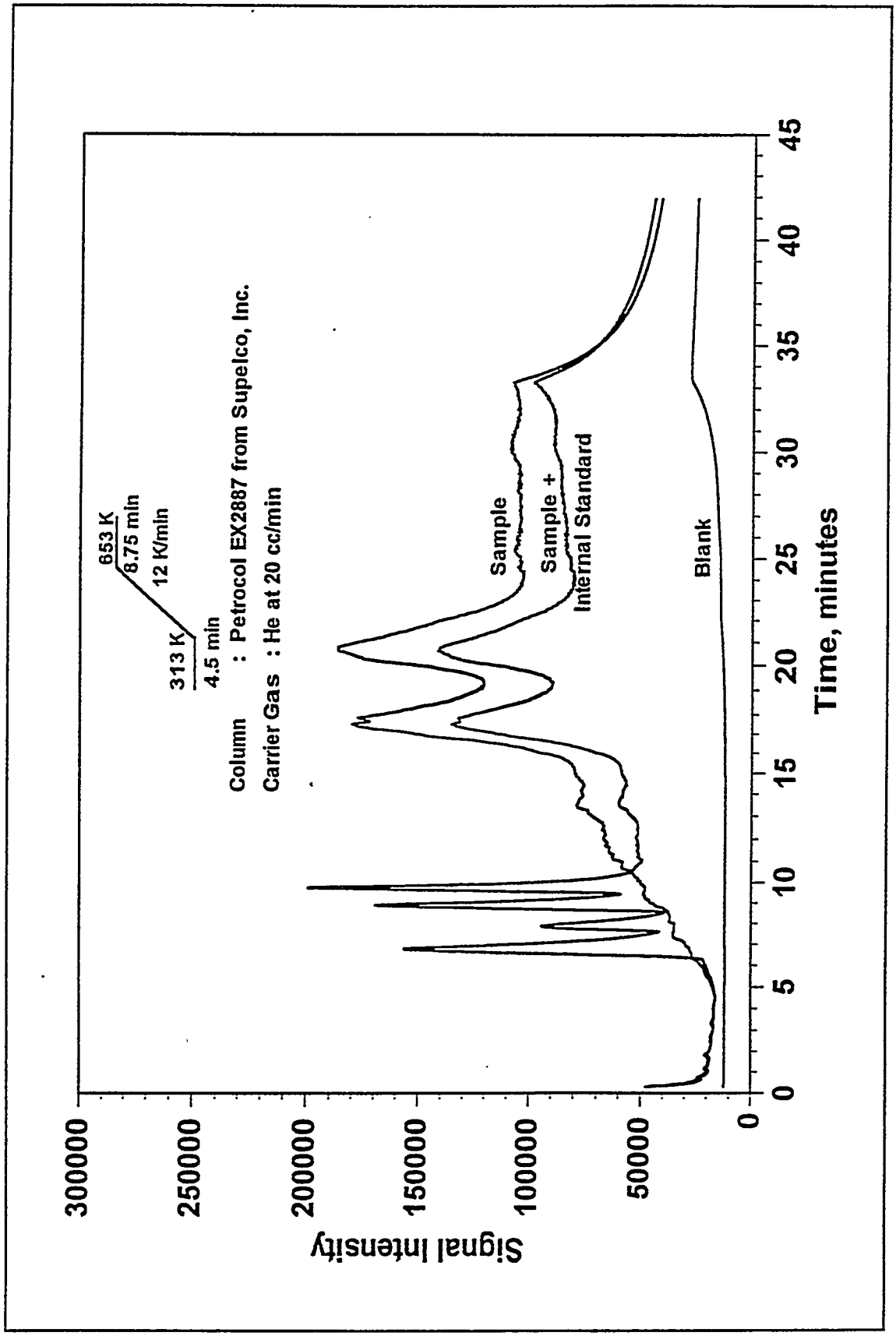
653 K
8.75 min
12 K/min
313 K
4.5 min
Column : Petrocol EX2887 from Supelco, Inc.
Carrier Gas : He at 20 cc/min
Sample
Sample +
Internal Standard
Blank
Signal Intensity
300000
250000
200000
150000
100000
50000
0
0
5
10
15
20
25
30
35
40
45
Time, minutes

Figure 38.

Boiling Point Distribution for Whiterocks Bitumen

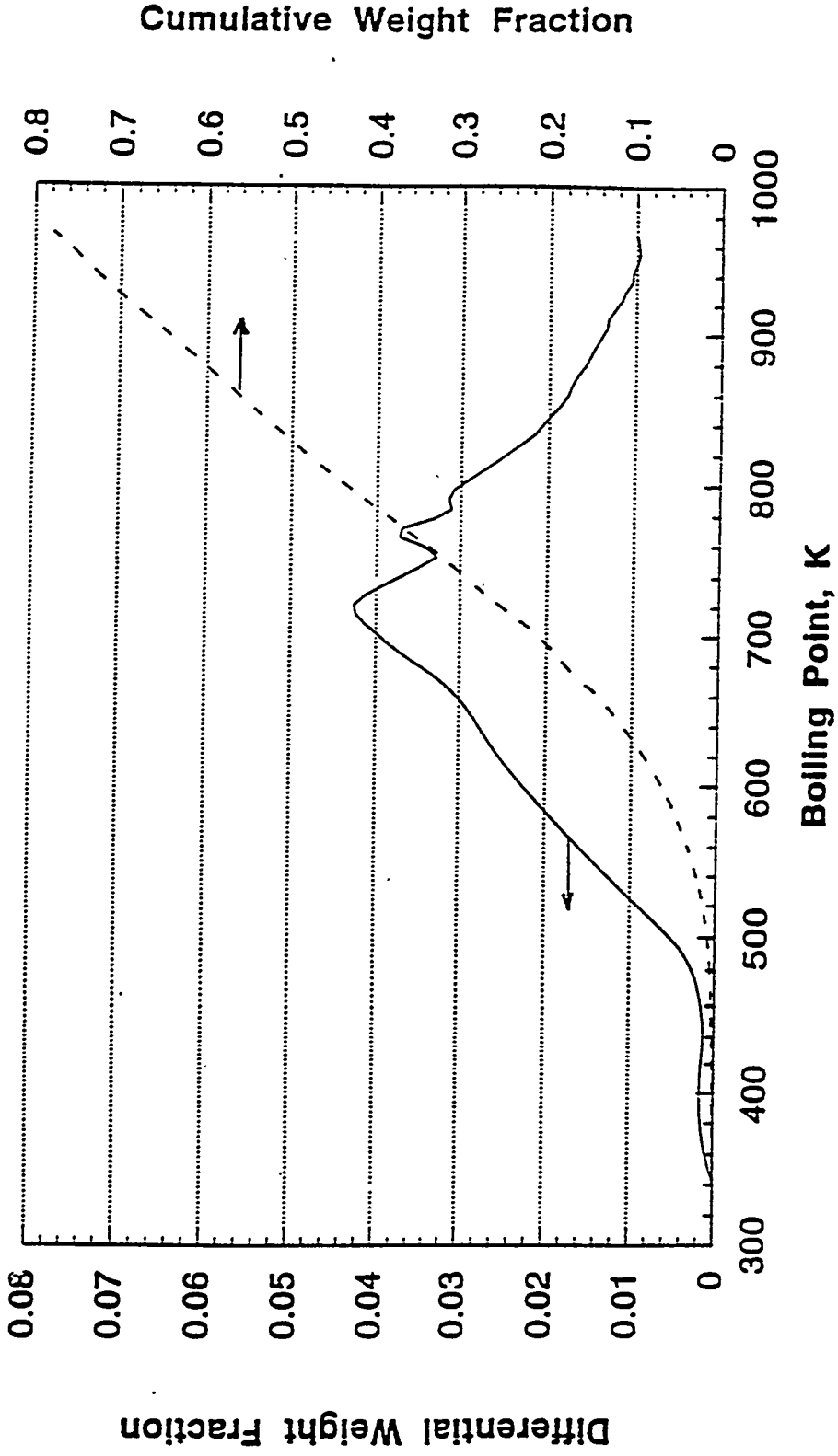
Cumulative Weight Fraction
0.8
0.7
0.6
0.5
0.4
0.3
0.2
0.1
0
1000
900
800
700
600
500
400
300
Boiling Point, K
0.08
0.07
0.06
0.05
0.04
0.03
0.02
0.01
0
Differential Weight Fraction

Table 13
Simulated Distillation Analyses for Bitumens Analyzed

Properties	Whiterocks Bitumen	Asphalt Ridge Bitumen	PR Spring Bitumen	Sunnyside Bitumen
Modified SIMDIS Procedure				
Volatility (< 811 K), wt%	46.6	53.5	45.4	40.9
Distillation Cuts, wt%				
< 477 K	0.5	1.3	0.4	0.6
477 K - 617 K	7.4	11.8	8.2	7.8
617 K- 811 K	38.7	40.4	36.8	32.5
811 K- 973 K	33.0	34.0	33.0	32.0
> 973 K	20.0	11.0	21.0	27.0

conducted by Hwang (63) and Subramanian (64), respectively. The SFE experiments for all four bitumens were carried out at five different operating conditions, a combination of three pressures (5.6, 10.4, and 17.3 MPa) and three temperatures (339, 380 and 422 K) with four conditions above the critical pressure and temperature of the solvent and one condition above the critical pressure but below the critical temperature of the propane. The typical operating conditions used for the SFE experiments are presented in Figure 39. The experiments were carried out at five similar conditions so that the influence of the nature of the bitumen on SFE yields and on the quality of the extract phases could be observed.

Experiments were conducted to measure the density of the commercial propane using the densitometer at the operating conditions used in this study. The measured densities of the propane are listed in Table 14. The propane density increased with increasing in pressure at constant temperature and decreased with increasing in temperature at constant pressure. Starling (67) developed an equation of state which was used to estimate the density of propane and other hydrocarbon gases. The propane densities for pressures and temperatures ranging from 1.97 MPa to 10.9 MPa and 355 to 477K; respectively, are presented in Figure 40. These curves were obtained by solving the equation of state developed by Starling (67). The propane densities predicted were less than the measured densities which is typical for cubic equations of state. The cubic equation of state predicts liquid densities lower than the experimentally measured one (68) and the deviation from the measured values differs for different equations of state (68, 69), hence the propane density was measured.

The SFE experiments were conducted with 50 g of bitumen (AR and SS) initially in the extractor. A known quantity of propane was charged to the extractor until the

Figure 39.

Chromatograms for the Whiterocks Bitumen Extract

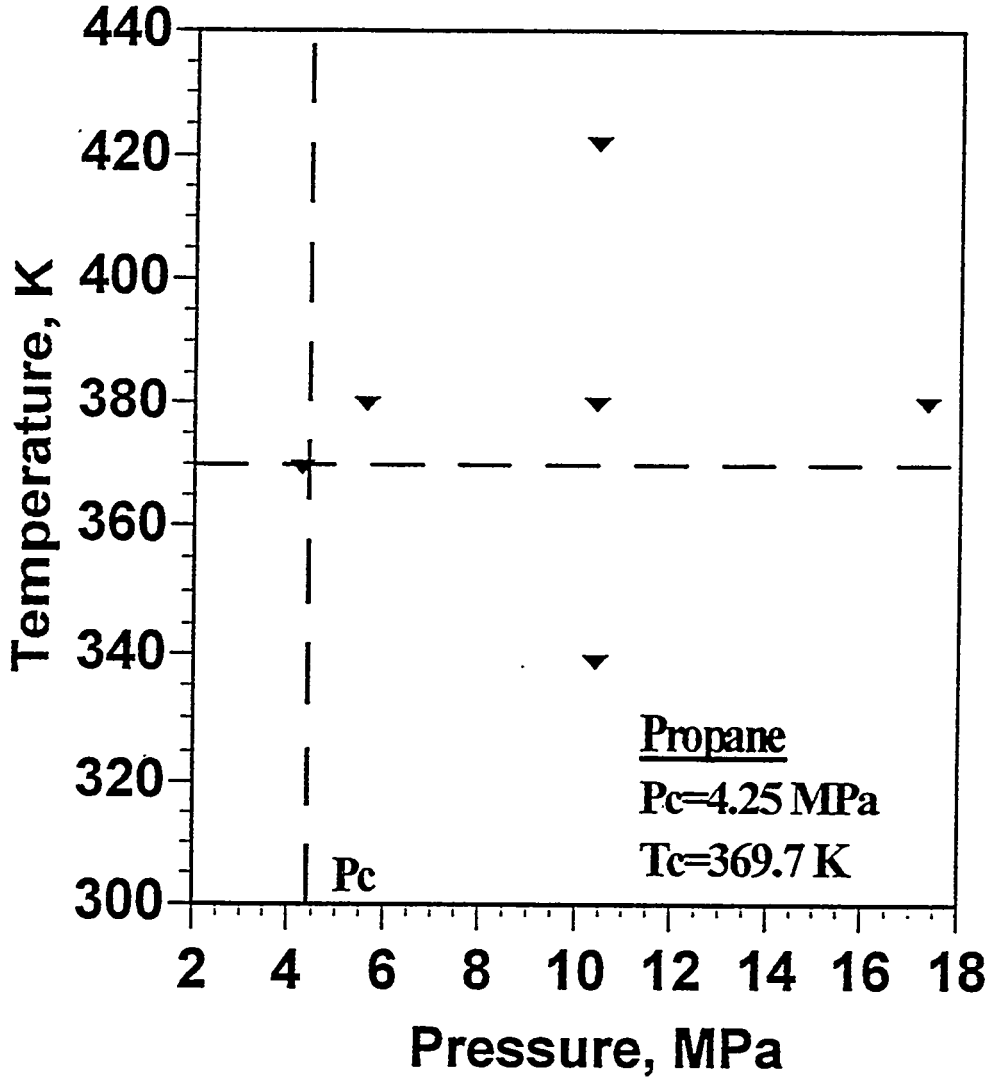
440
420
400
380
360
340
320
300
Temperature, K
2
4
6
8
10
12
14
16
18
Pressure, MPa
Pc
Propane
Pc=4.25 MPa
Tc=369.7 K

Figure 40.

Propane Density at Various Temperatures and Pressures (80)

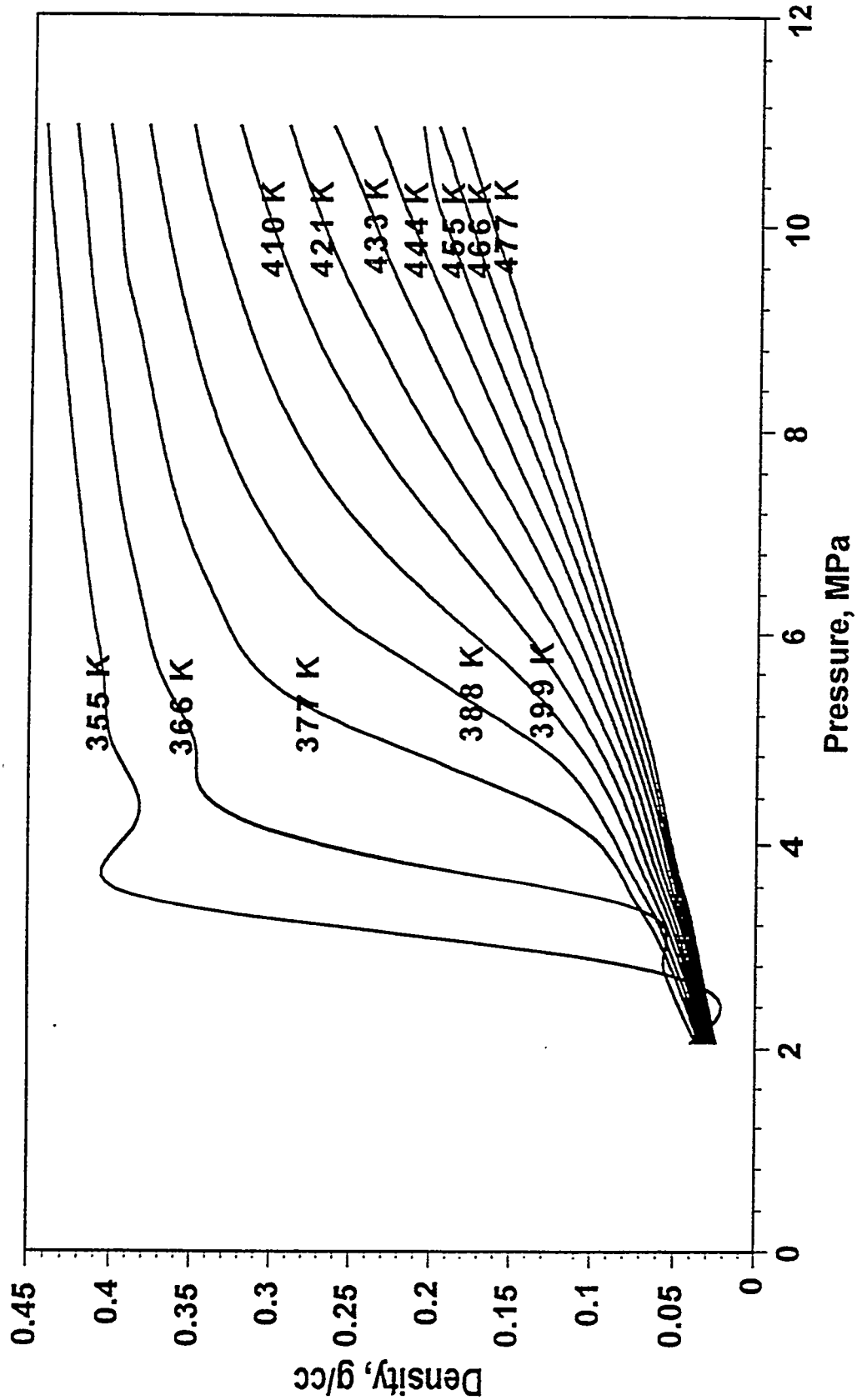
Density, g/cc
Pressure, MPa
0.45
0.4
0.35
0.3
0.25
0.2
0.15
0.1
0.05
0
0
2
4
6
8
10
12
355 K
366 K
377 K
388 K
399 K
410 K
421 K
433 K
444 K
455 K
466 K
477 K

Table 14

Measured Densities of Commercial Propane

		Density (g/cc)		
Temperature, K		339	380	422
Reduced Temperature		0.92	1.03	1.14
Pressure (MPa)	Reduced Pressure			
5.6	1.3	-	0.533	-
10.4	2.4	0.566	0.553	0.545
17.3	4.1	-	0.569	-

system was brought to the desired operating conditions. The initial solvent charging was performed using a positive displacement pump. Liquid samples were collected from the separator for every 25 liters of propane vented through the system. Six such samples were collected before the extraction was terminated. The extraction was terminated after window #6 because the extraction yield tapered down considerably and terminating extraction after a fixed number of windows (six) permitted meaningful comparisons of the compositions of the residual fractions. The extract phase samples were labeled as extract window #1 through #6. The hydrocarbon remaining in the extractor was collected as the residual fraction for further analysis.

Supercritical Fluid Extraction of Asphalt Ridge Bitumen

Hwang (63) and Subramanian (64) conducted SFE experiments and studied the SFE behavior of the bitumens from the WR and PRS deposits. This section will examine SFE extraction of the bitumen from the AR deposit whose physical and chemical properties are intermediate to those of the WR and PRS bitumens. The effect of process variables such as pressure, temperature and solvent density on the extraction yields of the AR bitumen has been determined.

Pressure Effect

The SFE experiments conducted to determine the influence of pressure on the SFE of AR bitumen were carried out at a constant temperature of 380 K (T_r=1.03) and three different pressures of 5.6 MPa (P_r=1.2), 10.4 MPa (P_r=2.3) and 17.3 MPa (P_r=4.1). The maximum cumulative extraction yield, 31.4 wt%, was achieved at 17.3 MPa (P_r=4.1) and 380 K (T_r=1.03). The extraction yield decreased with decreasing in pressure at

constant temperature 380 K (T_r=1.03) with yields of 24.5 wt% and 13.4 wt% achieved at 10.4 MPa (P_r=4.1) and 5.6 MPa (P_r=4.1), respectively. The amount extracted was quite sensitive to the solvent density: for every 1% change in the solvent density, there was 3% change in the cumulative extraction yield (6 windows). The effect of pressure on the extraction yield of AR bitumen is presented in Figure 41. The decrease in the overall extraction yield with decrease in pressure at constant temperature was attributed to the decrease in the solvent density with decrease in pressure (Table 14).

The extracted phase density was measured for all the SFE experiments for the AR bitumen-propane system using the data acquisition system incorporated into the SFE system. The measured extracted densities for the AR bitumen-propane system at all five operating conditions are plotted versus extraction time in Figure 42.

The extraction yield increased for the first three windows and decreased in the subsequent extraction windows (Figure 42). This trend is attributable to the extraction of lighter hydrocarbons initially and the change in the overall composition of the system with time. Propane has an affinity for the extraction of lighter hydrocarbons relative to heavier hydrocarbons (57). The lighter hydrocarbons were extracted initially and as the extraction proceeded, the system was depleted in lighter hydrocarbons (the SFE system is batch and continuous with respect to bitumen and solvent, respectively) and the remaining bitumen components in the extractor became heavier. As the hydrocarbons were extracted, the overall composition of the system changed continuously and became leaner in bitumen and richer in solvent. The lower affinity of propane for heavier hydrocarbons resulted in a reduction in the transfer of bitumen components from the oleic phase to the extract phase during the later part of the extraction. Furthermore, the lighter hydrocarbons acted as

Figure 41.

Effect of Pressure on SFE Yields with the Asphalt Ridge Bitumen

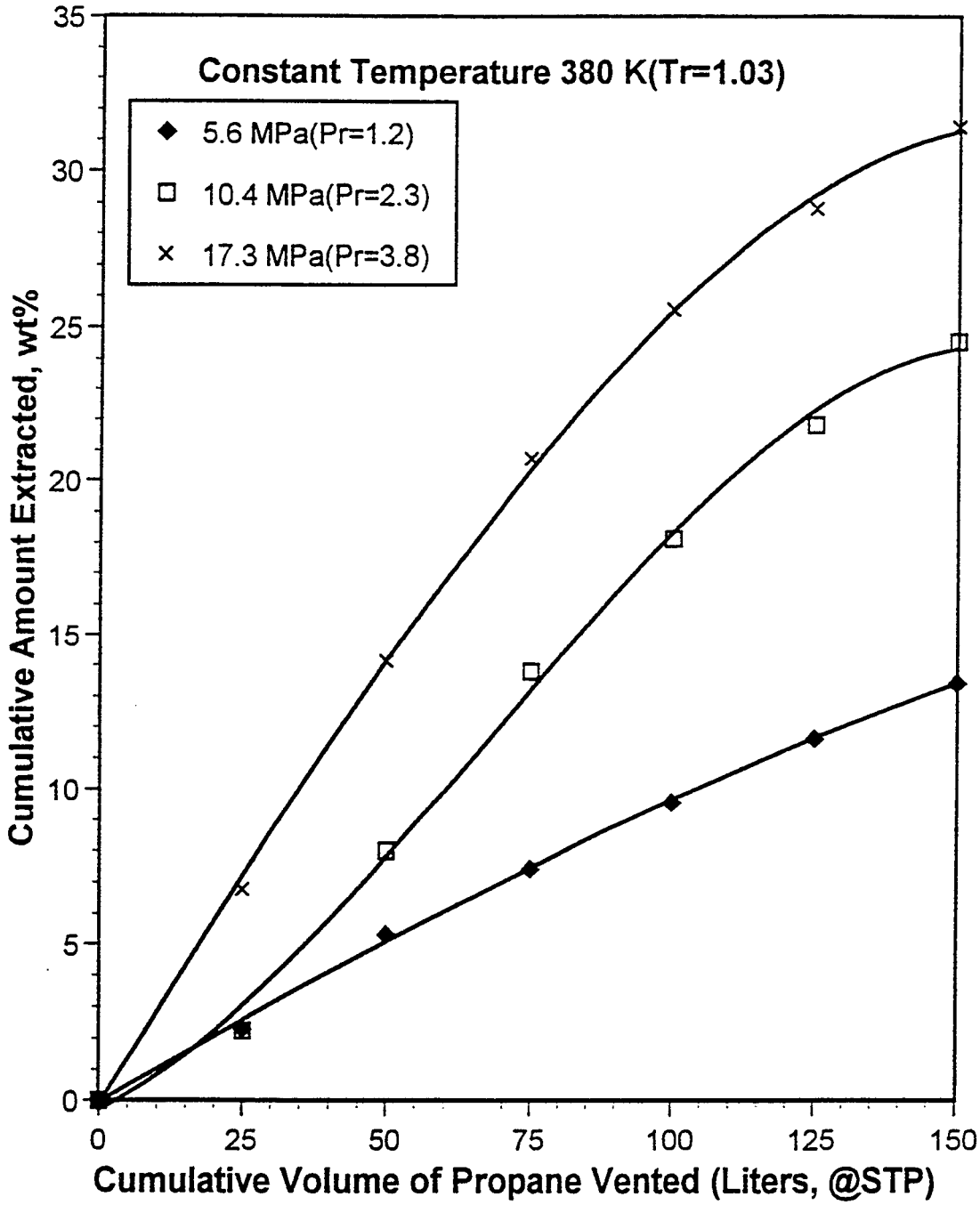
Constant Temperature 380 K(Tr=1.03)
5.6 MPa(Pr=1.2)
10.4 MPa(Pr=2.3)
17.3 MPa(Pr=3.8)
Cumulative Amount Extracted, wt%
Cumulative Volume of Propane Vented (Liters, @STP)
0
5
10
15
20
25
30
35
0
25
50
75
100
125
150

Figure 42.

Measured Extract Phase Density During SFE of the Asphalt Ride Bitumen with Propane as Solvent

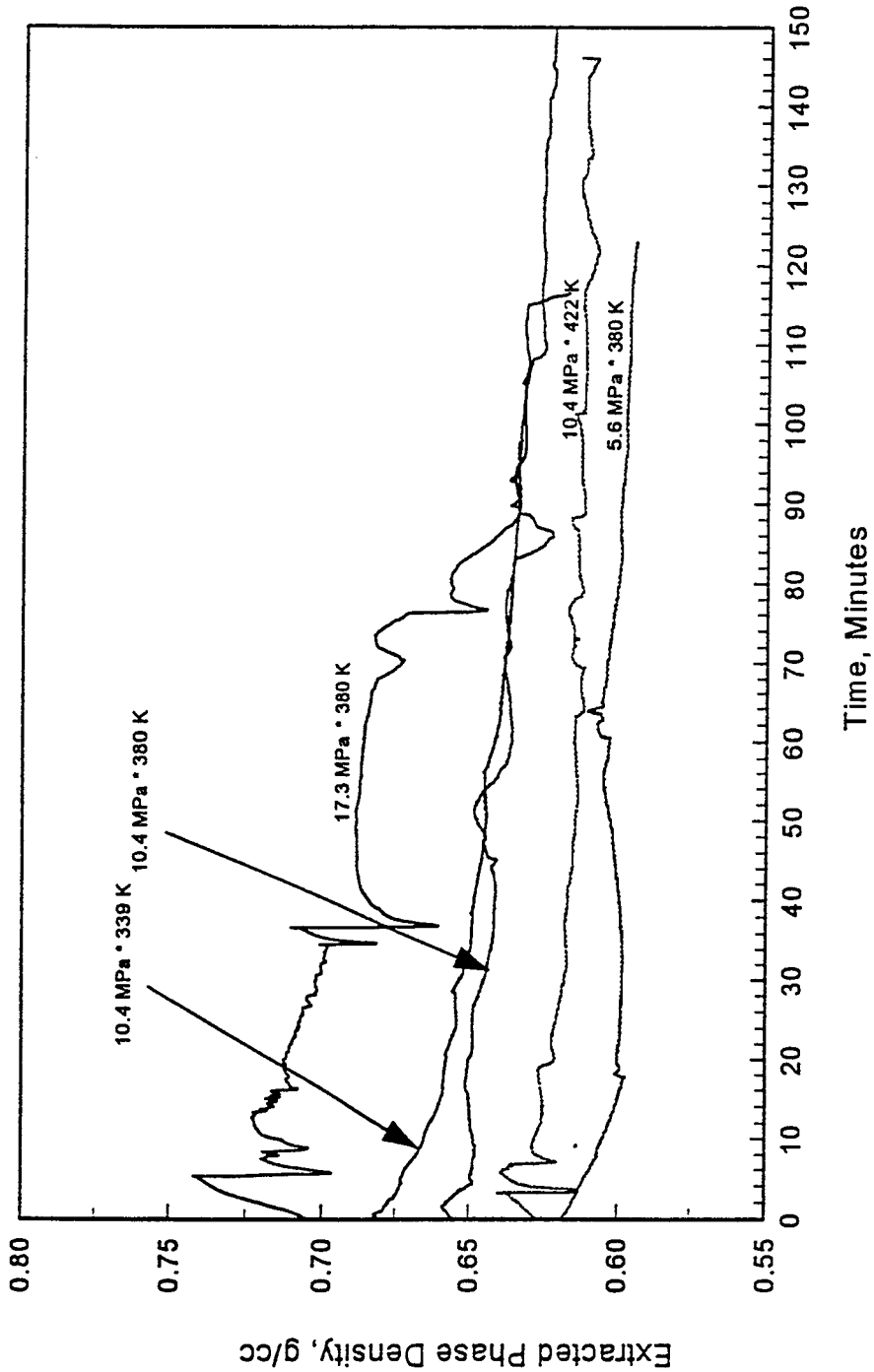
Extracted Phase Density, g/cc
0.80
0.75
0.70
0.65
0.60
0.55
0
10
20
30
40
50
60
70
80
90
100
110
120
130
140
150
Time, Minutes
10.4 MPa * 339 K
10.4 MPa * 380 K
17.3 MPa * 380 K
10.4 MPa * 422 K
5.6 MPa * 380 K

cosolubilizing agents for the heavier species; thus their depletion during the initial extraction periods produced a more refractory residual oleic phase which was less soluble in supercritical propane. Consequently the extraction yields decreased.

It is observed from the extract phase density plots (Figure 42) that the SFE experiments started with extract phase densities of 0.71, 0.66 and 0.62 g/cm^3 at pressures of 17.3 (P_r=4.1), 10.4 (P_r=2.3), and 5.6 MPa (P_r=1.2); respectively, at a constant temperature of 380 K (Tr=1.03). The pure solvent densities measured at these conditions were 0.569, 0.553 and 0.533 g/cm^3, respectively.

Temperature Effect

The extraction experiments were conducted to examine the influence of temperature on SFE of the AR bitumen at a constant pressure of 10.4 MPa (P_r=2.3) and at three different temperatures: 339 K (T_r=0.92), 380 K (T_r=1.03) and 422 K (T_r=1.14). The maximum cumulative extraction yield, 31.3 wt%, was obtained at 10.4 MPa (P_r=2.3) and 339 K (T_r=0.92). The cumulative extraction yield decreased with increase in temperature at constant pressure, that is, yields of 24.5 and 18.2 wt%, were achieved at 380 K (Tr=1.03) and 422 K (Tr=1.14), respectively (Figure 43). The decrease in extraction yield with increase in temperature at constant pressure was attributed to the decrease in solvent density with increase in temperature (Table 14) It is also observed from the extract density plots (Figure 42) that the extract phase density was highest at the lowest temperature 339 K, (T_r=0.92) and decreased with increase in temperature at constant pressure.

The extraction yield increased for the first four windows and decreased in the subsequent extraction windows (Figure 43). As explained in the previous section, this

Figure 43.

Effect of Temperature on SFE Yields with the Asphalt Ridge Bitumen

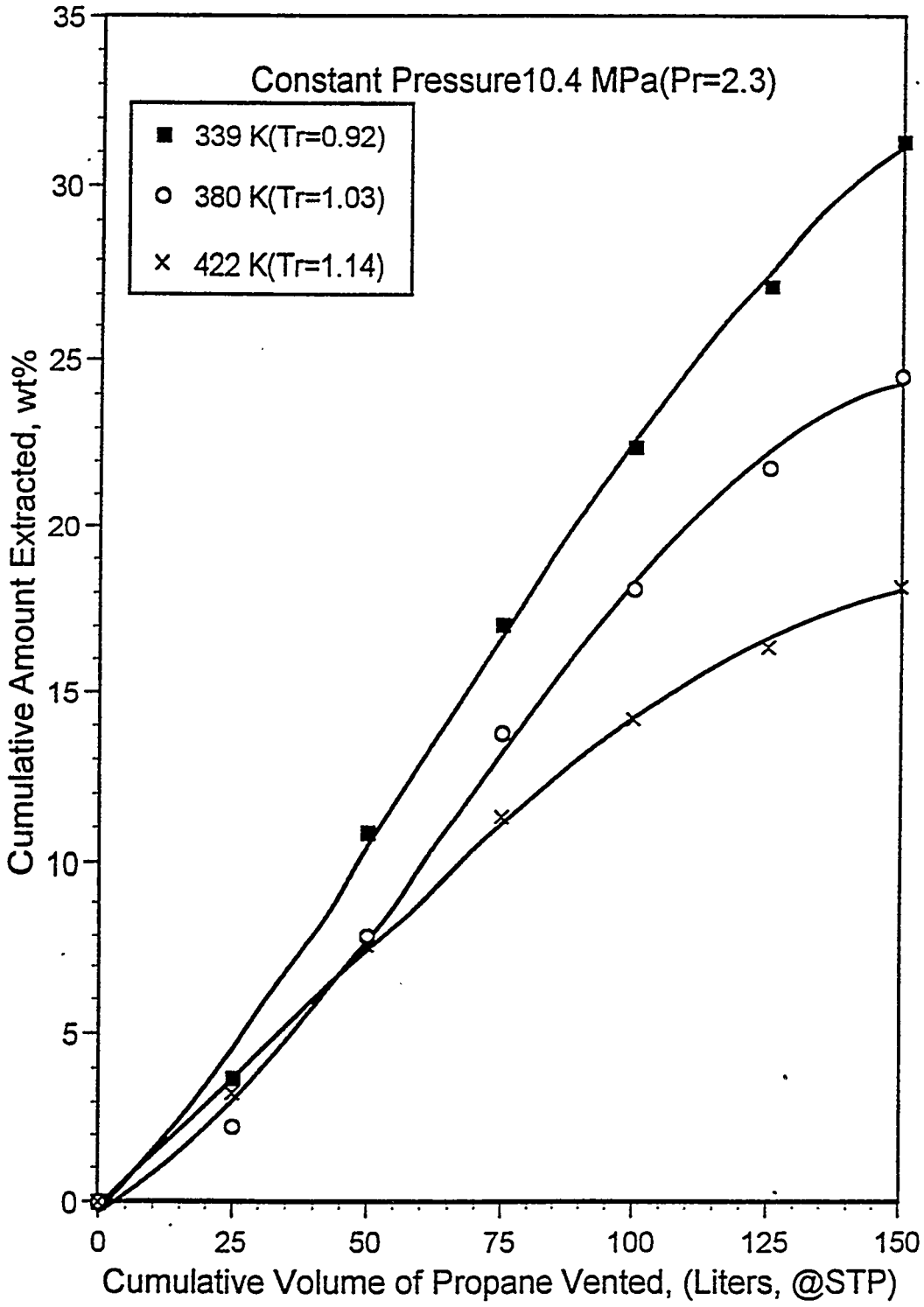
Constant Pressure10.4 MPa(Pr=2.3)
339 K(Tr=0.92)
380 K(Tr=1.03)
422 K(Tr=1.14)
Cumulative Amount Extracted, wt%
Cumulative Volume of Propane Vented, (Liters, @STP)
0
5
10
15
20
25
30
35
0
25
50
75
100
125
150

effect was related to the extraction of lighter hydrocarbons initially and the change in the overall composition of the system with time.

The initial extract phase densities were 0.680, 0.66 and 0.625 g/cm^3 at 339 (T_r=0.92), 380 (T_r=1.03), and 422 K (T_r=1.14), respectively at a constant pressure of 10.4 MPa (Pr=2.3) (Figure 42) whereas the pure solvent densities were 0.566, 0.553 and 0.545 g/cm^3; respectively. Thus, both the pure solvent density and the extract phase densities decreased with increase in temperature resulting in a decrease in the extraction yields.

Solvent Density Effect

The solvent densities measured at the five operating conditions are plotted (Figure 44) against the cumulative extraction yields obtained for SFE with the AR bitumen. It is observed from the plot that the cumulative extraction yields with AR bitumen increased as the pure solvent density increased. However, the maximum extraction yield obtainable using propane as the supercritical fluid would be equal to or less than the deasphalted oil obtained using liquid propane (70).

The pure solvent densities measured at the five operating conditions were 0.533, 0.566, 0.553, 0.545 and 0.569 g/cm^3; respectively, at 5.6 MPa and 380 K, 10.4 MPa and 339 K, 10.4 MPa and 380 K, 10.4 MPa and 422 K and 17.3 MPa and 380 K. While performing SFE experiments, the extract phase density was measured on a continuous basis using the data acquisition system. The initial extract phase densities were 0.62, 0.68, 0.66, 0.625 and 0.71 g/cm^3; respectively, at 5.6 MPa and 380 K, 10.4 MPa and 339 K, 10.4 MPa and 380 K, 10.4 MPa and 422 K and 17.3 MPa and 380 K. These values

Figure 44.

Effect of Solvent Density on SFE Yields with the Asphalt Ridge Bitumen

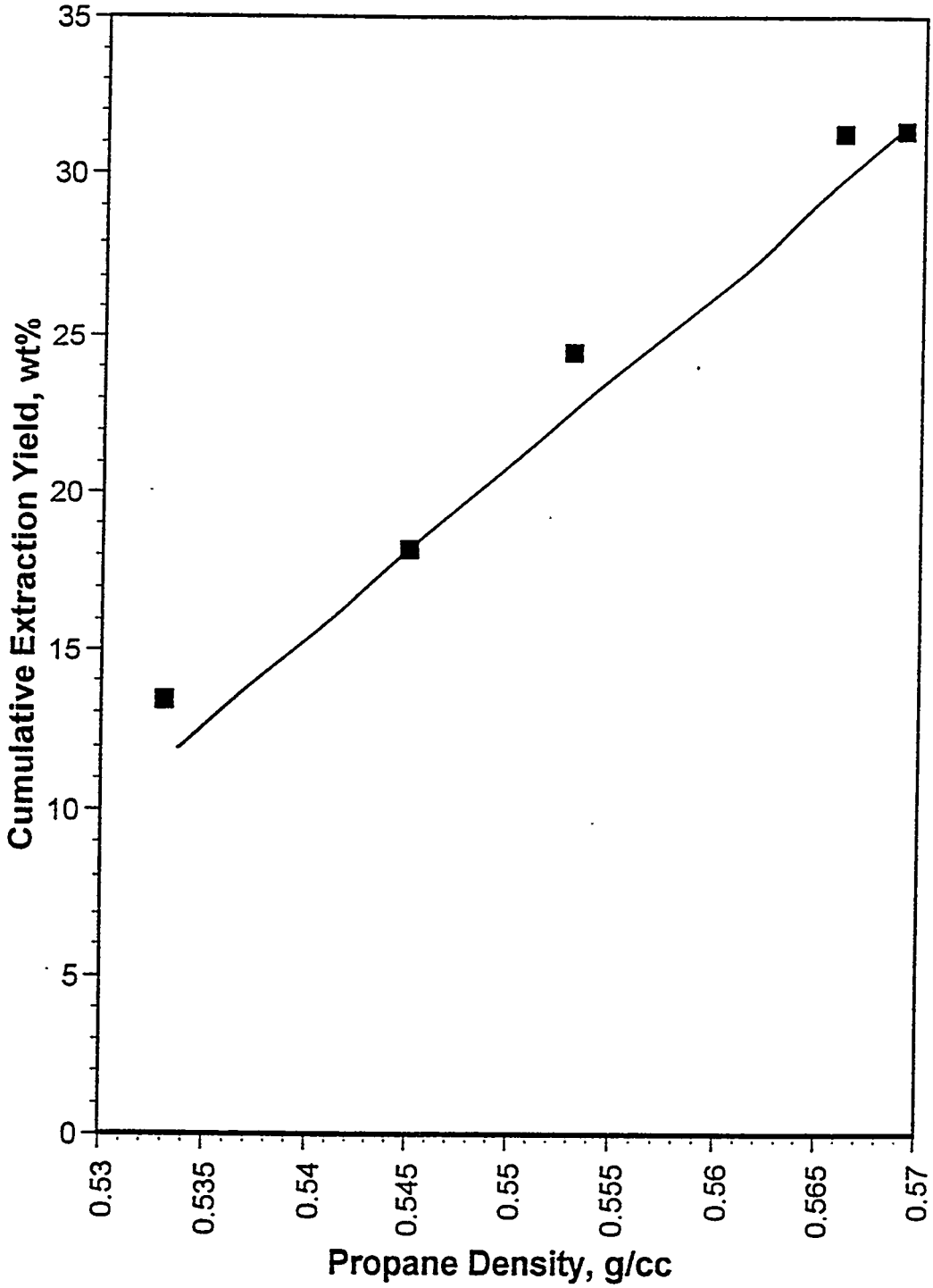
Cumulative Extraction Yield, wt%
35
30
25
20
15
10
5
0
0.53
0.535
0.54
0.545
0.55
0.555
0.56
0.565
0.57
Propane Density, g/cc

indicate that the higher the pure solvent density, the higher the initial extract phase density at the same temperature and pressure. The propane densities were varied by adjusting the pressure and temperature and the extraction capacity of the solvent increased with increased density. The propane densities at 10.4 MPa and 339 K and 17.3 MPa and 380 K were similar: 0.566 and 0.569 g/cm3; respectively. The cumulative extraction yields for the AR bitumen were likewise nearly the same: 31.3 and 31.4 wt%; respectively. These results indicate that the by maintaining the same extraction density through combinations of pressure and temperature, similar extraction yields could be obtained.

Another explanation could be provided for the increase in extraction yields with increase in solvent density. Johnston (71) indicated that the enhancement factor for hexamethylbenzene, 2-naphthnol, phthalic anhydride, anthracene and acridine increased exponentially with increase in density of carbon dioxide. The enhancement factor, a measure of the solubility of a solute in the vapor phase is directly governed by vapor pressures. This observation could be applied to SFE of bitumen using propane as solvent and the dependence of extraction yield on solvent density.

The propane solvent density can be increased either by increasing the pressure at constant temperature or by decreasing the temperature at constant pressure. The maximum propane solvent density obtainable under supercritical conditions is always less than the propane liquid density and hence the extraction capability will be less than that of liquid propane. Thus, it may be advantageous to operate the extraction in the liquid phase region of the solvent where the temperature and pressure will be less compared to the supercritical conditions and to separate the solvent from the extract phase at supercritical conditions.

The main advantages for operating under supercritical conditions are given below:

I. Extraction provides high selectivity

II. Selectivity towards extraction of a single compound or group of compounds could be varied by decreasing or increasing the solvent density by adjustment of the operating pressure and temperature

III. The supercritical solvent-solute separation is achieved by increasing the extract phase temperature when the extracted oil is no longer soluble in the solvent or by simple depressurization. In the case of a liquid solvent, the thermal energy must be added to the solvent to vaporize it from the solvent-extract phase mixture. Hence supercritical solvent processes are energy efficient. In case of commercial SFE process (72) to upgrade heavy oil, the energy savings are of the order of 30 to 50 % relative to conventional propane deasphalters which utilizes liquid propane.

Carbon Number Distribution for AR Bitumen Extract Phases

The extract samples obtained from SFE of the AR bitumen were subjected to simulated distillation analyses to determine the boiling point or carbon number distributions. The results obtained at a pressure of 17.3 MPa (P_r=4.1) and a temperature of 380 K (T_r=1.03) are presented in Figure 45. It is observed from the boiling point distributions of the extract phases that as the extraction proceeded heavier and heavier components were extracted. This was due to the semi-continuous (batch for solute and continuous for solvent) SFE system used for the extraction experiments where the lighter hydrocarbons were extracted initially. As the extraction proceeded, the extractor was depleted of lighter hydrocarbons and hence the heavier hydrocarbons were extracted in the

Figure 45.

Carbon Number Distributions for the Asphalt Ridge Bitumen, Extracts and Residual Fractions Obtained from SFE at 17.3 MPa (P_r=4.1) and 380 K (T_r=1.03)

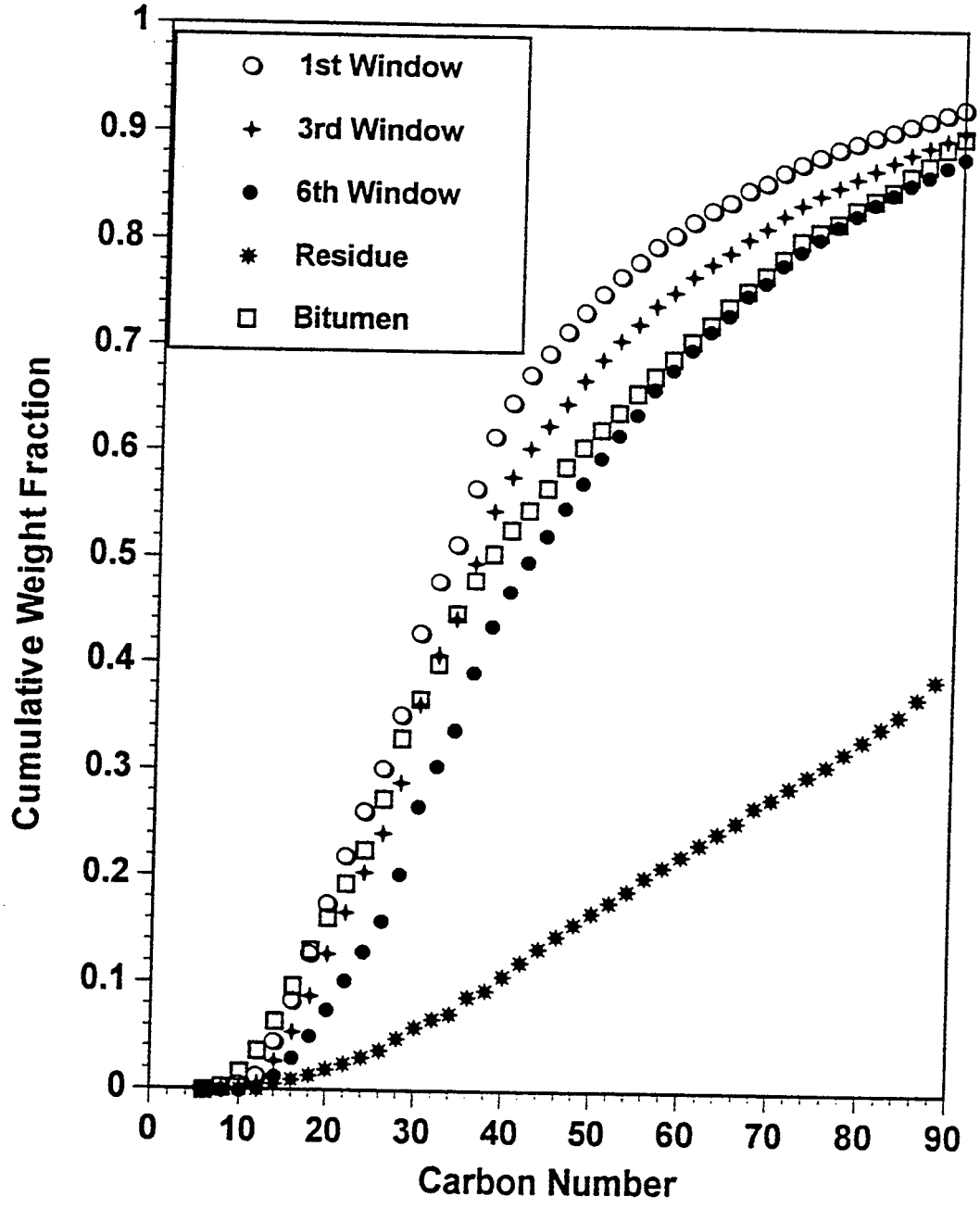
1st Window
3rd Window
6th Window
Residue
Bitumen
Cumulative Weight Fraction
Carbon Number
0
0.1
0.2
0.3
0.4
0.5
0.6
0.7
0.8
0.9
1
0
10
20
30
40
50
60
70
80
90

subsequent windows. This was also indicated by the simulated distillation curves shifting towards higher carbon numbers as the extraction window number increased (Figure 45). Furthermore, the extract phases were significantly upgraded liquids as indicated by the volatilities, approximately 70 wt%, compared to the original bitumen which was 53.5 wt% volatile. The residual fraction was only 20 wt% volatile. The volatiles are defined as the fraction boiling below 811 K.

The effects of temperature and pressure on compositional variation of the extract phases are presented in Figure 46. As the system pressure increased at constant temperature heavier extract fractions were obtained in the 2nd extraction window. At constant pressure, as the system temperature is increased, lighter extract liquids were obtained.

It is observed from the experimental results that at a constant temperature of 380 K (T_r=1.03), the extraction yield increased from 13.4 wt% (@5.6 MPa) to 31.4 wt% (@17.3 MPa) as the extraction pressure increased. At the same time the volatility (fractions boiling below 811 K) of the 2nd extraction window extract decreased from 85.2 wt% (@5.6 MPa) to 65.1 wt% (@17.3 MPa). The SFE system was operated on semicontinuous basis (bitumen and propane are batch and continuous respectively) and hence an increase in extraction yield with pressure means decrease in overall volatility (quality) of the extract phase as the solvent extracts heavier hydrocarbons. As the system temperature increased at constant pressure (10.4 MPa), the cumulative extraction yield decreased from 31.3 wt% (339 K) to 18.2 wt% (422 K). The volatility (quality) of the 2nd window extract phase increased from 73.1 wt% (339 K) to 83.9 wt% (422 K). Thus, it could be stated that at constant temperature, as the extraction pressure increased extraction

Figure 46.

Effect of Pressure and Temperature on the Carbon Number Distributions of the Second Extraction Window Obtained During SFE of the Asphalt Ridge Bitumen

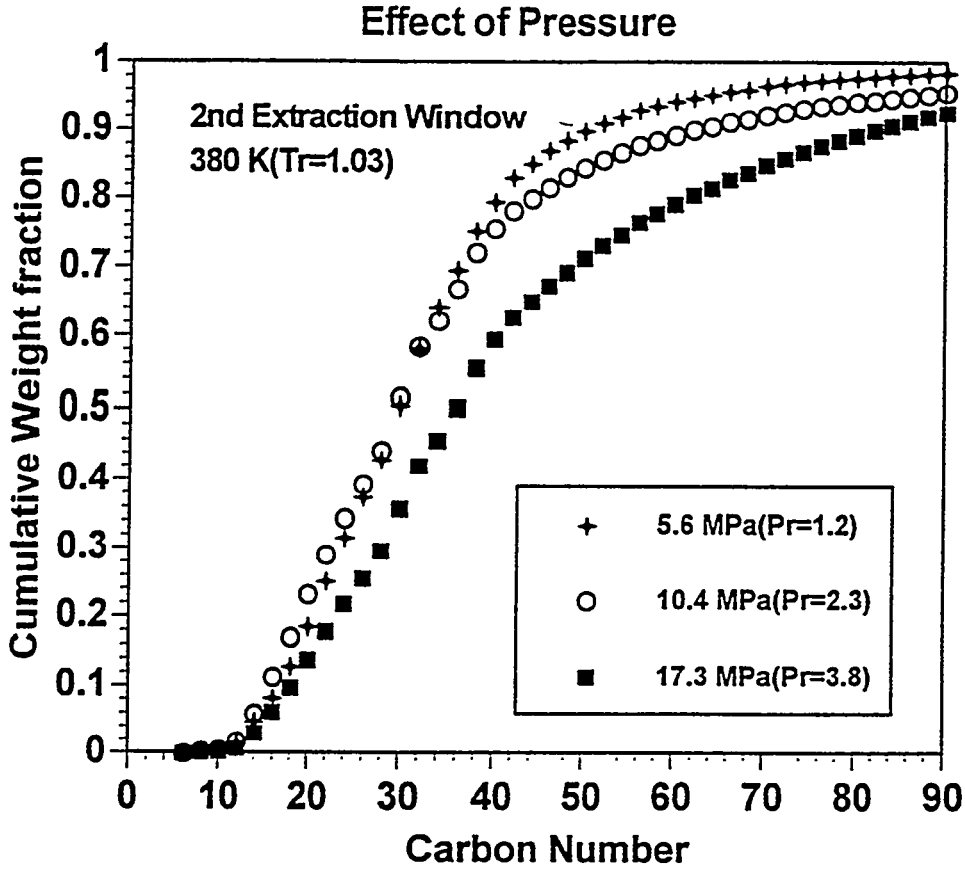
Effect of Pressure
2nd Extraction Window
380 K(Tr=1.03)
5.6 MPa(Pr=1.2)
10.4 MPa(Pr=2.3)
17.3 MPa(Pr=3.8)
Cumulative Weight fraction
Carbon Number
0
0.1
0.2
0.3
0.4
0.5
0.6
0.7
0.8
0.9
1
0
10
20
30
40
50
60
70
80
90

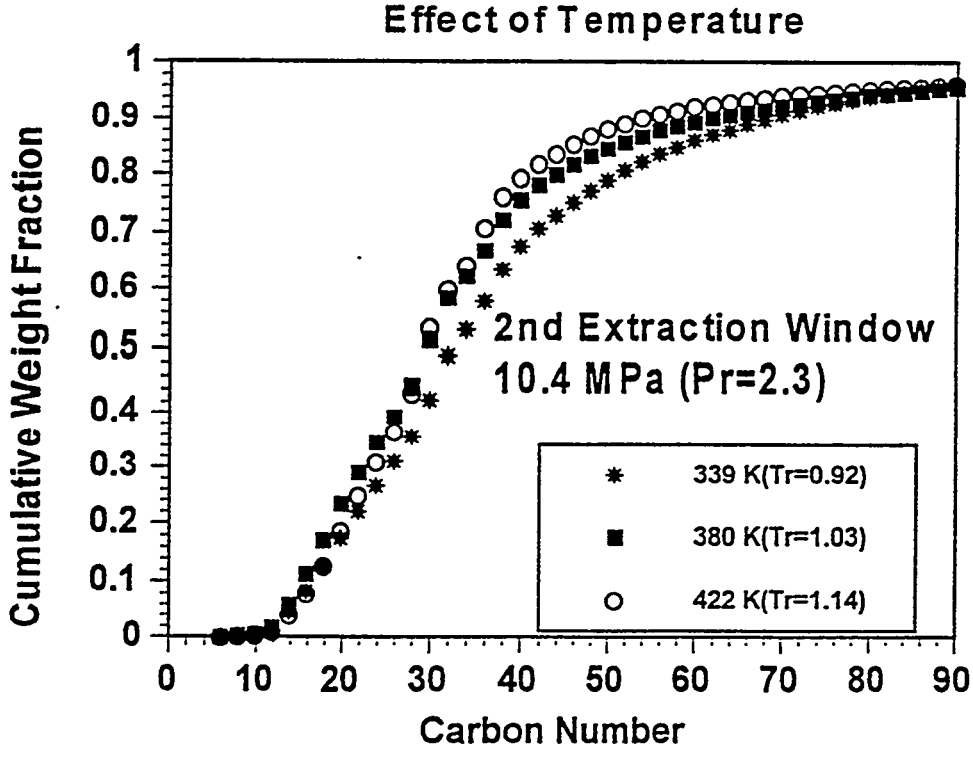
Effect of Temperature
2nd Extraction Window
10.4 MPa (Pr=2.3)
339 K(Tr=0.92)
380 K(Tr=1.03)
422 K(Tr=1.14)
Cumulative Weight Fraction
Carbon Number
0
0.1
0.2
0.3
0.4
0.5
0.6
0.7
0.8
0.9
1
0
10
20
30
40
50
60
70
80
90

yields increased and produced heavier and less volatile hydrocarbon liquids. In contrast, at constant pressure as the extraction temperature increased extraction yields decreased but produced refined and lighter hydrocarbon liquids.

Reproducibility

Reproducibility experiments were conducted using the AR bitumen at 10.4 MPa (P_r=2.3) and 339 K (T_r=0.92). The results obtained from two experiments are compared in Figure 47. It is observed from the experimental results that the difference between the extraction yields (for individual extraction windows) obtained for each of the six windows were within 5 % absolute margin. Hence, it was concluded that the experimental results are reproducible.

Supercritical Fluid Extraction of Sunnyside Bitumen

The physical and chemical properties such as specific gravity, Conradson carbon, pour point, viscosity at 343 K, pentane insolubles and 811 K plus (non volatile) fractions of the bitumen from the SS oil sands deposit are higher than those for the WR, AR and PRS bitumens. Hence, the SS bitumen was selected as representative of a lower quality bitumen for SFE studies.

Pressure Effect

The experiments intended to determine the influence of pressure on the SFE of bitumen from the SS oil sands deposit were conducted at a constant temperature of 380 K (T_r=1.03) and three different pressures, 5.6 MPa (P_r=1.2),10.4 MPa (P_r=2.3) and

Figure 47.

Reproducibility for SFE with the Asphalt Ridge Bitumen at 10.4 MPa (P_r=2.3) and 339 K (T_r=0.92)

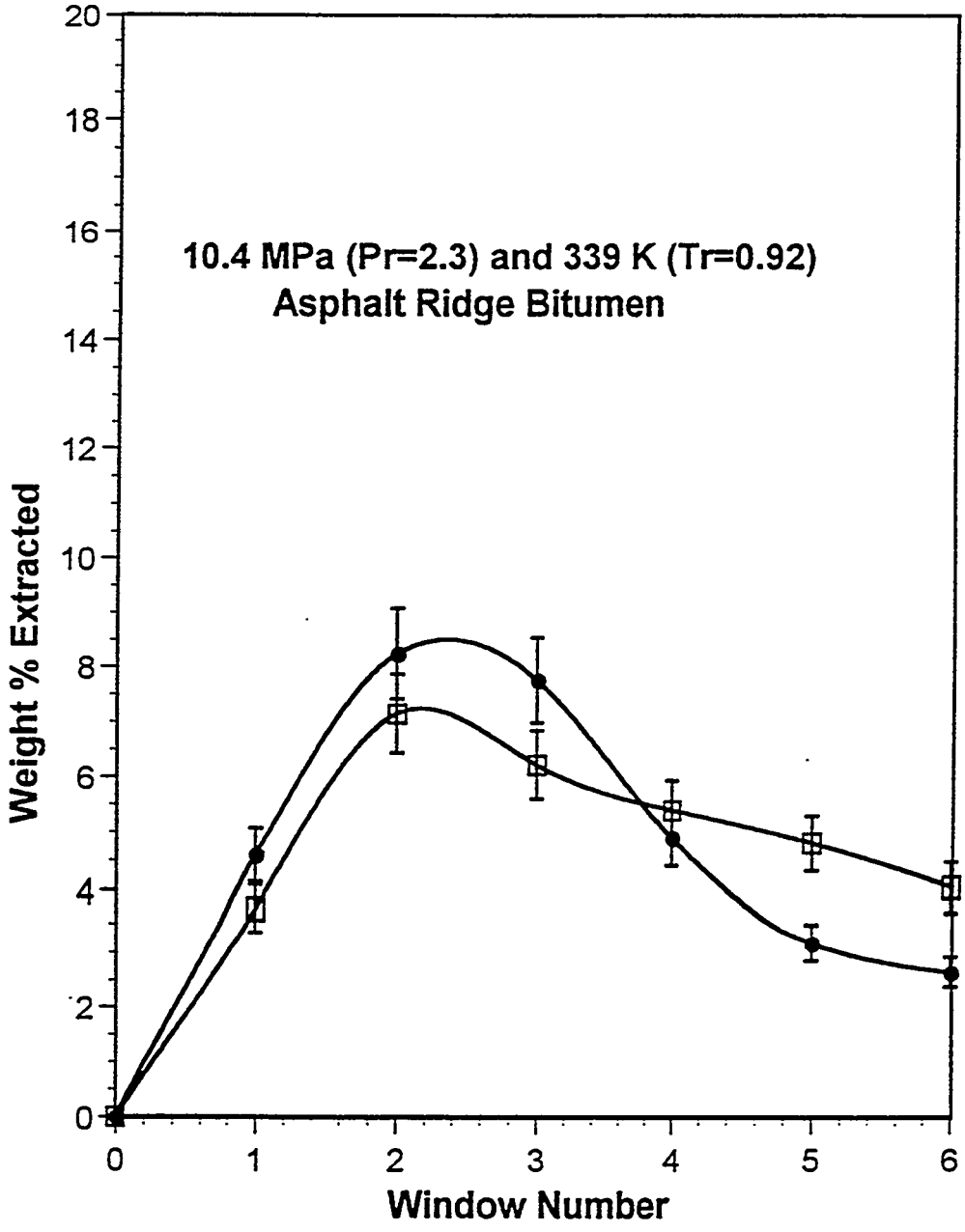
10.4 MPa (Pr=2.3) and 339 K (Tr=0.92)
Asphalt Ridge Bitumen
Weight % Extracted
Window Number
0
2
4
6
8
10
12
14
16
18
20
0
1
2
3
4
5
6

17.3 MPa (P_r=4.1). The maximum extraction yield, 23.7 wt%, was achieved at 17.3 MPa (P_r=4.1) and 380 K (T_r=1.03). The extraction yields decreased with decrease in pressure at constant temperature. Extraction yields of 14.8 and 12.0 wt% were obtained at 10.4 MPa (P_r=2.3) and 5.6 MPa (P_r=1.2), respectively (Figure 48). The decrease in the extraction yield with decrease in pressure was attributed to decrease in solvent density with decrease in pressure at constant temperature.

The extracted phase density was measured for all the SFE experiments for SS bitumen-propane system. The measured extract phase densities for the SS bitumen-propane system at all five operating conditions are plotted vs time in Figure 49.

The extraction yield increased for the first three extraction windows and decreased in the subsequent extraction windows (Figure 48). As discussed previously, this trend was presumed to be related to the extraction of lighter hydrocarbons initially and to the change in the overall composition of the system with time. Propane has an affinity for the extraction of lighter hydrocarbons compared to heavier hydrocarbons (57). The initial depletion of the lighter hydrocarbons led to a residual bitumen phase in the extractor which consisted of heavier components. As the extraction process proceeded, the overall composition in the extractor changed continuously to leaner in the bitumen component and richer in the solvent. The propane's lesser affinity for heavier hydrocarbons and the enrichment of solvent in the extractor resulted in decreased extraction of bitumen components during the later part of the extraction. The maximum differential extraction yield was also inferred by the maximum extract phase density (Figure 49). The extract phase density plots (Figure 49) indicated that the initial extract phase densities were 0.604, 0.58 and 0.571 g/cm^3 at pressures of 17.3 (P_r=4.1), 10.4 (P_r=2.3), and 5.6 MPa

Figure 48.

Effect of Pressure on SFE with the Sunnyside Bitumen

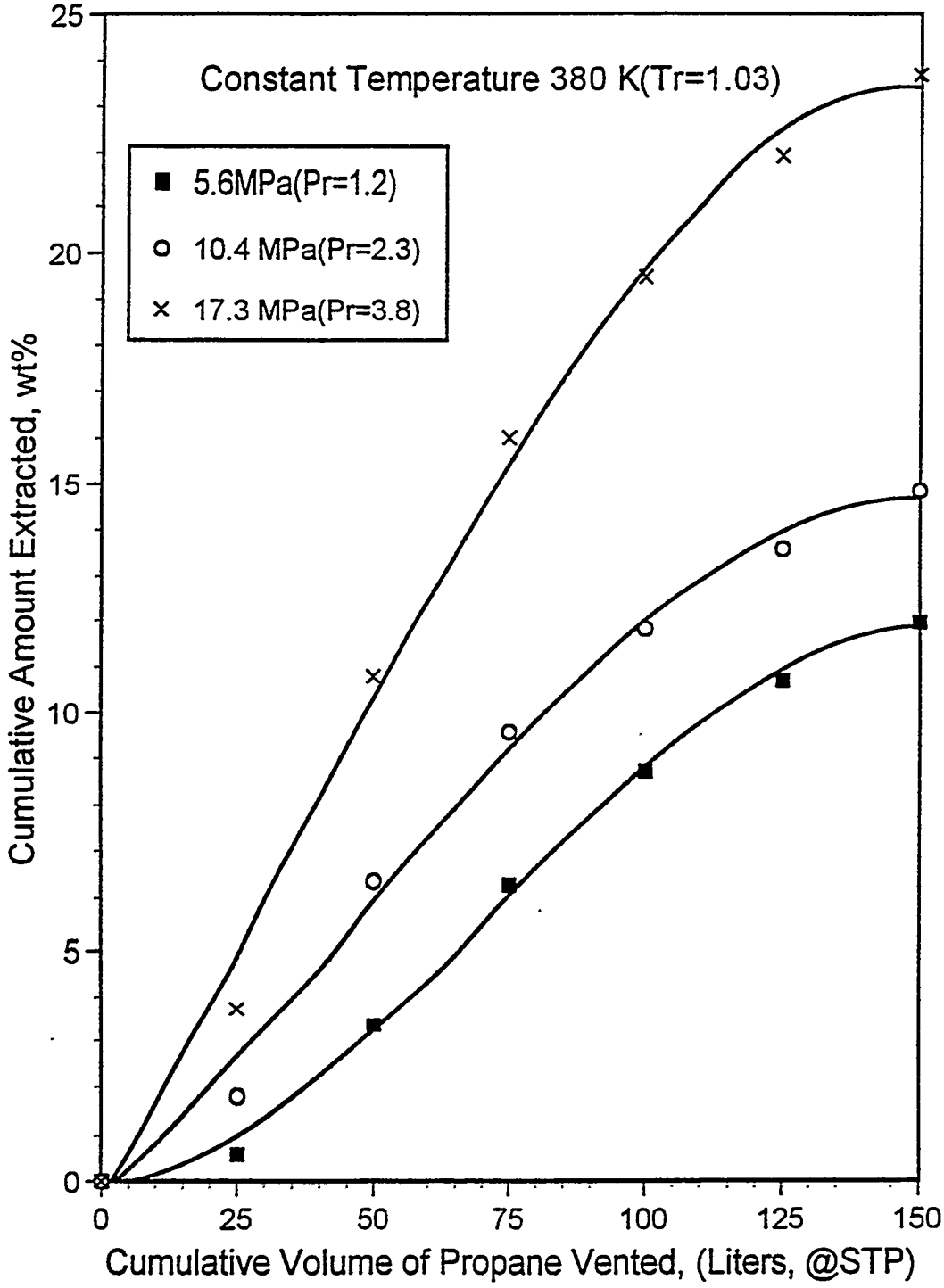
Constant Temperature 380 K(Tr=1.03)
5.6MPa(Pr=1.2)
10.4 MPa(Pr=2.3)
17.3 MPa(Pr=3.8)
Cumulative Amount Extracted, wt%
Cumulative Volume of Propane Vented, (Liters, @STP)
0
5
10
15
20
25
0
25
50
75
100
125
150

Figure 49.

Measured Extract Phase Densities During SFE of the Sunnyside Bitumen with Propane as Solvent

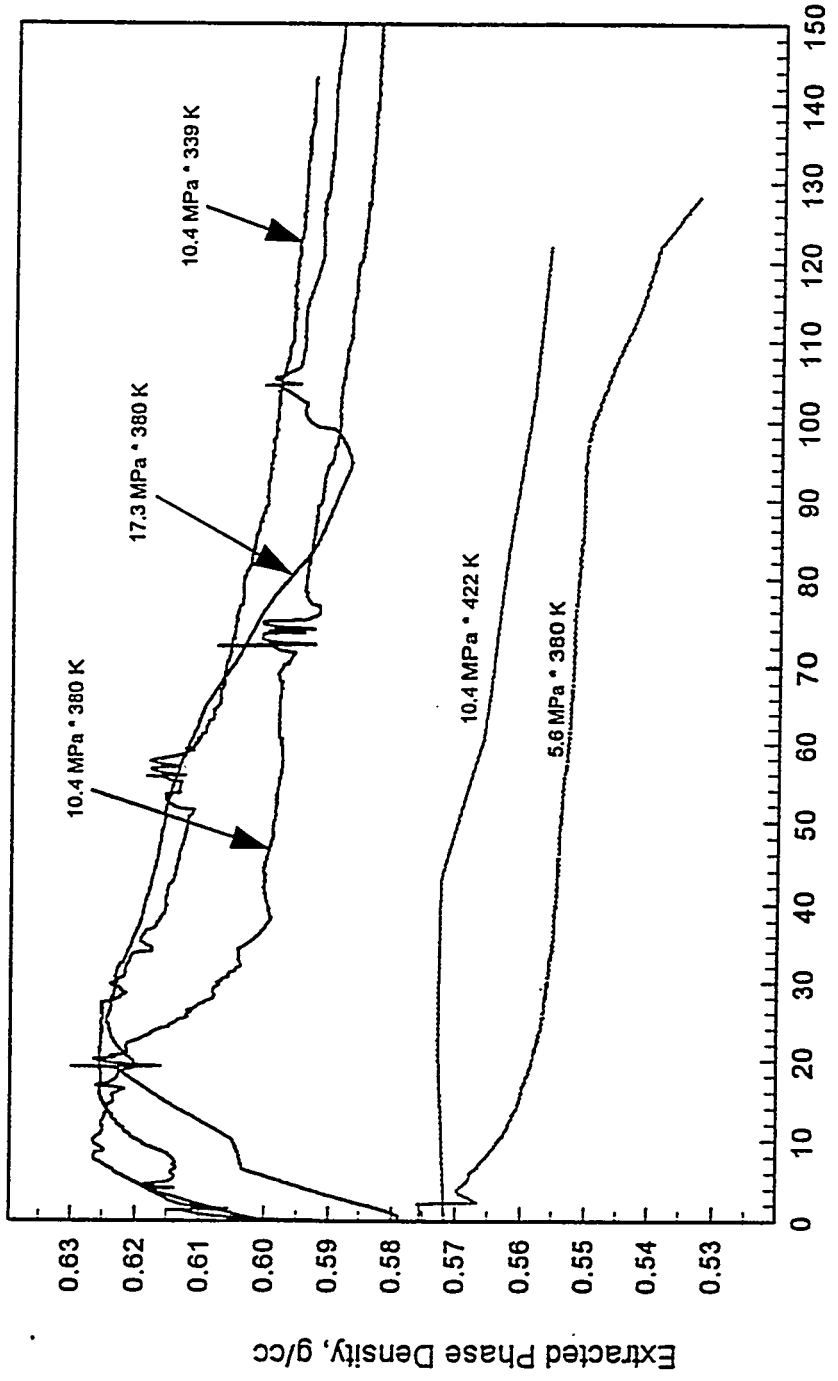
Extracted Phase Density, g/cc
0.63
0.62
0.61
0.60
0.59
0.58
0.57
0.56
0.55
0.54
0.53
0
10
20
30
40
50
60
70
80
90
100
110
120
130
140
150
Time, Minutes
10.4 MPa * 380 K
17.3 MPa * 380 K
10.4 MPa * 339 K
10.4 MPa * 422 K
5.6 MPa * 380 K

(P_r=1.2); respectively, at a constant temperature of 380 K (Tr=1.03). The comparable pure solvent densities were 0.569, 0.553 and 0.533 g/cm^3, respectively. Thus, once again, it was concluded that higher extraction yields were driven by higher propane densities and in fact can be correlated by the solvent densities.

Temperature Effect

The influence of temperature on SFE extraction yields with the SS oil sands bitumen was determined at a constant pressure 10.4 MPa (P_r=2.3) and three different temperature of 339 K (T_r=0.92), 380 K (T_r=1.03) and 422 K (T_r=1.14). The effect of temperature on the cumulative extraction yield is presented in Figure 50. The maximum extraction yield, 22.4 wt%, was obtained at 339 K (T_r=1.03). The extraction yields decreased with increase in temperature at constant pressure, 14.8 and 11.2 wt% at 380 K and 422 K; respectively. The decrease in the extraction yield was attributed to the decrease in the solvent density with increase in the temperature at constant pressure.

The extraction yield increased for the first four windows and decreased in the subsequent extraction windows (Figure 50). As explained in the previous section, this effect was attributed to the initial extraction of lighter hydrocarbons and the transition in the overall system composition to heavier components and an enrichment in solvent with time.

It is observed from the plots that the extractions were started with an extract phase densities of 0.602, 0.58 and 0.572 g/cm^3 at temperatures 339 (T_r=0.92), 380 (T_r=1.03), and 422 K (T_r=1.14); respectively, at a constant pressure of 10.4 MPa (Pr=2.3) (Figure 49). The pure propane solvent densities at these conditions were 0.566, 0.553 and 0.545

Figure 50.
Effect of Temperature on the SFE Yields with the Sunnyside Bitumen

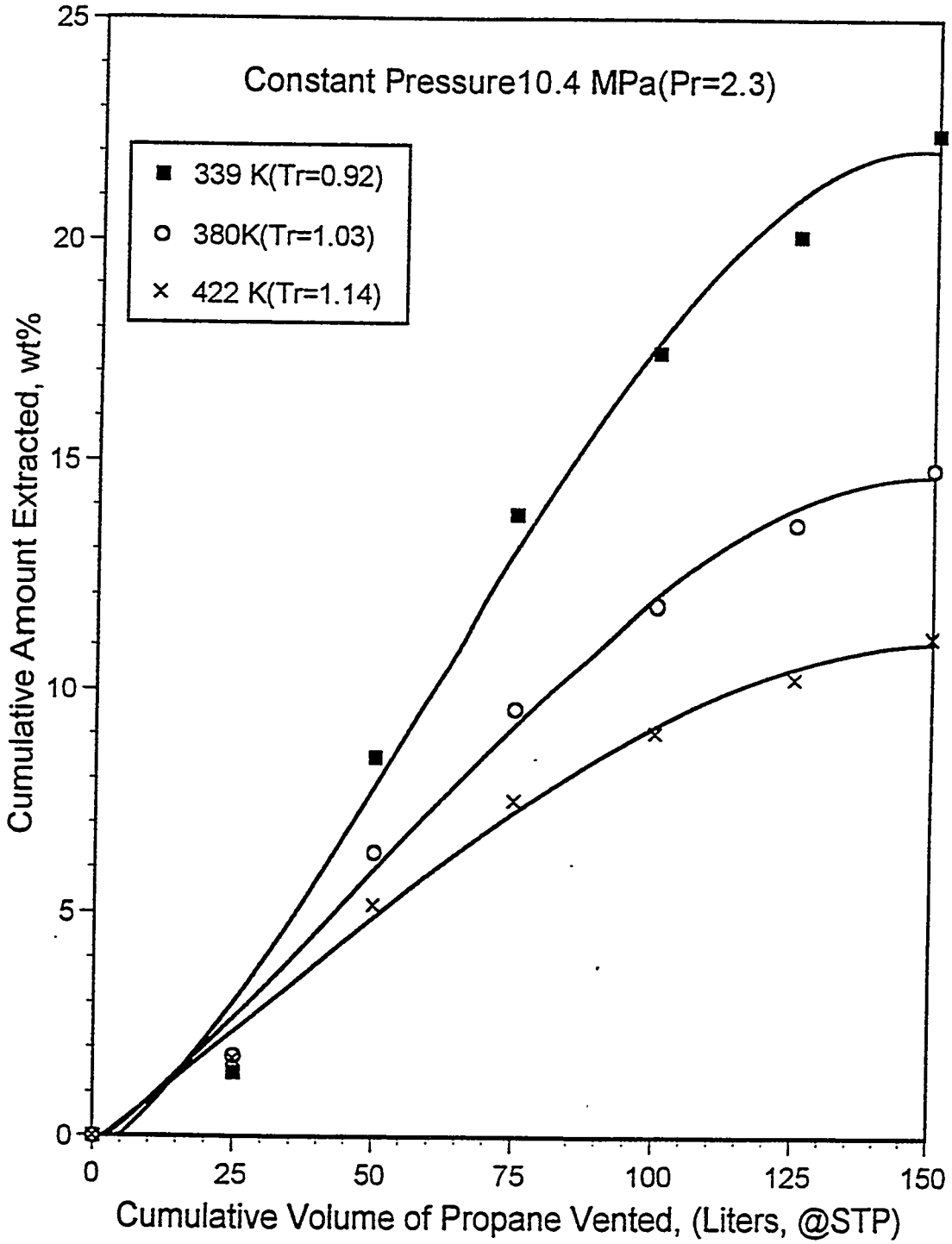
Constant Pressure10.4 MPa(Pr=2.3)
339 K(Tr=0.92)
380K(Tr=1.03)
422 K(Tr=1.14)
Cumulative Amount Extracted, wt%
Cumulative Volume of Propane Vented, (Liters, @STP)
0
5
10
15
20
25
0
25
50
75
100
125
150

g/cm^3, respectively. Thus, it is apparent that as the pure solvent density decreased with increase in temperature, the experimentally measured extract phase density also decreased which led to the decline in the carrying capacity of the solvent.

Solvent Density Effect

The solvent densities are plotted versus the cumulative extraction yields for the SS bitumen in Figure 51. The extraction yield increased with increase in solvent density during SFE of the SS bitumen using propane as solvent. It is observed from the plot that the cumulative extraction yields with the SS bitumen increased as the pure solvent density increased.

The pure solvent densities were measured at the five operating conditions. The extract phase densities were measured on a continuous basis during each extraction. The measured extract phase densities indicate that the starting densities were 0.571, 0.602, 0.58, 0.572 and 0.604 g/cm^3 at 5.6 MPa and 380 K, 10.4 MPa and 339 K, 10.4 MPa and 380 K, 10.4 MPa and 422 K and 17.3 MPa and 380 K; respectively. It was observed that the relationship between the pure solvent densities and the starting extract phase densities and operating variables was consistent; thus it was possible correlate the extraction yields by the pure solvent density. The propane density (Figure 40) could be varied by adjusting the extraction pressure and temperature. Thus, the propane densities at 10.4 MPa and 339 K and 17.3 MPa and 380 K were similar: 0.566 and 0.569 g/cm3, respectively. Furthermore, the cumulative extraction yields of SS bitumen, 22.4 and 23.7 wt%, corresponding to these densities indicated the significance of solvent density as a

Figure 51.

Effect of Solvent Density on Extraction Yields with the Sunnyside Bitumen

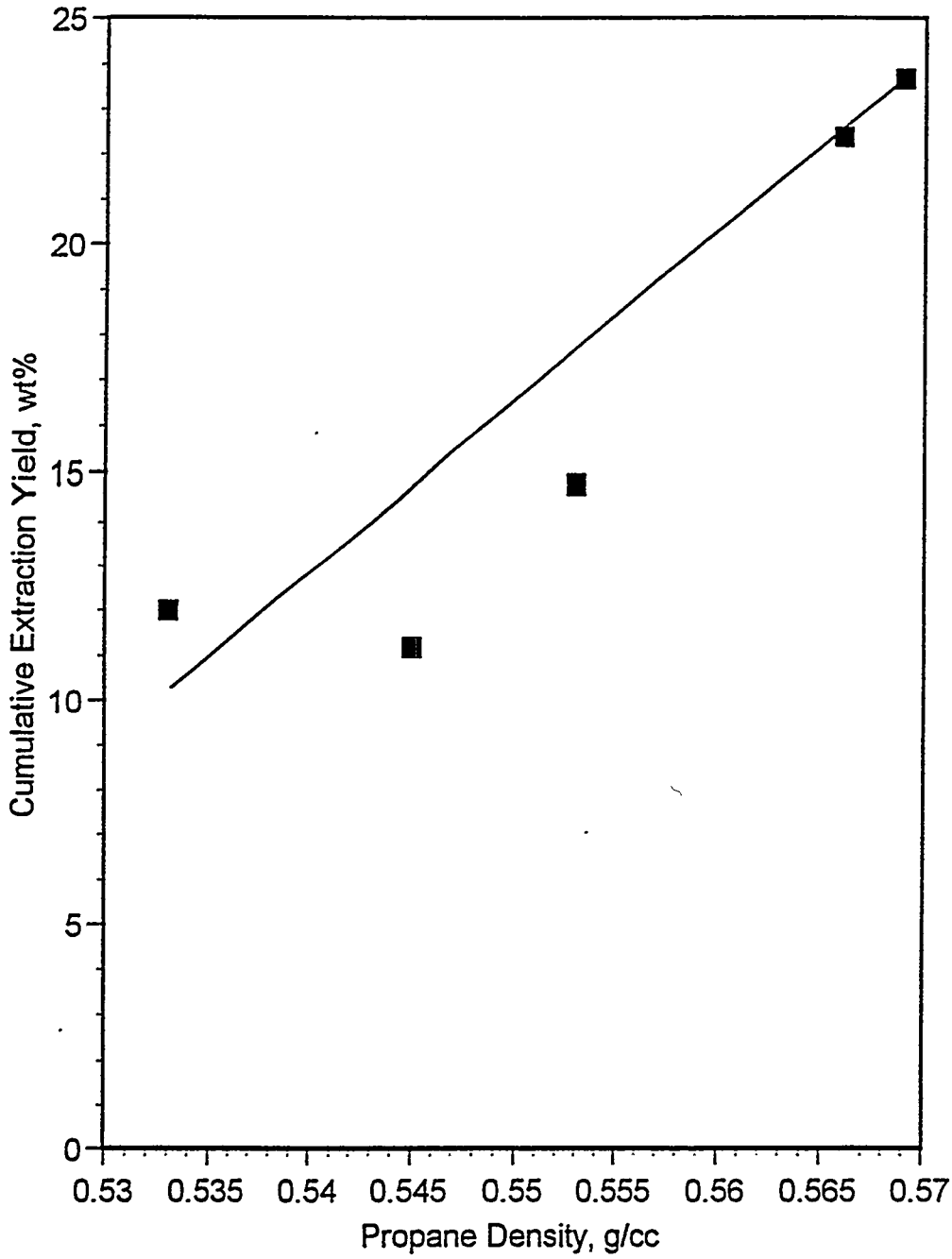
25
20
15
10
5
0
Cumulative Extraction Yield, wt%
0.53
0.535
0.54
0.545
0.55
0.555
0.56
0.565
0.57
Propane Density, g/cc

correlating parameter. If a combination of pressure and temperature is selected that maintains a fixed solvent density, similar extraction yields should result.

An alternate explanation, an increase in E with increase in solvent density, which was described relative to the extraction of the AR bitumen is also valid for the SS bitumen.

Carbon Number Distribution for SS Bitumen Extract Phases

The extract fractions obtained during SFE of the SS bitumen were analyzed using a modified simulated distillation technique to obtain boiling point and carbon number distributions up to 973 K (C_{90}). Carbon number distributions for the extract samples obtained from SFE of the SS bitumen at 17.3 MPa (P_r=4.1) and 380 K (T_r=1.03) are presented in Figure 52. As the extraction proceeded heavier and heavier components were extracted as indicated in Figure 52. The extract phases were significantly upgraded (volatilities ~ 80 wt%) compared to the original feedstock (volatility 40.9 wt%). The residual fraction was approximately 20 wt% volatile (fraction boiling below 811 K).

The effects of temperature and pressure on compositional variation of the extract phases are compared in Figure 53. As the system pressure increased at constant temperature heavier extract fractions were obtained. As the system temperature increased at constant pressure lighter extract liquids were obtained. It is observed from the experimental results that at constant temperature, as the extraction pressure increased, the extraction yield increased from 12.0 wt% (@5.6 MPa) to 23.7 wt% (@17.3 MPa). At the same time the volatility (fractions boiling below 811 K) of the 2nd extraction window extract decreased from 89.6 wt% (@5.6 MPa) to 63.1 wt% (@17.3 MPa). The SFE system was operated on a semicontinuous basis and hence the increase in extraction yield

Figure 52.

Carbon Number Distributions for the Sunnyside Bitumen and the Extract and Residual Fractions Obtained from SFE at 17.3 MPa (P_r=4.1) and 380 K (T_r=1.0[3])

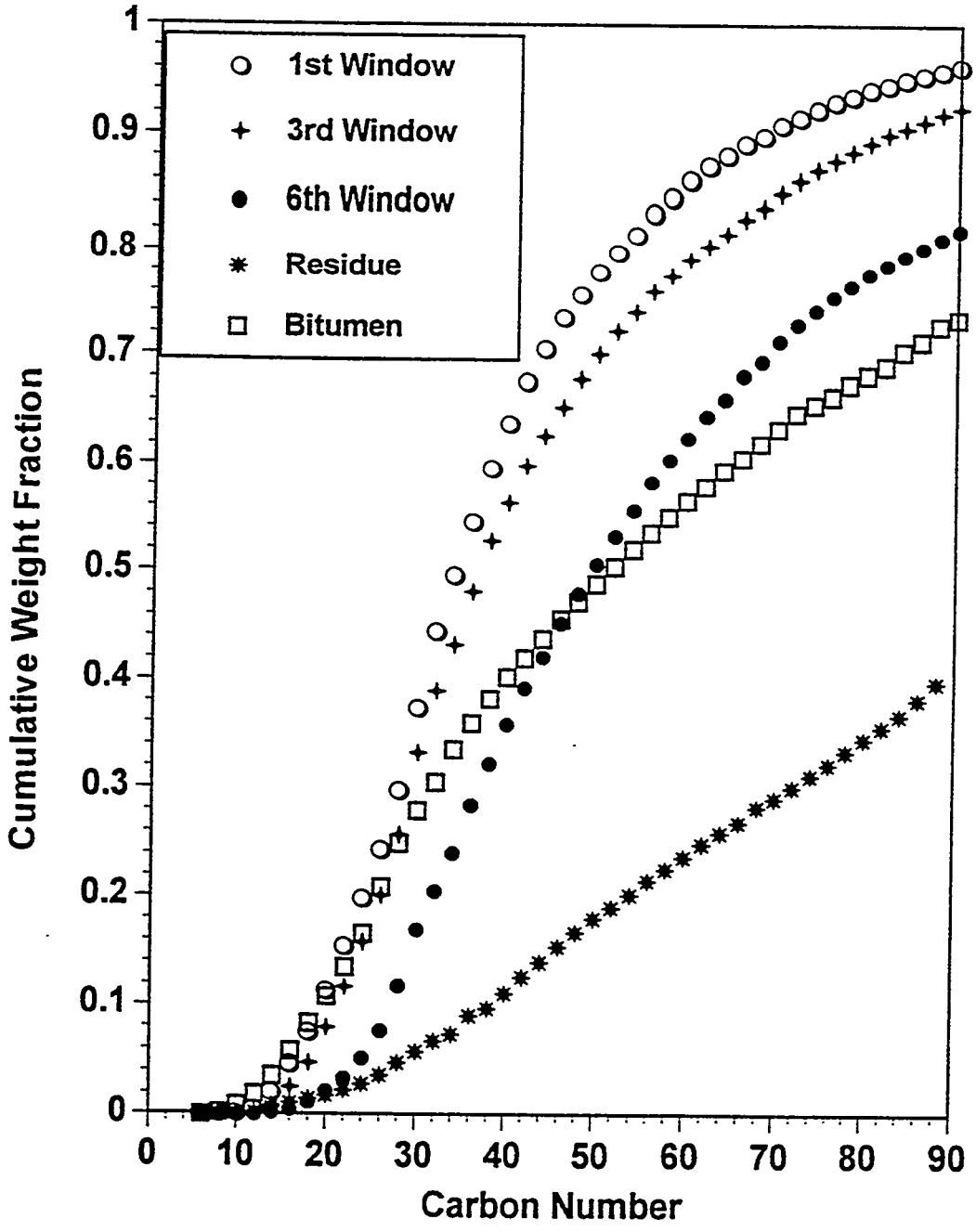
1st Window
3rd Window
6th Window
Residue
Bitumen
Cumulative Weight Fraction
Carbon Number
0
0.1
0.2
0.3
0.4
0.5
0.6
0.7
0.8
0.9
1
0
10
20
30
40
50
60
70
80
90

Figure 53.

Effect of Pressure and Temperature on the Carbon Number Distribution of the Second Extraction Windows Obtained from SFE with the Sunnyside Bitumen

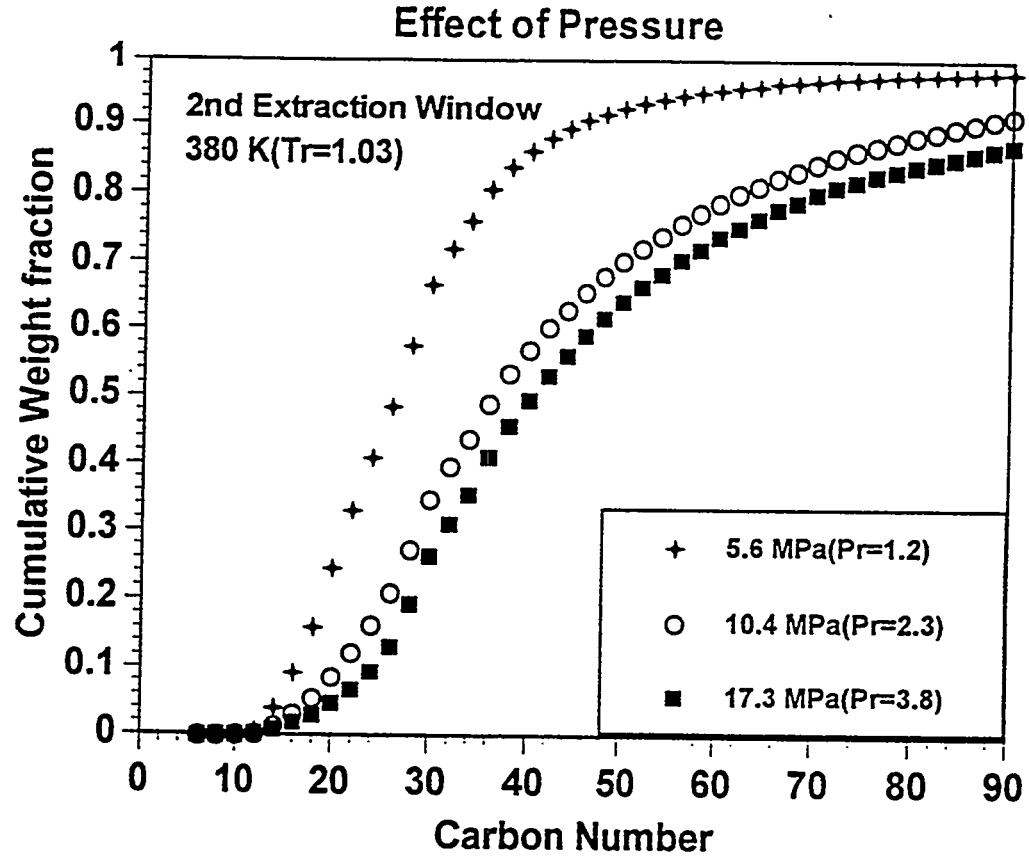
Effect of Pressure
2nd Extraction Window
380 K(Tr=1.03)
Cumulative Weight fraction
Carbon Number
5.6 MPa(Pr=1.2)
10.4 MPa(Pr=2.3)
17.3 MPa(Pr=3.8)

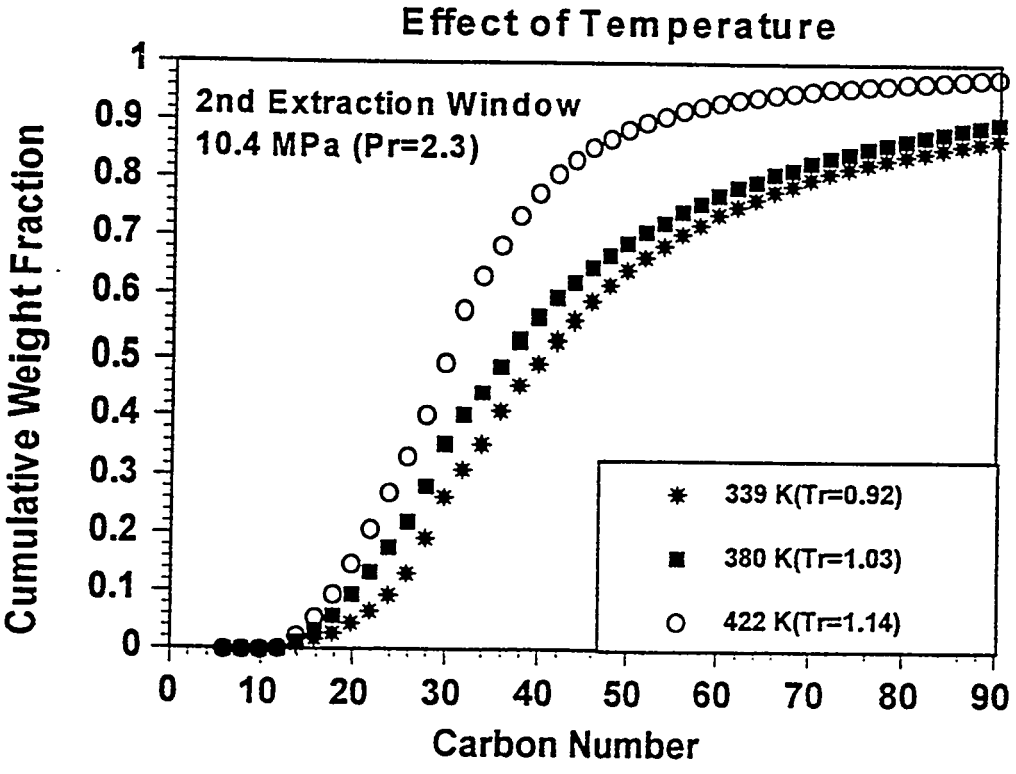
Effect of Temperature
2nd Extraction Window
10.4 MPa (Pr=2.3)
Cumulative Weight Fraction
Carbon Number
339 K(Tr=0.92)
380 K(Tr=1.03)
422 K(Tr=1.14)

with pressure led to a decrease in overall volatility (quality) of the extract phase. As the system temperature increased at constant pressure (10.4 MPa), the cumulative extraction yield decreased from 22.4 wt% (339 K) to 11.2 wt% (422 K). The volatility (quality) of the 2nd window extract phase increased from 62.4 wt% (339 K) to 83.4 wt% (422 K). Thus at constant temperature, as the extraction pressure increased the extraction yields increased and produced heavier or poorer quality hydrocarbon liquids. In contrast, at constant pressure as the extraction temperature increased extraction yields decreased but produced refined hydrocarbon liquids. These are similar to the observations made for the AR bitumen-propane system and hence these observations could be generalized for other feedstocks also.

Reproducibility

SFE experiments were conducted at 10.4 MPa (P_r=2.3) and 339 K (T_r=1.03) using the SS bitumen to demonstrate the reproducibility of the experimental results. The extraction yields obtained in these experiments are presented in Figure 54. The difference between the extraction yields is within 5% and hence it was concluded that the experimental results were reproducible.

Pressure Effect

Cumulative extraction yields were obtained for the four bitumens at a constant temperature of 380 K (T_r=1.03) and at three pressures 5.6 MPa (P_r=1.2), 10.4 MPa (P_r=2.3) and 17.3 MPa (P_r=4.1). Plots of cumulative extraction yields versus system pressure for the bitumens are presented in Figure 55. As the system pressure increased at constant temperature the cumulative extraction yields increased. As discussed before,

Figure 54.

Reproducibility for SFE with the Sunnyside Bitumen at 10.4 MPa (P_r=2.3) and 339 K (T_r=0.92)

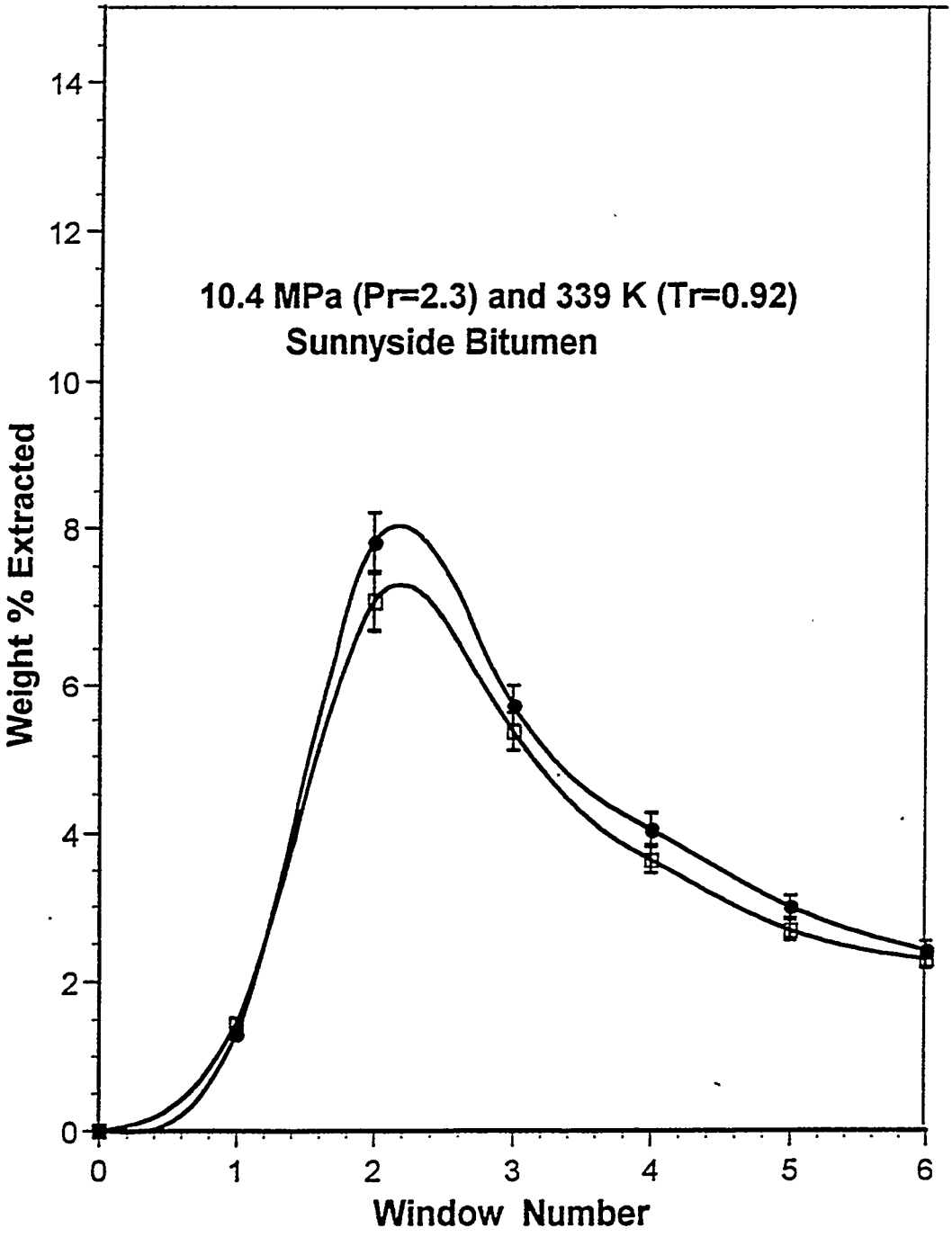
10.4 MPa (Pr=2.3) and 339 K (Tr=0.92)
Sunnyside Bitumen
Weight % Extracted
Window Number
0
2
4
6
8
10
12
14
0
1
2
3
4
5
6

Figure 55.

Effect of Pressure on the Extraction Yields for the Four Bitumens from the Uinta Basin at Constant Temperature 380 K (Tr=1.03)

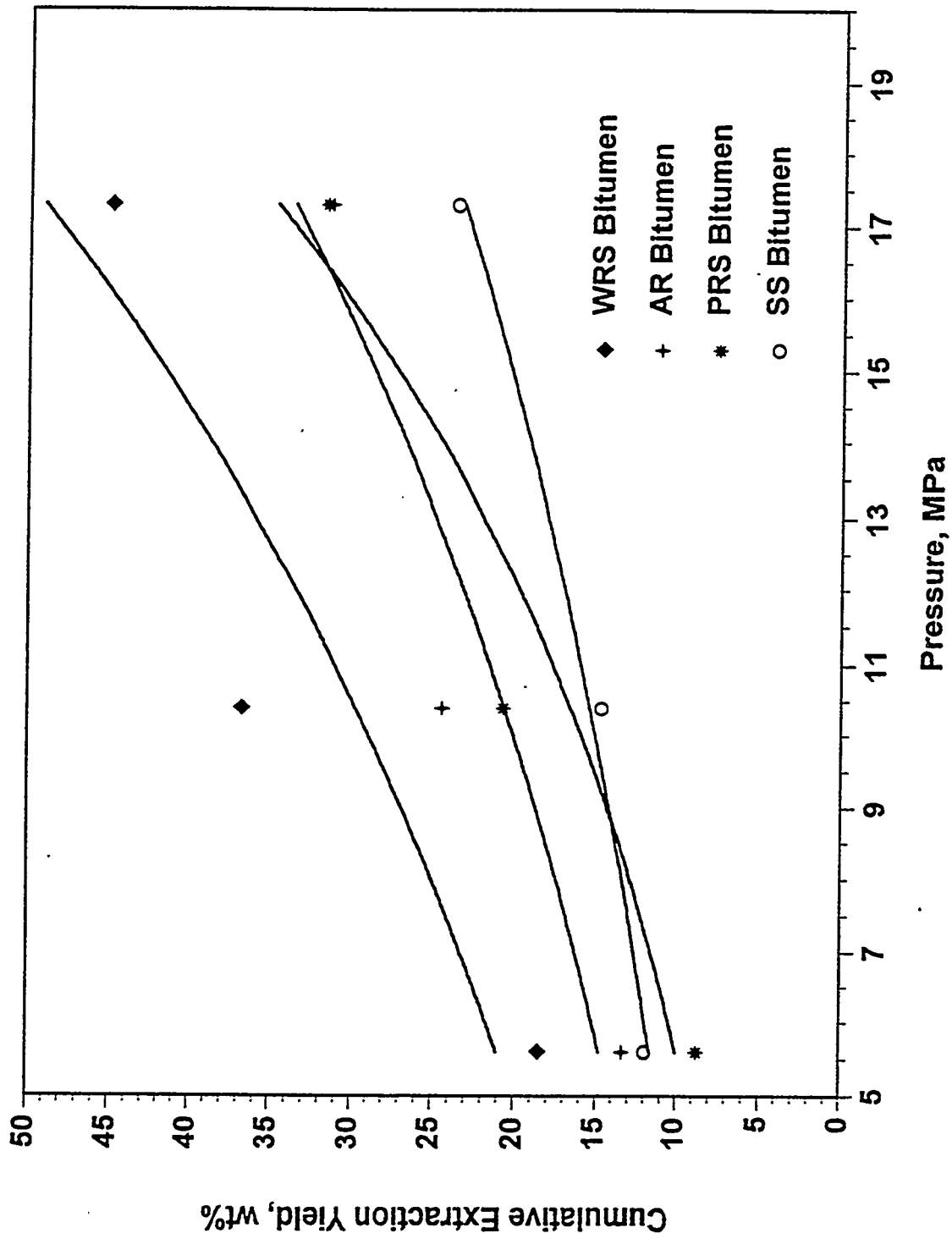
Cumulative Extraction Yield, wt%
0
5
10
15
20
25
30
35
40
45
50
5
7
9
11
13
15
17
19
Pressure, MPa
WRS Bitumen
AR Bitumen
PRS Bitumen
SS Bitumen

the increase in extraction yields has been attributed to the increase in the solvent density with increased pressure at constant temperature for a particular bitumen. Moreover, the WR bitumen gave the maximum yield at all three pressures, the AR bitumen gave the second highest yields, and the SS bitumen gave the lowest. The PRS extraction yields were intermediate between the yields for the AR and SS bitumens. The WR bitumen extraction yields were 6 to 10 % (absolute) more than those of the AR Bitumen. The AR bitumen yields were 1 to 5 % more than PRS bitumen. The PRS bitumen extraction yields were 1 to 7 % greater than the yields for the more refractory SS bitumen. The ranking for the four bitumens according to extraction yield as follows:

Whiterocks > Asphalt Ridge > PR Spring > Sunnyside

This ranking is similar to the ranking observed when the physical (specific gravity, Conradson carbon and viscosity) and chemical (asphaltene and resin contents) properties of the four bitumens are compared. The bitumen (WR) judged to possess superior physical and chemical properties gave greater extraction yields compared to the bitumen (SS) judged to possess inferior physical and chemical properties. Thus, the difference in the cumulative extraction yields amongst four bitumens at a particular temperature could be attributed to their physical and chemical properties.

Temperature Effect

The effect of temperature on the cumulative extraction yield at a constant pressure of 10.4 MPa (P_r=2.3) for the four bitumens is presented in Figure 56. As the system temperature increased at constant pressure, the cumulative extraction yield decreased for the four bitumens. The decrease in the extraction yields with increase in temperature was

Figure 56.

Effect of Temperature on the Extraction Yields for the Four Bitumens from the Uinta Basin at Constant Pressure 10.4 MPa (Pr=2.3)

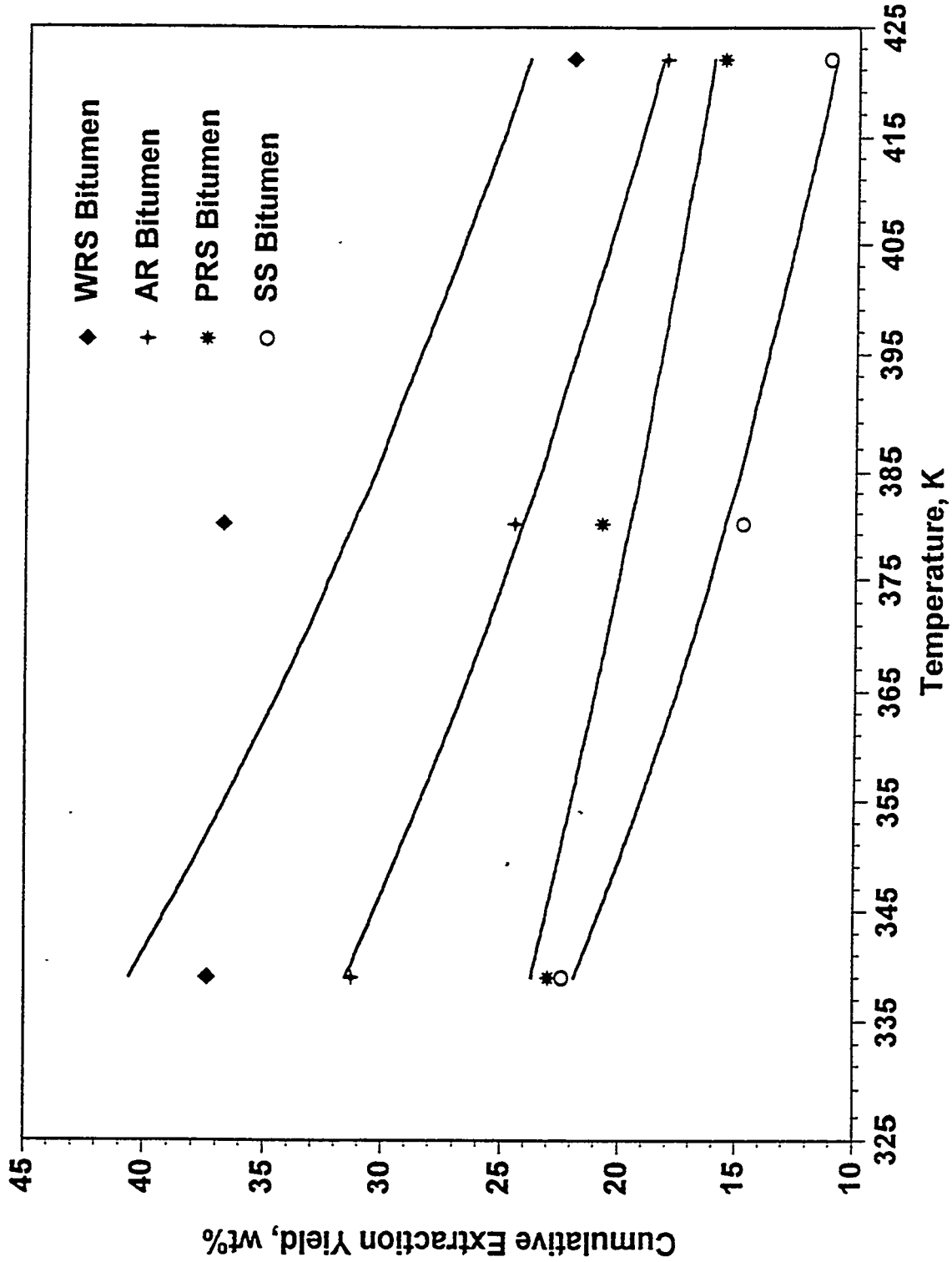
WRS Bitumen
AR Bitumen
PRS Bitumen
SS Bitumen
Cumulative Extraction Yield, wt%
Temperature, K
45
40
35
30
25
20
15
10
325
335
345
355
365
375
385
395
405
415
425

attributed to the decrease in solvent density as the temperature increased. The cumulative extraction yields for the WR bitumen were highest and were 10 to 12 wt% greater than those for the AR bitumen. The extraction yields of SS bitumen were lowest, and were 2 to 6 wt% less than those for the PRS bitumen. The AR bitumen and PRS extraction yields were intermediate with the former yields 2 to 7 wt% higher than that of PRS bitumen. Thus, the order as indicated by the extraction yields was as follows:

Whiterocks > Asphalt Ridge > PR Spring > Sunnyside

This ranking is similar to the ranking observed with the pressure effects. The cumulative extraction yields for the four bitumens should remain the same if the extraction yields were solely governed by the operating pressure and temperature of the SFE. However, it was observed that the four bitumens exhibited different extraction yields at the same operating conditions with the order as shown above. Thus, the extraction yields of the bitumen are not only governed by the operating parameters but also by the feedstock physical and chemical make up. The bitumen with the lowest specific gravity, Conradson carbon, viscosity, asphaltene and highest resin content (WR bitumen) exhibited higher extraction yields than the other three bitumens. The SS bitumen that had the highest specific gravity, Conradson carbon, viscosity, asphaltene and lowest resin content gave lowest extraction yield. The AR bitumen and PRS bitumen extraction yields were in the intermediate range with AR bitumen yield greater than those of the PRS bitumen. This was consistent with the perception that the AR bitumen was of a higher quality than the PRS bitumen. The effect of chemical make up of the bitumen on the extraction yield is discussed in detail in the subsequent sections.

Solvent Density Effect

The cumulative extraction yields at all five operating conditions for the four bitumens are plotted against the pure propane solvent density in Figure 57. The pure solvent densities were measured in a separate experiment and are reported in Table 14. The cumulative extraction yields increased with increase in solvent density. As indicated previously, the WR bitumen gave the highest extraction yields at all five operating conditions whereas the SS bitumen gave the lowest yields. Thus, the ranking of the four bitumens according to extraction yields:

Whiterocks > Asphalt Ridge > PR Spring > Sunnyside

was the same for each of the process variables studied: This would seem to indicate that it may be possible to link process extraction yields to key chemical and physical attributes of the bitumens.

The measured extract phase densities for the AR and SS bitumens at all the five operating conditions were plotted against extraction time and are presented in Figures 42 and 49, respectively. It can be observed from these plots that the starting extract phase densities at 17.3 MPa (P_r=3.2) and 380 K (T_r=1.03) were 0.71 and 0.604 g/cm3 for the AR and SS bitumens, respectively. The corresponding cumulative extraction yield for the AR bitumen was higher at 31.4 wt% compared to SS bitumen at 23.7 wt%. Thus, the higher extraction yield for the AR bitumen relative to the SS bitumen at same solvent density could be attributed to the chemical make up of the bitumens. Similar observations could be made for the AR bitumen at the other four operating conditions, where the starting extract phase density and corresponding extraction yields were higher than for the SS bitumen.

Figure 57.

Effect of Solvent Density on the Extraction Yields for the Four Bitumens from Uinta Basin

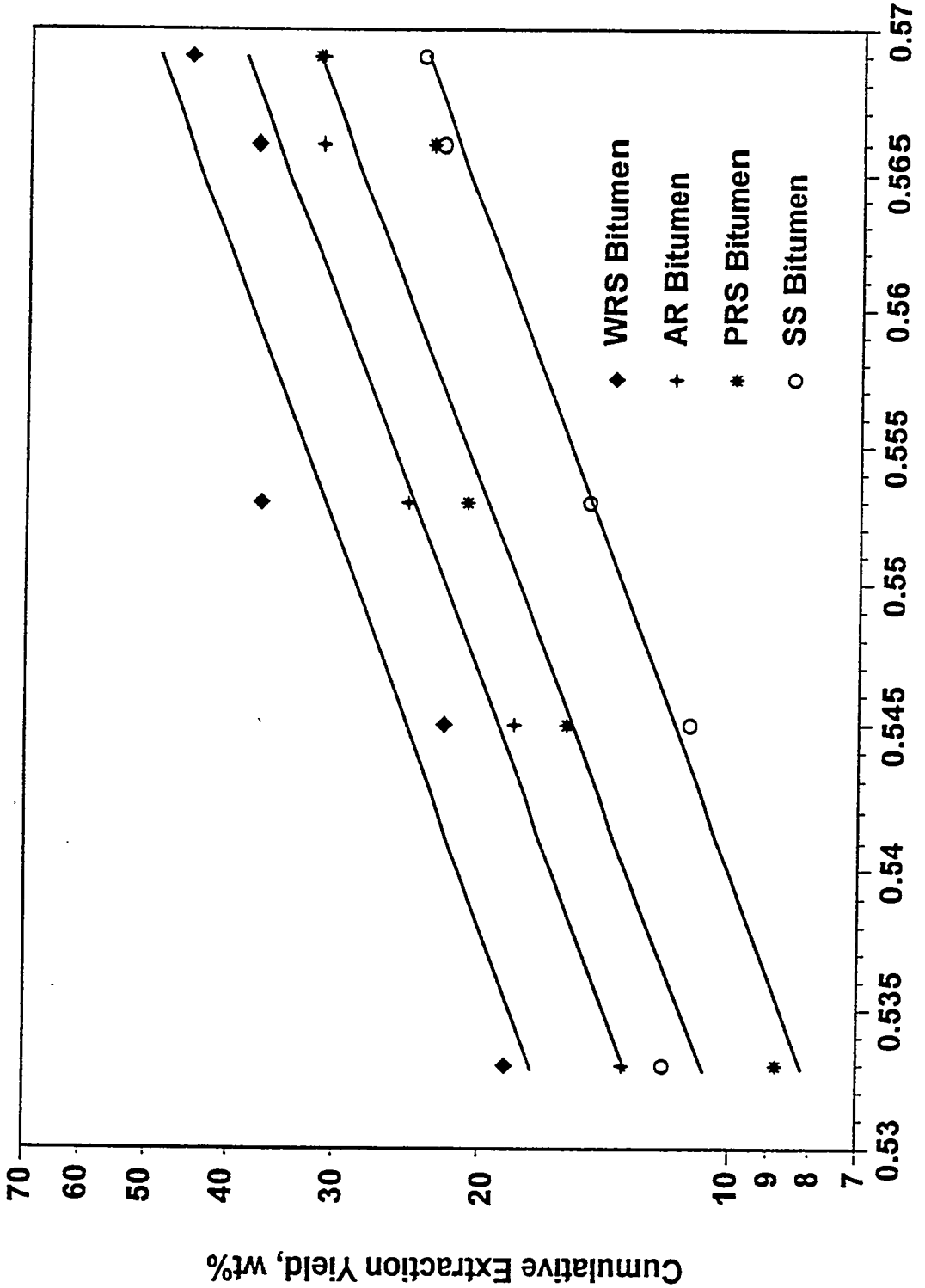
Cumulative Extraction Yield, wt%
70
60
50
40
30
20
10
9
8
7
0.53
0.535
0.54
0.545
0.55
0.555
0.56
0.565
0.57
Solvent Density, g/cc
WRS Bitumen
AR Bitumen
PRS Bitumen
SS Bitumen

Effect of Bitumen Asphaltene Content

The extraction yields were different for the four bitumens under investigation at the same temperature, pressure and solvent density. This could be attributed to the difference in the chemical nature of the bitumens (Table 11). The asphaltene contents of the four bitumens varied from 2.9 wt% (WR) to 23.6 wt% (SS). The cumulative extraction yields obtained at the five different operating conditions for the four bitumens were plotted against the asphaltene content of the feedstocks and are presented in Figure 58. It is observed from the plot that as the asphaltene contents of the bitumens increased from 2.9 wt% for the WR bitumen to 23.6 wt% for the SS bitumen, the cumulative extraction yields decreased.

The WR bitumen that had the lowest asphaltene (2.9 wt%) content gave the highest extraction yields at all five operating conditions. The SS bitumen with an asphaltene content of 23.6 wt% gave the lowest extraction yields. The AR (6.7 wt%) and PRS bitumens (19.3 wt%) extraction yields were intermediate with the AR extraction yields higher than the PRS yields at all five conditions.

It was established by Speight (65) that for a bitumen sample, the amount of asphaltene precipitated increased exponentially from 18 wt% to 48 wt% when the solvent was switched from pentane to propane. The difference in the propane and pentane soluble fractions is related to the resin molecules present in the bitumens. It should be noted that the highest resin content was 54.5 wt% for the WR bitumen whereas the lowest resin content was 36.8 wt% for the SS bitumen. The AR and PRS bitumens fall in the intermediate range with AR bitumen resin content (44.1 wt%) higher than the PRS bitumen resin content (43.8 wt%). Thus, the bitumen (WR) that had lowest pentane

Figure 58.

Relationship Between Asphaltene Content and Extraction Yield for the Four Uinta Basin Bitumens

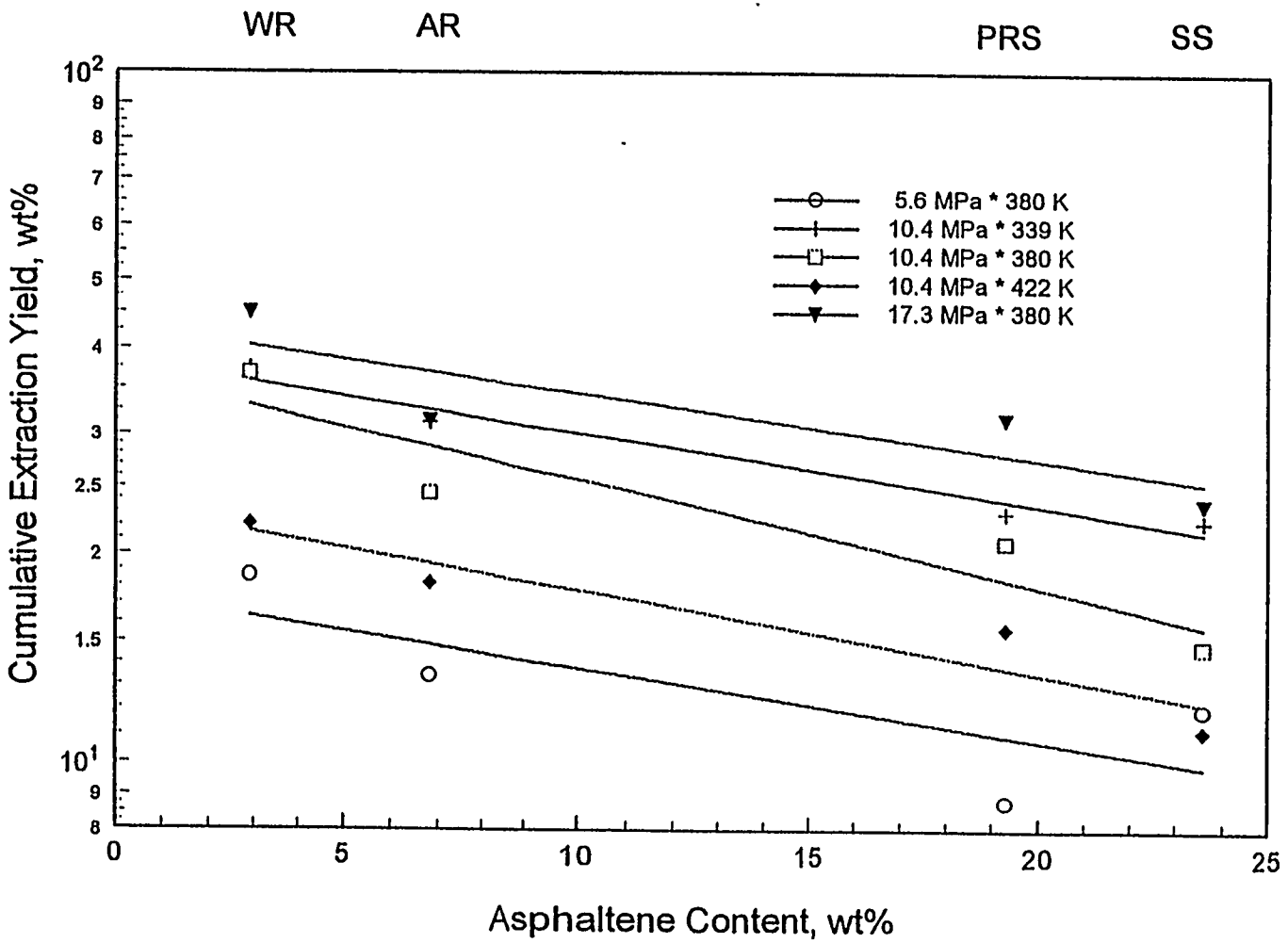
WR
AR
PRS
SS
5.6 MPa * 380 K
10.4 MPa * 339 K
10.4 MPa * 380 K
10.4 MPa * 422 K
17.3 MPa * 380 K
Cumulative Extraction Yield, wt%
Asphaltene Content, wt%
10^2
9
8
7
6
5
4
3
2.5
2
1.5
10^1
9
8
0
5
10
15
20
25

insolubles and highest resin content was expected (assuming equal increase in asphaltene content from pentane to propane insolubles) to have the lowest propane insolubles compared to the SS bitumen (highest pentane insolubles and lowest resin content). The AR and PRS bitumen propane insolubles were expected to fall in the intermediate range with AR bitumen propane insolubles lower than the PRS bitumen insolubles. As stated in the earlier section, the maximum extraction yield obtainable using supercritical propane will be equal to or less than the maximum deasphalted oil obtainable using liquid propane. Thus, the amount of propane soluble fractions available for extraction is in the order:

Whiterocks > Asphalt Ridge > PR Spring > Sunnyside

Thus, the WR bitumen that would have highest propane soluble fractions (largest fraction available for extraction since asphaltene was not extracted) gave a higher extraction yield than the other bitumens at all five operating conditions. The SS bitumen was extracted least and the AR and PRS bitumens extraction yields fell in the intermediate range with the AR bitumen yields higher than the PRS bitumen yields. The pentane insoluble test performed on the AR and SS extract samples (2nd window at 10.4 MPa and 339 K) did not yield any precipitate. Thus, the relationship established between the asphaltenes and extraction yields indicates that the asphaltenes (pentane insolubles) played a significant role in decreasing the extraction yield of bitumens and asphaltenes were not transferred to the extract phase.

Effect of Bitumen Resin Content

The resin contents of the four feedstocks are plotted against the cumulative extraction yields obtained for the SFE of the bitumens at the five different operating

conditions in Figure 59. It is observed from the plot that as the resin content of the feedstock decreased from 54.5 to 36.8 wt%, the cumulative extraction yields decreased. The WR bitumen had the highest resin content, 54.5 wt%, and the lowest asphaltene content, and gave the highest extraction yields relative to the other bitumens. The SS bitumen that had the lowest resin content (36.8 wt%) and the highest asphaltene content gave the lowest extraction yields at all the five operating conditions. The AR bitumen (44.1 wt%) extraction yields were lower than those of the WR bitumen and marginally higher than those of the PRS bitumen (43.8 wt%) at all five conditions. This trend is similar to the observation made for the asphaltene contents of the bitumens.

Effect of Bitumen Saturate and Aromatics Content

No clear trends were observed based on the saturates and aromatics contents of the bitumens. It was expected that the AR bitumen (saturates content 39.2 wt%) which had the highest saturates content should have given high extraction yields similar to those of the WR bitumen (saturates content 35.7 wt%); however, the WR bitumen gave higher extraction yields than the AR bitumen at all five operating conditions. The PRS (saturates content 33.4 wt%) and SS bitumens (saturates content 20.0 wt%) again gave intermediate extraction yields with the PRS bitumen yields lower than those of the AR bitumen and higher than those of the SS bitumen. It was also observed that the cumulative extraction yields for the WR, PRS and SS bitumens increased with increase in the volatility (fraction boiling below 811 K). It was expected that the AR bitumen with the greater volatility and the highest saturates content would exhibit higher extraction yields than the WR bitumen;

Figure 59.

Relationship Between Resin Content and Extraction Yield for the Four Uinta Basin Bitumens

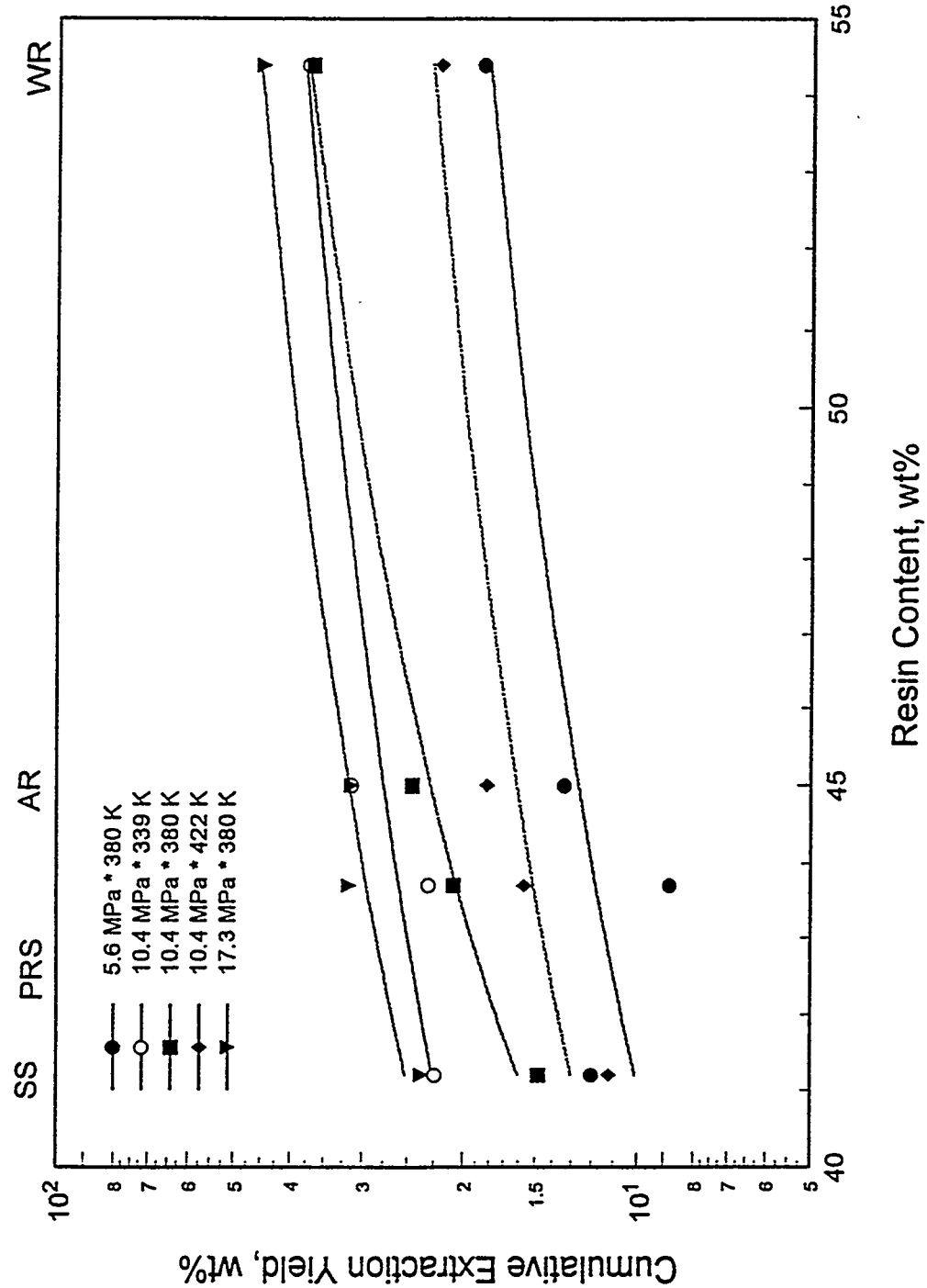
SS
PRS
AR
WR
5.6 MPa * 380 K
10.4 MPa * 339 K
10.4 MPa * 380 K
10.4 MPa * 422 K
17.3 MPa * 380 K
Cumulative Extraction Yield, wt%
Resin Content, wt%
10^2
10^1
8
7
6
5
4
3
2
1.5
8
7
6
5
40
45
50
55

however, the experimental results indicted that the AR yields were lower than those obtained for the WR bitumen at all five operating conditions.

An explanation for this behavior is proposed based on the boiling point distributions of the bitumen solubility fractions. A comparison has been made in Table 15 of the contributions from the solubility fractions to the volatility (<811 K) and to fraction boiling below 973 K for the four bitumens. It is observed from Table 15 that the WR, AR, PRS and SS bitumens volatilities were 46.6, 53.5, 45.4 and 40.9 wt%, respectively. As explained before, no clear trend was observed when an attempt was made to correlate cumulative extraction yields based on the volatilities of the bitumens. The fractions boiling below 811 K consisted of saturate, aromatics, resin and asphaltene solubility fractions. The contribution to the volatility from the asphaltene class of compounds was small compared to the contributions from other three solubility classes. The trend observed in Figure 60 could not be explained based on the estimated contribution to the volatility from the three solubility classes since the AR bitumen had a higher concentration of these classes than the WR bitumen (Table 15) which exhibited the apparent anomalous behavior.

All the extract phase samples were characterized using a simulated distillation technique with a maximum boiling point of 973 K. The AR and SS extract phase samples (2^{nd} extract window samples produced at 10.4 MPa and 339 K) were subjected to pentane insoluble analysis. The test results confirmed that these extract phase samples did not contain asphaltene solubility class compounds. Based on the boiling point distributions of the saturates, aromatics and resins fractions for the four bitumens, the contribution towards the bitumen solubility fractions boiling below 973 K was estimated on a prorated basis relative to the corresponding three solubility classes in the respective bitumens and is

Table 15

Comparison of Boiling Fractions for Four Bitumens

Properties	Whiterocks Bitumen	Asphalt Ridge Bitumen	PR Spring Bitumen	Sunnyside Bitumen
Asphaltenes[a], wt %	2.9	6.8	19.3	23.6
Saturates, wt %	35.7	39.2	33.4	20.0
Aromatics, wt %	7.0	9.0	3.6	15.1
Resins, wt %	54.5	44.1	43.8	36.8
Simulated Distillation				
Volatility(<811 K) of Bitumen, wt%	46.6	53.5	45.4	40.9
Volatility (<811 K) of Saturates, wt%	81.2	86.2	78.5	84.1
Volatility (<811 K) of Aromatics, wt%	28.5	23.2	40.9	30.2
Volatility (<811 K) of Resins, wt%	21.6	20.4	29.8	19.0
Contribution from Saturates + Aromatics and Resin towards Volatility (<811 K) of Bitumen[b]	42.7	44.9	40.7	28.4
Boiling Fraction (< 973 K) of Bitumen, wt%	78.7	90.1	78.1	73.4
Boiling Fraction (< 973 K) of Saturates, wt%	99.8	100.0	99.4	99.6
Boiling Fraction (< 973 K) of Aromatics, wt%	71.4	56.5	80.3	72.9
Boiling Fraction (< 973 K) of Resins, wt%	56.3	54.7	62.4	55.0
Contribution from Saturates + Aromatics and Resin towards Boiling Fraction (< 973 K) of Bitumen[b]	71.3	68.40	63.4	51.2

[a] Pentane Insolubles

[b] Estimated on prorated basis

Figure 60.

Relationship Between Saturates Content and Extraction Yield for the Four Uinta Basin Bitumens

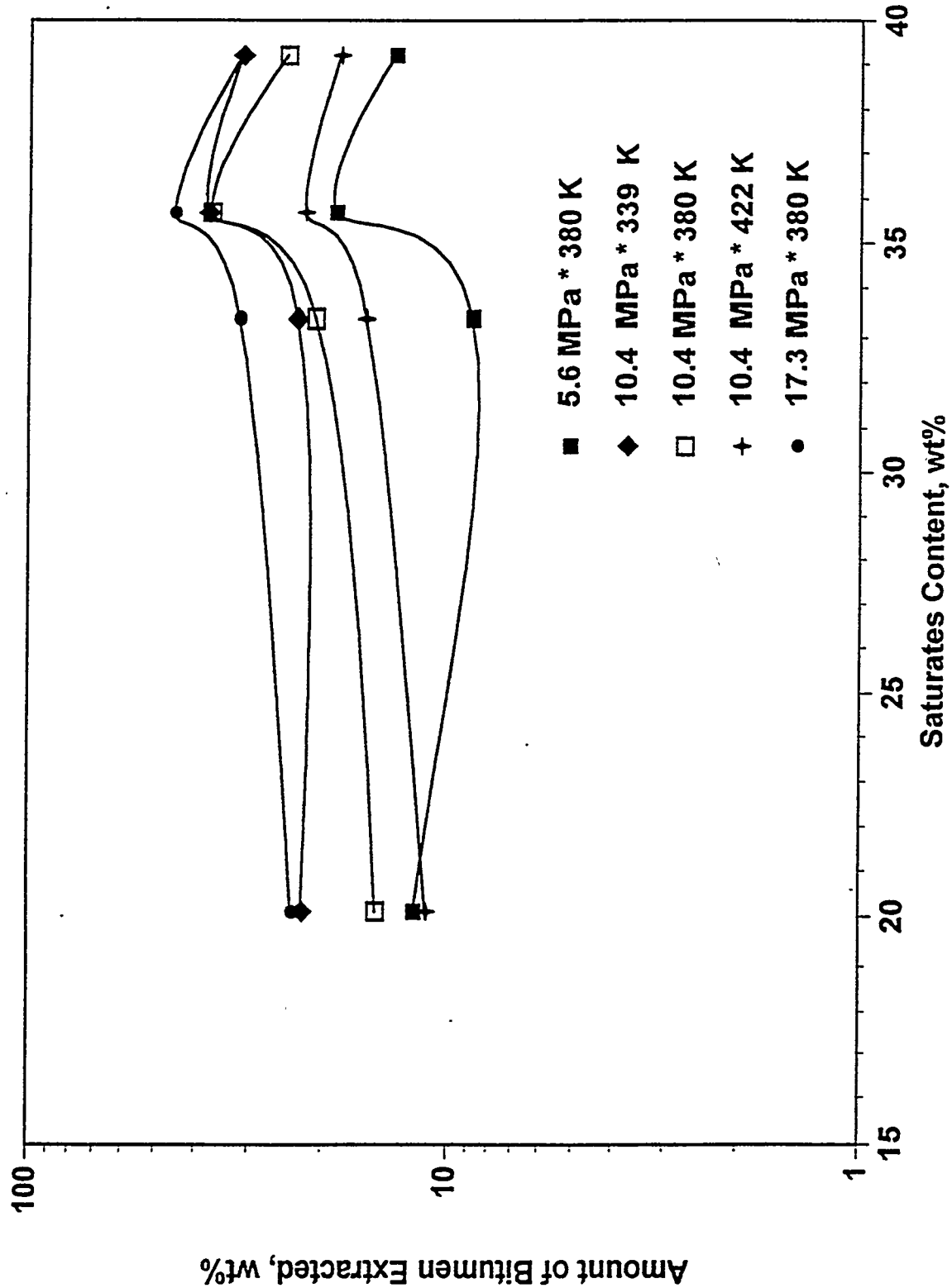
Amount of Bitumen Extracted, wt%
100
10
1
15
20
25
30
35
40
Saturates Content, wt%
5.6 MPa * 380 K
10.4 MPa * 339 K
10.4 MPa * 380 K
10.4 MPa * 422 K
17.3 MPa * 380 K

presented in Table 15. These estimated values indicated that the WR bitumen had the highest extractable (saturates, aromatics and resins) 973 K minus fraction: 71.3 wt% and the SS bitumen had the lowest extractable 973 minus fraction: 51.2 wt%. The AR and PRS bitumens extractable 973 K minus fractions fell in the intermediate range with the AR bitumen 973 K minus fraction (68.4 wt%) higher than that of the PRS bitumen (63.4 wt%). The experimental results also indicated that at all five extraction conditions, the WR bitumen yield was greater than those obtained for the other three bitumens. The refractory SS bitumen gave the lowest extraction yields whereas the AR and PRS bitumen were in the intermediate range with the AR bitumen yields greater than the yields for the PRS bitumen.

Thus, the cumulative extraction yield trend obtained from the SFE of the four bitumens using propane as solvent was controlled by the extractable solubility class compounds present in the 811 K plus and 973 K minus range.

Compositional Analyses of Residual Fraction

The residual fractions in the extractor at the completion of each extraction experiment were fractionated into saturates, aromatics, resins and asphaltenes using adsorption chromatography. The fractionation technique is outlined in Appendix D. The fractionations of the residual fractions were performed to determine the nature of the material left behind in the extractor.

The results of the compositional and elemental analyses of the residual fractions obtained from SFE of the four bitumens at five different operating conditions are presented in Tables 16 through 19.

Table 16
Summary of Extraction Yields and Residual Fractions Analyses for the Whiterocks Bitumen

Pressure (MPa)	5.6	10.4	10.4	10.4	17.3
Reduced Pressure	1.2	2.3	2.3	2.3	4.1
Temperature (K)	380	339	380	422	380
Reduced Temperature	0.92	1.03	1.03	1.03	1.14
Solvent Density, g/cc	0.533	0.566	0.553	0.545	0.569
Product Yields (wt%)					
Extract Phase	20.0	40.0	39.0	24.0	48.0
Residual Phase	79.0	59.0	58.0	73.0	50.0
Residual Phase SARA Analyses					
Saturates & Aromatics, wt%	24.9	15.5	20.1	27.0	0.0
Resins, wt%	63.7	74.5	64.5	62.2	76.5
Asphaltenes, wt%	11.4	10.0	15.4	10.8	23.5
Asphaltenes, wt% (Expected)	3.7	4.9	5.0	4.0	5.8
Residual Phase Elemental Analysis[a]					
C, wt%	86.8	86.7	86.7	86.7	86.8
H, wt%	11.0	10.8	10.8	11.1	10.6
N, wt%	1.8	2.0	2.0	1.8	2.1
S, wt%	0.5	0.5	0.5	0.5	0.5
H/C Atomic Ratio	1.52	1.50	1.49	1.53	1.46

a) Normalized to 100%

Table 17
Summary of Extraction Yields and Residual Fractions Analyses for the Asphalt Ridge Bitumen

Pressure (MPa)	5.6	10.4	10.4	10.4	17.3
Reduced Pressure	1.2	2.3	2.3	2.3	4.1
Temperature (K)	380	339	380	422	380
Reduced Temperature	0.92	1.03	1.03	1.03	1.14
Solvent Density, g/cc	0.533	0.566	0.553	0.545	0.569
Product Yields (%)					
Extract Phase	13.4	31.3	24.5	18.2	31.4
Residue Phase	86.6	68.7	75.5	81.8	68.6
Residual Phase SARA Analyses					
Saturates, wt%	22.6	5.5	13.3	18.8	4.1
Aromatics, wt%	3.5	1.6	2.3	4.9	1.4
Resins, wt%	58.9	60.0	61.9	59.5	56.5
Asphaltene, wt%	15.0	33.0	22.5	16.8	38.0
Asphaltene, wt% (Expected)	7.8	9.9	9.0	8.3	9.9
Residual Phase Elemental Analysis[a)]					
C, wt%	87.38	87.29	87.00	87.11	87.18
H, wt%	10.90	10.50	10.66	11.00	10.91
N, wt%	1.21	1.73	1.85	1.42	1.43
S, wt%	0.50	0.49	0.49	0.47	0.48
H/C Atomic Ratio	1.50	1.44	1.47	1.51	1.50

a) Normalized to 100.0 %

Table 18
Summary of Extraction Yields and Residual Fractions Analyses for the PR Spring Bitumen

Pressure (MPa)	5.6	10.4	10.4	10.4	17.3
Reduced Pressure	1.2	2.3	2.3	2.3	4.1
Temperature (K)	380	339	380	422	380
Reduced Temperature	0.92	1.03	1.03	1.03	1.14
Solvent Density, g/cc	0.533	0.566	0.553	0.545	0.569
Product Yields (%)					
Extract Phase	8.8	23.0	20.8	15.7	31.7
Residual Phase	91.2	77.0	79.2	84.3	68.3
Residual Phase SARA Analyses					
Saturates & Aromatics, wt%	29.3	22.7	10.0	21.0	10.8
Resins, wt%	50.3	42.0	53.8	52.6	37.1
Asphaltenes, wt%	20.4	35.3	36.2	26.4	52.0
Asphaltenes, wt% (Expected)	21.2	25.1	24.4	22.9	28.3
Residual Phase Elemental Analysis[a)]					
C, wt%	87.4	87.4	87.3	87.3	87.4
H, wt%	11.0	10.5	10.8	11.0	10.6
N, wt%	1.1	1.4	1.3	1.1	1.4
S, wt%	0.5	0.7	0.6	0.6	0.6
H/C Atomic Ratio	1.50	1.44	1.47	1.50	1.44

a) Normalized to 100%

Table 19
Summary of Extraction Yields and Residual Fractions Analyses for the Sunnyside Bitumen

Pressure (MPa)	5.6	10.4	10.4	10.4	17.3
Reduced Pressure	1.2	2.3	2.3	2.3	4.1
Temperature (K)	380	339	380	422	380
Reduced Temperature	0.92	1.03	1.03	1.03	1.14
Solvent Density, g/cc	0.533	0.566	0.553	0.545	0.569
Product Yields (%)					
Extract Phase	12.0	22.4	14.8	11.2	23.7
Residual Phase	88.0	77.6	85.2	88.8	76.3
Residual Phase SARA Analyses					
Saturates, wt%	13.3	3.3	5.4	16.7	1.3
Aromatics, wt%	7.3	1.2	3.5	6.8	1.5
Resins, wt%	51.5	37.1	35.9	40.2	37.0
Asphaltene, wt%	37.9	58.4	55.2	36.3	60.3
Asphaltene, wt% (Expected)	26.8	30.4	27.7	26.6	30.9
Residual Phase Elemental Analysis[a)]					
C, wt%	87.41	87.20	87.31	87.32	86.72
H, wt%	10.40	10.14	10.28	10.60	9.86
N, wt%	1.08	1.42	1.17	1.02	1.41
S, wt%	1.11	1.23	1.24	1.05	1.23
H/C Atomic Ratio	1.43	1.39	1.41	1.46	1.36

a) Normalized to 100%

Saturates Content of Residual Fractions

A partial SARA analysis was performed on the residual fractions from the SFE of the WR and PRS bitumens by Subramanian (64) without fractionating the saturates and aromatics into saturates, aromatics I and II using neutral alumina. Hence, the results were reported as saturates and aromatics. However, the residual fractions from SFE of the AR and SS bitumens were subjected to complete fractionation into saturates, aromatics, resins and asphaltenes.

The saturates and aromatics contents of the WR and PRS bitumen are compared with the saturates and aromatics contents of their respective residual fractions obtained at all five operating conditions in Figures 61 and 62. The solvent densities are plotted against the saturates and aromatic contents instead of operating variables pressure and temperature, because the extraction yields were proportional to the solvent density, which represents the severity of operation in SFE processes. The saturates and aromatics contents of the residual fractions for the WR and PRS bitumens were lower than the saturates and aromatics contents of the respective bitumens, and in general decreased with increase in solvent density (severity of operation). Thus, it was concluded that as the solvent density or the severity of operation or the extraction yields increased more and more of the saturates and aromatics were extracted. It has also been pointed out in the earlier sections that the cumulative extraction yields increased with increase in the solvent density meaning more of the saturates and aromatics were removed in the process. Moreover, the resin contents (Tables 16 through 19) of the residual fractions obtained during the SFE of four bitumens were higher than the resin contents of the original bitumens except for the PRS bitumen at two operating conditions where the solvent densities are higher compared to the

Figure 61.

Effect of Solvent Density on the Extraction of Saturates and Aromatics from the Whiterocks Bitumen

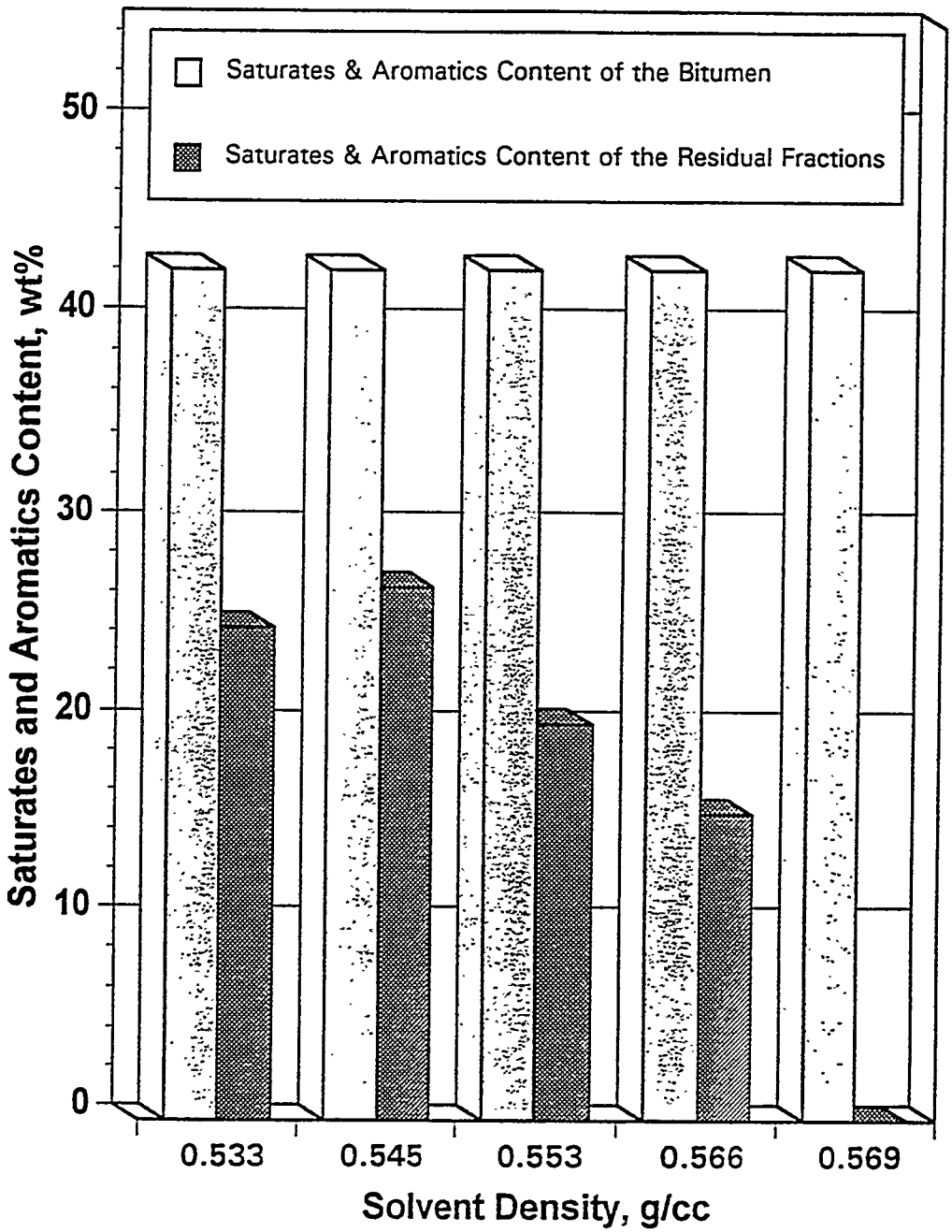
Saturates & Aromatics Content of the Bitumen
Saturates & Aromatics Content of the Residual Fractions
Saturates and Aromatics Content, wt%
50
40
30
20
10
0
0.533
0.545
0.553
0.566
0.569
Solvent Density, g/cc

Figure 62.

Effect of Solvent Density on the Extraction of Saturates and Aromatics from the PR Spring Bitumen

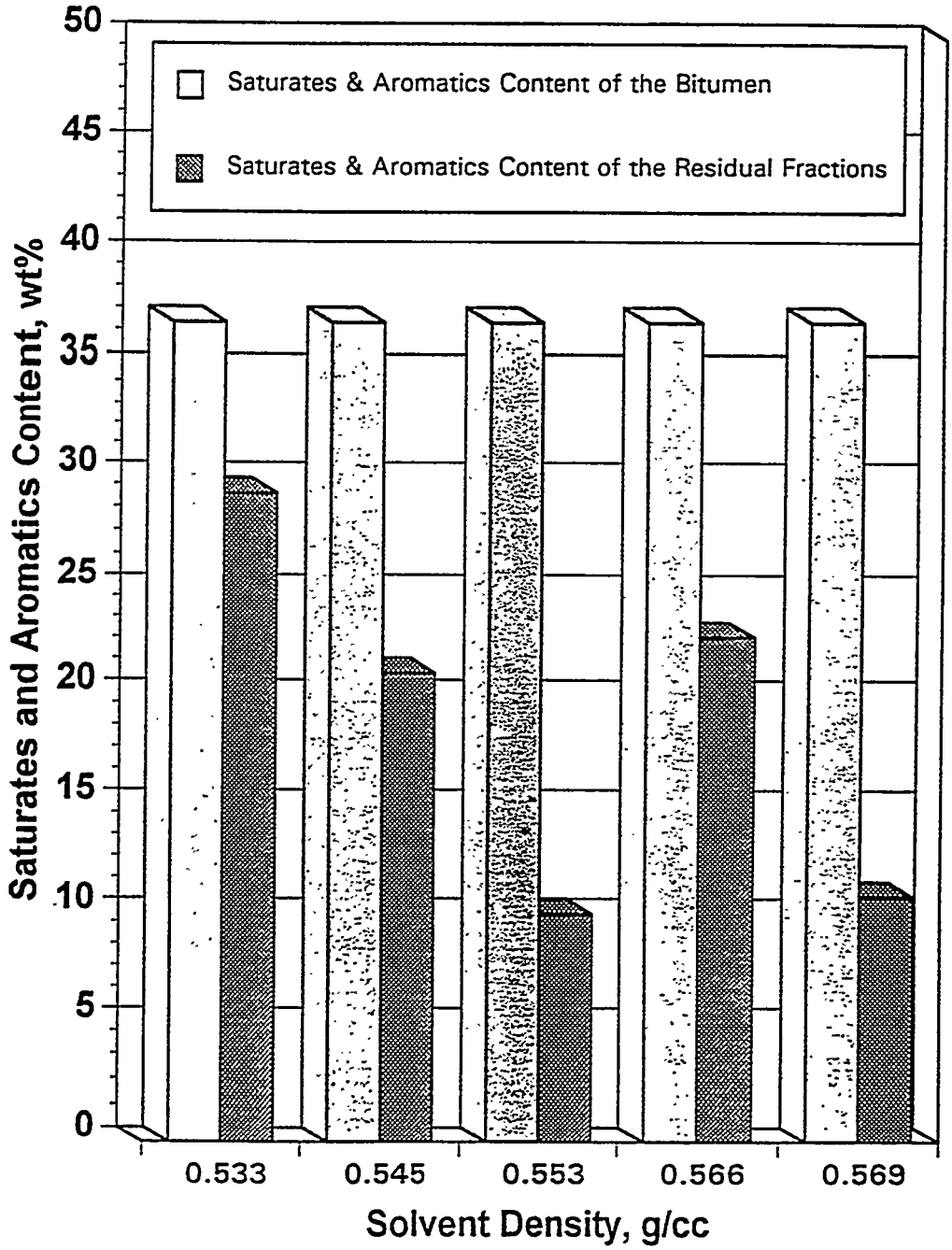
Saturates & Aromatics Content of the Bitumen
Saturates & Aromatics Content of the Residual Fractions
Saturates and Aromatics Content, wt%
50
45
40
35
30
25
20
15
10
5
0
0.533
0.545
0.553
0.566
0.569
Solvent Density, g/cc

other three conditions. This indicates that the contribution to the extract phases from resins was less than that from the saturates and aromatics. Analyses of selected extract samples indicated that no asphaltenes (pentane insolubles) were present. Thus, it was concluded that propane preferentially extracted saturates and aromatics from bitumens at the expense resins and asphaltenes.

The saturates contents of the AR and SS bitumens and the respective residual fractions have been plotted and are presented in Figures 63 and 64. The trends are similar to those reported for the WR and PRS bitumens. This led to the conclusion that the saturates and aromatics were preferentially extracted by propane compared to the asphaltenes and resins.

Asphaltene Content of Residual Fractions

The residual fractions of the four bitumens after SFE were mixed with excessive amounts of n-pentane to yield pentane insolubles, i.e., asphaltenes. The asphaltene content of the residual fractions was examined to determine the effect of process variables on the removal or rejection of the asphaltenes and also to investigate the nature of the unextracted residual fraction.

The measured asphaltene content of the residual fractions is compared with the expected asphaltene content of the residual fractions and the asphaltene content of the respective bitumens in Figures 65 through 68. The expected asphaltene contents of the residual fractions were calculated on a prorated basis relative to the amount of bitumen charged to the extractor and assuming that all the asphaltenes remained in the residual fractions. Selected extract samples from SFE of the AR and SS bitumens at 10.4 MPa

Figure 63.

Effect of Solvent Density on the Extraction of Saturates from the Asphalt Ridge Bitumen

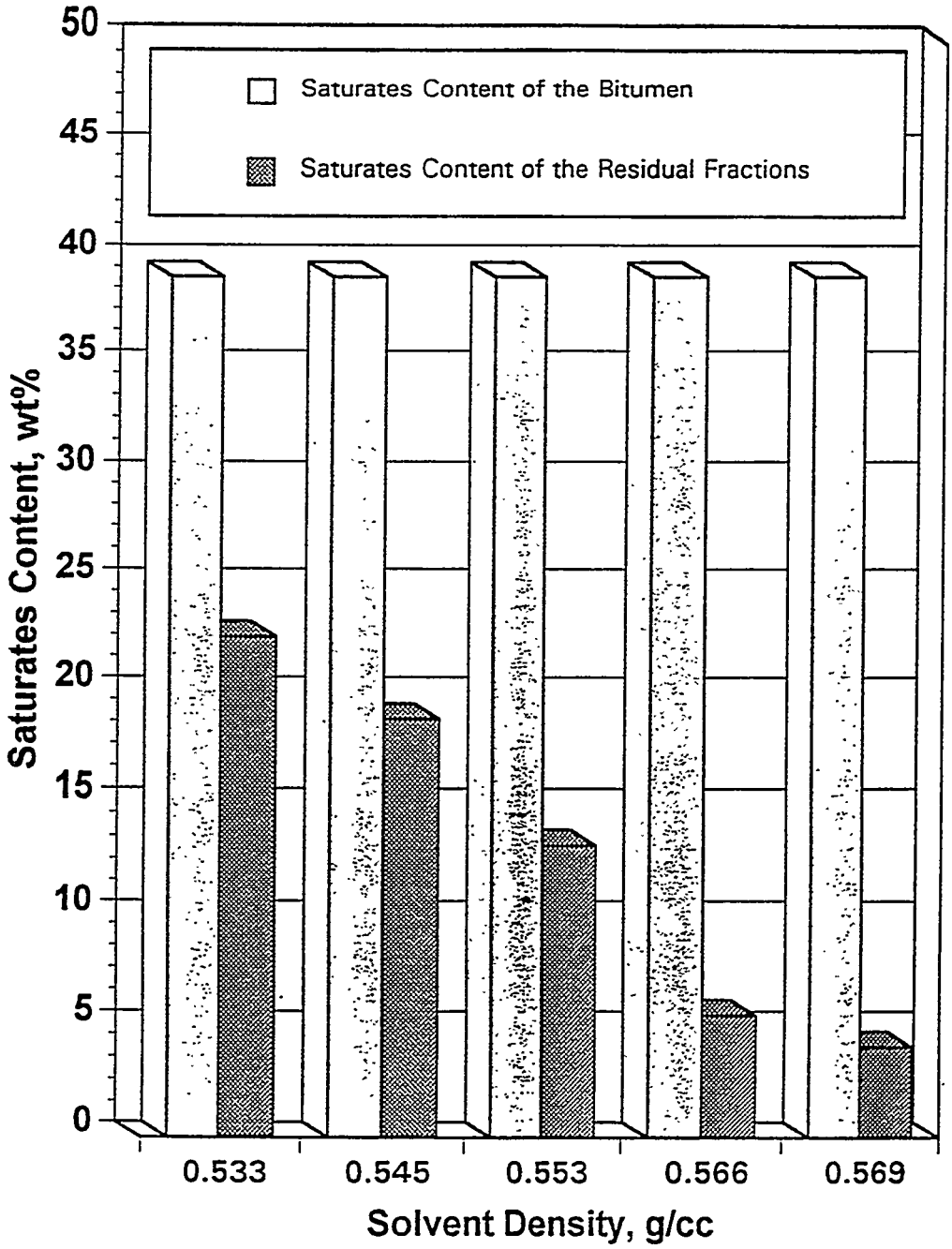
Saturates Content of the Bitumen
Saturates Content of the Residual Fractions
Saturates Content, wt%
50
45
40
35
30
25
20
15
10
5
0
0.533
0.545
0.553
0.566
0.569
Solvent Density, g/cc

Figure 64.

Effect of Solvent Density on the Extraction of Saturates from the Sunnyside Bitumen

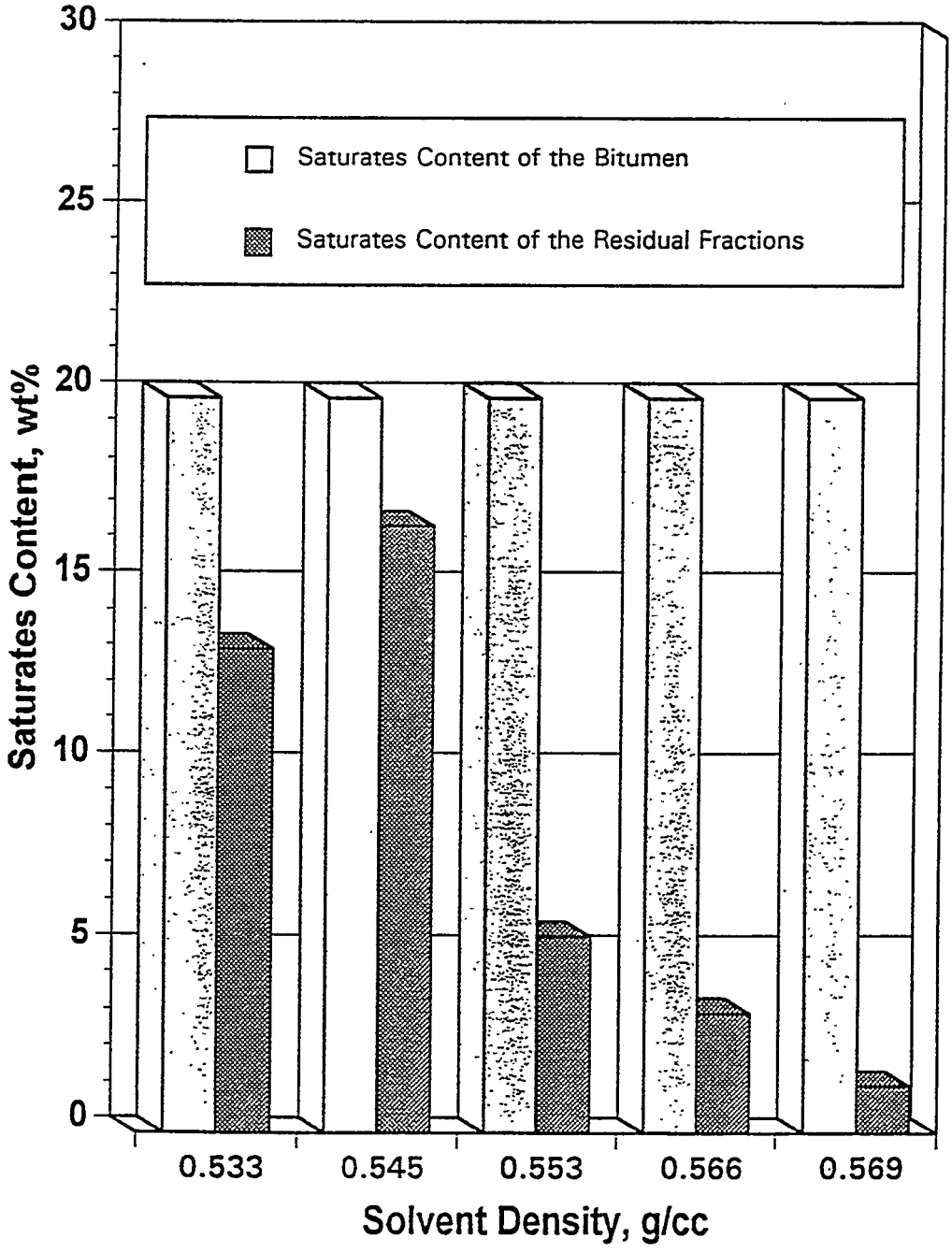
30
25
20
15
10
5
0
Saturates Content, wt%
Saturates Content of the Bitumen
Saturates Content of the Residual Fractions
0.533
0.545
0.553
0.566
0.569
Solvent Density, g/cc

Figure 65.

Effect of Solvent Density on the Extraction of Asphaltenes from the Whiterocks Bitumen

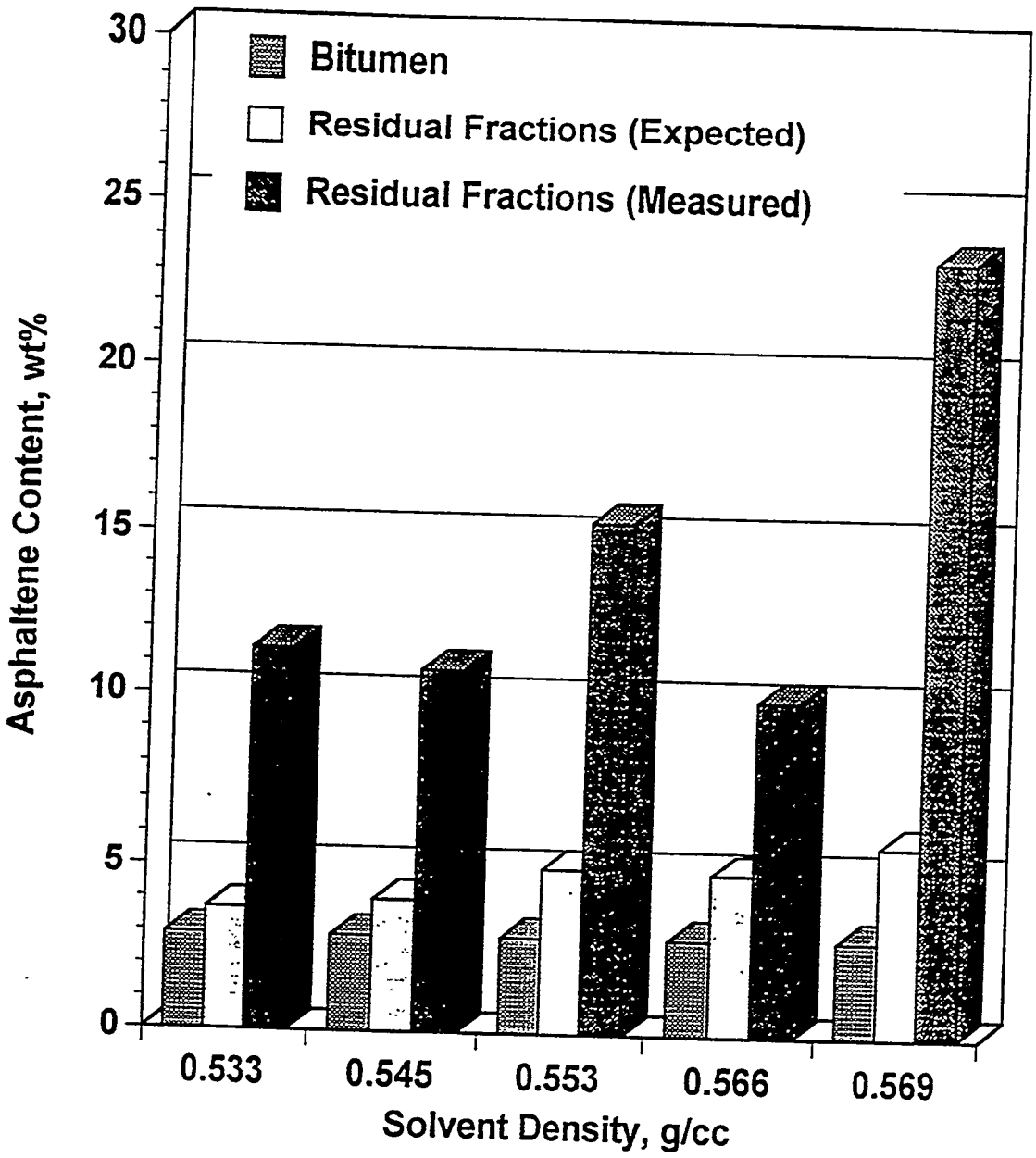
Bitumen
Residual Fractions (Expected)
Residual Fractions (Measured)
Asphaltene Content, wt%
30
25
20
15
10
5
0
0.533
0.545
0.553
0.566
0.569
Solvent Density, g/cc

Figure 66.

Effect of Solvent Density on the Extraction of Asphaltenes from the Asphalt Ridge Bitumen

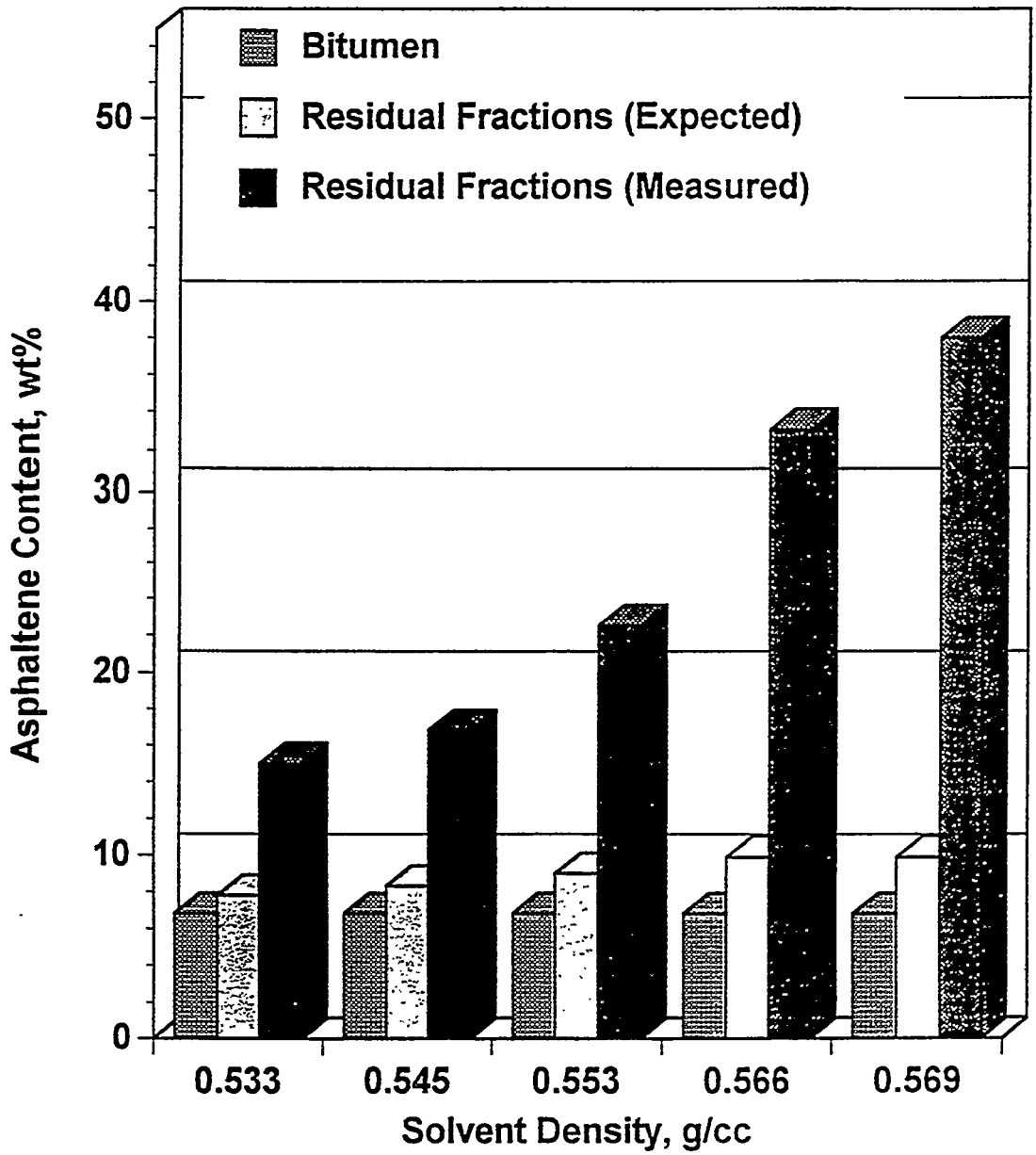
Bitumen
Residual Fractions (Expected)
Residual Fractions (Measured)
Asphaltene Content, wt%
0
10
20
30
40
50
0.533
0.545
0.553
0.566
0.569
Solvent Density, g/cc

Figure 67.

Effect of Solvent Density on the Extraction of Asphaltenes from the PR Spring Bitumen

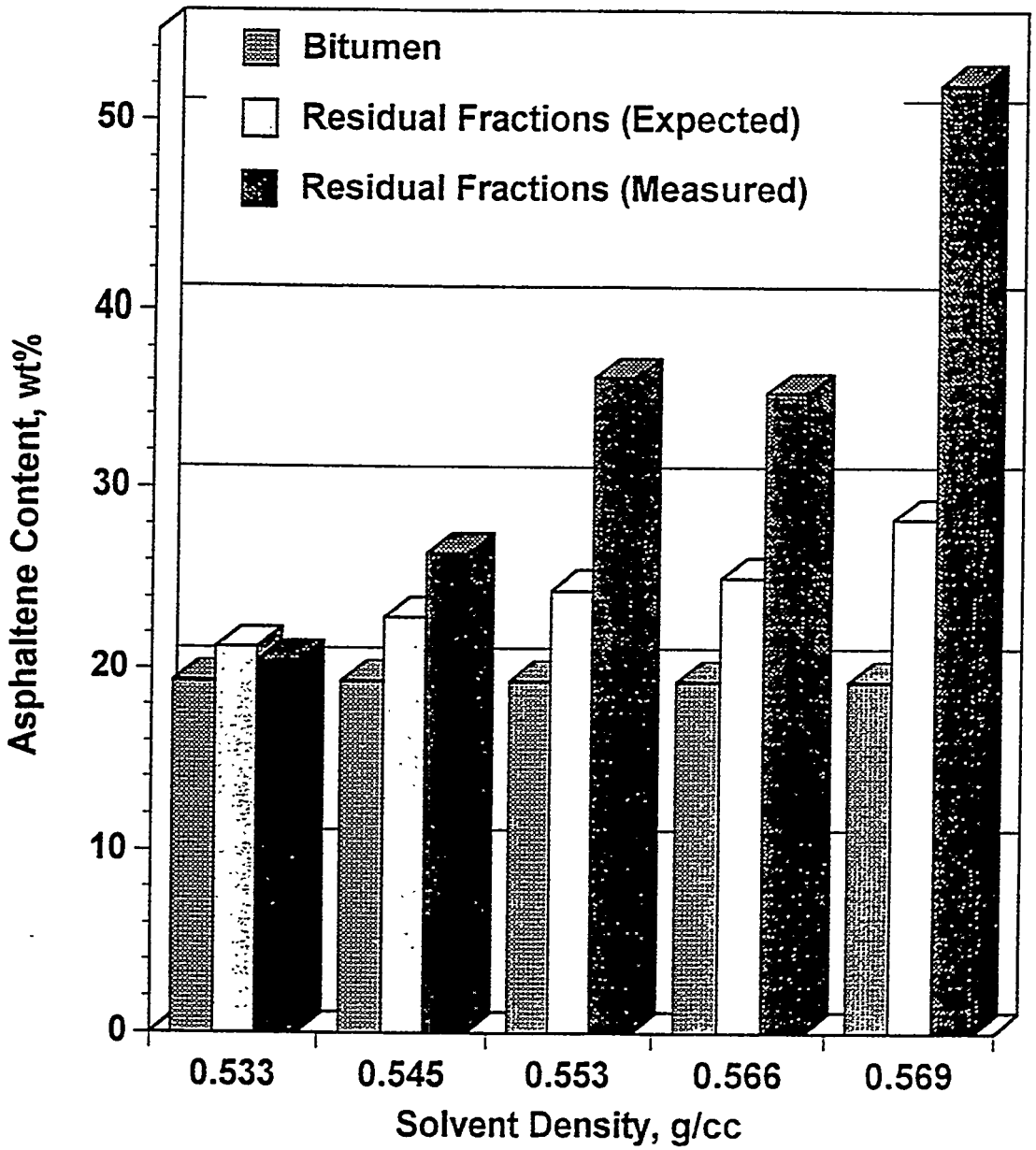
Bitumen
Residual Fractions (Expected)
Residual Fractions (Measured)
Asphaltene Content, wt%
0
10
20
30
40
50
0.533
0.545
0.553
0.566
0.569
Solvent Density, g/cc

Figure 68.

Effect of Solvent Density on the Extraction of Asphaltenes from the Sunnyside Bitumen

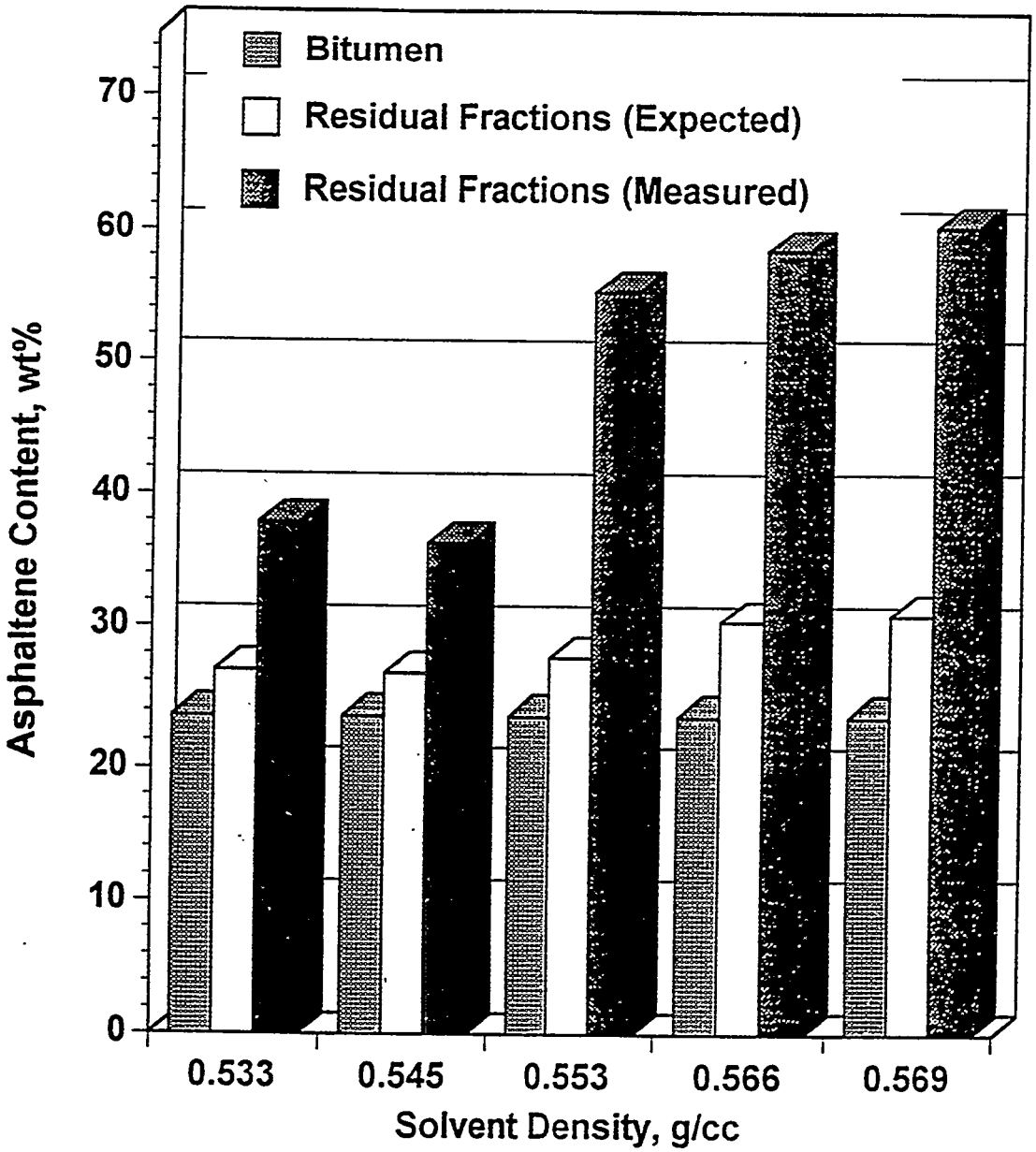
Bitumen
Residual Fractions (Expected)
Residual Fractions (Measured)
Asphaltene Content, wt%
70
60
50
40
30
20
10
0
0.533
0.545
0.553
0.566
0.569
Solvent Density, g/cc

(P_r=2.3) and 339 K (T_r=1.03) were analyzed and there was no evidence that asphaltenes were transferred to the extract phases.

The asphaltene contents of the residual fractions for the four bitumens were much higher than those of the bitumens and the expected asphaltene contents which had been calculated on a prorated basis. An explanation for this phenomenon can be generated by revisiting the literature. Nellensteyn (72) proposed initially a colloidal model for the heavy asphaltic material present in naturally occurring crude oils. According to him, the asphaltic materials were made up of micelles covered or shielded from the bulk of the oil by adsorbed resins (cosolubilizing agents) and other hydrocarbon materials. The micelles were assumed to be dispersed in the hydrocarbon medium. He also suggested that the precipitating properties of asphaltic materials in different solvents are related to the surface tension. Swanson (73) and Witherspoon and Munir (74) suggested that the resins help asphaltenes stay dissolved in the distillate portion of the naturally occurring crude oil, heavy oil, bitumen, etc. Dickie and Yen (75) proposed that the petroleum resins act as an interface between the polar asphaltenes and relatively nonpolar oil fractions in petroleum. Koots and Speight (76) proposed that the resin fractions play major role in maintaining the asphaltenes in a colloidal state in crude oils. Leontaritis and Mansoori (77) proposed a thermodynamic model of the colloidal state to predict the onset of asphaltene flocculation. Mitchell and Speight (78) indicated that asphaltene precipitation increased exponentially with a decrease in carbon number in the paraffinic solvent used for precipitation. Thus, the composition of the asphaltene precipitated using different solvents was different. The asphaltene molecular weight increased and the H/C atomic ratio decreased with increase in the carbon number of the paraffinic solvent used for precipitation. There are other

process variables such as the ratio of solvent-to-feedstock, the precipitation temperature and the contact time that influence the amount of asphaltene precipitated.

Thus, the interaction between resins and asphaltenes is the key to the colloidal suspension of the asphaltenes in oil. This interaction is disturbed by the addition of a nonpolar solvent, the equilibrium that existed between the resin (soluble in the nonpolar solvent) and asphaltenes (insoluble in the nonpolar solvent) was disturbed, and permitted the aggregation of asphaltene molecules and their precipitation from solution. The analysis of the residual fractions produced in the SFE process indicated the presence of saturates, aromatics, resins and pentane insolubles when propane was used as the solvent. At the same time, the propane-free extract phases consisted of saturates, aromatics and resins and no asphaltenes or pentane insolubles. During the SFE process, the resins or the cosolubilizing agents that kept the asphaltenes in solution in the original bitumen were transferred to the extract phase. Without these resin molecules, some of the asphaltene that did not precipitate from the original bitumen (while performing pentane insolubles) was precipitated after the bitumen sample was subjected to SFE. The observation made here was also observed by Koots and Speight (76) while studying the relationship between resin and asphaltenes in bitumen or crude oils. While using pentane and heptane as solvent, the Athabasca bitumen yielded 17 and 11 wt% of asphaltenes, respectively. Thus, 35 % of the pentane insolubles remained in solution when heptane was used as the solvent. An attempt was made to dissolve the pentane insolubles in heptane; however, only 10 % of the pentane insoluble dissolved. When resins were added, such that the asphaltene-resin ratio was same as that of the original bitumen, 33 % of the pentane insoluble asphaltenes were soluble in pentane. The authors also observed similar effects using other hydrocarbon

solvents. Thus, the removal of resins (cosolubilizing agents)resulted in an increase in the pentane insolubles in the residual fractions obtained from SFE of bitumens using propane.

The measured asphaltene content of the residual fractions increased with increase in the solvent density for all the four bitumens (Figures 65 through 68). This correlated well with the increased extraction yields with increase in solvent density for the four bitumens and also with the decrease in the saturate and aromatic contents of the residual fractions. Thus, it was concluded that the resins (cosolubilizing agents) that kept the asphaltenes suspended in the original bitumen have been removed during SFE.

Elemental Analyses

The elemental (C, H, N and S) analyses of the residual fractions for the bitumens are reported in Tables 16 through 19 for the WR, AR, PRS and SS bitumens, respectively. The nitrogen and sulfur compounds are primarily present in the resin and asphaltenes with the exception of sulfur in small quantities in the oils (saturates plus aromatics). The nitrogen and sulfur compounds have a tendency to concentrate in the asphaltenes relative to resins (79). However, an exception to this trend was observed in the case of sulfur (79). It has been observed from the solubility fractions of the SFE residual fractions that saturates and aromatics were extracted preferentially compared to resins and asphaltenes. The analyses of the extract samples indicated the absence of asphaltenes. Thus the pentane insolubles which contain the increased amounts of asphaltenes and consequently nitrogen and sulfur were left behind in the residual fractions. The resins were transferred to the extract phase; however, the relative amount of extraction was less compared to the extraction of saturates and aromatics (saturates and aromatics content decreased in the

residual fractions compared to the original bitumens) . This was also indicated by the increase in the resin contents of the residual fractions compared to the original resin content of the bitumens. Thus, the heteroatoms such as sulfur and nitrogen that are predominantly contained in the asphaltenes, and to a lesser extent in the resins, were concentrated in the residual fractions. The nitrogen and sulfur concentrations of the residual fractions were consistently higher than the nitrogen and sulfur contents of the bitumen confirming that the heteroatoms are concentrated in the unextracted residual fractions. This is an important observation relevant to the quality of the upgraded hydrocarbon liquids produced in the SFE process. Elemental analyses of the extract samples need to be performed to quantify the amount of heteroatoms present in the extract samples; however, the quantities of the extract samples produced in this study were not sufficient to permit elemental analyses.

The H/C atomic ratios of the residual fractions are compared with the H/C ratios of the bitumens in Figures 69 through 72 for the WR, AR, PRS and SS bitumens; respectively. The H/C ratios of the residual fractions were lower than the H/C ratios of the bitumens. Furthermore, as the solvent density increased and concomitantly the extraction yields, the H/C atomic ratio of the residual fractions decreased for the four bitumens implying that the saturates and aromatic compounds were preferentially extracted compared to the polar resins and asphaltenes. This was confirmed by an observed reduction in the saturates and aromatic contents of the residual fractions compared to the original bitumen.

Figure 69.

Relationship Between Pure Solvent Density and the Residual Fraction H/C Atomic Ratio for the Whiterocks Bitumen

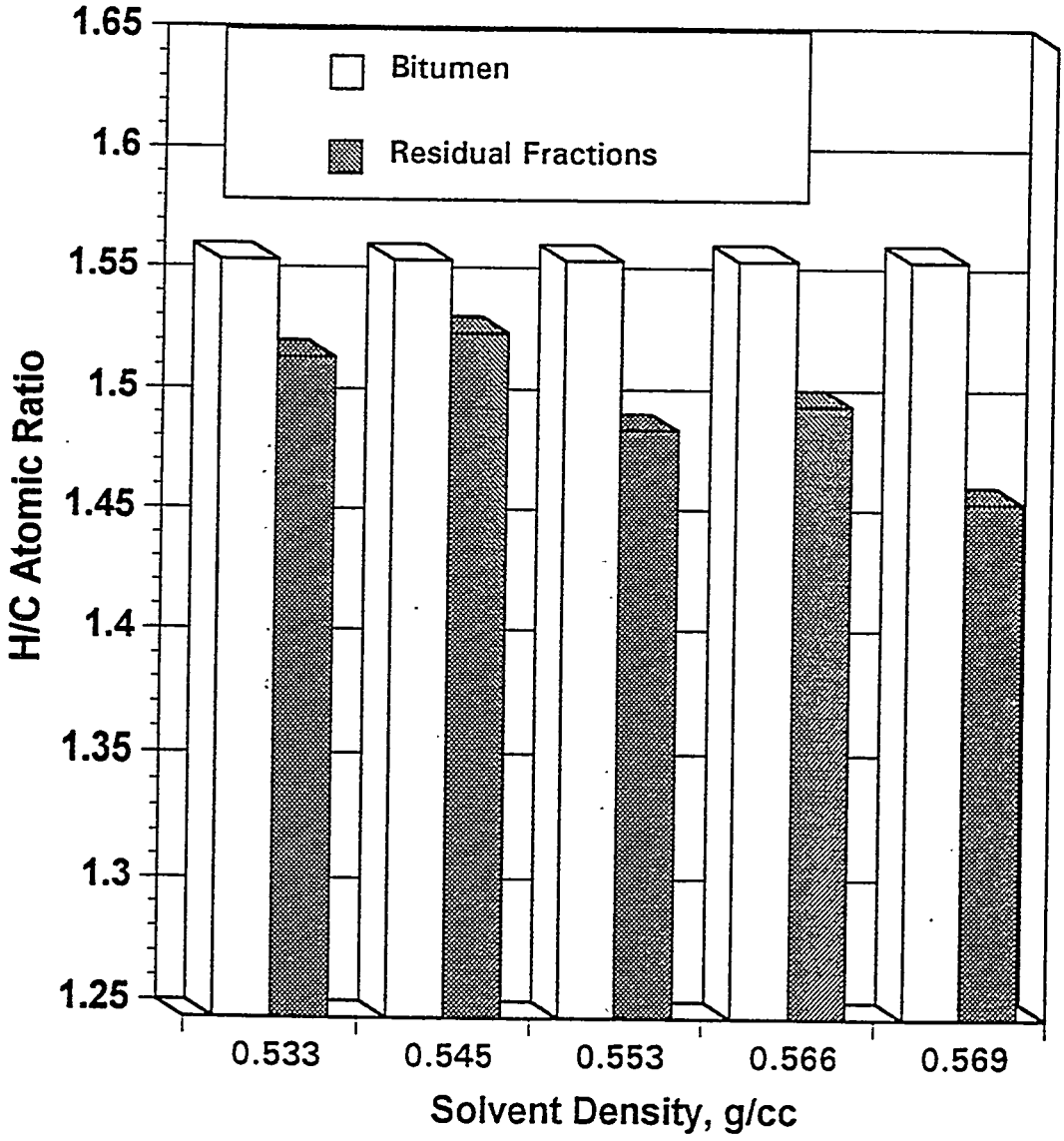
1.65
1.6
1.55
1.5
1.45
1.4
1.35
1.3
1.25
H/C Atomic Ratio
Bitumen
Residual Fractions
0.533
0.545
0.553
0.566
0.569
Solvent Density, g/cc

Figure 70.

Relationship Between Pure Solvent Density and the Residual Fraction H/C Atomic Ratio for the Asphalt Ridge Bitumen

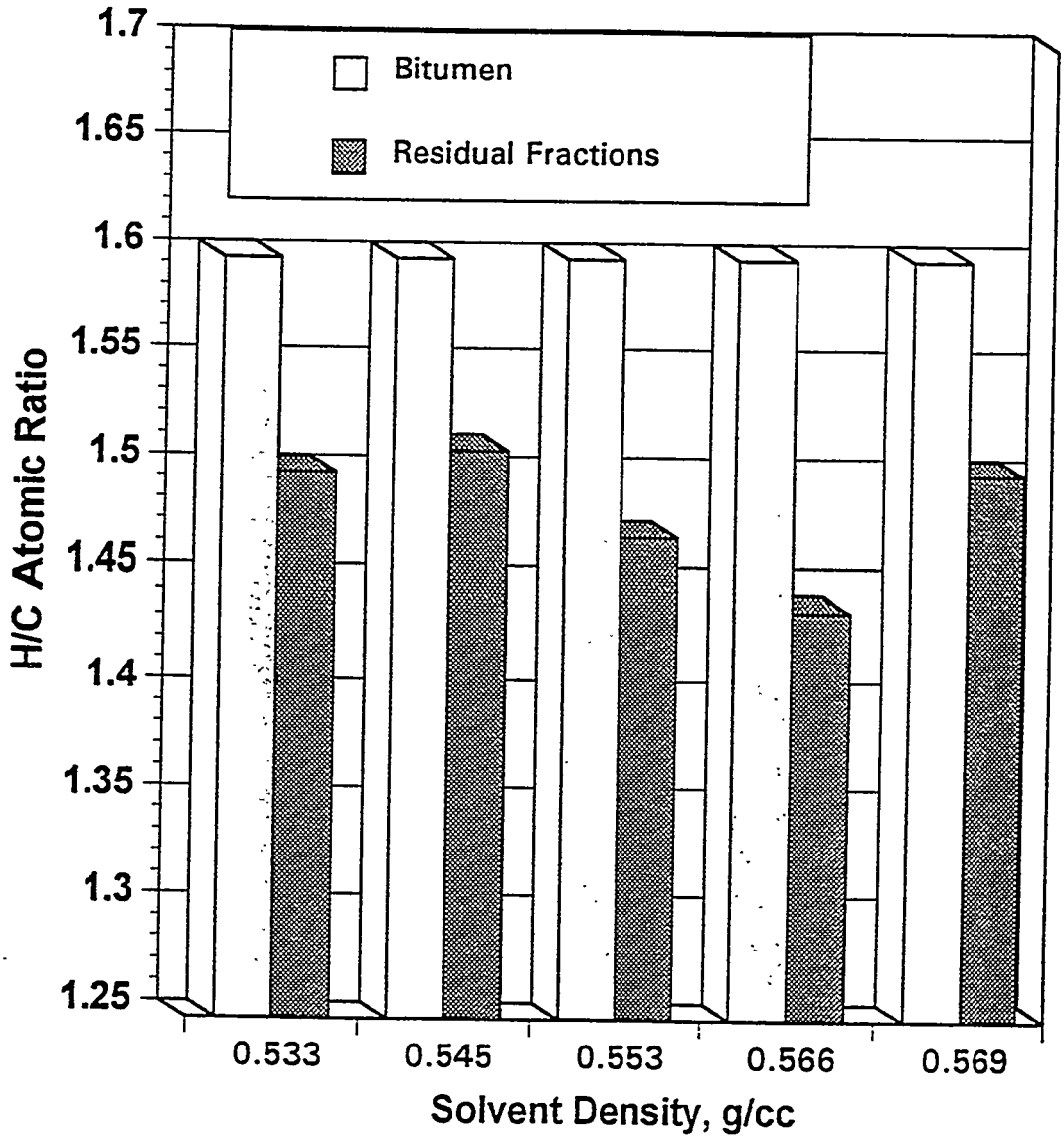
Bitumen
Residual Fractions
H/C Atomic Ratio
1.7
1.65
1.6
1.55
1.5
1.45
1.4
1.35
1.3
1.25
0.533
0.545
0.553
0.566
0.569
Solvent Density, g/cc

Figure 71.

Relationship Between Pure Solvent Density and the Residual Fraction H/C Atomic Ratio for the PR Spring Bitumen

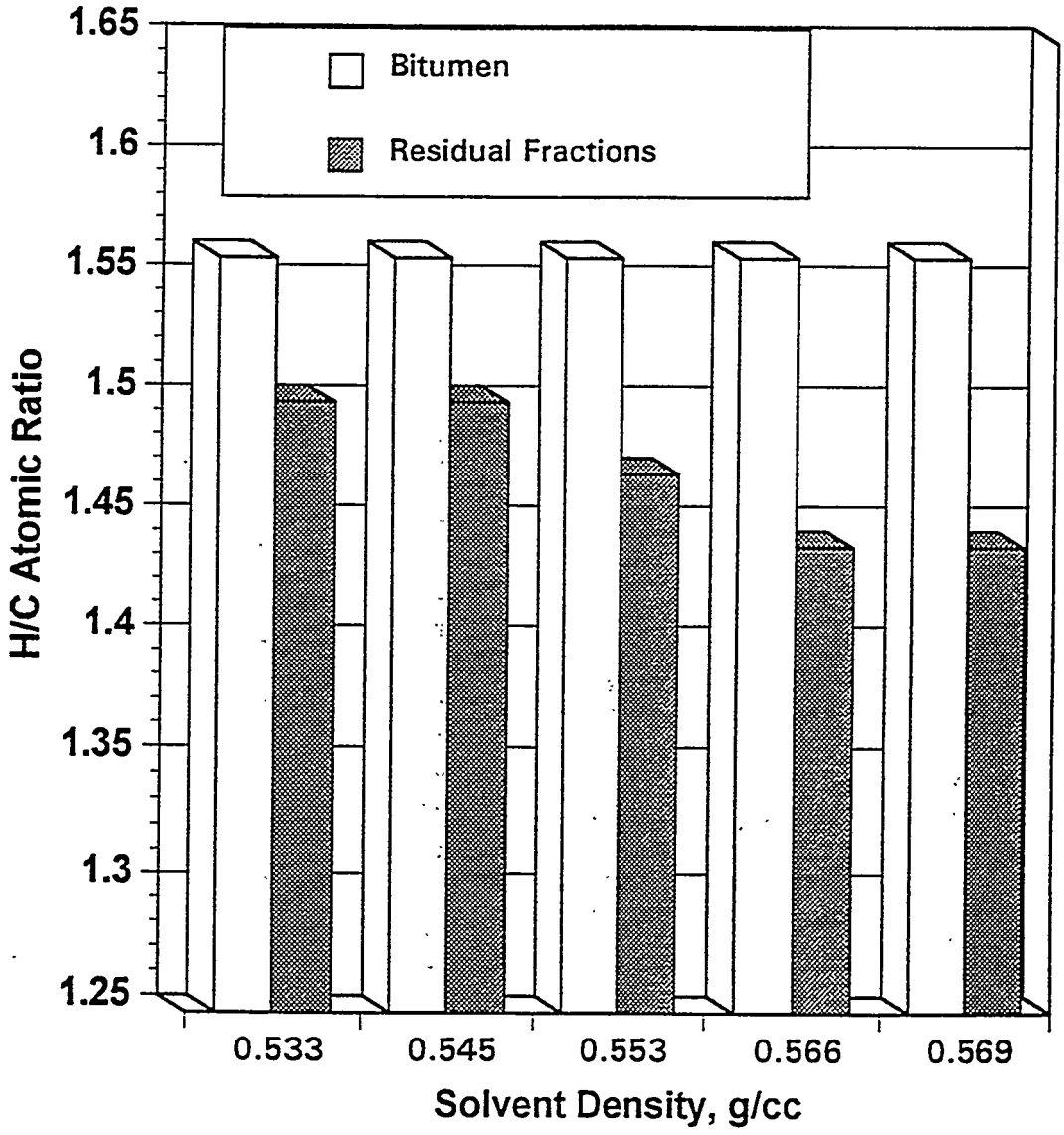
1.65
1.6
1.55
1.5
1.45
1.4
1.35
1.3
1.25
H/C Atomic Ratio
Bitumen
Residual Fractions
0.533
0.545
0.553
0.566
0.569
Solvent Density, g/cc

Figure 72.

Relationship Between Pure Solvent Density and the Residual Fraction H/C Atomic Ratio for the Sunnyside Bitumen

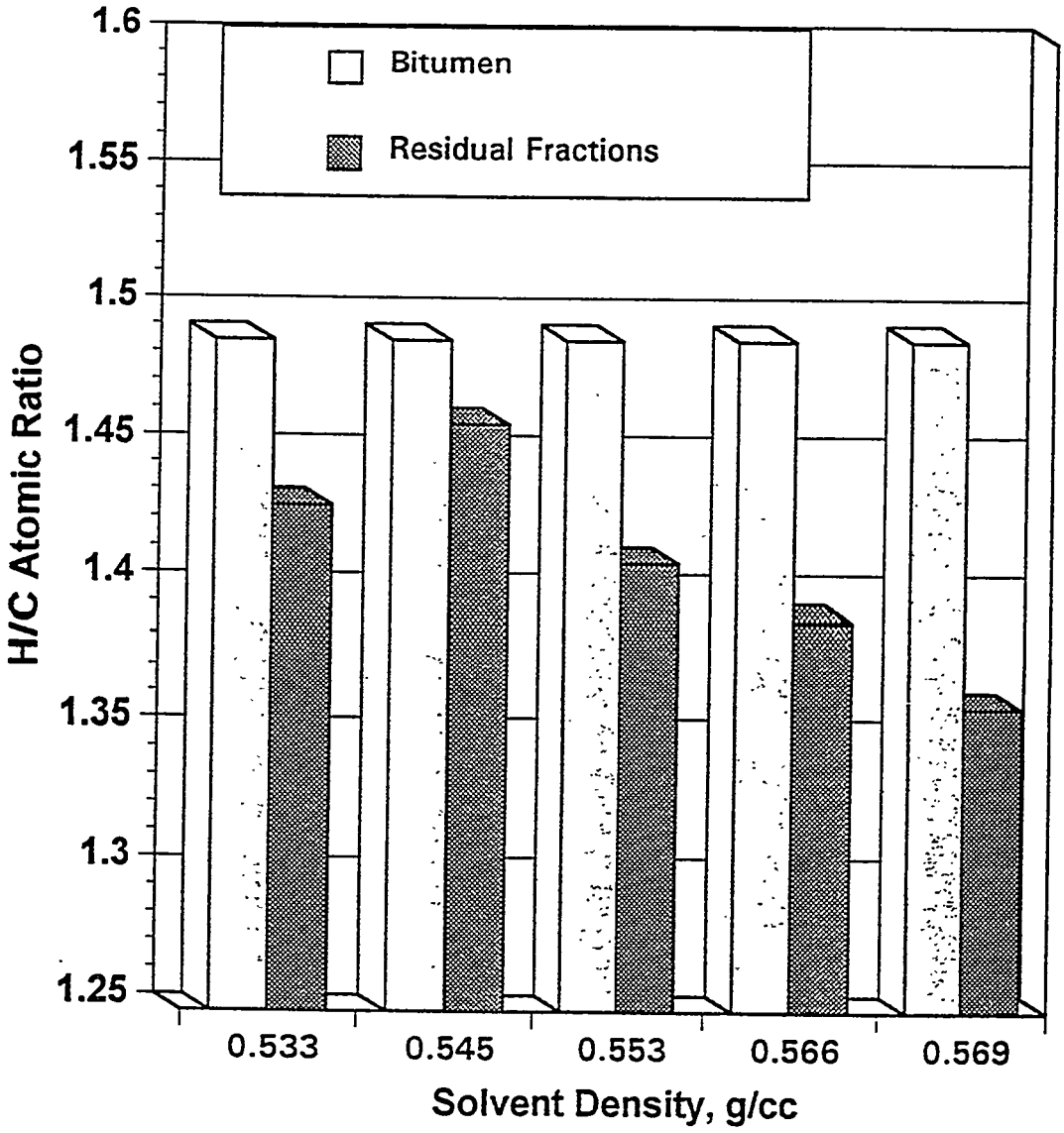
1.6
1.55
1.5
1.45
1.4
1.35
1.3
1.25
H/C Atomic Ratio
Bitumen
Residual Fractions
0.533
0.545
0.553
0.566
0.569
Solvent Density, g/cc

Modeling SFE Using Continuous Thermodynamics Principle

An attempt has been made to model the supercritical fluid extraction of oil sands bitumen with propane as solvent using the principle of continuous thermodynamics. The pseudocomponent lumps used to represent the bitumen in modeling were arbitrarily specified whereas continuous thermodynamic principles uses mathematically selected quadrature points to represent the complex hydrocarbon mixtures. The critical properties were estimated at these quadrature points and flash calculations were conducted using the Peng-Robinson (62) equation of state to simulate the supercritical extraction process and understand the effect of bitumen composition on the SFE yields. The choice of the proper continuous distribution function and the number of quadrature points required to represent ultra heavy oils such as bitumen was very critical for the success of the modeling process.

SUMMARY AND CONCLUSIONS

The supercritical fluid extraction (SFE) apparatus was successfully used to conduct studies with two bitumens from the Asphalt Ridge (AR) and Sunnyside (SS) oil sands deposits of Utah. The existing system (63, 64) was modified by switching the backpressure valve located upstream of the extractor to downstream of the extractor between the densitometer and the low pressure separator to achieve better pressure control of the system. A data acquisition system was installed to monitor the flowrate of the solvent gas flowing out of the system and also to measure the density of the extract phase on a continuous basis.

The SFE experiments were carried out at five different sets of operating conditions using the Asphalt Ridge and Sunnyside bitumens and the following conclusions were drawn:

a) The cumulative extraction yields for both the Asphalt Ridge and Sunnyside bitumens increased with increase in pressure at constant temperature;

b) The cumulative extraction yields of the two bitumens decreased with increase in temperature at constant pressure.

c) The extraction yields increased with increase in propane solvent density.

d) The liquid products obtained from SFE of both the bitumens were upgraded liquids which were approximately 80 wt% volatile.

e) Higher molecular weight extract phases were obtained by increasing the system pressure at constant temperature. Lighter and upgraded liquids were obtained by increasing the temperature at constant pressure.

The bitumens from four major Utah deposits, Whiterocks, Asphalt Ridge, PR Spring and Sunnyside were subjected to SFE using propane as the solvent. The effect of pressure,

temperature, solvent density, and feed compositions on extraction yields and residual fraction characteristics has been investigated. The cumulative extraction yields for the four bitumen increased with increase in pressure at constant temperature and decreased with increase in temperature at constant pressure. In general, higher extraction yields were obtained at higher solvent density for all four bitumens.

The cumulative extraction yields decreased with increase in the asphaltene content and were directly proportional to the feed resin content of the feedstock at all five operating conditions. Except for the Asphalt Ridge bitumen, the extraction yields increased with an increase in feed volatility and saturates content of the bitumens. Saturates and aromatics were preferentially extracted compared to asphaltene and resins. This was confirmed by the reduction in the H/C ratio of the residual fraction. The higher the solvent density, the greater the extent of removal of saturated and aromatic compounds during SFE of all four bitumens.

Modeling of the supercritical extraction of oil sands bitumen was attempted using continuous thermodynamics along with the Peng-Robinson equation of state. A process flow diagram was developed for upgrading bitumen recovered by the surface mining and aqueous flotation recovery technique. Optimization has been attempted using the modeling procedure to obtain operating conditions such as solvent-to-bitumen ratio, pressure and temperature for supercritical extraction and separation using propane as solvent and the Asphalt Ridge and Sunnyside bitumens as feedstocks.

The modeling results predicted preferential extraction of saturates, and aromatics relative to resins were consistent with the experimental observation.

FUTURE ACTIVITIES

The supercritical fluid extraction studies will be discontinued due to the termination of the University of Utah Oil Sands Research and Development Program by the U.S. Department of Energy. The database on the Whiterocks, Sunnyside, PR Spring and Asphalt Ridge bitumen will be published for the benefit of the technical community in a series of journal articles currently in preparation.

Compositional Analysis of Bitumens and Bitumen-Derived Products

Principal Investigator: F.V. Hanson
Co-Principal Investigator: M.D. Deo
Graduate Student: M. Subramanian

INTRODUCTION

Bitumens are ultraheavy oils with API gravity values less than 10°API and viscosity values greater than 10,000 cp at reservoir conditions. Whether the bitumens are produced by surface recovery (81,82) or by in-situ (83) processes, their characterization is important for the development of recovery process employed to convert them to refinery feedstocks. Some of the processes used for upgrading bitumens and bitumen-derived heavy oils include coking (54,55), hydrotreatment (84), and supercritical fluid extraction (SFE) (63,64). Ryu (85) has extensively reviewed the literature on bitumen upgrading processes.

Boduszinski (86,89) reported a method for heavy oil characterization using both chromatographic and spectroscopic techniques and has suggested the use of the sequential elution fractionation (SEF) technique for extending the atmospheric equivalent boiling point (AEBP) beyond 704°C(1300°F) to as high as 1648°C(2998°F). Correlations (89) are available to estimate the mid-AEBP using the H:C atomic ratio or specific gravity of fractions obtained from SEF of hydrocarbons boiling above 704°C(1300°F). This permits complete characterization of petroleum crude oils and residual fractions. Bukka and co-workers (58,66) reported solubility class fractions of selected bitumens from the Uinta Basin of Utah. The fractions were separated using a sequence of solvents of increasing polarity. The separated solubility fractions were classified as saturates, aromatics I, aromatics II, resins I, resins II, and asphaltenes. The analyses of the fractions obtained from the Whiterocks, Asphalt Ridge, and Sunnyside bitumens led to the recommendation

that the Whiterocks deposit be subjected to subsequent development studies based on the lower asphaltene content.

The boiling point distributions of oils can be determined using the ASTM D2892 (90) procedure. Distillation is carried out at a 5:1 reflux ratio on a column that contains 15 theoretical plates. Gas chromatographic simulated distillation (SIMDIS) techniques such as ASTM D2892 were developed to reduce the time required for boiling range analysis. The ASTM D2887 (91) simulated distillation procedure provided the means to determine boiling point distributions of oils containing components boiling below 538°C(1000°F). ASTM D5307-92 (92) was subsequently developed to account for the uneluted portion of the oil, based on the mathematical procedure originally proposed by Worman and Green (93). Neer and Deo (94) established the mathematical equivalence between this procedure and the more intuitive lever arm rule to quantitate the uneluted fraction. ASTM D2887 and D5307 make use of packed columns to determine the boiling point distributions of oils up to 538°C(1000°). It should be possible to elute heavier fractions of oils and to obtain boiling point (or equivalent carbon number) distributions up to about 700°C(1292°F) using capillary columns with high phase ratios (approximately 500) or equivalent packed columns. The development of this technique would be particularly useful for analysis of heavy oils and bitumens that typically contain greater than 50 wt% material boiling above 538°C(1000°F).

The objective of this paper is to demonstrate the viability of using short, high-phase-ratio capillary columns for the characterization of ultraheavy oils and bitumens. The ASTM D5307 method has been extended to higher boiling point components and thus, to higher carbon numbers. The modified technique has been used to analyze bitumens from the Whiterocks, Asphalt Ridge, PR Spring, and Sunnyside oil sands deposits of the Uinta Basin (Utah). Four extract phases and four residues generated during SFE of the bitumens with propane (63,64) have been analyzed, and

the boiling range distributions have been reported.

EXPERIMENTAL

Gas Chromatography

A Hewlett-Packard Model 5890 Series II gas chromatograph (GC) (Palo Alto, CA) was used to analyze the samples in this study. The chromatograph was equipped with on-column injection and a flame-ionization detector (FID). A schematic of the GC setup is presented in Figure 73. Helium was used as the carrier gas. Air, hydrogen, and nitrogen were used to sustain the FID flame. Injections were performed using the Model A 7673 automatic sampler from Hewlett-Packard. The signals from the detector were sent to an IBM-PC through a Hewlett-Packard 3396 Series II integrator using a Hewlett-Packard file server program. The signals were integrated and were stored as report files for further computations. A Microsoft Windows based SIMDIS program was developed in-house to read the sliced and calibration data and to obtain the boiling point distributions for totally and partially eluted samples.

A Petrocol EX-2887 fused-silica capillary column (5 m x 0.53-mm i.d.; 0.1-μm film thickness; phase ratio = 1325) from Supelco (Bellefonte, PA) was used to characterize Whiterocks and PR Spring bitumens and the four extracts and residues. A Model Petrocol 2887 column from Supelco with 0.5-μm film thickness (phase ratio = 265) was used to analyze the Asphalt Ridge and Sunnyside bitumens to achieve improved resolution because this column has a lower phase ratio. The recommended maximum operating temperature of the columns was 380°C(716°F).

The initial oven temperature was maintained at 35°C(95°F) for 4.5 min, increased at a constant rate of 12°C/min to a final oven temperature of 380°C(716°F), and held there for 8.75 min. The detector was maintained at 400°C(752°F) during the entire analysis. The temperature

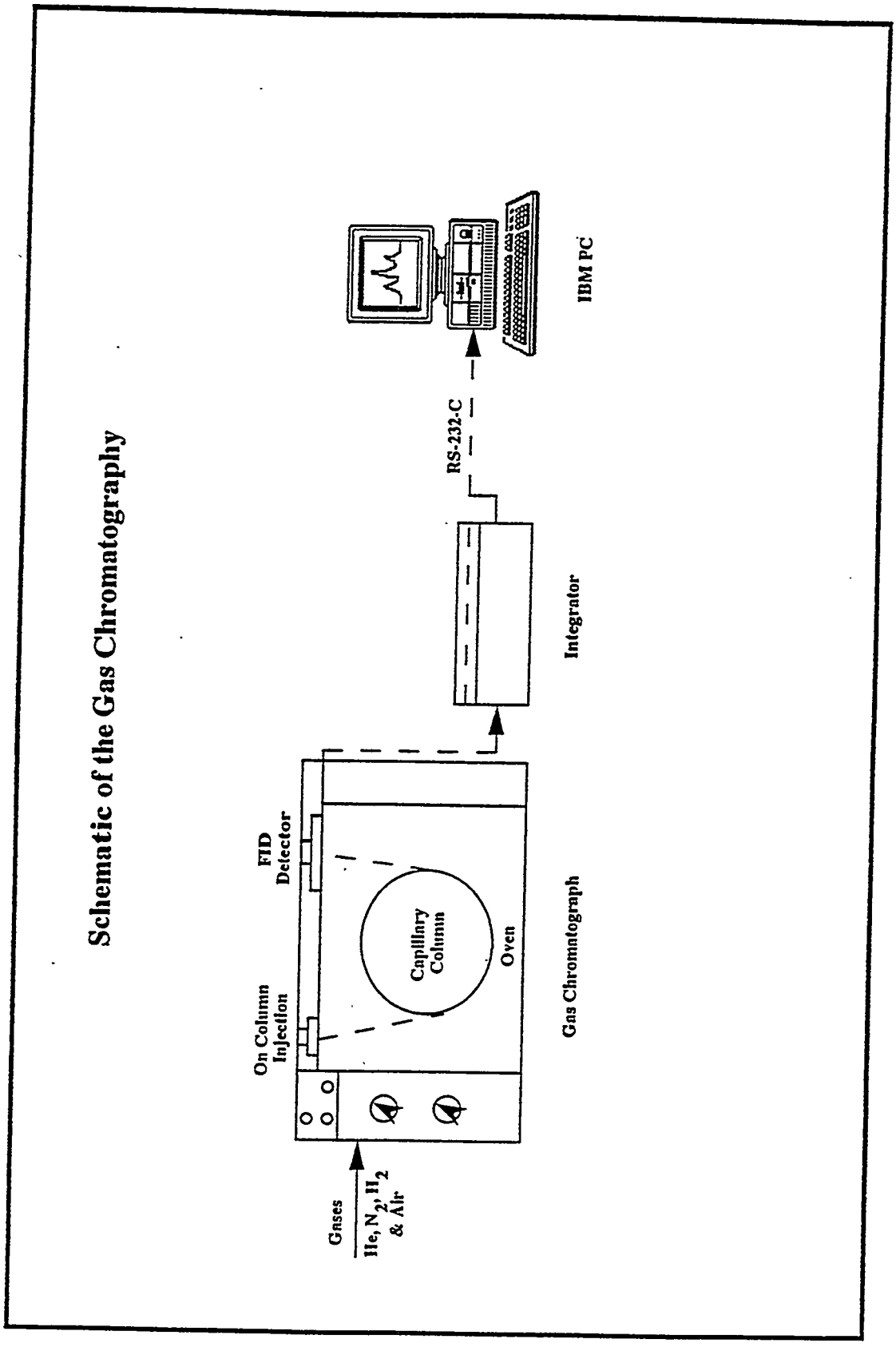

Figure 73. Schematic of the gas chromatography system.

of the injector was initially maintained at 200°C(392°F) for 2.0 min, increased at 10°C/min to a final temperature of 400°C(752°F), and held at 400°C(752°F) until the end of the oven program. The oven and injector temperature programs are reported in Table 20. The carrier gas flow rates were maintained at 20 and 13cc/min for the Petrocol EX-2887 and 2887 columns, respectively.

A 10-μL syringe from Hewlett-Packard and a nanoliter adapter kit were used in the automatic sampler to reduce the injection volume to 0.2 μL of sample. Polywax 655, a calibration mixture from Supelco, was used to calibrate the column. Polywax 655 is a blend of polyethylene oligomers with a carbon number range of C_{10} to C_{110} in even-number increments. The chromatogram of the Polywax 655 calibration standard for the Petrocol EX-2887 column is presented in Figure 2. The peaks for carbon numbers C_{20}, C_{30}, C_{40}, C_{50}, C_{60}, C_{70}, C_{80}, and C_{90} were observed at approximately 13.5, 19.0, 23.5, 27.5, 29.5, 31.0, 33.0, and 35.5 min, respectively (Figure 74). The retention times for earlier peaks (with a carbon number less than 20) were obtained using different calibration mixtures from Supelco. Separate calibration runs using Polywax 655 were carried out with the Petrocol 2887 column used to analyze the Asphalt Ridge and Sunnyside bitumen samples.

The relationship between carbon number and retention time was obtained from the calibration mixtures. The boiling point of hydrocarbons (C_{10} to C_{90}) were obtained from TRC Thermodynamic Tables (95). The relationship between the boiling point and retention time is nearly linear and is presented in Figure 75. A Hewlett-Packard internal standard, which contained C_{14}, C_{15}, C16, and C_{17} normal alkanes, was used in approximately a 1:10 weight ratio with the samples to permit calculation of the uneluted portion of the sample.

Table 20

Temperature Program for Simulated Distillation

	Initial Temperature (°C)	Initial Time (min)	Ramp (°C/min)	Final Temperature (°C)	Final Time (min)
Oven	35	4.5	12.0	380	8.75
Injector	200	2.0	12.0	400	20.0

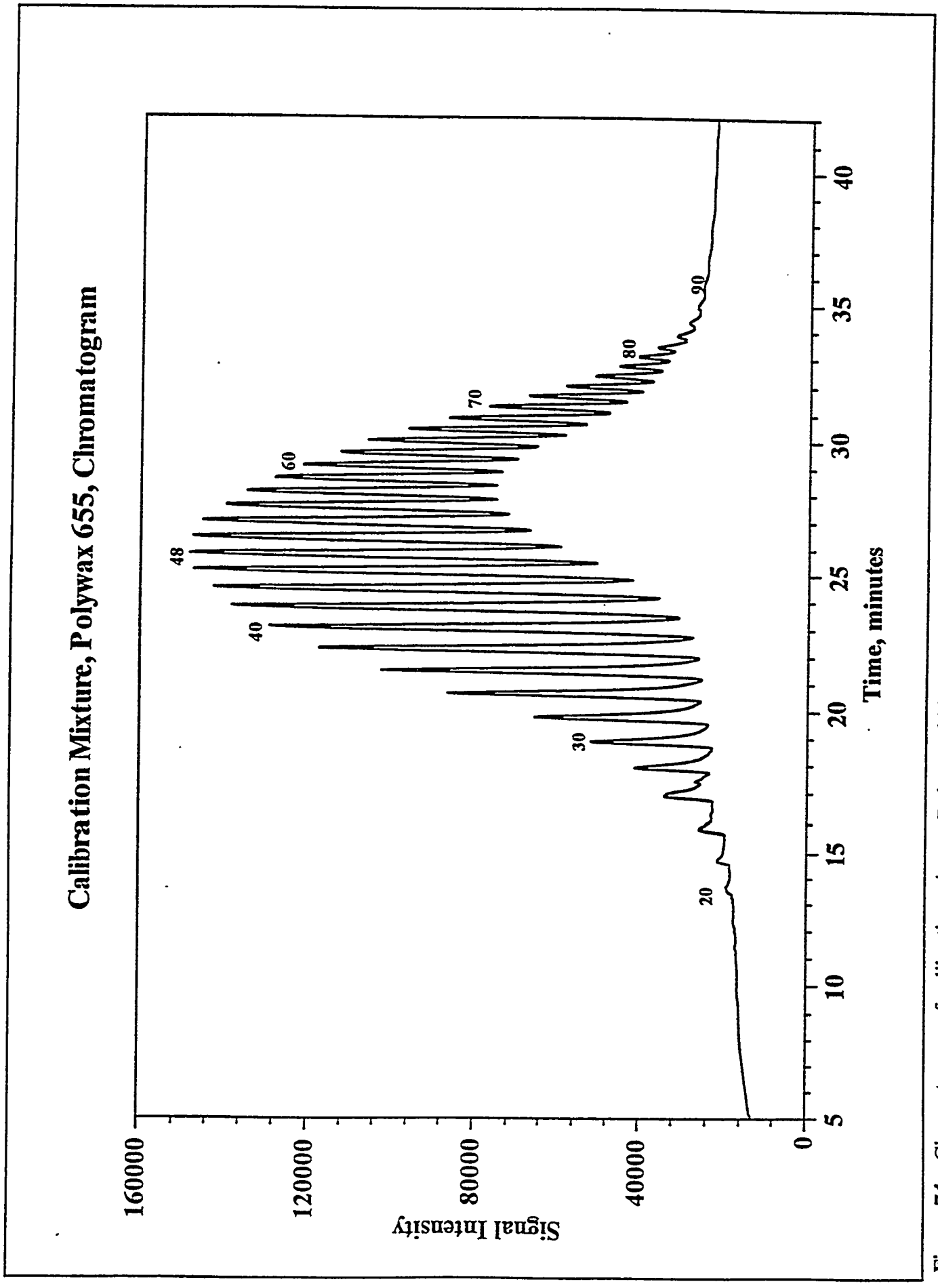

Figure 74. Chromatogram of calibration mixture Polywas 655 on a Petrocol EX2887 column (Supelco). The carrier gas was helium at a flow rate of 20 cc/min. The initial temperature was 35°C. It was held for 4.5 min, increased at 12°C/min to 380°C, and held 8.75 min.

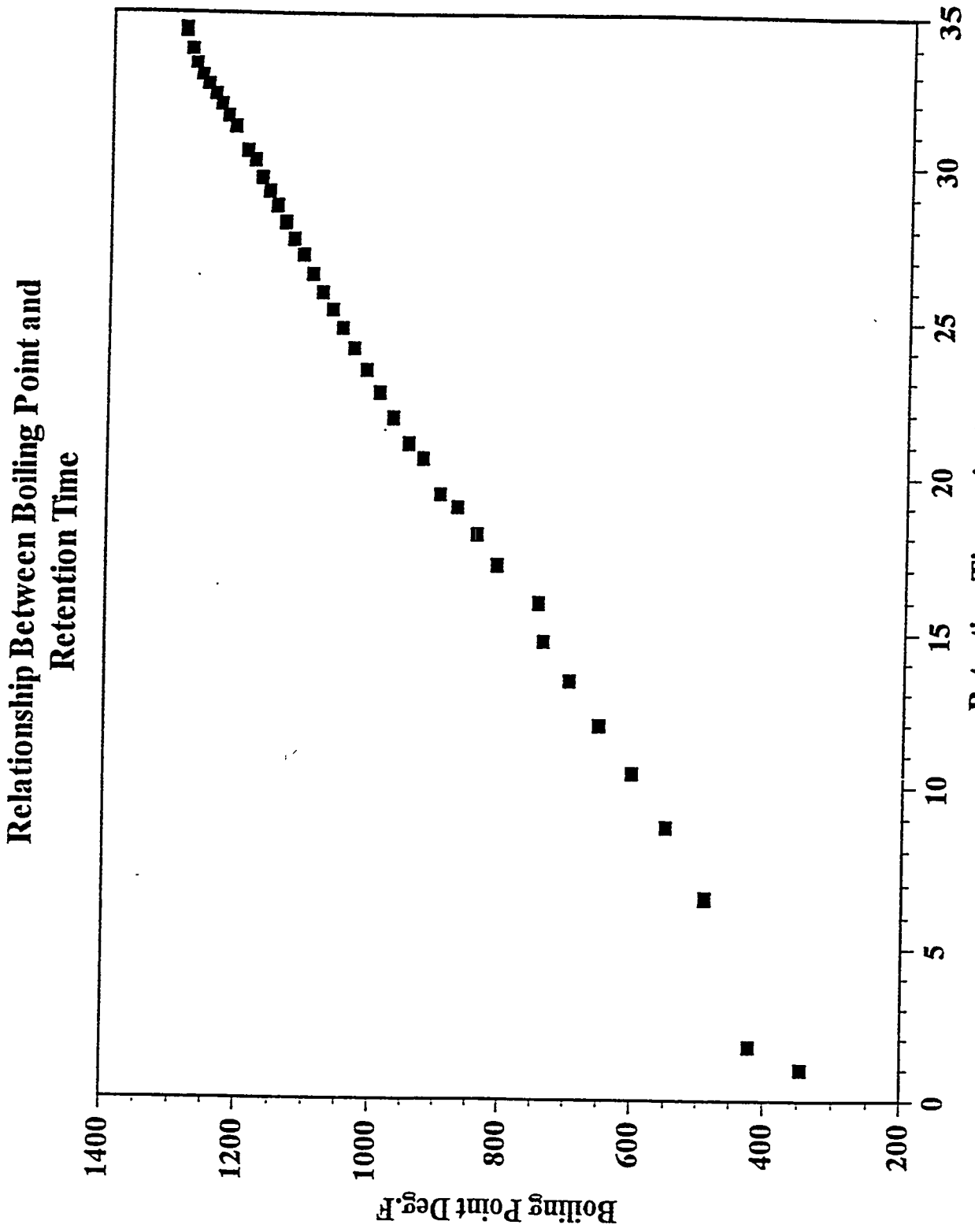

Figure 75. Plot of the relationship between boiling point and retention time.

Samples

Four Uinta Basin bitumens from the Whiterocks, Asphalt Ridge, PR Spring, and Sunnyside deposits were analyzed in this study. The bitumens were extracted from the crushed oil sands ores in a conventional Dean-Stark extraction apparatus using toluene as the solvent. The bitumen-toluene solution was concentrated in a rotary evaporator, and the toluene was removed from the solution at 80°C(176°F). The physical and chemical properties of the bitumens are presented in Table 21. The extract samples for all four bitumens were obtained by SFE using propane as the solvent at 5.6 Mpa and 193°C(380°F). The residual samples were obtained by SFE of the four bitumens at 17.3 Mpa and 193°C(380°F). The supercritical fluid extraction procedure has been described in detail elsewhere (64). The objective of this work was to demonstrate the applicability of the chromatographic technique to materials lighter and heavier than bitumens. The extract samples were viscous light hydrocarbons, containing mainly saturates, aromatics, resins, and little or no asphaltenes. Asphaltenes were pentane insolubles obtained by a technique (96) prescribed by Syncrude Canada Ltd. Resins were measured using the technique described by Bukka and co-workers (58,66). The residual samples were black powders at ambient temperatures and consisted primarily of asphaltenes and resins and contained small amounts of saturates and aromatics. The residual samples were expected to contain 80 to 90 wt% of 538°C(1000°F) plus fractions. The bitumens and residual samples were diluted by adding 50-100 wt% of carbon disulfide to facilitate injection using the automatic sampler. The extent of dilution varied for individual samples to permit easy flow into the syringe. The extract phase samples were injected without dilution. However, due to their viscous nature, the turret tray of the automatic sampler was maintained at 60°C(140°F) using a constant temperature water circulation bath. The automatic sampler viscosity parameter was maintained at 7 for syringe rinsing and injection.

Table 21

Typical Physical and Chemical Properties of Bitumen

Properties	Whiterocks Bitumen	Asphalt Ridge Bitumen	PR Spring Bitumen	Sunnyside Bitumen
Specific Gravity (288/288 K)	0.98	0.985	1.005	1.015
API Gravity, °API	12.9	12.1	9.3	7.9
Conradson Carbon, wt %	9.5	13.9	14.17	15.0
Pour Point, K	327	320	319	348
Viscosity, @ 343 K	4,825	5,050	47,000	173,000
Asphaltenes[a], wt %	2.9	6.8	19.3	23.6
Saturates, wt %	35.7	39.2	33.4	20.0
Aromatics, wt %	7.0	9.0	3.6	15.1
Resins, wt %	54.5	44.1	43.8	36.8
Molecular Weight	653	426	670	593
Elemental Analysis[b]				
C, wt %	87.0	86.9	87.0	86.8
H, wt %	11.2	11.6	11.3	10.8
N, wt %	1.4	1.7	1.3	1.1
S, wt %	0.4	0.4	0.4	0.7
H/C Atomic Ratio	1.56	1.60	1.56	1.49

a) Pentane Insolubles

b) C, H, N, S analyses normalized to 100%

Results and Discussion

Once a boiling point versus retention time calibration curve has been established for a given column at prescribed conditions, the following procedure permits calculation of the boiling point distribution of a given sample to the upper limit of the calibration curve. The curve used in this study (Figure 75) gave retention times of hydrocarbons boiling up to 700°C(1292°F). The uneluted portion of the sample, which in this case corresponds to species boiling above 700°C(1292°F), was calculated using chromatograms of the sample and chromatograms of the sample containing a known weight of the internal standard (typically 10 wt%). The baseline signal was subtracted from both the sample and sample containing the internal standard chromatograms before the uneluted fractions were calculated according to the following procedure (92).

The total area of the chromatogram was calculated from Equation 1:

$$A_T = [(I_A \times R) - I_B] \times \left[\frac{1 - W}{W}\right] \quad (15)$$

where A_T is the total area under the chromatogram, $R = (B - I_B)/(A - I_A)$; W is the weight of the internal standard divided by the sum of the weights of the sample and the internal standard (18); A is the area of the internal standard chromatogram up to 700°C(1292°F), B is the area of the sample chromatogram up to 700°C(1292°F); I_A is the area of the internal standard segment of the internal standard chromatogram; and I_B is the area of the internal standard segment of the sample chromatogram.

The weight fractions of different boiling point or carbon number segments were calculated

using to total chromatogram area according to Equation 2:

$$W_n = \left[\frac{B_n - B_{n-1}}{A_T} \right] \quad (16)$$

where W_n is the weight fraction of the sample eluted between carbon numbers n and n - 1; and B is the area of the sample chromatogram up to a given carbon number.

The chromatograms of the Whiterocks and PR Spring bitumens are presented in Figures 76 and 77. Chromatograms of the sample plus the internal standard are also shown in Figures 76 and 77. The chromatograms indicate that even at high temperatures, negligible column bleed was observed. It should be noted that C_{90}, which has a boiling point of 700°C(1292°F), elutes at around 35.5 min. Thus, the procedure essentially divides the sample chromatograms into boiling point fractions up to 35.5 min plus a non-eluted fraction that boils above 700°C(1292°F). It should be noted that packed columns (instead of capillary columns) are employed in ASTM D5307, and the technique extends only to a boiling point of 538°C. The differential and cumulative boiling point distributions of the Whiterocks bitumen are shown in Figure 78. A comparison of the amounts of the 538°C(1000°F) plus fractions of the bitumens, as determined by the conventional D5307 analyses, and the 700°C(1292°F) plus fractions, as determined by the procedure reported herein, is presented in Table 22. The Whiterocks bitumen has a 538°C(1000°F) plus fraction of 53 wt% and a 700°C(1292°F) plus fraction of 20 wt%. Thus, by using the technique described in this paper, it was possible to characterize (within the limits of simulated distillation analysis) 80 wt% of the Whiterocks bitumen; that is, 33 wt% more than would have been possible using ASTM D5307. Similarly, 89 wt% of the Asphalt Ridge bitumen

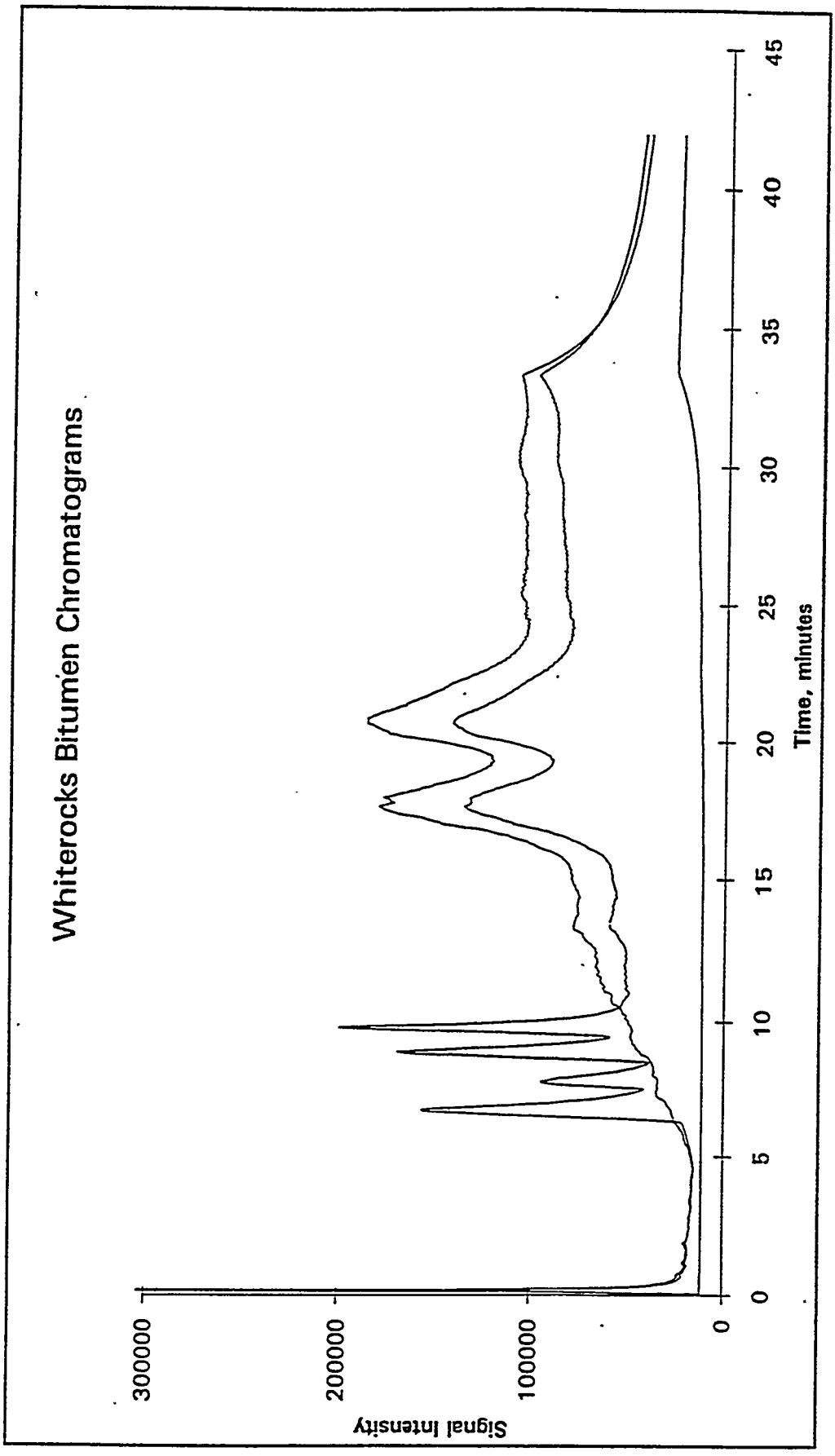

Figure 76. Chromatograms of Whiterocks Bitumen

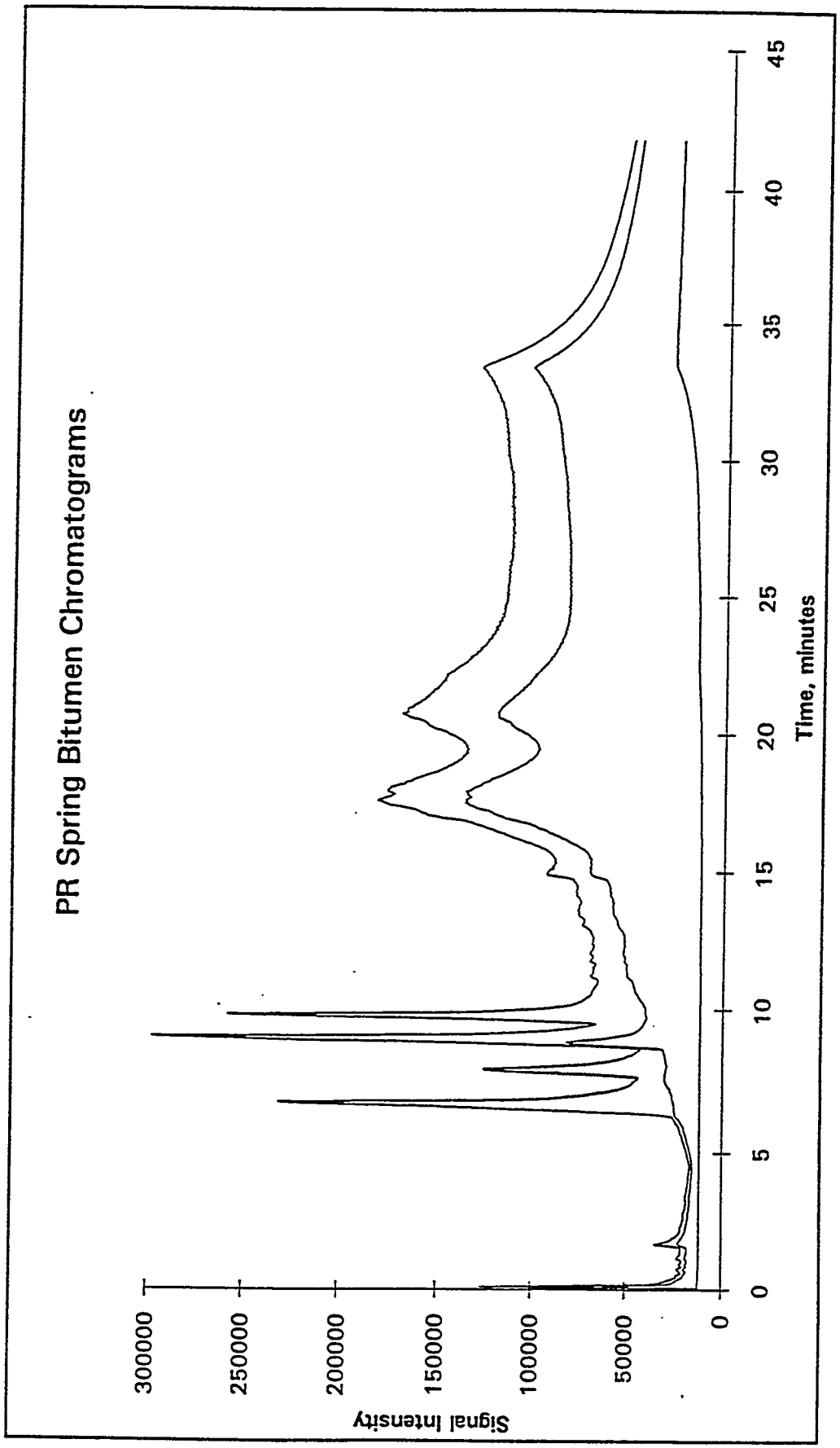

Figure 77. Chromatograms of PR Spring Bitumen

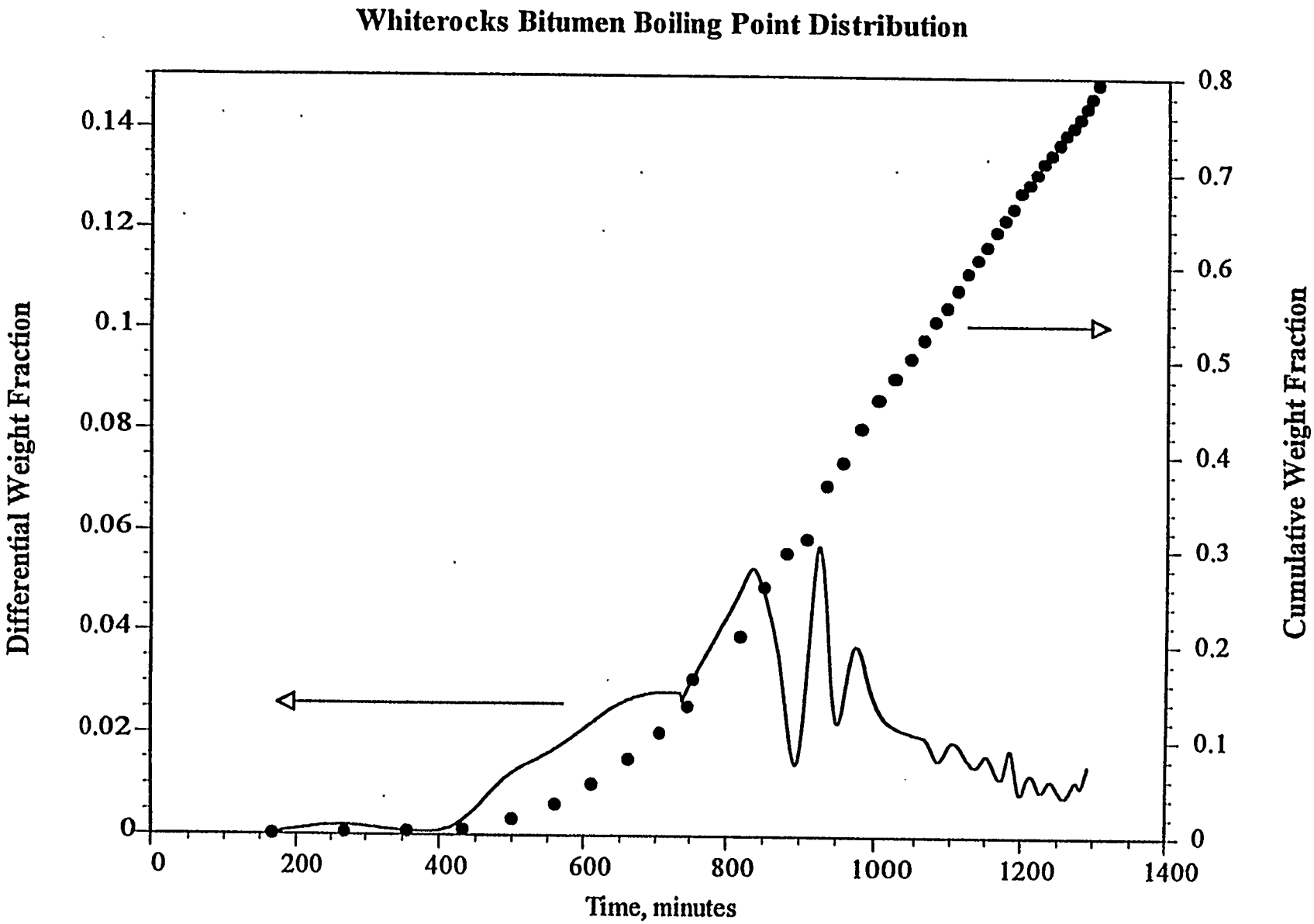

Figure 78. Boiling Point Distribution of Whiterocks Bitumen

Table 22

Comparison of the Extended Method Results

Samples	Weight Fraction	
	1000°F+	1292°F+
Whiterocks Bitumen	0.53	0.20
Asphalt Ridge Bitumen	0.45	0.11
PR Spring Bitumen	0.54	0.21
Sunnyside Bitumen	0.59	0.27
Whiterocks Extract	0.08	0.0
Asphalt Ridge Extract	0.16	0.0
PR Spring Extract	0.12	0.0
Sunnyside Extract	0.18	0.0
Whiterocks Residue	0.88	0.58
Asphalt Ridge Residue	0.87	0.61
PR Spring Residue	0.86	0.59
Sunnyside Residue	0.87	0.61

(34 wt% more than ASTM D5307), and 73 wt% of the Sunnyside bitumen (32 wt% more than ASTM D5307) were characterized by the proposed method. In general, it was possible to characterize approximately one-third more of these heavy oil samples than would have been possible by conventional ASTM analyses. The distillation cuts, thus obtained, for the four bitumens are presented in Table 23.

If an oil contains a small amount of material boiling above 538°C(1000°F), it should be possible to characterize 100% of the sample using the proposed method. This is illustrated using the proposed method. This is illustrated using the extract phases obtained by the SFE of four bitumens with propane. The chromatogram for the extract phase from the Whiterocks bitumen is shown in Figure 79. Analyses with internal standard (analogous to those described in the previous paragraph) for these extract samples revealed that these extracts did not contain any hydrocarbon heavier than C_{90}. The 538°C(1000°F) plus weight fractions of the Whiterocks, Asphalt Ridge, PR Spring, and Sunnyside extracts were 0.08, 0.16, 0.12, and 0.18, respectively. However, all four extract phases were totally eluted with the upper boiling point of 700°C(1292°F). Thus, the procedure developed in this paper allows for complete characterization of samples that consist of relatively small fractions boiling above 538°C(1000°F). The boiling point distribution of the extract phase from Whiterocks bitumen is shown in Figure 80.

The method can also be applied to extremely heavy petroleum residue. Residual fractions of the four bitumens recovered after SFE with propane were used to illustrate this point. Approximately 90 wt% of each of these residues boiled above 538°C(1000°F), as shown in Table 22. The extended SIMDIS technique helped characterize 42 wt% of the Whiterocks residue, 39 wt% of the Asphalt Ridge residue, 41% of the PR Spring residue, and 39% of the Sunnyside residue (Table 22). Thus, the technique permitted the characterization of an additional 30 wt%

Table 23
Distillation Cuts for Four Bitumens Analyzed

	Bitumen Source			
	Whiterocks	Asphalt Ridge	PR Spring	Sunnyside
ASTM D5307				
Volatility (<538°C), wt%	46.6	53.5	45.4	40.9
Distillation cuts (wt%)				
< 204°C	0.5	1.3	0.4	0.6
204 - 344°C	7.4	11.8	8.2	7.8
344 - 538°C	38.7	40.4	36.8	32.5
> 538°C	53.4	46.5	54.6	59.1
Modified SIMDIS procedure				
Volatility (<538°C), wt%	46.6	53.5	45.4	40.9
Distillation cuts (wt%)				
< 204°C	0.5	1.3	0.4	0.6
204 - 344°C	7.4	11.8	8.2	7.8
344 - 538°C	38.7	40.4	36.8	32.5
538 - 700°C	33.0	34.0	33.0	32.0
> 700°C	20.0	11.0	21.0	27.0

Figure 79.

Chromatograms for the Whiterocks Bitumen Extract Phase

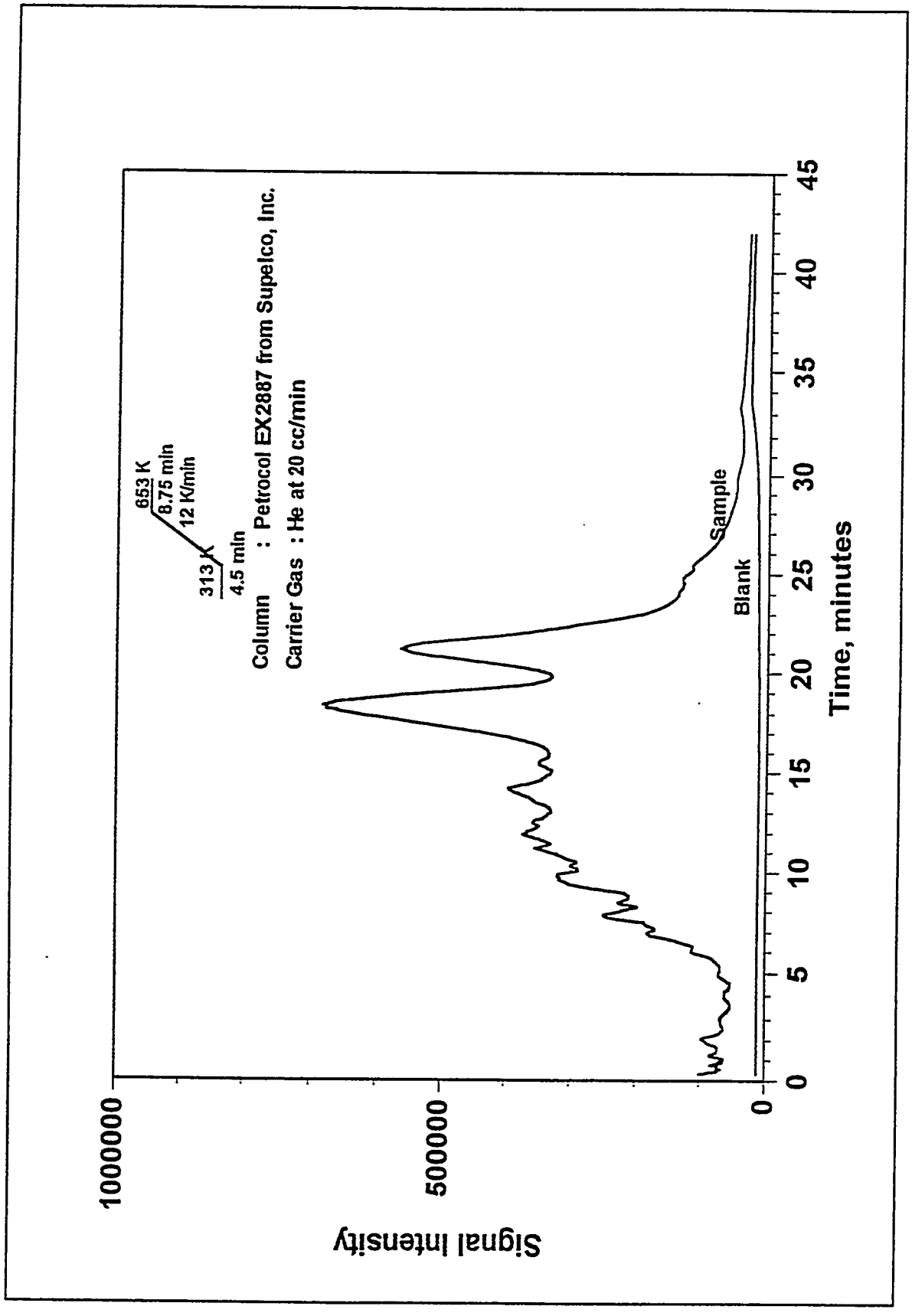
653 K
8.75 min
12 K/min
313 K
4.5 min
Column : Petrocol EX2887 from Supelco, Inc.
Carrier Gas : He at 20 cc/min
Sample
Blank
Signal Intensity
1000000
500000
0
0
5
10
15
20
25
30
35
40
45
Time, minutes

Figure 80.

Boiling Point Distribution for the Whiterocks Bitumen Extract

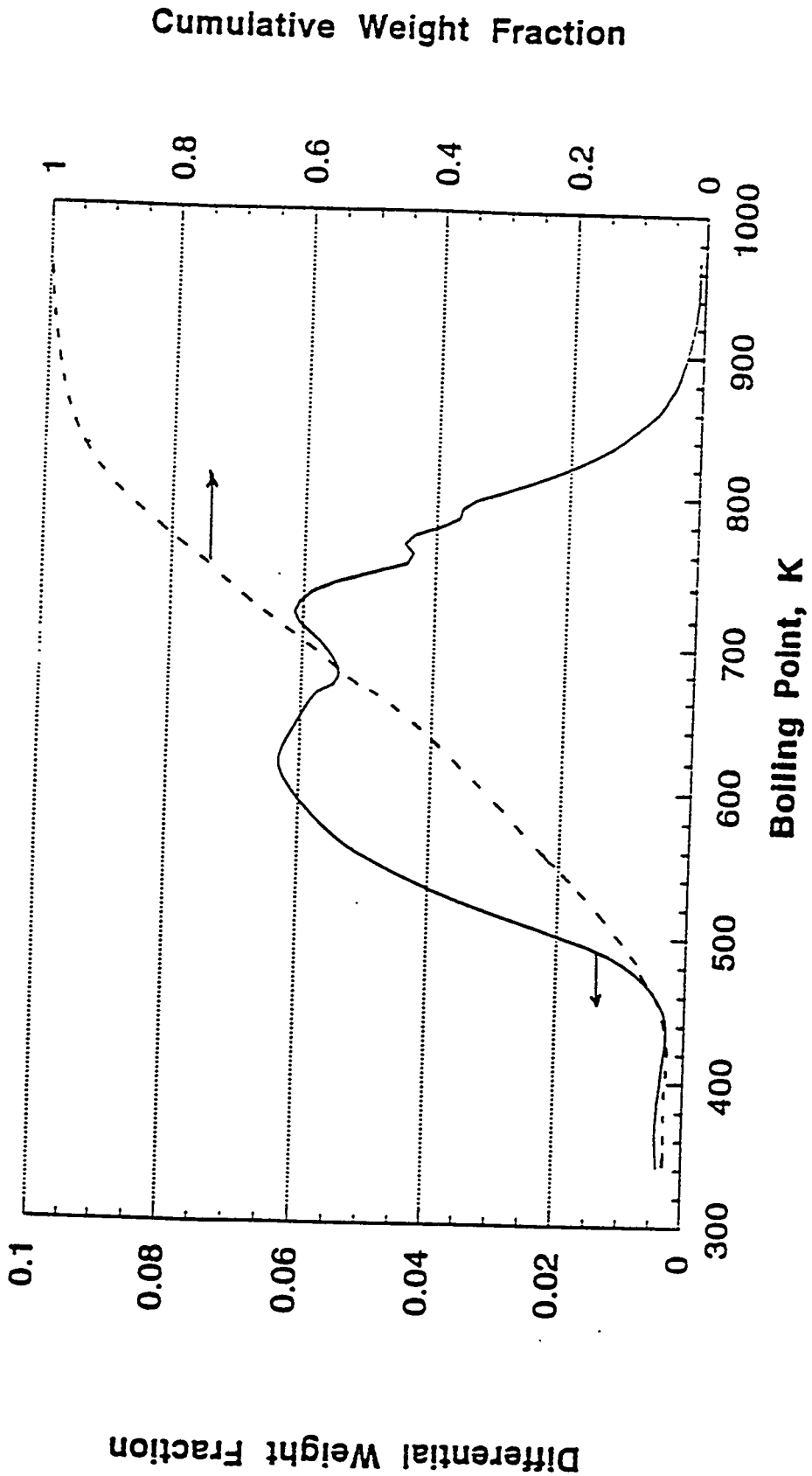
Cumulative Weight Fraction
1
0.8
0.6
0.4
0.2
0
0.1
0.08
0.06
0.04
0.02
0
300
400
500
600
700
800
900
1000
Boiling Point, K
Differential Weight Fraction

of the residual fractions. The chromatograms of the Whiterocks bitumen residual fraction and the boiling point distributions are presented in Figures 81 and 82, respectively. The carbon number distributions for the Whiterocks, Asphalt Ridge, PR Spring and Sunnyside bitumens and their saturates, aromatics and resins fractions are presented in Figures 84 through 87.

Summary and Conclusions

Boiling point distributions up to 700°C(1292°F) and an estimate of the 700°C(1292°F) plus fraction for the ultraheavy oils can be obtained using capillary columns with high phase ratios. Applicability of this technique was demonstrated using ultraheavy oils (bitumens) from the Uinta Basin in Utah, which had volatilities (538°C minus fractions)of 55 wt% or less. The method allowed for the characterization of 30-35 wt% more of the bitumen and bitumen residual fractions obtained by SFE than would have been possible using the ASTM D5307-92 method. Characterization of extract phases with volatilities of 90 wt% was also demonstrated.

Figure 81.

Chromatograms for the Whiterocks Bitumen Residual Fraction

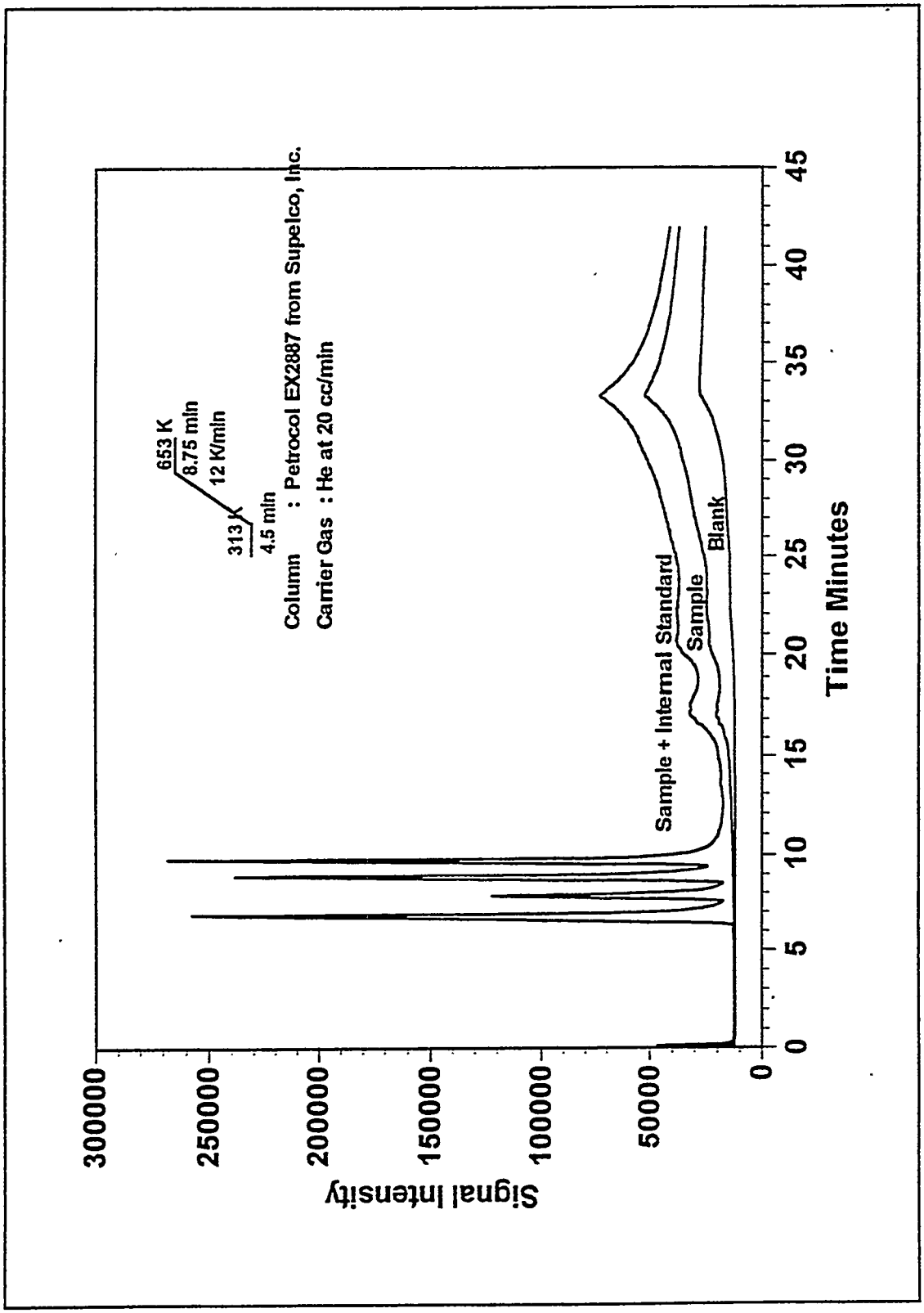
653 K
8.75 min
12 K/min
313 K
4.5 min
Column : Petrocol EX2887 from Supelco, Inc.
Carrier Gas : He at 20 cc/min
Sample + Internal Standard
Sample
Blank
Signal Intensity
Time Minutes
300000
250000
200000
150000
100000
50000
0
0
5
10
15
20
25
30
35
40
45

Figure 82.

Boiling Point Distribution for the Whiterocks Bitumen Residual Fraction

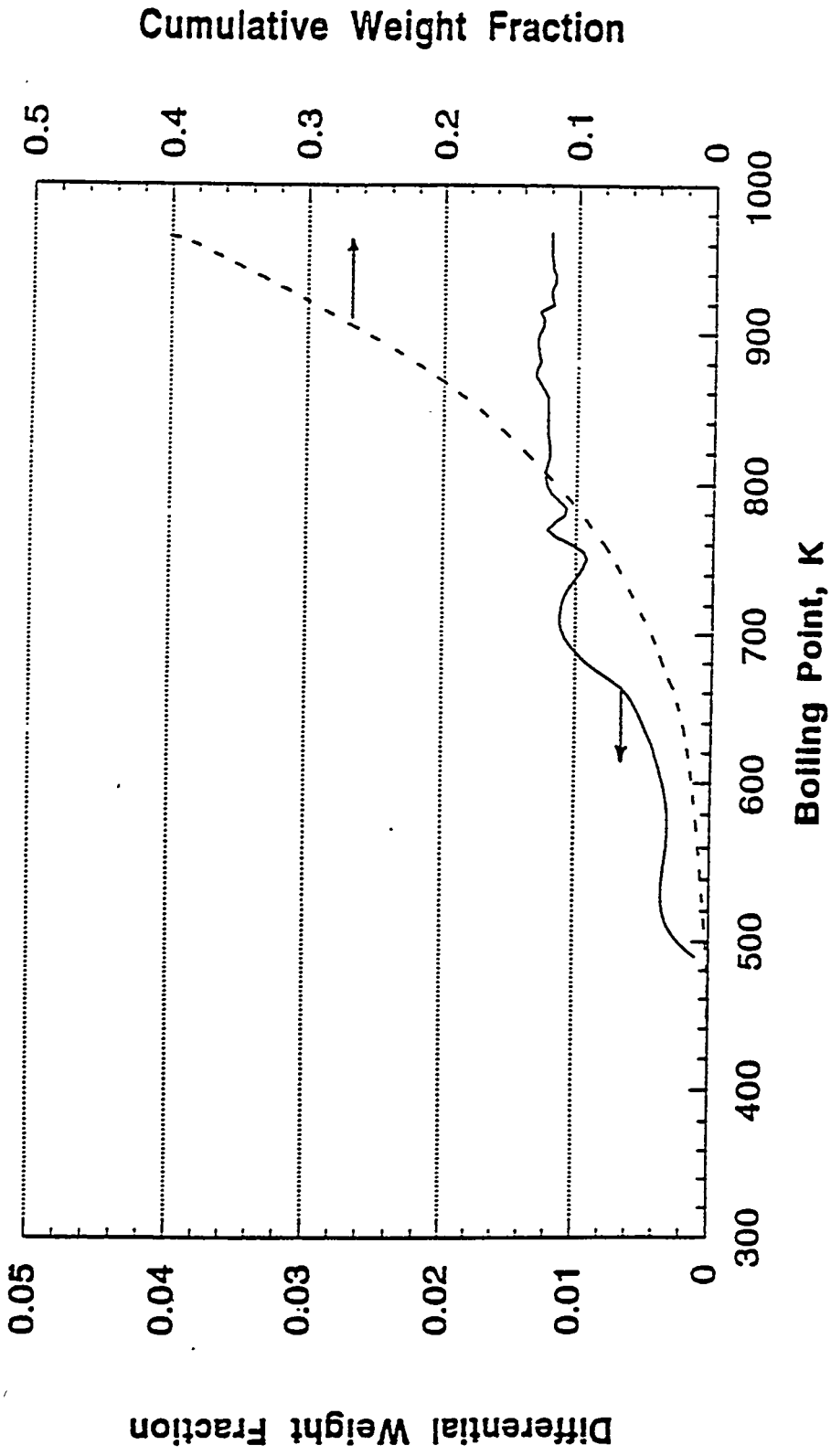
Cumulative Weight Fraction
0.5
0.4
0.3
0.2
0.1
0
1000
900
800
700
600
500
400
300
Boiling Point, K
0.05
0.04
0.03
0.02
0.01
0
Differential Weight Fraction

Figure 84.

Carbon Number Distributions for the Whiterocks Bitumen and the Saturates, Aromatics and Resins Solubility Fractions

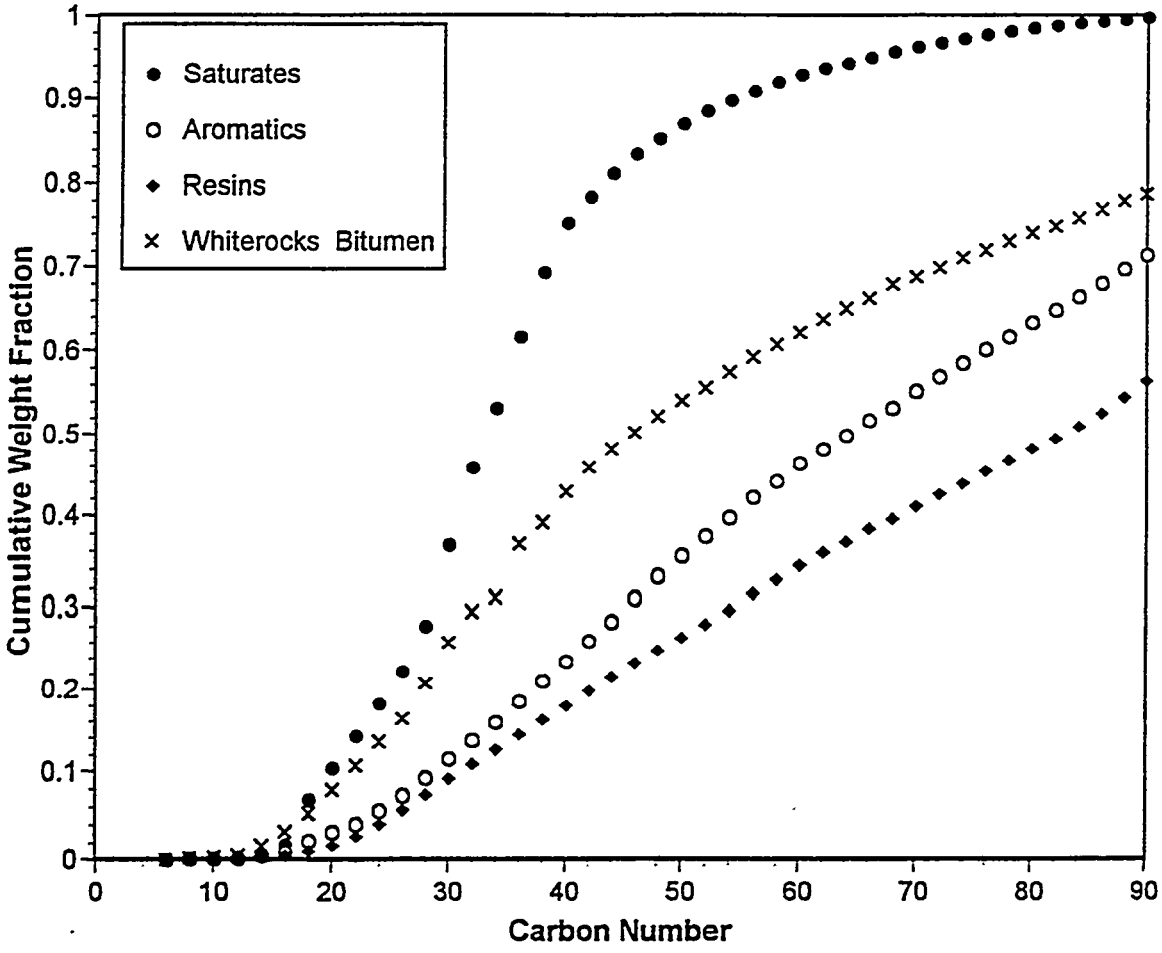
Saturates
Aromatics
Resins
Whiterocks Bitumen
Cumulative Weight Fraction
Carbon Number
0
0.1
0.2
0.3
0.4
0.5
0.6
0.7
0.8
0.9
1
0
10
20
30
40
50
60
70
80
90

Figure 85.

Carbon Number Distributions for the Asphalt Ridge Bitumen and the Saturates, Aromatics and Resins Solubility Fractions

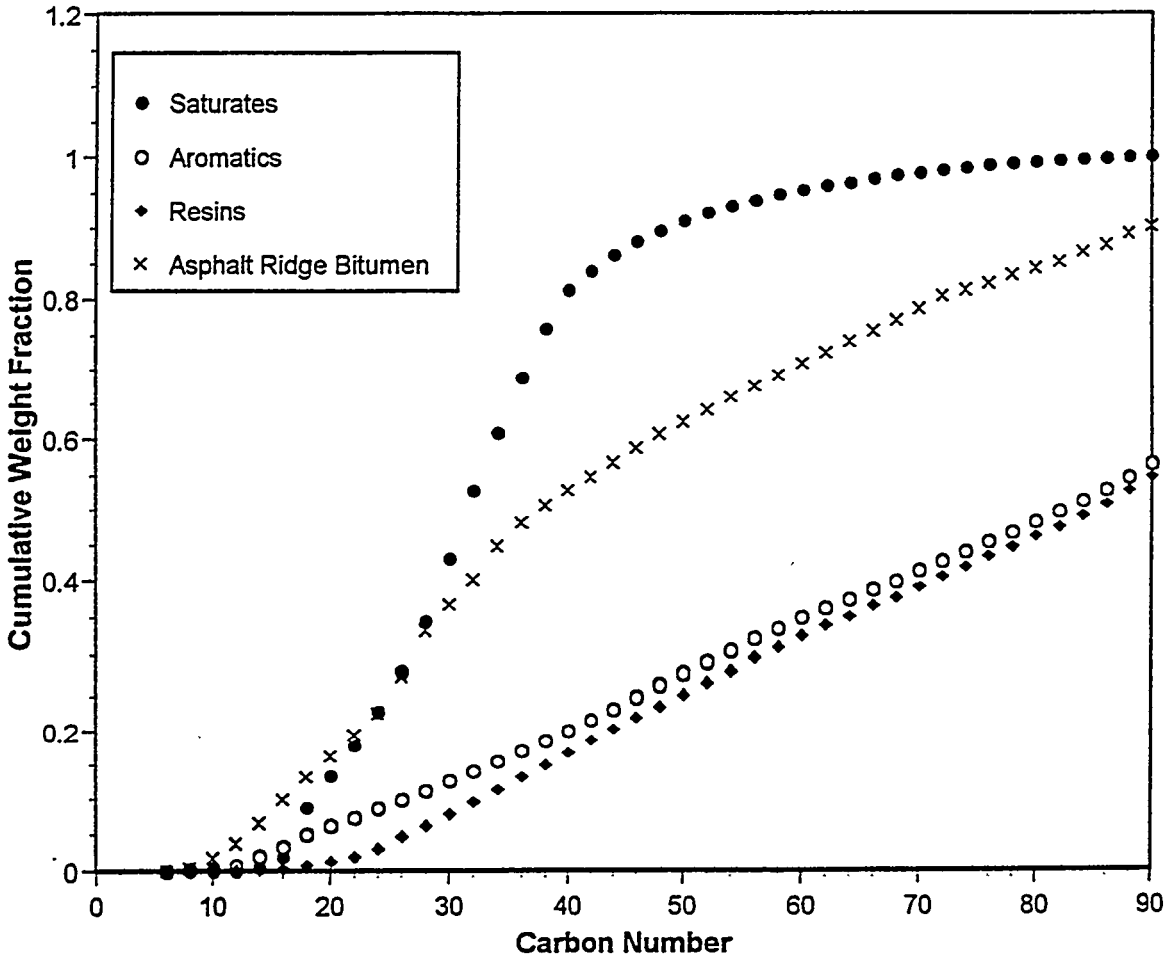
Saturates
Aromatics
Resins
Asphalt Ridge Bitumen
Cumulative Weight Fraction
Carbon Number
0
0.2
0.4
0.6
0.8
1
1.2
0
10
20
30
40
50
60
70
80
90

Figure 86.

Carbon Number Distributions for the PR Spring Bitumen and the Saturates, Aromatics and Resins Solubility Fractions

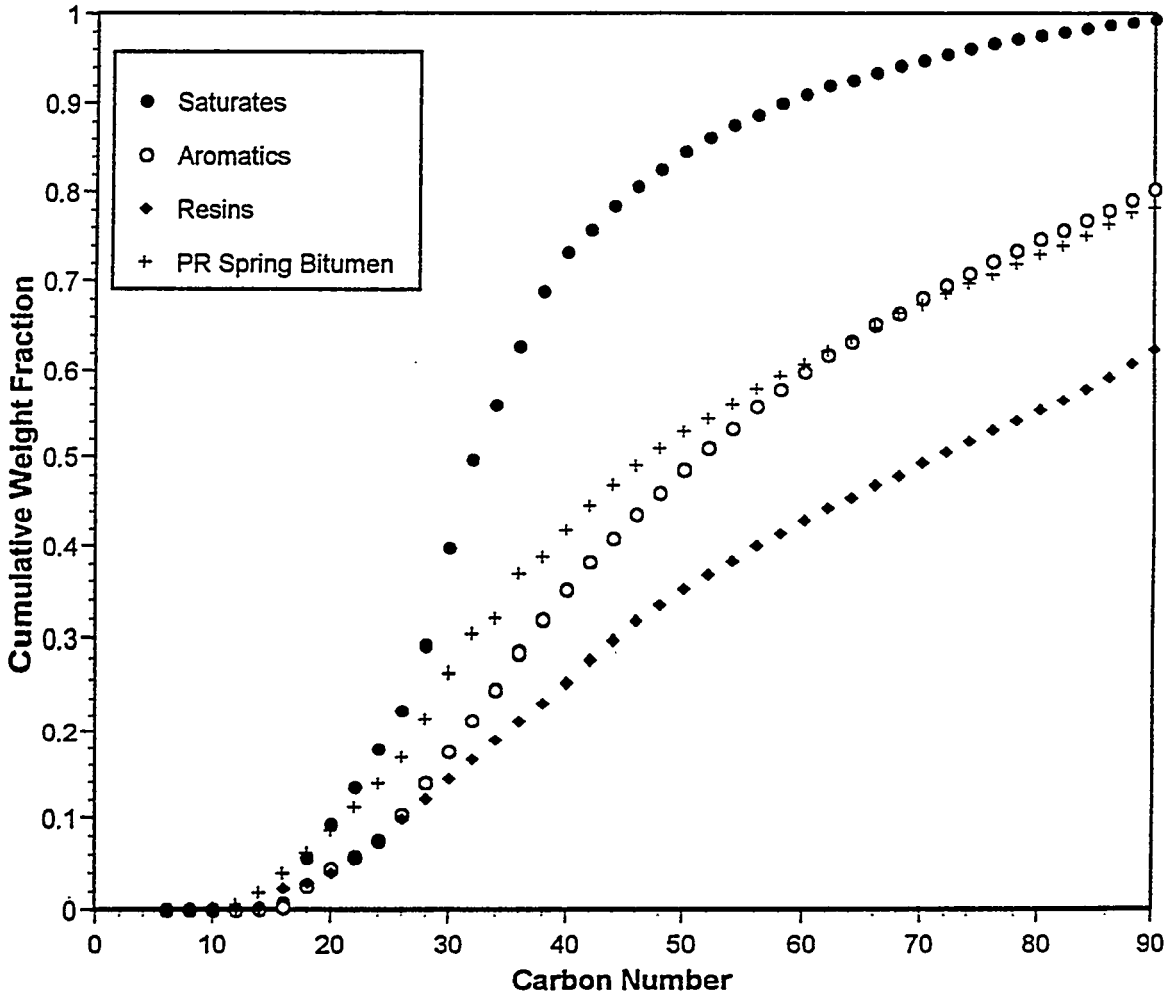
Saturates
Aromatics
Resins
PR Spring Bitumen
Cumulative Weight Fraction
Carbon Number
0
0.1
0.2
0.3
0.4
0.5
0.6
0.7
0.8
0.9
1
0
10
20
30
40
50
60
70
80
90

Figure 87.

Carbon Number Distributions for the Sunnyside Bitumen and the Saturates, Aromatics and Resins Solubility Fractions

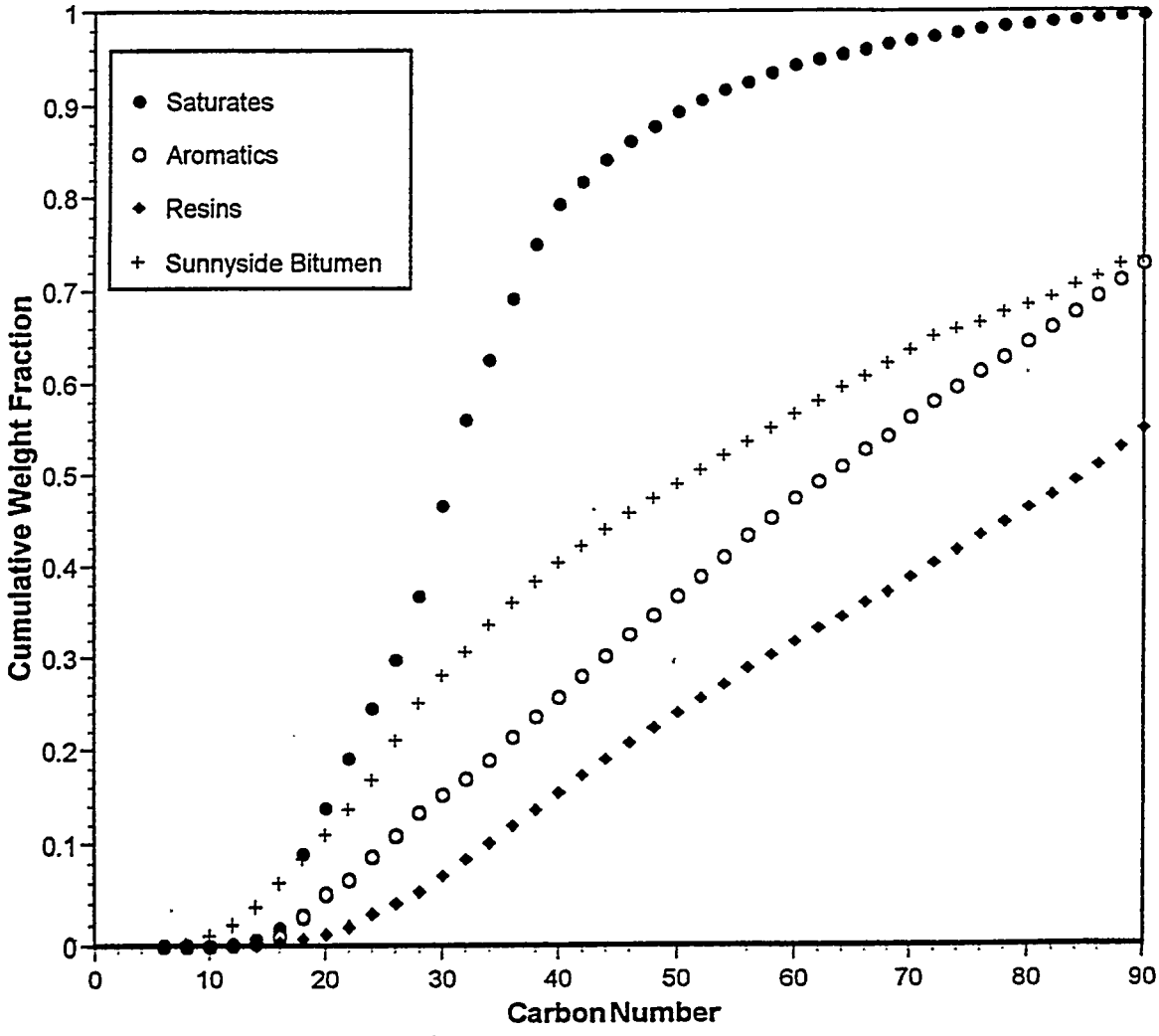
Saturates
Aromatics
Resins
Sunnyside Bitumen
Cumulative Weight Fraction
Carbon Number
0
0.1
0.2
0.3
0.4
0.5
0.6
0.7
0.8
0.9
1
0
10
20
30
40
50
60
70
80
90

FLUIDIZED BED PYROLYSIS OF OIL SANDS IN A THREE-INCH DIAMETER FLUIDIZED BED

Principal Investigator: F.V. Hanson
Co-Principal Investigator: J.V. Fletcher
Graduate Student: Qiming Tang

INTRODUCTION

Because of the special properties of oil sands, these materials cannot be recovered by conventional petroleum reservoir production techniques. The lack of sufficient reservoir energy and the viscous nature (>10,000 cp) of the reservoir fluid prevents movement through the formation to a production well (97). Also, the unconsolidated structure of oil sands deposits means that conventional underground mining methods, such as the room-and-pillar technique for mining of oil shale and coal cannot be used (98).

The methods used for the recovery of heavy oil from oil sand can be classified into two broad categories: in-situ recovery techniques and surface mining-recovery processes. The oil sands recovery method of choice is determined by cost, recoverability, and bitumen content.

In-situ processes recover bitumen-derived heavy oils from oil sands reservoirs by thermal and/or chemical means. The mobilized reservoir fluid is lifted to the surface for subsequent processing and upgrading. Typically thermal in-situ recovery techniques include steam injection, partial combustion, and combustion (99, 100). The costs associated with surface mining of oil sands are related to the thickness of the overburden which must be stripped to expose the oil sands. Generally, an overburden-to-pay zone ratio less than or equal to unity is required to justify a surface mining-recovery operation (101). Surface mining recovery processes involve open pit

mining of the oil sands ore at the surface followed by extraction and upgrading of the bitumen and disposal of the coked sands. In-situ recovery schemes can be employed where surface mining is not economically feasible.

Mining Surface Oil Sands Recovery Technologies

Surface recovery technology is the dominant method applied for the recovery of hydrocarbon values from oil sands (98). Surface recovery schemes include open pit mining of the oil sands, transportation of the ore from the mine site to the processing plant, and extraction and upgrading of the bitumen. The surface recovery of oil sands can be classified into two distinct categories. The first involves the use of water or solvents or a combination of both to separate the bitumen from oil sands (102, 103). The second category includes the various thermal processes used to produce bitumen-derived heavy oils from oil sands. The thermal processing of oil sands is carried out in a nonoxidizing environment (104, 105). The liquid products are upgraded and are of a higher quality than the bitumen recovered by aqueous separation or solvent extraction. The feasibility of an individual surface mining-recovery process is subject to economic constraints related to the pricing of conventional crude oil.

Thermal Processing Recovery Technologies

Surface thermal processing methods involve the heating of the mined oil sands to high temperatures (usually around 723 to 823 K) in a nonoxidizing environment (106). The high molecular weight hydrocarbon species in the bitumen undergo thermal decomposition reactions to form low molecular weight (about 370 to 500) compounds which volatilize to form gaseous and liquid products at high temperature. Simultaneously, a portion of the bitumen is polymerized to form a carbonaceous residue or coke. Thus pyrolysis of oil sands is a molecular weight reduction process. The liquid products produced during pyrolysis are of higher quality than the bitumens

obtained by solvent extraction processes. The terms *flash distillation, pyrolysis, retorting, cracking, volatilization, destructive distillation, coking,* and *carbonization* are frequently used interchangeably in discussing this process. The thermal process recovery methods can be classified into two general groups, direct heating and indirect heating, depending on whether the pyrolysis and combustion steps are carried out in one or two reactors. The thermal processes can further be subdivided into fluidized bed and rotary kiln reactor systems.

Fluidized bed pyrolysis was initially investigated by Gishler (107), in which fluidized bed technology was applied successfully to the flash distillation of oil from Alberta oil sands on a laboratory scale. The oil recovered represented 76 wt% of the bitumen fed to the reactor. A pilot plant reactor was developed and operated based on this process (108). The liquid yield for the pilot plant was over 80 wt% based on the bitumen fed. The Lurgi-Ruhr gas process has been adapted to the pyrolysis of oil sands (109). The process included the recirculation of clean, burned sand as a heat carrier. The oil yield was reported to be above 90 wt%. A direct heating process with pyrolysis and combustion in a single unit has also been investigated. In this case, the liquid yield was in excess of 83 wt% at a pyrolysis temperature of 744 K (110).

Rotary Kiln Pyrolysis Process

The rotary kiln process is an alternative to the fluidized bed pyrolysis process for the production of bitumen-derived heavy oils from oil sands. A single rotating vessel for the recovery of bitumen from oil sands was developed and patented (111, 112). Hanson et al. (113) studied pyrolysis of the Whiterocks oil sands in a rotary kiln reactor. The influence of process variables on the product distribution and yields was investigated. The trends reported for the effect of reactor temperature and solids retention time were similar to those reported for fluidized bed pyrolysis of the Whiterocks oil sands in laboratory scale reactors (114). A maximum liquid yield

of 69 wt% relative to the bitumen fed was achieved at a kiln temperature of 798 K and a solids retention time of 10 min (105).

Fluidized Bed Pyrolysis Process

Two-stage fluidized bed pyrolysis process studies have been conducted at the University of Utah (115-118). The process involved two units: a fluidized bed pyrolysis reactor and a coked sands combustion reactor. The oil sands were fed to the top of the upper pyrolysis reactor and underwent pyrolysis to produce a bitumen-derived heavy oil. The coked sands were transferred to the lower combustion chamber where the coke was burned. Heat was transferred from the combustion chamber to the pyrolysis zone by potassium heat pipes. The potassium was vaporized in the combustion zone and condensed in the pyrolysis zone. The results indicated that the liquid yield increased as the temperature increased in the range of 713 to 773 K, and as the solid residence time increased (117). Smart (117) reported that a maximum liquid yield would be expected to be obtained at solid retention times of around 9 min.

Oil sands pyrolysis using fluidized bed processes have been investigated by Hanson and co-workers (50, 51, 106, 114, 119-121). The process variables studied included reactor temperature, fluidizing gas velocity, solids retention time, oil sands source, and alternate fluidization modes.

Prescreened oil sands were fed continuously from the discharge feeders located on top of the reactors in the fluidized bed pyrolysis process studies. Oil sands particles fell directly into the fluidized bed, and the bitumen underwent pyrolysis to form hydrocarbon vapors, gases, and a carbonaceous residue on the sand particles. Vapor and gases were carried out by the nitrogen fluidizing gas, whereas the coke remained on the sand surface. The coked sands were withdrawn from the reactor by a solids control valve or a modified L-valve. The continuous flow reactor

systems were operated to maintain the bed hold-up constant. This was accomplished using a differential pressure controller.

The yields of bitumen-derived liquids were primarily dependent on the pyrolysis temperature and on the solids retention time which was determined by the oil sands feeding rate and the bed hold-up. The liquid products decreased with increased pyrolysis temperature and increased with decreased solids retention time. The total liquid yields and product distribution appeared to be independent of the fluidizing gas velocity in the range of velocities investigated. The amount of bitumen converted to coke on the sand was relatively insensitive to process variables; however, it was dependent upon the source of the feed sands. Most of the oil sands exhibited maximum total liquid yields at pyrolysis temperatures in the range 773-798 K.

It was concluded from these oil sands pyrolysis investigations (50, 51, 106, 114, 119-121) that the most important pyrolysis process variables were the pyrolysis temperature and the solids retention time. Temperature appeared to be more significant than the solids retention time in determining the product distribution and yields and the quality of the total liquid products (104).

EXPERIMENTAL APPARATUS AND PROCEDURES

The fluidized bed reactor (FBR) oil sands pyrolysis system was a laboratory scale, continuous flow reactor. The apparatus consisted of a fluidized bed reactor, an oil sands feeder, an electric furnace, a solids withdrawal L-valve, liquid recovery condensers, and measurement and control instrumentation. The unit will be described in detail in this chapter.

Fluidized Bed Experimental Apparatus

Fluidized Bed Reactor Pyrolysis Apparatus

Schematics of the fluidized bed reactor when operated in the push and pull fluidization modes (121) are presented in Figures 88 and 89, respectively. Nitrogen was used as the fluidizing and purge gas in all pyrolysis experiments. The fluidizing gas was preheated and evenly distributed in the windbox and passed through the gas distributor into the pyrolysis zone. The purge gas flowed continuously through the coked sands receiver. The purpose of maintaining a positive purge gas pressure in the coked sands receiver was to prevent air leaks and the combustion of the carbonaceous residue on the coked sands.

The reactor was loaded with screened coked sands at the beginning of each experiment. The amount was established by the ratio of the intended height of the settled bed to the reactor diameter (H/D). The appropriate H/D ratio had been previously determined in the preliminary fluidization studies conducted with the coked sands. The reactor temperature was raised to the desired pyrolysis temperature, and the coked sands were fluidized to establish hydrodynamic and thermal stability in the bed. The oil sands feed was introduced into the reactor stepwise by increasing the feeder speed in increments until the desired feed rate was obtained. Oil sands were fed continuously at the top of the reactor and dropped through the expansion chamber into the fluidized bed due to gravity. Once a steady state condition was attained, data

Figure 88.

Schematic of the Fluidized Bed Reactor Pyrolysis Push Mode

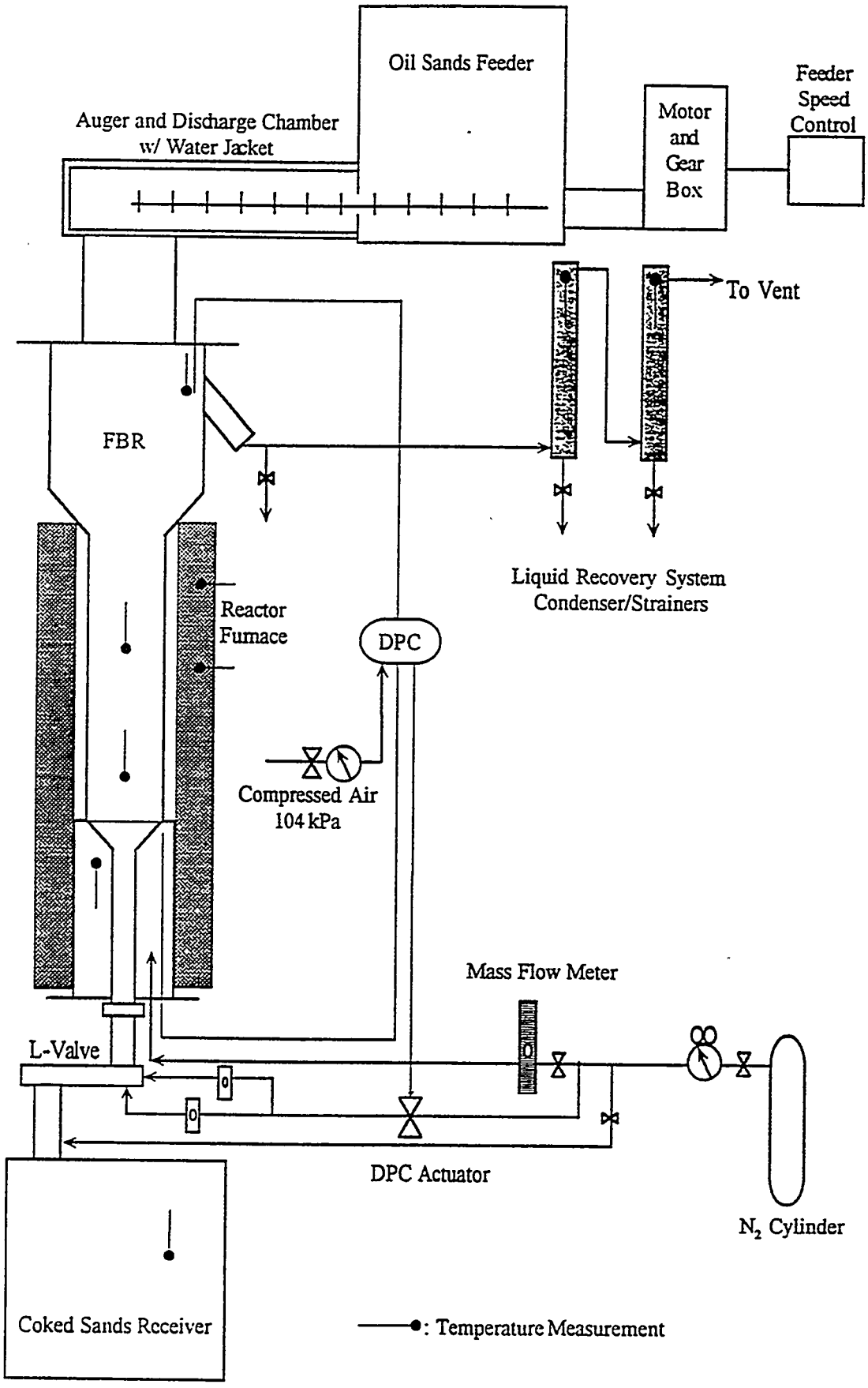
Oil Sands Feeder
Feeder Speed Control
Motor and Gear Box
Auger and Discharge Chamber w/ Water Jacket
To Vent
FBR
Liquid Recovery System Condenser/Strainers
Reactor Furnace
DPC
Compressed Air 104 kPa
Mass Flow Meter
L-Valve
DPC Actuator
N2 Cylinder
Coked Sands Receiver
: Temperature Measurement

Figure 89.

Schematic of the Fluidized Bed Reactor Pyrolysis Pull Mode

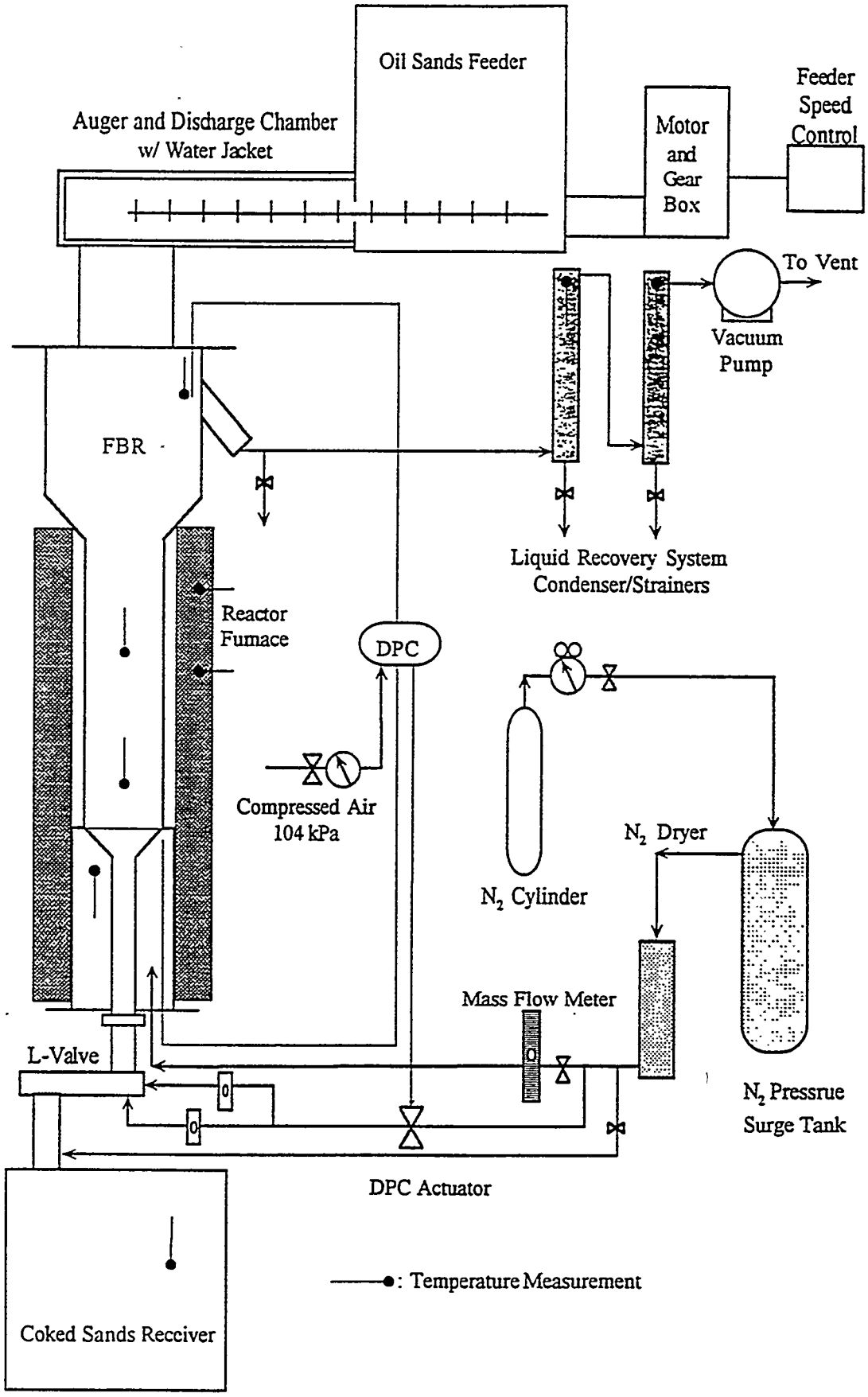
Oil Sands Feeder
Auger and Discharge Chamber
w/ Water Jacket
Motor
and
Gear
Box
Feeder
Speed
Control
To Vent
Vacuum
Pump
FBR
Liquid Recovery System
Condenser/Strainers
Reactor
Fumace
DPC
Compressed Air
104 kPa
N2 Cylinder
N2 Dryer
Mass Flow Meter
L-Valve
N2 Pressrue
Surge Tank
DPC Actuator
: Temperature Measurement
Coked Sands Receiver

logging was started and the run initiated. Initial liquid, solid, and gas samples were collected at the start of the steady state operation.

The fluidized bed hold-up was maintained at a constant value by a solids withdrawal L-valve. The differential pressure drop across the bed was monitored and controlled. Pressure taps were located at the exit of the disengager and in the windbox underneath the gas distributor. When the differential pressure exceeded the set-point, a signal was sent to an actuator which caused the nitrogen to flow into the L-valve and coked sands were withdrawn from the reactor. Since the pyrolysis reaction is an endothermic reaction, thermal energy was supplied to the reactor by means of an electrical furnace which had four separate heating zones.

The mixture of coked sands and oil sands in the reactor were fluidized by preheated nitrogen, and the bitumen was pyrolyzed. The heavy oil vapors and entrained fine particles were carried out of the disengager into the liquid recovery system. The entrained particles and liquids were separated in the recovery system, and the liquids were withdrawn from the condensers. The liquid recovery system consisted of a condensing pipe and two water cooled liquid filter-condensers in series. The noncondensable hydrocarbon gases flowed through a transfer line and two water cooled condensers. The condensate-free gas was sampled and vented to the stack.

Fluidized Bed Reactor Assembly

Fluidized Bed Reactor

The fluidized bed reactor was fabricated from 304 stainless steel with a flange welded to each end. The reactor consisted of the main body, the windbox, and the disengager sections. Main body section had a 7.62 cm inside diameter (ID) and was 76.2 cm long with a maximum throughput of 3 to 4 kg/h depending upon the individual oil sands feedstock. The expansion chamber was intended to reduce the superficial gas velocity above the bed which allowed fine particles to fall back into the bed. The

windbox was designed to preheat nitrogen to the pyrolysis temperature. The conical gas distributor located between the fluidized bed and the windbox was intended to evenly distribute the gas across the reactor.

A stainless steel ring, 7.62 cm ID by 11.43 cm OD and 0.95 cm thickness, was welded to the reactor wall between the reactor and windbox sections. A 3 mm deep by 3 mm wide groove at a diameter of 8.89 cm was machined on the bottom side of the ring. The edge of the distributor fitted into the groove to form a seal which prevented by-passing of the fluidization gas.

Fluidizing Gas Distributor

Thirty-two evenly distributed holes, 0.16 cm in diameter, were drilled through the 304 stainless steel conical gas distributor perpendicular to the surface. The holes were drilled in a staggered pattern consisting of three sets of holes at different depths in the cone: 14, 10, and 8 proceeding from shallowest to the deepest set (see Figure 90). The holes provided a nominal open surface area of 1.4 % based on the reactor cross-sectional area. The gas distributor, sand withdrawal pipe, and bottom flange were welded into one piece. The sand withdrawal pipe was 2.54 cm ID with standard pipe threads. Thus the height of the gas distributor could be adjusted. The distributor was installed in the reactor and adjusted to fit into and seal the groove. Also, a flexible graphitic packing material which could withstand 3033 K under nonoxidizing conditions from Palmetto was used as a sealant between the edge of the distributor and the groove machined into the interior ring. The bottom flange had a nitrogen inlet fitting (0.64 cm ID) and three NPT fittings (0.32 cm ID) for control and monitoring of temperatures and pressures.

Oil Sands Feeding System

The oil sands feeder was a standard commercial bin discharge feeder manufactured by Acrison, Inc. A schematic of the feeder and the control system has been presented by Hanson et al. (122). The original Acrison Model BDF-1-C/2 feeder

Figure 90.

Schematic of the Gas Distributor for Fluidized Bed Reactor

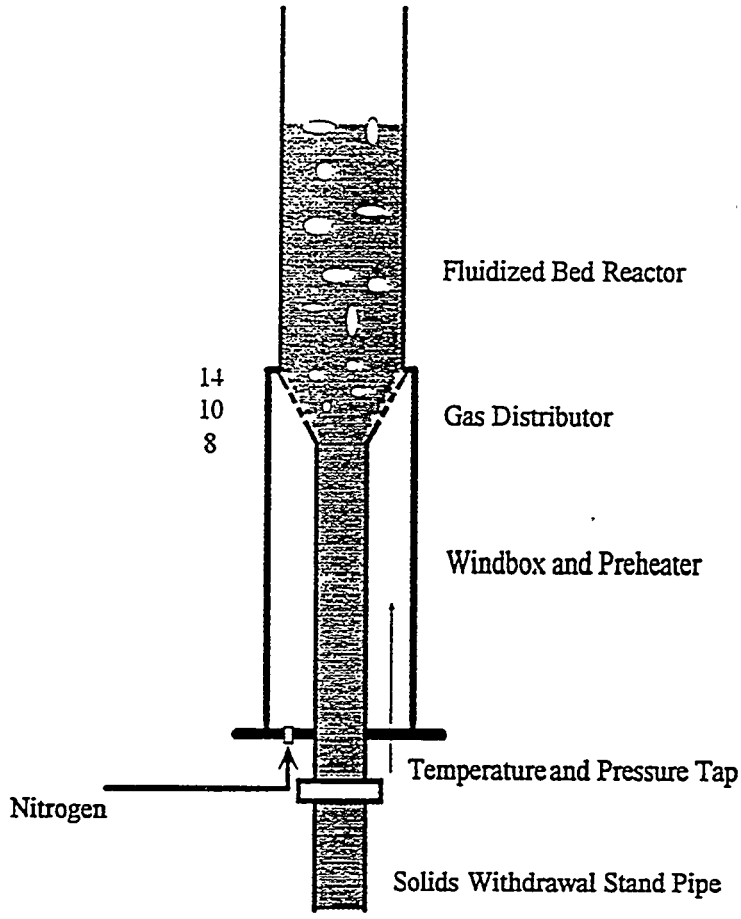
Fluidized Bed Reactor
14
10
8
Gas Distributor
Windbox and Preheater
Temperature and Pressure Tap
Nitrogen
Solids Withdrawal Stand Pipe

was equipped with a C-auger. The standard C-auger plugged because of the unique feeding characteristics of oil sands. The feeder was modified by increasing the auger diameter and by reducing the length of the auger. An E-size auger was used to eliminate the tendency of the oil sands to fill the gap between the auger and auger housing and to maintain constant feed rates. The length of the discharge cylinder was reduced from 45.72 to 30.48 cm and the auger housing was equipped with a water-cooled jacket (Figures 88 and 89).

A 10.16 cm long and 10.16 cm ID heat resistant rubber clamp was used to connect the reactor and the feeder downspout to reduce heat transfer from the pyrolysis reactor to the feeder. The water jacket was used to maintain the auger housing temperature below 290 K.

The feeder specifications were as follows:

- Acrison bin discharge volumetric feeder Model BDF-1-E/2, SN 91380-1.
- Digital variable speed SCR/DC controller Model 050-1A operatingrange of 0-99.9 %.
- 373W DC motor.
- 0.0286 m^3 feed hopper.

The auger was a stainless steel solid shaft. The discharge cylinder was equipped with an auger end bearing and a stainless steel 10.16 cm downspout. The discharge downspout cover had two 0.64 cm NPT fittings equipped with feed-through were used for temperature monitoring and control.

Gas Introduction System

The reactor was designed to operate in a non-oxidizing inert gas environment at atmospheric pressure and at temperatures up to 823 K. Cylinder nitrogen was used as the fluidizing gas, aeration gas, and purge gas in all the experiments. A mass flow meter from OMEGA, Model FMA-5611, and a Whitey needle valve were to monitor and control the flow rate of fluidizing gas, respectively. Aeration nitrogen to the L-

valve was regulated by two Matheson flow meters, Model 1050, with 0-7.5 LPM flow tubes and aluminum utility valves. The flow meters were connected to an air-to-close Type 78S control valve supplied by Research Controls with an M-trim and a 21 to 103 kPa pressure range. The coked sands receiver was purged with nitrogen to prevent spontaneous ignition of the carbonaceous residue on the coked sands withdrawn from the reactor.

Compressed building air was used as the supply gas for the differential pressure control unit. The line pressure was regulated to 207 kPa by a brass Whitey needle valve and a Model 14R air regulator from Schrader Bellows.

Modified Solids Withdrawal L-valve

A schematic of the modified L-valve is presented in Figure 91. The coked sands withdrawal system consisted of an L-valve and a solids receiver. The coked sands were intermittently withdrawn from the bed to maintain a constant inventory in the reactor. The L-valve was similar to that used for the 15.24 cm diameter fluidized bed reactor (121).

The L-valve assembly was constructed from 2.54 cm ID 304 stainless steel Schedule 40 pipe and cross and tee fittings. The length of the downcomer was 45.72 cm, and the horizontal section was 10.16 cm. There were two nitrogen injection ports in this modified L-valve. The main aeration point was positioned at the center line of the horizontal section behind the downcomer (Point A) and the auxiliary gas injection port was located on the center line of the downcomer and below the horizontal pipe (Point B). The purpose of the second injection port was to facilitate the withdrawal of coked sands and to assist in the removal of large lumps, whenever the main injection port (Point A) did not provide sufficient surge energy to purge coked sands from the valve.

The coked sands receiver was a modified 30-gallon commercial barrel. The lid of the drum had two 0.32 cm NPT half couplers which were used as a thermocouple

Figure 91.

Schematic of the L-valve and the Solids Receiver System

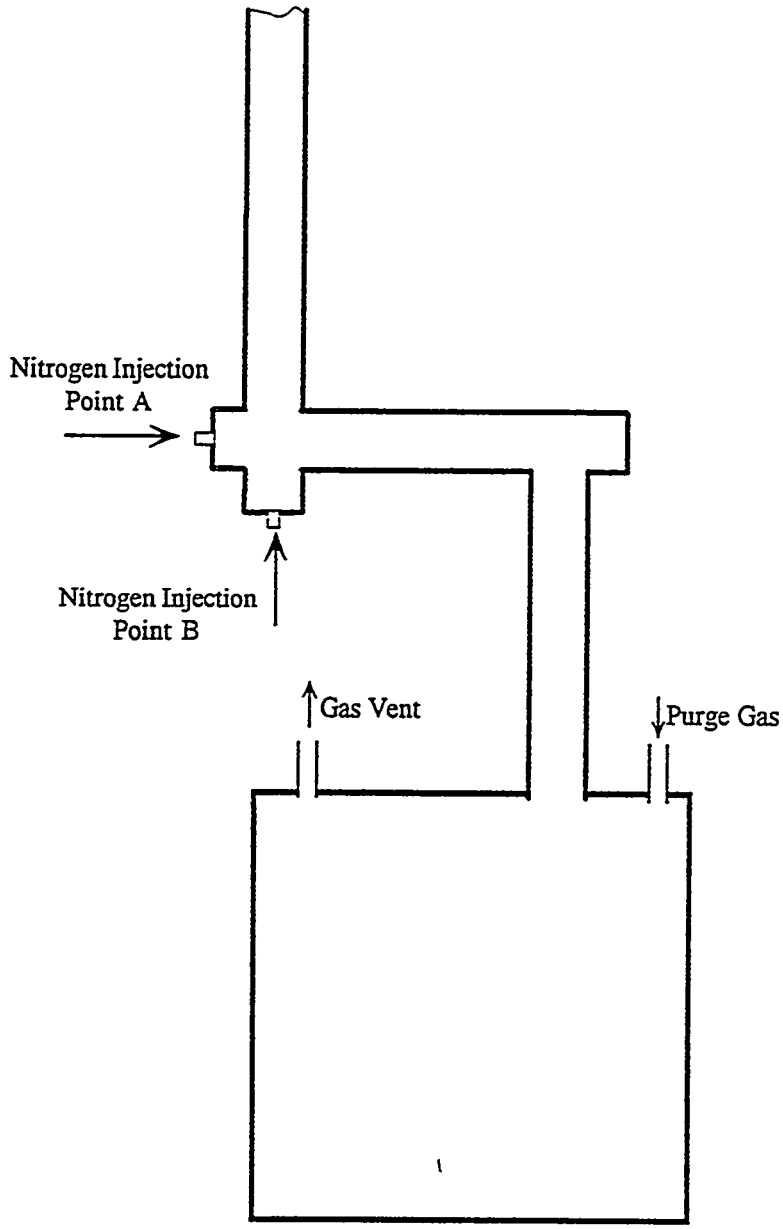
Nitrogen Injection
Point A
Nitrogen Injection
Point B
Gas Vent
Purge Gas

feed through for temperature measurement and as the purge gas vent. The L-valve was connected to the coked sands receiver by a 15.2 cm long 2.54 cm diameter flexible pipe.

Process Control and Monitoring Instrumentation

The process variables, including temperatures, pressures, and flow rates of gases and solids, were controlled and monitored during the course of an experiment. Provision was made for both manual and automatic control.

Liquid Product Recovery System

The purpose of the liquid product recovery system was to condense the maximum amount of liquids from the gas stream and to separate the entrained sand particles from the liquid product. A schematic of the liquid product recovery system for solids-liquids-gas separation is presented in Figure 92.

The recovery system included three components: the prestrainer trap to collect heavy liquids and two liquid recovery strainers in series. The prestrainer trap was made from 2.54 cm stainless steel pipe fittings with a 0.64 cm NPT Speedy valve for withdrawal of condensed liquids. Insulation materials were wrapped on the condenser pipe to maintain a constant temperature.

The product vapors were carried along with the nitrogen sweep gas as it passed through the prestrainer trap into the first liquid collection strainer which had been fabricated from modified high pressure water purifiers. The perforated stainless steel strainer was 8.89 cm in diameter and was 45.72 cm long with an open area of 58%. The inner strainer screen and its cover were connected by a twist pin lock and sealed by an O-ring gasket. The liner of the cylinder was a 200 mesh stainless steel screen which functioned as a solid-liquid-gas separation device. The second strainer was fitted with two Rosedale 10.16 cm diameter 25 micron prewetted multifilament polyester bags to capture the fine oil mist present in the gas stream after the first strainer.

Figure 92.

Schematic of the Liquid Recovery System

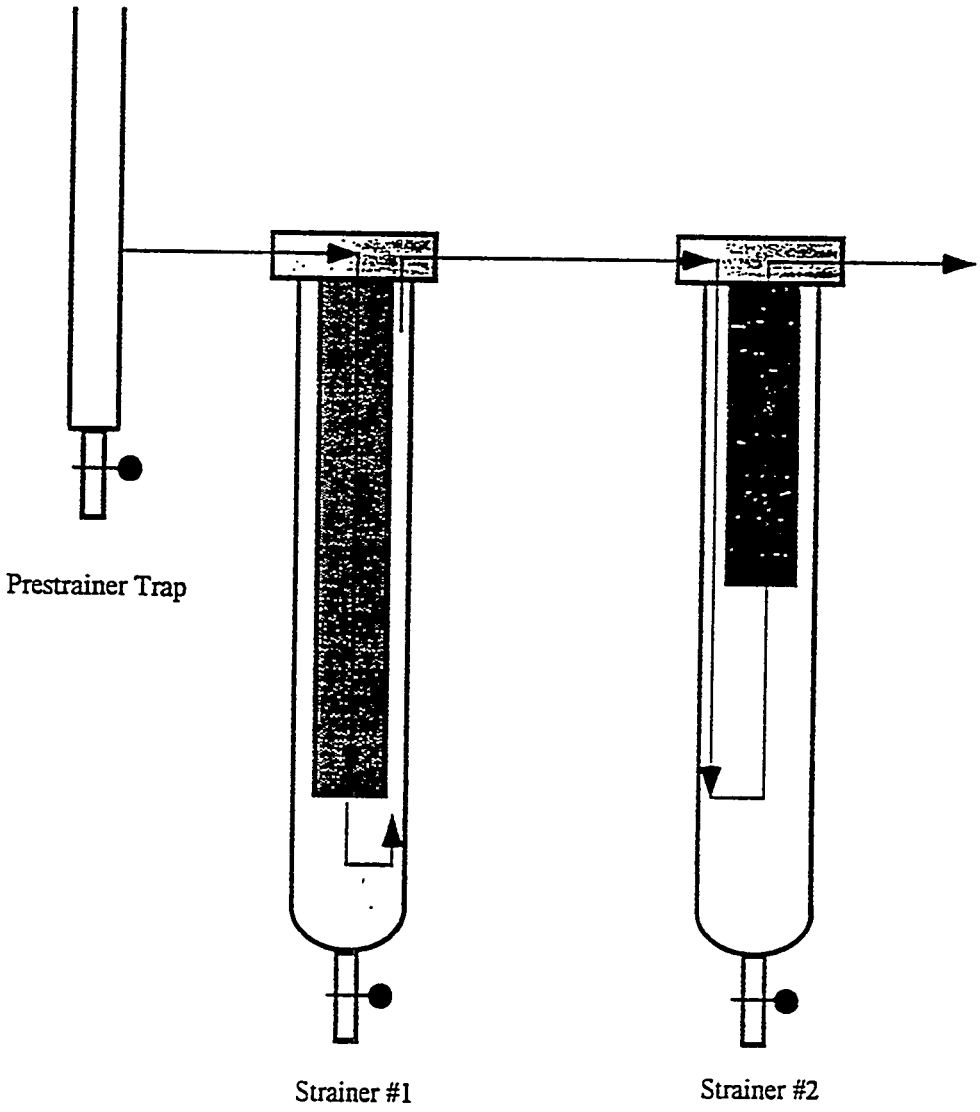
Prestrainer Trap
Strainer #1
Strainer #2

The vapor product stream passed into the strainer, penetrated the screen and passed out through the outlet. The entrained solid particles were retained inside the screen and the mist condensed to form the liquid product after penetrating the screen. The liquid accumulated at the bottom of the first strainer. The second strainer filter had two 25 micron prewetted filter bags which adsorbed almost all of the light liquids at room temperature. Both strainers had bottom drain valves for liquid removal. The chromatographic analysis indicated only trace amounts of C_5^+ hydrocarbons were present in the vented gas stream.

Electrical Furnace

The thermal energy required for the oil sands pyrolysis reaction was provided by a 14 kW four-zone electrical furnace Model M-5048-S-V manufactured by Lindburg. The furnace had four separate heating zones which could be controlled at different temperatures as required. The furnace was powered by four two-phase 20A 240V AC circuits. The silicon carbide heating elements were wrapped thermal resistant wires. Each of the power circuits was controlled by a temperature controller and a solid state relay. The power supply wiring to the furnace and control panel were installed by University of Utah Campus Utility Services.

Bed Height Determination

The bed height was an indirect measurement; that is, it was determined by the bed hold-up divided by the coked sands packed density and the reactor cross-sectional area. The particle bulk density was determined by placing a weighed amount of coked sands into a 10.2 cm ID transparent glass column and measuring the height of the sands. The particle bulk density was obtained by the weight of the sands loaded into the column divided by the volume it occupied. Using the particle bulk density, the reactor cross-sectional area, and the weight of sands loaded into the reactor the settled bed height was calculated from the following relationship:

$$H = \frac{W_b}{\rho_{bk} A} \qquad (17)$$

The bed height was usually expressed as a dimensionless parameter of H/D, which is the ratio of the bed height to the reactor diameter.

Stepwise Oil Sands Feeding During Pyrolysis

A typical feeder speed pattern (QTPRS05) is shown in Figure 93. After the fluidized bed reactor was loaded with 1750 g screened coked sands and the desired temperature (i.e., 773 K) was established in the settled bed, fluidizing gas was introduced into the reactor at 10 LPM. The pressure drop across the bed gradually built up. Steady state fluidization was usually attained after 20 minutes with the bed of coked sands. The bed temperature did not exhibit significant fluctuations during this period. Oil sands feeding from the Acrison feeder was started after stable fluidization was achieved at the desired temperature and fluidization gas flow rate. Oil sands feed rates were increased to the desired level in step increments. Normally, a higher oil sands feed rated required a longer time to reach steady state. Once a steady state condition was attained, the motor speed set point was once again incrementally increased. The temperature and differential pressure of a typical steady state condition (QTPRS05) were 773±3 K and 2.27±0.06 kPa. The operating parameters indicated that the system had the capacity to supply sufficient energy for the pyrolysis of oil sands at all the feed rates investigated. The differential pressure control and solids withdrawal system were continuously monitored, and coked sands were intermittently removed by means of the L-valve.

Product Analysis Methods

The pyrolysis products of the PR Spring oil sands included the total liquid product, the C_1-C_4 light hydrocarbon gases, and a carbonaceous residue on the spent

Figure 93.

Schematic of Stepwise Oil Sands Feeding Method

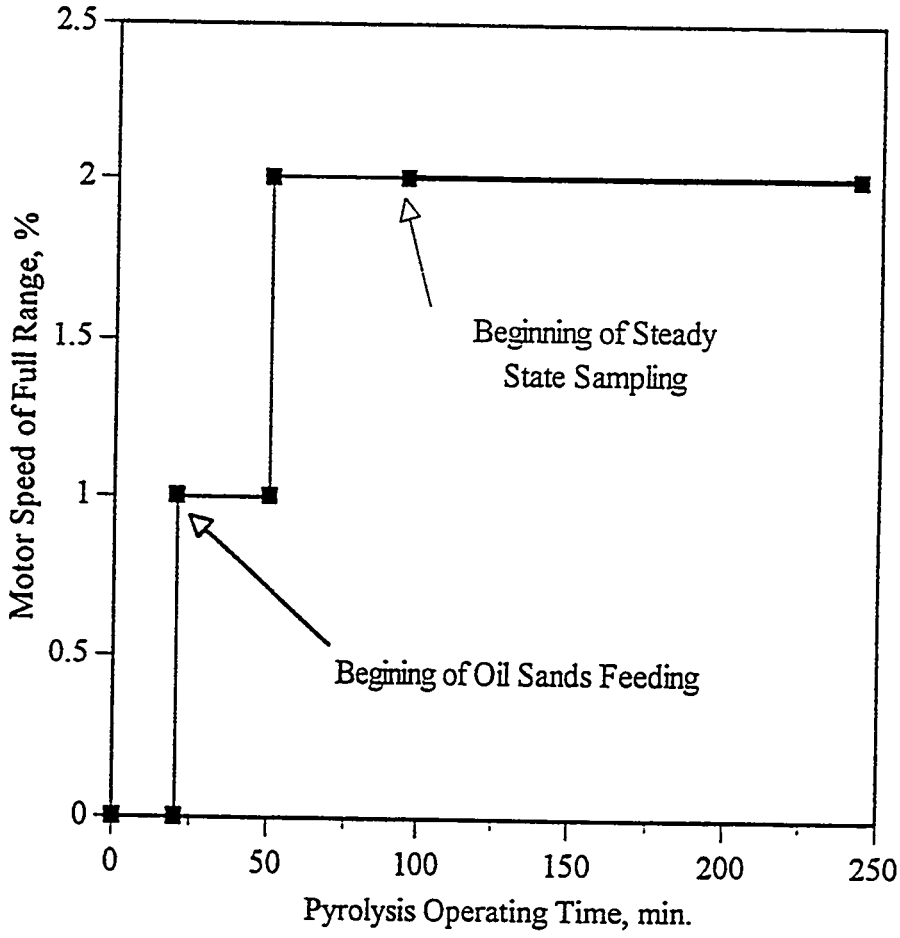
2.5
2
1.5
1
0.5
0
Motor Speed of Full Range, %
Beginning of Steady
State Sampling
Begining of Oil Sands Feeding
0
50
100
150
200
250
Pyrolysis Operating Time, min.

sands which is also referred to as coke. The mass balance calculations were based on the bitumen fed to the reactor. An experiment was considered successful when the bitumen mass balance was over 90 wt%. Experiments were rejected when the mass balance was less than 90 wt%.

Gas Sample Analysis

The pyrolysis hydrocarbon (HC) gases leaving the liquid recovery systems contained mainly nitrogen and small amounts of hydrocarbon gases ranging from C_1 to C_6. The HC gas species were identified and quantified using a Hewlett Parkard 5890A gas chromatograph equipped with a thermal conductivity detector (TCD) and a microprocessor. A 80/100 SUPELCO chromsorb 102 column (3.18 mm diameter by 6.1 m long) was used for gas separation in this investigation. Helium was used as both the carrier and reference gas. The recommended carrier and reference gas flow rates were 20 and 30 ml/min, respectively, and the inlet pressure was 6.80 kPa. The hydrocarbon species thermal response factors for the TDC were determined and calculated by the method proposed by Dietz (123) and Rosie and Barry (124). The actual response factors for this investigation were obtained from Tang (125) and Nagpal (106). The HC gas analysis was conducted in two steps to compare the relative ratios of each species. The low sensitivity signals were sent to an IBM-XT computer with data acquisition software and were used to obtain the relative ratio of nitrogen and methane. At high sensitivity, the nitrogen peak was off the integrated range, but the relative amounts of all low concentration species were quantified. The Visualized GC software collected and integrated each hydrocarbon peak. The fractions of each individual compound were computed by combining data for the two-step analyses.

Coke and Extractables Analysis

The coked sands samples from each pyrolysis experiment were prepared by cone and quartering the coked sands collected in the sands receiver and the reactor during the experiment (126). The coke content was determined according to the

method reported by Wang (114) and Shun (120). Two crucibles which contained 2 g coked sands samples were placed into a muffle furnace at 823 K for 16 hours, transferred to a desiccator, and cooled to ambient temperature. The crucibles were weighed and the total combustibles were determined by difference. The crucibles were removed from the dessicator and weighed every 2 hours until the second decimal did not change.

A 20 g coked sands sample was charged to a tared thimble and put into a vacuum dryer overnight at 378 K at the same time. The sample was removed from the dryer and weighed every two hours until the second decimal did not change. The weighed thimble containing the coked sands sample was placed in a Soxhlet extraction apparatus and extracted for 48 hours using toluene as a solvent. The thimble was placed into the vacuum dryer overnight and dried at 378 K to evaporate the residual toluene. The toluene extractables were determined by difference. The coked sands withdrawn from the reactor was checked for toluene extractables to ensure correct reporting of the product distributions and bitumen mass balances. The amounts of toluene extractables in this investigation were generally negligible; that is, no measurable quantities of extractables were detected using a five decimal place analytical balance.

Liquid Product Analysis

Selected physical and chemical properties of the bitumen and the pyrolysis liquid products were determined. The properties included simulated distillation; specific and API gravities; viscosities; Conradson carbon residues and ash contents; pour points; C, H, N, and S elemental analyses; nickel and vanadium metal contents; and molecular weights. The analytical methods used to determine the properties of the samples were adopted from the ASTM standard methods and the Syncrude Analytical Methods (127). The elemental, metals, and molecular weight analyses were performed by Galbraith Laboratories, Inc., Knoxville, Tennessee.

Bitumen Mass Balance Calculation

The pyrolysis runs using the PR Spring oil sands feed were carried out in a laboratory scale fluidized bed reactor system. The mined oil sands ore was crushed and screened through a 0.32 cm sieve and air dried in a 1.8 m by 3.0 m rectangular polyethylene box prior to being loaded into the feeder storage bin.

Mass balance calculations included the bitumen-derived heavy oil yield, the C_1-C_4 hydrocarbon gas yield, and carbonaceous residue yield. The calculations reported were based on a bitumen saturation of 10 wt% water-free basis which was determined by Soxhlet extraction of a cone and quarted sample over a 48-hour period using toluene as a solvent.

Material balances ranged from 90 to 110 wt% based on bitumen fed to the reactor. The best mass balances obtained were 100 wt%. If the mass balance was not 100 wt%, the yields were normalized to 100 wt%.

Product Gas Analyses and Yield Calculations

The qualitative and quantitative analyses of the product gases were determined using a Hewlett-Packard 5890A gas chromatograph. The molar ratios are the same as the volume ratios for the gaseous compounds. The computation of the amount of each compound was based on the nitrogen flow rate. The assumption was made that all nitrogen present in the process gas was from fluidizing gas. Also, it was assumed that a negligible amount of hydrogen gas was produced during the process; thus the product gas yields were reported on a nitrogen and hydrogen free basis.

Since nitrogen was used as an inert gas, its flow into the system equaled its flow out of the system; thus it was treated as an internal standard for the calculation of product gas composition. The following equations were used to determine the weight of each compound in the gas stream based on the steady-state samples taken during the pyrolysis process.

The quantitative analysis for the C_1 to C_6 yields were calculated as follows:

Mass ratio (MR) calculation

$$MR = \left(\frac{A_{N_2}}{A_{CH_4}}\right)_{LS}\left(\frac{A_{CH_4}}{A_i}\right)_{HS} = \frac{A_{N_2}}{A_i} \qquad (18)$$

Mass of a single gas specie

$$M_g = T_{ss} \times V_{STP} \times \frac{T_{STP}}{T} \times MR \times MW_i \qquad (19)$$

where MR is the nitrogen to specie i mass ratio based on the integrated area; A is the integrated area which was corrected by compound response factors; LS and HS indicate the low sensitivity and high sensitivity chromatographs, respectively; T_{SS} is the total steady state sample collection time, min; V is the nitrogen volumetric flow rate, LPM; T is the temperature, K; MW is the molecular weight, g/mol; and STP is the standard temperature and pressure of 273.15 K and 1 atm.

The hydrocarbon gas and coke yields in the bitumen mass balance were assumed to represent 100% recovery in the process. Thus, the losses were presumed to be liquid products. Some of the hydrocarbon vapors may have condensed in the section intended to isolated the feeder downspout from the reactor expansion chamber (Figure 88). It is possible that a portion of the vapor products condensed on the wall in that section. This would result in a loss of liquid products and a low mass balance.

Solids Retention Time Calculation

Oil sands feed rate was computed based on the coked sands produced during the mass balance period. The coked sands production rate was calculated by weighing total coked sands produced during the mass balance period of the experiment divided by the

duration of the run. Bed hold-up was indirectly determined by averaging the bed hold-up in the reactor before or after the experiment.

$$\theta_s = \frac{W_b}{F} = \frac{1000}{4633.7/121} = 26.1\,\text{min} \qquad (20)$$

where $_s$ is the solids retention time, min; W_b is the bed hold-up, g; and F is the oil sands feed rate, g/min.

RESULTS AND DISCUSSION

Although the fluidized bed process has been adopted to the pyrolysis of Utah oil sands, a series of equipment and operating problems had always been associated with this process. The problems included plugging of oil sands feeder, clogging of solids withdrawal valves, slugging of the bed, and loss of liquid products from the recovery system (50, 51, 114, 119, 120). A 15.2 cm diameter fluidized bed reactor system was designed and tested by Fletcher (121). The system was operated successfully in oil sands pyrolysis studies with the Whiterocks oil sands (121) and the PR Spring oil sands (106). Acrison dry-materials feeders provided reproducible oil sands feed rates (122). The L-valve used as a solids withdrawal device solved the solids removal problem (121). A novel pull fluidization mode eliminated bed slugging (121).

A 7.62 cm diameter reactor was used to investigate the continuous fluidized bed pyrolysis of the PR Spring oil sands under regular fluidization conditions. The objective was to investigate reproducible oil sands feeding with a small Acrison feeder, to evaluate the performance of an intermittent solids discharge L-valve on a small diameter fluidized bed reactor, to develop an effective liquid products recovery system, and to conduct a process variable study with the PR Spring oil sands. The fluidization studies included fluidization and defluidization experiments with Group B sands (128), an investigation of the fluidization characteristics of the bed under different fluidization modes, determination of the minimum fluidization velocity at elevated temperatures, and determination of the performance of the tapered gas distributor during fluidization. The pyrolysis process variable study with the PR Spring oil sands ore was intended to determine the influence of reaction temperature and feed sands retention time on the product distribution and yields and on the total liquid product quality. The results of these studies are described in detail in this chapter.

Coked Sands and Oil Sands Feeding

A Model BDF-1 commercial bin discharge dry-materials feeder from Acrison was used in the oil sands feeding study and as the oil sands feeder in the process studies. The feeder was capable of having the auger and auger housing changed. Thus variations in auger size and type and in the discharge cylinder could be studied.

Oil sands are silica particles coated by a viscous hydrocarbon, called bitumen. The rheological characteristics of the bitumen-impregnated sandstone changes as it is transported through the screw feeder. A coating of compacted oil sands formed on the feeder auger and the inner wall of the discharge chamber in the laboratory scale and semipilot plant scale oil sands pyrolysis studies (119, 120) due to shear and frictional forces. The feed rates decreased with time, and eventually the discharge chambers were plugged by the oil sands mixtures. The plugging problem was temporarily solved by using a feed that consisted of oil sands premixed with coked sands produced in the previous pyrolysis experiments (51, 105, 118). However, increasing the sand content of the feed mixture reduced the average bitumen content and increased the sensible heat requirement for the sands in the reactor. The objective in this investigation was to develop the ability to feed oil sands directly to a small diameter reactor without diluents.

Coked Sands Feeding Study

The initial feeder studies were conducted with spent coked sands. The coked sands used were produced from the previous fluidized bed pyrolysis study with the Whiterocks oil sands (119). The coked sands consisted of the sand granules coated with a carbonaceous residue and were nonsticky, free flowing materials similar to regular sand grains.

The coked sands calibration curves using a C-auger are presented in Figure 94. These curves indicated that the Acrison BDF-1 feeder gave linear and reproducible feed rates over the complete range of motor speeds when handling dry materials. The

Figure 94.

Feeder Calibration Curves Using a Solid Flight C-auger with the Whiterocks Coked Sands

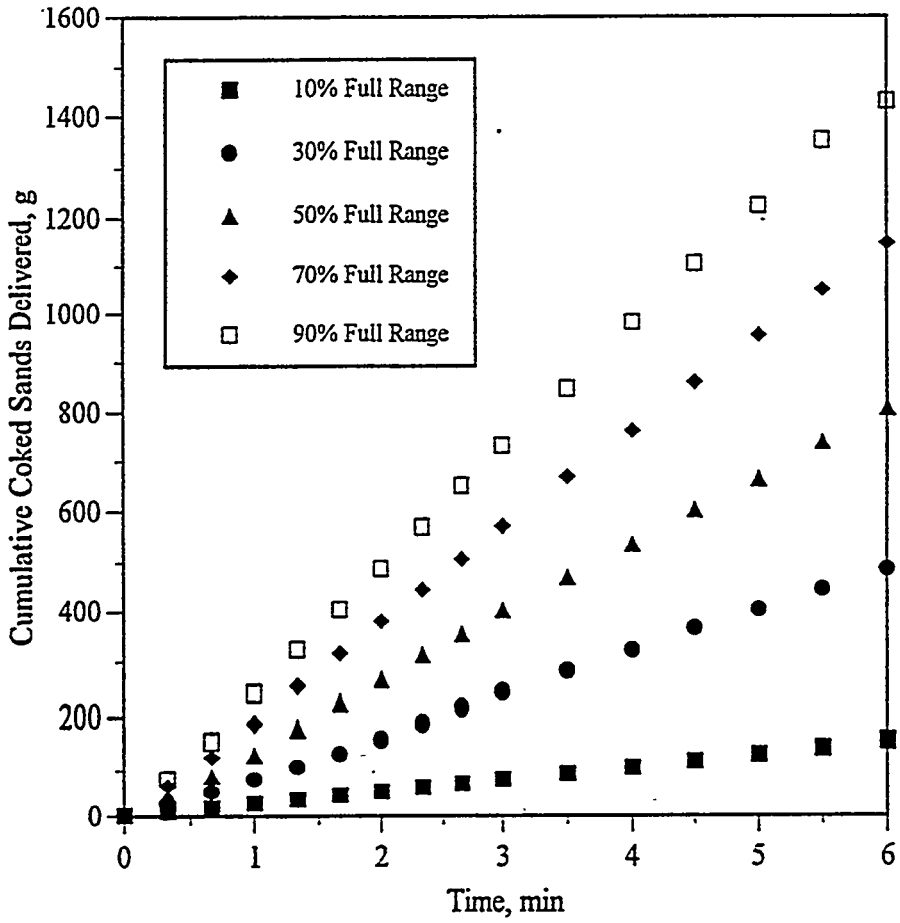
10% Full Range
30% Full Range
50% Full Range
70% Full Range
90% Full Range
Cumulative Coked Sands Delivered, g
Time, min
0
200
400
600
800
1000
1200
1400
1600
0
1
2
3
4
5
6

feed rates of coked sands can be determined from the slopes of the lines in Figure 94 for a given motor speed. The coked sands feeder studies demonstrated that the feeder could successfully handle dry oil sands related materials.

Oil Sands Feeding Study

The mined and crushed ores from the Whiterocks and PR Spring oil sands deposits were used for the feeder calibration-studies. The mined ore was crushed and screened to provide particle size ranges below 6.4 and 3.2 mm for the Whiterocks and PR Spring ores, respectively. The bitumen saturations for the Whiterocks and PR Spring ores were 7 and 10 wt%, respectively. Samples were air dried for more than 30 days to evaporate gravitational moisture.

As mentioned previously, the unique characteristics of oil sands caused unstable feeding rates with laboratory scale screw feeders. The auger configurations (diameter, shape, and length) were important factors affecting oil sands feeding. The auger diameters increased according to the alphabetical sequence (C, D, E, F) in Table 24. The void volume-to-surface area between the auger and the inner auger housing increased as the alphabetic order. The surface area included the inner surface of the cylindrical auger housing and the area on both faces of the auger flights. The void volume included the cylindrical annulus between the outer edge of the auger flights and the inside wall of the auger housing and the volume between the faces of auger flights. The C- and D-augers were classified as small size augers and E-and F-augers were classified as large size augers for the purpose of this study. The C- and D-augers had smaller gaps between the inner surface of the discharge chamber and the auger edge than the E- and F-augers.

The C-auger also had a relatively smaller gap than the D-auger, which appeared to cause the C-auger to plug more quickly than the D-auger. The plot of the cumulative weights of Whiterocks oil sands fed with the C- and D-augers at various conditions are presented in Figures 95 and 96, respectively. The tests for both augers indicated that

Table 24. Auger Specifications for Acrison BDF-1 Feeder

Auger	Diameter, cm	Configuration	Coating	Water Cooling	Length, cm	Testing Result
C	0.95	solid flight	none	yes	45.7	failed
D	2.54	solid flight	none	yes	45.7	failed
E	3.49	solid flight	none	yes	30.5	success
F	4.45	solid flight	yes	none	45.7	success
F	4.45	helical	none	none	45.7	success

Figure 95.

Oil Sands Feeder Test Using a Solid Flight C-auger with the Whiterocks Oil Sands

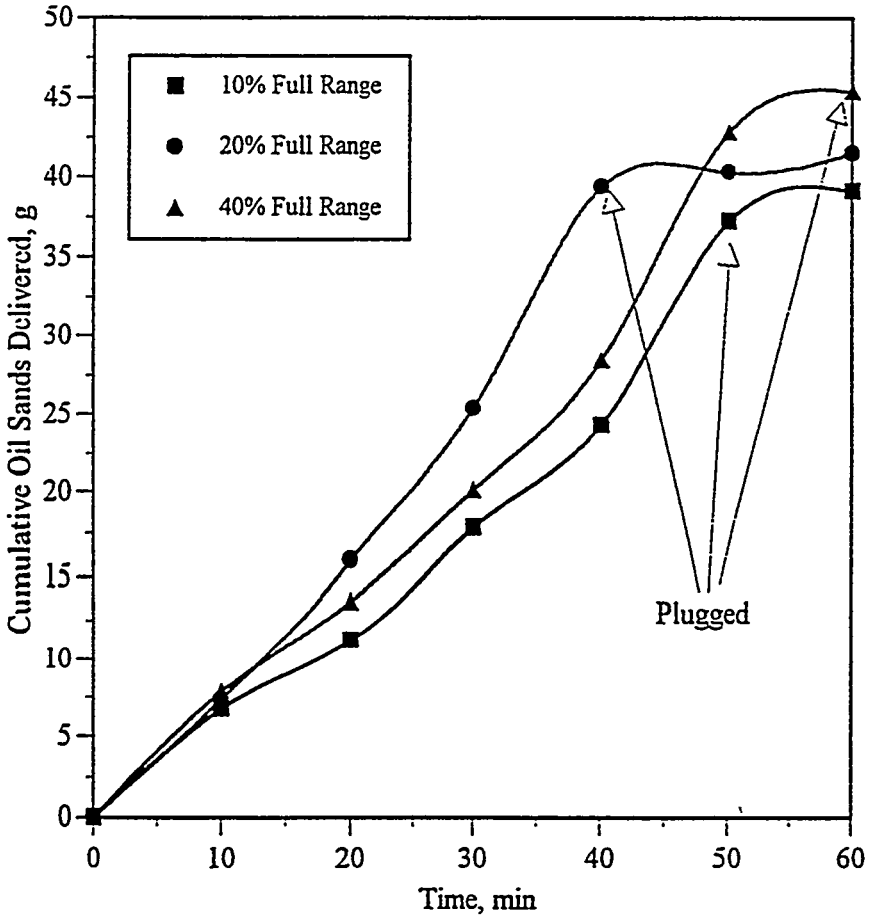
10% Full Range
20% Full Range
40% Full Range
Cumulative Oil Sands Delivered, g
Time, min
Plugged
0
5
10
15
20
25
30
35
40
45
50
0
10
20
30
40
50
60

Figure 96.

Oil Sands Feeder Using a Solid Flight D-auger with Whiterocks Oil Sands

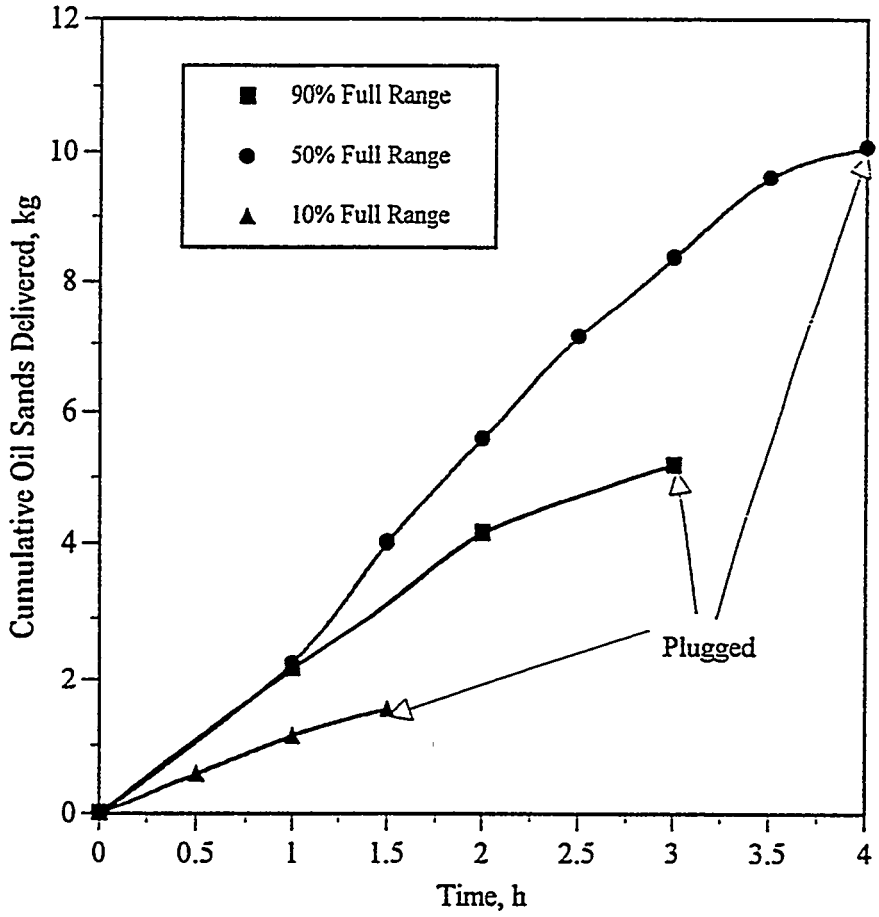
90% Full Range
50% Full Range
10% Full Range
Cumulative Oil Sands Delivered, kg
Time, h
Plugged
0
2
4
6
8
10
12
0
0.5
1
1.5
2
2.5
3
3.5
4

feeding ceased when the auger plugged. The results for both the C- and D-augers indicated that neither was capable of feeding undiluted oil sands for a sustained period of time at a constant rate. The feed rate of oil sands decreased with time and eventually the auger plugged even though feeding persisted for a longer time with the D-auger than with the C-auger. It was presumed that the smaller the ratio of the void volume-to-surface area the greater the tendency for the auger to plug. When plugging occurred oil sands were no longer delivered, although the auger was still rotating. It was noted that the space between the auger surface and the inner wall of discharge chamber was filled with compacted oil sands when the auger-discharge cylinder assembly was removed. The auger and discharge cylinder were cleaned and replaced on the feeder.

The effect of reducing the annular gap space was evaluated with the C-auger when bronze and PVC sleeves were placed in the discharge cylinder to reduce the gap between the auger flights-edge and the cylinder wall. The results of these tests are presented in Figure 97. This change gave no improvement in feeding and in fact made the situation worse because the actual space for oil sands movement had been reduced.

Oil sands feeding was a result of the relative movement between the stationary discharge cylinder and the rotating auger, which provided the driving force to move the oil sands from the feeder hopper to the discharge downspout. The mechanical shear and friction forces acting on the oil sands caused the movement of the material through the auger-housing assembly. A layer of bitumen-impregnated oil sands which may have been enriched in bitumen coated the inside wall of the cylinder and built-up on the auger flights at the same time. When the space between the auger and the discharge cylinder was less than the size of the oil sands lumps, these lumps accumulated near the entrance of the discharge chamber. Shear stress and frictional forces caused the lumps to grow larger than the transportation space provided for a specific auger size. The result was to stop the feeding of oil sands.

Figure 97.

Oil Sands Feeder Test Using a Solid Flight C-auger with Inserted Sleeves with the Whiterocks Oil Sands

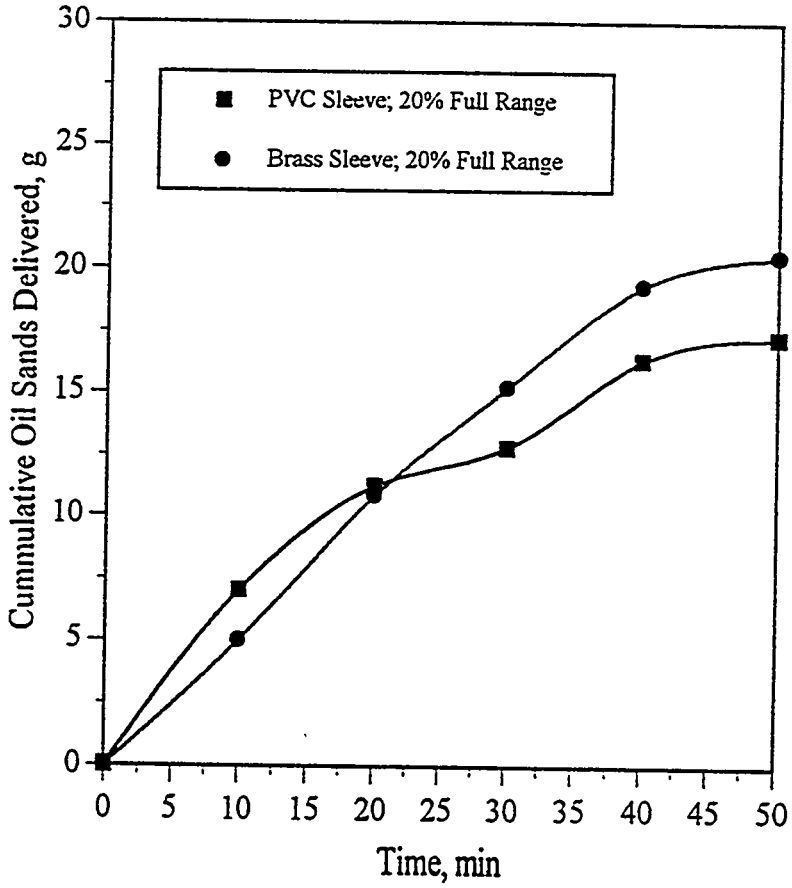
PVC Sleeve; 20% Full Range
Brass Sleeve; 20% Full Range
Cummulative Oil Sands Delivered, g
Time, min
0
5
10
15
20
25
30
35
40
45
50

The mass of oil sands delivered at various auger speeds and feed rates for the solid flight and helical F-augers are presented in Table 25. The experiments were conducted with a solid flight F-auger with a nonstick fluorocarbon polymer coating layer and with a helical F-auger. The feed rates were more stable when large size solid flight and helical augers were used. Thus the feed rates can be predicted from calibration curves for these augers using a linear regression technique. The F-augers were operated continuously over a 4-hour period and for total feeding times up to 15 hours. The results indicated that minor variations in the feed rates occurred and were caused by adhesive and agglomeration tendencies of oil sands. The results indicated that both augers performed in a similar manner based on a statistical analysis of the data in Table 25 and that neither the coated solid flight F-auger nor the helical F-auger gave improved feeding characteristics compared with an uncoated solid flight E-auger.

The results of an oil sands feeder test using the E-auger are presented in Figure 98. The solid flight E-auger was specified and purchased based on the test results with the C-, D-, and F-augers. The statistical analysis indicated that the E-auger performed better than the F-auger. It is possible the performance difference between the C-, D-, and F-augers and the E-auger was related to the nature of the oil sands ore fed. The Whiterocks ore were used as the feed sands with the C-, D-, and F-augers whereas the PR Spring ore was used with the E-auger. Visual observation indicated the PR Spring oil sands was less likely to agglomerate. The particle size distribution may also have played a role: the PR Spring oil sands were crushed and screened to pass through a 3.2 mm mesh sieve, and the Whiterocks oil sands were screened through a 6.4 mm mesh sieve. The larger size of the oil sands particles coupled with the tendency for particle agglomeration with the Whiterocks ore may have been responsible for the plugged augers. The oil sands feed rates using the E-auger at various motor speeds are presented in Table 26. The E-auger gave the longest continuous run, 5 hours, at pyrolysis conditions, and had a cumulative successful feeding time of over 100 hours. The feed

Table 25. Statistical Analysis of Average Feed Rates for F-Augers

Type of Auger	Solid Flight F-auger			Helical F-auger			
Auger Speed Set-Point, %	1.0	10.0	20.0	4.0	5.0	10.0	20.0
No. of Data Points	14	14	14	4	4	4	4
F_{avg}, kg/h	1.2	3.5	6.3	1.3	1.7	6.0	8.2
σ_{n-1}	0.10	0.05	0.16	0.08	0.04	0.15	0.39
σ_{n-1}/F_{avg}, %	8.3	1.5	2.5	6.1	2.1	2.6	4.7

F_{avg} is average feeding rate, kg/h

σ_{n-1} is standard deviation

Table 26. Statistical Analysis of Average Feed Rates for E-Auger

Auger Speed Set-Point, %	2.0	5.0	10.0	20.0
No. of Data Points	6	6	6	6
F_{avg}, kg/h	1.9	5.4	10.8	21.7
σ_{n-1}	0.046	0.01	0.06	0.14
σ_{n-1}/F_{avg}, %	2.4	0.27	0.52	0.63

F_{avg} is average feeding rate, kg/h

σ_{n-1} is standard deviation

Figure 98.

Oil Sands Feeder Test Using a Solid Flight E-auger with the PR Spring Oil Sands

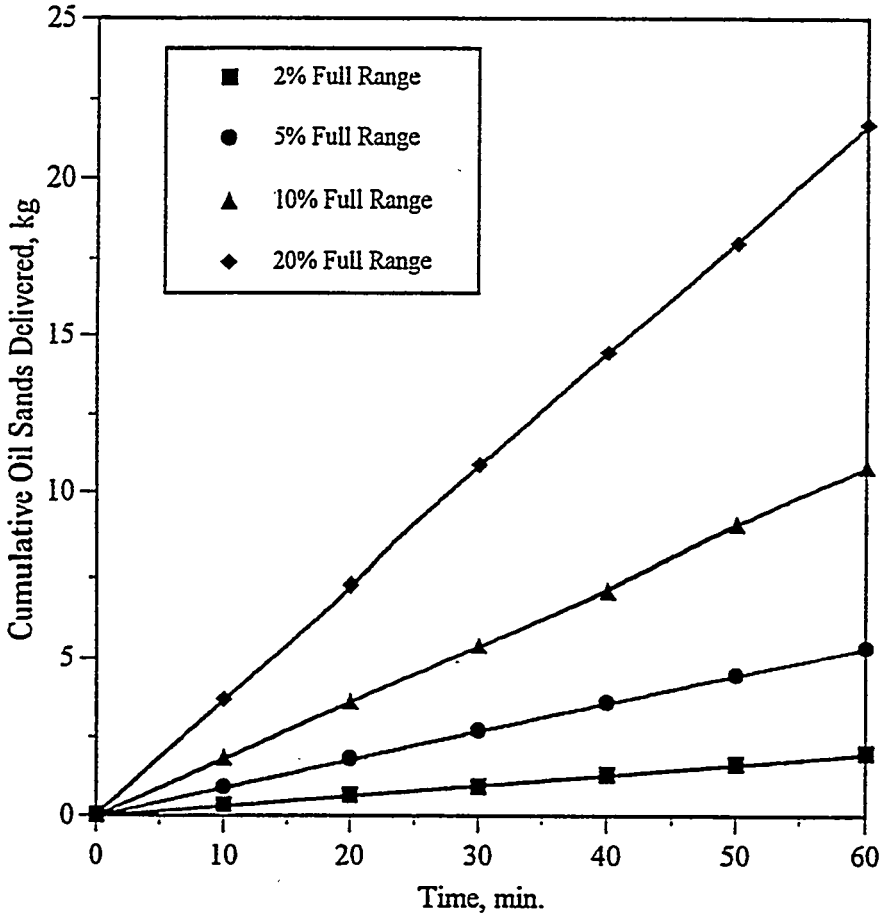
2% Full Range
5% Full Range
10% Full Range
20% Full Range
Cumulative Oil Sands Delivered, kg
Time, min.
0
5
10
15
20
25
0
10
20
30
40
50
60

rates were maintained during experiments with virtually no discernible change. The feed rates were proportional to motor speed setting in the test range.

A water jacket was installed for continuous cooling of the auger housing to maintain the discharge housing temperature at 290 K in the summer and 285 K in the winter which was 5 to 10 K below the ambient laboratory temperature in each case.

The crushed and screened PR Spring oil sands ore used in the feeder study had a loose structure and narrow particle size distribution which resulted in more stable feed rates compared with the more compact crushed run-of-mine oil sands ore. The Acrison BDF-1 feeder with solid flight E- and F-augers and a helical F-auger provided linear and predictable feed rates. The length of the discharge chamber and the ratio of void volume-to-surface area, including auger and inner housing surface areas, were the primary constraints during feeder operation. The shorter the lengths of the discharge chamber and augers and the larger the ratio of the void volume-to-surface area, the more reproducible and linear the feed rates were.

Increasing the motor speed caused the feed rates to increase; however, it also increased the shear stress and frictional forces and eventually led to reduced feed rates when agglomeration occurred. Low auger speeds were adequate for feeding the oil sands ores. A large auger was required to provide reproducible feed rates and sustained oil sands feed rates. The preferred Acrison feeder auger was the solid flight E-auger fitted with a 30.5 cm long water jacketed discharge chamber (previously a 45.7 cm standard discharge cylinder was used) based on reactor design requirements and the feeder studies. The cumulated operating hours were over 120 and the longest run lasted for 5 hours. The results showed a good linearity and reproducibility for the E-auger.

Pneumatic L-Valve as a Solids Withdrawal Device

Knowlton and Hirsan (129), Frick and Novak (130), Geldart and Jones (131), Fletcher (121), and Yang and Knowlton (132) have reported on the applications of an

L-valve as a solids flow control device. Knowlton and Hirsan (129) used it as a solids recycling system for a circulating fluidized bed reactor. Geldart and Jones (131) conducted extensive experimental work to determine the different factors that effect the performance of L-valves and to develop L-valve design procedures. Fletcher (121) reported on the use of an L-valve to withdraw Group B sands (128) from a high temperature fluidized bed oil sands pyrolysis reactor. Recently, Yang and Knowlton (132) analyzed and correlated data which led to proposed L-valve equations for calculation of solids flow rates.

L-valves are different from traditional mechanical solids withdrawal valves. They do not have moving mechanical parts within the system. The L-valves consist of a vertical section and a horizontal section in conjunction with one or more gas injection points. Aerating gas is introduced into the L-valve through injection taps. The geometric shape of the L-valve combined with the aerating gas flow is used to start and stop solids withdrawal from a process vessel.

A reliable spent coked sands withdrawal system is critical to the maintenance of bed inventory and operation of a fluidized bed oil sands pyrolysis reactor. Solids withdrawal valves can be classified into two categories: mechanical control valves and nonmechanical aerated L-valves. Mechanical valves previously evaluated included a Foxboro P50 air-to-close model actuator with an open and shut valve (119). The control signal was provided by a differential pressure controller (DPC) which measured the differential pressure across the fluidized bed in the reactor. When the differential pressure exceeded the set-point, a signal was sent to the actuator which opened the valve to discharge solids from the reactor. Generally, the mechanical valve failed to close properly after repeated cycles due to solids retention in the valve housing. Fletcher (121) introduced a nonmechanical L-valve as a spent sand withdrawal device on the large diameter fluidized bed reactor. It successfully controlled the bed inventory and the solids withdrawal rate from the reactor.

The control principle of L-valves was similar to that used with mechanical valves. Signals from the DPC controlled the flow of the aeration gas to the L-valve to control the rate of solids withdrawal from the bed so as to maintain a constant pressure drop across the bed. The advantages of nonmechanical L-valves included no mechanical parts in direct contact with the solids and the controlled withdrawal of solids due to the geometric configuration and sensitivity of the aerating gas flow rate control. The aeration gas flow was regulated by an open and shut mechanical valve.

Experimental Set-up

The L-valve solids withdrawal device is depicted in Figure 88. It consisted of a pneumatic L-valve, a nitrogen gas supply, and pressure regulating and monitoring devices. The L-valve downcomer, horizontal section, and cross connector were made of 2.54 cm 304 stainless steel pipe and fittings for uses at elevated temperatures. Injection gas was introduced through a 6.4 mm tubing and NPT connectors. The aeration gas flow rates were controlled and metered by two FM1050 flowmeters equipped with utility valves supplied by Matheson.

The coked sands used in the L-valve studies were produced previously during fluidized bed pyrolysis of the Whiterocks oil sands (119). The sand granules were coated with a carbonaceous residue and were a multisized Group B sands (128). The physical properties and the particle size distribution of the sands are summarized in Tables 27 and 28, respectively. The average particle diameter was calculated from the following equation:

$$d_p = \left(\sum \frac{x_i}{d_{p,i}}\right)^{-1} \qquad (17A)$$

where d_p is the average particle diameter of the coked sands, m, $d_{p,i}$ is the average diameter of the particles between the two sieves, m, and x_i is the weight fraction of

Table 27. Whiterocks Coked Sands Physical Properties

Mean particle size (d_p), μm	153
Particle density (ρ_p), kg/m^3	2440
Bulk density (ρ_{bk}), kg/m^3	1450
Bulk packed Voidage (ε_{bk})	0.405
Minimum fluidization Voidage (ε_{mf})	0.408

Table 28. Whiterocks Coked Sands Particle Size Distribution

Sieve No.	Sieve size, μm	$d_{p,i}$, μm	x_i, wt%	$x_i/d_{p,i}$
Under	<75	38.5	5.8	0.129
200	75	90.5	6.1	0.068
140	106	115.5	8.1	0.070
120	125	137.5	11.9	0.086
100	150	165	11.0	0.067
80	180	196	27.7	0.141
70	212	231	8.7	0.038
60	250	275	9.7	0.035
50	300	327.5	3.1	0.009
45	355	427.5	2.4	0.006
35	500	605	1.1	0.002
25	710	3456	4.3	0.001

coked sands having a diameter of $d_{p,i}$. The mean particle size was determined to be 153 μm.

According to the coked sands particle size analysis, 95.7 wt% of the particles was less than 500 μm. The sands contained 4.3 wt% rock chips and coked sands lumps which bridged at the neck of the downcomer, caused segregation in the fluidized bed, and plugged the withdrawal system. The oil sands particles could have agglomerated to form large lumps during pyrolysis and would not be expected to break down into individual particles in their passage through the bed. Agglomeration of the feed oil sands and subsequent cementation of the agglomerates due to coking were the main cause of malfunctions of the mechanical withdrawal devices and led to modifications of the L-valve design in term of the cross-sectional area of the L-valve and the addition of a second aeration point.

The downcomer and horizontal sections of the L-valve were fabricated from 2.54 cm Schedule 40 stainless steel pipe to circumvent plugging due to larger particles. The 60° slope of the tapered gas distributor facilitated gravitational flow of the solids into the downcomer and eliminated distributor dead volume at the wall of the reactor.

After filling the L-valve with coked sands, the aeration gas flow rate was set at a predetermined value. Solids withdrawn from the L-valve were collected for specified time intervals and weighed. The solids flow rate was measured five times and an average value calculated. The aeration gas rate was increased in a stepwise manner during the course of an experiment.

Characteristics of Solids Flow in L-valves

Solids flow patterns in L-valves had been studied by Knowlton and Hirsan (129), Geldart and Jones (131), and Yang and Knowlton (132). When aeration gas is injected into an L-valve, solids do not begin to move immediately at low gas injection rates. A threshold aeration rate is required to initiate solids flow. The threshold value will vary with the configuration of the L-valve, the location of the injection points and the solids

properties. After the critical aeration rate is attained, increasing the aeration gas rate to the L-valve leads to a solids flow rate increase. Once the gas flow rate increases to a certain value, the solids flow rate reaches a maximum value and a further increase in the gas rate may actually reduce the solids flow rate.

The solids flow rate in an L-valve is zero at very low aeration gas flow rates and the solids in both the vertical and horizontal sections remain stationary. The solids flow patterns (Figure 99) in an L-valve are usually described in term of three regimes (129, 131). At low gas flow rates only the sands at the top of the horizontal section flowed while the balance of the sands in the horizontal section remained stationary (Figure 99[a]). In addition, a small portion of the vertical section flowed at low gas flow rates. However, significant size segregation occurred when multisized particles were present in the horizontal section with the smaller particles reporting to the top layer of sands in the horizontal pipe where solids appeared to move in ripples. At medium gas flow rates the stationary region of particles decreased and a relative large portion of the solids moved through the horizontal section (Figure 99[b]) Dunes and ripples in the sand enlarged and moved at relatively higher frequencies. The entire solids in the L-valve were in motion at high aeration rates (Figure 99[c]). The segregated layers and the demarcation between the flowing and stagnant phases disappeared. The maximum solids flow rate was accompanied by streaming and flow fluctuations with a further increase in the gas injection rates. When the L-valve horizontal section was sufficiently long, the motion of the solids formed dunes and the frequency of the cycles dramatically increased.

Results and Discussion

The L-valves can be classified as automatic solids flow L-valves or external gas facilitated L-valves depending upon the length of the horizontal section. When the horizontal section of an L-valve is shorter than 1.5 times the downcomer pipe diameter, the L-valves do not require gas injection to facilitate solids flow. Solids automatically

Figure 99.

Schematic of Solids Flow Patterns in the L-valve (131)

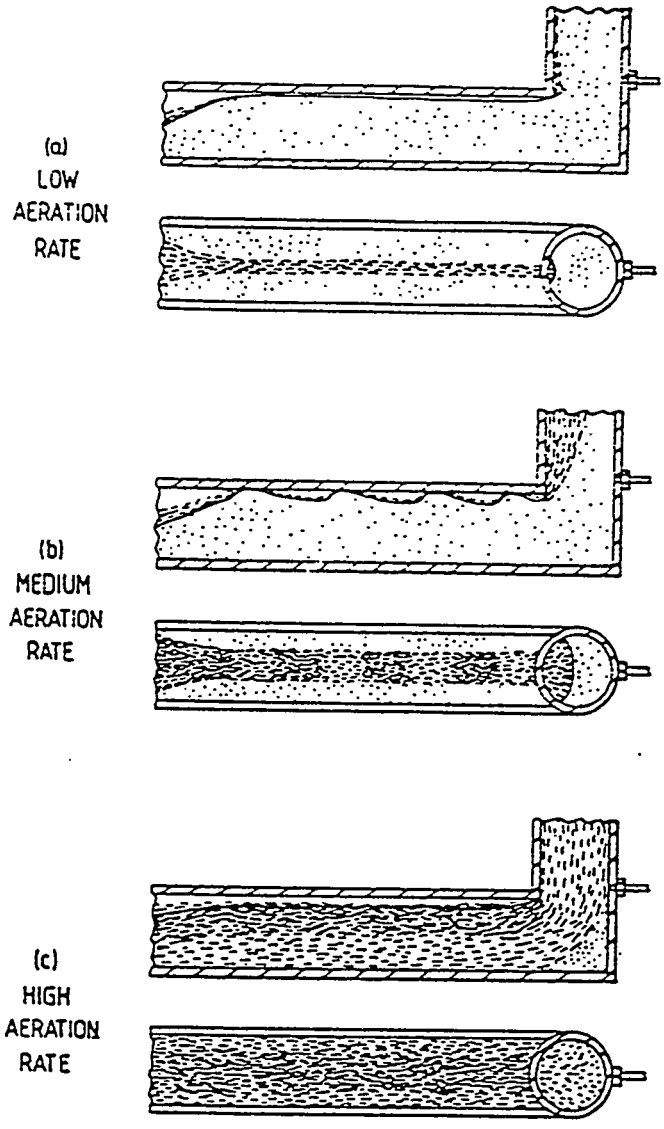
(a)
LOW
AERATION
RATE
(b)
MEDIUM
AERATION
RATE
(c)
HIGH
AERATION
RATE

flow out due to gravity and the length of the vertical section do not affect the solids flow rates. It was concluded in the present study that the horizontal section of an L-valve should be greater than the critical value of 1.5 times its diameter to permit control of the solids flow rate. The critical value is defined as the minimum length requirement to control the solid flow. The height of downcomer did not affect solids flow rates in the range of interest. Varying cylinder downstream pressure in the range 34 to 207 kPa did not change solids initial flow point at a given gas injection rate because the solids were discharged to an ambient pressure receiver. The preferred cylinder pressure was 41 to 55 kPa.

Three different lengths of the horizontal section were tested in these experiments: 11.4 cm, 19.1 cm, and 34.3 cm. The effect of the length of the horizontal section on solids flow rates is presented in Figure 100. The solids transfer rates decreased as the length of the horizontal section increased at a fixed aeration rate. As the length of the horizontal section increased the more kinetic energy consumed to transfer the solids in the horizontal pipe instead to discharge particles. The solids transfer rate increased as the aeration rate increased to a certain point and then leveled off for sufficiently long horizontal pipe sections, i.e., the 34.3 cm long horizontal section. This was related to the energy consumed in accomplishing the horizontal transfer of solids.

The changes in solids flow rates with injector location are presented in Figure 101. The variation in the position of the aerating gas injector along the center line of the horizontal section affected solids flow rates. A maximum solids flow rate was obtained with the injection point located 1.3 cm behind the center line of the downcomer. When the injection point was moved in either direction the solids flow rate decreased. If the injector was moved forward, the solids flow rate decreased faster than if it was moved in the opposite direction. The aerating gas did not affect the solids flow rate when the injection point was positioned 2.54 cm in front of the center line of the downcomer. The injection gas flow rate was an important parameter in the design and the operation

Figure 100.

Effect of the Lengths of the Horizontal Section on the Solids Flow Rates with the Injector Port Located 1.3 cm behind the Center Line of the Vertical Section

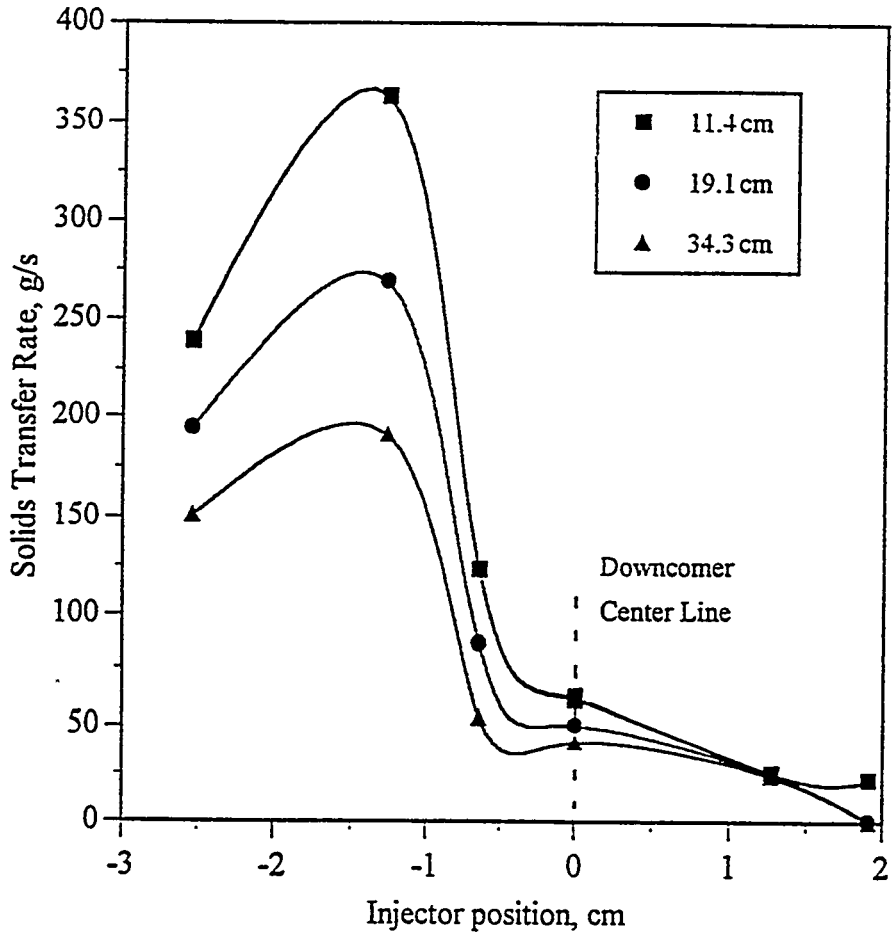
400
350
300
250
200
150
100
50
0
-3
-2
-1
0
1
2
Solids Transfer Rate, g/s
Injector position, cm
11.4 cm
19.1 cm
34.3 cm
Downcomer
Center Line

Figure 101.

Effect of the Injection Port Location on the Solids Flow Rate with Different Horizontal Section Lengths at a Fixed Aeration Rate of 4.5 LPM

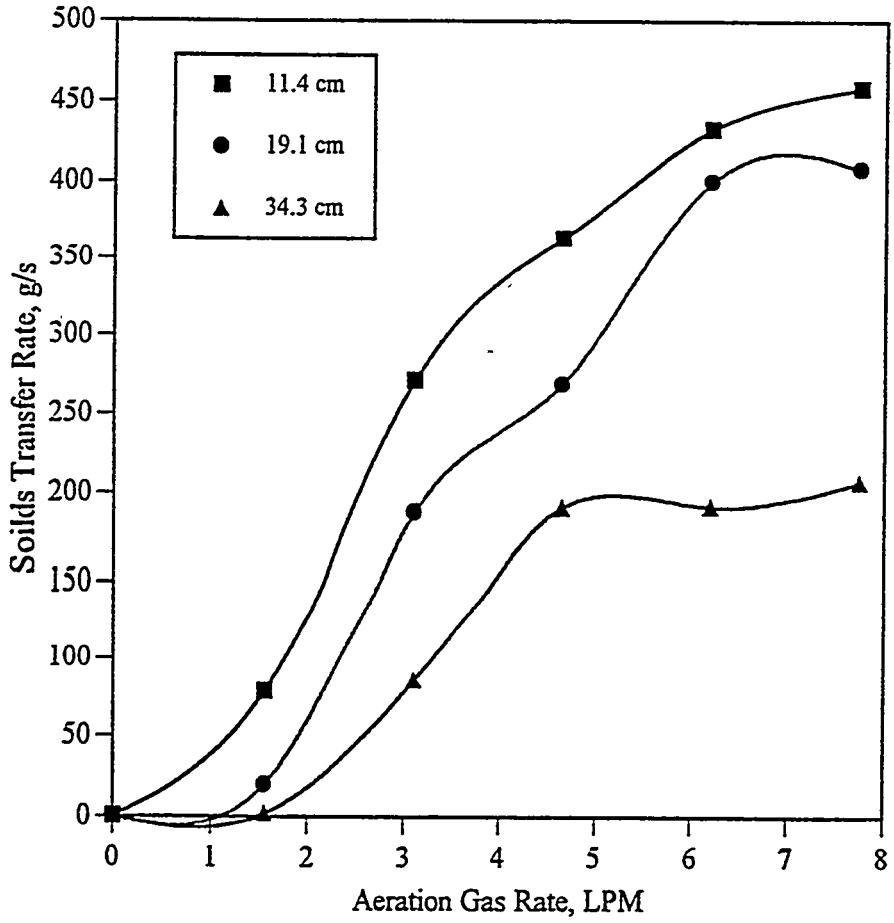
11.4 cm
19.1 cm
34.3 cm
Soilds Transfer Rate, g/s
Aeration Gas Rate, LPM
500
450
400
350
300
250
200
150
100
50
0
0
1
2
3
4
5
6
7
8

of the L-valve. Initial solids breakthrough occurred at a nitrogen flow of 1.5 LPM with the injection point located 1.3 cm behind the center line of the downcomer. The amount of coked sands which remained in the L-valve was determined by its angle of repose. If the injector projected beyond the coked sands slope-boundary defined by the angle of repose, the injected gas discharged into the empty region of the horizontal section of the L-valve. As the injector moved backward into the coked sands pile, more and more coked sands were carried out by aeration gas and reached a maximum value at 1.3 cm behind the center line of downcomer. However, further backward movement of injector decreased the solids transfer rates, because part of the energy consumed in horizontal transport.

The solids flow rate (Figure 100) increased as the gas flow rate increased. The solids fluxes ranged from 0 to 90.4 g/cm^2s, whereas the discharge rate ranged from 0 to 460 g/s throughout the test range. When injection gas rates increased from 0 to 7.5 SLPM, the solids transfer rate reached 458 g/s and leveled off with the 11.4 cm horizontal section. The solids flow rates increased from 0 to 408 g/s with a 19.1 cm horizontal section and from 0 to 207 g/s with a 34.3 cm horizontal section. The solids transfer rate decreased as the length of the horizontal section increased at constant gas injection rate. This effect was related to the energy required to transport the solids through the horizontal section: increasing the length of the horizontal section led to the consumption of more energy in the horizontal transfer pipe.

An attempt was made to correlate these results using the Yang and Knowlton (132) method. However, large deviations resulted because the Yang and Knowlton (132) method was established for large solids flow rates and the method was reported to be inaccurate at low solids flow rates.

The following conclusions were drawn from the L-valve studies. The diameter of the vertical and horizontal sections of the L-valve should be equal to or greater than 2.54 cm. The experimental results indicated that lumps formed in the pyrolysis process

did not plug the valve. The solids flowed out automatically by gravity when the length of the horizontal section of the L-valve was less than 1.5 times its diameter. A minimum amount of injection gas which varied with the lengths of the horizontal section (Figure 101) was required to initiate solids flow. Gas injection into the horizontal section behind the center line of downcomer was an effective way to control the solids flow rate. The length of the downcomer section of the L-valve did not affect solids flow rate, whereas the length of the horizontal section of the L-valve had a significant effect on solids flow rates. Secondary gas injection facilitated solids flow in the presence of coked sands lumps which formed during pyrolysis.

An L-valve with two aeration injection ports (Figure 91) was fabricated using an 11 cm long 2.54 cm pipe for the horizontal section and fittings for the fluidized bed system. The injection gas flow rate was 4 SLPM, the solids flow rate was 50 g/s, and aeration time lasted for 2 seconds. The valve intermittently discharged coked sands at 90-second intervals to maintain the fluidized bed hold-up constant for a settled-bed H/D of 2 and a solids retention time of 30 min. The auxiliary aeration injector was located underneath of the vertical section to permit solids flow when lumps were present in the coked sands.

Coked Sands Fluidization Studies

The fluidization studies conducted in the 7.62 cm diameter fluidized bed reactor had the following objectives:

- test the reactor system capability and performance, especially the tapered gas distributor;
- examine the fluidization regimes and determine the range of operating variables in which channeling and slugging were absent;
- determine the preferred bed hold-up and fluidizing gas flow rate;
- determine the relationship between H/D, fluidization mode, and reactor temperature;

- determine the minimum fluidization velocity at elevated temperatures; and,
- determine the appropriate fluidizing gas velocity for oil sands pyrolysis based on the coked sands minimum fluidization velocity.

Characteristics of Fluidization

Consider a column or a reactor that is filled with loose packed solids up to a certain level, H. If a fluid is introduced in the bottom of the reactor upward through the bed of solids, the bed gradually expands and the pressure drop across the bed increases with an increase in the gas velocity in the fixed bed regime. The particles are in a static state and exhibit no relative movement. The pressure drop across the bed is proportional to the gas velocity in the fixed bed regime. As the fluidizing gas rate increases the pressure drop across the bed increases and the particles are partially suspended by the gas in the bed leading to a further expansion.

When the fluid velocity is increased beyond this point, the pressure drop fluctuates around a constant value equal to the mass per unit area of the bed and the particles begin to move about freely with frequent collisions. The suspended solids exhibit properties usually attributed to liquids. The onset of fluidization is observed when the drag force exerted by the upward moving fluid stream balances the mass of the particles in the bed. The pressure drop at this point should be equivalent to

$$\Delta P = \frac{W_b}{A_b} \qquad (18A)$$

where W_b is the mass of the particles in the bed and A_b is the cross-sectional area of the reactor.

The pressure drop at minimum fluidization is given by

$$\Delta P_{mf} = H_{mf}(1-\varepsilon_{mf})(\rho_p - \rho_g) \qquad (19A)$$

where H_{mf} is the height of the expanded bed at minimum fluidization, ε_{mf} is the voidage of the expanded bed at minimum fluidization, ρ_P and ρ_g are the densities of the solids and fluidizing gas, respectively.

The minimum fluidization velocity is determined by extrapolating the straight line pressure drop for a packed bed until it reaches the horizontal line corresponding to the bed hold-up per unit cross-sectional area or the value of the pressure drop across the bed of solids acting on the bed.

Geldart (128) classified powders into four categories according to particle-gas fluidization characteristics: group A, B, C, and D. Geldart's group B particles have a mean particle size between 40 to 500 μm and particle densities between 1,400 and 4,000 kg/m^3 and are sandlike particles. The coked sands produced during oil sands pyrolysis is a group B sand: the coked sands had an average particle size of 153 μm and a particle density of 2440 kg/m^3.

Fluidized Bed Pressure Analyses

The system arrangement and pressure analysis for the conventional push, the reduced pressure, and the pull modes of fluidization are presented in Figures 102 to 104, respectively. The pressure in the fluidized bed reactor is the system pressure and is the pressure above the bed. The system pressure in conventional push mode fluidization is the same as the ambient pressure. The system pressure is less than the ambient pressure in the reduced pressure fluidization mode. The windbox (plenum) pressure is the sum of the reactor pressure and differential pressure drops across the bed and the distributor.

Conventional Push Mode Fluidization

The solids particles in the bed were at the ambient atmospheric pressure. Fluidizing gas was introduced into windbox and then passed through gas distributor upward through the bed (Figure 102). A pressure equal to the bed loading must be established in the windbox to fluidize particles above the gas distributor. This pressure drop

Figure 102.

Pressure Analysis for Push Mode Fluidization

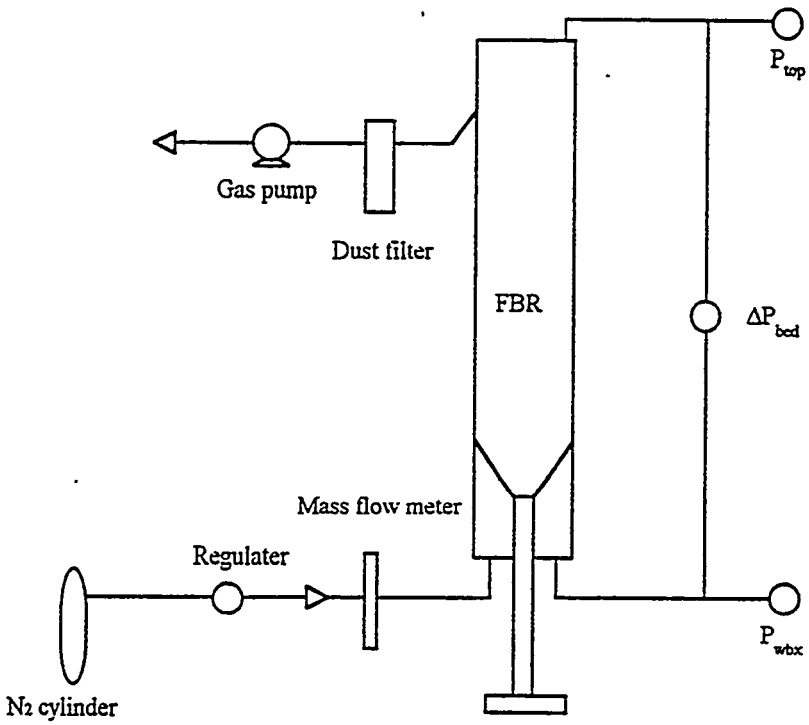

$P_{cor}=P_{atm}-4.1kPa(const.)$

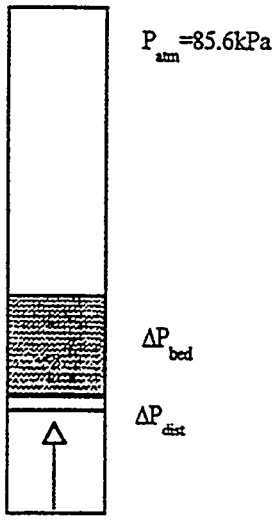

$P_{top}<P_{wbx}$

$P_{wbx}=P_{atm}+\Delta P_{bed}+\Delta P_{dist}-4.1$ kPa

should be equal to the sum of the pressure drop across the bed and pressure loss in the distributor. The absolute pressure analysis for the conventional push mode of fluidization was as follows:

$$P_{amb} = 85.1\,kPa$$

$$P_{rxr} = P_{amb}$$

$$P_{wbx} > P_{rxr}$$

$$P_{wbx} > P_{amb}$$

$$P_{wbx} = P_{rxr} + \Delta P_b + \Delta P_{dist}$$

The pressure drop across the fluidizing gas distributor was negligible. The pressure drop, P_{dist}, was 0.03 kPa at gas flow rate of 5.5 cm/s (15 LPM).

Reduced Pressure Mode Fluidization

The sealed reactor system was operated at an absolute pressure lower than ambient pressure by means of vacuum pump pulling gas out of system (Figure 103). The pressure in the freeboard region had a value of 81.5 kPa. The absolute pressure analysis for reduced pressure mode fluidization is as follows:

$$P_{amb} = 85.6\,kPa$$

$$P_{amb} > P_{rxr}$$

$$P_{rxr} = P_{amb} - 4.1\,kPa = 81.5\ kPa$$

$$P_{wbx} > P_{rxr}$$

$$P_{wbx} > P_{amb}$$

$$P_{wbx} = P_{rxr} + \Delta P_b + \Delta P_{dist}$$

Figure 103.

Pressure Analysis for Reduced Pressure Mode Fluidization

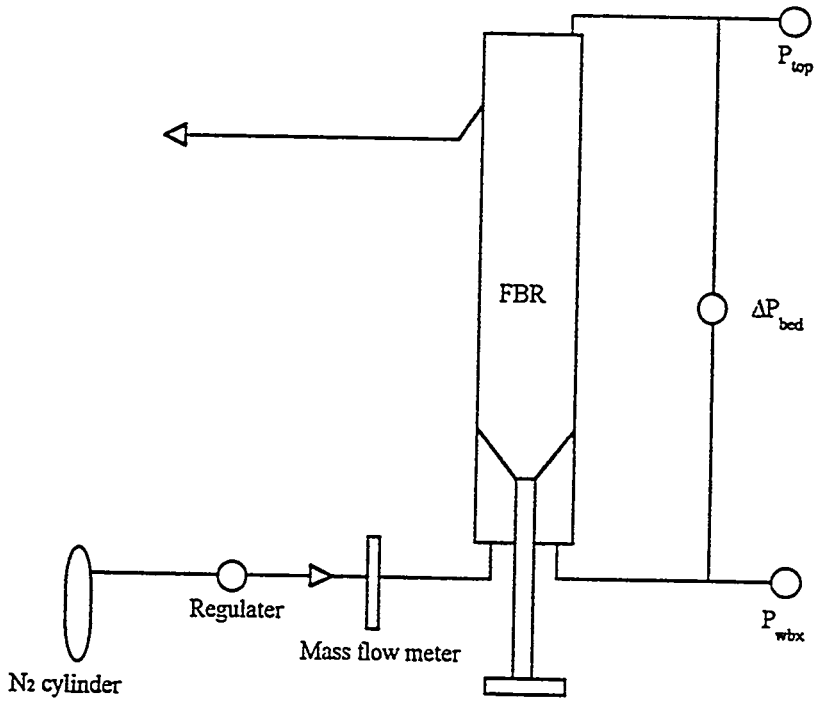

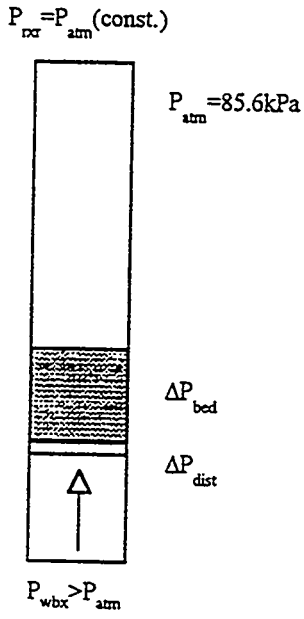

$$P_{wbx} = P_{atm} + \Delta P_{bed} + \Delta P_{dist}$$

The windbox pressure is dependent on the pressure drop across the bed. If the two terms of ΔP_b and ΔP_{dist} exceeded the 4.1 kPa, the windbox pressure could be higher than the ambient pressure. The difference between the two flow modes is the system pressure. The system pressure affects the minimum fluidization velocity by changing the fluidizing gas density. The reduced pressure mode fluidization provides an environment in which the minimum fluidization velocity occurs at a lower superficial gas velocity.

Pull Mode Fluidization

The pull mode of fluidization was developed for fluidization of wide particle size distribution sands by Fletcher (121). The windbox pressure was the ambient pressure. Fluidization of the bed inventory was accomplished by pulling the fluidizing gas through the windbox and gas distributor into the bed by means of a vacuum pump in the exit line from the reactor expansion chamber (Figure 104). Fluidization gas used in the pull fluidization was ambient air. The absolute pressure analysis for pull mode fluidization was as follows:

$$P_{amb} = 85.6\,kPa$$

$$P_{wbx} = P_{amb}$$

$$P_{amb} > P_{rxr}$$

$$P_{wbx} > P_{rxr}$$

$$P_{rxr} = P_{wbx} - (\Delta P_b + \Delta P_{dist})$$

Figure 104.

Pressure Analysis for Pull Mode Fluidization

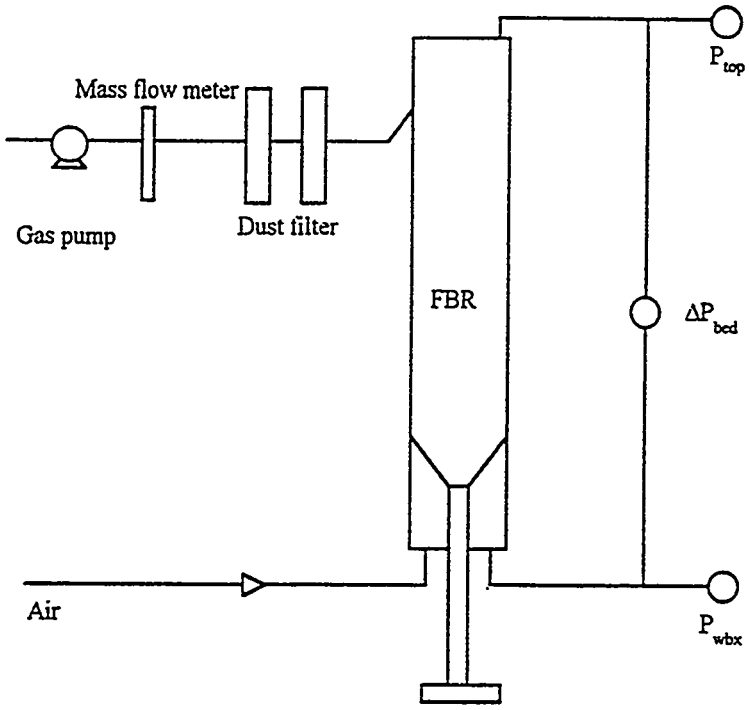
Mass flow meter
Gas pump
Dust filter
FBR
P_{top}
ΔP_{bed}
Air
P_{wbx}

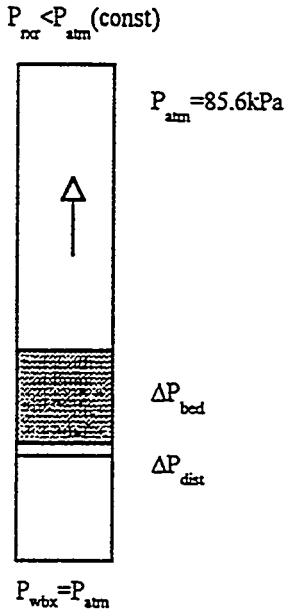
$P_{rxr} < P_{atm}$ (const)
P_{atm}=85.6kPa
ΔP_{bed}
ΔP_{dist}
$P_{wbx}=P_{atm}$

Experimental Determination of the Minimum Fluidization Velocity

The fluidization studies were conducted using the Whiterocks coked sands produced in a 10.2 cm fluidized bed reactor (119). Several techniques have been developed to interpret the experimental minimum fluidization velocity (U_{mf}) (128, 133-135). The minimum fluidization velocity is defined as the gas velocity at which the pressure drop across the bed is equal to the bed hold-up per unit cross-sectional area (M/A). This value is the point of intersection of the fluidization curve and the horizontal line equal to M/A (136-138). The intersection was taken on the descending portion of the curve beyond the transition point from the fixed to the fluidized bed during which the particles unlock. The experimental U_{mf} values in this study were determined at the intersections of the fluidization curve beyond the maximum and the horizontal line corresponding to the theoretical M/A values.

The differential pressure measured across the reactor was the sum of the pressure drops across the fluidized bed and the gas distributor. Normally, the bed pressure drop would be calculated by deducting the pressure drop across the gas distributor; however, the experimental results indicated that the distributor pressure drop was less than the experimental uncertainty in terms of pressure drop measurements; therefore the correction was not made. The net pressure drop across the gas distributor at a gas velocity of 5.5 cm/s (15 LPM) was 0.03 kPa at a bed pressure drop of 1.63 kPa (H/D=1.5).

The fluidization and defluidization experiments were conducted at various H/D ratios and for three distinct fluidization modes. Fluidization and defluidization curves

for various H/D ratios in the push and reduced pressure fluidization modes are presented in Figures 105 to 108. Values of U_{mf} at ambient temperature (294 K) using nitrogen as the fluidizing gas are tabulated in Table 29.

The minimum fluidization velocity is a function of both particle and fluid properties. Once the particles (coked sands), temperature, and fluidizing gas (nitrogen) were specified U_{mf} should be fixed. The H/D ratios did not affect the U_{mf} which was expected. The experimental U_{mf} values reported in Table 30 were obtained for different fluidization modes and different fluidization gases. However, the density and viscosity of fluidizing gases are very similar for nitrogen and ambient air. The fluidization and defluidization curves at an H/D of 2.5 under the pull fluidization mode are presented in Figure 109.

The U_{mf} for the push mode fluidization was greater than U_{mf} for the reduced pressure mode fluidization. This observation has been confirmed by several researchers (139-140) during the reduced pressure fluidization studies. Their findings indicated that the U_{mf} decreased in the reduced pressure environment. The push mode of fluidization is essentially the conventional fluidization method in which pressure above the bed is the ambient pressure. The reduced pressure mode was achieved using a vacuum pump in the exit line leaving the product recovery train. The ambient pressure due to the altitude of the Salt Lake City area is 85% of atmospheric pressure at sea level. Thus the ambient pressure in these studies was 85.1 kPa. The vacuum pump installed in the exit of the reactor system maintained a system pressure of 81.5 kPa or 4.1 kPa vacuum. Fluidization at system pressures below the ambient pressure was identified as the reduced pressure fluidization mode.

Pressure exerts a significant influence on the fluidizing gas density. The relationship of pressure and gas density can be reasonably expressed by the ideal gas law at ambient pressure and temperature. The gas density decreased from 0.9853

Figure 105.

Coked Sands Fluidization at Various H/D Values
Push Mode Fluidization
Nitrogen Fluidizing Gas, 294 K, 85.6 kPa

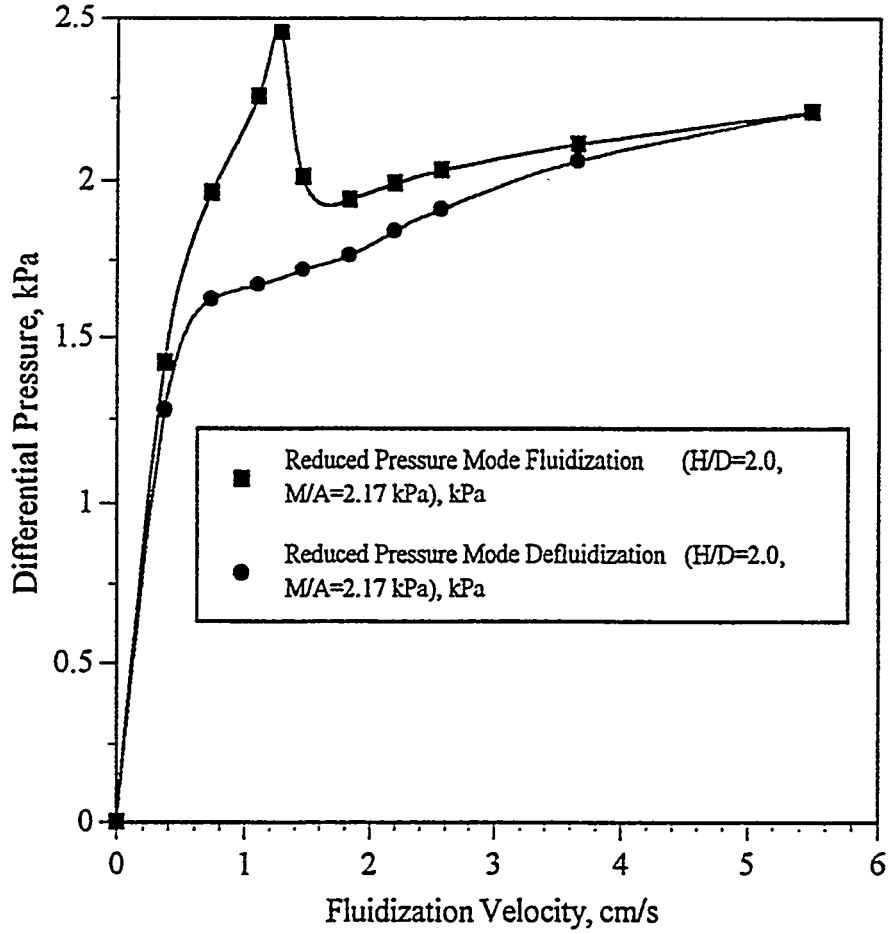
2.5
2
1.5
1
0.5
0
0
1
2
3
4
5
6
Differential Pressure, kPa
Fluidization Velocity, cm/s
Reduced Pressure Mode Fluidization (H/D=2.0, M/A=2.17 kPa), kPa
Reduced Pressure Mode Defluidization (H/D=2.0, M/A=2.17 kPa), kPa

Figure 106.

Coked Sands Fluidization and Defluidization at H/D=2.0
Push Mode Fluidization
Nitrogen Fluidizing Gas, 294 K, 85.6 kPa

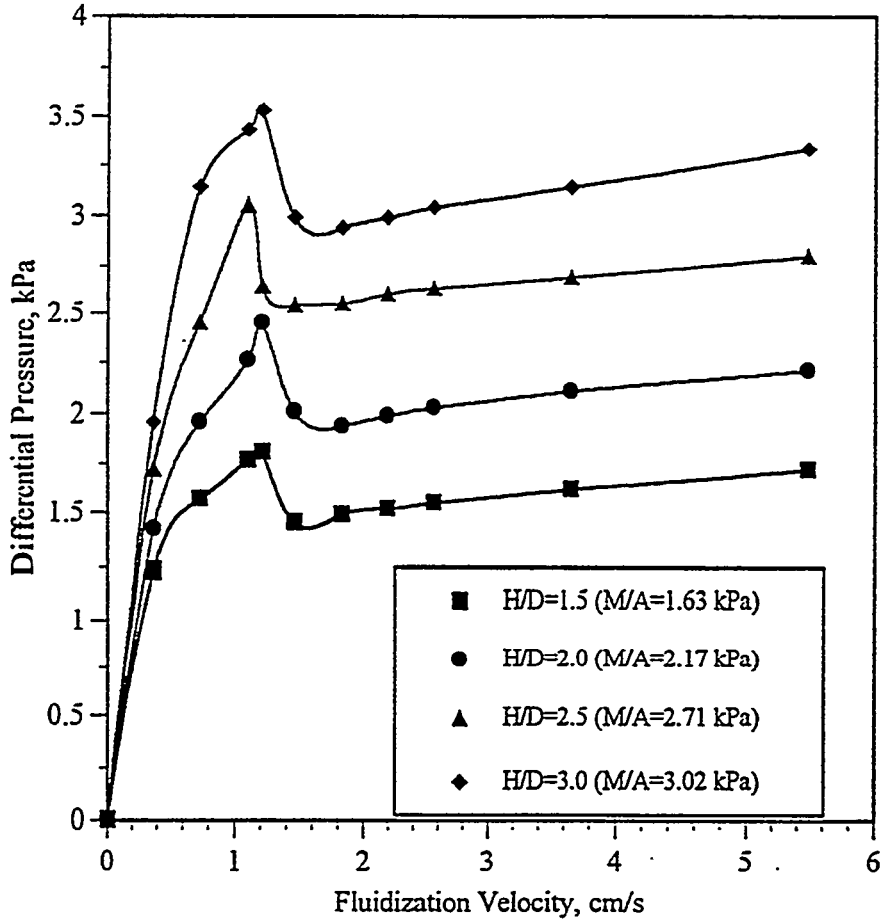
Differential Pressure, kPa
Fluidization Velocity, cm/s
0
0.5
1
1.5
2
2.5
3
3.5
4
0
1
2
3
4
5
6
H/D=1.5 (M/A=1.63 kPa)
H/D=2.0 (M/A=2.17 kPa)
H/D=2.5 (M/A=2.71 kPa)
H/D=3.0 (M/A=3.02 kPa)

Figure 107.

Coked Sands Fluidization at Various H/D Values
Reduced Pressure Mode Fluidization
Nitrogen Fluidizing Gas, 294K, 81.5 kPa

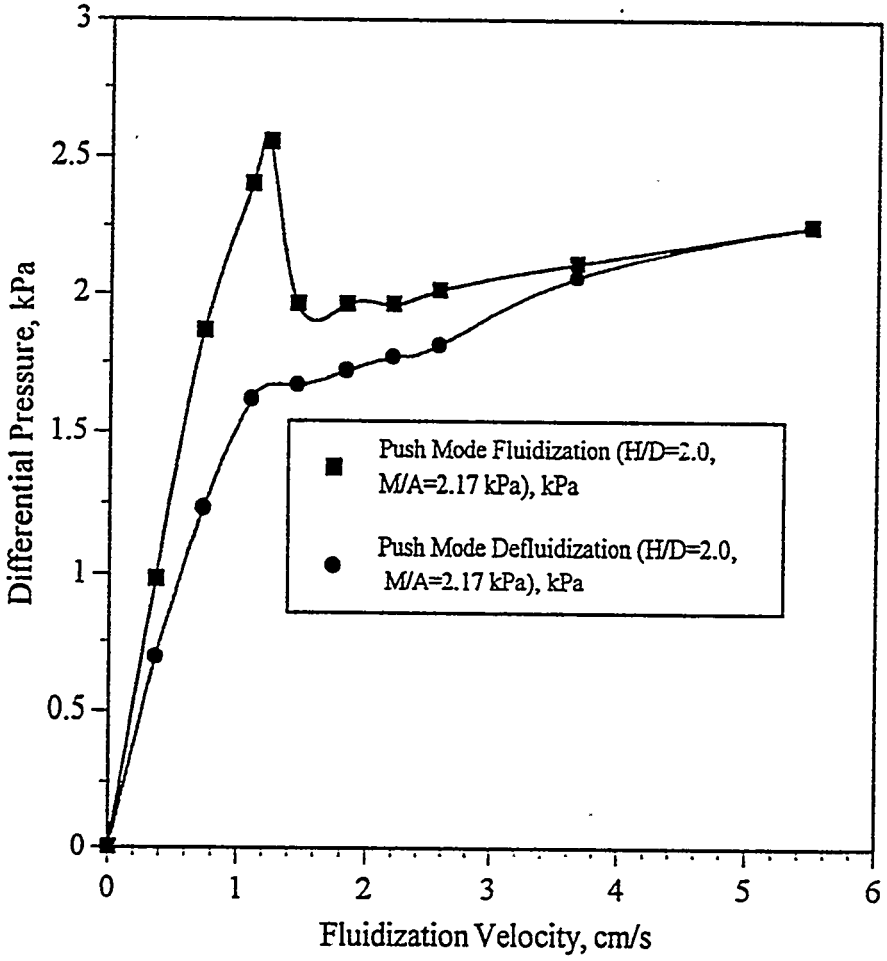
Differential Pressure, kPa
Fluidization Velocity, cm/s
0
0.5
1
1.5
2
2.5
3
0
1
2
3
4
5
6
Push Mode Fluidization (H/D=2.0, M/A=2.17 kPa), kPa
Push Mode Defluidization (H/D=2.0, M/A=2.17 kPa), kPa

Figure 108.

Coked Sands Fluidization and Defluidization at H/D=2.0
Reduced Pressure Mode Fluidization
Nitrogen Fluidizing Gas, 294K, 81.5 kPa

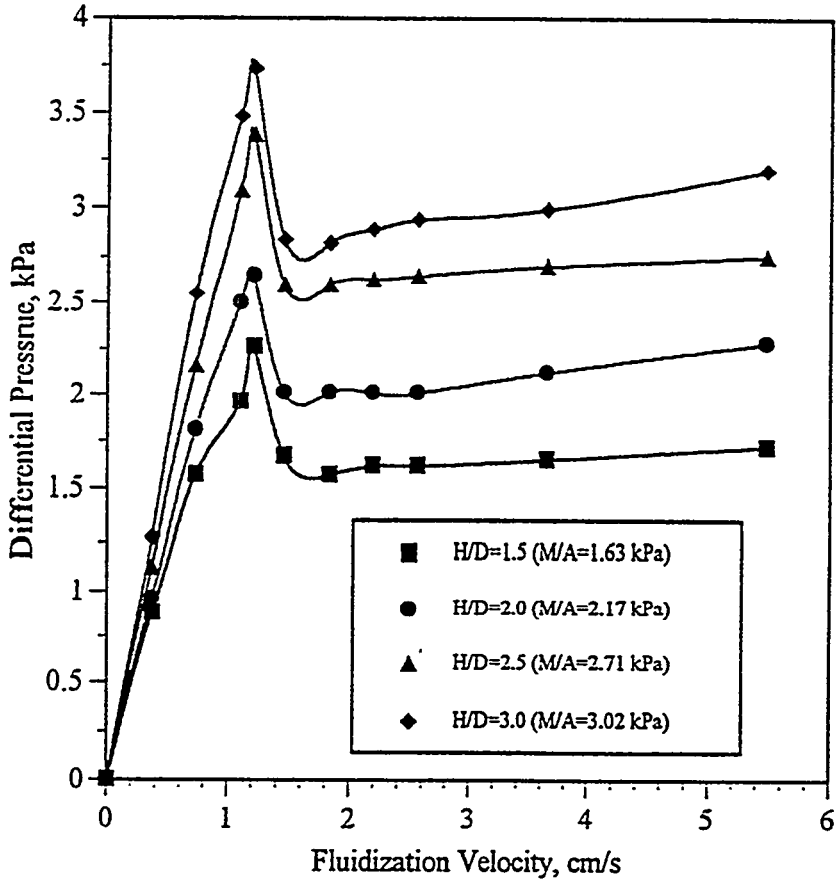
Differential Pressrue, kPa
Fluidization Velocity, cm/s
0
0.5
1
1.5
2
2.5
3
3.5
4
0
1
2
3
4
5
6
H/D=1.5 (M/A=1.63 kPa)
H/D=2.0 (M/A=2.17 kPa)
H/D=2.5 (M/A=2.71 kPa)
H/D=3.0 (M/A=3.02 kPa)

Table 29. Experimental U_{mf} Using Nitrogen Fluidizing Gas

	M/A, kPa	Push Mode, cm/s	Reduced Pressure Mode, cm/s
H/D=1.5	1.63	1.43	1.30
H/D=2.0	2.17	1.40	1.37
H/D=2.0*	2.17	1.40	1.30
H/D=2.5	2.71	1.41	1.37
H/D=3.0	3.02	1.41	1.40
Average U_{mf}, cm/s	--	1.41	1.35
σ_{n-1}, cm/s	--	0.01	0.04
σ_{n-1}/U_{mf}, %	--	0.7	3.0

*: reproducibility test.

Table 30. Experimental U_{mf} at Different Flow Modes

Flow Mode	Push Mode	Reduced Pressure Mode	Pull Mode
Fluid Media	Nitrogen	Nitrogen	Air
U_{mf}, cm/s	1.41	1.35	1.62

Figure 109.

Coked Sands Fluidization and Defluidization at H/D=2.5
Pull Mode Fluidization
Air Fluidizing Gas, 294 K, 81.5 kPa

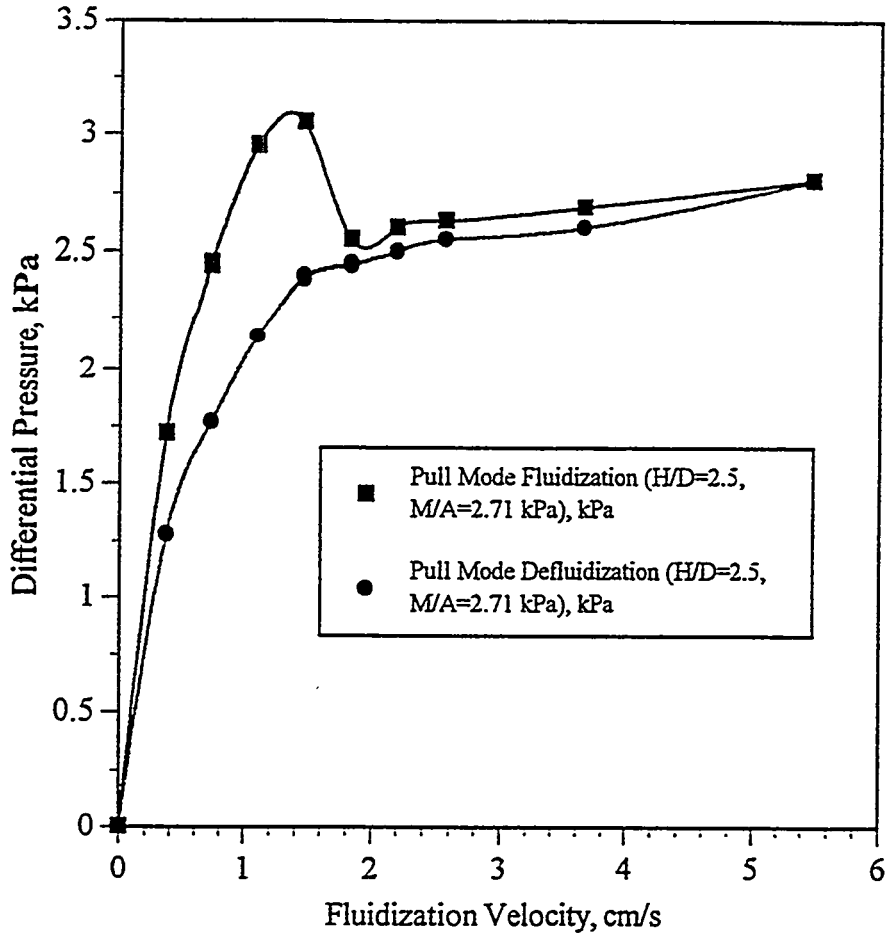
Differential Pressure, kPa
Fluidization Velocity, cm/s
0
0.5
1
1.5
2
2.5
3
3.5
0
1
2
3
4
5
6
Pull Mode Fluidization (H/D=2.5, M/A=2.71 kPa), kPa
Pull Mode Defluidization (H/D=2.5, M/A=2.71 kPa), kPa

kg/m^3 at ambient pressure to 0.9377 kg/m^3 at the reduced pressure fluidization operating pressure.

The minimum fluidization velocity under pull mode fluidization, 1.62 cm/s, was greater than those observed for the other two modes. The pull fluidization mode was presumed to induce a loosely packed bed a higher bed voidage under minimum fluidization conditions. The increases in bed voidage in pull mode were confirmed from studying of Ergun equation (142).

In conclusion, U_{mf} under reduced pressure fluidization was lower than U_{mf} under push mode fluidization, and it is presumed that this difference is related to the reduction in the fluidizing gas density. U_{mf} under the pull mode fluidization was higher than U_{mf} under the push mode fluidixation. An attempt to explain the difference was based on changes in bed voidage at minimum fluidization.

Prediction of Minimum Fluidization Velocity

The experimentally determined minimum fluidization velocities were discussed in the previous section. Several empirical and semitheoretical methods have been developed for the calculation of U_{mf} (121, 143). The mathematical expressions can be derived in term of the Reynolds number at minimum fluidization and the Archimedes number to give a dimensionless form:

$$Re_{mf} = f(Ar) \text{ or } Ar = f(Re_{mf}) \qquad (20A)$$

$$Ar = \frac{\rho_g d_P^3 (\rho_P - \rho_g) g}{\mu_g^2} \qquad (21)$$

$$Re_{mf} = \frac{d_p U_{mf} \rho_g}{\mu_g} \qquad (22)$$

The well-established Ergun equation (142) and the characteristic dimensionless number (Ar/Re_{mf}) are frequently used to correlate minimum fluidization velocities. The Ergun equation was originally developed as a universal correlation for the pressure losses across packed beds of spherical particles.

Two types of correlation (144) can be used correctly to describe the behavior of a fluidized bed at the minimum fluidization velocity.

$$\text{I.}\quad \frac{Ar}{Re_{mf}} = CAr^{m} \tag{23}$$

where $C = f(\varepsilon_{mf}, \phi_s, \mu_g, \rho_p, \rho_g)$ and $0.5 < m < 1.0$ and where ε_{mf} is the bed voidage at minimum fluidization; ϕ_S is the particle sphericity; ρ_g is the gas density, kg/m^3; ρ_p is the particle density, kg/m^3; and μ_g is the gas viscosity, g/cm-s.

The left-hand side of equation 24 is the characteristic dimensionless group Ar/Re_{mf} which is a measure of minimum fluidization velocity of the system: a function of the particles to be fluidized and the fluidizing gas. The right-hand side of the equation is composed of a constant determined by particle size, density, voidage, sphericity, and the particle Ar number.

$$\text{II.}\quad Ar = C_1 Re_{mf} + C_2 Re_{mf}^{n} \tag{24}$$

where $C_1, C_2 = f(\varepsilon_{mf}, \phi_s)$ and $1.5 < n < 2.0$

The Ergun equation (142) was given by

$$\frac{\Delta P}{H_{mf}} = 150\frac{(1-\varepsilon_{mf})^2}{\phi_s^2 \varepsilon_{mf}^3}\frac{\mu U_{mf}}{d_p^2} + 1.75\frac{(1-\varepsilon_{mf})}{\phi_s \varepsilon_{mf}^3}\frac{\rho_g g U_{mf}^2}{d_p} \tag{25}$$

which can be recast in dimensionless form as follows:

$$\frac{Ar}{Re_{mf}} = 150\frac{1-\varepsilon_{mf}}{\phi_s^2\varepsilon_{mf}^3} + \frac{1.75}{\phi_s\varepsilon_{mf}^3}Re_{mf} \qquad (26)$$

Thus $C_1 = 150\frac{1-\varepsilon_{mf}}{\phi_s^2\varepsilon_{mf}^3}$ and $C_2 = \frac{1.75}{\phi_s\varepsilon_{mf}^3}$

Solving the quadratic Ergun equation the following form is obtained:

$$Re_{mf} = (c_1^2 + c_2 Ar)^{0.5} - c_1 \qquad (27)$$

where C_1, C_2, c_1, and c_2 are functions of ϕ_S and ε_{mf}. Thus the minimum fluidization velocity is a function of the properties of the bed material and fluidization gas properties. The values of the constants in the Wen-Yu correlation (145) were $C_1=11$, $C_2=14$, $c_1=33.7$, and $c_2=0.0408$. The calculated values of U_{mf} in the push fluidization and the reduced pressure fluidization were 1.46 cm/s and 1.39 cm/s, respectively, using the Wen-Yu equation (Equation 27). This equation is not adequate to predict U_{mf} under pull mode fluidization, because the lump constants, c_1 and c_2, contain bed voidage, which infers that the ε_{mf} is considered to be a constant in the Wen-Yu equation.

Interpretation of Fluidization Curves

The fluidization curves for tapered gas distributors are different from conventional fluidization curves obtained with a flat distributor (146-148). The fluidization curve for a cone-shaped distributor in continuous operation with coked sands is presented in Figure 110.

Packed Bed Regime — O to A

When gas flowed upwards through a packed bed reactor which was loaded with a certain amount of coked sands the pressure drop across the bed gradually increased

Figure 110.

Interpretation of Fluidization Curves for a Cone-shaped Distributor in Continuous Operation with Coked Sands

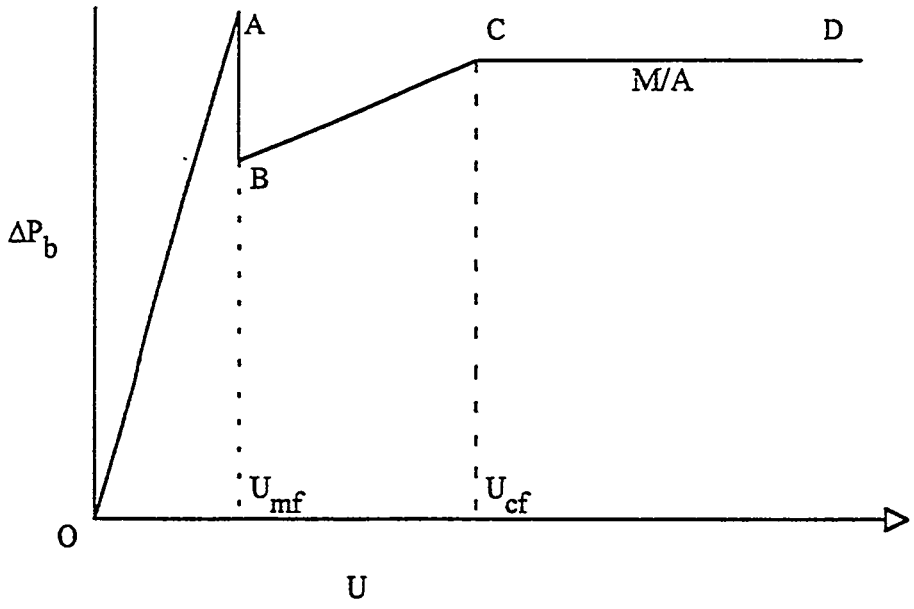
A
C
D
M/A
B
ΔP_b
U_{mf}
U_{cf}
O
U

with gas velocity according to Ergun equation (142). The bed was in a quiescent state in the packed bed regime. The increase in pressure drop versus gas velocity depended upon bed inventory and how firmly the bed was packed. The packed bed pressure drop curve with conical gas distributor was as similar as that with flat gas distributor in the packed bed regime.

Transition Regime — A to B

As the fluidizing gas velocity increased, the pressure drop across the bed declined: and the differential pressure across the bed decreased from a maximum value at (A) to a minimum value at (B). A "hump" in the curve was recorded particularly during the first attempt to fluidize the bed, or if the settled bed was left undisturbed for a relatively long period of time. This pressure rise was attributed to pressure drop required to free or unlock the compacted or interlocked particles in the transition from a packed bed to a fluidized bed. This phenomena has usually been associated with the fluidization of Geldart's Group B particles (128) for both flat and conical gas distributors.

As soon as the pressure drop reached the maximum value (A), the bed began to segregate into a fluidized inner column and downward moving outer column. It was presumed that the momentum of fluidizing gas which passed through holes in the cone was about 70 times higher than the momentum associated with the fluidization velocity (~2 m/s) and would keep it toward the center of the reactor This phenomena was attributed to the conical design of the gas distributor. The orientation of the distributor orifices (Figure 90) caused the gas to flow toward the center of the bed which formed an inner fluidized column. Thus, the distributor set up a preferential flow path in the bed through which large quantities of gas flowed.

Once the bed pressure drop curve reached its maximum value at A, the pressure drop fell to B. The experimental pressure at a point A was in the range of 95 to 110%

of the pressure drop equivalent to the mass of the bed divided by the cross-sectional area of the reactor (M/A), whereas at point B it was about 85 to 90% of M/A.

Partial Inner Column Fluidization Regime — B to C

The solids flow pattern at B was reported to resemble channeling due to the fact that the pressure drop was 10 to 15% below the calculated M/A value (133). After the bed pressure drop fell to the minimum value B, increasing gas velocity led to increased the pressure drop from B to C. Particles were continuously transferred from the upward-moving inner region of the column to the downward-moving outer region of the column. The outer column region decreased and the pressure drop recovered as the fluidization gas velocity increased. The excess gas flow, $U-U_{mf}$, expanded the partial fluidization region.

Fully Developed Fluidization Regime — C to D

The entire bed was fluidized, and the bed pressure drop was equivalent to the bed hold-up per unit cross-sectional area when the fluidizing gas velocity attained the value equal to the complete fluidization velocity, U_{cf}. U_{cf} was about two to three times the minimum fluidization velocity in this study. The fluidization curve was similar to that with flat gas distributor. The complete fluidization velocity can be calculated according to Geldart (128) even though the method was developed for fluidization of multisized particles in a system with a flat gas distributor.

The pressure-fluidizing gas curve with cone-shaped gas distributor indicated that the curve was different than that of flat-plated distributor. The tapered gas distributor provided a preferential pathway perpendicular to the surface of the distributor which allowed the gas to flow toward the centerline of the reactor. In contrast, the fluidizing gas flow with flat-plated distributor was upward. Thus, the configuration of the tapered gas distributor affected the fluidization characteristics. This influence on the pressure drop across the bed diminished as the fluidization velocity reached the

complete fluidization regime. The fluidization curve with tapered gas distributor was the same as that with flat-plated distributor.

Elevated Temperature Fluidization

Although many of the applications of fluidization involve high temperature operations, most of the correlations developed for the prediction of minimum fluidization velocities have been obtained at ambient conditions (137, 138, 149). Examinations of the correlations over a board temperature range have shown a significant deviation between predicted and measured velocities when gas densities and viscosities corresponding to the operating conditions were used (150-152). The minimum fluidization velocity (Table 31) decreased with increased fluidized bed temperature with the coked sands produced during the pyrolysis of the Whiterocks oil sands in a fluidized bed reactor (119).

Elevated temperature fluidization studies were conducted at 423, 523, and 623 K to determine the effect of reactor temperature on the minimum fluidization velocity. These temperatures were below the coke ignition temperature to prevent the spontaneous ignition of the carbonaceous residue on the sand grains. Furthermore, nonoxidizing nitrogen was used as the fluidizing gas in these push mode fluidization studies. The temperature dependence of nitrogen viscosity and density used to compute the predicted U_{mf} were reported by White (153) and are given as follows,

$$\mu_g = -1.189 \times 10^{-11} T^2 + 4.832 \times 10^{-8} T + 4.394 \times 10^{-6} \text{ (kg/m-s)} \qquad (28)$$

$$\rho_g = 338.8 \times T^{-0.9987} \text{ (kg/m}^3\text{)} \qquad (29)$$

where R^2=1.00 for both correlations. The experimental and predicted minimum fluidization velocities are presented in Table 31 and Figure 111.

Table 31. Values of Minimum Fluidization Velocities at Elevated Temperatures

Bed Temperature, K	Experimental U_{mf}, cm/s	Predicted U_{mf}[a], cm/s
297	1.41	1.46
423	1.2	1.32
523	1.0	1.12
623	0.75	0.99

a: predicted minimum fluidization velocities were calculated from Ergun equation.

Figure 111.

Minimum Fluidization Velocity at Elevated Temperatures with Whiterocks Coked Sands

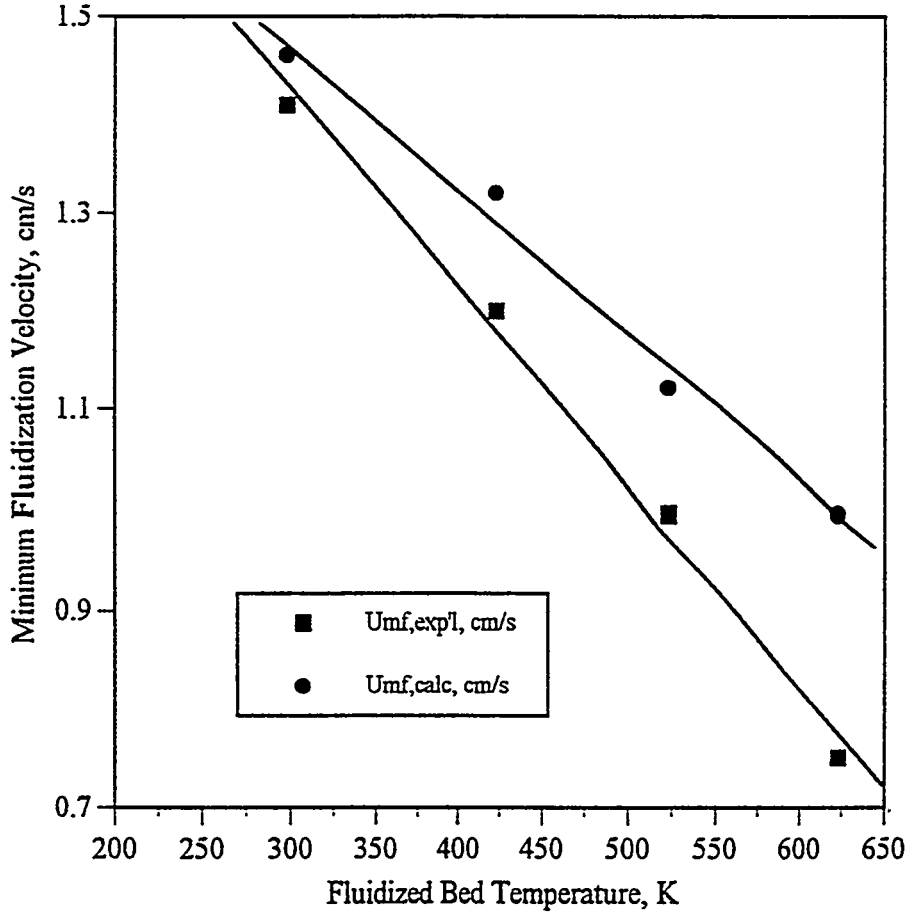
1.5
1.3
1.1
0.9
0.7
Minimum Fluidization Velocity, cm/s
200
250
300
350
400
450
500
550
600
650
Fluidized Bed Temperature, K
Umf,exp'l, cm/s
Umf,calc, cm/s

The minimum fluidization velocity is dependent upon a number of parameters, such as fluid density (ρ_g), fluid viscosity (μ_g), particle sphericity (ϕ_S), voidage at minimum fluidization velocity (ε_{mf}), and particle density (ρ_p). When the temperature and pressure of the system are fixed, these parameters are constants. The characteristic dimensionless numbers Ar and Re_{mf} for coked sands at ambient temperature and pressure can be determined. However, the use of parameters measured at room temperature may not be justified for the prediction of U_{mf} at elevated temperatures.

All the U_{mf} calculations are based upon the equality of pressure drop per unit cross-sectional area as given by the Ergun equation (142). If the voidage at minimum fluidization velocity, ε_{mf}, and the particle shape factor, ϕ_S, are known, the original Ergun equation (142) could provide a better prediction of U_{mf} than its simplified variations. However, both voidage and sphericity are parameters which are difficult to determine for a given system. Practically, both factors may be mutually interdependent.

When the temperature of a fluidized bed is changed, the most obvious changes were in the properties of the fluidizing gas. The gas density and viscosity significantly affect the performance of gas-solid fluidization systems and, concomitantly, U_{mf}. The density of the gas, ρ_g, decreases and the viscosity, μ_g, increases with temperature.

Fluidized beds operate in the laminar flow region at low particle Reynolds numbers where Re_{mf} is less than 20 (144). The viscous term in the Ergun equation is predominant and the kinetic term is negligible in this regime. The Ergun equation can be rearranged to give

$$\frac{Ar}{Re_{mf}} = 150\frac{1-\varepsilon_{mf}}{\phi_s^2\varepsilon_{mf}^3} \qquad (30)$$

U_{mf} is a function of gas viscosity; that is, Umf $\propto 1/\mu$. Since the gas viscosities are proportional to T^{n} where n is usually between 0.6 and 1.0 (150), U_{mf} is also a function of temperature. The U_{mf} of coked sands at elevated temperature study were fallen into this category, where gas viscosity is the important variable.

The system is in the turbulent flow region at high particle Reynolds numbers over 1000 (128). The kinetic term in the Ergun equation (142) predominates and the viscous term is negligible. Thus, the Ergun equation reduces to

$$\frac{Ar}{Re_{mf}} = \frac{1.75}{\phi_s \varepsilon_{mf}^3} Re_{mf} \qquad (31)$$

and U_{mf} is primarily determined by kinetic energy losses. Since U_{mf} is proportional to the square root of the fluidizing gas density, the temperature dependence is a function of $T^{0.5}$.

The experimental minimum fluidization velocity at the elevated temperatures invested can be expressed by the following equation in the temperature range from 290 to 623 K.

$$U_{mf} = 2.03 - 2.02 \times 10^{-3} T \text{ (cm/s)} \qquad (32)$$

where $R^2 = 1.00$.

The predictions from existing correlations tend to overestimate the minimum fluidization velocity at elevated temperatures (150). Bed voidage (ε_{mf}) increased with temperature for Geldart's group B particles (137, 151, 154), especially for particles in the size range from 90 to 110 μm. Mii et al. (152) studied the U_{mf} at 673 K with air and nitrogen and indicated that the experimental U_{mf} was 2 cm/s whereas the predicted U_{mf} was 4 cm/s. The discrepancies between the predictions and experimental data

increased as the temperature increased. The experimental results at elevated temperatures indicated that the minimum fluidization velocity was less than the predicted values and that the deviation increased as the temperature increased.

Variations in bed voidage with temperature appeared to be another factor in determining the dependence of the minimum fluidization velocity on temperatures. It is presumed that fluidized bed voidage changed as the bed temperature increased and, consequently, the minimum fluidization velocity with temperatures. The characteristics of the particulate phase was determined by the interparticle force in the bed. The growth of bed voidage at minimum fluidization condition with increasing temperature demonstrated the possibility of attaining an increasingly looser arrangement of the sand particles. This arrangement increased the fluidity of particle.

The experimental results in this study suggested that the minimum fluidization velocities decreased as bed temperature increased at elevated temperatures. The minimum fluidization velocity was determined by the viscous energy loss term in the Ergun equation at low particle Reynolds numbers. Other relevant parameters, such as mf and s, might also impact the minimum fluidization velocity. The rise in operating temperature led to an increase in the fluidity of the fluidized bed. Calculations confirmed that the system was well within the laminar flow region when the particle Reynolds numbers were less than 10.

Comparison of Pull Mode Fluidization Characteristics with Different Coked Sands

The coked sands produced during pyrolysis of the Whiterocks oil sands in a fluidized bed reactor (119) and the PR Spring coked sands produced in this study were used to investigate the feasibility of the pull mode fluidization in a small fluidized bed reactor. A surge tank with a gas dryer was installed to provide continuous nitrogen flow to the reactor at constant ambient pressure to maintain the pull mode fluidization. A schematic of the system was presented in Figure 89.

The fluidization curves for the Whiterocks and the PR Spring coked sands are presented in Figure 112. The two types of coked sands studied exhibited different fluidization characteristics in the pull mode. The fluidization curve using the Whiterocks coked sands was similar to a push mode fluidization curve. It displayed distinct packed bed and fluidized bed regimes. In contrast, the fluidization curve for the PR Spring coked sands exhibited a gradual transition from the packed bed to the fluidized bed regimes. The slope of pressure drop in the packed bed portion with the Whiterocks coked sands was greater than with the PR Spring coked sands. The transition from the packed bed to the fluidized bed was not apparent during fluidization with the PR Spring coked sands.

The beds were allowed to settle for 30 min and a second set of fluidization curves were obtained for both coked sands. The fluidization curves were quite similar to Figure 112. Two distinct regimes were still apparent with the Whiterocks coked sands, whereas once again the PR Spring coked sands did not exhibit an observable transition from the packed bed to the fluidized bed regime. The pressure drop across the bed developed gradually with the PR Spring coked sands as the fluidizing gas velocity was increased, which indicated that the fluidization of the PR Spring coked sands underwent a gradual transition from partially to fully developed fluidization. The pressure drop was fully developed and attained a value equivalent to the bed hold-up per unit area with further increase in the nitrogen flow rate for the PR Spring coked sands. These observation may be related to the that the PR Spring and Whiterocks coked sands samples had different particle size distributions. The PR Spring coked sands (106) had a broad particle size distribution whereas the particle size distribution of the Whiterocks coked sands was relatively narrow. The results indicated that both coked sands operated successfully in a pull mode fluidization.

The differential pressure drop across the bed for a fluidized bed operated in the pull mode at a constant bed inventory is shown in Figure 113. A significant amount of

Figure 112.

Comparison of Pull Mode Fluidization Curves with Whiterocks and PR Spring Coked Sands

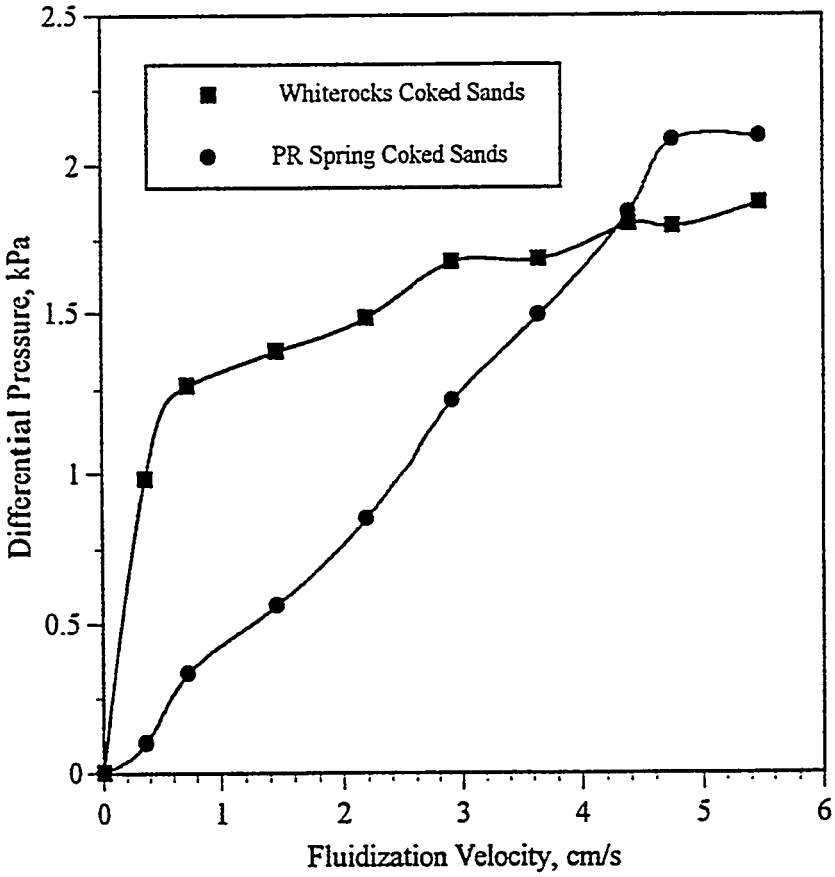
Whiterocks Coked Sands
PR Spring Coked Sands
Differential Pressure, kPa
Fluidization Velocity, cm/s
0
0.5
1
1.5
2
2.5
0
1
2
3
4
5
6

Figure 113.

Continuous Operation in Pull Mode Fluidization at H/D=2.0 With PR Spring Coked Sands

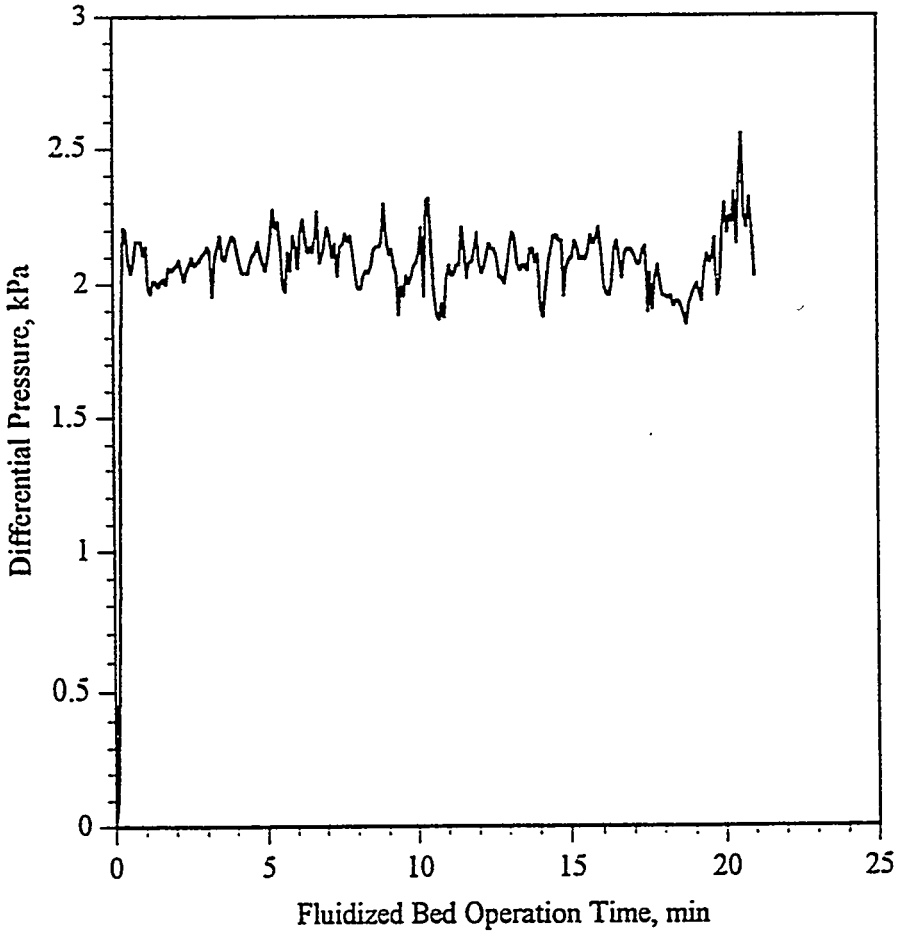
Differential Pressure, kPa
3
2.5
2
1.5
1
0.5
0
0
5
10
15
20
25
Fluidized Bed Operation Time, min

fluidizing gas flow rate was required to achieve a fully developed fluidized bed pressure drop: twice the minimum fluidization velocity was required to maintain a bed pressure drop equal to M/A in the pull mode for the PR Spring coked sands (Figure 112). Pull mode fluidization was not practical compared with push mode fluidization and fluidization quality was not as good as in the push mode operation for this reactor system.

Effect of Pyrolysis Variables on Product Distributions and Yields

The fluidized bed reactor system operated in the bubbling regime under pyrolysis conditions. This conclusion was based on the coked sand fluidization and defluidization studies at ambient and elevated temperatures for different flow modes. The process variables investigated in the oil sand pyrolysis studies included the bed temperature, the solids retention time, and the fluidizing gas velocity. Previous researchers, (50, 51, 114, 119-121), established the range of reactor temperatures and solids retention times expected to influence the product distribution and yields. These investigations also confirmed that the fluidized gas velocity had no significant effect on product yields in the range of conditions studied.

In this study, a series of experiments was conducted in which

- the reproducibility of the reactor system was established;
- the effect of reactor temperatures at constant solids retention time was studied;
- the effect of solids retention times at constant reactor temperature was studied;

and,

- the maximum reactor throughput with the PR Spring oil sands at pyrolysis conditions was established.

Reproducibility of Fluidized Bed Pyrolysis

Two experiments (QTPRS11 and QTPRS13) were conducted at a reactor temperature of 773 K and solids retention times of 26.0 and 27.2 minutes to test the reproducibility of the operating and experimental procedures for the fluidized bed

system at elevated temperatures under pyrolysis conditions. The process operating conditions, the product distribution and yields, and selected liquid product properties are presented in Table 32. The temperature and differential pressure of the bed for these two experiments were controlled by four temperature controllers and a differential pressure controller. The temperatures for the two experiments were 773±2 and 773±3 K. The solids retention times for the two experiments controlled by the differential pressure controller and the oil sands feeder auger speed. The differential pressures across the bed were 2.24±0.11 and 2.19±0.10 kPa for QTPRS11 and QTPRS13, respectively. The auger speeds of the two experiments were 2.0% of the full speed. The solids retention times in the runs were 27.2 and 26.0 minutes and were considered the same for purposes of the reproducibility evaluation. The minor difference of 1.2 minutes of the solids retention times was caused by oil sands feed rate fluctuations and did not change the conclusions regarding reproducibility.

Selected bitumen-derived liquid properties were determined for the two experiments to evaluate the reproducibility of the experimental procedures. The normalized product distribution and yields for the two experiments were very close. Specific and API gravities, pour points, viscosities, and Conradson carbon residues were in fairly good agreement, and the simulated distillation results indicated that the two liquid products had similar boiling range distributions. The results indicated that the fluidized bed pyrolysis system was reliable and reproducible.

Effect of Pyrolysis Temperature on Product Distribution and Yields

The pyrolysis temperature is the most significant process variable which affects the product distribution and yields in thermal cracking processes, especially in the pyrolysis of oil sands. A series of experiments using the PR Spring oil sands as feed were conducted, in which the reactor solids retention time and fluidizing gas velocity were held constant at 30±1 min and 10 SLPM (standard liter per minute), respectively. The

Table 32. Reproducibility of Product Distribution and Yields with the PR Spring Oil Sands in a Fluidized Bed Pyrolysis Reactor

Experiment I.D.	QTPRS11	QTPRS13
Date	10/17/94	10/21/94
T_b, K	773±2	773±3
T_R, min.	27.2	26
ΔP_b, kPa	2.24±0.11	2.19±0.10
Auger Speed, %	2.0	2.0
U_f, LPM	10	10
U_f/U_{mf}	2.6	2.6
Steady State Run, min.	120	121
Bitumen Mass Balance		
Gases, wt%	3.1	2.9
Liquids, wt%	83.3	78.5
Coke, wt%	12.9	13.3
Extractables, wt%	trace	trace
Total Mass Bal., wt%	99.3	94.7
Normalized Yields		
Gases, wt%	3.1	3.0
Liquids, wt%	83.9	82.9
Coke, wt%	13.0	14.1
Extractables, wt%	trace*	trace*
Total Yields, wt%	100	100
Specific Gravity (288/288K)	0.9360	0.9408
API Gravity (288 K)	19.7	18.9
Viscosity (298 K), cp	210	320
Pour Point, K	257	263
Conradson Carbon, wt%	3.3	4.5
Ash, wt%	0.0	0.1
Simulated Distillation		
IBP-477 K, wt%	3.1	2.8
477-617 K, wt%	18.9	18.2
617-811 K, wt%	56.3	56.6
>811 K, wt%	21.7	22.4
Volatility, <811, wt%	79.3	77.6
Elemental Analysis		
Carbon, wt%	86.97	87.28
Hydrogen, wt%	12.24	11.88
Nitrogen, wt%	0.50	0.54
Sulfur, wt%	0.29	0.30
H/C Ratio		
Molecular Weight, g/mol	364	383
H/C atomic Ratio	1.69	1.63

Trace: Toluene extractable amount less than 0.01 g.

effect of reactor temperature on the product distribution and yields in the push mode fluidization are presented in Figure 114 and Table 33.

The normalized total hydrocarbon liquid yields ranged from 76.0 wt% at 723 K to 81.8 wt% at 798 K. The liquid yield increased as reactor temperature increased from 723 to 773 K. An apparent maximum liquid yield of 84.2 wt% was obtained at 773 K. The total liquid yield decreased from 84.2 to 81.8 wt% as the reactor temperature increased from 773 to 798 K. The light gas yield steadily increased from 1.5 wt% at 723 K to 5.1 wt% at 798 K. The coke yield decreased from 21.9 to 13.1 wt% as the reactor temperature increased from 723 to 773 K. The coke yield was insensitive to reactor temperature above 773K. Similar product distribution and yields were obtained with the PR Spring oil sands in a large diameter fluidized bed reactor pyrolysis study (106).

The thermal decomposition of bitumen during oil sands pyrolysis in a fluidized bed reactor is a set of complex chemical reactions. The proposed mechanisms for bitumen pyrolysis consists primarily of thermal cracking reactions (51, 155); however, Shun (120) reported that the Circle Cliffs oil sands mineral matter exhibited catalytic cracking activity at pyrolysis conditions. The apparent catalytic effect led to a significant reduction in the bitumen-derived liquid yields. The liquid yields obtained in this study were higher and the gas yields were lower than those reported in previous pyrolysis studies using various oil sands (50, 51, 114, 119, 120). The reason for higher liquid yields in this investigation was presumed to be related to the attainment of the bubbling fluidization regime in the reactor.

The lowest normalized liquid yield, 76 wt%, was obtained at a reactor temperature of 723 K and a solids retention time of 29 minutes. The amount of toluene extractables leaving the reactor in the coked sand was 0.6 wt%, whereas the coke yield was 21.9 wt%. The liquid yields were lower at low temperatures due to the reduced severity of the pyrolysis reactions as the temperature decreased. The higher coke yield and the presence of toluene extractables on the coked sand indicated that some higher molecular

Figure 114.

Effect of Pyrolysis Temperature on the Product Distribution and Yields for the PR Spring Oil Sands in a Fluidized Bed Reactor

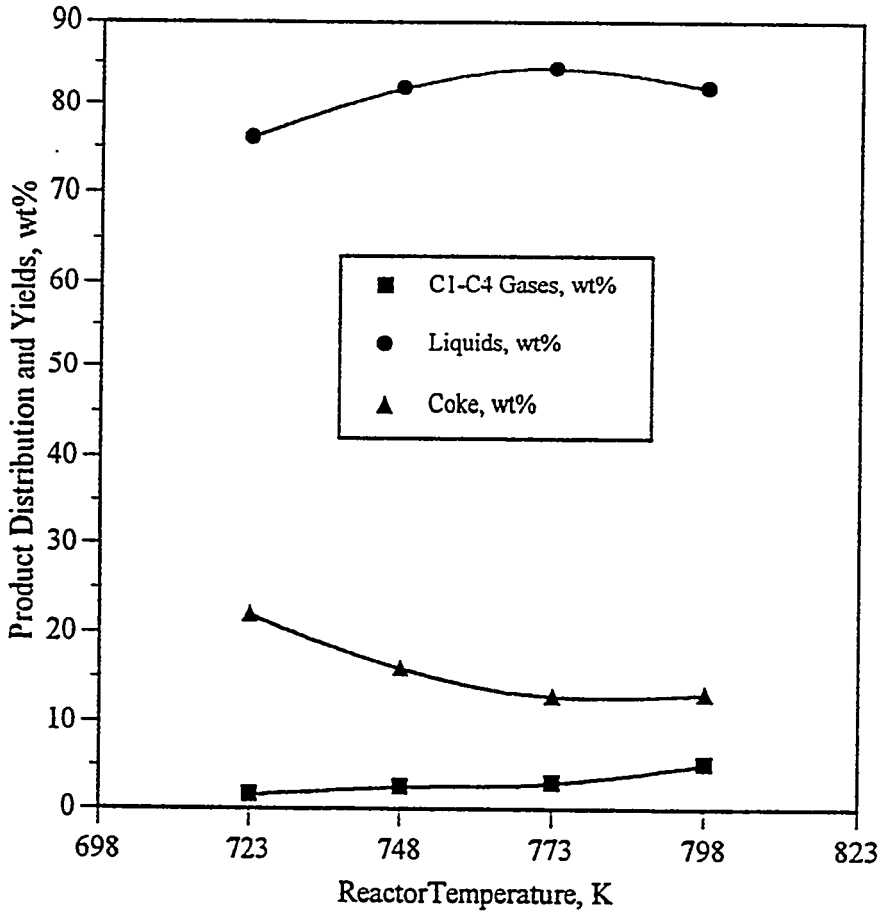
90
80
70
60
50
40
30
20
10
0
Product Distribution and Yields, wt%
C1-C4 Gases, wt%
Liquids, wt%
Coke, wt%
698
723
748
773
798
823
ReactorTemperature, K

Table 33. Effect of Pyrolysis Temperature on Product Distribution and Yields for the PR Spring Oil Sands in a Fluidized Bed Reactor

Experiment I.D.	QTPRS17	QTPRS16	QTPRS05	QTPRS14
Date	11/05/94	11/04/94	09/27/94	11/01/94
T_b, K	723±4	748±3	773±3	798±3
T_R, min.	29	31	29	30.9
ΔP_b, kPa	2.43±0.07	2.47±0.15	2.27±0.06	2.38±0.15
Auger Speed, %	2.0	2.0	2.0	2.0
U_f, LPM	10	10	10	10
U_f/U_{mf}	2.6	2.6	2.6	2.6
Steady State Run, min.	120	121	148	122
Bitumen Mass Balance				
Gases, wt%	1.5	2.2	2.9	4.9
Liquids, wt%	73.7	76.3	85.0	78.6
Coke, wt%	21.2	14.8	13.0	12.6
Extractables, wt%	0.5	trace	trace	trace
Total Mass Bal., wt%	96.9	93.3	100.9	96.2
Normalized Yields				
Gases, wt%	1.5	2.4	2.9	5.1
Liquids, wt%	76.0	81.8	84.2	81.8
Coke, wt%	21.9	15.9	12.9	13.1
Extractables, wt%	0.6	trace	trace	trace
Total Yields, wt%	100.0	100.0	100.0	100.0

weight species were not converted to evaporable liquids at reactor temperatures below 723 K. The overall bitumen pyrolysis reaction is frequently represented as follows:

$$\text{Bitumen} \xrightarrow{Pyrolysis} \text{Condensable Hydrocarbon Vapors}(C_5^+ \text{ Liquids}) + \text{Hydrocarbon Gases } (C_1 + C_4) + \text{Coke}$$

Conceptually (not mechanistically) the pyrolysis can be represented as a combined vaporization and pyrolysis/vaporization scheme:

$$\text{Bitumen}(< T_v) \xrightarrow{Vaporization} \text{Condensable Hydrocarbon Vapors (Liquids)}$$

$$\text{Bitumen}(> T_v) \xrightarrow{Pyrolysis} \text{Bitumen Derived Heavy Oils(BDHO) on Sand Grains} + \text{Condensable Hydrocarbon Vapors (Liquids)} + \text{Hydrocarbon Gases } (C_1 - C_4) + \text{Coke}$$

The BDHO intermediate can undergo further reaction to produce coke and/or vapor phase products or it can vaporize:

$$\text{BDHO} \xrightarrow{Vaporization} \text{Condensable Hydrocarbon Vapors (Liquids)}$$

$$\text{BDHO} \xrightarrow{Pyrolysis} \text{Condensable Hydrocarbon Vapors (Liquids)} + \text{Hydrocarbon Gases } (C_1 - C_4) + \text{Coke}$$

If the reactor is operated at a temperature where the rate of coke formation is greater than the rate of BDHO vaporization and pyrolysis, then the coke yield would be expected to increase at this temperature at the expense of liquid yield. The longer the BDHO remains in contact with the sand surface the greater the tendency to form coke whereas once the reaction products are vaporized they are rapidly swept out of the

reactor. The conceptual pyrolysis scheme was invoked to explain the observed trends in product distribution as a function of temperature: the bitumen-derived liquid yields increased and coke yields decreased as the reactor temperature increased from 723 to 773 K. A maximum liquid yield of 84.2 wt% was obtained at 773 K. The coke yields remained unchanged as the reactor temperature increased from 773 to 798 K. However, secondary vapor phase cracking of condensable vapors to gas may have shifted the liquid and gas yields and consequently, the product distribution.

Effect of Solids Retention Time on Product Distribution and Yields

The average solids retention time (θ_s) in the fluidized bed reactor was defined as the bed hold-up divided the oil sands feed rate.

$$\theta_s = \frac{W_b}{F} \qquad (32A)$$

The solids retention time can be varied by changing the bed hold-up or by adjusting the oil sands feed rates. The solids retention time in this study was changed and controlled by changing the feed-auger speed while the bed hold-up was held constant. The feed rate of oil sands was not precisely controlled compared to reactor temperature because the auger speed control operated in the low range from 1.5 to 3.0 % of full range and the E-auger was relatively large based on the feed rate. The average solids retention times exhibited minor differences even though the auger speed control was set to the same value in different runs. A series of solids retention time experiments using the PR Spring oil sands was conducted to determine the effect of solids retention time on product distribution and yields and total liquid product quality.

The effect of solids retention time on the product distribution and yields in the push mode of fluidization are presented in Table 34 and Figure 115. The average solids

Table 34. Effect of Solids Retention Time on Product Distribution and Yields for the PR Spring Oil Sands in a Fluidized Bed Reactor

Experiment I.D.	QTPRS08	QTPRS13	QTPRS05	QTPRS04
Date	10/10/94	10/21/94	09/27/94	09/23/94
T_b, K	773±6	773±3	773±3	773±2
T_R, min.	18.5	26	29	39
ΔP_b, kPa	2.20±0.26	2.19±0.10	2.27±0.06	2.30±0.09
Auger Speed, %	3.0	2.0	2.0	1.5
U_f, LPM	10	10	10	10
U_f/U_{mf}	2.6	2.	2.6	2.6
Steady State Run, min.	52	121	148	180
Bitumen Mass Balance				
Gases, wt%	3.6	2.9	2.9	3.7
Liquids, wt%	79.8	78.5	85.0	84.4
Coke, wt%	16.4	13.3	13.0	12.9
Extractables, wt%	trace	trace	trace	trace
Total Mass Bal., wt%	99.8	94.7	100.9	101.1
Normalized Yields				
Gases, wt%	3.6	3.0	2.9	3.7
Liquids, wt%	80.0	82.9	84.2	83.5
Coke, wt%	16.4	14.1	12.9	12.8
Extractables, wt%	trace	trace	trace	trace
Total Yields, wt%	100.0	100.0	100.0	100.0

Figure 115.

Effect of Average Solids Retention Time on the Product Distribution and Yields for the PR Spring Oil Sands in a Fluidized Bed Reactor

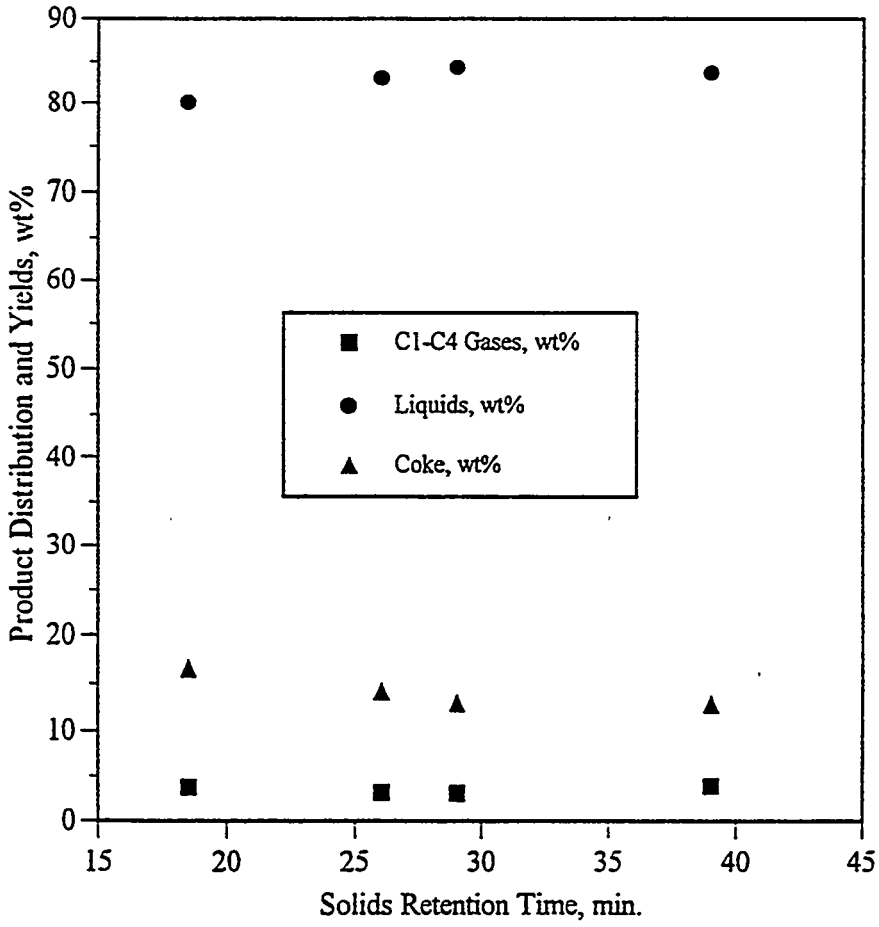
Product Distribution and Yields, wt%
Solids Retention Time, min.
C1-C4 Gases, wt%
Liquids, wt%
Coke, wt%
0
10
20
30
40
50
60
70
80
90
15
20
25
30
35
40
45

retention time was varied from 18.5 min to 39 min, whereas the reactor temperature was held constant at 773 K. The liquid yields increased with solids retention time from 80.0 wt% at an 18.5 min average retention time to a maximum value of 84.2 wt% at a 29 min average retention time. The liquids decreased slightly to 83.5 wt% as the average retention time increased further to 39 min.

The total liquid yields increased as the solids retention time increased at constant reactor temperature. The gas yield was insensitive to changes in solids retention times: it only increased from 3.6 wt% at 18.5 to 3.7 wt% at 39 min. The coke yield decreased from 16.4 to 12.9 wt% as the solids retention time increased from 18.5 to 29 min. The coke yield was constant as the solids retention time increased further from 29 to 39 min.

Changes in the solids retention time at a fixed bed inventory affected the bitumen-to-nitrogen feed ratio in the fluidized bed. An increase in solids retention time reduced the bitumen fed-to- nitrogen ratio. The tendency of low vapor pressure species being swept out increased in a nitrogen-rich environment. The vapor phase retention time was constant at about 8 seconds as the average solids retention time increased from 18.5 to 39 min at constant fluidizing gas rate of 10 SLPM. The solids retention time was 140 to 280 times greater than the vapor phase retention time. The pyrolysis reactions occurred in dense and diluted solid phases with minimal secondary cracking reactions in the vapor phase. Secondary cracking in the gas phase would be expected to be unchanged for a given fluidizing gas flow rate at a fixed temperature.

Study of Short Solids Retention Time

The short solids retention time experiments were conducted using the PR Spring oil sands as feed sand to determine the limits of the fluidized bed pyrolysis reactor regarding oil sands throughput and the attendant effects on the product distribution and yields. The results of a pair of experiments are presented in Table 35. Two experiments were conducted at different conditions: QTPRS08 was conducted at a reactor temperature of 773 K and a solids retention time of 18.5 min, and QTPRS12 was conducted at a reactor temperature of 798 K and a solids retention time of 20 minutes. The first experiment operated at steady state for 52 minutes, and the second one operated at steady state for 86 minutes. The coke yields for two experiments were higher than corresponding longer solids retention time runs (QTPRS05 and QTPRS14) at 723 K and 798 K, respectively. The normalized product distributions were nearly the same which was unexpected given the significance of temperature as a variable in pyrolysis reactions.

The reactor temperature and pressure fluctuations also increased in magnitude and frequency when the solids retention time was decreased. The onset of reactor plugging was detected in these experiments based on the differential pressure across the bed. This indicated that the reactor system was not capable of sustained long-term operation at solids residence times less than 20 min as indicated by differential pressure instabilities in the reactor. Although the furnace supplied enough heat through the wall of the reactor at short solids residence time ($\leq$ 20 min), the reactor shut down due to plugging. The magnitude of the temperature fluctuations in the runs of QTPRS08 and QTPRS12 was $\pm$6 K, which was 2 to 3 K (or 70 to 100%) greater than for typical stable pyrolysis experiments, i.e., QTPRS05 or QTPRS04. The differential pressure across the bed in runs QTPRS08 and QTPRS12 was 2.20 kPa. The variations around the set-point were $\pm$0.26kPa. The differential pressure variations for stable pyrolysis experiments were typically less than 0.1 kPa. Thus the instabilities

Table 35. Effect of Short Solids Retention Time on Product Distribution and Yields for the PR Spring Oil Sands in a Fluidized Bed Reactor

Experiment I.D.	QTPRS08	QTPRS12
Date	10/10/94	10/20/94
T_b, K	773±6	798±5
T_R, min.	18.5	20
ΔP_b, kPa	2.20±0.26	2.15±0.22
Auger Speed, %	3.0	3.0
U_f, LPM	10	10
U_f/U_{mf}	2.6	2.6
Steady State Run, min.	52	86
Bitumen Mass Balance		
Gases, wt%	3.6	3.6
Liquids, wt%	79.8	74.1
Coke, wt%	16.4	13.3
Extractables, wt%	Trace	trace
Total Mass Bal., wt%	99.8	91.1
Normalized Yields		
Gases, wt%	3.6	4.0
Liquids, wt%	80.0	81.4
Coke, wt%	16.4	14.6
Extractables, wt%	Trace	trace
Total Yields, wt%	100.0	100.0

were two to three times higher at short solids retention times than these were for stable pyrolysis experiments at longer retention times.

A portion of the oil sands particles fed to the reactor were several times greater than the screen size (3.2 mm) used to prepare the feed sands. This was related to agglomeration of oil sands particles during transport through the feeder auger at the higher feed rates due to auger induced shear and frictional forces. The agglomerates formed during feeding did not disperse into smaller particles until the pyrolysis reactions were completed and in some instances were bound together by coke. The large oil sands lumps could not be fluidized in the reactor which limited heat and mass transfer between the solids and the fluidized phases and disrupted the bubbling fluidization mode. The incompletely reacted bitumen-residue wetted sand particles caused the bed to plug.

Characteristics of the Total Liquid Products

The quality of the hydrocarbon liquids produced in the fluidized bed pyrolysis process was dependent on the operating variables as reflected by their physical and chemical properties (82, 104). The pyrolysis of the PR Spring oil sands in this work gave high bitumen-derived total liquid product yields (76-84 wt%) with low gas yields (2-5 wt%) relative to those from the other Uinta Basin oil sands deposits (50, 51, 114, 119, 120). Based on bitumen fed to the reactors, liquid yields ranged from 17 to 75 wt% and gas yields ranged from 15 to 22 wt% in small diameter fluidized bed pyrolysis process studies. A maximum yield of 75 wt% was obtained using PR Spring Rainbow I oil sands (51) and a minimum of 17 wt% of liquid yield was found using Circle Cliffs oil sands (120). Shun (120) reported that the catalytic characteristics of the host rock led to the low liquid yields. The total liquid yields in this study were similar to the liquid yields (77-90 wt%) reported for large diameter fluidized bed reactor (15.2 cm) studies (106, 121) in which slugging and channeling were absent. The reasons probably relate to the nature of the oil sands and the fluidization regimes in

which the fluidized bed reactor was operated. The previous small fluidized bed reactors (3.8 and 10.2 cm diameter) had a tendency to slug, especially the 10.2 cm diameter reactor (119). Heat transfer was greatly hindered in the slugging regime where the piston movement of bulk sand also caused poor mass transfer (135). In oil sands pyrolysis this could result in inefficient removal of the vapor phase from contact with the sand particles in the plug, thus leading to the secondary cracking of product vapors and a shift to high gas and low liquid yields. The fluidized bed reactor used in this study was operated in the bubbling fluidization regime as confirmed in fluidization studies. The improved quality of fluidization in this system may be a factor which led to the high liquid and low gas yields. Bubbling fluidization is characterized by good heat and mass transfer and decreased retention time of vapor products in the reactor which suppresses secondary cracking during pyrolysis. This should further lead to a better quality of bitumen-derived liquid products. The same trend was obtained in a large diameter fluidized bed reactor (106, 121).

The determination of liquid product properties was undertaken to assertion the influence of the process variables (i.e., reactor temperature and solids retention time) on the quality of the liquid products. Ultimately, these analyses will aide in the determination of the preferred process scheme for upgrading and refining of bitumen-derived liquid products. The effect of the pyrolysis process variables on liquid properties will be discussed with respect to oil sands pyrolysis to determine the extent of upgrading between the liquids and the bitumen.

Effect of Reactor Temperature on the Liquid Product Quality

A series of experiments was performed to determine the influence of reactor temperature on the liquid product properties. The effect of temperature on the physical and chemical properties of the total liquid quality was studied in the temperature range from 723 to 798 K at a fixed solids retention time of 30±1 minutes. The effect of

reactor temperature on the properties of the total liquid products produced from the PR Spring oil sands in a fluidized bed reactor are presented in Table 36.

The API gravity of bitumen derived liquid products steadily decreased from 19.6°API at a reactor temperature of 723 K to 19.0°API at 798 K. The API gravity of the bitumen on the feed oil sands was 11.2°API. The increase in the API gravity of the PR Spring total liquid products relative to the bitumen was related to the severity of the thermal decomposition reactions at the pyrolysis temperatures.

The effect of reactor temperature on the viscosity of the liquid products from the PR Spring oil sands was also investigated. The viscosity of the liquid products decreased from 298 cp at 723 K to 247 cp at 798 K at a constant solids retention time of 30±1 min. The decrease in viscosity with increasing temperature was consistent with the API gravity data. The slight decline in viscosity with temperature was probably related to a slight increase in the severity of thermal cracking as the reactor temperature increased from 723 to 798 K.

The Conradson carbon residue of the liquid products increased with reactor temperature from 3.4 wt% at 723 K to 4.5 wt% at 798K. This was a significant decrease relative to the bitumen (16.1 wt%) and represented a major improvement in the quality of the bitumen-derived heavy oils relative to the bitumen. The ash content for each sample was insignificant (<0.1 wt%) and was related to the entrainment of fine particles in the fluidizing gas and heavy oil vapors. Fluidizing gas velocity was held constant in each experiment at 10 LPM. Hence, the ash content in the liquid products due to fines entrainment was expected to be independent of process conditions. The ash contents indicated that the fluidizing gas velocity was low enough to minimize entrainment and that the condenser/strainer system was functioning as designed.

The pour points of the liquid products were independent of the reactor temperature. The lower pour points of the liquid products relative to the bitumen were consistent

Table 36. Effect of Reactor Temperature on the Properties of the Total Liquid Products Produced from the PR Spring Oil Sands in a Fluidized Bed Reactor

Experiment I.D.	QTPRS17	QTPRS16	QTPRS05	QTPRS14	Bitumen
Date	11/05/94	11/04/94	09/27/94	11/01/94	
T_b, K	723±4	748±3	773±3	798±3	
T_R, min.	29	31	29	30.9	
ΔP_b, kPa	2.43±0.07	2.47±0.15	2.27±0.06	2.38±0.15	
Specific Gravity (288/288K)	0.9364	0.9379	0.9391	0.9400	0.9913
API Gravity (288K)	19.6	19.4	19.2	19.0	11.2
Viscosity (298K), cp	298	282	277	247	3492*
Pour Point, K	262	262	260	257	339
Conradson Carbon Residue, wt%	3.4	3.9	3.7	4.5	16.1
Ash, wt%	0.1	0.0	0.1	0.1	3.2
H/C Atomic Ratio	1.70	1.69	1.68	1.67	1.60
Simulated Distillation					
IBP-477 K, wt%	2.7	2.9	2.7	3.3	0.2
477-617 K, wt%	17.9	17.6	19.4	19.2	5.5
617-811 K, wt%	56.9	56.6	55.3	56.6	30.6
>811 K, wt%	22.6	22.9	22.6	20.9	63.7
Volatility (<811 K), wt%	77.4	77.1	77.4	79.1	36.3
Elemental Analysis					
Carbon, wt%	86.92	86.96	87.03	87.14	86.99
Hydrogen, wt%	12.29	12.28	12.18	12.06	11.63
Nitrogen, wt%	0.51	0.50	0.50	0.51	1.08
Sulfur, wt%	0.28	0.26	0.29	0.29	0.30
Molecular Weight	365	373	376	366	809
Nickel, ppm	6	8	10	12	78
Vanadium, ppm	<5	<5	<5	<5	18

*: Bitumen viscosity measured at 363 K.

with the thermal cracking of heavy molecular species at pyrolysis temperatures in the range 723 to 798 K.

Simulated distillation data for the liquid products produced in the temperature range from 723 to 798 K are presented in Table 36 and Figure 116. The boiling point distributions and liquid product yields did not change significantly with reactor temperature. This is similar to the results reported by Dorius [1984] for the fluidized bed pyrolysis of PR Spring oil sands. The gasoline (IBP-477 K), middle distillates (477-617 K), and the gas oil (617-811 K) fractions were insensitive to reactor temperature. The volatility of liquid products increased from 77.4 to 79.1 wt% as the reactor temperature increased from 723 to 798 K. The residuum (>811 K) fraction decreased from 22.6 wt% to 20.9 wt% as the reactor temperature increased from 723 to 798 K.

The influence of reactor temperature on H/C atomic ratios of the total liquid products was consistent with the trend observed for viscosities and API gravities. The heteroatom contents of the liquid products were little influenced by changes in reactor temperature. The increase in the H/C ratios of the total liquid products was related to carbon rejection via the formation of the carbonaceous residue on the sand grains during pyrolysis.

Effect of Solids Retention Time on the Liquid Product Quality

A set of experiments was conducted to study the effect of solids retention time on liquid product properties using the PR Spring oil sands as feed. The study was conducted by varying solids retention time from 18.5 to 39 min at a fixed reactor temperature of 773±3 K. The effect of solids retention time on the total liquid product quality is presented in Table 37.

Figure 116.

Effect of Reactor Temperature on the Simulated Distillation of the Total Liquid Products Produced from the PR Spring Oil Sands in a Fluidized Bed Reactor

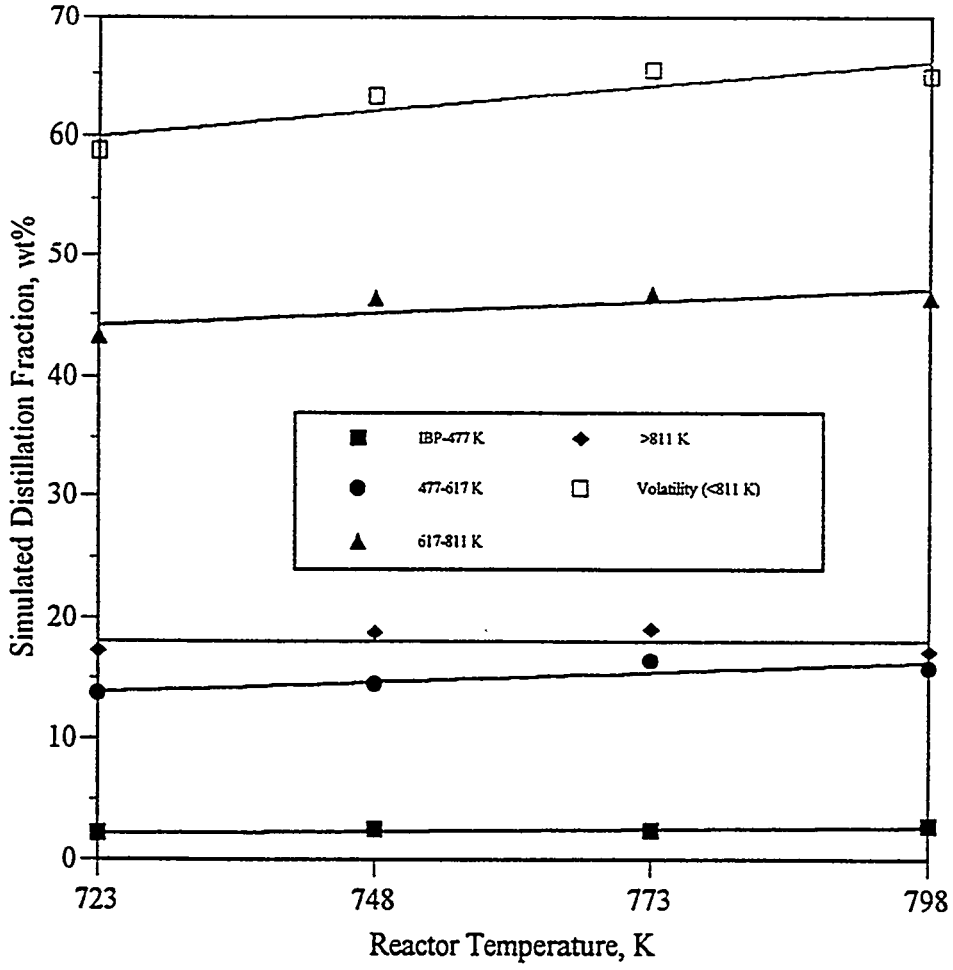
70
60
50
40
30
20
10
0
723
748
773
798
Simulated Distillation Fraction, wt%
Reactor Temperature, K
IBP-477 K
477-617 K
617-811 K
>811 K
Volatility (<811 K)

Table 37. Effect of Average Solids Retention Time on the Properties of the Total Liquid Products Produced from the PR Spring Oil Sands in a Fluidized Bed Reactor

Experiment I.D.	QTPRS08	QTPRS13	QTPRS05	QTPRS04	Bitumen
Date	10/10/94	10/21/94	09/27/94	09/23/94	
T_b, K	773±6	773±3	773±3	773±2	
T_R, min.	18.5	26	29	39	
ΔP_b, kPa	2.20±0.26	2.19±0.10	2.27±0.06	2.30±0.09	
Specific Gravity (288/288K)	0.9300	0.9408	0.9391	0.9417	0.9913
API Gravity (288K)	20.7	18.9	19.2	18.8	11.2
Viscosity (298K), cp	231	320	277	311	3492*
Pour Point, K	258	263	260	262	339
Conradson Carbon Residue, wt%	2.6	4.5	3.7	4.0	16.1
Ash, wt%	0.1	0.1	0.1	0.1	3.2
H/C Atomic Ratio	1.71	1.63	1.68	1.67	1.60
Simulated Distillation					
IBP-477 K, wt%	3.1	2.8	2.7	2.9	0.2
477-617 K, wt%	22.2	18.2	19.4	18.9	5.5
617-811 K, wt%	58	56.6	55.3	55.3	30.6
>811 K, wt%	16.8	22.4	22.6	22.9	63.7
Volatility (<811 K), wt%	83.2	77.6	77.4	77.1	36.3
Elemental Analysis					
Carbon, wt%	86.84	87.28	87.03	87.08	86.99
Hydrogen, wt%	12.37	11.88	12.18	12.12	11.63
Nitrogen, wt%	0.51	0.54	0.50	0.50	1.08
Sulfur, wt%	0.28	0.30	0.29	0.30	0.30
Molecular Weight	353	383	376	379	809
Nickel, ppm			10		78
Vanadium, ppm			<5		18

*: Bitumen viscosity measured at 363 K.

Since the 18.5 min run (QTPRS08) was terminated when the reactor plugged, it was not considered as a successful run. Thus, the effect of solids retention time on total liquid product quality only considered 26, 29, and 39 min retention time runs. As indicated in the fluidization study, the superior bubbling fluidization suppressed the secondary cracking. The solids retention time did not exhibit any clear influence on the properties of the liquid products. This phenomena was also observed from large diameter fluidized bed reactor (106).

Extent of Upgrading as Reflected in Total Liquid Product Quality

It is essential to understand that total liquid quality improved significantly during fluidized bed pyrolysis in the 7.62 cm fluidized bed reactor. A comparison of the physical and chemical properties of the liquid product produced at 773 K and a solids retention time of 29 min and the PR Spring bitumen is presented in Table 38.

Significant changes occurred during fluidized bed pyrolysis. The specific gravity of the bitumen was higher than that of liquid products. The API gravity improved from 11.2 to 19.2°API. The viscosity of the liquid product decreased several orders of magnitude relative to the bitumen feed. The pour point of liquid product was markedly reduced during pyrolysis. The API gravity, 19.2°API; the viscosity, 277 cp at 298 K; and the pour point, 260 K indicated that the total liquid product produced at 773 K and a solids retention time of 29 min was pipeline quality petroleum liquid. The Conradson carbon residue decreased by a factor of four from 16.1 wt% to 3.7 wt%. The boiling point distribution indicated that during pyrolysis the volatility increased from 36 to 77 wt%, whereas the resid content was reduced from 64 to 33 wt%.

Improvement in the liquid quality occurred because of thermal cracking of high molecular weight materials to smaller compounds. This was observed as a reduction in molecular weight process. An increase in H/C atomic ratio indicated that the liquid quality increased during pyrolysis. The nitrogen contents of the liquid products decreased by approximately 50%. This observation was significantly different from the trends reported previously [Hanson and Oblad, 1988] regarding the fate of nitrogen heteroatoms during oil sands pyrolysis. The nitrogen contents of the total liquid products produced in the small diameter (50, 51, 114, 120) and large diameter (106, 119, 121) fluidized beds were little different from that of bitumen. It was presumed that nitrogen containing heteroatomic species were deposited in the carbonaceous residue on the sand grains during thermal cracking and coke formation. The sulfur contents of the total liquid products were little different from that of the bitumen which was consistent with the results reported previously (104). Inorganic material, such as metals and ash, were significantly decreased. The reduction in Conradson carbon residue, resid content, and metals were a reflection of the significant upgrading accomplished during pyrolysis of the oil sands.

Liquids produced from the fluidized bed pyrolysis process were significantly upgraded relative to the bitumen. The experimental results indicated that it was technically feasible to use the fluidized bed pyrolysis process to recover an upgraded bitumen-derived liquid product. Pyrolysis followed by hydrotreating may reduced the overall costs of upgrading to synthetic crude oil relative to aqueous extraction followed by coking and/or hydrotreating.

SUMMARY AND CONCLUSIONS

A fluidized bed reactor system was designed, installed, and operated for the pyrolysis of the PR Spring oil sands under push mode fluidization. A number of previously reported problems with oil sands pyrolysis in a small diameter reactor (<15.2 cm) were resolved through improved oil sands feeding, coked sands withdrawal with a modified aerated L-valve, and a modified liquid recovery system. The following conclusions were drawn from this investigation.

The coked sands feeding study indicated that commercial Acrison model BDF-1 bin discharge feeders were capable of feeding dry coked sands. An E-auger with a water-cooled discharge cylinder (30.5 cm long) operated at low auger speeds, 1-3% full range, was successfully used to feed undiluted PR Spring oil sands. The water-cooled E-auger exhibited reproducible feed rates and an appropriate correlation between oil sands feed rate and the auger speed was established.

A modified aerated L-valve with two aeration ports was used as a solids withdrawal device. The secondary aeration port facilitated the transfer of large particles from the downcomer to the coked sands receiver and resolved the L-valve solids withdrawal plugging problems. The L-valve study indicated that the device was suitable for controlling and metering solids removal in a small diameter fluidized bed pyrolysis reactor.

A series of fluidization and defluidization experiments with multisized coked sands was conducted to establish the regime in which the reactor operated during oil sands pyrolysis. The coked sands fluidization studies indicated that the bed operated in the bubbling regime, which was different from previous studies in which the slugging regime predominated.

Three different fluidization modes were investigated in the system: conventional push, reduced pressure, and pull fluidization modes. Pressure analyses were performed for three fluidization modes.

The minimum fluidization velocity was 1.41 cm/s in push fluidization mode and 1.35 cm/s in reduced pressure fluidization mode. The difference between the push and reduced pressure fluidization modes was related to the reactor pressure. The decrease in fluidizing gas density at the bed pressure in the reduced pressure mode relative to the push mode led to the decreased U_{mf}. The minimum fluidization velocities for both modes were predicted using the Wen-Yu empirical equation (145). The calculated values of U_{mf} in the push and reduced pressure fluidization modes were 1.46 cm/s and 1.39 cm/s, respectively.

The tapered gas distributor gave a unique fluidization curve which had four separate regimes: packed bed, transition, partial inner column fluidization, and fully developed fluidization. The partial inner column fluidization distinguishes a tapered gas distributor from a conventional flat plate distributor. The fluidizing gas velocity during pyrolysis was achieved in a fully developed fluidization regime characterized by bubbling fluidization.

Elevated temperature fluidization at push fluidization mode suggested that the ambient temperature empirical correlations, and even the Ergun equation deviated significantly from results. The deviation increased dramatically with an increase in fluidization temperatures. The effect of temperature on minimum fluidization velocity for coked sands was correlated to $U_{mf} = 2.03 - 2.02 \times 10^{-3} T$ cm/s in the temperature range of 294 to 623 K.

Fluidization during continuous feeding and withdrawal indicated that the PR Spring coked sands can be fluidized in the small fluidized bed reactor under pull fluidization mode.

The pyrolysis study demonstrated that upgraded bitumen-derived liquids can be produced during oil sands pyrolysis in a fluidized bed. The reproducibility study indicated that process variable results for fluidized bed pyrolysis of oil sands can be duplicated. The product distributions and yields and liquid product qualities at the

same reactor temperature and solids retention time were in good agreement for the two experiments.

The major focus of this investigation was the pyrolysis of the PR Spring oil sands and the study of the influence of process variables (temperature and solids retention time) on product distributions and yields and total liquid product properties. The bitumen-derived liquid yields increased as reactor temperature increased at fixed solids retention time, passed through a maximum, and decreased as reactor temperature continued to increase. The coke yields decreased and the hydrocarbon gas (C_1 to C_4) yields increased as reactor temperature increased. A maximum liquid yield of 84.2 wt% was obtained at a reactor temperature of 773 K and a solids retention time of 29 min with the PR Spring oil sands. The liquid yields increased as the solids retention time increased at a fixed reactor temperature. The coke yields increased as solids retention time decreased. The C_1 to C_4 gas yields were insensitive to solids retention time Reactor temperature exerted a greater influence than solids retention time on the total liquid product liquid properties. Even though pyrolysis significantly affected the liquid product properties relative to bitumen, the effects of changes in reactor temperature and solids retention time were minor. Its was presumed that the reactor operated in the bubbling fluidization which is characterized by superior heat and mass transfer. In oil sands pyrolysis this could facilitate the release of hydrocarbon vapor from the sand particles, reduce secondary cracking, and dampen the process variable effects observed in slugging reactors. The total liquid properties indicated that substantial upgrading occurred during the pyrolysis process, that is, significant improvements on API gravities, specific gravities, viscosities, Conradson carbon residues, and pour points were achieved. The extent of upgrading was also indicated by improved liquid volatilities, metal contents, and molecular weights. The sulfur of the total liquid products was little different from that of the bitumen and was independent of the process conditions. However, there was a reduction of

approximately 50% for the nitrogen contents. This effect has not been previously reported for either the large or small diameter reactors regardless of the origin of the feed oil sands.

The pyrolysis studies indicated that the preferred recovery sequence would be oil sands pyrolysis followed by hydrotreating of the total liquid products to reduce the heteroatom concentrations.

FLUIDIZED BED PYROLYSIS OF OIL SANDS IN A LARGE DIAMETER REACTOR

Principal Investigator: F.V. Hanson
Co-Principal Investigator: J.V. Fletcher
Graduate Student: S. Nagpal

INTRODUCTION

Pyrolysis of oil sands in a fluidized bed reactor has been investigated by various researchers (50, 51, 108, 114-117, 119-121, 156). The basic process involves the following three steps: feeding oil sands to a heated fluidized bed, condensation and collection of the cracked and distilled heavy oil fractions and continuous withdrawal of coked sand from the reactor. The bitumen on the oil sands undergoes the following overall reaction:

Bitumen ----------> a. Liquid + b. Coke + c. Gases

In the above equation, a, b and c are the weight fractions based on unit weight of bitumen reacted. Various operating parameters have been found to effect the product distribution and yields (i.e., a, b and c) from these reactors. These variables include the reactor temperature, solids retention time in the reactor, nature of the oil sands, the fluidizing gas flowrate, the nature of the fluidizing gas, the chemical and physical nature of host rock, the reactor loading (height-to-diameter ratio (H/D) of the settled bed), and the design of the reactor.

Pyrolysis of Oil Sands

A systematic study to develop the scientific and engineering data base necessary for commercialization of Utah's tar sand deposits was started in 1973 at the University of Utah (82, 157). The emphasis of this program was on water-assisted (45, 158-160); and thermal recovery technologies (104, 113, 161, 162); upgrading of the bitumen derived heavy oils and

characterization of hydrocarbon liquid products and bitumens (163).

The initial fluidized bed investigators at the University of Utah were carried out by Weeks (115), Jayakar (116), and Venkatesan (51). A 5-cm ID fluidized bed reactor capable of processing up to 2.27 kg/h of oil sands (164) was constructed. The reactor system included two coupled fluidized beds - one for pyrolysis of oil sands and the other for combustion of coked sand. Heat was transferred from the combustion bed to the pyrolysis bed by a heat pipe which contained potassium as the heat transfer fluid. These studies were conducted with the crushed and mixed ore from the Tar Sand Triangle and Asphalt Ridge oil sands deposits. The product yields were reported to be dependent upon the reactor temperature. A temperature of 773 K was found to maximize the liquid yields. However, less than 80% of the bitumen fed to the reactor could be accounted for in this exploratory study.

Venkatesan (50) constructed a bench scale fluidized bed pyrolysis reactor (3.6 cm ID). The reactor was designed to process a maximum of 2.5 kg/h of oil sands. Effects of reactor temperature and solids residence time on product distribution and yields were investigated with crushed and sized oil sands from the Sunnyside and Tar Sand Triangle deposits. It was concluded that a reactor temperature of about 723 K gave the maximum liquid yield of 61% (based on bitumen fed to the reactor) with the Sunnyside oil sand feed. The temperature for maximum liquid production was found to shift to 798 K in the case of Tar Sand Triangle oil sand feed. The liquid yields were inversely related to the solids retention times. It was predicted that a maximum liquid yield of about 80% could be achieved at the preferred reactor temperature and retention times in the range of 12-16 min (165). Detailed chemical and physical property analyses of the liquid products were carried out. The API gravity and viscosity were found to decrease with reactor temperature while the Conradson carbon residue and volatility were found to increase.

Wang (114) conducted runs with Whiterocks and Tar Sand Triangle oil sands in the reactor constructed by Venkatesan (50) and reported similar trends in product distribution. The maximum liquid yield with the Whiterocks oil sands was obtained at a lwo solids residence time and a reactor temperature of about 798 K. A correlation based on regression analysis was developed to fit the experimental yield data. It was predicted that a liquid yield of about 80% could be achieved at a solids retention time of 12 min and a pyrolysis temperature in the range from 803 K to 823 K. A primary conclusion of this study was that the liquid yield was more dependent on the solids retention time than on any other parameter in laboratory scale reactors.

Smart (117) investigated the effect of reactor temperature and solids residence time on the pyrolysis of oil sands in a mini-pilot scale fluidized bed reactor (10.8-cm ID). This reactor was scaled up from the design of Jayakar (116) and Weeks (115). Three oil sands were investigated - PR Spring, Whiterocks and Sunnyside. The reactor temperature was varied from 713 K to 773 K and the solids retention time ranged from 30 to 48 min. Since the number of satisfactory runs with Whiterocks and Sunnyside oil sands were too few to establish interpretable trends, only the PR Spring runs were used to determine the effects of process variables on the product distribution and yields. The liquid and gas yields were reported to increase with temperature while the coke yield decreased. Similarly, an increase in solids residence time resulted in an increase in liquid yields. These results were contrary to the trends observed by other workers (50, 51, 114). In terms of liquid properties, the API gravity did not indicate any trend with reactor temperature whereas the viscosities decreased from 2000 to 500 cp as the temperature increased from 713 to 773 K.

Dorius (51) followed up on the work of Venkatesan (50) and Wang (114) and investigated the pyrolysis of Whiterocks (WR), PR Spring Rainbow-I (PRS-RI), PR Spring Rainbow - II (PRS-

RII) and PR Spring South (PRS-S) oil sands. The reactor temperatures at which maximum liquid yields were obtained were 798 K for PRS-RI and PRS-RII and 823 K for PRS-S. The difference in these two temperatures was attributed to the highly asphaltic nature of PRS-S bitumen as compared to the other two bitumens (104). Dorius (51) expanded on the regression analysis of Wang (114) and developed a set of correlations to predict product yields which correlated the experimental data better. Moreover, the asphaltene content, Conradson carbon residue and the H/C ratio of the bitumen were determined to have a very strong influence on the product distribution (166). The effect of operating parameters on the liquid quality was also determined. The results were similar to those reported by Venkatesan (51).

Sung (119) constructed 4-in diameter glass fluidized bed and pilot plant fluidized bed reactors to study the hydrodynamics of coked sand fluidization and the pyrolysis of the Circle-Cliffs oil sands, respectively. A 21-h long production run with Whiterocks oil sands was also carried out. The liquid yield during the production run with Whiterocks oil sands was 45 wt%.

Shun (120) rebuilt the reactor system originally constructed by Venkatesan (51) and conducted pyrolysis runs with the Circle Cliffs oil sands. The product distribution and yield patterns in these experiments were found to be very different from those of earlier investigations with other oil sands. A maximum liquid yield of 35.9 wt% was obtained at a reactor temperature of 823 K and solids residence time of 15 min. The gas yields were found to be much higher (30-35 wt%) than those previously reported. Furthermore, the recovered total liquid product contained a large amount of condensed water. The low liquid yield, high gas yield and the product water were attributed to the unusual chemical nature of the mineral substrate/host rock. The host rock contained kaolinite which released large amounts of bound water at pyrolysis temperatures. The activated kaolinite was presumed to have catalytically cracked the produced

liquid-boiling range vapors (104).

Deo et al. (167) reexamined the fluidization data of some of the previous studies (50, 51, 114, 120) and determined that the fluidization regime (based on the criterion proposed by Clift (168) in each case was in the slugging regime instead of the intended bubbling regime. Fletcher (121) constructed a pilot scale fluidized bed reactor capable of processing up to 20 kg/h of oil sands. Various hydrodynamic studies were carried out and a new correlation for predicting the minimum fluidization velocity (U_{mf}) was proposed (121). The effect of temperature on U_{mf} was also investigated and a new correlation was determined. The new reactor system incorporated some of the features of a commercial oil sands processing unit. Instead of electrical heating, the reactor used a propane burner as the source of heat. The burner flue gases were used to fluidize the bed instead of nitrogen as in previous studies. Care was taken to ensure that the bed operated in the bubbling fluidization regime by operating in the "pull" mode rather than the conventional "push" mode (121). Pyrolysis of Whiterocks oil sands was investigated in the temperature range from 723 to 798 K and the solids residence times between 30 to 76 minutes. There was a substantial increase in the maximum liquid yields as compared to the previous studies in the bench scale fluidized bed reactors (50, 51, 114, 115, 117, 119, 120); 85% vs. 70%. The gas yields were lower (5% vs. 20%) and the coke yield also showed a minor reduction. Moreover, no significant trends were observed in the product distribution and yields with respect to the reactor temperature and solids retention time. The difference may be related to the CO_2 and steam rich fluidizing gas and the better quality of fluidization in the reactor or to a combination of the two.

Bhadkamkar (156) conducted pyrolysis experiments with Whiterocks oil sands in a coupled fluidized bed reactor system (117) and obtained liquid yields ranging from 50.0 to 74.6 wt%. The maximum liquid yield (74.6 wt%) was obtained at a solids residence time of 12 min and a reactor

temperature of 734 K. The C_5-C_6 yield from the reactor was significant (13 to 49 wt%) indicating a high degree of secondary cracking. However, no discernable trends in product yields with respect to process parameters could be established.

General Trends in Product Yields and Quality

Most researchers agree that there are two important operating parameters that affect the product yields from the pyrolysis reaction in a fluidized bed reactor (104). These are the reactor temperature and the solids residence times.

Reactor Temperature

The liquid product yields have been plotted in Figure 117. The effect of reactor temperature on liquid yields can be analyzed to two different methods.

1. Subdivision I: Figure 117 can be divided into three distinct regions based on the amounts of liquid product yields. These regions are presented in Figure 118. Region I contains results with liquid yields higher than 75%, Region II has liquid yields between 45% to 75% and Region III consists of all results with liquid yields less than 45%. The bulk of the results lie in Region II (50, 51, 114, 117). Region III has results of only one researcher (120). The uncharacteristically lwo liquid yields of Shun (120) were attributed to the unusual nature of the Circle Cliffs oil sands and the small reactor diameter which could have resulted in slugging in the bed. Sung (119) reported higher liquid yields with Circle Cliffs oil sands in a large diameter fluidized bed. The results included in Region I of Figure 118 are those of Fletcher (121). The reason for high liquid yields is not clear at this stage. However, superior fluidization quality and steam and CO_2 rich fluidization gas have been proposed as possible explanations (121).

2. Subdivision II: Regions II and III in Figure 118 can be divided into sub-Regions IV and

Figure 117

Liquid Yields vs. Reactor Temperature

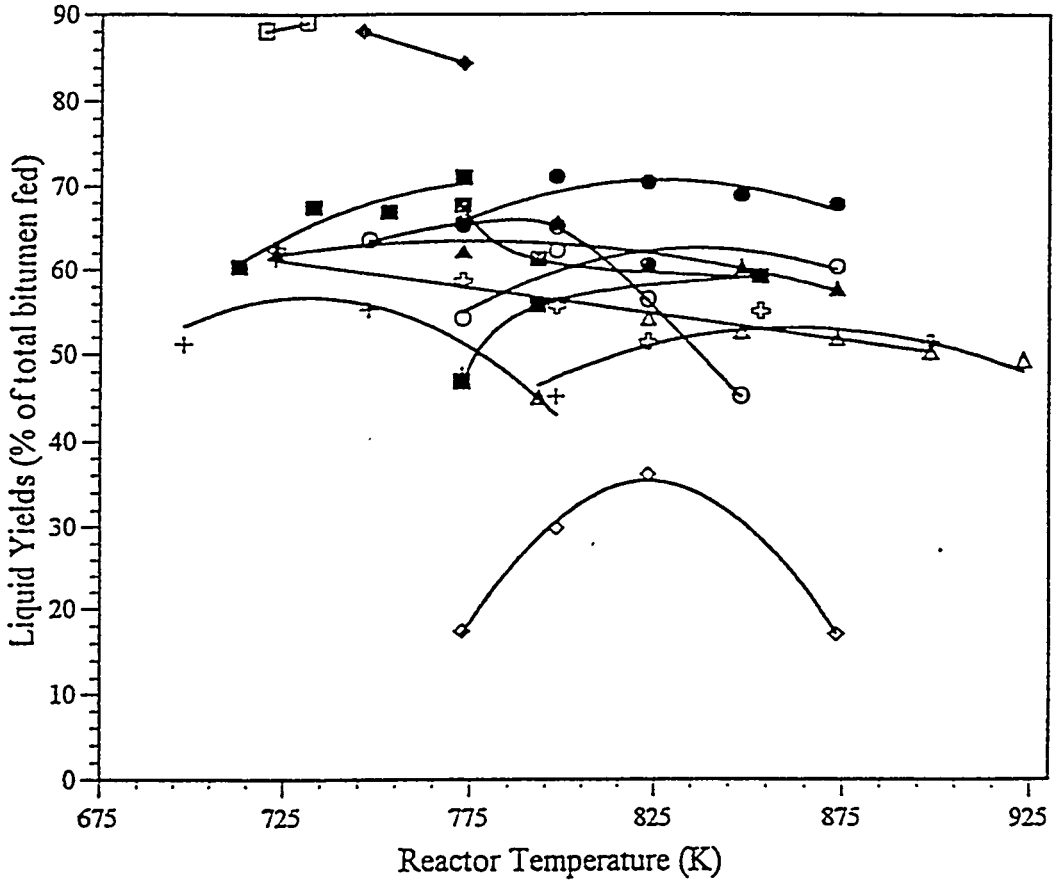

■	PRS, Smart (1984) (t-res=48 min)	◇	CC, Shun (1990) (t-res=15 min)
●	PRS-R1, Dorius (1985)(t-res=20 min)	+	SS, Venkatesan (1980) (t-res= 27min)
▲	TST, Wang (1983) (t-res=25 min)	✣	TST, Venkatesan (1980) (t-res= 27 min)
◆	WR, Fletcher (1992) (t-res=30 min)	⊙	WR, Cha (1991) (t-res=21 min)
□	WR, Fletcher (1992) (t-res=46 min)	▣	WR, Dorius (1985) (t-res=25 min)
○	PRS-R2, Dorius (1985) (t-res=20 min)	⧈	WR, Wang (1983)(t-res = 25 min)
△	PRS-S, Dorius (1985) (t-res=27 min)		

Figure 118

Liquid Yields vs. Reactor Temperature: Regions I to II

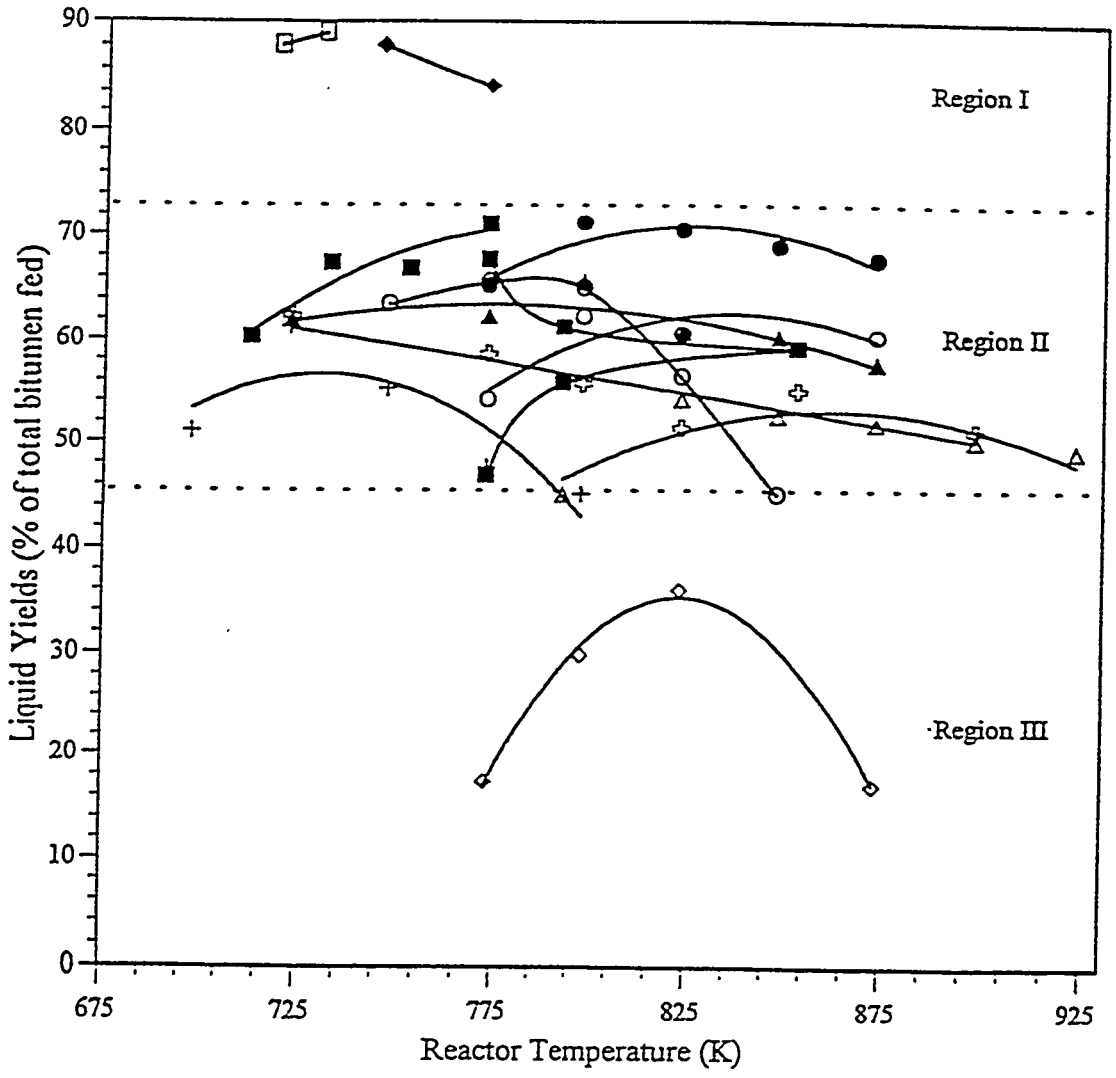

■	PRS, Smart (1984) (t-res=48 min)	◇	CC, Shun (1990) (t-res=15 min)
●	PRS-R1, Dorius (1985)(t-res=20 min)	+	SS, Venkatesan (1980) (t-res= 27min)
▲	TST, Wang (1983) (t-res=25 min)	✣	TST, Venkatesan (1980) (t-res= 27 min)
◆	WR, Fletcher (1992) (t-res=30 min)	⊙	WR, Cha (1991) (t-res=21 min)
□	WR, Fletcher (1992) (t-res=46 min)	■	WR, Dorius (1985) (t-res=25 min)
○	PRS-R2, Dorius (1985) (t-res=20 min)	■	WR, Wang (1983)(t-res = 25 min)
△	PRS-S, Dorius (1985) (t-res=27 min)		

V (Figure 119). During the pyrolysis process, two competing sets of reactions take place simultaneously. The first set of reactions involve primary cracking and distillation of heavy fractions of bitumen. The distilled heavy oil is subjected to secondary cracking at long reaction times and high temperatures. In Region IV, the liquid yield increases with an increase in reactor temperature. It is presumed that in this temperature range, the heavy oil is being distilled. Hence, with increase in temperature, the rate of distillation becomes more rapid. However in Region V, this trend is reversed. This is due to increased cracking of heavy oil to light oil and gases at high temperatures. Hence, there exists a temperature at which the liquid yields are maximized. Though this optimum temperature depends on the nature of oil sands, it is usually found to lie at the common boundary of Regions IV and V (798 to 823 K).

Solids Residence Time

With the exception of Smart, most researchers (50, 51, 114, 120) agreed that the liquid yields decrease with an increase in solids retention time in the reactor (Figure 120). The proposed explanation (51) for this trend is that an increase in solids residence time leads to thermal cracking of the undistilled portion of the bitumen on the oil sands. Fletcher (121), however, did not report significant trends in liquid yields with solids retention time. It was generally agreed (50, 114) that a residence time of about 12-16 min might be preferred for the pyrolysis of oil sands in a fluidized bed reactor.

Generalized observations based on the oil sands pyrolsysi studies are as follows:

1. Fluidizing gas flowrate did not affect the product distribution directly.
2. The gas yield increased with an increase in the reactor temperature while the coke yield, which is a function of the nature of oil sands, remained constant.

Figure 119

Liquid Yields vs. Reactor Temperature: Regions IV to V

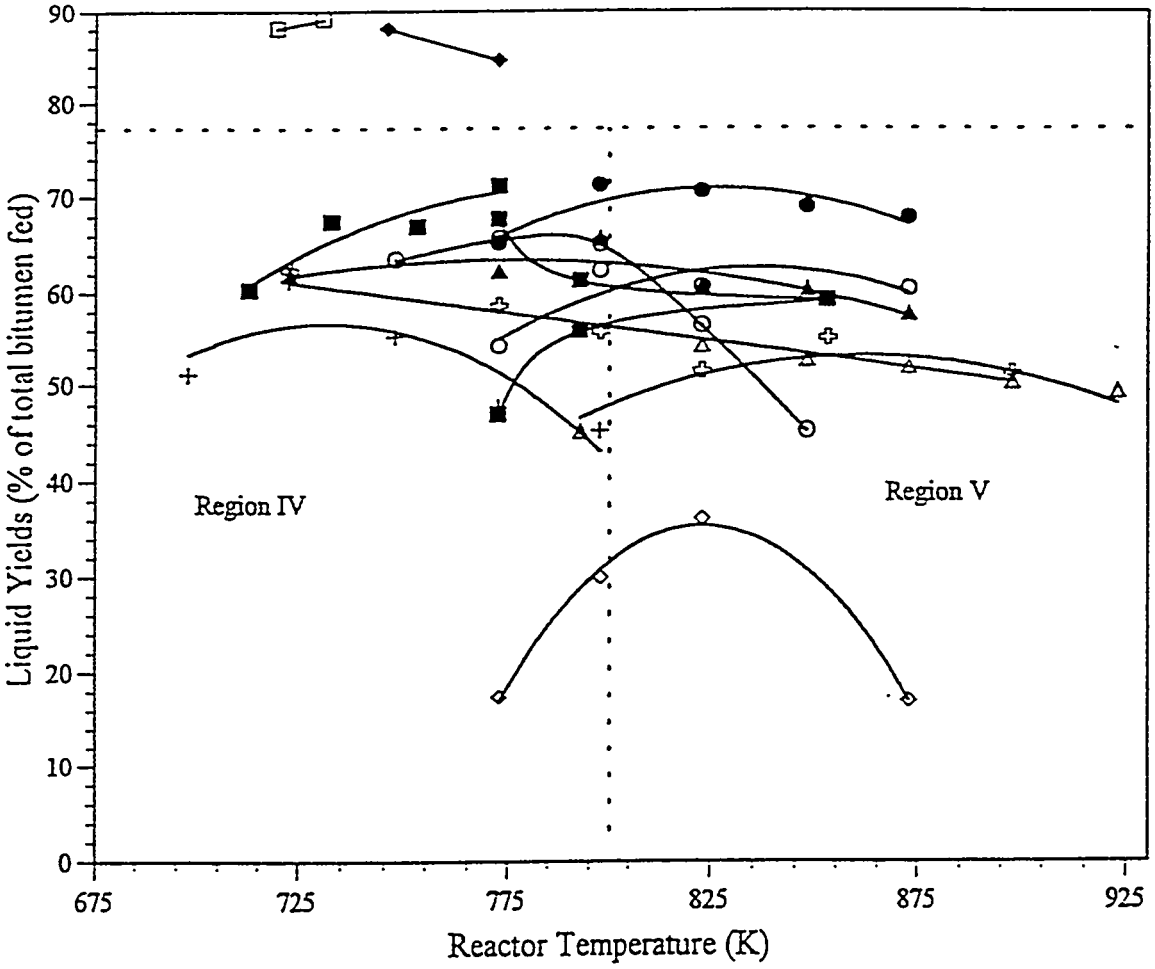

■	PRS, Smart (1984) (t-res=48 min)	◇	CC, Shun (1990) (t-res=15 min)
●	PRS-R1, Dorius (1985)(t-res=20 min)	+	SS, Venkatesan (1980) (t-res= 27min)
▲	TST, Wang (1983) (t-res=25 min)	✣	TST, Venkatesan (1980) (t-res= 27 min)
◆	WR, Fletcher (1992) (t-res=30 min)	⊙	WR, Cha (1991) (t-res=21 min)
□	WR, Fletcher (1992) (t-res=46 min)	■	WR, Dorius (1985) (t-res=25 min)
○	PRS-R2, Dorius (1985) (t-res=20 min)	■	WR, Wang (1983)(t-res = 25 min)
△	PRS-S, Dorius (1985) (t-res=27 min)		

Figure 120

Liquid Yields vs. Solids Residence Time

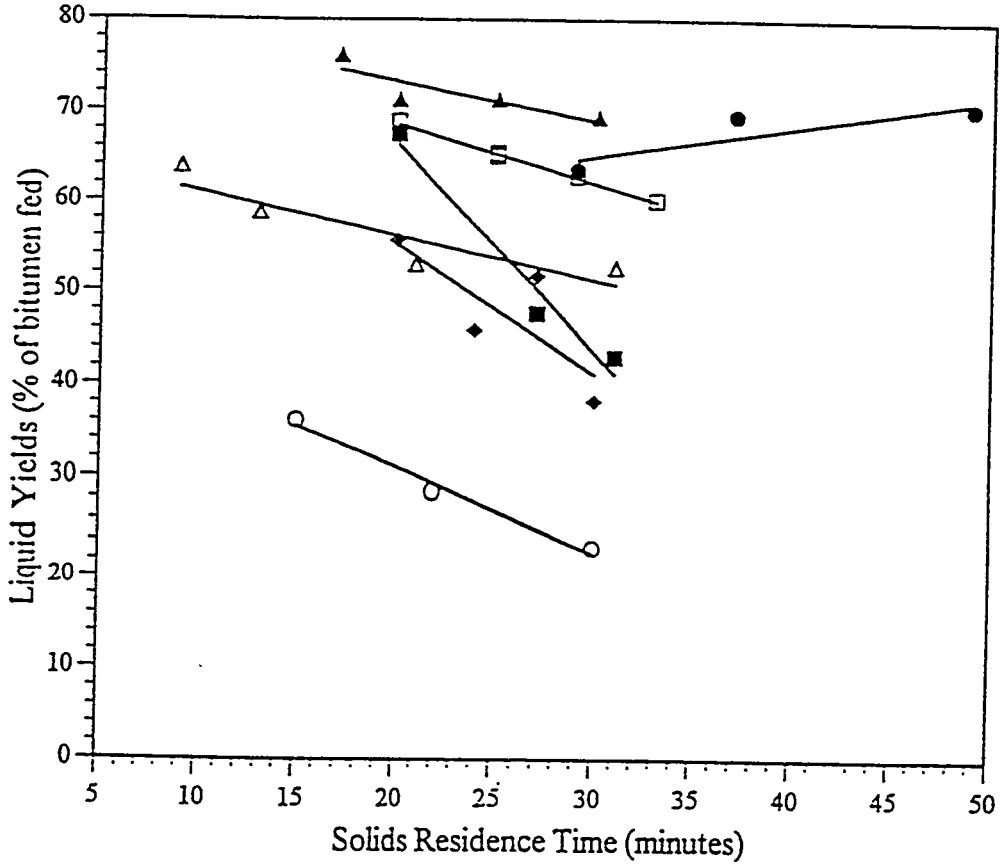

■	SS, Venkatesan (1980) (T=773K)	□	TST, Wang (1983) (T=798K)
●	PRS, Smart (1984) (T=773K)	○	CC, Shun (1983) (T=823K)
▲	PRS-R1, Dorius (1985) (T=798K)	△	WR, Cha (1991) (T=798K)
◆	PRS-S, Dorius (1985) (T=873K)		

3. The nature of oil sands had a direct bearing on the product distribution. The higher the asphaltene content or Conradson carbon residue of the bitumen, the lower the liquid yield and the higher the coke yield. The structure and chemical nature of the host rock also influenced the yields (as was evident from Circle Cliffs oil sand studies [119, 120]).
4. Reactor diameter and loading (H/D ratio) determined the fluidization regime which in turen influenced the liquid yields.
5. The reactor temperature influenced the quality of liquid product. In general, an increase in reactor temperature led to a reduction in viscosity, pour point and API gravity and an increase in volatility and Conradson carbon residue.
6. It is probably not technically feasible to process oil sands in a fluidized bed at temperatures below 723 K.

Rotary Kiln Process

The rotary kiln process has been studied by Cha (105) as an alternative to the fluidized bed process for the pyrolysis of oil sands. The process variable data obtained in an exploratory study (169) indicated that rotary kiln pyrolysis could be a feasible alternative to a fluidized bed thermal process for the production of an upgraded bitumen-derived heavy oil from oil sands. The product distribution and yields obtained with the rotary kiln process appeared to be better than most contemporary fluidized bed processes. Hanson et al. (113) reported on the pyrolysis of Whiterocks oil sands in a commercially available rotary kiln. The effect of temperature and retention times on the product yields were found to be very similar to the trends obtained for the fluidized bed. The maximum liquid yield of 68.7 wt% was obtained for the fluidized bed. The maximum liquid yield of 68.7 wt% was obtained at a temperature of 798 K and a solids retention time of 10 min. This compared favorably with the results obtained by the previous fluid-bed

researchers (50, 51, 114, 117). However, Fletcher (121) obtained much higher liquid yields with the same feed in a large diameter (15.2-cm ID) fluidized bed reactor. His maximum yield of 89% (by weight) was greater than the yield obtained from the rotary kiln with Whiterocks oil sands. In terms of quality of the liquid product obtained, the two processes were comparable. The only significant difference lay in the volatility of the liquids. The rotary kiln liquid product was reported to be 100% volatile (boiling point less than 813 K) (113) whereas the fluidized bed liquid product was about 80-85% volatile (121).

The advantages of the rotary kiln process (as applied to pyrolysis of oil sands) relative to the fluidized bed process are as follows.

1. Rotary kilns are commercially available as opposed to fluidized beds which must be specifically designed for a particular application.
2. It is easier to operate rotary kilns as compared to fluidized beds. The control of solids residence time is much easier and more precise.
3. The fluidized bed may not operate in the intended regime. For example, in small diameter beds, there is a tendency for the bed to slug. This could affect the extent of solids mixing in the bed which would influence the product distribution. This problem is obviously absent in rotary kilns.
4. If an agglomerated mass of oil sands is fed to a fluidized bed, it is likely to de-fluidize the bed which could lead to severe coking of the oil sands in the bed and bed plugging. Rotary kilns are more versatile and can process wider size-distribution oil sand ores than fluidized beds.
5. Withdrawl of coked sand from a rotary kiln is continuous whereas in a fluidized bed the coked sand generally exits in spurts. There is also an increased likelihood of plugging of

the exit pipe in fluidized beds.

Although the rotary kiln process exhibits a number of advantages relative to a fluidized bed, in light of the higher yields obtained by Fletcher (121), the fluidized bed pyrolysis studies were extended.

EXPERIMENTAL

Deo et al. (167) reported that most of the oil sands pyrolysis fluidized bed reactors had a tendency to operate in the slugging regime instead of the bubbling regime which is more desireable. Fletcher (121) constructed a 15.2 cm ID reactor which was capable of operating in the bubbling regime over a wide range of fluidization gas flow rates and bed H/D ratios. The details of design calculations, construction and installation are available elsewhere (121).

The pilot scale fluidized bed reactor was modified for this investigation. A schematic of the system (after modifications) is presented in Figure 120. The oil sands were fed to the fluidized bed reactor by a bin-discharge dry materials feeder (Acrison BDF 1.5 H/2). The fluidized bed was heated by two propane burners attached to the reactor jacket. The burner flue gases were split into two streams. The first stream was pulled into the bed through the wind box by the gas pump. These gases served to fluidize the bed and to directly transfer heat to the oil sands (direct retort heating). The second stream traversed a swirling path along the reactor jacket and provided the additional heat required for pyrolysis through the reactor wall (indirect retort heating).

Bitumen on the oil sands underwent pyrolysis reactions at the high temperatures prevailing in the reactor. Approximately 85% of the bitumen was distilled off or cracked to lower molecular weight hydrocarbon liquids and gases and the remaining 15% formed a carbonaceous residue on the sand. The hydrocarbon vapors were carried over to the product recovery system where the heavier hydrocarbons and moisture in the fluidizing gas were condensed. The uncondensed gases were vented through the chimney.

The pressure drop across the bed increased as the bed hold-up/height increased. The nitrogen control valve on the L-valve was activated and the coked sand was withdrawn from the reactor and was transferred to the coked sand receiver returning the pressure drop (and hence the

bed hold-up) to the preset value. The propane supply to the burners was regulated by a PID controller to ensure that the reactor temperature remained steady during the course of a run.

Modifications in the Burner System

One of the most frequent problems encountered in operating this pilot scale fluidized bed (121) was the failure of the burner system. This was precipitated by direct exposure of the burner sleeve to unusually high temperatures (as high as 1300K). In this study, it was decided to use PR Spring oil sands which have a higher (10 wt%) bitumen saturation than the Whiterocks oil sands (7 wt%) which were used in the previous investigation (121). This increase in bitumen saturation marginally increased the thermal energy requirements of the reactor. Furthermore, it was intended to reduce the solids residence times in the reactor in this study. Both of these factors contributed to an increase in the heat requirement of the system. Thus, the burner/heat supply section of the reactor was redesigned and rebuilt.

It appeared that a single burner would be overloaded if used to provide the entire energy demand of the reactor. Hence, it was decided to divide the heat load between two burners. It was expected that apart from reducing the thermal stress, this new configuration (as shown in Figure 120) would lead to a more uniform temperature profile along the circumference of the reactor and would be capable of providing a greater amount of heat than the previous single burner system (121).

Design of Burner Sleeves

The primary design assumptions and constraints were as follows:

1, The inner wall of the burner (i.e., the ceramic tube) was at a temperature of 1773 K Fletcher (121) reported burner sleeve temperatures of approximately 1273K.

2. The outer layer (ceramic wool) was in contact with stationary, ambient air at 294 K.

Figure 120A

Schematic of the Fluidized Bed Pyrolysis System

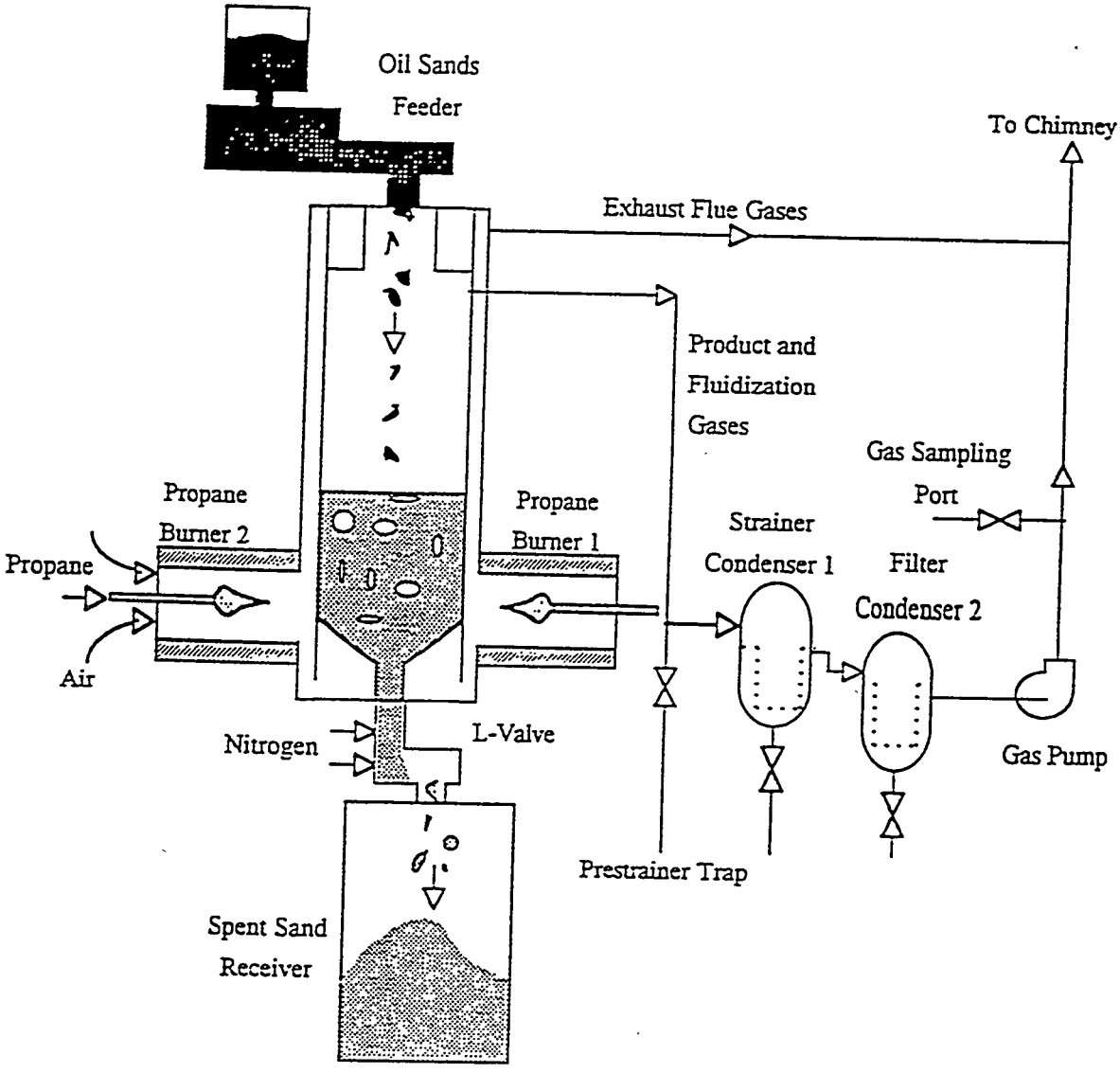
Oil Sands
Feeder
To Chimney
Exhaust Flue Gases
Product and
Fluidization
Gases
Gas Sampling
Port
Propane
Burner 2
Propane
Propane
Burner 1
Strainer
Condenser 1
Filter
Condenser 2
Air
Nitrogen
L-Valve
Gas Pump
Prestrainer Trap
Spent Sand
Receiver

3. The diameter of the whole assembly should not exceed 45.7 cm since that posed problems in installation.

These assumptions and constraints were employed in the heat transfer calculations using various combinations of refractory materials and thicknesses. The lognitudinal-section of the burner sleeve is shown in Figure 121. The outer wall of each burner was an 20.3-cm ID SS 304 pipe. It was covered by a thick layer of insulating ceramic fiber (*Inswool HP*). The inner wall was a mullite ceramic ($3Al_2O_3.2SiO_2$) tube. Mullite is a dense ceramjic material with excellent high temperature and thermal shock properties and can withstand temperatures up to 2000 K. The annular space between the ceramic tube and the outer wall was filled with a castable refractory: *Kast-O-Lite 30 Plus* (trade name) which is an alumina based compound capable of withstanding temperatures up to 2000 K.

Casting and Curing the Refractory

The refractory was obtained in the form of a white granular material. It was mixed with water in a ratio of one gallon of water per 100 lb of refractory. The mixing was carried out in a cement mixer. When the mixture reached a uniform consistency it was poured into the annular region between the outer SS 304 pipe and the inner ceramic tube. A cement vibrator was used to remove trapped air bubbles in the cast and to ensure uniform distribution of the refractory in the annulus. The cast was air dried for 48 h. At this stage the cast had solidified. This was followed by more rigorous thermal curing which was carried out at Lotec, Inc. The following manufacturere recommended temperature program was used to cure the refractory:

1. The refractory was heated to a temperature of 523 K at a rate of 40 K/h. The refractory was held a 523 K for 4 h.
2. The temperature was increased at a rate of 40 K/h to 873 K and was held at this

Figure 121

Longitudinal Section of the Burner Sleeve

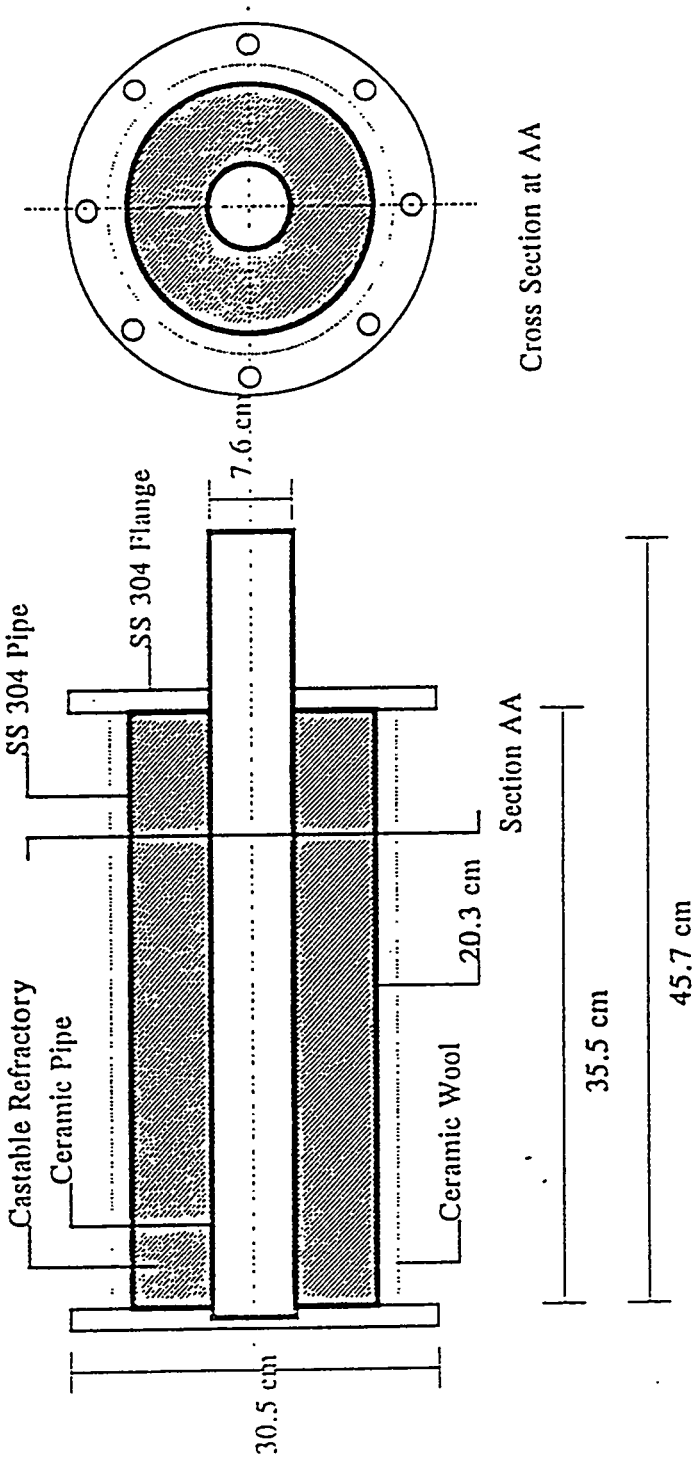
Cross Section at AA
7.6 cm
SS 304 Flange
SS 304 Pipe
Castable Refractory
Ceramic Pipe
Ceramic Wool
20.3 cm
Section AA
35.5 cm
45.7 cm
30.5 cm

temperature for 36 h.

The refractory was dry after the above heat treatment and the burners were ready to be installed on the reactor furnace.

Design of Burners

The burners were designed to provide a combination of premixed and diffusion flames. This kind of flame was found to be extremely effective in the past (121) since it combines the advantages of both types of flames. A premixed flame is capable of burning fuel at a very high rate as compared to the diffusion type whereas it is easier to control the fuel/oxidizer ratio in a diffusion flame. Controlling this ratio was critical in this application since excess oxygen could lead to excessive formation of coke in the reactor during the pyrolysis reaction and to oxidation of the produced hydrocarbon vapors.

A commercial weed burner was modified to serve as the burner. Premixing of the air-fuel stream was achieved by installing a tee (with an open top) in the fuel line. The burner nozzle was located in the center of this tee. The nozzle was fabricated by drilling a 0.08-cm hole (drill bit 67) in a brass swagelok cap. As the gas passed through the nozzle at a high velocity, air was drawn through the open end of the tee. The fuel/oxidizer ratio was maintained close to stoichiometric by positioning the flame deep inside the burner sleeve and controlling the amound of air allowed to diffuse into the burner housing. This was achieved by varying the open area available at the end of the burner sleeve. A portable oxygen analyzer (Bacharach OXOR II) was installed in the product gas line to monitor the amount of oxygen in the flue gas.

Installation

The two burners were located on opposite sides of the reactor. Furthermore, the burners were welded tangentially along the burner wall to prevent impingement of flue gases from one

Figure 122

Longitudinal Section of the Complete Burner Assembly

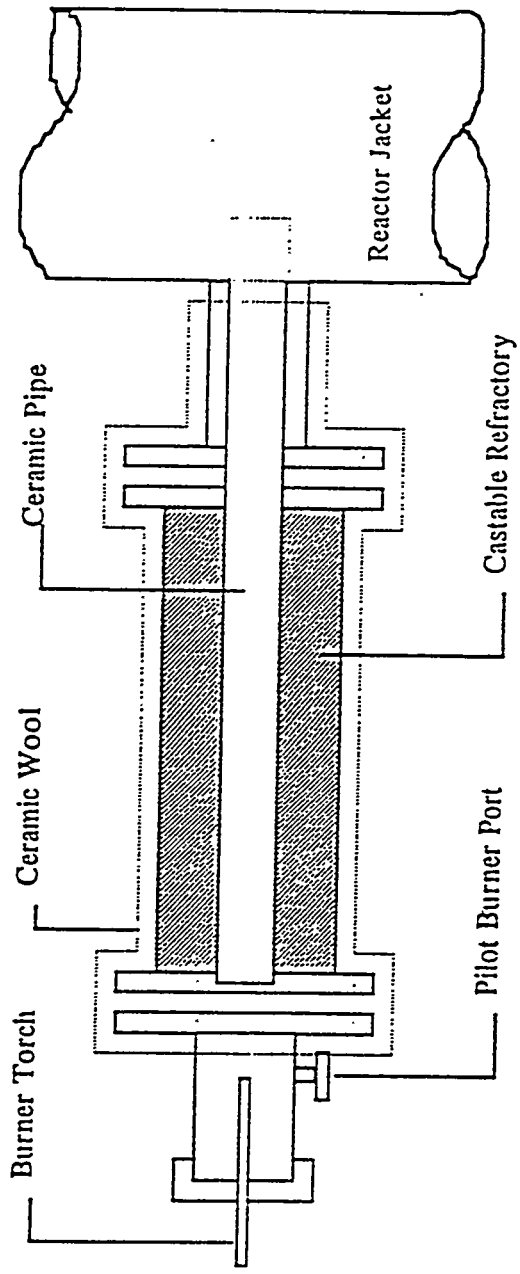
Reactor Jacket
Ceramic Pipe
Castable Refractory
Ceramic Wool
Pilot Burner Port
Burner Torch

capable of providing thermal energy at higher rates than the previous single-burner system.

Experimental Procedures

The oil sands used in this investigation were mined from the Utah Pit in the PR Spring oil sands deposit in Utah. The oil sands were originally in the form of a consolidated sandstone. These rocks were crushed in a jaw crusher and sieved through a 0.64-cm (1/4") sieve. A representative sample was obtained by the coning and quartering technique recommended by Kenkel (170). The oil sands feed was air dried for at least 24 h before being loaded in the feeder. The burner start up procedure, the standard operating procedure, and the reactor shutdown procedure have been described in detail by Nagpal (106).

Product Collection

Following termination of a run it took approximately 16 h for the reactor temperature to decline to about 373 K. The condensers and the prestrainer trap were drained. The traps located before and after the gas pump were checked for traces of liquid product. The nitrogen flow to the L-valve was switched on to drop the bed into the coke receiver. The bed thermocouple was pulled out and the feeder was disconnected from the reactor. Residual oil sands from the reactor were dropped in to the L-valve. The reactor was disconnected and the partially pyrolyzed oil sands were collected. The distillables in the partially pyrolyzed oil sands were extracted with toluene in a Soxlet extractor. The gas samples, collected during the run, were analyzed immediately after the run to minimize contamination from the ambient air.

Process Variable Studies

It has been demonstrated conclusively (50, 51, 104) that the bed temperature and solids residence time are the only two operating parameters that significantly effect the product yields and quality. The effect of these parameters was investigated in this study. The bed temperature

was varied from 723 to 808 K whereas the solids residence time ranged between 20 and 50 min. The effect of each parameter was studied independently. The reactor temperature was varied at a constant solids residence time of 30±3 min in the first set of experiments. The temperature was maintained at 773 K whereas the solids residence time was varied from 20 to 50 min in the second set of experiments. An attempt was made to reduce the residence time to 10 min; however, the heat requirement for such experiments was such that it was difficult to maintain a constant temperature throughout the course of a run.

Mass Balance Calculations

Mass balance calculations were carried out based on the bitumen or hydrocarbon content of oil sands. These calculations involved the following steps: estimation of bitumen fed to the reactor, determination of liquid, gas and coke yields, and determination of the amount of unpyrolyzed bitumen recovered from the reactor after the run.

The amount of coked sand collected at the end of the run was used to back calculate the amount of bitumen fed to the reactor. The amount of coke on coked sand was determined by burning a representative sample of coked sand in a muffle furnace. The amount of clean sand fed to the reactor was calculated as follows:

$$\text{Clean sand (kg)} = \text{Coked sand (kg)} \times (1\text{-Coke\%}/100)$$

The bitumen saturation of the oil sands was known (from Soxlet extraction) to be 10 wt%. Hence, the amount of oil sands and bitumen fed to the reactor in the entire run was calculated from the amount of clean sand and the bitumen saturation.

The liquid product from the run was collected in the two condensers and the prestrainer trap (Figure 120A). A small amount of liquid condensed in the traps located before and after the

gas pump occasionally (121). However, virtually no liquid was recovered from these traps in this study. After the liquid was drained, the condensers were opened and any remaining heavy oils were collected. The oil collected from the prestrainer trap was very heavy and tarlike. The liquid from the condensers contained 25-40 wt% water. The oil and water usually separated into two layers with oil forming the top layer. Hence, the oil was recovered using a sepratory funnel. Sometimes some pockets of water would remain in the oil. The oil was refrigerated overnight and the water removed from the samples using a pipet in such cases. The total amount of liquid was determined by combining oils recovered from the two condensers and the prestrainer trap.

Two gas samples were collected during each run. The gases were analyzed in a gas chromatograph (Hewlett-Packard 5890A) with a thermal conductivity detector (TCD) and 80/100 mesh Chromosorb 102 Supelco column. The peaks were identified by comparing the retention time of the peaks in the chromatograph with the standard sample chromatograph. The following temperature program was followed for the gas chromatograph run to achieve a satisfactory degree of resolultion.

Initial Time:	248 K
Initial Time:	5 min
Rate:	10 K/min
Final Temperature:	508 K
Final Time:	20 min

The nitrogen concentration in the gas samples was greater than 70 mol% whereas the concentration of the pyrolysis gases (C_1 to C_4) was less than 2 mol%. Therefore, it was not possible to integrate these peaks at the same level of detector sensitivity (to integrate the C_1 to C_4 peaks) and the other at low sensitivity (to integrate the nitrogen peak). The CO_2 peak was

integrated in both chromatograms. Hence, the hypothetical area of the nitrogen peak at low sensitivity was calculated as follows:

$$N_2(HS) = N_2(LS)\left(\frac{CO_2(HS)}{CO_2(LS)}\right) \qquad (33)$$

where HS infers High Sensitivity and LS infers Low Sensitivity. The peak areas were then corrected using the response factors.

Corrected Peak Area of A = Actual Peak Area of A / Response Factor of A

The response factors obtained from literature (124) were found to give erroneous results. Hence, the GC response factors were determined specifically for this study. The corrected peak areas were added and then normalized to determine the molar concentration of each compound. Using the molar concentrations and the average gas flow at ambient conditions, the total mass of pyrolysis gas formed in the run was calculated. The calculation of the amount of pyrolysis gas formed in the run SNPRS-13 is summarized in Table 39.

The coked sand obtained in the coke receiver was agitated vigorously to obtain a representative sample. Twenty grams of this sample were weighed out in a crucible and heated to a temperature of 373 K under vacuum to remove moisture. The sample was then combusted at 823 K for 16 h. The percentage coke on coked sand was hence determined. The test was repeated to ensure that the amount of coke on coked sand was established within $\pm 5\%$.

At the end of each run about 500 to 1000 g of a mixture of partially pyrolyzed oil sands and coked sand was removed from the L-valve. Typically the amount of hydrocarbon in this mixture constituted less than 3% of the total bitumen mass balance. The bitumen in this mixture

Table 39
Gas Analysis of Run SNPRS13

Low Sensitivity Gas Analysis

Gas	Area
N2	1.3441
CO2	0.2042

Ratio of Areas N2/CO2 = 6.5823

Gas Flow (LPH)	Time (min)	Temperature (K)	Pressure (atm)	Moles
5380	86	298	0.86	271.24

Total Gas Analysis

Gas	MW	Area	RF*	Area/RF	Vol %	Moles	Mass (g)
N2	28	36.5073	35.1	1.0404	76.27	206.87	5792
O2	32	2.1644	37.3	0.0580	4.25	11.54	369
CO	28	3.4629	43.6	0.0928	6.81	18.46	517
CH4	16	0.2710	36.0	0.0062	0.46	1.24	20
CO2	44	5.5463	63.8	0.1541	11.29	30.63	1348
C2H6	30	0.1343	64.0	0.0021	0.15	0.42	13
C2H4	28	0.1685	48.0	0.0026	0.19	0.52	15
C3H8	44	0.1488	104.0	0.0031	0.23	0.62	27
C3H6	42	0.2789	86.0	0.0027	0.20	0.53	22
n-C4H10	58	0.0736	142.0	0.0009	0.06	0.17	10
1-C4H8	56	0.1682	114.0	0.0012	0.09	0.24	13
1-C5H10	70	0.0000	164.0	0.0000	0.00	0.00	0
n-C5H12	72	0.0000	206.0	0.0000	0.00	0.00	0
n-C6H14	86	0.0000	213.0	0.0000	0.00	0.00	0
1-C6H12	84	0.0000	165.0	0.0000	0.00	0.00	0

* Response Factor as Calculated in Appendix C

Moles of Pyrolysis Gas Produced in the Run = 3.73
Mass of Pyrolysis Gas Produced in the Run (g) 120

Table 40
Input Data File of Run SNPRS13

Name of run:	snprs13
Date:	Aug 9,94

Please Supply the Following Measured Parameters

1. Weight of coked sand collected (g): 19473

2. Average weight of spent sand in bed (g): 8500

3. Liquid Product (g):

a. Pre-strainer Trap:	76.37
b. Condenser # 1:	1245.79
c. Condenser # 2:	278.57
d. From reactor:	49.45

4. Coke on coked sand (%): 1.61

5. Type of tar sand used (WR = 1 or PRS = 2): 2

6. Gas Analysis:

a. Low sensitivity analysis:

Comp.	Area
N2	1.3441
CO2	0.2042

b. High sensitivity analysis:

Comp.	Area
O2	2.1644
CO	3.4629
CH4	0.271
CO2	5.5463
C2H6	0.1343
C2H4	0.1685
C3H8	0.1488
C3H6	0.2789
C4H10	0.0736
C4H8	0.1682
C5H10	0
C5H12	0
C6H14	0
C6H12	0

7. Gas Flowrate (LPH): 5380

8. Length of the run (minutes): 86

9. Ambient Pressure (kPa): 86

10. Ambient Temperature (K): 298

11. Bed Temperature (K): 773

12. Feed Rate (%): 6.00

Table 41
Results of Mass Balance Calculations of Run SNPRS13

Mass Balance Calculations for Run: snprs13

Date: Aug 9,94

Conditions for the run:

Bed Temperature (K):	773
Feed Rate (%):	6.00
Average Residence Time (min):	34

Overall Mass Balance:

Total Tar Sand Fed (g):	21288
Coked Sand Recovered (g):	19473
Total Bitumen Fed (g):	2129

Products Recovered (g):

Liquid:	1600.7
Gas:	119.6
Coke:	313.5

Liquid Yield (wt%):	79
Gas Yield (wt%):	6
Coke Yield (wt%):	15

Bitumen Accounted For (g): 2083

Bitumen Mass Balance Closing (wt%): 98

Pyrolysis Gas Analysis:

	Vol%	Mass %
CH4	33	17
C2H6	11	10
C2H4	14	12
C3H8	17	23
C3H6	14	19
n-C4H10	5	8
1-C4H8	6	11
1-C5H10	0	0
n-C5H12	0	0
n-C6H14	0	0
1-C6H12	0	0

was estimated by extraction with toluene in a Soxlet extractor. This amount of bitumen was not added to the product yields but was estimated only for the purpose of closing the mass balance.

Once each of the above amounts had been determined, the product yields and the overall bitumen mass balance was calculated. A spreadsheet program was used to calculate the overall mass balance and yields. The input data sheet and the final output for the run SNPRS-13 are shown in Table 40 and Table 41, respectively.

Liquid Sample Preparation

The liquid products were recovered from three different points in the equipment: the prestrainer trap and the two condensers. It was necessary to obtain a single representative sample of the liquid to evaluate the effect of process parameters on the quality of liquid product. The three oil samples were blended proportionally to obtain a single sample after the removal of moisture from the product. The mixture was heated to 323 K and stirred to prepare a uniform sample. This sample was used to determine the quality of the liquid products. It was suspected that some of the samples might be contaminated with entrained coked sand fines. Hence, about 20 ml of the blended liquid sample were filtered through a Whatman Grade 4 filter paper to prepare samples for viscosity and simulated distillation analyses.

Liquid Product Analyses

The following chemical and physical analyses were carried out on the liquid samples to determine the effect of process variables on liquid quality and the extent of upgrading of bitumen-derived liquid relative to the bitumens.

1. Specific gravity: The specific gravity was measured using a capillary stoppered pyknometer as specified in the ASTM method number D-70. The specific gravity was measured at 293 K.

2. Pour point: The pour point was determined by the ASTM D97-66 method.

3. Conradson carbon residue: The conradson carbon residue and ash contents were measured by the Syncrude Analytical Method 5.4 (171) in order to determine the coking tendencies of pyrolysis liquid products.

4. Viscosity: The viscosity was measured at a temperature of 298 K using the Brookfield DV II+ viscometer. A CP-40 cone was used. A Brookfield TC500 temperature bath was used to maintain the sample at the constant temperature. The effect of sample temperature on the viscosity was also investigated for one sample (run id SNPRS16).

5. Simulated distillation The boiling fractions of the liquid product were characterized by simulated distillation. This was performed on a Hewlett Packard (HP) 5890 Series II gas chromatograph with a flame ionization detector (FID) and a Supelco Petrocol column. The weight percent boiling up to 477 K (400°F) was defined as the naphtha fraction. The fraction boiling between 477 and 616 K (400 and 650°F) was the middle distillate and the fraction between 616 and 811 K (650 and 1000°F) was the gas oil. The residuum consisted of the fraction boiling above 811 K (1000°F). The ASTM D2887 method was followed for calculating the fractions for totally elutable chromatograms.

6. Elemental and other analyses: The carbon, hydrogen, kjeldahl-nitrogen and sulphur contents of all the samples were determined (analyses performed by Galbraith Laboratories Inc.). Additional analyses (including nickel and vanadium contents and molecular weight [3 point method using benzene solvent]) were carried out on the bitumen and one liquid product sample (run id SNPRS13) to determine the extent of upgrading of bitumen.

7. Asphaltene content: Asphaltenes were defined as n-pentane insolubles and were determined according to the method reported by Subramanian (1994) for heavy oils and bitumens.

RESULTS AND DISCUSSION

The pilot scale fluidized bed reactor system (121) was modified and used for the pyrolysis of mined and crushed oil sands from the PR Spring oil sands deposit which is located in Uinta Basin (Utah). The effect of process parameters (reactor temperature and solids residence time) on product were carried out to study the effect of process parameters on the liquid quality and the extent of bitumen upgrading. The kinetic model for bitumen pyrolysis of Deo et al. (167) was modified to explain the results of this investigation. The yields and properties of the products obtained in the large diameter fluidized bed and the rotary kiln (105) reactors were also compared.

The details of the hydrodynamic and feeder calibration studies, the pyrolysis process variable experiments, the product distributions and yields, the liquid product qualities, the kinetics of pyrolysis reaction, and the influence of hydrodynamics on the reactor performance are discussed.

Determination of Minimum Fluidization Velocity

The fluidization regime is directly linked to the fluidization gas velocity. This affects the mass and heat transfer characteristics in the bed and hence the performance of the fluidized bed reactor. Therefore, it was essential to determine the minimum fluidization velocity (U_{mf}) to define the regime of operation.

It was necessary to determine the mean particle size diameter (d_p) to theoretically calculate the minimum fluidization velocity. Hence, a sample of coked sand was sieved to determine d_p. A representative sample of coked sand was obtained using a 1/16 sample splitter. The analysis was carried out according to the ASTM STP 447B standard method (ASTM Committee E-29, 1985). US Standard wire mesh sieves and a ro-tap mechanical shaker were used for the sieve analysis. An important parameter in sieve analysis is the total sieving time (ASTM Committee

E-29) since extended sieviing time can lead to attrition and fines generation. The time of analysis is determined by trial and error and varies from one material to another. The Sieve analysis was carried out for four different time intervals: 5, 10, 15 and 20 min. The particle size distributions obtained at sieving times of 10 and 15 min were nearly identical. However, the particle size distribution obtained with 20 min sieving time was a little finer indicating attrition had occured. Hence, an "end point" of 10 min was selected. The particle size distribution is presented in Figure 123. The calculation of mean particle diameter as determined by sieve analysis is reported in Table 42.

The above analysis established the mean particle size of the coked sand to be 132 $\pm$ 3μm. Various empirical correlations are available in the literature for predicting the minimum fluidization velocity (143, 172-174; Grewal and Gupta,k 1989). The minimum fluidization velocity was determined by using the following equations provided by Fletcher et al., (1992).

$$Ar=\frac{d_p^3 g^* \rho_g(\rho_s-\rho_g)}{\mu_g^2} \qquad (34)$$

$$Re_{mf}=\frac{Ar}{1400} \qquad (35)$$

$$U_{mf}=\frac{\mu_g Re_{mf}}{d_p \rho_g} \qquad (36)$$

The minimum fluidization velocity for the coked sand obtained from pyrolysis of PR Spring oil sands in the large diameter fluidized bed reactor was predicted to be 1.64 cm/s at

Figure 123

Particle Size Distribution of Coked Sand from PR Spring Oil Sands

(Sample Size = 410 g, Sieving Time = 10 min)

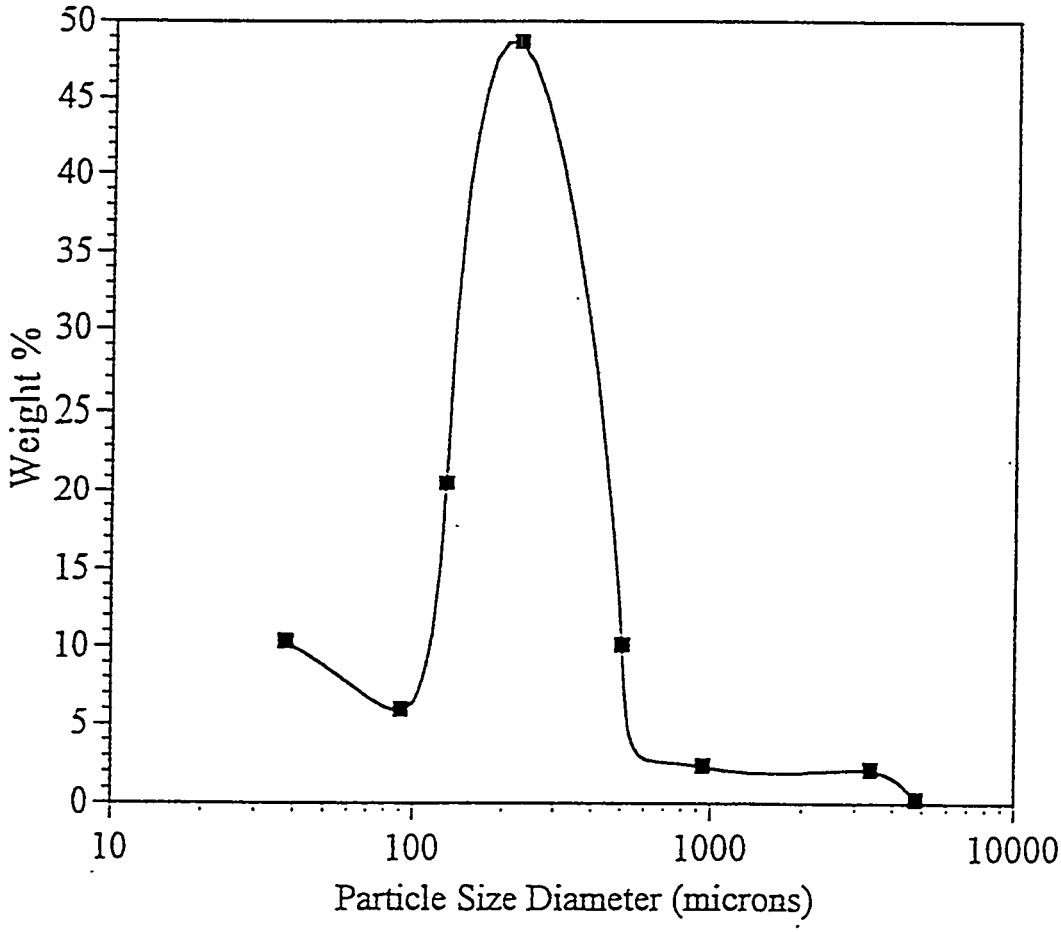
50
45
40
35
30
25
20
15
10
5
0
Weight %
10
100
1000
10000
Particle Size Diameter (microns)

Table 42
Sieve Analysis of Coked Sand from PR Spring Oil Sands

US Standard No.	Mesh Size (micro-m)	dpi (micro-m)	Weight of Sieve (g)	Weight of sand &sieve (g)	Weight of Sand (g)	100(Xi)	Xi/dpi
4	4750	5175	429.8	430.7	0.9	0.2	4.24178E-07
16	1180	2965	424.9	433.7	8.8	2.1	7.23893E-06
25	710	945	330.6	339.9	9.3	2.3	2.40031E-05
50	300	505	349.9	391.2	41.3	10.1	0.000199469
100	150	225	382.1	581.3	199.2	48.6	0.00215935
140	106	128	381.6	465.5	83.9	20.5	0.001598704
200	75	91	371.4	395.7	24.3	5.9	0.000654898
pan	0	38	366.4	408.7	42.3	10.3	0.00275122
				Sand Recovered (g):	410		

Sieving Time: 10 min

Sample Size: 410 g

Average Particle Diameter (microns) = 135

ambient conditions with air as the fluidizing gas.

Fluidization studies were conducted on beds with H/D ratios ranging from 1.7 to 4. It was found that the minimum fluidization velocity in all cases lay between 1.5 to 1.6 cm/s. A fluidization curve (pressure drop vs. fluidization gas flow rate) for an H/D ratio of 2.2 is shown in Figure 124. An interesting observation in this plot are the fluctuations in pressure drop in the region between the point of incipient fluidization and the point corresponding to the M/A value of the bed. This is a typical observation in the fluidization of multi-sized paritcle beds (121, 175). The large particles remain defluidized at the point of minimum fluidization. As the gas flowrate is increased the larger particles become fluidized. This leads to pressure fluctuations and an increase in the average pressure drop across the bed. As more particles get fluidized, the pressure drop value approaches the M/A value.

The pyrolysis experiments were carried out at a gas superficial velocity corresponding to a U/U_{mf} value of approximately 5 and an H/D ratio of 1.9. The bed operated in the bubbling fluidization regime and provided excellent solids mixing at this gas velocity.

Feeder Calibration

The oil sands were fed to the reactor by a commercially available bin discharge feeder (Acrison Model BDF 1.5-H/2). The feeder was calibrated to determine the feeding rates as a function of the motor speed. The determination of a correlation between the feeding rates and the motor controller set points was essential to the establishment of reproducible solids residence times in the fluidized bed reactor. The feeder was calibrated using a representative sample of oil sands that was air dried for at least 24 h prior to being placed in the feeder hopper. The feeder was calibrated at four different motor speeds: 5%, 10%, 15% and 25% of the maximum feeder speed. The higher motor speeds were not investigated because it was intended to conduct the pyrolysis

Figure 124

Fluidization Curve for PR Spring Coked Sand

("Pull" Mode of Fluidization, Fluidization Gas: Air, Bed Mass = 7 kg)

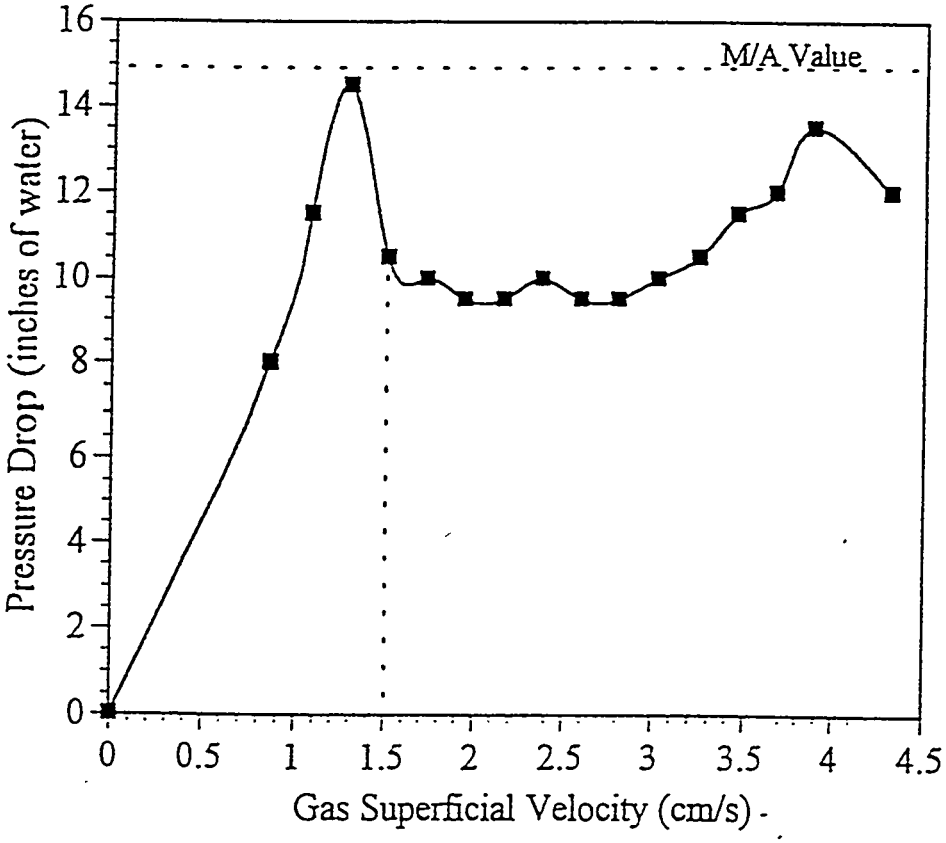
M/A Value
Pressure Drop (inches of water)
Gas Superficial Velocity (cm/s)
0
2
4
6
8
10
12
14
16
0
0.5
1
1.5
2
2.5
3
3.5
4
4.5

experiments at feeding rates corresponding to 5-10% of maximum motor speed. The cumulative amount of oil sand fed was measured as a function of time at each motor speed. The feeder auger housing was water cooled to maintain the oil sands nearly isothermal during their transit through the auger. Increased temperatures due to shear forces on oil sand granules in the auger have been reported to make the oil sands sticky thereby making them difficult to feed (122).

The feeder calibration curves for the PR Spring and Whiterocks oil sands are presented in Figures 125 and 126, respectively. A comparison of the two figures indicate that the feeding rates of PR Spring oil sands are higher than that of Whiterocks oil sands for the same motor speed. The cumulative amounts of oil sands remained linear ($R^2 > 0.99$) for both the oil sands over the time range investigated indicating constant feed rates. The feeder motor controller set point was varied between 4% and 7% of full scale during the pyrolysis experiments.

Effect of Process Parameters on Product Distribution

A total of sixteen pyrolysis experiments were conducted in the large diameter fluidized bed reactor with PR Spring oil sands feed. Only the runs with an overall bitumen material balance in the range 88 to 109 wt% were accepted for studying the effect of process variables on the product yields, distribution and quality. The high bitumen mass balances (109 wt% each) achieved in runs SNPRS11 and SNPRS12 are probably due to oil sands which stuck to the sides of the reactor and underwent partial pyrolysis. This was, however, not accounted for in the mass balance calculations. It is expected that in long term continuous operation of the fluidized bed pyrolysis process, the contribution of this source of error would be negligible. The low bitumen mass balances (88 to 92 wt%) in runs SNPRS5, SNPRS8 and SNPRS10 may have been related to leakage of air into the reactor leading to the combustion of the hydrocarbon vapors.

The reactor temperature and solids residence time have been reported to be the two most

Figure 125

Feeder Calibration Curves for PR Spring Oil Sands

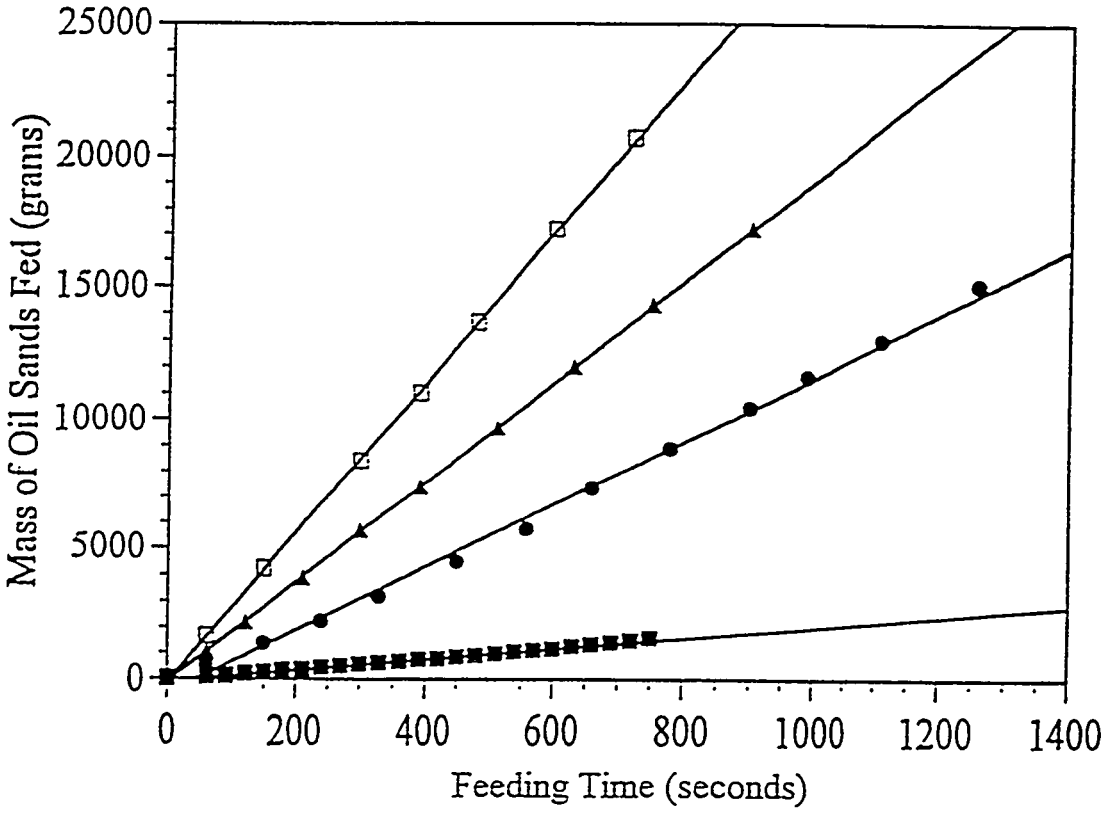
25000
20000
15000
10000
5000
0
Mass of Oil Sands Fed (grams)
0
200
400
600
800
1000
1200
1400
Feeding Time (seconds)

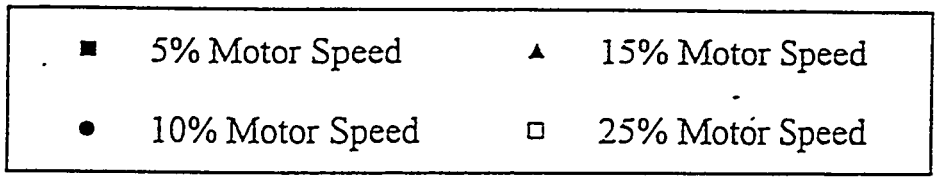
5% Motor Speed
15% Motor Speed
10% Motor Speed
25% Motor Speed

Figure 126

Feeder Calibration Curves for Whiterocks Oil Sands

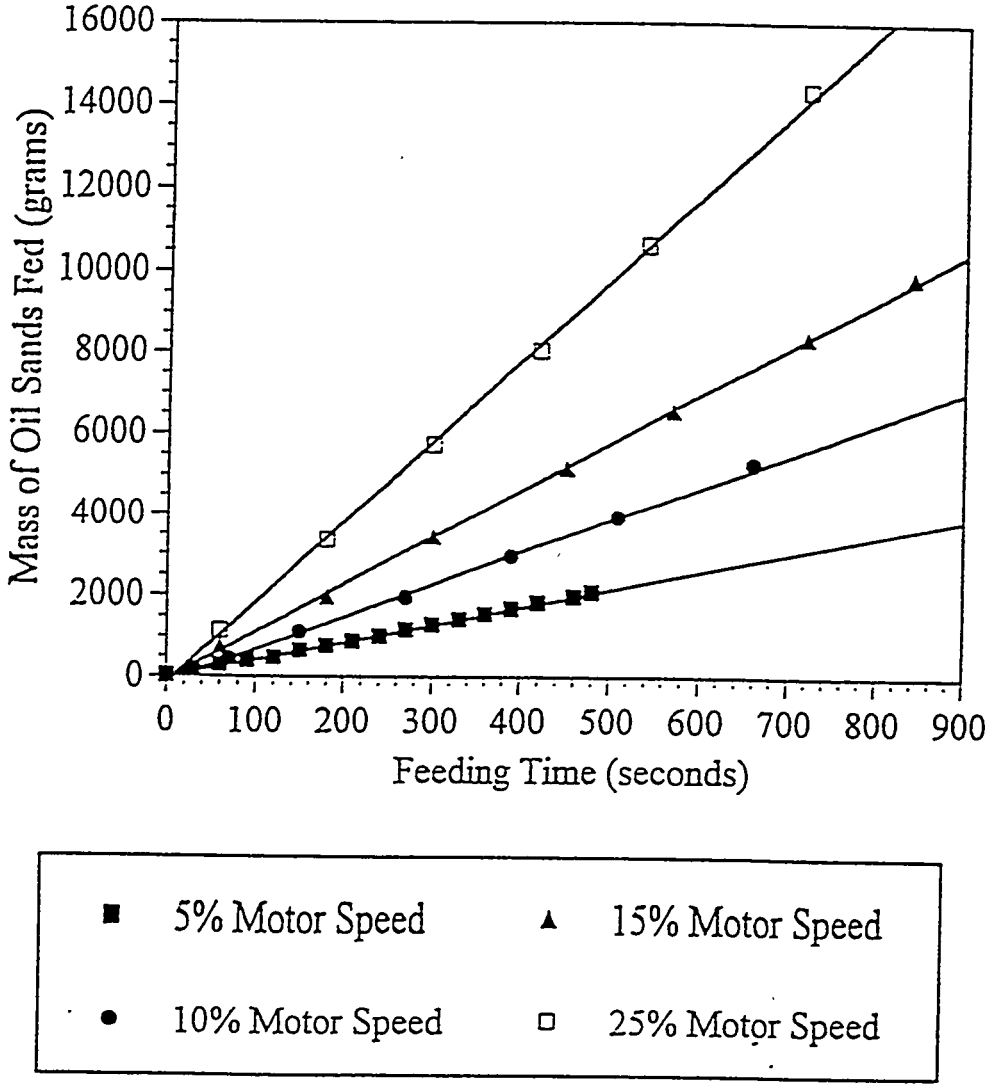
16000
14000
12000
10000
8000
6000
4000
2000
0
Mass of Oil Sands Fed (grams)
0
100
200
300
400
500
600
700
800
900
Feeding Time (seconds)
5% Motor Speed
15% Motor Speed
10% Motor Speed
25% Motor Speed

important process parameters influencing the product distribution and yields and the liquid product qualities during the pyrolysis of oil sands in a fluidized bed reactor (104, 120, 121). The product distribution and yields were reported to be independent of fluidization gas velocity (51). Thus, the influences of reactor temperature and solids residence times were the focus of this study.

Effect of Reactor Temperature on Product Distribution and Yields

Five runs were made to study the effect of reactor temperature on product distribution and yields. The bed temperature was varied from 723 K (450°C) to 808 K (535°C). The fluidization gas velocity and the solids residence time were maintained constant at 5380 $\pm$ 141.6 LPH (190 $\pm$5 SCFH) and 31$\pm$3 min, respectively. The reactor loading was also constant with H/D (bed height to diameter ratio) fixed at 1.9.

The effect of reactor temperature on product distribution and yields is presented in Table 43 and Figure 127. The analyses of the pyrolysis gas products obtained in this study are reported in Appendix F. The liquid (C_5 + fraction), gas (C_1 to C_4) and coke yields appeared to be independent of reactor temperature over the range studied (723 to 808 K). This observation is inconsistent with the results reported in the earlier investigations of pyrolysis of oil sands in laboratory scale fluidized bed reactors (50, 51, 114, 117, 119, 120) and a pilot scale (15.2 cm ID) rotary kiln reactor (105, 113). The liquid product yields showed an apparent maxima with respect to reactor temperature in the laboratory scale reactors and in the rotary kiln reactor. The maxima usually lay between 798 and 823 K depending on the nature and origin of the oil sands. Moreover, the liquid yields obtained in these reactors varied between 55 and 71 wt% depending upon the bitumen saturation of the oil sands fed to the reactor.

However, no such liquid yield maxima was observed in this study. Also, the liquid yields obtained in the large diameter fluidized bed reactor were higher, ranging from 77% to 81%, than

Table 43

Effect of Reactor Temperature on Product Yields and Distribution

(Solids Residence Time: 31 ± 3 minutes, Gas Flowrate:

5380 ± 141 SLPH, Feed: PR Spring Oil Sands)

Run ID	Temperature (K)	Product Yields (normalized wt%)		
		Liquid	Gas	Coke
SNPRS16	723	81	3	16
SNPRS5	748	78	1	21
SNPRS10	755	80	2	18
SNPRS13	773	79	6	15
SNPRS11	808	77	6	17

Figure 127

Effect of Reactor Temperature on Product Yields

(Feed: PR Spring Oil Sands, Solids Residence Time: 31±3 min)

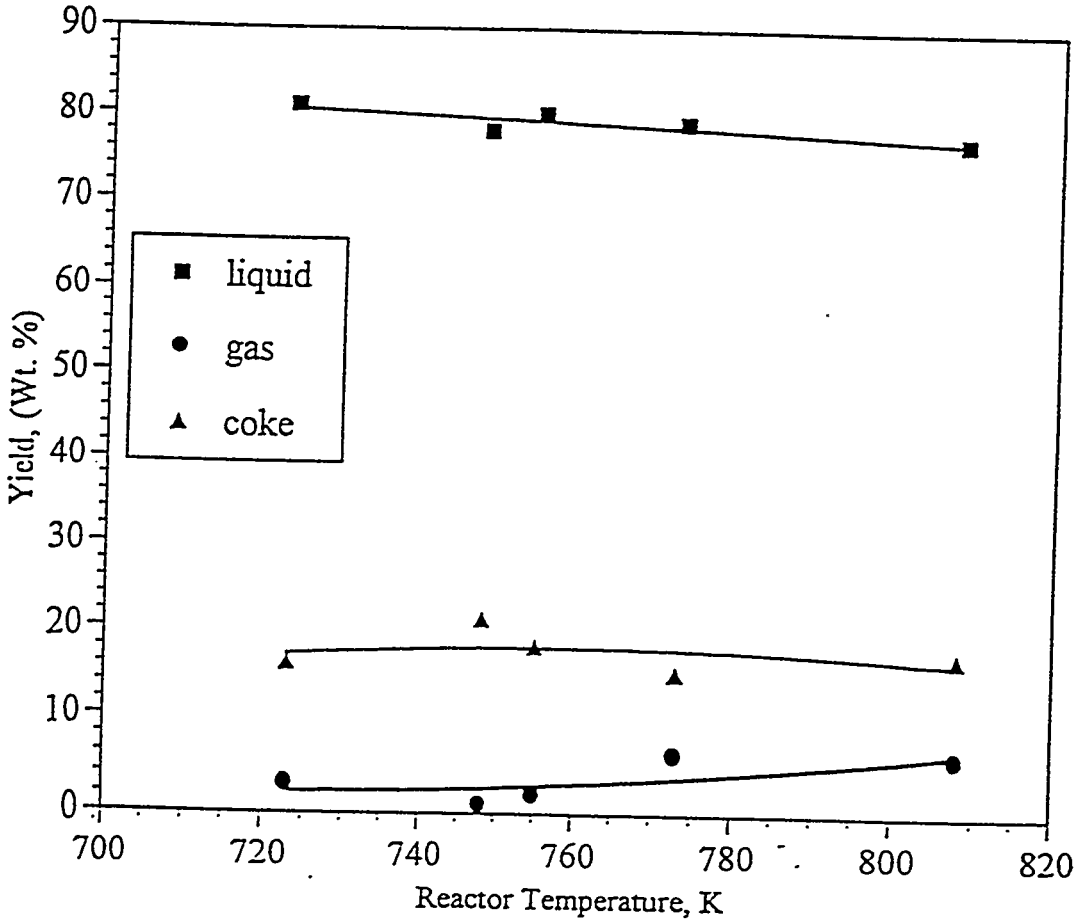
90
80
70
60
50
40
30
20
10
0
Yield, (Wt. %)
liquid
gas
coke
700
720
740
760
780
800
820
Reactor Temperature, K

those reported for laboratory scale reactors. The gas yields were lower: 1-6 wt% in this study as opposed to 15-22 wt% in this study confirming the speculation (51) that coke yields were dependent upon the nature and origin of the oil sands and not on processing conditions.

The liquid product yields declined from 81 to 77 wt% as the reactor temperature increased from 723 to 808 K. TGA studies reported by Lin (1988) indicated that the maximum liquid yields were obtained at pyrolysis temperatures between 723 and 748 K. This observation is in concurrence with the results obtained in this study. The reduction of 4% in liquid yields over a range of reactor temperatures from 723 to 808 K is minor. The gas yield increased from a minimum of 1% to a maximum value of 6%. Both of these trends can be explained on the basis of increased secondary cracking of heavy oils at high temperatures to form light oil and gas.

Effect of Solids Residence Time on Product Distribution and Yields

The average solids residence time (θ) in the fluidized bed reactor was defined as follows:

$$\theta = \frac{W}{F} \qquad (37)$$

where:

W = mass of the sand inventory in the bed (kg)

F = feed rate of oil sands (kg/min)

The solids residence time was determined as follows. The cumulative mass of coked sand recovered at the end of the run was measured. The mass of oil sands fed to the reactor during the run was back calculated. The average feed rate was determined by dividing the mass of oil sands fed by the total time of the run. The mass of sand inventory in the bed (W) was fixed at the beginning of the run and was maintained constant by controlling the pressure drop across the bed

Table 44

Effect of Solids Residence Time on Product Yields and Distribution

(Temperature: 773 K, Gas Flow: 5380 ± 141 SLPH)

(Feed: PR Spring Oil Sands)

Run ID	Residence Time	Product Yields (normalized wt%)		
	(min)	Liquid	Gas	Coke
SNPRS12	20	80	3	18
SNPRS13	34	79	6	15
SNPRS14	40	82	3	15
SNPRS9	50	81	6	13

Figure 128

Effect of Solids Residence Time on Product Yields

(Feed: PR Spring Oil Sands, Reaction Temperature: 773 K)

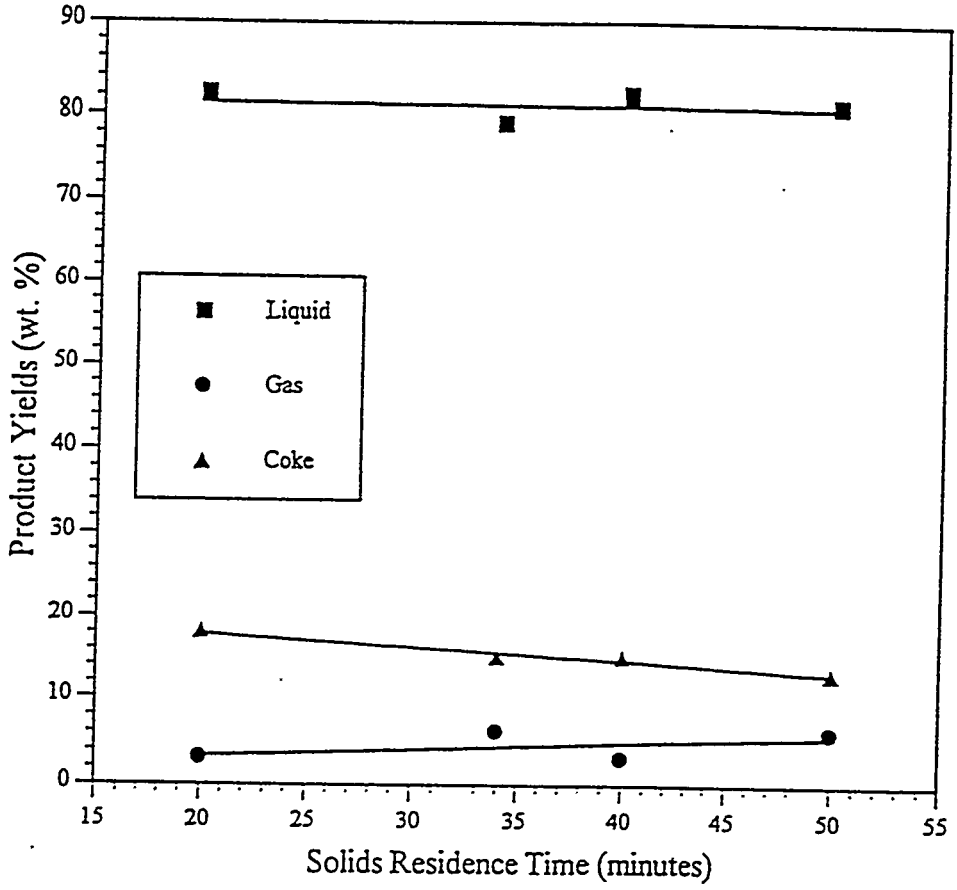
Product Yields (wt. %)
90
80
70
60
50
40
30
20
10
0
Liquid
Gas
Coke
15
20
25
30
35
40
45
50
55
Solids Residence Time (minutes)

during the course of the run. The solids residence time was calculated from the above expression.

The solids residence time could be varied by two methods: by changing the bed hold up (W) or by changing the oil sands feed rate (F). During the course of this investigation the solids residence time was varied by a combination of both methods.

The solids residence time in the reactor was varied from 20 to 50 min at a constant temperature of 773K. The fluidization gas flow rate was maintained constant at 5380$\pm$141.6 LPH (190$\pm$5 SCFH) (U/U_{mf} ~5) in all runs.

The effect of solids residence time on the product distribution and yields is shown in Table 44 and Figure 128. The product yields did not exhibit any apparent trend with the solids residence time in the range investigated. The liquid yields ranged from 79 to 81 wt% and the gas and coke yields were nearly constant at 3-6 wt% and 13-18 wt%, respectively. These observations differ from those reported for pyrolysis experiments carried out in laboratory scale fluidized bed reactors (104, 119) and the rotary kiln reactor (105). The liquid yields decreased but the gas yields increased as the solids residence time was increased in the laboratory scale fluidized bed reactor. The difference in results is attributed to the difference in the hydrodynamic characteristics of the laboratory scale reactors and the large diameter fluidized bed reactor and is discussed in the following section.

Discussion

The results of this investigation can be explained by studying the pyrolysis reaction mechanism and the bubbling bed hydrodynamics in the large diameter fluidized bed reactor.

Pyrolysis Reaction Mechanism

Various reaction schemes (65, 105, 118, 148, 167, 176, 177) have been proposed for the pyrolysis of oil sands and oil shale. Deo et al. (167) proposed a kinetic model to explain the

results obtained from pyrolysis experiments carried out in laboratory scale fluidized bed reactors (104). According to this model, the pyrolysis process occurs via three steps:

1. Asphaltenes ----------> a. Coke + b. Heavy Oil
2. Maltenes ----------> c. Heavy Oil + d. Gas
3. Heavy Oil ----------> e. Light Oil + f. Gas

The first reaction accounts for the cracking and condensation reactions involving asphaltenes (pentane insolubles) to form heavy oils and the carbonaceous residue on the sand grains. The heavy oil constituents volatilize and are transferred to the gas phase. Neurock et al. (178) conducted pyrolysis experiments with asphaltene fractions and determined the kinetic pathways for this series of reactions. They determined that coke and heavy oil are the two most important products of asphaltene pyrolysis. The second reaction accounts for volatilization of a portion of the maltene fraction (pentane solubles), the cracking of high molecular weight constituents and gases, and the subsequent volatilization of the produced heavy oil. The third reaction accounts for secondary cracking of the bitumen-derived heavy oil produced from the first two reactions.

An examination of the rate constants reported for the three reactions (167, 177) indicates that the rates of the first two reactions are higher by more than an order of magnitude than the third reaction (at 723 K, k_1: 1.6 h^{-1}, k_2: 86.2 h^{-1}, k_3: 0.1 h^{-1} and at 803 K, k_1: 30.6 h^{-1}, k_2: 342.5 h^{-1}, k_3: 1.7 h^{-1}). The third reaction becomes significant only at high temperatures ($>$ 773 K) and long reaction times ($>$ 10 min). This explains the existence of an apparent maxima in liquid yields with respect to reactor temperature reported for most laboratory scale fluidized bed oil sand pyrolysis studies (Figure 117). Also long reaction times lead to greater secondary cracking which explains the previously observed reduction in liquid yields and increase in gas yields with solids

residence time at a fixed reactor temperature (Figure 44). Conesa et al. (178) reported that long solids residence times and high temperatures favored the secondary cracking reactions resulting in higher gas yields during pyrolysis of polyethylene in a fluidized bed reactor. The relationship between the reaction time and solids residence time is explained in the next section.

The gas yields obtained in this study were significantly lower (1-6 wt% versus 15-22 wt% in the rotary kiln and smaller fluidized bed reactors) (82, 104, 119, 120). It was presumed that the secondary cracking reactions were suppressed in the large diameter fluidized bed and that the primary cracking and volatilization reactions (reactions 1 and 2) should be sufficient to explain the results of this study. The hypothesis was tested by calculating the product yields based on the first two reactions only. The kinetic parameters and the stoichiometric coefficients used in the simplified model are given in Table 45. The rate constants were adapted from Phillips et al. (177) and Deo et al. (167) except that the activation energy for reaction 2 was reduced by 20% in this simplified model compared to the previous model (167) to achieve a better fit of the data. The stoichiometric constants were determined from the best fit of the experimental data.

The yields of coke, liquid, and gas products from this simplified kinetic model have been plotted as functions of temperature and residence times in Figures 129 and 130, respectively. The simplified model predicts that for reactor temperatures above 750 K and reaction times above 5 min the product yields remain more or less constant. This observation agrees reasonably well with the experimental results obtained in this study in the range of solids residence time from 20 to 50 min. The slight reduction in liquid yields (from 81 to 77 wt%) with temperature in the experimental results is likely due to secondary cracking of heavy oil. It is proposed that although the secondary cracking is suppressed, it is not entirely eliminated.

Table 45

Rate Constants[1] and Stoichiometric Coefficients for the Model

$$k_1 = 1.16 \times 10^{13} \exp\left(\frac{-178,000}{RT}\right) (h^{-1})$$

$$k_2 = 8.85 \times 10^{7} \exp\left(\frac{-83,200}{RT}\right) (h^{-1})$$

a = 0.8, b = 0.2, c = 0.93, d = 0.07

[1]Adapted from Phillips et al. (1985) and Deo et al. (1991)

Figure 129

Results of Simplified Model vs. Experimental Results:

Effect of Reactor Temperature on Product Yields

(Reaction Time = 30 min)

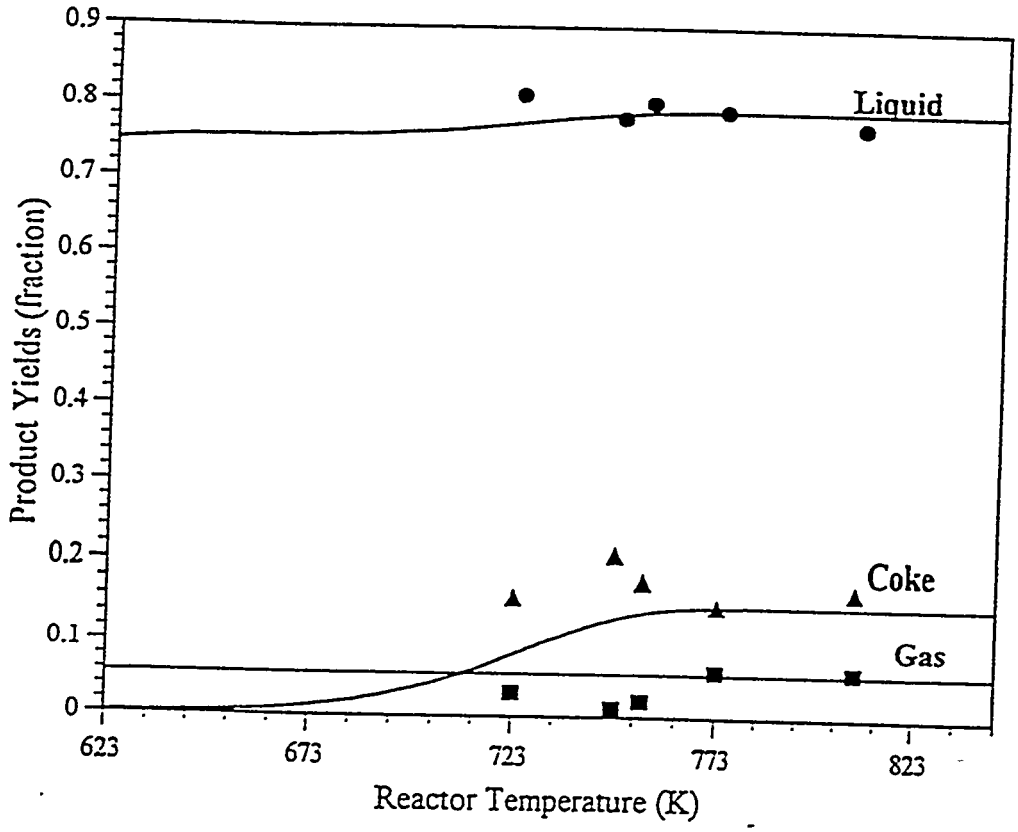
0.9
0.8
0.7
0.6
0.5
0.4
0.3
0.2
0.1
0
Product Yields (fraction)
Liquid
Coke
Gas
623
673
723
773
823
Reactor Temperature (K)

Figure 130

Results of Simplified Model vs. Experimental Results:

Effect of Reactor Time on Product Yields

(Reaction Temperature = 773 K)

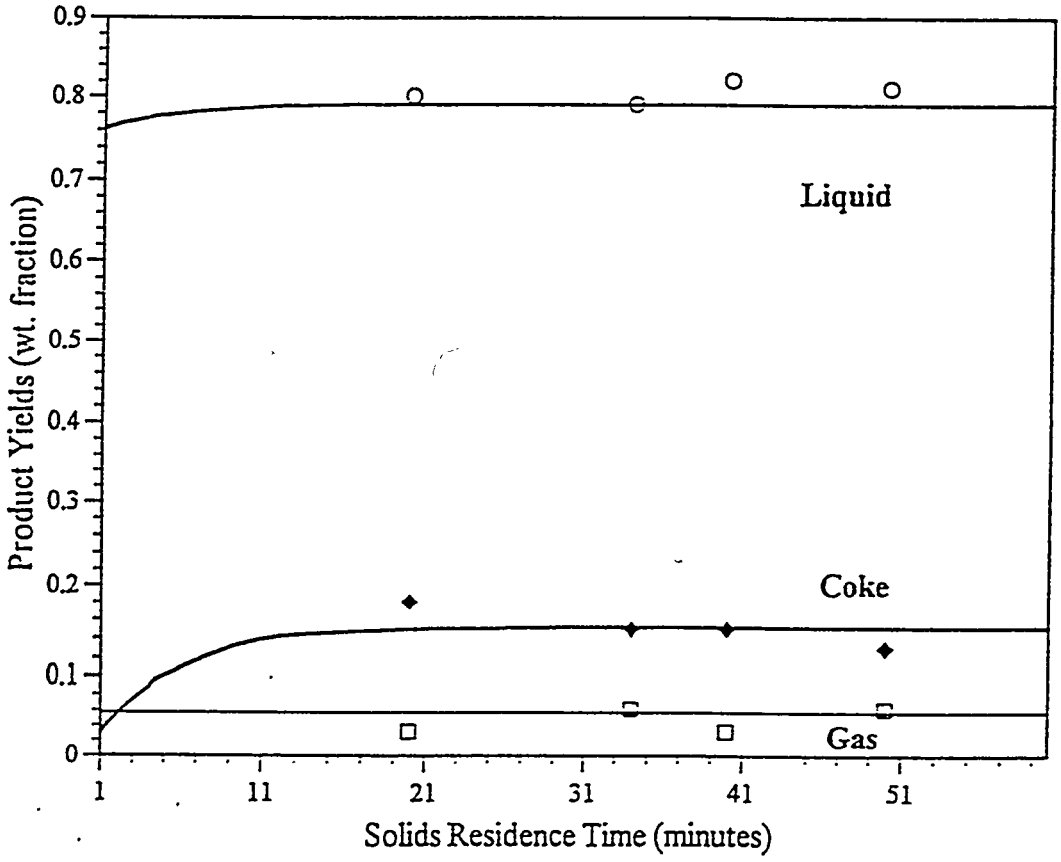
0.9
0.8
0.7
0.6
0.5
0.4
0.3
0.2
0.1
0
Product Yields (wt. fraction)
Liquid
Coke
Gas
1
11
21
31
41
51
Solids Residence Time (minutes)

Mass Transfer in Bubbling Fluidized Beds

Three distinct phases have been identified in the fluidized beds (135). Most of the gas flow through the bed occurs in the form of bubbles. This is called the bubble phase. A fraction of the gas maintains the solids in a suspended state. In this phase, the solids are essentially in the state of minimum fluidization. This phase is called the emulsion phase. As the bubble pushes through the emulsion phase, the particles move aside as would an incompressible inviscid fluid resulting in a region of high particle concentration surrounding the bubble. This phase is called the cloud phase. A schematic of these phases is presented in Figure 131.

The primary pyrolysis reactions of oil sand bitumens take place at the surface of the sand grains and the secondary cracking reactions take place in the gas phase (167). Gas flow through the emulsion phase being minimal (135), the pyrolysis products are transferred from the solid surface to the emulsion phase, from the emulsion phase to the cloud phase and finally from the cloud phase to the bubble phase. The products are then swept from the reactor by the bubbling gas. Kunii and Levenspiel (135) have reported that the rate controlling step in this process is the mass transfer to the bubble phase. Hence, the total reaction time for pyrolysis is dependent on the time taken for this step.

One of the primary motivations for the design and fabrication of the 15.2 cm ID reactor by Fletcher (121) was that the previous laboratory scale fluidized bed reactors (50, 51, 114, 120) had a tendency to operate in the slugging regime instead of the bubbling regime (161). The large diameter fluidized bed operated in the bubbling regime at bed loadings corresponding to H/D ratios in excess of four (121).

The rate of mass transfer between the emulsion and bubble phases is strongly dependent on the bubble phase mass transfer area available. In slugging beds the bubbles become very large

Figure 131

Mass Transfer from Emulsion Phase to Bubble Phase in a Fluidized Bed Reactor

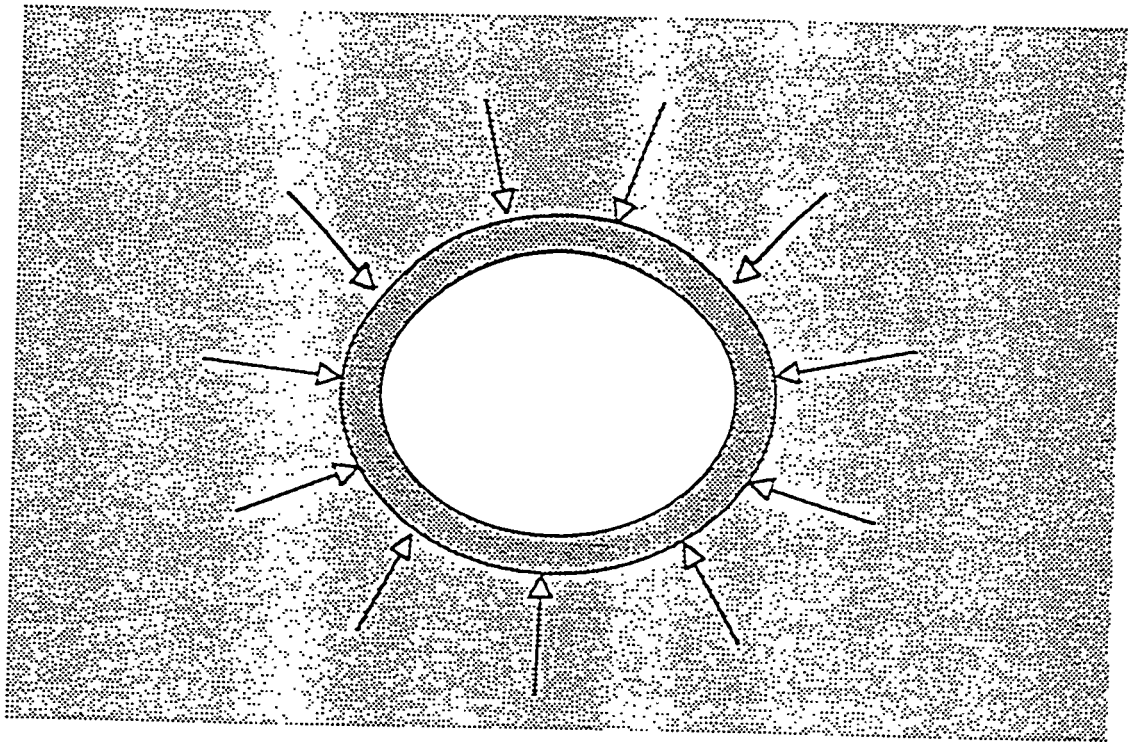

Emulsion Phase

Cloud Phase

Bubble Phase

which lowers the total mass transfer area and hence, the rate of removal of cracked and distilled oil from the emulsion phase. This also provides the time required for the slower heavy oil secondary cracking reactions (represented by reaction 3) to produce light oil and gas. The increase in the FBR reactor diameter to 15.2 cm ID and the "pull" mode of operation (121) led to a superior quality of fluidization and elimination of slugging in this reactor. Availability of a high interfacial mass transfer area between the cloud phase and the bubble phase led to a faster removal of primary cracked and distilled oil from the reactor which was responsible for the increased liquid yields. The secondary cracking reactions could not proceed to a significant extent due to the reduction in the total pyrolysis reaction time. Hence, an increase in reactor temperature had no effect on product distribution and yields as observed in this study.

Peterson and Ghishler (108) carried out coking of oil sands from Bitmont and Abasand oil sands in a 15 cm ID reactor and reported liquid yields of 84 to 86 wt% in the range of reactor temperature of 773 to 798 K. These results are similar to those obtained by Fletcher (121) and those obtained in this study in the large diameter fluidized bed reactor. Suppression of secondary cracking reactions due to elimination of wall effects in the large diameter reactor could be responsible for the high liquid yields obtained by Peterson and Ghishler (179).

The pyrolysis reaction time is indirectly related to the solids residence time in the bed. An increase in solids residence time results in an increase in the solid-vapor contact time. Carberry (180) determined that for sequential reactions (of the bitumen pyrolysis type) the liquid yields decrease with an increase in the gas-solid contact time. This observation explains the results of the earlier laboratory scale reactors (Figure 120). In slugging beds, the rate of mass transfer of primary cracked and distilled heavy oil from the emulsion phase to the bubble phase being low, the effective solid-vapor contact time is increased. This resulted in an increase in pyrolysis

reaction time which led to an increase in secondary cracking. This was probably responsible for the decrease in liquid yields and increase in gas yields. In the large diameter fluidized bed, the rapid removal of primary cracked and distilled liquid products led to an invariant product distribution with respect to solids residence time.

Characterization of Liquid Products

One of the objectives of this investigation was to perform complete physical and chemical analyses of the liquid products. The quality of the liquid products influences the choice of subsequent processing steps for further upgrading and refining. Moreover, knowledge of the effect of process parameters on the nature of the liquid products may provide insight into the pyrolysis reaction scheme and helps in determining the optimum set of process conditions for the pyrolysis process. It also provides information about the extent of bitumen upgrading achieved in the fluidized bed pyrolysis process.

The trends in product quality will be discussed in relation to the pyrolysis reaction scheme discussed in the previous section.

Effect of Reactor Temperature on Liquid Product Quality

The quality of liquid products as a function of the pyrolysis temperature is shown in Table 46. The effect of reactor temperature on the boiling point distribution of the liquid product is shown in Figure 132. The overall volatility of the liquids increased slightly (from 80 to 85 wt%). The gasoline and the gas oil fractions remained nearly constant and ranged from 3.1 to 3.9 wt% and from 55 to 59 wt%, respectively. The middle distillate fraction increased from 18 to 24 wt% while the residuum fraction decreased from 20 to 14 wt% as the reactor temperature increased from 723 to 808 K. These trends indicate that at high temperatures, secondary cracking of the

Table 46

Effect of Reactor Temperature on Liquid Product Quality

(Solids Residence Time = 31 ± 3 minutes, PR Spring Oil Sands Feed)

	SNPRS16	SNPRS5	SNPRS10	SNPRS13	SNPRS11
Temperature (K)	723	748	755	773	808
Simulated Distillation					
Volatility (wt%)	80.0	82.7	81.9	80.3	85.6
<477 K (wt%)	3.1	3.4	3.4	3.9	3.7
477-616 K (wt%)	18.7	20.1	21.6	20.8	24.8
617-811 K (wt%)	58.3	59.2	57.0	55.5	57.0
>811 K (wt%)	20.0	17.3	18.1	19.7	14.4
Properties					
Viscosity @ 298 K (cp)	507	347	369	420	259
Specific Gravity @ 293 K	0.96	0.94	0.94	0.94	0.94
Conradson Carbon (wt%)	2.8	2.3	2.8	3.3	3.2
Pour Point (K)	284	285	274	277	267
Asphaltenes (wt%)	4.4	2.3	1.7	1.8	2.7
Maltenes (wt%)	95.6	97.7	98.3	98.2	97.3
Elemental Analysis					
C (wt%)	86.12	86.15	86.71	85.34	85.32
H (wt%)	12.13	12.25	12.49	11.66	11.54
S (wt%)	0.29	0.28	0.29	0.29	0.29
N (wt%)	0.54	0.52	0.52	0.52	0.56
H/C (atomic ratio)	1.69	1.71	1.73	1.64	1.62

Figure 132

Effect of Reactor Temperature on Simulated Distillation of Liquid Products

(PR Spring Oil Sands Feed, Solids Residence Time = 31±3 min)

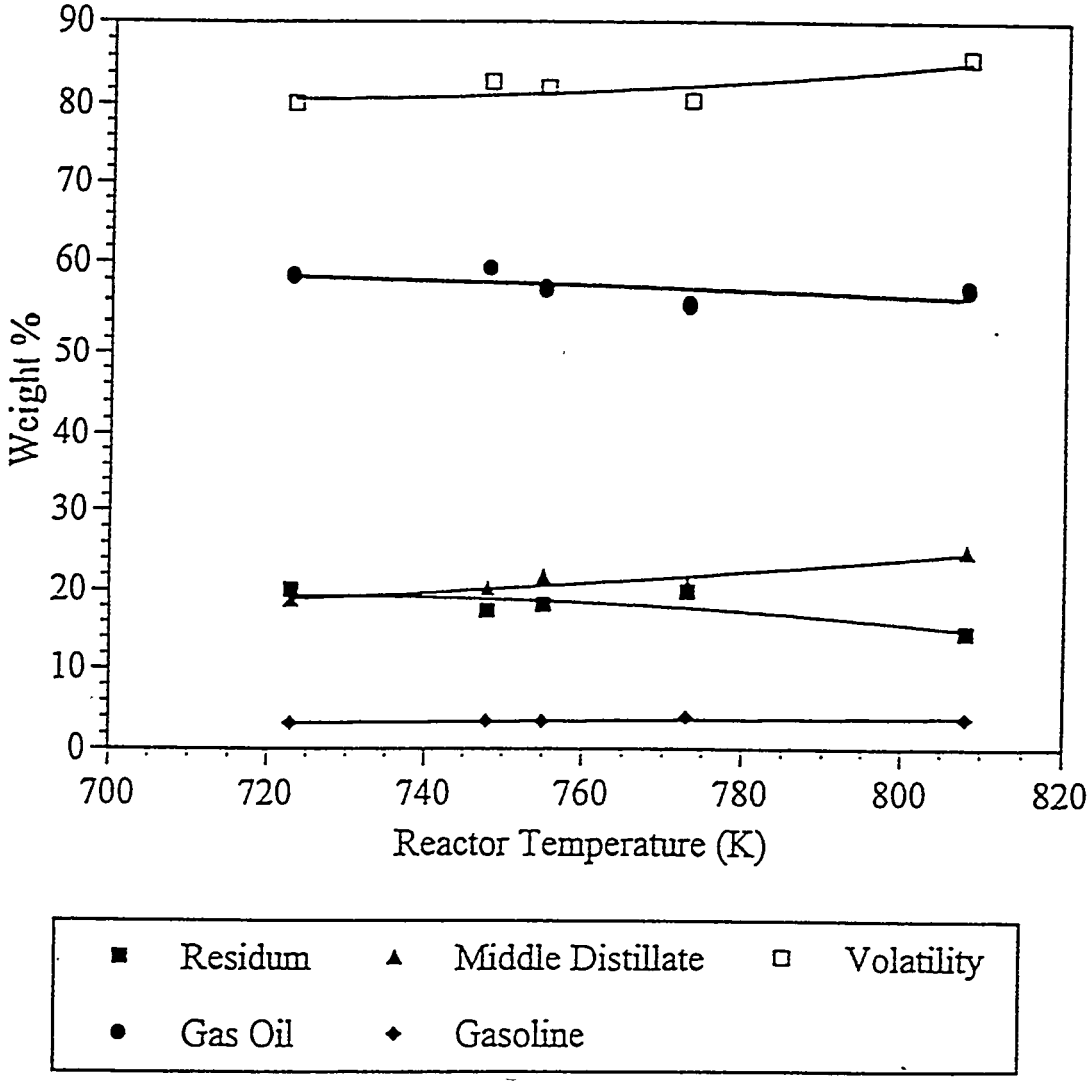
90
80
70
60
50
40
30
20
10
0
Weight %
700
720
740
760
780
800
820
Reactor Temperature (K)
Residum
Middle Distillate
Volatility
Gas Oil
Gasoline

residuum fraction to lighter fractions takes places. However, only a slight increase (5 wt%) in the overall volatility of the liquid products with reactor temperature indicates that secondary cracking was suppressed even at high temperatures because of the rapid removal of the primary cracked and distilled products.

The trends obtained in viscosity and pour point (Figures 133 and 134, respectively) can also be explained by this argument. Increased secondary cracking at high temperatures led to slightly lighter and a less viscous liquid products.

The specific gravity (Figure 135) of the liquid product reduced with increase in the reactor temperature in the range 723 to 755 K but remained nearly constant in the range 755 to 808 K. This plateau could be due to the condensation reactions of aromatic free radicals to form higher molecular weight aromatics (65).

The Conradson carbon residue of the liquid products increased slightly as the reactor temperature increased (Figure 136). The polynuclear aromatics (PNA) with alkyl side chains which constitute the asphaltene fraction of the bitumen (65) undergo cracking reactions at high reactor temperatures. The alkyl side chains are severed and removed from the reactor as lighter products. Hence, an increase in cracking leads to an increase in the aromaticity of the liquid products which form precursors for coke. This is reflected in an increase in the Conradson carbon residue of the liquid products as the severity of the reaction increased.

The asphaltene (n-pentane insolubles) content of the liquid product decreased with increase in reactor temperature up to 775 K and increased beyond 780 K (Figure 137). The decrease was probably due to the conversion of PNAs to aromatics (as explained above) as the reactor temperature increased. At high reactor temperatures ($>$780 K) formation of coke precursors due to condensation reactions of aromatic free radicals results in an increase in the total asphaltene

Figure 133

Effect of Reactor Temperature on Viscosity of Liquid Products

(PR Spring Oil Sands Feed, Solids Residence Time = 31±3 min)

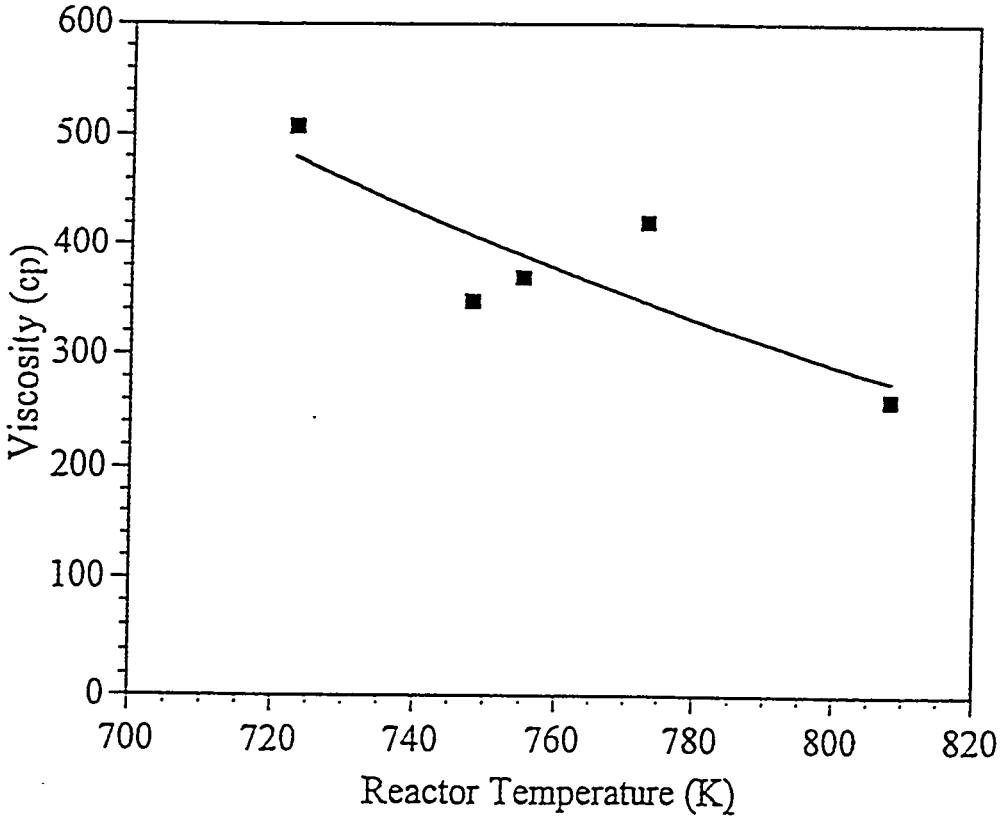
600
500
400
300
200
100
0
Viscosity (cp)
700
720
740
760
780
800
820
Reactor Temperature (K)

Figure 134

Effect of Reactor Temperature on Pour Point of Liquid Products

(PR Spring Oil Sands Feed, Solids Residence Time = 31±3 min)

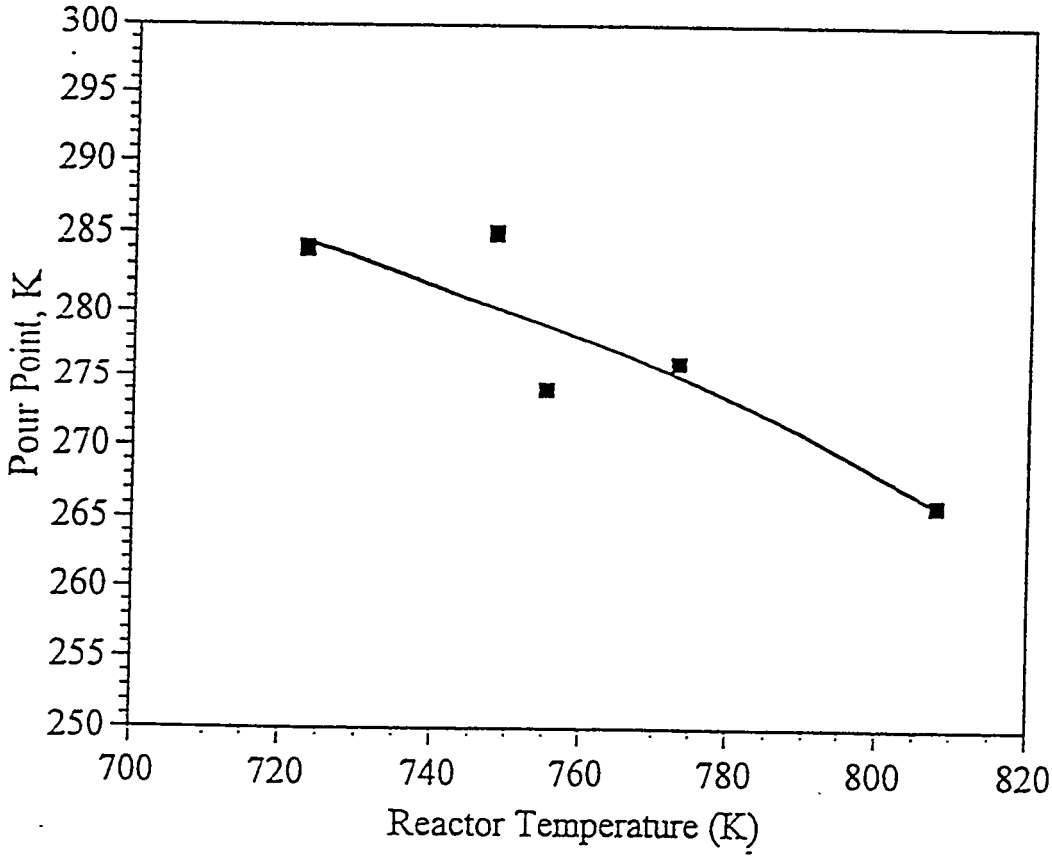
300
295
290
285
280
275
270
265
260
255
250
Pour Point, K
700
720
740
760
780
800
820
Reactor Temperature (K)

Figure 135

Effect of Reactor Temperature on Specific Gravity of Liquid Products

(PR Spring Oil Sands Feed, Solids Residence Time = 31±3 min)

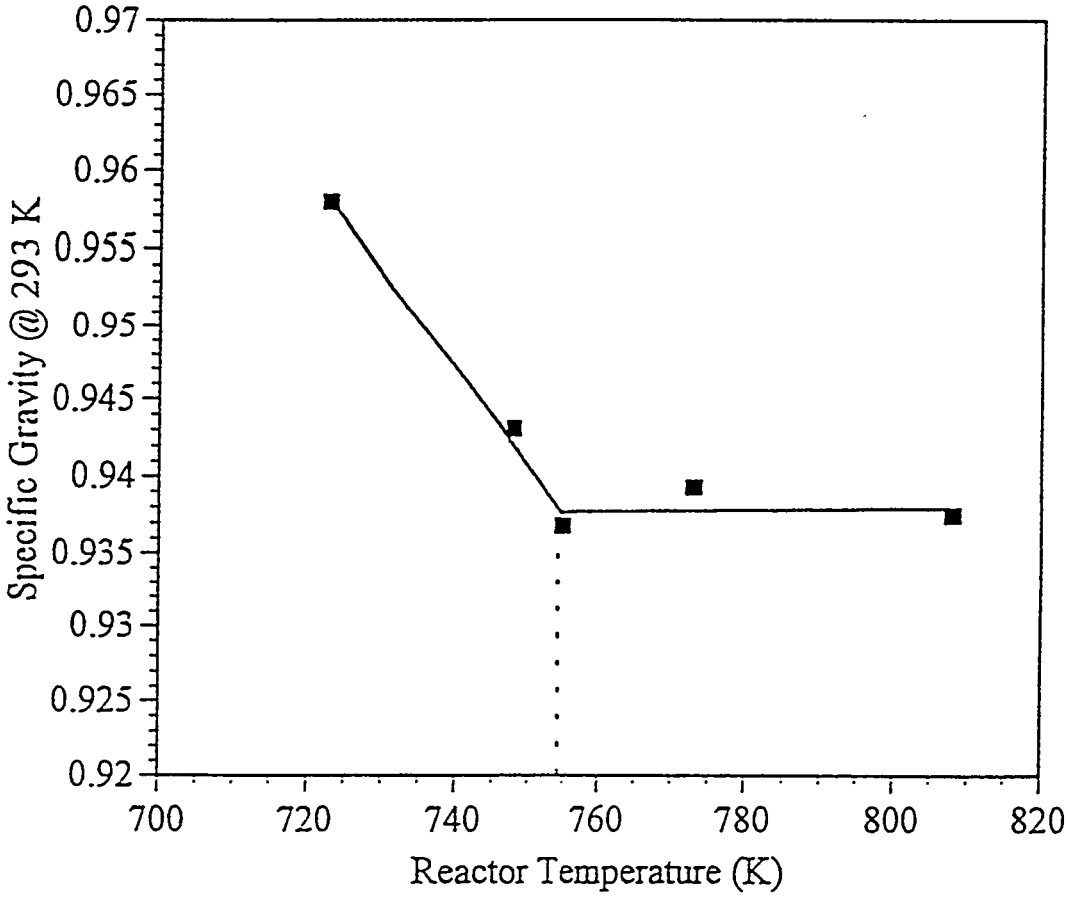
0.97
0.965
0.96
0.955
0.95
0.945
0.94
0.935
0.93
0.925
0.92
Specific Gravity @ 293 K
700
720
740
760
780
800
820
Reactor Temperature (K)

Figure 136

Effect of Reactor Temperature on Conradson Carbon Residue

of Liquid Products

(PR Spring Oil Sands Feed, Solids Residence Time = 31±3 min)

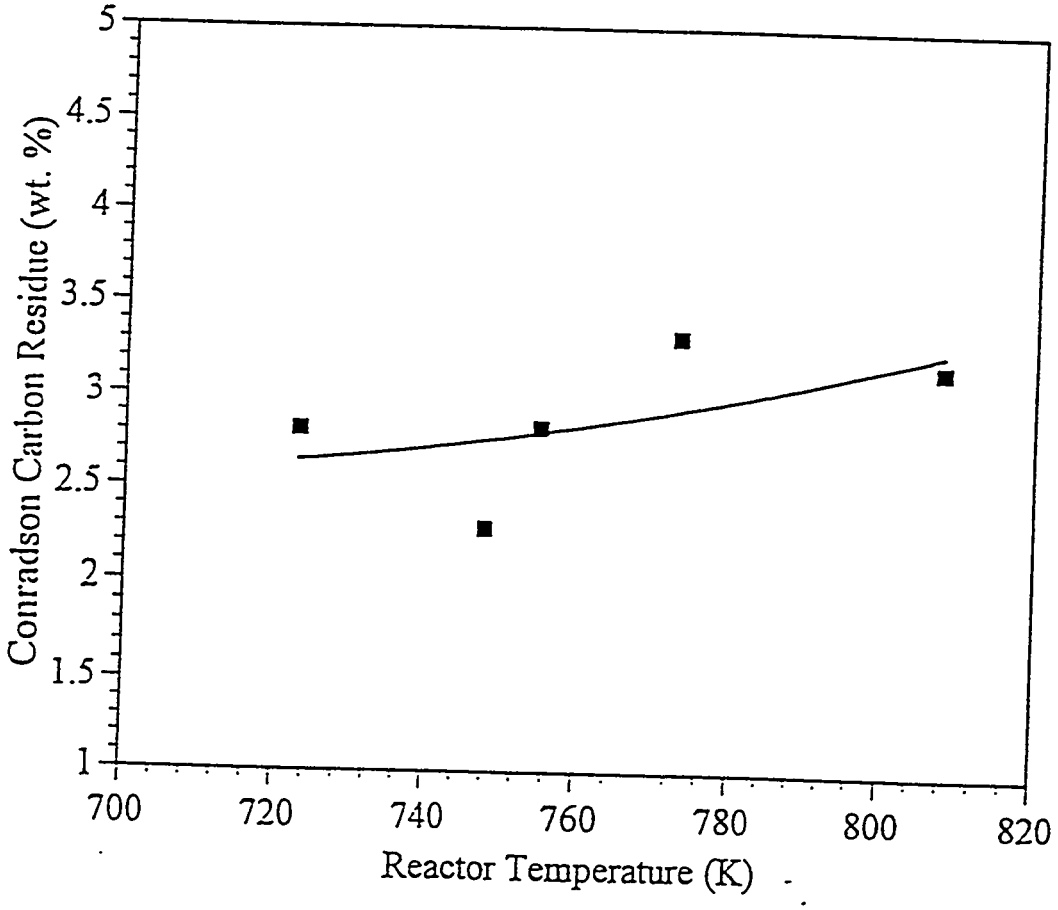
Conradson Carbon Residue (wt. %)
5
4.5
4
3.5
3
2.5
2
1.5
1
700
720
740
760
780
800
820
Reactor Temperature (K)

Figure 137

Effect of Reactor Temperature on Asphaltene Content of Liquid Products

(PR Spring Oil Sands Feed, Solids Residence Time = 31±3 min)

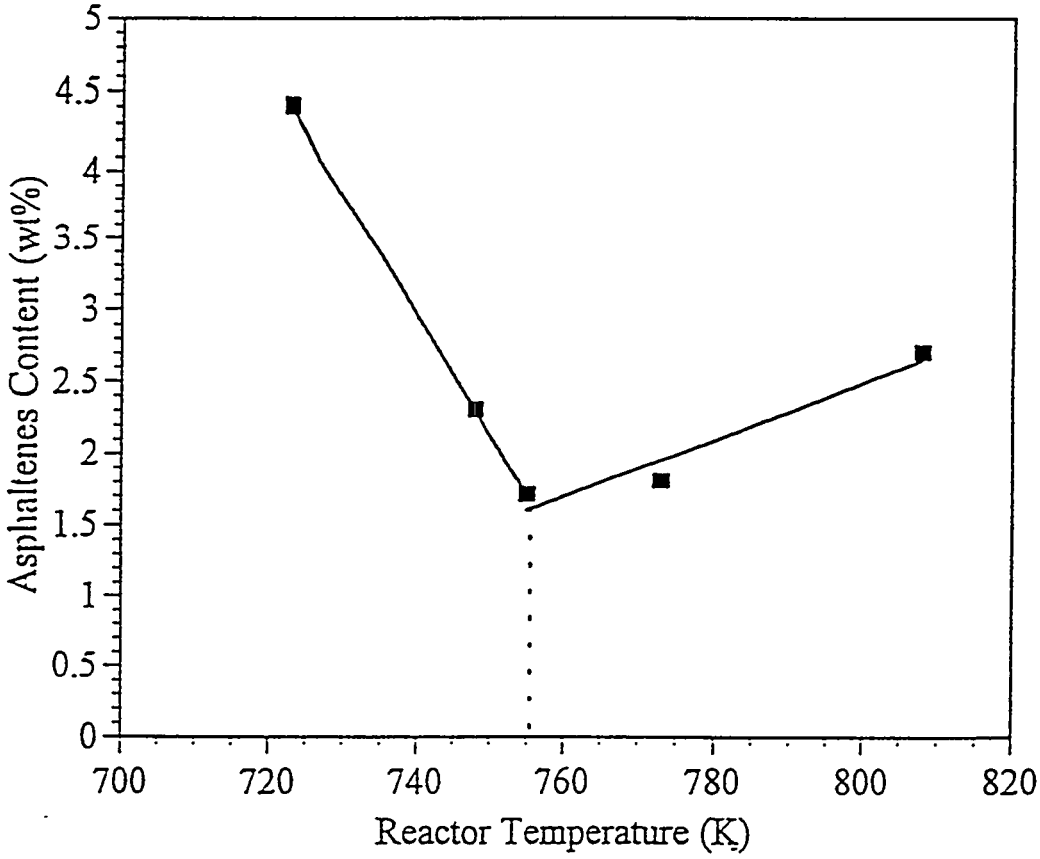
Asphaltenes Content (wt%)
5
4.5
4
3.5
3
2.5
2
1.5
1
0.5
0
700
720
740
760
780
800
820
Reactor Temperature (K)

content of the liquid product.

The effect of reactor temperature on the H/C ratio of the liquid products is shown in Figure 138. The H/C ratio increased as the reactor temperature increased from 723 to 755 K and decreased as the reactor temperature increased from 755 to 808 K. As the reactor temperature is increased from 723 to 755 K, the high molecular weight compounds crack to form heavy oil and coke. This leads to a net increase in the H/C ratio of the liquid product since the hydrogen deficient species are depositing on the sand grains as coke. As the temperature increased beyond 755 K, the alkyl chains attached to the asphaltic and resinous naphthenoaromatic species are severed and removed from the reactor as high H/C lower molecular weight products. Hence, the overall H/C ratio decreases because of increased formation of high H/C gas products at higher temperatures.

The nitrogen and sulphur contents of the liquid product did not exhibit trends with reactor temperature and remained nearly constant at approximately 0.5 and 0.3 wt%, respectively.

Effect of Solids Residence Time on Liquid Product Quality

The effect of solids residence time on the quality of the liquid product is shown in Table 47. There were no apparent trends in liquid quality with increasing solids residence time. Due to the superior quality of fluidization and rapid removal of primary cracked products from the reactor, the solids residence time did not exert any clear influence on the quality of the liquid products. This trend is in concurrence with the proposed kinetic and hydrodynamic explanation for the trends.

Extent of Bitumen Upgrading

A significant advantage of the use of thermal methods (fluidized bed and rotary kiln

Table 47

Effect of Solids Residence Time on Liquid Product Quality

(Reactor Temperature = 773 K, PR Spring Oil Sands Feed)

	SNPRS12	SNPRS13	SNPRS14	SNPRS9
Solids Res. Time (min)	20	34	40	50
Simulated Distillation				
Volatility (wt%)	84.8	80.3	80.2	84.2
<477 K (wt%)	4.5	3.9	4.1	3.9
477-616 K (wt%)	23.9	20.8	20.6	22.1
617-811 K (wt%)	56.4	55.5	55.6	58.2
>811 K (wt%)	15.2	19.7	19.8	15.8
Properties				
Viscosity @ 298 K (cp)	183	420	431	212
Specific Gravity @ 293 K	0.96	0.94	0.95	0.95
Conradson Carbon (wt%)	2.5	3.3	3.3	2.6
Pour Point (K)	279	277	277	273
Asphaltenes (wt%)	1.9	1.8	2.8	1.7
Maltenes (wt%)	98.1	98.2	97.2	98.3
Elemental Analysis				
C (wt%)	86.15	85.34	-	85.83
H (wt%)	11.98	11.66	-	11.97
S (wt%)	0.29	0.29	-	0.31
N (wt%)	0.54	0.52	-	0.52
H/C (atomic ratio)	1.67	1.64	-	1.67

processes) over other surface recovery methods is the upgrading of bitumen during the pyrolysis process. The physical and chemical properties of the liquid products from this study were determined and compared to the bitumen properties. The extent of bitumen upgrading achieved in this study is shown in Table 48.

There is a marked difference between the physical properties of the liquid product and the bitumen. The specific gravity of the liquid product was lower than that of the bitumen. A similar trend was observed for the pour point of the two liquids. The liquid product is about three orders of magnitude less viscous than the bitumen. The volatility of the liquid product is 80 wt% as against 36 wt% for the bitumen. All of these trends can be explained on the basis of thermal cracking of high molecular weight compounds in the bitumen to form lighter compounds.

The higher H/C atomic ratio of the pyrolyzed liquid indicates the extent of upgrading. The nitrogen and sulphur contents are significantly lower indicating that a portion of the hetroatoms were deposited on the sand grains along with the coke. The liquid products had a lower trace metal content than the bitumen which suggested that most of the trace metals in the bitumen are concentrated in the coke product. The marked reduction in the asphaltene and Conradson carbon residue contents of the bitumen during the pyrolysis process was indicative of the thermal conversion of the asphaltenes to aromatics and light gases as explained earlier.

The high degree of upgrading achieved in the pyrolysis process was reflected by the improvement in the liquid product properties over the bitumen. The high volatility and low asphaltenes, Conradson carbon residue, hetroatoms, and trace metals contents of the liquid products indicate that they could be upgraded to refinery feedstock quality by hydrotreating (51, 163).

Table 48

Extent of Bitumen Upgrading

Properties	PR Spring Bitumen	Total Liquid Product (Run ID SNPRS13, T = 773 K, Θ = 34min)
Specific Gravity	1.005 @ 288 K [a]	0.939 @ 293 K
Conradson Carbon (wt%)	14.2[a]	3.3
Pour Point (K)	319[a]	277
Viscosity (cp)	870,000 @ 311 K[a]	420 @ 298 K
Asphaltenes[b] (wt%)	19.3[a]	1.8
Maltenes (wt%)	80.7[a]	98.2
Elemental Analysis		
C (wt%)	84.0	85.3
H (wt%)	10.6	11.7
S (wt%)	0.43	0.29
N (wt%)	0.91	0.52
Ni (ppm)	38	< 4.5
V (ppm)	6	< 4.5
H/C atomic ratio	1.52	1.64
Molecular Weight, g mole^{-1}	924	441
Simulated Distillation		
Volatility (wt%)	45.4[a]	80.2
< 477 K (wt%)	0.4[a]	3.9
477 - 616 K (wt%)	8.2[a]	20.8
617 - 811 K (wt%)	36.8[a]	55.5
> 811 K (wt%)	54.6[a]	19.8

[a] Data from Subramanian (1994)

[b] As Pentane insolubles

Comparison of Fluidized Bed and Rotary Kiln

Pyrolysis Processes

Cha (105) and Hanson et al. (113) reported on pyrolysis studies using the Whiterocks oil sands in a 15.2 cm ID rotary kiln reactor. A maximum liquid yield of 65.5 wt% was reported at a temperature of 773 K and a residence time of 21 min. The gas and coke yields for these conditions were 13.0 wt% and 21.5 wt%, respectively (105). Pyrolysis experiments in a 15.2 cm ID fluidized bed reactor with the Whiterocks oil sands by Fletcher (121) resulted in a liquid product yield of 84.5 wt% at similar process conditions. A liquid product yield of 80 wt% was obtained in this investigation with PR Spring oil sands (which has a higher asphaltene content, 19.3 wt% [64] compared to 11.4 wt% for the Whiterocks bitumen [113]) at 773 K and a solids residence time of 20 min.

The product distribution and the properties of the liquid products from the 15.2 cm ID rotary kiln and fluidized bed pyrolysis experiments are compared in Table 49. The yields of liquid products obtained in the large diameter fluidized bed reactor studies were approximately 15-20 wt% higher than the liquid product yield from the rotary kiln reactor at similar process conditions. However, the rotary kiln liquid product was higher in API gravity and volatility and lower in viscosity and pour point indicating a slightly greater extent of upgrading.

These trends are consistent with the proposed explanation of the impact of kinetics of the pyrolysis reaction and hydrodynamic characteristics of the large diameter fluidized bed reactor on the product distribution and yields. The high interfacial contact area between the emulsion phase and the bubble phase in the 15.2 cm ID fluidized bed reactor leads to rapid removal of the primary pyrolysis products from the reactor thereby suppressing the secondary cracking reactions. In contrast, there is almost no gas flow through the rotary kiln solids and the mass transfer rate

Table 49

Comparison of Liquid Products from Rotary Kiln and Fluidized Bed

	Fluidized Bed (This Work)	Rotary Kiln (Cha, 1991)	Fluidized Bed (Fletcher, 1992)
Feed Source	PR Spring	Whiterocks	Whiterocks
Process Conditions			
Temperature (K)	773	773	773
Residence Time (min)	20	20	20
Product Yields			
Liquid (wt%)	80	65	85
Gas (wt%)	3	13	9
Coke (wt%)	18	22	6
Properties			
API Gravity	15.9	22.3	19.0
Conradson Carbon (wt%)	2.4	1.3	2.3
Viscosity @ 298 K	183	76	-
Pour Point (K)	279	251	-
Asphaltenes[a] (wt%)	1.9	3.3	3.6
Maltenes (wt%)	98.1	96.7	96.4
Simulated Distillation			
Volatility (wt%)	84.8	100	85.6
< 477 K (wt%)	4.5	7.7	1.3
477 - 617 K (wt%)	23.9	24.3	33.8
617 - 811 K (wt%)	56.4	68.0	50.8
> 811 K (wt%)	15.2	0.0	14.4

[a]As pentane insolubles

from the solid phase to the vapor phase above the surface of the solids is reduced. Thus the effective residence time of produced heavy oils in the vicinity of the sand grains is increased and secondary cracking reactions become significant leading to lower liquid yields, higher gas yields and higher extent of upgrading.

Preferred Process Conditions

The liquid product yields were independent of the reactor temperature and solids residence time. However, the liquid product analyses indicated that the produced liquids were substantially upgraded at high reactor temperatures (> 748 K). The liquid product obtained at a reactor temperature of 723 K was significantly less upgraded as compared to the liquid products obtained at higher reactor temperatures (high specific gravity, high viscosity, high pour point, etc.). Hence, based on these observations, a reactor temperature of 748 K and a solids residence time of 20 min or less is recommended for pyrolysis of oil sands in a fluidized bed reactor. The fluidization gas flow corresponding to approximately five times the minimum fluidization velocity (U_{mf}) should be maintained.

SUMMARY AND CONCLUSIONS

This investigation has conclusively demonstrated that the fluidized bed pyrolysis of oil sands has certain clear advantages over other surface recovery methods. Bitumen obtained from the hot-water process is considerably less upgraded as compared to the liquid product obtained in the fluidized bed thermal process. The environmental problems associated with tailing ponds in the hot water process and waste solvent disposal in the solvent recovery method are also eliminated in this process. The liquid product yields obtained in this investigation were considerably higher than those obtained from the rotary kiln pyrolysis reactor (105).

The tasks completed during this investigation and the results and conclusions of the pyrolysis experiments are summarized as follows.

1. A two-burner system was designed, constructed, installed and successfully operated for pyrolysis of PR Spring oil sands in the large diameter fluidized bed reactor. The new burner system performed well under high thermal stress and was able to provide heat input sufficient to achieve solids residence times of as low as 20 min. The adjustable burner supports successfully supported the weight of the burner assembly and provided sufficient flexibility to account for the reactor expansion at high temperatures.

2. Pyrolysis experiments with PR Spring oil sands feed were conducted in the modified large diameter fluidized bed reactor. The effect of reactor temperature and solids residence time on product yields and quality was determined. The

reactor temperature and solids residence time did not have any apparent effect on the product distribution and yields.

3. The liquid product yields obtained in this study were significantly higher than those obtained from laboratory scale fluidized beds (104) and rotary kiln reactors (105, 113).

4. The trends in the process variable studies and the high liquid yields have been explained by a combination of the kinetics of the pyrolysis reaction and the hydrodynamic characteristics of the large diameter fluidized bed reactor when operated in the pull mode. It is proposed that the secondary cracking reactions were suppressed in this reactor by rapid removal of primary cracked pyrolysis products. This was due to the increased interfacial mass transfer area between the emulsion phase and the bubble phase because of the improvement in the quality of fluidization achieved in the large diameter fluidized bed reactor as compared to the laboratory scale fluidized bed reactors.

5. A simplified two-reaction pyrolysis network was proposed which fit the experimental product yield data reasonably well for a bubbling fluidized bed.

6. The liquid products obtained in this study were found to be considerably upgraded as compared to the bitumen on the oil sands fed to the reactor.

7. The reactor temperature was found to influence the liquid product quality to some extent. Viscosity, specific gravity, and pour points of the liquid product decreased with increase in the pyrolysis temperature while volatility increased. The Conradson carbon residues of the produced liquids were nearly insensitive to

pyrolysis temperature.

8. The solids residence time (Θ) did not appear to influence the liquid product quality.

9. The rotary kiln and fluidized bed pyrolysis processes were compared with respect to the product yields and liquid product quality. The liquid product yields obtained from the large diameter fluidized bed reactor were higher than those from the rotary kiln pyrolysis reactor (approximately 80 wt% as compared to 65 wt%). However, the rotary kiln liquid product was slightly more upgraded in terms of volatility, API gravity, and viscosity. The rotary kiln process variable data base is not sufficient to prepare the technical and economic evaluations required to select the rotary kiln or fluidized bed as the preferred pyrolysis reactor.

10. Based on the product yields and liquid product quality, a reactor temperature of 748 K (475°C) and a solids residence time of 20 min are recommended for continuous operation of the fluidized bed pyrolysis process.